

Durham E-Theses

The walls boundary fault zone and the Møre Trøndelag fault complex:: a case study of two reactivated fault zones.

Watts, Lee Mark

How to cite:

Watts, Lee Mark (2001) *The walls boundary fault zone and the Møre Trøndelag fault complex:: a case study of two reactivated fault zones.*, Durham theses, Durham University. Available at Durham E-Theses Online: <http://etheses.dur.ac.uk/3878/>

Use policy

The full-text may be used and/or reproduced, and given to third parties in any format or medium, without prior permission or charge, for personal research or study, educational, or not-for-profit purposes provided that:

- a full bibliographic reference is made to the original source
- a [link](#) is made to the metadata record in Durham E-Theses
- the full-text is not changed in any way

The full-text must not be sold in any format or medium without the formal permission of the copyright holders.

Please consult the [full Durham E-Theses policy](#) for further details.

Academic Support Office, Durham University, University Office, Old Elvet, Durham DH1 3HP
e-mail: e-theses.admin@dur.ac.uk Tel: +44 0191 334 6107
<http://etheses.dur.ac.uk>

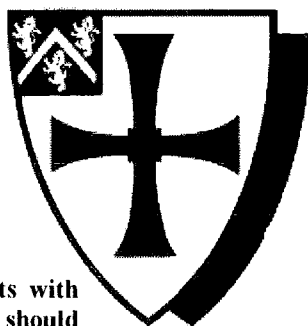
**The Walls Boundary Fault Zone and
the Møre-Trøndelag Fault Complex:
a Case Study of Two Reactivated Fault Zones.**

by

Lee Mark Watts

**A thesis submitted in fulfilment of the requirements of the University of
Durham for the degree of Doctor of Philosophy**

**Department of Geological Sciences
University of Durham**



The copyright of this thesis rests with the author. No quotation from it should be published in any form, including Electronic and the Internet, without the author's prior written consent. All information derived from this thesis must be acknowledged appropriately.

2001



28 MAY 2002

Declaration

No part of this thesis has been previously submitted for a degree at this, or any other university. The work described in this thesis is entirely that of the author, except where reference is made to previously published work.



Lee M. Watts

Department of Geological Sciences,

University of Durham

November 2001

©Lee M. Watts

The copyright of this thesis rests with the author. No quotation or data from it should be published without the author's prior written consent and any information derived from it should be acknowledged.

Abstract

It is commonly observed that ancient faults or shear zones can become reactivated again and again, either within the same or even superimposed tectonic episodes, yet millions of years apart. Rocks of the continental crust show such effects particularly well, owing to their longevity, because through their buoyancy, continental rocks resist recycling back into the Earth's mantle over long time-scales. The Møre-Trøndelag Fault Complex (MTFC), Central Norway and the Walls Boundary Fault (WBF), Shetland, were studied to elucidate the kinematic, geometric and textural evolution, in order to assess fault linkages, fault-rock preservation styles and the controlling factors on fault reactivation

The WBF is a crustal-scale, reactivated fault that separates distinctively different basement terranes; the Caledonian front to the west from Dalradian type rocks to the east. The WBF initiated as a late-Caledonian sinistral strike-slip fault (c.100-200km offset) associated with the development of mylonites and cataclasites. Dextral strike-slip reactivation (c.65km) in the Permo-Carboniferous related to inversion of the Orcadian Basin and led to the development of cataclasite and fault gouge assemblages. Later dip-slip and finally sinistral strike-slip (c.15km, Tertiary?) reactivation were localised within earlier formed fault gouges.

The ENE-WSW-trending MTFC in Central Norway is a 10-20 km wide, steeply dipping zone of fault-related deformation. The MTFC has a prolonged and heterogeneous kinematic history. The complex comprises two major fault strands: the Hitra-Snåsa Fault (HSF) and the Verran Fault (VF). These two faults seem to have broadly initiated as part of a single system of sinistral shear zones during Early Devonian times (409 ± 12 Ma). Sinistral transtensional reactivation (dated as Permo-Carboniferous; 291 ± 14 Ma) of the ENE-WSW-trending HSF and VF led to the development of cataclasites and pseudotachylites together with the formation of N-S-trending faults leading to the present day brittle fault geometry of the MTFC. Several later phases of reactivation were focused along the VF and N-S linking structures during the Mesozoic probably related to Mid-Late Jurassic / Early Cretaceous rifting and Late Cretaceous / Early Tertiary opening of the North Atlantic.

Based on apparent offshore trends, it has been suggested that the MTFC and the WBF may have been linked at some stage during their evolution and subsequent reactivation. This is consistent with the present study, as early Devonian movements along both the WBF and the MTFC are sinistral. Differences in the magnitude, dynamics and senses of displacement in the Permo-Carboniferous, however, seem to militate against linkage of these faults in the late Palaeozoic. There is no compelling evidence for direct Mesozoic or Tertiary linkage, although both structures were reactivated to some extent during these times. It seems that the formation and reactivation of the WBF and MTFC were associated with broadly similar regional tectonic processes and therefore, to some extent, share similar kinematics. Although both the MTFC and the WBF show clear proof of repeated reactivated, superficially similar geometries or alignments should not be used as a basis for correlating structures, in the absence of direct kinematic evidence.

Displacements along the MTFC and the WBFZ are repeatedly localised along the earlier formed fault rocks, suggesting that these fault rocks are intrinsically weak compared to the surrounding rocks. A complex interaction exists between the geometrical properties of the fault network and fault-zone weakening mechanisms operative within fault rocks around the level of the frictional-viscous transition. Together these factors control fault reactivation in the long term. In the case of reactivated, sub-vertical, strike-slip fault zones the preservation and exhumation of these fault rocks both depend on the architecture and magnitude of later reactivations.

Acknowledgements

Firstly, I'd like to thank my supervisor's Bob Holdsworth (even if he does support Man Utd.) for his guidance, enthusiasm and encouragement, David Roberts (Norwegian Geological Survey) for his help in the field, vast knowledge of regional geology and amazing capacity to spot typos, and Tony Dore (Statoil UK) for financial assistance and stimulating discussions. Sarah Sherlock (Open University) is thanked for carrying out, much appreciated, fault-rock dating analyses of samples from Norway. Eric Condcliffe is thanked for help with SEM work and Laurence Warr is also thanked for carrying out XRD analyses on fault gouges from Norway. Other unsung heroes of the Geology Dept. (Karen Atkinson, Gary Wilkinson, Dave Stevenson and Alan Carr) are thanked for technical assistance.

Cheers to the liquor-hungry mob a.k.a. grad. soc. pool club (Geoff, Alex, Ed, Rich, Dave, Phyto and many others) for some very memorable nights. In particular, the mauling of Van Mildert and the ruck that followed, and the narrow defeat in the final of the trophy. I'd also like to thank the post-grads in Durham (Phil, Dave, Rich, Ade, Abi, Jules, Helen and other hang-ons) for some memorable, if clouded evenings. Cheers to the dept. five-a-side team, whom over the years, have transformed from the whipping boys to mid-table obscurity and now to a side to be feared!

Thanks to Elin, Odd, Juliet and Jan for letting us try out the luxurious Sjøhus and boat, introducing me to the delights of supping wine while fishing on the fjord after a long day in the field, and generally showing us a great time in Trøngsundet, and introducing us to the many crazy 'locals'. Many thanks to John at the Westing's in Shetland for saving us from camping in freezing Shetland, and providing us with convenient, comfy accommodation above the bar!

Thanks to Mum, Dad, Nan and Grandad for their love and support over the years. Finally, I'd like to thank Janine for her love and support, and such a fantastic time over the years here in Durham and on fieldwork.

The Walls Boundary Fault Zone and the Møre-Trøndelag Fault Complex: a Case Study of Two Reactivated Fault Zones.

CHAPTER 1. INTRODUCTION	1
1:1 INTRODUCTION AND AIMS	1
1:2 THE CONTINENTAL LITHOSPHERE.....	3
1:2:1 <i>The strength of the continental lithosphere</i>	5
1:3 FAULT ZONE REACTIVATION	6
1:4 FAULT ROCK DEFINITIONS AND SHEAR SENSE INDICATORS.....	6
1:5 METAMORPHISM ALONG FAULTS AND SHEAR ZONES.....	12
1:5:1 <i>Metamorphic classification scheme</i>	12
1:5:2 <i>Fluid transport in fault zones</i>	12
1:6 DEFORMATION MECHANISMS	16
1:6:1 <i>Frictional deformation mechanisms</i>	17
1:6:2 <i>Viscous deformation mechanisms</i>	19
1:6:2:1 Diffusive mass transfer (DMT)	20
1:6:2:2 Crystal plasticity	21
1:6:3 <i>Mineral strength behaviour</i>	23
1:6:4 <i>Aggregate strength and behaviour</i>	25
1:6:5 <i>Frictional to viscous creep transition</i>	27
1:7 FAULT-ZONE WEAKENING MECHANISMS	28
1:7:1 <i>Transient, syn-tectonic weakening mechanisms</i>	28
1:7:1:1 High pore-fluid pressure.....	28
1:7:1:2 Hydrolytic weakening	29
1:7:1:3 Generation of transient, fine grained reaction products.....	29
1:7:1:4 Transformational plasticity and volume change.....	30
1:7:1:5 The introduction of melt.....	30
1:7:1:6 Shear heating.....	31
1:7:2 <i>Long-term weakening mechanisms</i>	31
1:7:2:1 Favourable orientation of a pre-existing anisotropy	31
1:7:2:2 Reaction softening.....	33
1:7:2:3 Fabric softening.....	33
1:7:2:3a Foliation weakening	34
1:7:2:3b Development of crystallographic fabrics.....	34
1:7:2:4 Grain-size reduction.....	35
1:7:2:5 Fluid-assisted DMT.....	35
1:8 DATA COLLECTION.....	36
1:8:1 <i>Fieldwork methods</i>	36
1:8:2 <i>Microstructural methods</i>	36
1:8:3 <i>Major element geochemistry</i>	37

1:8:4 $^{40}\text{Ar}/^{39}\text{Ar}$ laserprobe dating.....	37
1:9 OUTLINE OF THESIS	37
CHAPTER 2. THE GEOLOGY OF SHETLAND.....	39
2:1: ONSHORE GEOLOGY	41
2:1:1 <i>Caledonian and Older Basement west of the WBF</i>	41
2:1:1:1 Lewisianoid basement associated with the Caledonian Front	41
2:1:1:2 Sand Voe Group.....	44
2:1:1:3 Hillswick Group.....	44
2:1:1:4 Queyfirth Group.....	44
2:1:1:5 Metamorphic rocks of the Walls Peninsula.....	45
2:1:2 <i>East Mainland Succession</i>	45
2:1:2:1 Yell Sound Division.....	45
2:1:2:2 Moine-Dalradian boundary zone.....	46
2:1:2:3 The Scatsta Division	46
2:1:2:4 The Whiteness Division	47
2:1:2:5 The Clift Hills Division.....	47
2:1:3 <i>The Unst Ophiolite</i>	48
2:1:3:1 Metamorphic Rocks	48
2:1:3:2 Lower Nappe.....	48
2:1:3:3 Mélange Zones.....	49
2:1:3:4 Upper Nappe	49
2:1:3:5 The Phyllite Group.....	49
2:1:3:6 Skaw Granite.....	50
2:1:4 <i>Regional Synthesis of Caledonian and Older Basement</i>	50
2:1:4 <i>Devonian Sandstones</i>	51
2:1:4:1 Central Group.....	51
2:1:4:2 Western Group	53
2:1:4:3 Eastern Group	54
2:1:5 <i>Plutonic rocks</i>	54
2:1:5:1 Eastern Late-orogenic Complexes.....	54
2:1:5:1a Graven Complex	54
2:1:5:1b Brae Complex	55
2:1:5:1c Spiggie Complex.....	55
2:1:5:2 Western Post-orogenic Complexes.....	55
2:1:5:2a Northmaven Complex	55
2:1:5:2b Sandsting Complex	56
2:1:6 <i>Regional Synthesis of Devonian</i>	56
2:2 OFFSHORE GEOLOGY	58
2:2:1 <i>Shetland Platform</i>	58
2:2:1:1 West Fair Isle Basin.....	58
2:2:1:2 East Fair Isle basin	60

2:2:1:3 Unst and Fetlar basins	60
2:2:1:4 Sandwich Basin	60
2:2:2 <i>Viking Graben (VG) and East Shetland Basin (ESB)</i>	61
2:2:2:1 West Shetland Basin (WSB)	61
2:2:2:2 Faroe-Shetland Basin (FSB).....	62
2:2:3 <i>Regional Synthesis of Offshore Geology</i>	62
2:3 WALLS BOUNDARY FAULT SYSTEM.....	63
2:3:1 <i>Melby Fault (MF)</i>	63
2:3:2 <i>Nestings Fault (NF)</i>	63
2:3:3 <i>Walls Boundary Fault</i>	63
2:3:3:1 Onshore	64
2:3:3:2 Offshore	64
2:3:4 <i>Regional Synthesis of WBF</i>	67
CHAPTER 3. WALLS BOUNDARY FAULT SYSTEM, SHETLAND	69
3:1 THE WALLS BOUNDARY FAULT ZONE: LOCALITY DESCRIPTIONS AND STRUCTURE	69
3:1:1 <i>Ollaberry</i>	69
3:1:1:1 Protolith lithologies	72
3:1:1:1a Queyfirth Group	72
3:1:1:1b Graven plutonic rocks	72
3:1:1:2 Fault rocks	73
3:1:1:2a Cataclasites east of the WBF	73
3:1:1:2b Cataclastic rocks west of the WBF.	73
3:1:1:2c Fault gouges	74
3:1:1:3 Fault rock distribution and age relationships.....	74
3:1:1:3a West of the WBF core	76
3:1:1:3b East of WBF core.....	76
3:1:1:3c WBF Core	76
3:1:1:4 Protolith structure outside the WBFZ.....	77
3:1:1:5 Fault zone structure west of the WBFP	79
3:1:1:5a Domain A (160-130m west of the WBFP).....	79
3:1:1:5b Domain B (130-60m west of the WBFP).....	83
3:1:1:5c Domain C (fault core to 60m west of WBFP)	90
3:1:1:6 Fault zone structure east of the WBFP.	95
3:1:1:7 Kinematic summary and discussion	98
3:1:2 <i>Sullom, Lunnister and the Ness of Haggrister.</i>	101
3:1:2:1 Protolith lithologies.....	103
3:1:2:1a Granodiorite	103
3:1:2:1b Metasedimentary rocks	105
3:1:2:1c Gneissose rocks	105
3:1:2:2 Fault rocks.....	106
3:1:2:2a Mylonites	106

3:1:2:2b Cataclasites west of WBFP.....	107
3:1:2:2c Cataclasites east of the WBFP derived from granodiorite.....	107
3:1:2:2d Cataclasites west of WBF derived from schists	108
3:1:2:3 Fault rock distribution and age relationships, south side of the Ness of Haggrister.....	109
3:1:2:3a West of the WBF core.....	110
3:1:2:3b East of the WBF core.....	110
3:1:2:3c WBF core.....	110
3:1:2:4 Protolith Structure outside WBFZ.....	114
3:1:2:5 Fault zone structure southern side of the Ness of Haggrister	114
3:1:2:5a West of the WBF core.....	114
3:1:2:5b East of the WBF core.....	119
3:1:2:5c WBF Core.....	121
3:1:2:6 Fault rock distribution and age relationships, north of the Ness of Haggrister.....	123
3:1:2:6a West of the WBFP	123
3:1:2:6b East of the WBFP	126
3:1:2:7 Fault zone structure north of the Ness of Haggrister	126
3:1:2:7a West of WBFP	126
3:1:2:7b East of WBFP	135
3:1:2:7 Kinematic summary and discussion	135
<i>3:1:3 Brae Isthmus</i>	<i>140</i>
3:1:3:1 Protolith lithologies.....	142
3:1:3:1a Granodiorite.....	142
3:1:3:1b Limestone	142
3:1:3:1c Hornblende schists	143
3:1:3:2 Fault rocks.....	143
3:1:3:2a Cataclasite derived from hornblende schist.....	143
3:1:3:2b Foliated cataclasites	143
3:1:3:2c Cataclasite derived from limestone	144
3:1:3:2d Fault gouges.....	144
3:1:3:3 Fault rock distribution and age relationships.....	144
3:1:3:3a East of the WBF core	144
3:1:3:3b West of the WBF core.....	145
3:1:3:3c WBF core.....	145
3:1:3:4 Fault zone structure.....	146
3:1:3:4a East of the WBFP.....	146
3:1:3:4b West of the WBFP	148
3:1:3:5 Kinematic summary and discussion	149
<i>3:1:4 Papa Little.....</i>	<i>151</i>
3:1:4:1 Protolith lithologies.....	151
3:1:4:1a Gneissose rocks west of the WBF.....	151
3:1:4:1b Pegmatitic granite.....	154
3:1:4:1c Limestone.....	154
3:1:4:1d Yell Sound Division rocks	154
3:1:4:2 Fault rocks.....	155
3:1:4:2a Cataclasites west of the WBFP	155

3:1:4:2c Cataclasites east of the WBF.....	155
3:1:4:2c Fault gouges.....	156
3:1:4:3 Fault rock distribution and age relationships.....	156
3:1:4:3a East of the WBF core.....	156
3:1:4:3c West of the WBF core.....	156
3:1:4:3c WBF core.....	157
3:1:4:4 Fault zone structure.....	160
3:1:4:4a East of the WBF core.....	160
3:1:4:4b West of the WBF core.....	161
3:1:4:4c WBF core.....	162
3:1:4:5 Kinematic summary and discussion.....	163
<i>3:1:5 Aith Voe.....</i>	<i>165</i>
3:1:5:1 Protolith lithologies.....	165
3:1:5:1a Gneisses and schists.....	165
3:1:5:1b Sandstones and Volcanic rocks.....	167
3:1:5:1c Granite.....	167
3:1:5:2 Fault rocks.....	168
3:1:5:2a Marble mylonite.....	168
3:1:5:2b Phyllonitic rocks.....	168
3:1:5:2c Cataclasite.....	168
3:1:5:2d Fault gouge.....	170
3:1:5:3 Fault rock distribution and age relationships.....	170
3:1:5:3a West of the WBF core.....	170
3:1:5:3b East of the WBF core.....	171
3:1:5:3 c WBF core.....	171
3:1:5:4 Fault zone structure.....	172
3:1:5:4a West of WBF core.....	172
3:1:5:4b East of the WBF core.....	174
3:1:5:5 Kinematic summary and discussion.....	176
<i>3:1:6 Ness of Bixter.....</i>	<i>178</i>
3:1:6:1 Protolith lithologies.....	178
3:1:6:1a Calcareous schists.....	178
3:1:6:1b Sandstones.....	178
3:1:6:1c Granite.....	180
3:1:6:1d Pegmatite.....	180
3:1:6:2 Fault rocks.....	180
3:1:6:2a Cataclasite.....	180
3:1:6:2b Breccia.....	181
3:1:6:2c Fault gouge.....	181
3:1:6:3 Fault rock distribution and age relationships.....	181
3:1:6:3a West of the WBF core.....	182
3:1:6:3b East of the WBF core.....	182
3:1:6:3c The WBF core.....	183
3:1:6:4 Fault zone structure.....	186
3:1:6:4a West of the WBF core.....	186

3:1:6:4b East of the WBF core.....	189
3:1:6:4c WBF core.....	190
3:1:6:5 Kinematic summary and discussion	192
<i>3:1:7 Seli Voe and Sand</i>	<i>195</i>
3:1:7:1 Protolith lithologies.....	195
3:1:7:1a Metasedimentary rocks	195
3:1:7:1b Granite west of WBFP	197
3:1:7:1c Sandstones.....	198
3:1:7:1d Granodiorite east of WBFP.....	198
3:1:7:2 Fault rocks.....	198
3:1:7:2a Blastomylonites.....	198
3:1:7:2b Cataclasites	199
3:1:7:2c Foliated cataclasites	201
3:1:7:2d Fault gouge	201
3:1:7:3 Fault rock distribution and age relationships.....	201
3:1:7:3a East of WBF core.....	202
3:1:7:3b West of WBF core	205
3:1:7:3c WBF core.....	205
3:1:7:4 Fault zone structure.....	206
3:1:7:4a East of WBF core.....	206
3:1:7:4b West of WBF core	214
3:1:7:5 Kinematic summary and discussion	214
<i>3:1:8 Red Ayre.....</i>	<i>217</i>
3:1:8:1 Protolith lithology	217
3:1:8:1a Granite.....	217
3:1:8:2 Fault rocks.....	217
3:1:8:2a Mylonites	217
3:1:8:2b Cataclasites	219
3:1:8:2c Fault gouge.....	219
3:1:8:3 Fault rock distribution and age relationships.....	220
3:1:8:4 Structure.....	220
3:1:8:5 Kinematic summary and discussion	223
<i>3:1:9 Summary</i>	<i>225</i>
3:2 THE NESTING FAULT: LOCALITY DESCRIPTION AND STRUCTURE	226
<i>3:2:1 Wadbister Voe</i>	<i>226</i>
3:2:1:1 Protolith lithologies.....	228
3:2:1:1a Whiteness Division rocks west of the NF	228
3:2:1:1b Whiteness Division rocks east of the NF	228
3:2:1:2 Fault Rocks	229
3:2:1:2a Breccia.....	229
3:2:1:2b Fault gouge.....	229
3:2:1:3 Fault rock distribution and age relationships.....	229
3:2:1:3a West of the NF core	229
3:2:1:3a East of the NF core.....	230

3:2:1:3c NF core.....	230
3:2:1:4 Fault zone structure.....	230
3:2:1:4a West of the NF core	230
3:2:1:4b East of the NF core	234
3:2:1:4c NF core.....	234
3:2:1:5 Kinematic summary and discussion	238
3:3 THE MELBY FAULT: LOCALITY DESCRIPTION AND STRUCTURE.....	239
3:3:1 <i>Melby</i>	239
3:3:1:1 Protolith lithologies.....	241
3:3:1:1a West of the MF trace.....	241
3:3:1:1b East of the MF trace.....	241
3:3:1:2 Fault rocks.....	241
3:3:1:2a Phyllonites.....	241
3:3:1:2b Fault gouge	243
3:3:1:3 Fault rock distribution and age relationships.....	243
3:3:1:3a East of the MF trace	243
3:3:1:3b West of the MF trace.....	243
3:3:1:3 Fault zone structure.....	243
3:3:1:3a East of the MF trace	243
3:3:1:3b West of the MF trace.....	244
3:3:1:4 Kinematic summary and discussion	244
CHAPTER 4. FAULT ROCK TEXTURES AND MICROSTRUCTURES: WBFZ	246
4:1 PROTOLITHS	247
4:1:1 <i>Banded gneiss</i>	247
4:1:2 <i>Queyfirth Group</i>	249
4:1:3 <i>Devonian sandstones</i>	250
4:1:4 <i>Plutonic rocks</i>	250
4:1:4:1 Sullom and the Ness of Haggrister.....	250
4:1:4:2 Brae Isthmus	252
4:2 PRIMARY FAULT-ROCK ASSEMBLAGES	252
4:2:1 <i>Mylonitic rocks</i>	253
4:2:1:1 Sand to Seli Voe blastomylonites.....	253
4:2:1:1a Metamorphic conditions and operative deformation mechanisms	254
4:2:1:2 Lunnister mylonites.....	254
4:2:1:2a Felsic mylonites	254
4:2:1:2b Mafic protomylonites.....	258
4:2:1:2c Metamorphic conditions during mylonitisation.....	259
4:2:1:2d Operative deformation mechanisms.....	260
4:2:2 <i>Cataclastic rocks</i>	262
4:2:2:1 Lunnister cataclasites	262
4:2:2:1a Operative deformation mechanisms and localisation	264

4:2:2 Brae Isthmus foliated cataclasites	264
4:2:2a Metamorphic conditions during cataclasis	266
4:2:2b Operative deformation mechanisms.....	266
4:3 SECONDARY FAULT-ROCK ASSEMBLAGES	267
4:3:1 <i>Seli Voe to Sand banded cataclasites</i>	267
4:3:1:1 Operative deformation mechanisms	269
4:3:2 <i>Ollaberry cataclasites</i>	269
4:3:2:1 Operative deformation mechanisms	269
4:3:3 <i>Sullom, Lunnister and Ness of Haggrister cataclasites</i>	270
4:3:3:1 Operative deformation mechanisms	272
4:3:4 <i>Cataclasites derived from Devonian sandstones</i>	272
4:3:4:1 Operative deformation mechanisms	273
4:3:5 <i>Fault gouge</i>	273
4:3:5:1 Incohesive fault gouge	273
4:3:5:2 Cohesive fault gouge.....	274
4:4 SUMMARY	274

CHAPTER 5. THE GEOLOGY OF THE FOSEN PENINSULA 275

5:1 THE SCANDINAVIAN CALEDONIDES	275
5:1:1 <i>Autochthon / Parautochthon</i>	277
5:1:2 <i>Lower Allochthon</i>	280
5:1:2.1 <i>Banded Gneiss Complex on Fosen Peninsula</i>	280
5:1:3 <i>Middle Allochthon</i>	281
5:1:5 <i>Uppermost Allochthon</i>	283
5:1:6 <i>Regional synthesis of the Scandinavian Caledonides</i>	283
5:2 LATE-OROGENIC COLLAPSE AND DEVONIAN BASINS.....	287
5:2:1 <i>Stratigraphy of the Bjugn basin</i>	287
5:2:2 <i>Structure within the Bjugn basin</i>	291
5:2:3 <i>Høybakken detachment (HD)</i>	291
5:2:4 <i>Regional Synthesis of Late-orogenic collapse</i>	293
5:3 THE MØRE-TRØNDELAG FAULT COMPLEX	296
5:3:1 <i>The MTFC onshore</i>	297
5:3:2 <i>The MTFC offshore</i>	301
5:3:2:1 <i>Beitstadfjorden Basin</i>	301
5:3:2:2 <i>Edøylfjorden Basin</i>	302
5:3:2:3 <i>Møre Basin</i>	305

CHAPTER 6. THE MØRE-TRØNDELAG FAULT COMPLEX..... 308

6:1 LANDSAT™ INTERPRETATION OF THE MØRE-TRØNDELAG FAULT COMPLEX (MTFC)	308
6:2 REGIONAL STRUCTURE ACROSS THE MTFC	312
6:2:1 <i>Protolith lithology</i>	312
6:2:2 <i>Meffellet to Trongsvundet traverse</i>	313
6:2:2:1 Domain A	316
6:2:2:2 Domain B	316
6:2:2:3 Domain C	320
6:2:2:4 Domain D	322
6:2:2:5 Summary of structural domains	322
6:3 THE HITRA-SNÅSA FAULT ZONE: LOCALITY DESCRIPTIONS AND STRUCTURE	324
6:3:1 <i>Meffellet section</i>	324
6:3:1:1 Fault rocks	326
6:3:1:1a Mylonite	326
6:3:1:1b Cataclasite	327
6:3:1:1c Pseudotachylite	327
6:3:1:2 Fault rock distribution and age relationships	327
6:3:1:2a Hitra Snåsa Fault core	328
6:3:1:3 Fault zone structure	332
6:3:1:3a NW of Hitra Snåsa Fault core	332
6:3:1:3b SE of Hitra-Snåsa Fault core	343
6:3:1:3c Hitra-Snåsa Fault core	353
6:3:1:4 Kinematic summary and discussion	357
6:3:2 <i>Hamnardalen quarry and road cut</i>	361
6:3:2:1 Fault rocks	361
6:3:2:1a Protomylonite	361
6:3:2:1b Cataclasite	363
6:3:2:2 Fault rock distribution and age relationships	363
6:3:2:3 Fault zone structure	364
6:3:2:4 Kinematic summary and discussion	368
6:3:3 <i>Follavatnet traverse and Brattreitelva stream section</i>	371
6:3:3:1 Fault rocks	373
6:3:3:1a Mylonites	373
6:3:3:2 Fault zone structure	376
6:3:3:2a NW of the HSFP trace [Locality A]	376
6:3:3:2b NW of the HSFP trace [Locality B]	377
6:3:3:2c SE of the HSFP trace [Locality C]	379
6:3:3:2d SE of the HSFP trace [Locality D]	379
6:3:3:4 Kinematic summary and discussion	381
6:4 THE VERRAN FAULT ZONE: LOCALITY DESCRIPTIONS AND STRUCTURE	383

6:4:1 Air photograph interpretation of the Verran Fault Zone, N of Verrasundet.....	385
6:4:2 Skaudalen stream section.....	387
6:4:2:1 Protolith lithology	387
6:4:2:2 Fault rocks: nature, distribution and age relationships	389
6:4:2:2a Mylonite.....	389
6:4:2:2b Zeolite- and calcite-mineralised breccias	389
6:4:2:3 Fault zone structure.....	390
6:4:2:4 Kinematic summary and discussion	390
6:4:3 Ormsetvatnet road section	392
6:4:3:1 Fault rocks: nature, distribution and age relationships	392
6:4:3:1a Cataclasite	393
6:4:3:1b Zeolite- and calcite-mineralised breccias	393
6:4:3:2 Fault zone structure.....	393
6:4:3:3 Kinematic summary and discussion	396
6:4:4 Hydro station.....	396
6:4:4:1 Fault rocks: nature, distribution and age relationships	396
6:4:4:1a Cataclasite	397
6:4:4:1b Zeolite- and calcite-mineralised breccias	397
6:4:4:2 Fault zone structure.....	397
6:4:4:3 Kinematic summary and discussion	399
6:4:5 Outcrops along the 720 road section	400
6:4:5:1 Fault rocks: nature, distribution and age relationships	400
6:4:5:1a Cataclasite	400
6:4:5:1b Zeolite- and calcite-mineralised breccias	400
6:4:5:1c Grey fault gouge.....	402
6:4:5:2 Fault zone structure.....	402
6:4:5:3 Kinematic summary and discussion	406
6:4:6 Verrabotn stream section	407
6:4:6:1 Fault rocks: nature, distribution and age relationships	407
6:4:6:1a Quartz and epidote cataclasites	407
6:4:6:1b Zeolite- and calcite-mineralised breccias	407
6:4:6:1c Grey fault gouge.....	409
6:4:6:2 Fault zone structure.....	409
6:4:6:3 Kinematic summary and discussion	411
6:4:7 Verrasundet exposures.....	412
6:4:7:1 Fault rock distribution and age relationships.....	413
6:4:7:2 Fault zone structure.....	413
6:4:7:3 Kinematic summary and discussion	416
6:4:8 Verran Fault Core, Finesbekken.....	416
6:4:8:1 Fault rocks.....	417
6:4:8:1a Cataclasite	417
6:4:8:1b Indurated gouge	419
6:4:8:1c Zeolite- and calcite-mineralised breccias	419
6:4:8:1d Grey gouge.....	419

6:4:8:1e Blue-grey gouge.....	420
6:4:8:2 Fault rock distribution and age relationships.....	420
6:4:8:3 Fault zone structure.....	424
6:4:8:4 Kinematic summary and discussion.....	429
6:4:9 <i>Rautingdalen Fault</i>	430
6:4:9:1 Fault rocks.....	430
6:4:9:1a Cataclasite.....	432
6:4:9:1b Zeolite- and calcite-mineralised fault gouge.....	432
6:4:9:1c Zeolite- and calcite-mineralised breccia.....	432
6:4:9:2 Fault rock distribution and age relationships.....	434
6:4:9:3 Fault zone structure.....	436
6:4:9:4 Kinematic summary and discussion.....	438
6:5 <i>Summary of the Verran Fault</i>	439
CHAPTER 7. FAULT ROCK TEXTURES AND MICROSTRUCTURES: MTFC	441
7:1 HITRA-SNÅSA FAULT ZONE: TEXTURES AND MICROSTRUCTURES.....	441
7:1:1 <i>Protolith</i>	441
7:1:2 <i>Mylonite</i>	444
7:1:2:1 Mefjellet mylonites.....	444
7:1:2:1a Metamorphic conditions during mylonitisation.....	446
7:1:2:1b Operative deformation mechanisms.....	446
7:1:2:2 Follavatnet and Brattreitelva mylonites.....	448
7:1:2:2a Marble mylonite.....	448
7:1:2:2b Mylonites derived from feldspathic psammites.....	450
7:1:3 <i>Cataclasite</i>	453
7:1:3:1 Operative deformation mechanisms.....	455
7:1:4 <i>Pseudotachylite</i>	455
7:1:4:1 Localisation mechanism and generation of pseudotachylite.....	458
7:2 ⁴⁰ Ar/ ³⁹ Ar LASERPROBE DATING OF PSEUDOTACHYLITE AND HOST ROCK SAMPLES	459
7:2:1 <i>Sample preparation</i>	459
7:2:2 <i>Sample analysis</i>	460
7:2:3 <i>Results</i>	460
7:3 SUMMARY.....	467
7:4 VERRAN FAULT ZONE: TEXTURES AND MICROSTRUCTURES	467
7:4:1 <i>Protolith</i>	468
7:4:2 <i>Mylonite</i>	471
7:4:2:1 Metamorphic conditions during sinistral shear.....	471
7:4:2:2 Operative deformation mechanisms.....	471
7:4:3 <i>Cataclasite</i>	472
7:4:3:1 Operative deformation mechanisms.....	473
7:4:4 <i>Indurated fault gouge</i>	475
7:4:4:1 Operative deformation mechanisms.....	476

7:4:5 Zeolite- and calcite-mineralised breccia.....	476
7:4:5:1 Operative deformation mechanisms	476
7:4:6 Grey fault gouge.....	478
7:4:7 Blue-grey fault gouge.....	478
7:5 SUMMARY	479
7:6 MAJOR ELEMENT GEOCHEMISTRY OF FAULT ROCKS.....	479
7:6:1 Major element composition.....	482
7:6:2 Protolith-normalised composition.....	482
CHAPTER 8. DISCUSSION AND CONCLUSIONS	485
8:1 THE WALLS BOUNDARY FAULT SYSTEM	485
8:1:1 Kinematic evolution and fault-rock sequence	485
8:1:2 Timing, regional implications and displacement magnitudes.....	489
8:1:3 Textural and microstructural evolution	495
8:2 THE MØRE-TRØNDELAG FAULT COMPLEX	498
8:2:1 Kinematic evolution, fault-rock sequence and timing	498
8:2:1:1 Summary.....	502
8:2:2 Timing, regional implications and displacement magnitudes.....	503
8:2:3 Textural and microstructural evolution	509
8:3 REGIONAL SYNTHESIS AND POSSIBLE FAULT-ZONE LINKAGES.....	513
8:4 LOCALISATION AND WEAKENING PROCESSES	519
8:4:2 'Weak' fault rocks.....	521
8:4:2 Geometric controls on reactivation.....	523
8:5 EXHUMATION AND PRESERVATION OF FAULT ROCKS ALONG MULTIPLY REACTIVATED FAULTS.....	524
8:6 CONCLUSIONS	528
REFERENCES	530

Chapter 1. Introduction

1:1 Introduction and aims

The deformation of much of the Earth's continental crust is characteristically heterogeneous. It is widely recognised that major faults and shear zones in the continental crust preserve evidence of repeated localisation of displacement or *reactivation* over long periods of geological time (Holdsworth et al. 1997). Both geological and geophysical observations suggest that reactivation often occurs in preference to the formation of new structures. This strongly implies that reactivated fault zones may be weak relative to their surroundings.

Crustal-scale, reactivated fault zones strongly influence the location and architecture of a wide range of geological features, such as rift basins and orogenic belts (Rutter et al. 2001). Fault zones also act as conduits for the focused migration of fluids, and play an important role in understanding the location and emplacement of hydrocarbons, ore deposits and igneous intrusions (Rutter et al. 2001 and references therein). Also, a great deal of active seismicity is associated with displacements along reactivated fault zones and therefore can represent one of the most important geological hazards. Geophysical observations along neotectonic structures have provided insights into the mechanical behaviour of continental faults and shear zones. For example, geophysical evidence from the San Andreas Fault, such as in-situ stress and heat flow measurements, suggest that this fault moves under very low shear stresses, and this is consistent with the fault zone being weak relative to the surrounding rocks (Zoback et al. 1987). Geological evidence to support the various weakening mechanisms proposed for the weakness of this structure is scarce (Scholz 1990; Wintsch et al. 1995).

Several authors have suggested that operative weakening mechanisms along long-lived reactivated fault zones must affect a major part of the lithosphere (Watterson 1975) and, in particular, the main load-bearing regions or strongest parts of the



lithosphere (Stewart et al. 1999, 2000; Holdsworth et al. 2001; Imber et al. 2001). Therefore, field studies of neotectonic and upper crustal fault zones are unlikely to provide insights into long-term weakening mechanisms. Exhumed basement faults and shear zones, which expose deeper parts of the crust, are central to understanding the factors that control fault reactivation over long periods of geological time. Recent studies of deeply exhumed, crustal-scale, reactivated fault zones (Butler 1995; Imber et al. 1997; Stewart et al. 1997, 1999, 2000; Imber 1998; Holdsworth et al. 2001) have identified long-term weakening mechanisms such as *reaction softening*, which involves the alteration and retrograde metamorphism of fault rocks in the presence of hydrous fluids, and the onset of grain-size sensitive, *diffusion-dominated deformation mechanisms*. Such processes are thought to weaken the fault zone and lead to these structures being susceptible to reactivation in the long term.

In light of this, there have been relatively few attempts (Sibson 1977b; Butler 1995; Stewart 1997; Imber 1998) to describe the kinematic and structural evolution of reactivated basement fault zones, and, in particular the spatial and temporal relationships between successive generations of fault rocks. This thesis is concerned with two, crustal-scale reactivated basement fault zones that occur along the North Atlantic margin, the Walls Boundary Fault Zone, Shetland, and the Møre-Trøndelag Fault Complex, Central Norway. These structures appear to have controlled the location and architecture of several hydrocarbon prolific, offshore sedimentary basins of Mesozoic age. It has been suggested in the literature, often based on no direct evidence, that these structures have been reactivated several times and have been linked at some stage during their evolution and subsequent reactivation (Norton et al. 1987; Ziegler 1987; Grønlie and Roberts 1989; Seranne 1992b; Blystad 1995). Both fault zones are well exposed and provide an excellent opportunity to study fault reactivation on a variety of scales. The principal aims of this thesis are to:

- Unravel the kinematic, geometric, textural and microstructural evolution of both structures.
- Establish the regional tectonic context for both fault zones and assess fault linkages between Norway and Shetland.
- Provide insights into the controlling factors on fault reactivation.

1:2 The continental lithosphere

The understanding of the overall structure and mechanical behaviour of the continental lithosphere is central in assessing the significance of basement fault zones and reactivation.

The continental lithosphere is typically 100 to 150km thick, comprising an upper zone (30 to 40km thick) of quartzo-feldspathic crust that overlies the thick, olivine-rich upper mantle. This lithological stratification has important consequences for the rheology of the continental lithosphere (Molnar 1988).

The overlying quartzo-feldspathic crust is significantly less dense than the underlying olivine-dominated upper mantle. The resulting buoyancy of the quartzo-feldspathic crust prevents continental lithosphere from being subducted into the olivine-dominated upper mantle (Sutton and Watson 1986). Therefore, the continental lithosphere is old in both absolute terms and relative to the oceanic crust. Consequently, ancient mechanical anisotropies in the continental lithosphere, such as faults and shear zones, have great longevity and may be reactivated leading to the characteristically heterogeneous deformation observed in the continental crust and lithosphere. These ancient faults and shear zones divide the continental crust into a series of 'blocks' and 'flakes', which can deform to some extent independently of each other. As a result, crustal deformation patterns are characteristically complex and result in: (a) localisation of strain along long-lived faults and shear zones, which separate blocks of relatively undeformed crust, and (b) kinematic partitioning of regional deformation into different components of the total strain field (Dewey et al. 1986; Figure 1.1)

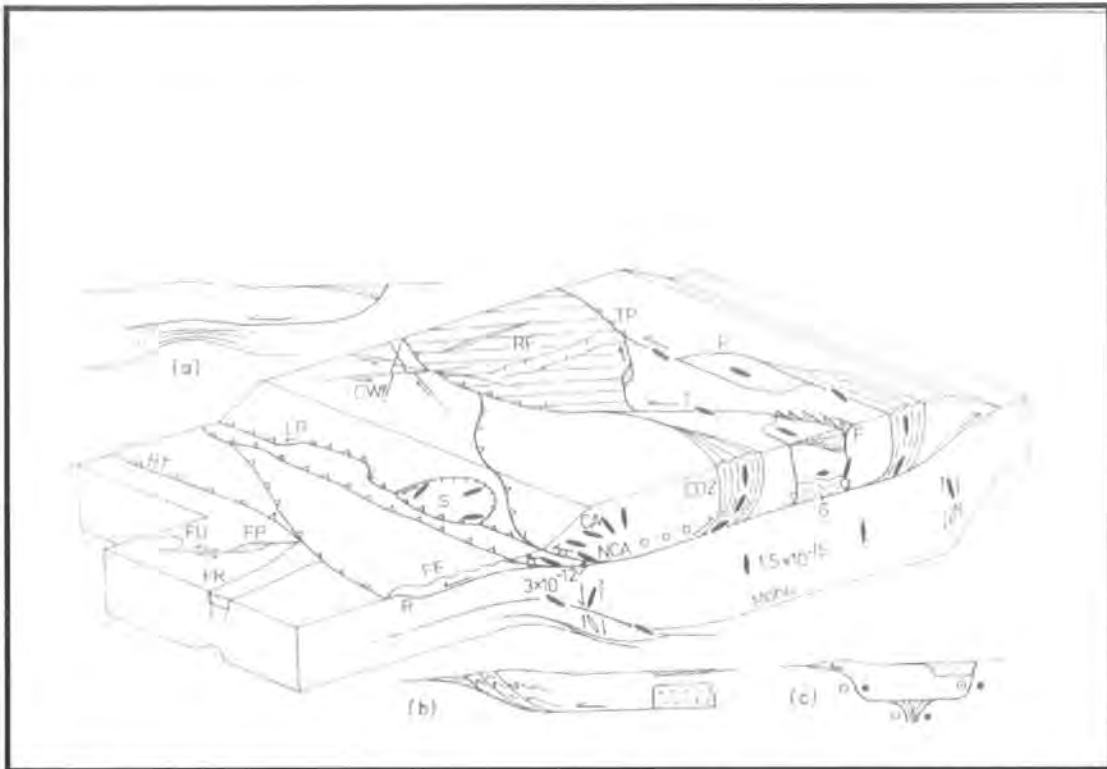


Figure 1.1 Schematic diagram illustrating the components of a continental (collisional) deformation zone after Dewey et al. (1986). BT-basement thrust, CA-coaxial strain, CDZ-convergent deformation zone, CW-conjugate wrenching, F-flower structures, FF-foreland folding, FP-foreland pull apart, FR-foreland rift, FU-foreland uplift, G-granite, LR-lateral ramp, NCA-non-coaxial strain, P-Pull-apart, R-ramp, RF-rigid flake, S-surge zone, T-transform, TP-tranpression, small circles - large earthquake hypocentres.

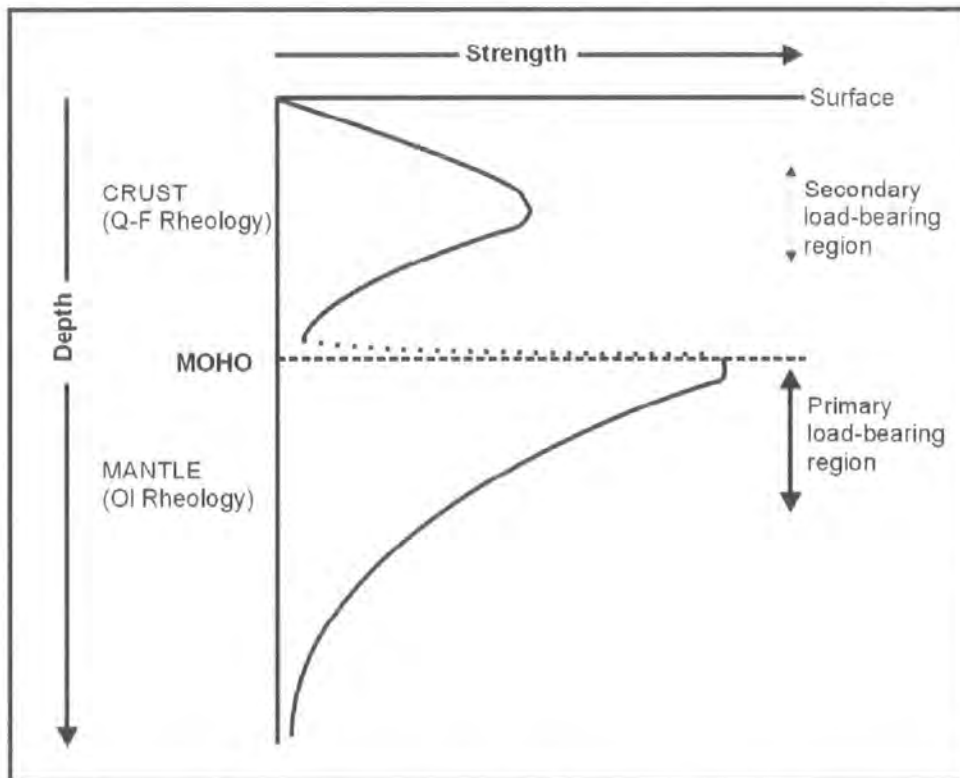


Figure 1.2 Not to scale. Schematic strength versus depth profile for average continental lithosphere showing the main load-bearing regions in the upper mantle and the mid-crust (after Molnar 1988).

1:2:1 The strength of the continental lithosphere

The continental lithosphere comprises three rheologically different layers: a seismogenic upper crust; an aseismic lower crust; and a strong, occasionally seismic uppermost mantle (Figure 1.2).

In the upper, seismogenic part of the crust, deformation occurs by frictional processes. Both the temperature and the frictional strength of the upper crust increase with depth (Figure 1.2). Above a critical temperature, viscous creep mechanisms become operative, and as a result the lower crust deforms in an essentially aseismic, ductile manner (Sibson 1983), and decreases in strength dramatically with increasing temperature (Figure 1.2).

The Moho separates quartzo-feldspathic continental crust from the underlying olivine-dominated upper mantle, and corresponds to a sharp increase in strength (Figure 1.2; primary load-bearing region). The increase in strength is due to the fact that at any given temperature olivine is significantly stronger than either quartz or feldspar (Evans and Goetze 1979).

The strength maximum in the upper mantle represents the primary load-bearing region in the lithosphere as a whole, whilst the strength maximum in the overlying crust (i.e., secondary load-bearing region) corresponds with the frictional to viscous creep (“brittle-ductile”) transition. Consequently, deformation processes active around the frictional to viscous creep transition are likely to affect the strength of the crust, but are unlikely to affect the strength of the lithospheric mantle.

Several authors have noted that many reactivated fault zones preserve fault rocks which appear to have developed around the level of the frictional to viscous creep transition (Imber et al. 1997; Stewart et al. 2000; Holdsworth et al. 2001). On the basis of the observations outlined above, Imber et al. (1997) suggested that basement reactivation fundamentally influences deformation within the crust.

1:3 Fault zone reactivation

In ancient settings, reactivation is defined as '*the accommodation of geologically separable displacement events (at intervals >1Ma) along pre-existing structures*' (Holdsworth et al. 1997). Two distinct types of reactivated faults were recognised: those which display different senses of relative displacement for successive events are said to have experienced geometric reactivation (Figure 1.3A); whilst those which display similar senses of relative displacement for successive events are said to have experienced kinematic reactivation (Figure 1.3B).

Figure 1.4 summarises the four main groups of generally reliable criteria that can be used to recognise reactivation along basement faults and shear zones: stratigraphic, structural, geochronological and neotectonic (Holdsworth et al. 1997).

In the literature, a number of unreliable criteria have been used to infer reactivation along pre-existing structures. Most of these suggestions have been based upon apparent similarities in trend, dip or the 3D shape of structures (see Holdsworth et al. 1997 and references therein). This group of speculative criteria are termed *geometric similarity*.

1:4 Fault rock definitions and shear sense indicators

In the field it is often difficult to identify operative deformation mechanisms within a fault rock. As a result, Sibson (1977) proposed a purely descriptive classification of fault rocks (Figure 1.5). Sibson (1977) divided fault rocks into those with a random fabric and those with a foliation. The products of frictional deformation are termed 'cataclastic fault rocks' (Sibson 1977). Cataclastic fault rocks usually contain a random fabric and include fault gouge, breccia, cataclasites and pseudotachylites. Fault gouge is an incohesive rock composed mostly of very fine-grained clay minerals, with few wall rock fragments. When more than 30% of an incohesive fault rock is composed of angular fragments from the wall rock, surrounded by a fine-grained matrix, the rock is defined as a breccia. Cataclasite series rocks are cohesive fault rocks formed during frictional deformation. When less than 30% of the fault rock volume is composed of fragments set within a fine-grained matrix, the rock is defined as a cataclasite. There is usually a complete gradation in grain size from the

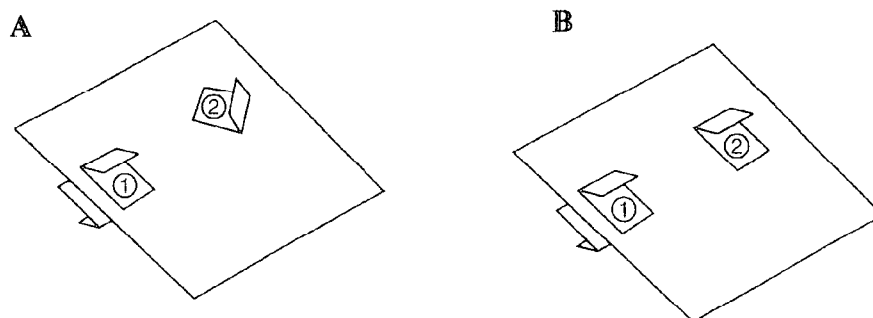


Figure 1.3 (A) Geometric reactivation; reactivated structures display *different* senses of relative displacement for successive events. (B) Kinematic reactivation, reactivated structures display *similar* senses of relative displacement for successive events (after Holdsworth et al. 1997).

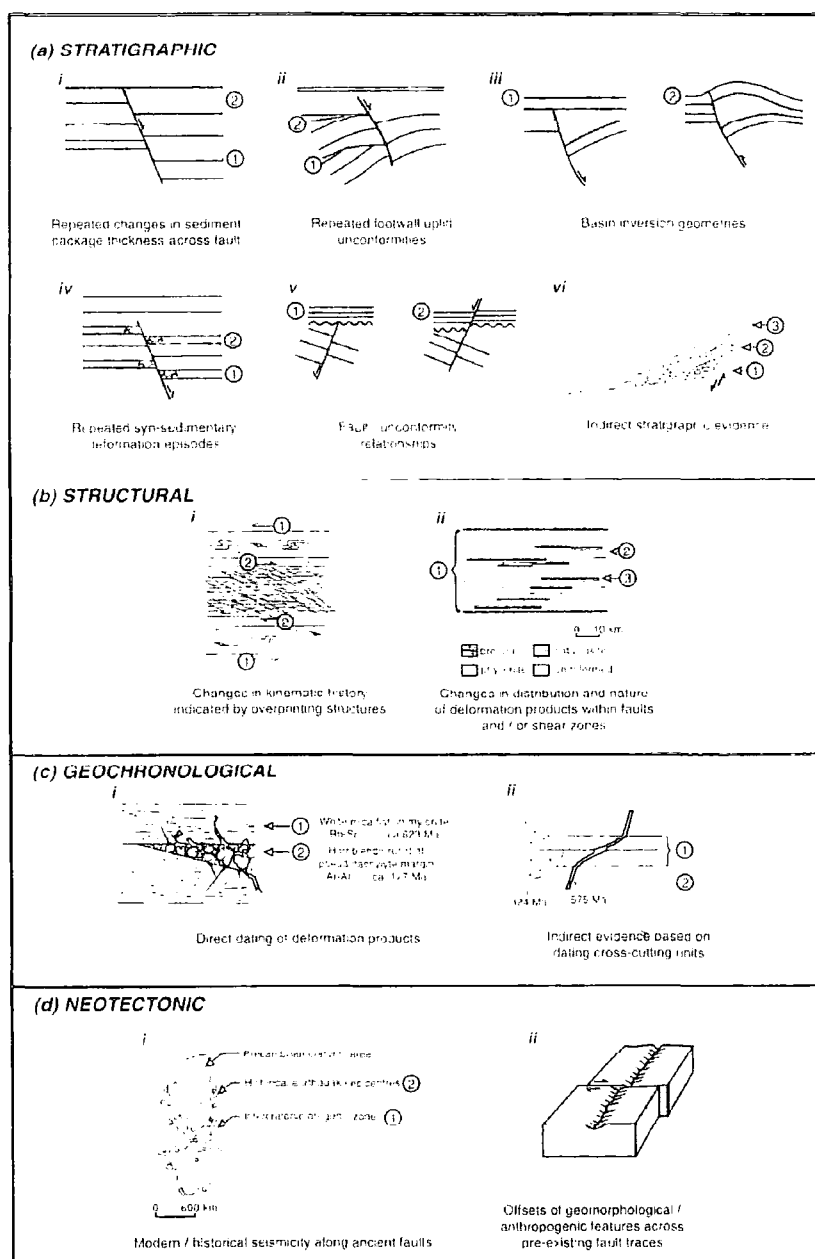


Figure 1.4 The criteria considered reliable for recognising reactivation: stratigraphic, structural, geochronological and neotectonic (after Holdsworth et al. 1997).

		RANDOM FABRIC			FOLIATED			
INCOHESIVE			Fault breccia (visible fragments >30% rock mass)		?			
			Fault gouge (visible fragments <30% rock mass)		?			
COHESIVE	Nature of matrix	Glass	Pseudotachylite		?			
		Tectonic reduction in grain size dominates grain growth by recrystallisation and neomineralisation	Crush breccia (fragments > 0.5cm) Fine crush breccia (fragments 0.1 – 0.5cm) Crush microbreccia (fragments < 0.1cm)			0 – 10%		
						Proportion of matrix		
			Protomylonite	10 – 50%				
				Cataclasite series	Phyllonite varieties			Mylonite Series
						90 –		
			Cataclasite			Ultra – mylonite		
				Ultracataclasite				
					?			
		Grain growth pronounced				Blastomylonite		

Figure 1.5 Textural classification of fault rocks (after Sibson 1977).

fragments to the matrix. Pseudotachylite is a cohesive rock that occurs as distinct dark veins of glassy material, formed as a result of frictional melting. It contains very fine-grained mineral or wall rock fragments which are surrounded by glass or devitrified glass. Mylonite series rocks are primarily produced by viscous deformation (Sibson 1977) and include mylonite, phyllonite and blastomylonite. A mylonite is a foliated and usually lineated rock that shows evidence for strong viscous deformation (White et al. 1980; Passchier and Trouw 1996). Many mylonites contain porphyroclasts, which are remnants of resistant mineral grains. A commonly used mylonite classification is based on the percentage of matrix compared to porphyroclasts (Sibson 1977). Rocks with 10-50% matrix are classified as *protomylonites*, rocks with 50-90% matrix are classified as *mylonites*, and rocks with >90% matrix are classified as *ultramylonites*. A phyllonite is a fine-grained, phyllosilicate-rich mylonite. Blastomylonites are mylonites that have undergone significant grain growth. Figure 1.6 shows the typical depth distribution of fault rocks along a notionally vertical, crustal-scale fault zone. In this study, fault-rock names refer to textures observed in the field and do not have any mechanistic implications (Figure 1.5).

The direction of movement along a fault or shear zone is usually assumed to lie parallel to striations, slickenfibres or stretching and mineral lineations. When the movement direction has been established, it is necessary to determine the sense of shear (sinistral or dextral strike-slip, normal, reverse or oblique). In the absence of direct evidence, such as offset geological markers, the asymmetric geometry of structures can be used to determine the sense of shear (Figure 1.7B), in surfaces viewed parallel to the movement direction and normal to the foliation or fault surface (Simpson and Schmid 1983; Hanmer and Passchier 1991). Fracture orientations can be used to determine shear sense by the development of Riedel structures. After a study based on simple shear experiments, subsidiary shear fractures called Riedel shears can also be used to determine shear sense (Riedel 1929; Hancock 1985; Passchier and Trouw 1996). Riedel structures are commonly used in this study and are identified by their kinematics and geometry with respect to the principal displacement direction, which is parallel to the fault boundary (Figure 1.7A). Riedel structures are divided into R, R', P and Y shears, each with a characteristic orientation and shear sense relative to the fault boundary (Passchier & Trouw 1996).

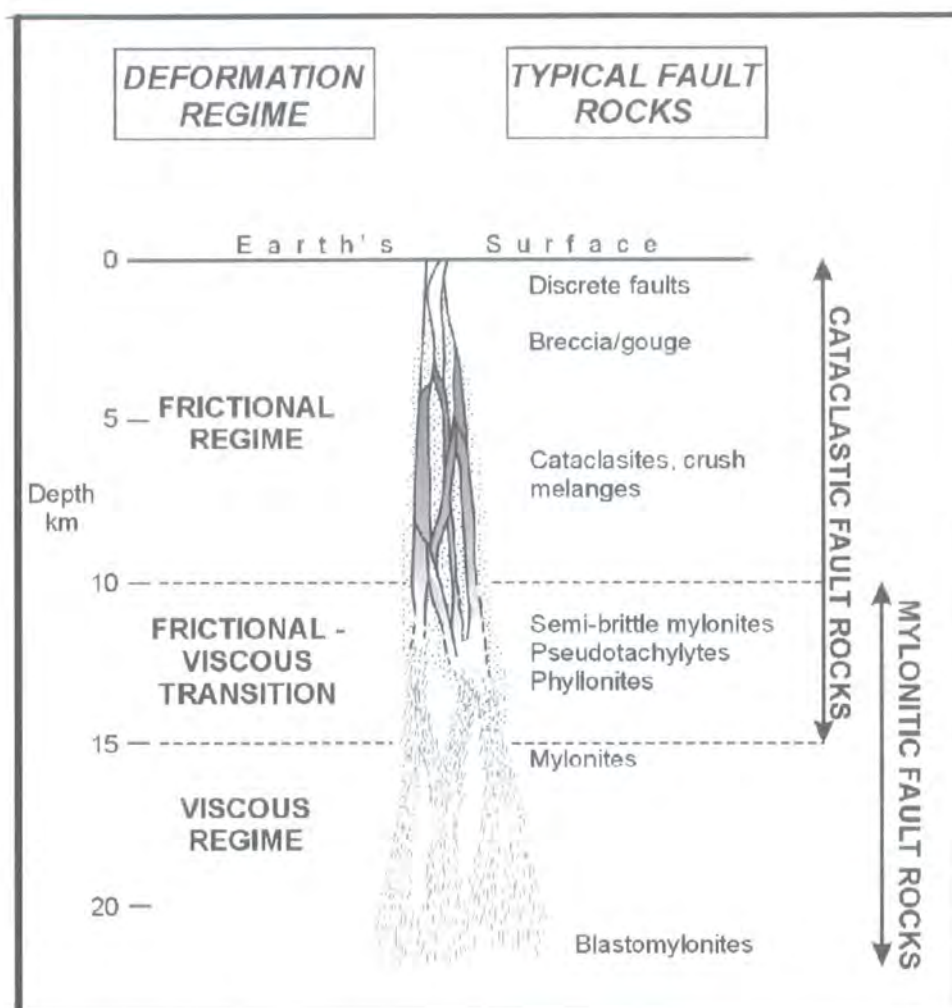


Figure 1.6 Conceptual model of a notional vertical, crustal-scale fault zone. Narrow brittle-frictional faults with a range of cataclastic fault-rock products pass with increasing depth into foliated mylonitic rocks in which intracrystalline plastic and diffusion-accommodated viscous flow processes progressively dominate (after Holdsworth et al. 2001).

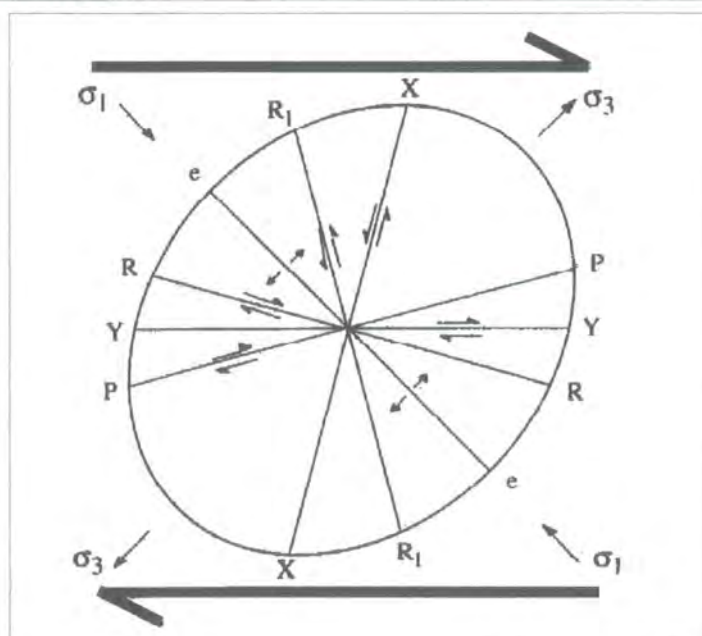


Figure 1.7A Subsidiary en-echelon structures that may occur within fault zones during simple shear. R and R1 = Riedel and conjugate Riedel shears. P-shears, X-shears, Y-shears, extension joints (e) (after Hancock 1985).






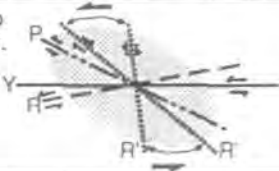
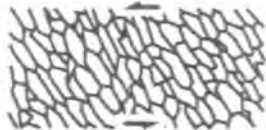


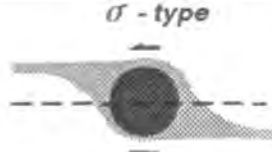
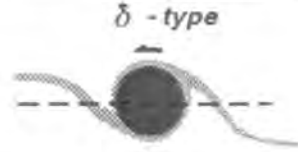
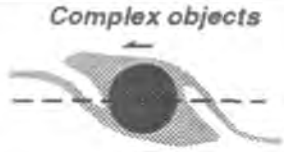

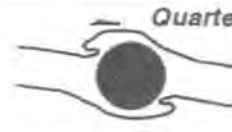





Scale		Type of kinematic indicator			
Macroscopic	External		Rotation of external foliation: Passive foliations may be rotated towards the fabric attractor in non-coaxial flow. Subsidiary shears: orientations of synthetic/anti-synthetic subsidiary shears can determine shear sense. (see diagram below)		
	Internal		Sense of fold overturning & vein asymmetry	 A view parallel to the lineation may show veins that are asymmetrically folded (if vein orientation was parallel to shortening) or boudinaged (if vein was orientated parallel to the extension direction). Fold vergence direction should give shear sense.	
Microscopic	Kinematic indicators formed by mainly frictional processes		 'Domino-faulting' is a common type of brittle deformation of rigid porphyroclasts. An asymmetric shape is created by development of antithetic faults.		Rigid porphyroclasts may also be faulted by synthetic shears.   Y: Y shears (synthetic) R: Riedel shears (synthetic) P: P shears (synthetic) R': anti-Riedel shears (anti-synthetic) : range of anti-Riedel shears (applicable to all scales)
	Kinematic indicators formed by mainly viscous creep processes	Shear zone fabrics	Grain-shape fabrics 	S-C fabrics 	S-C' fabrics 
		Mantled porphyroclasts	 σ - type	 δ - type	 Complex objects
		Quarter structures	 Concentrations of mica that lie in the shortening direction.	 Microfolds in the quarters that lie in the extensional direction.	 In K-feldspar, myrmekite is common in the rim lying in the shortening direction.
		Mica-fish & garnet spirals	 Single mica crystals in deformed rocks often display asymmetries that can be used as shear sense indicators	 Spiral inclusion trails often occur in garnets, formed as the garnets trapped inclusions during growth and rotated in response to simple shear. Their shape can determine if the garnet rotated clockwise (under dextral shear) or anticlockwise (under sinistral shear).	
		Pressure shadows and fibres	 Rigid fibres Asymmetry to pressure shadows mantling a porphyroclast and crystal fibres within the pressure shadows may be used as kinematic indicators.	 Deformable fibres	

Figure 1.7B Shear sense indicators (compiled by Stewart 1997 from Passchier and Trouw 1996 and Simpson and Schmid 1983).

1:5 Metamorphism along faults and shear zones

Reactivated basement faults and shear zones are commonly the site of intense, localised retrograde (e.g., Imber et al. 1997) or prograde metamorphism (e.g., Holdsworth 1994). Fault-related deformation in most high-grade basement rocks is retrogressive as it occurs at mid to upper crustal depths in the presence of fluids. Retrograde metamorphism involves the chemical breakdown of high-grade, 'unstable', anhydrous minerals (e.g., pyroxene) to low-grade assemblages of 'stable' hydrous minerals (e.g., phyllosilicates) in the presence of a fluid phase.

1:5:1 Metamorphic classification scheme

It is possible to assign each fault rock to a particular metamorphic facies, once the stable, syn-tectonic mineral assemblage has been identified. The metamorphic classification scheme used in this thesis is based on that published by Yardley (1994). The relationship between metamorphic facies, pressure/ temperature space and the critical mineral assemblages is summarised in Figure 1.8.

1:5:2 Fluid transport in fault zones

Fault zones provide permeability pathways for fluid flow and are often sites of extensive fluid-related alteration and mineralisation. Such permeability is a result of the dilatant nature of frictional deformation processes that occur in the middle to upper crust. The most important mechanism that promotes fluid flow through fault zones is *seismic pumping* (Sibson et al. 1975; Sibson 1993). As seismic events occur along faults, the resultant dilatancy and the development of the fracture network enables fluid to escape from the fault zone, causing a drop in fluid pressure. The drop in fluid pressure promotes the inward migration of fluids causing a renewed build up of fluid pressure. The increase in fluid pressure reduces the frictional resistance of the fault surfaces. This promotes seismic failure as the increase in fluid pressure reduces

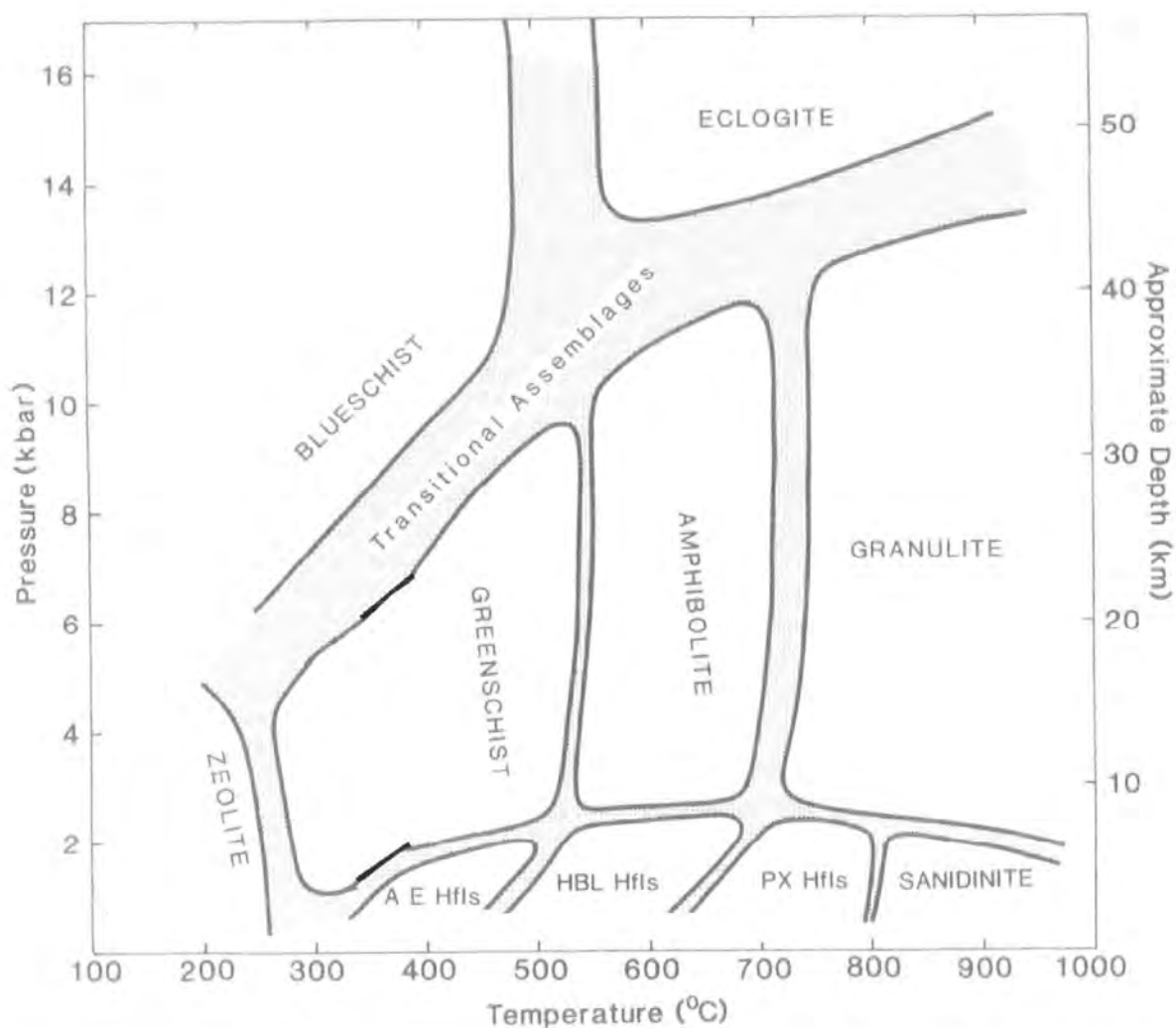


Fig. 2.8 Pressure-temperature diagram showing the fields of the various metamorphic facies. Details of the characteristic assemblages are given in Chapter 4 (Table 4.1). Abbreviations used are: HfIs = hornfels, A E = albite-epidote, HBL = hornblende, PX = pyroxene, PREH-PUMP = prehnite-pumpellyite.

Figure 1.8 Simplified metamorphic classification scheme used in this thesis (after Yardley 1994).

the effective normal stress causing a corresponding decrease in the frictional resistance, which promotes seismic failure along the fault surface. Seismic failure releases fluids and the process starts again.

Another important fluid transport process in the middle to upper crust is *fault valve behaviour* (Sibson 1990). Cyclic changes in fluid pressure during the seismic cycle, controls faulting in the fault valve model. Fault valve behaviour requires a constant input of fluids into the system and a regional permeability barrier, which maintains high pore-fluid pressures within the fault zone. The fault valve model consists of five distinct phases (Figure 1.9; after Sibson 1990).

- Input of fluid leads to an increase in fluid pressure along the sealed fault zone.
- Fluid pressure (hydrostatic) locally exceeds lithostatic pressure and leads to tensile fracturing within the fault zone.
- Shear hydraulic fracture occurs along the fault zone.
- Fluid release occurs along shear fractures within the fault zone.
- Fluid pressure diminishes and mineralisation occurs along the fault surface. The fault zone seals and the cycle begins again.

This behaviour can be recognised in the field by the mutual cross-cutting relationships between several generations of tensile veins and shear hydraulic fractures within fault zones. Other processes in the middle to upper crust include, convection through fracture networks and the influx of hydrothermal fluids.

In the middle to lower crust, fluid flow is channelled into actively deforming faults and shear zones, due to the rheological and permeability contrasts between the wall rocks and fault rocks (Oliver 1996). The most important mechanism in the middle crust is thought to be *dilatancy pumping* (Etheridge et al. 1983), which is driven by changes in fluid pressure. Cyclic variations in pore-fluid pressure during macroscopically ductile deformation may result in hydraulic fracture. Voids (i.e., dilatancy) may be created due to movement along irregular fracture surfaces. The resulting change in hydraulic head during the creation of voids will promote fluid flow. Fluid flow depends on the connectivity of the fractures, while the direction of

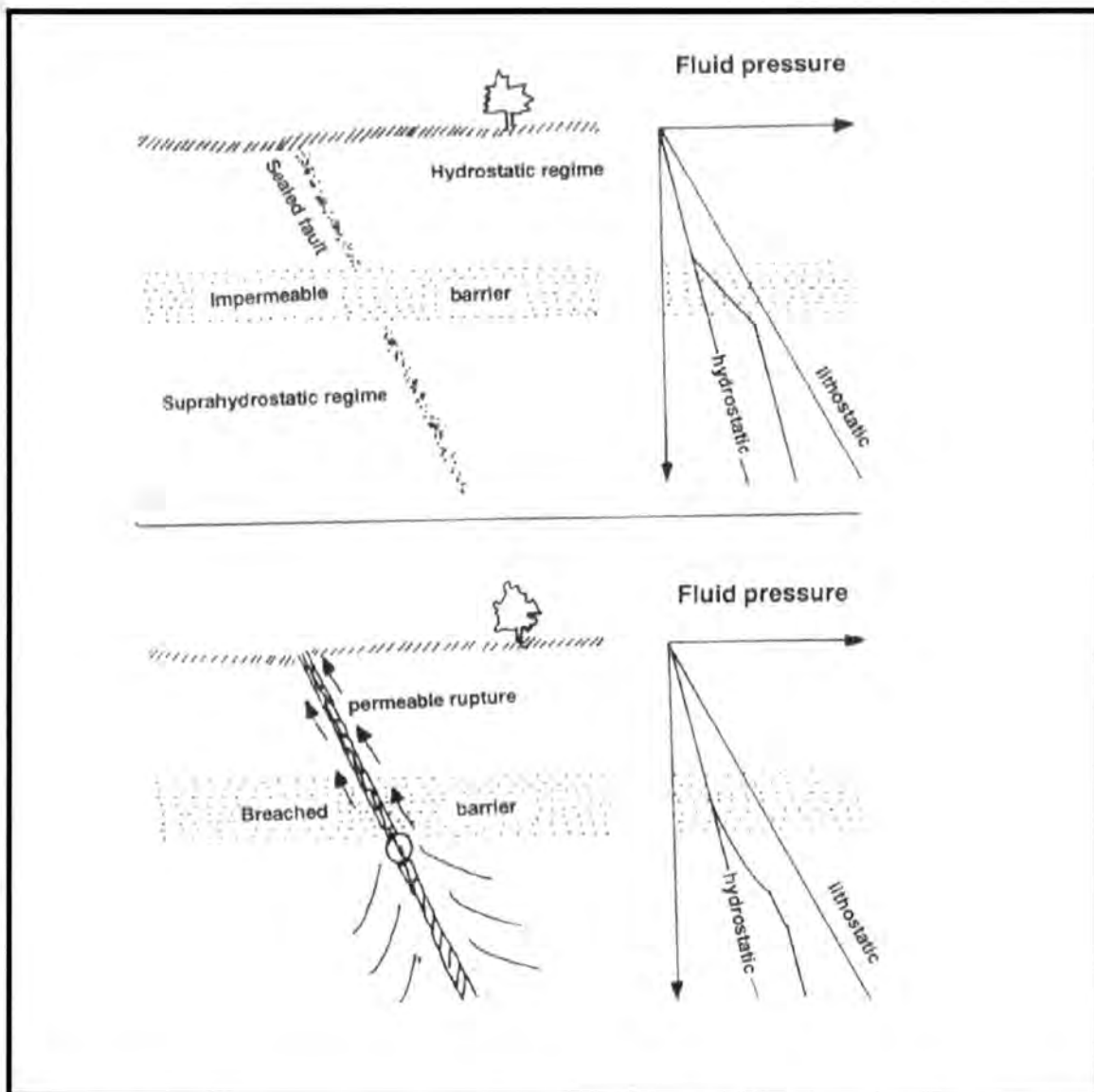


Figure 1.9 Schematic diagram to show the model conditions for fault valve behaviour (after Sibson 1990).

flow is controlled by the orientation of the permeability pathway (Sibson 1996). Other fluid-transport processes in the middle to lower crust include fluid infiltration along grain boundaries (e.g., McCaig and Knipe 1990) and the presence of microporous minerals (e.g., David et al. 1995).

1:6 Deformation mechanisms

In order to understand the rheological evolution of reactivated basement fault zones and identify fault-zone weakening processes, it is of utmost importance to determine the operative deformation mechanisms, prior to, during and after reactivation (White et al. 1986). Before outlining deformation mechanisms, it is worth outlining the use of the terms *brittle* and *ductile*, which have been used imprecisely in the literature, resulting in confusion (Rutter 1986). Ductility is a measure for the capacity of a material to deform by uniformly distributed flow (Schmid and Handy 1991), whilst brittle is defined as '*the breaking of rocks along well defined planes or zones*' (Twiss and Moores 1992). It is important to be specific about the scale of observation when using the terms brittle and ductile. For example, a fine-grained fault rock may display a macroscopic deformation which is accommodated by uniformly distributed flow, which may therefore be termed ductile. However, at microscopic scales or smaller, deformation and grain-size reduction may be accommodated by cataclasis and fracturing. In light of this, any fault rock may be described as ductile at a suitable scale of observation. Therefore, the term ductile is a phenomenological concept (Rutter 1986; Schmid and Handy 1991). Conversely, brittle, describes fracturing and crack development and is thus a mechanistic concept.

There are many variables which act together to create the conditions under which deformation occurs. There are two main groups of variables, lithological controls which are imposed by the characteristics of the rock, and controls which are imposed by the environment (Knipe 1989). Lithological controls include grain size, mineralogy, dislocation population, microcrack population, porosity and permeability. Environmental controls include temperature, pressure, stress, strain rate, fluid pressure and fluid composition. The combination of these factors give rise to material processes acting within grains or at grain boundaries which combine in various ways

resulting in the different deformation mechanisms described in the following sections. The inter-relationships of the factors outlined above are described in Figure 1.10 (after Knipe 1989).

The following section outlines the principal operative deformation mechanisms that are known to occur within the continental crust, and briefly describes their microstructural characteristics. There are two main groups of deformation mechanisms: (a) pressure-sensitive *frictional* mechanisms and (b) pressure-insensitive, thermally activated *viscous creep* mechanisms (Figure 1.11; Schmid and Handy 1991). The relationship between strength, deformation regime and fault rocks for a notional, vertical, crustal-scale fault zone is shown in Figure 1.6.

1:6:1 Frictional deformation mechanisms

Frictional deformation mechanisms are dominant in the upper c. 10km of the continental crust (Figure 1.6) and include the processes such as *fracture*, *frictional grain-boundary sliding*, *cataclasis* and *frictional melting* (Sibson 1977; Knipe 1989). The frictional strength of rocks increases proportionally to the effective normal strength, and thus depth (Figure 1.11).

Fracture mechanisms involve the nucleation and propagation of cracks, along which displacement may occur as deformation progresses. For a detailed review of mechanisms of fracture nucleation and propagation see Lloyd and Knipe (1992) and references therein.

Frictional grain-boundary sliding involves the sliding and rolling of grains past one another. Sliding takes place when the frictional resistance between grains is overcome and cohesion between the grains is lost (Knipe 1989). Deformation is dependent on the amount and strength of intergranular cement and typically occurs at low effective stress (low confining pressure and/ or high pore-fluid pressure). In general, the grains do not display evidence for intergranular deformation. Grain-boundary sliding without fracturing is common in fault gouges where pore-fluid pressures are high due to the presence of clay minerals. Grain-boundary sliding is

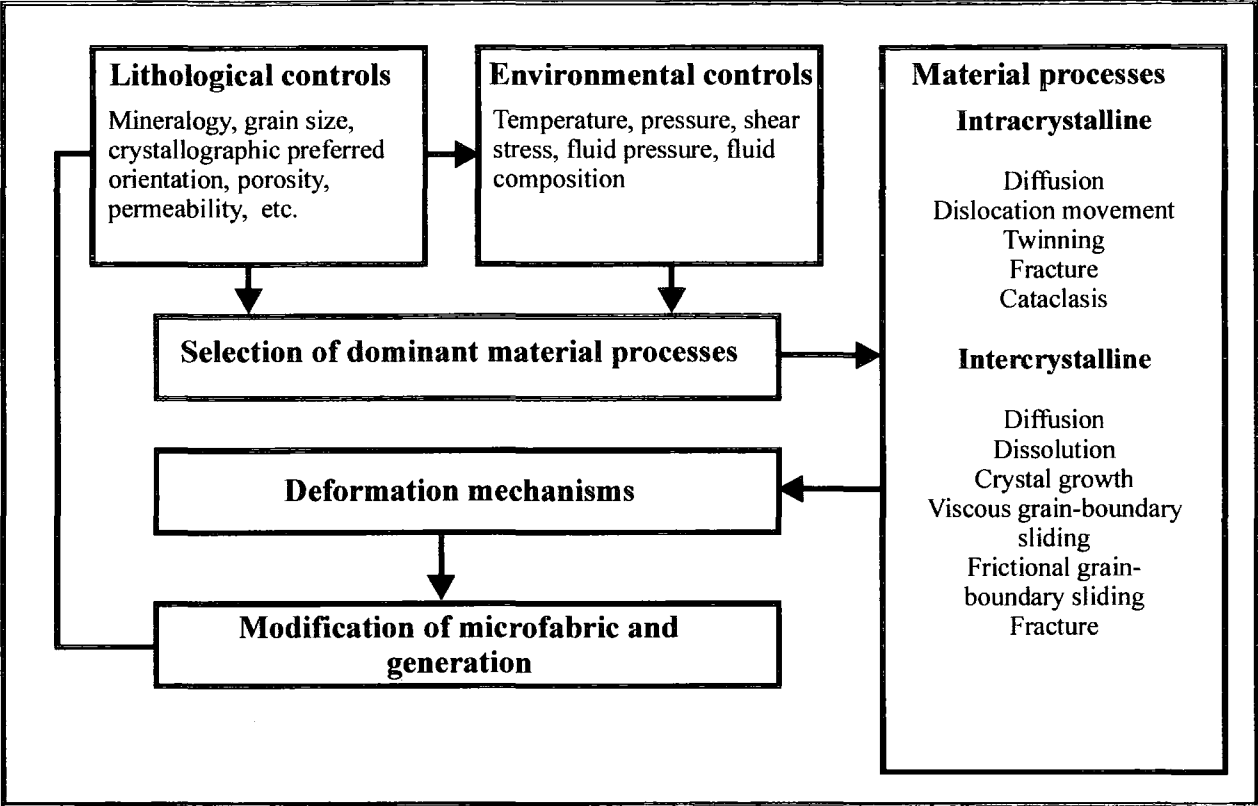


Figure 1.10 Flow chart to show the variables affecting the material behaviour of a deforming rock mass. Note the feedback between deformation processes and microstructural evolution of the rock (after Knipe 1989).

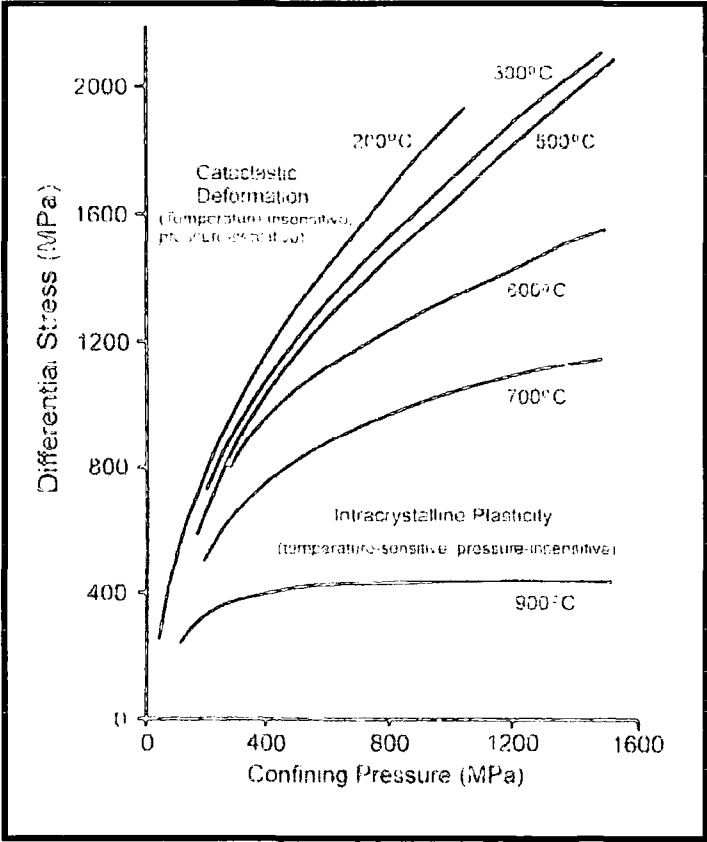


Figure 1.11 (A) Simplified representation of the data of Tullis and Yund (1977) for the ultimate strength of the Westerly granite at a strain rate of 0.0001/second. Strength in the brittle regime (up to 300°C) is insensitive to temperature, but sensitive to confining pressure. At higher temperatures, deformation is increasingly sensitive to temperature and a reduction in pressure sensitivity as intracrystalline plastic processes begin to dominate.

particularly important in the generation of deformation bands within unconsolidated sediments (Hesthammer et al. 2000 and references therein).

Cataclasis or cataclastic flow involves grain-scale fracturing, frictional sliding along fracture surfaces, frictional grain-boundary sliding and grain rotation (Knipe 1989). Cataclasis occurs at moderate confining pressures and relatively high pore-fluid pressures, and is likely to be an important deformation mechanism within the uppermost 5 to 10km of the crust (Sibson 1983; Knipe 1989). Cataclasis involves significant dilatancy (i.e., volume change) and therefore has implications for fluid transport properties for cataclastically deformed rocks (Knipe 1989). Cataclastically deformed rocks are characterised by randomly orientated, angular to rounded clasts which ‘float’ in a fine-grained cataclastic matrix. Cataclasis may be localised or may accommodate macroscopically ductile flow over broader areas.

Frictional sliding converts elastic strain and kinetic energy into heat. At high (seismic) strain rates (10^{-2} to 1 ms^{-1}), frictional sliding may result in localised *frictional melting* ($>1000^\circ\text{C}$) of the wall rocks along fault planes (Spray 1995). Friction-generated melts rapidly cool to crystallise as pseudotachylite. Magloughlin and Spray (1992) summarised pseudotachylite as a rock that shows “*a particular assemblage of mesoscale and microscale characteristics, including typically dark, aphanitic veins showing intrusive relationships, sharp boundaries, included clasts and crystals of the host rock and, critically, an association with faults or shear zones. The veins may contain glass, microlites, spherulites, vesicles, amygdales and embayed lithic fragments and show chilled margins*”. In general, frictional melting is thought to be promoted in dry, fluid-absent conditions (Sibson 1977). However, in a more recent study, Magloughlin (1992) suggested that some frictional melts may also be generated in fluid-rich environments.

1:6:2 Viscous deformation mechanisms

Viscous deformation mechanisms are pressure insensitive and thermally activated (Figure 1.11), and are characterised by linear, exponential or power-law relationships between stress and strain rate. Viscous creep mechanisms comprise two groups of

deformation mechanisms: (a) *diffusive mass transfer* and (b) *crystal plasticity* (Knipe 1989).

1:6:2:1 Diffusive mass transfer (DMT)

DMT processes involve the diffusional transport of material away from regions of high intergranular normal stress (source) to areas of relatively low intergranular normal stress (Rutter 1983; Knipe 1989). There are two fundamental groups of DMT processes; solid-state (Nabarro-Herring and Coble creep) and fluid assisted. Solid-state DMT processes involve the transport of material through the crystal lattice (Nabarro-Herring creep) or along grain boundaries (Coble creep), without the involvement of a fluid phase. If a fluid phase is involved in the transport of material, the process is termed fluid-assisted DMT (e.g., pressure solution and mass transport). Mechanisms that drive diffusion reflect the presence of a chemical potential gradient, which is induced by stress variations (Wheeler 1987), fluid pressure gradients (McCaig and Knipe 1990) or by variations in the internal strain energy of grains (Wintsch et al. 1995). DMT processes are promoted by high temperatures (increased rates of solid-state diffusion during Nabarro-Herring and Coble creep), fine grain sizes (increased grain boundary surface area and decreased diffusion pathways), low strain rates and/ or the presence of a chemically active fluid phase (dissolved material is easily transported within a fluid phase).

Knipe (1989) considered fluid-assisted DMT to be a three-stage process involving (a) source mechanisms, (b) diffusion mechanisms, and (c) sink mechanisms.

Source mechanisms dictate how material enters a diffusion pathway. Pressure-solution processes are the most important source mechanism during fluid-assisted DMT. Pressure solution (chemical dissolution of material) leads to the formation of stylolites, transected grains, dissolution seams, slaty cleavages and crenulation cleavages (Passchier and Trouw 1996). *Diffusion mechanisms* control how material is transported from source to sink regions. During fluid-assisted DMT, material is either transported along grain boundaries (e.g., pressure-solution creep, Rutter 1983) or in a bulk fluid flowing through the rock (e.g., mass transport, McCaig and Knipe 1990).

Voids, fluid inclusions (along grain boundaries), localised growth of retrograde minerals and veins are all characteristic of diffusion mechanisms (Passchier and Trouw 1996). *Sink mechanisms* are, in general, sites of localised dilatation and comprise veins and strain shadows (beards) adjacent to rigid porphyroclasts. Newly precipitated minerals can be different from consumed minerals; this effect is known as *incongruent pressure solution* (Beach 1979).

1:6:2:2 Crystal plasticity

Crystal plasticity involves the accumulation of strain by intracrystalline processes by the movement of dislocations (linear defects) and mechanical twinning (Figure 1.12).

At relatively low temperatures (<0.5 melting temperature), crystal plastic deformation is accommodated predominantly by the movement of dislocations along slip planes, which is known as *dislocation glide* (Knipe 1989). At these temperatures, dislocations build up to form dislocation tangles, which restrict further movement of dislocations through the lattice. This leads to *work hardening*, which is commonly observed to be the precursor to brittle fracturing and frictional sliding (Lloyd and Knipe 1992). Patchy undulose extinction and the development of crystallographic fabrics are characteristic of dislocation glide. At higher temperatures (>0.5 melting temperature) and/ or lower strain rates, work hardening is counteracted by thermally activated *recovery processes*, such as *dislocation climb* (Knipe 1989), which rearrange defects to lower the internal strain energy of a crystal. Recovery is predominantly achieved by dislocation climb, which involves the diffusive movement of defects to higher or lower slip planes (Williams et al. 1994). Sweeping, undulose extinction, deformation lamellae and subgrains are indicative of recovery (Passchier and Trouw 1996). Subgrains develop as dislocations are arranged into a planar boundary, which separates slightly misoriented regions of the crystal lattice (e.g., Figure 1.12).

In addition to recovery, the rock may experience *dynamic recrystallisation*, which also reduces the dislocation density or the internal strain energy of the crystal during deformation. Recrystallisation involves the development of new, relatively strain free

grains at the expense of older, highly-strained, work-hardened grains. Drury and Urai (1990) recognised two mechanisms of dynamic recrystallisation: (a) *Subgrain rotation recrystallisation* and (b) *grain-boundary migration recrystallisation*.

Subgrain rotation recrystallisation results from the addition of an increasing number of dislocations at a subgrain boundary, which causes a progressive misorientation of the crystal lattice. At misorientations of $>10^\circ$, the subgrain transforms into a newly recrystallised grain (Figure 1.12). 'Core' and 'mantle' structures are characteristic of subgrain rotation recrystallisation (White 1976). These structures comprise relatively undeformed porphyroclasts, which are mantled by aggregates of fine subgrains and dynamically recrystallised grains.

Grain-boundary migration recrystallisation involves the migration of a grain boundary that separates a highly-strained grain (high dislocation density) from an unstrained grain (low dislocation density) of the same material (Drury and Urai 1990). The boundary migrates into the highly-strained grain, leaving the unstrained grain behind. This process reduces the dislocation density and therefore the internal strain energy. Aggregates of interlobate grains with highly irregular grain boundaries are characteristic of grain-boundary migration recrystallisation (Passchier and Trouw 1996).

1:6:3 Mineral strength behaviour

The deformation mechanisms described previously in sections 1:6:1 and 1:6:2 are active in virtually all minerals. However, differences in the crystal lattice structure and melting temperature of minerals lead to differences in strength. Hence, a mineral's response to an applied deformation is largely controlled by the prevailing physical conditions (i.e., pressure and temperature). Figure 1.13, after Stewart (1997), summarises the operative deformation mechanisms and resultant microstructures for different minerals at varying temperatures. It is important to note that the fault rock fabrics are not wholly dependent on temperature, since other environmental controls such as, lower strain rates, higher finite strains and fluid compositions have the same effect as increasing temperature (see section 1:6; Figure 1.10).






Temperature	100°C	200°C	300°C	400°C	500°C	600°C	700°C
Quartz	Brittle fracturing, pressure solution and solution transfer of material are dominant processes. Features include fractures in grains, evidence for pressure solution and deposition of material sometimes in veins.		Dislocation glide dominant. Dislocation climb becomes important. 'Sweeping' undulose extinction and deformation lamellae	Dislocation climb dominant and recovery and dynamic recrystallization important. Dynamic recrystallization mechanism may change with increasing temperature from SR dominant to combination of SR and GBM recrystallization. Pressure solution may still occur. Fine recovery & recrystallization textures; oblique foliations may develop in the SR and GBM regime.	Rapid recovery and recrystallization. Prism slip ($\{m\}\langle c \rangle$) becomes important. Secondary grain growth may occur. Dynamic recrystallized assemblages, grains have a strain-free appearance.		
Feldspar	Brittle fracturing and cataclastic flow. Angular grain fragments with variable clast size. Grain-scale faults and bent cleavage planes & twins. Patchy undulose extinction actually due to submicroscopic crushing.		Internal fracturing assisted by minor dislocation glide. Flame perthite may be present. Tapering deformation twins, undulose extinction and bent twins.	Dislocation glide possible & recrystallization becomes important, esp. around margins. Micro-kinking abundant. Core & mantle structures.	Dislocation climb and glide relatively easy. Both SR and GBM recrystallization occur. Myrmekite abundant. Core and mantle structures still occur but the boundary between the core and recrystallizing mantle is less pronounced. Myrmekite abundant, especially along foliation planes. Flame perthite is absent. Fracturing is uncommon.		
Micas	Micas deform by slip on $\{001\}\langle 001 \rangle$ or $\{001\}[001]$. Slip accommodated by pressure solution, fracturing, kinking and folding.		Biotite experiences viscous creep above 250 °C. Muscovite is generally more resistant to deformation and forms mica-fish.				
Calcite	<p>Pressure solution dominant at low grades if water is present. Deformation twinning becomes important from very low grades onwards.</p> <div><div><p>Type I deformation twins</p></div><div><p>Type II deformation twins</p></div><div><p>Type III deformation twins</p></div><div><p>Type IV deformation twins</p></div><div></div></div>						

Figure 1.13 The mechanical behaviour of common minerals in response to deformation at different temperatures (after Stewart 1997, compiled from Passchier and Trouw 1996). Note that an increase in the fluid content and a decrease in strain rate will have the same effect as increasing temperature. Grey shading - crystal plastic and DMT processes (viscous creep).

1:6:4 Aggregate strength and behaviour

Rocks consist of aggregates of different minerals, which respond to deformation in different ways under the same physical conditions. Therefore, the strength of a rock is largely determined by the proportions of its constituent minerals, some of which may be relatively weak whilst others are relatively strong. Handy (1990) characterised the deformation effects on polymineralic rocks, and defined three microstructural and mechanical behaviours as a result of deformation, based on the ratios of the strength of strong minerals to weak minerals and the proportion of those weak minerals present in the rock (Figure 1.14).

Handy (1990) characterised three domains:

- (a) *Domain 1, Load-bearing framework.* In this field the strong phase is dominant and provides a **load-bearing framework** separating isolated pockets of the weak phase. The aggregate strength is controlled by grain size, shape and the distribution of the weak phase.
- (b) *Domain 2, Boudin-matrix field.* Here, elongate grains of the stronger phase are set within a weaker matrix. The relative strength of both phases is low. Both phases are rheologically active, representing a matrix-controlled **interconnected weak-layer** rheology.
- (c) *Domain 3, Clast-matrix field.* Higher mineral strength ratios and greater than 20% volume of the weak phase lead to relatively undeformed clasts (strong phase), which are surrounded by the weak phase. This leads to a matrix-controlled, **interconnected weak-layer** rheology.

Deformation and metamorphic processes tend to break down the load-bearing framework (Domain 1) to generate an interconnected weak-layer rheology, even if the weak phase is only subordinate (see section 1:7:2:3a for discussion).

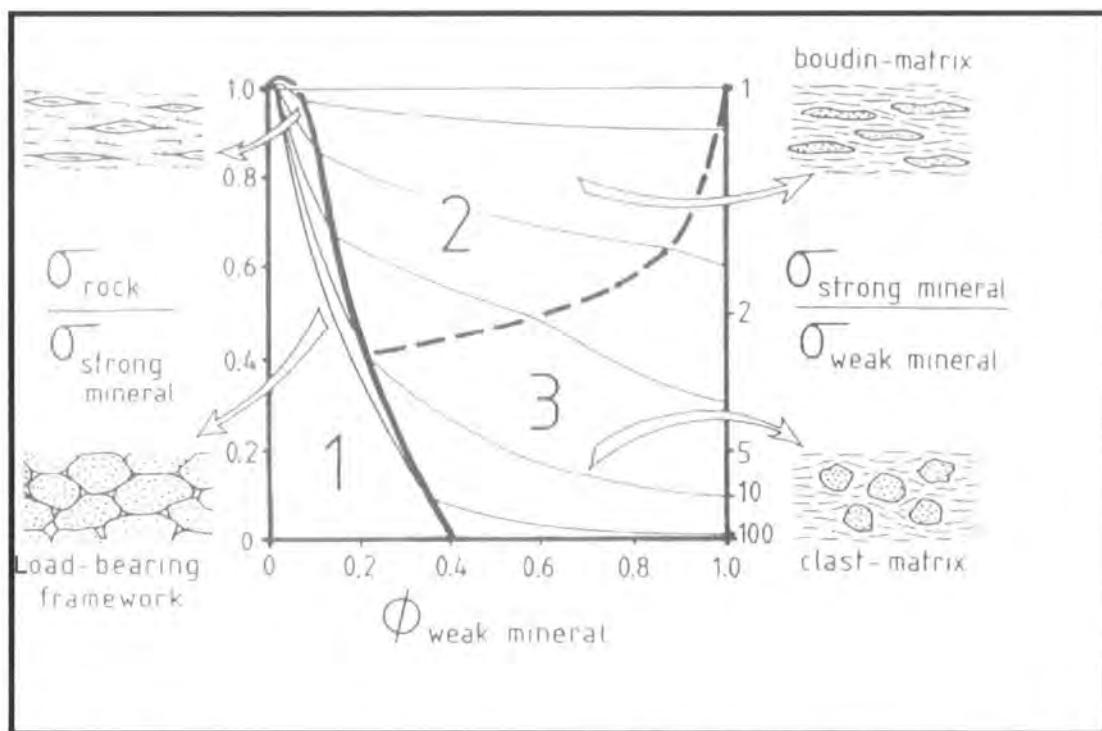


Figure 1.14 The characterisation of polyphase aggregate behaviour in solid-state deformation (after Handy 1990). ϕ - volume proportion, σ -strength.

1:6:5 Frictional to viscous creep transition

Reactivated fault zones if exposed may show evidence for both frictional and viscous deformation. The frictional to viscous creep transition separates seismogenic upper crust, which deforms primarily by frictional processes, and an essentially aseismic crust that deforms principally by viscous creep mechanisms (Schmid and Handy 1991). This change in the dominant deformation mechanism is controlled by increasing temperature with depth. However, different minerals have different activation energies with respect to the onset viscous deformation. At a given temperature, a 'weak' mineral may deform by viscous creep while a 'strong' mineral will deform by frictional processes, and will act as a rigid mineral. Therefore, the nature and style of deformation in rocks is a function of the relative proportion of weak phases present. As a result, the mechanical behaviour of the frictional to viscous creep transition is extremely complex (Schmid and Handy 1991).

The position of the frictional to viscous creep transition, with increasing strain, is unlikely to remain at the same depth due to the complex interactions between fault rock textures, mineralogy and environmental variables (Figure 1.10; Knipe 1989; Schmid and Handy 1991; Stewart et al. 1999, 2000; Holdsworth et al. 2001; Imber et al. 2001).

Handy (1990) suggested that in rocks which contain 20% or more by volume of a weak phase, there is likely to be a strain-dependent switch from frictional to viscous deformation mechanisms as the rock evolves from a 'load-bearing framework' to an 'interconnected weak-layer' rheology (Figure 1.14; section 1:6:4). Therefore, in highly-strained rocks the transition from frictional to viscous deformation will occur over a narrow depth range (Schmid and Handy 1991). In rocks which contain <20% volume of a weak phase, frictional processes (cataclasis) may be dominant. Cataclasis results in extreme grain-size reduction. If cataclasis is localised and the cataclasite matrix consists of 20% or more of the rock, an interconnected weak-layer microstructure may develop. Such grain-size reduction may lead to the onset of grain-size sensitive DMT mechanisms. As a consequence, the frictional to viscous creep

transition may change depth with increasing strain (Imber et al. 1997, 2001; Stewart et al. 1999, 2000; Holdsworth et al. 2001).

Imber et al. (1997) also documented that syn-tectonic retrograde metamorphism and the growth of new mineral phases will alter the mechanical properties of the frictional to viscous creep transition (see section 1:7:2:2).

1:7 Fault-zone weakening mechanisms

There are two fundamentally different groups of fault-zone weakening mechanisms, *transient*, *syn-tectonic* and *long term* (Holdsworth et al. 1997). Long-term weakening mechanisms are both syn-tectonic and semi-permanent, causing weakening over long periods of geological time. Transient, syn-tectonic weakening mechanisms are those processes that are only operative during active deformation. In the following section, only those weakening mechanisms that are likely to be operative along reactivated basement fault zones are described. More detailed reviews of fault-zone weakening mechanisms are presented in Rubie (1990) and Wintsch et al. (1995).

1:7:1 Transient, syn-tectonic weakening mechanisms

1:7:1:1 High pore-fluid pressure

An increase in pore-fluid pressure causes a decrease in the effective normal stress across a pre-existing fault surface, and therefore decreases the critical shear stress needed for frictional sliding. As a result, high pore-fluid pressures across a pre-existing fault causes brittle failure under differential stress conditions that in dry rocks would be stable (Byerlee 1978). Therefore, highly overpressured faults are thought to be relatively weak. Rice (1992) suggested that high pore-fluid pressures may explain the apparent weakness of the San Andreas Fault. Wintsch et al. (1995) concluded that high pore-fluid pressures would be unlikely to explain this weakness in the long term,

as no mechanism is known that will maintain high pore-fluid pressures over long periods of geological time.

1:7:1:2 Hydrolytic weakening

Tullis and Yund (1980), on the basis of experimental work, suggested that the addition of trace amounts of water may reduce the activation energy, and hence, the temperature at which dislocation creep operates in quartzo-feldspathic rocks. In other words, trace amounts of water can significantly enhance the activity of crystal-plastic deformation mechanisms, at a given temperature and pressure (Tullis and Yund 1980). The temperature at which the onset of crystal plasticity occurs in experimentally deformed 'wet' rocks, is dependent on pressure, strain and strain rate. Therefore, hydrolytic weakening may result in the shallowing and narrowing of the frictional to viscous creep transition in rocks which are not highly overpressured. However, in highly overpressured, fluid-saturated crust, where rocks are likely to deform by fluid-assisted DMT, it is unclear how significant the effects of hydrolytic weakening will be (Imber 1998).

1:7:1:3 Generation of transient, fine grained reaction products

The development of new, fine-grained reaction products at the start of a metamorphic reaction can cause weakening (Rutter and Brodie 1985). Brodie and Rutter (1985) carried out experimental studies which suggested that significant decreases in stress are associated with shear-zone location during the development of fine-grained reaction products. Rutter and Brodie (1985) attributed this weakening to the onset of diffusion-dominated, grain-size sensitive mechanisms within shear zones. These weakening mechanisms are likely to be short-lived. If the rock remains at sufficiently high temperatures, grain growth is likely to occur, which will suppress diffusion-dominated deformation mechanisms as the surface area is reduced.

1:7:1:4 Transformational plasticity and volume change

Metamorphic phase changes may enhance the plasticity of a deforming rock by promoting a change in volume from one phase to another. Volume change may create localised stresses which assist intracrystalline plasticity (Brodie and Rutter 1985). Long-term weakening is unlikely by this method, as it requires repeated recycling through the phase change (Rubie 1990).

1:7:1:5 The introduction of melt

Several authors have suggested a link between magma emplacement and the weakening of the continental crust (Hollister and Crawford 1986; Davidson et al. 1994), and more significantly the concentration of strain where melt is present. Scholz (1990) suggested that the frictional resistance to brittle failure along a fault may drop if the fault is filled with melt or hot fluids. Also, strength estimates for natural rocks that experienced anatectic flow indicate that melts weaken the continental crust, particularly at depths where they spread laterally beneath low-permeability layers or along active shear zones with a pronounced mylonite foliation (Handy et al. 2001 and references therein). Hollister and Crawford (1986) suggested that melts may enhance strain localisation. However, strain localisation does not necessarily coincide with weakening; rocks can harden during localisation if deformation involves a component of dilation during melting (Hobbs et al. 1990) or syn-tectonic metamorphic reactions (Brodie and Rutter 1985; Wintsch 1995; Wibberley 1999). In more recent studies, Handy et al. (2001), noted that an acute weakening associated with diminished stress only occurs during short periods of crustal veining. Handy et al. (2001) point out that cooling and crystallisation is rapid and hardens the crust, to strengths of at least as great as and, in some cases, greater than, its pre-melting strength. Therefore, the introduction of melts may lead to localisation and short-term, syn-tectonic weakening, but is unlikely to operate over long periods of geological time.

1:7:1:6 Shear heating

If localised deformation along a fault or shear zone is rapid, a syn-tectonic weakening may occur due to shear heating as a result of friction (Scholz 1990). The syn-tectonic generation of sufficient heat within a fault zone can lead to deformation at lower shear stresses than in the surrounding country rock. This process is unrealistic in the long term, as later reactivations along basement fault zones occur a long period after inception of the fault zone, and any effects of shear heating are likely to be very short-lived.

1:7:2 Long-term weakening mechanisms

1:7:2:1 Favourable orientation of a pre-existing anisotropy

If a fault zone is inherently weak in the long term, the orientation of a pre-existing fault with respect to the newly imposed stress regime is likely to control reactivation. Reactivation may occur in the brittle regime if the fault lies in a near ideal orientation to the regional stress field, as the difference in strength may be small (Etheridge et al. 1986). Other authors believe that faults fail under a much greater variety of orientations for the same stress. The failure criterion for most rocks is the same as most rocks share similar frictional properties. The failure criterion is termed *Coulomb fracture criterion* (Byerlee 1978). Potential for reactivation can be assessed by comparing the coefficient of internal friction for the fault rock with the intact wall rock. For example, a fault may contain gouge which will have a lower coefficient of friction than the surrounding wall rock. At low confining pressures, deformation will occur along the pre-existing fault (Figure 1.15). However, at increasing depths and under greater confining pressures it will become easier to form a new fault rather than reuse the pre-existing structure (Figure 1.15). The problem for the application of this theory is that it assumes deformation occurs in the brittle regime following Coulomb fracture criterion. However, deformation along crustal-scale, reactivated fault zones also occurs within the viscous regime and near the frictional to viscous creep transition, and therefore this method cannot be applied in a direct sense to the entire

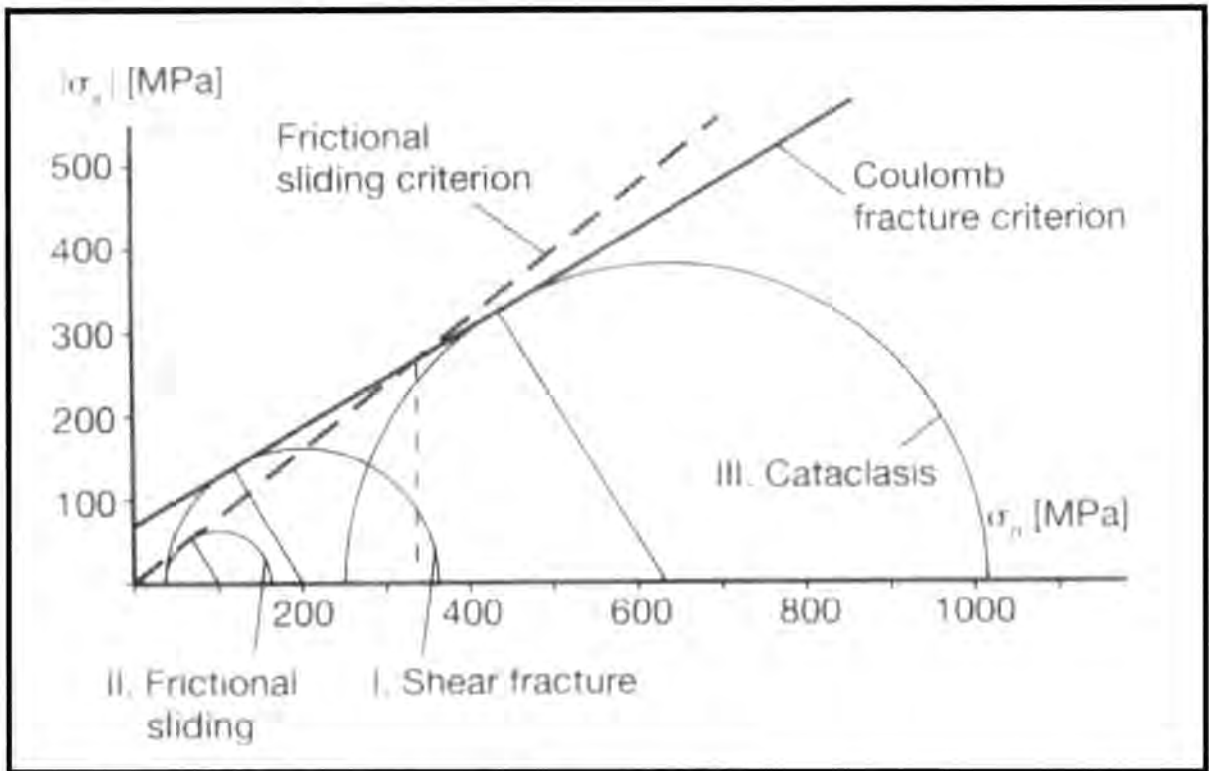


Figure 1.15 Mohr circle diagram to show Coulomb fracture criterion (solid line) and for frictional sliding on a pre-existing fault surface (dashed line). 1 - Mohr circle of critical stress for shear fracture. 2 - Mohr circle of critical stress for frictional sliding along fracture surface at low confining pressure. 3 - Mohr circle of critical stress for cataclastic flow. Note - fracturing requires lower differential stress than frictional sliding at the same confining pressure. Data for Weber Sandstone (after Twiss and Moores 1992).

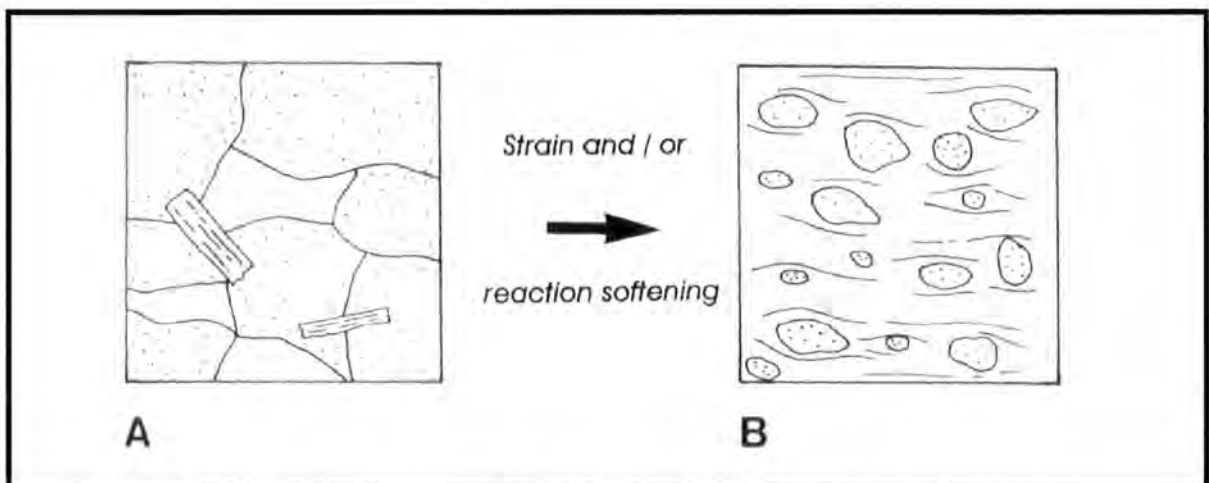


Figure 1.16 Schematic diagram illustrating foliation weakening. (A) Load-bearing framework microstructure (LBF). Stipple - interlocking strong phase, plane and dashed ornament - weak phase. (B) Interconnected weak layer microstructure (IWL). Stipple-strong phase (forming isolated, rigid porphyroclasts), dashed ornament - weak phase. (compiled by Imber 1998 from Handy 1990).

fault zone. The concept of favourably orientated weak zones in the lower crust and upper mantle may be applicable where viscous flow laws operate (Silver 1996). The range in favourable orientations, dominant mechanisms and how they change in character with depth are presently unknown.

1:7:2:2 Reaction softening

The process of reaction softening results in the replacement of relatively 'strong' minerals by *intrinsically weak* minerals during syn-tectonic metamorphism (Rubie 1990; Wintsch et al. 1995; Imber et al. 1997; Wibberley 1999). Single muscovite grains, deformed in experiments, accommodate strain by dislocation glide over a wide range of temperature and pressure conditions. Muscovite (biotite and chlorite) grains have low activation energies with respect to dislocation glide, and are likely to be weak over a wide range of crustal depths (Mares and Kronenberg 1993). Also, well foliated, micaceous rocks appear to be significantly weaker than massive, quartzo-feldspathic rocks deformed in experiments at similar pressure, temperature and strain rate conditions (Shea and Kronenberg 1993). Therefore, the syn-tectonic, chemical breakdown of feldspar aggregates to white mica, and hornblende to chlorite, constitutes an important reaction softening process (Wintsch et al. 1995; Imber et al. 1997). Other important reaction softening processes involve the precipitation of water-swelling clay minerals and zeolite minerals along upper-crustal fault zones (Byerlee 1978), as a result of hydrothermal alteration during frictional deformation (Warr et al. 2001). Several authors have attributed the weakness of faults to the presence of low-friction clay minerals (Morrow et al. 1992 and references therein), whilst others have noted the occurrence of clay minerals along active faults (Zoback et al. 1987; Wintsch 1995).

1:7:2:3 Fabric softening

Fabric softening includes two main processes, foliation weakening (Jordan 1987) and the development of crystallographic fabrics (White et al. 1986).

1:7:2:3a Foliation weakening

Undeformed basement rocks are usually characterised by relatively strong minerals, such as hornblende and feldspar, which isolate pockets of relatively weak minerals, such as quartz and biotite, to form a granoblastic texture. Therefore, the rheology of most undeformed basement rocks is controlled by the rheological behaviour of strong minerals, and thus forms a load-bearing framework microstructure (LBF) (Figure 1.16A; section 1:6:4; Handy 1990). As the rock starts to deform, the strong minerals (e.g., feldspar and hornblende) remain rigid and deform predominantly by fracturing (Handy 1990). However, relatively weak mineral phases (e.g., quartz and mica) deform in a crystal-plastic manner. The plastically deformed minerals become more stretched with increasing strain to such an extent that the weak phase becomes interconnected, and wraps around isolated, rigid porphyroclasts. In such rocks, the rheology of the deformed aggregate will be controlled by the rheology of the weak phase, leading to the development of an interconnected weak-layer microstructure (IWL) (Figure 1.16B). Schmid and Handy (1991) suggested that such IWL microstructures only develop if the weak phase constitutes 20% or more by volume of the undeformed protolith (see Figure 1.14). Therefore, a switch from an LBF-dominated rheology to an IWL-rheology will weaken the fault rocks relative to the undeformed protoliths of the same composition. This process is known as *foliation weakening* (Handy 1992). In many cases, reaction softening, through the development of highly aligned aggregates of phyllosilicate minerals, will enhance the process of foliation weakening (Jordan 1987; Handy 1990; Imber et al. 1997).

1:7:2:3b Development of crystallographic fabrics

The formation of crystallographic fabrics occurs during crystal-plastic deformation and results in the alignment of crystallographic axes of a particular phase. Deformed minerals become aligned depending on (a) which intracrystalline slip systems were operative (which depends on mineralogy, pressure, temperature and strain rate), and (b) the kinematics and the direction of movement along the fault or shear zone (Law 1990). For example, phyllosilicate grains often become aligned parallel to the mylonite foliation and are therefore oriented conveniently for grain-boundary sliding (White et al 1986). However, crystallographic axes in quartz mylonites are oriented obliquely to the shear-zone boundary (Law 1990). In such cases, if the kinematics

during reactivation correspond to the kinematics of the previous deformation event, the slip systems within the previously deformed grains may be ideally oriented for easy intracrystalline deformation. If the kinematics are different during successive deformations a strong crystallographic fabric is unlikely to weaken the fault or shear zone (White et al. 1986).

1:7:2:4 Grain-size reduction

Grain-size reduction in a fault or shear zone, either by cataclasis or dynamic recrystallisation, is likely to promote the onset of grain-size sensitive deformation, such as DMT processes (see following section, 1:7:2:5). Also, fine-grained rocks (which have a larger grain boundary surface area) are more susceptible to metamorphism and therefore reaction softening (section 1:7:2:2) than coarse-grained rocks of the same composition (Brodie and Rutter 1985). Therefore, grain-size reduction is essential to the operation of grain-size sensitive mechanisms, and contributes significantly to fault-zone weakening. However, the importance of grain-size reduction in the long term depends on whether the fault zone remains at sufficiently low temperatures to suppress grain growth during post-tectonic static recrystallisation (Imber 1998).

1:7:2:5 Fluid-assisted DMT

Localised grain-size reduction and/ or the influx of fluids into a fault zone may promote the onset of grain-size sensitive, fluid-assisted DMT mechanisms (Imber et al. 1997, 2001; Imber 1998; Stewart et al. 1999, 2000; Holdsworth et al. 2001; see section 1:6:2:1). Grain-size sensitive mechanisms, such as DMT, are able to sustain higher strain rates than crystal-plastic mechanisms at the same pressure, temperature and stress regime (Handy 1989 and references therein). In other words, fine-grained fault rocks which deform by diffusion-dominated creep are able to deform under much lower stresses than rocks at the same strain rate by crystal-plastic mechanisms. Consequently, fine-grained, fluid-rich fault zones are expected to be weak.

1:8 Data collection

1:8:1 Fieldwork methods

Reconnaissance studies were carried out on all exposures along the Walls Boundary Fault System and the Møre-Trøndelag Fault Complex in the study areas to identify key fault strands for more detailed studies. Key fault strands were primarily mapped at 1:10,000 scale. Further studies involved detailed baseline mapping, cross-sections and structural logging on a variety of scales (1:1,000 to 1:5) in complex areas of the fault zones. Projected cross-sections used in areas of patchy exposure involved the projection of structural data onto a 2D vertical surface (oriented normal to the fault zone) to provide an accurate record of fault rock distribution and structure within parts of the fault zones. Structural logs were used to document fault rock distribution and structural relationships. A structural log is a 1D traverse through the fault zone, and usually oriented normal to the fault zone or foliation and normal to the slickenside or stretching lineations, exposure permitting. Each log comprises (a) a sketch which records overprinting and structural relationships, (b) a geometric log comprising structural data, and (c) a lithological log which records fault rock distribution. Samples of key fault rocks were collected for microstructural and textural observations, and are located on the structural logs. Each log was photographed at a variety of scales. The structural logs in this thesis vary in scale depending on the complexity of the fault zone and the amount of exposure.

1:8:2 Microstructural methods

Thin-sections of fault-rock samples were studied under a variety of magnifications using an optical transmitted light microscope. Selected samples were analysed using the backscatter detector attached to a CamScan scanning electron microscope (SEM) in the Electron Microscopy Unit at the University of Leeds. Semi-quantitative analyses of selected minerals were obtained using the energy dispersive X-ray detector attached to the SEM.

1:8:3 Major element geochemistry

Major element concentrations were determined using the XRF at the Department of Geological Sciences, University of Durham. Samples were crushed, powdered and dried, then fused to form glass discs, using standard techniques. The fusion discs were analysed using a Philips PW1400 XRF machine using peak and background intensity measurements. This was conducted using the Philips X41 software package and a suite of international standards

1:8:4 $^{40}\text{Ar}/^{39}\text{Ar}$ laserprobe dating

Fault-rock dating techniques carried out by Sarah Sherlock at The Open University, UK are outlined in section 7:2.

1:9 Outline of thesis

Following this introductory chapter, the thesis comprises:

- **Chapter 2** – an introduction to the regional geology of Shetland and a summary of previous work on the Walls Boundary Fault Zone (WBFZ) and other regionally significant faults that are part of the Walls Boundary Fault System (WBFS).
- **Chapter 3** – describes the kinematic and structural evolution of the WBFZ and other regionally significant faults within the WBFS based on detailed analysis of fault rock distribution and structures at a series of key localities.
- **Chapter 4** – describes fault rock microstructures and textures from key localities along the WBFZ in order to provide a detailed textural and microstructural evolution exhibited by fault rocks along key strands of the fault zone.
- **Chapter 5** – an introduction to the regional geology of the Fosen Peninsula, Central Norway and a summary of previous work on the Møre-Trøndelag Fault Complex (MTFC).

- **Chapter 6** - describes the kinematic and structural evolution of the MTFC based on detailed analysis of fault rock distribution and structures at a series of key localities.
- **Chapter 7** - describes fault rock microstructures and textures from key localities along the two principal faults of the MTFC (Hitra-Snåsa Fault and Verran Fault), in order to provide a detailed textural and microstructural evolution exhibited by fault rocks along key strands of the fault zone. $^{40}\text{Ar}/^{39}\text{Ar}$ laserprobe dating of pseudotachylite and host-rock mylonite samples will be presented in order to constrain the timing of 'early' fault rocks formed along the MTFC.
- **Chapter 8** – this chapter provides a synthesis of kinematic, structural and microstructural evolution of the two reactivated basement fault zones studied: the WBFZ and the MTFC. The processes and factors that control deformation, localisation and reactivation along basement-reactivated fault zones is discussed.

Chapter 2. The Geology of Shetland

The Shetland Islands (Figure 2.1) lie 300km north of Aberdeen and 300km to the west of Bergen. In total there are 120 islands stretching N-S over a distance of 110km and 50km across from east to west at their widest point.

Shetland is part of a basement window surrounded by Devonian and younger sedimentary rocks. The islands provide an important link between the Scottish, Norwegian and East Greenland portions of the Caledonian Orogen. Shetland is transected by a major strike-slip fault system, which includes the Walls Boundary Fault (WBF) that juxtaposes a segment of the Caledonian front to the west against Moine-Dalradian type rocks to the east. The rocks of the Caledonian front to the west of the WBF are unconformably overlain by Devonian sedimentary and volcanic rocks, and are cut by Late Devonian granites. The succession of Moine-Dalradian type sedimentary rocks to the east of the WBF were metamorphosed during the Caledonian orogeny, overthrust by an ophiolite complex, intruded by Early Devonian granites, and are unconformably overlain by Middle Devonian sandstones.

Offshore, Permo-Triassic basins, bounded by N-S-striking faults (e.g., Viking Graben, West Shetland and Faroe Shetland Basins; Figure 2.1), dissect the remnants of Devonian basins and Caledonian basement. Late Jurassic rifting affected the Viking Graben accompanied by the deposition of syn-rift sediments and footwall uplift of the Shetland platform. Thick sequences of Cretaceous and Tertiary rocks overlie Jurassic rocks of the Viking Graben and are intercalated with volcanic rocks within the Faroe Shetland Basin. Regional uplift of the mainland and offshore basins took place during the Early Tertiary as a result of magmatic underplating related to opening of the North Atlantic.

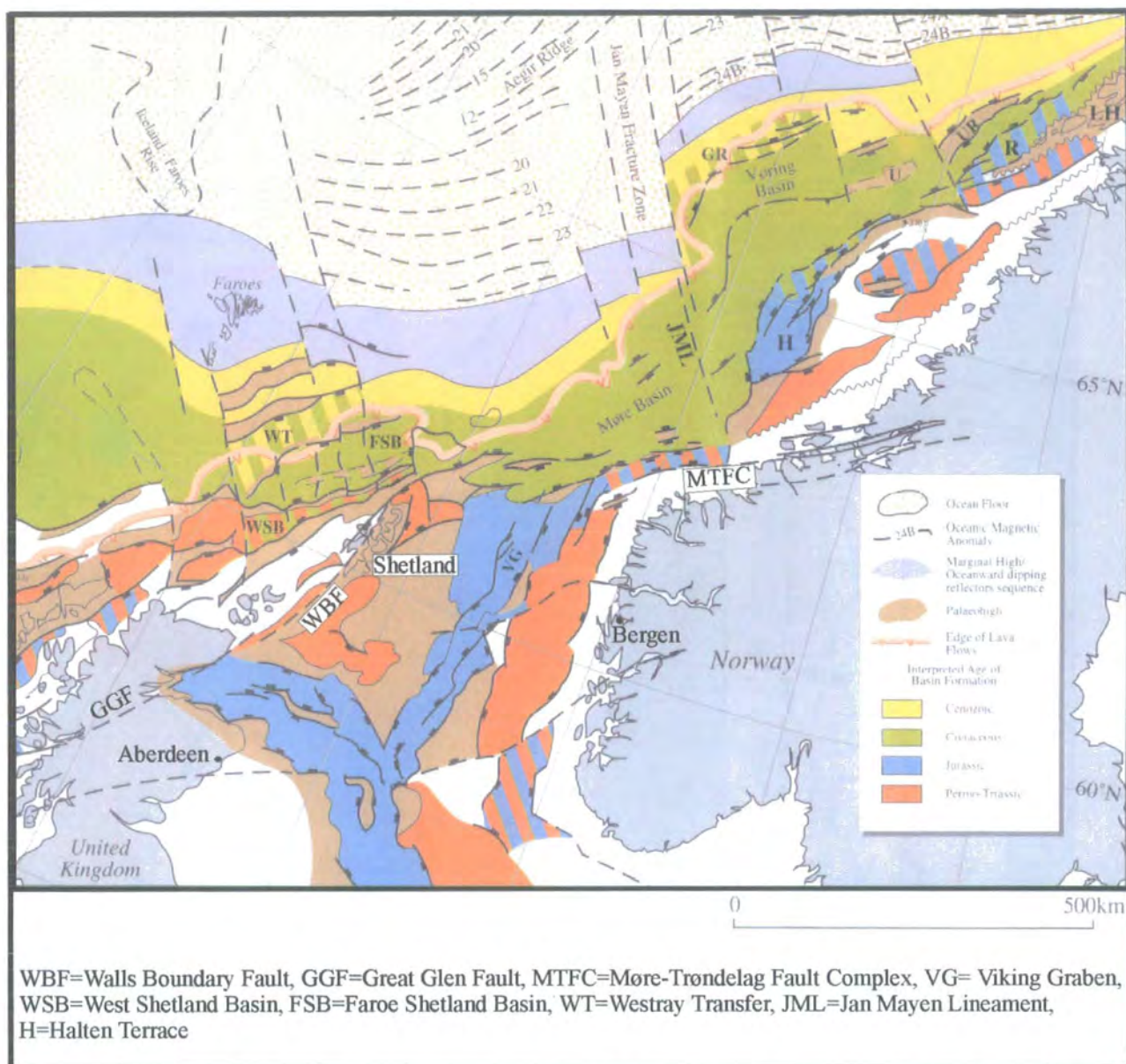


Figure 2.1 Map to show the location of the Shetland Isles and the major offshore basins of the Northeast Atlantic margin (adapted from Doré et al. 1997b).

2:1: Onshore Geology

2.1:1 Caledonian and Older Basement west of the WBF

Basement rocks west of the WBF comprise Lewisian gneisses, Moine cover rocks, the Queyfirth Group and the metamorphic rocks of the Walls Peninsula (Figure 2.2).

2:1:1:1 Lewisinoid basement associated with the Caledonian Front

The Caledonian Front in Shetland is defined by the Wester Keolka shear zone (WKSZ) (Pringle 1970). This structure is a ductile thrust dipping about 60° to the east with a top-W sense of shear and it is thought to be equivalent to the Moine Thrust in Northwest Scotland (Pringle 1970; Andrews 1985). In the North Roe area, the WBF trace lies only 4km east of the Caledonian Front (Figure 2.3). Basement gneisses west of the WKSZ have the same appearance of being autochthonous basement to the Caledonides as have the Lewisian gneisses of Northwest Scotland (Flinn 1985). Aeromagnetic anomalies over Northwest Shetland are almost identical to those over the Lewisian of Northwest Scotland (Flinn 1969).

The Lewisian basement gneisses in the area are subdivided into two groups. To the west of the WKSZ, the autochthonous Western Gneisses are felsic banded orthogneisses with accessory hornblende that are cut by foliated pegmatites. The Western Gneisses have yielded a minimum age of 2900Ma (Flinn 1985). To the east, the Lewisinoid Eastern Gneisses form inliers of schistose, banded, hornblende-rich gneisses intercalated with cover rocks of the Sand Voe and Hillswick Groups. In places they are acidic, feldspar rich, and contain fine bands of hornblende-rich rocks. Serpentinites commonly occur, ranging in thickness from a few centimetres to many tens of metres. East of the WKSZ is a 800m-thick succession of amphibolite-facies, psammitic metasedimentary rocks belonging to the Sand Voe Group, interleaved with tectonically banded slices of Eastern gneisses (Figure 2.3; Holdsworth et al. 1994).

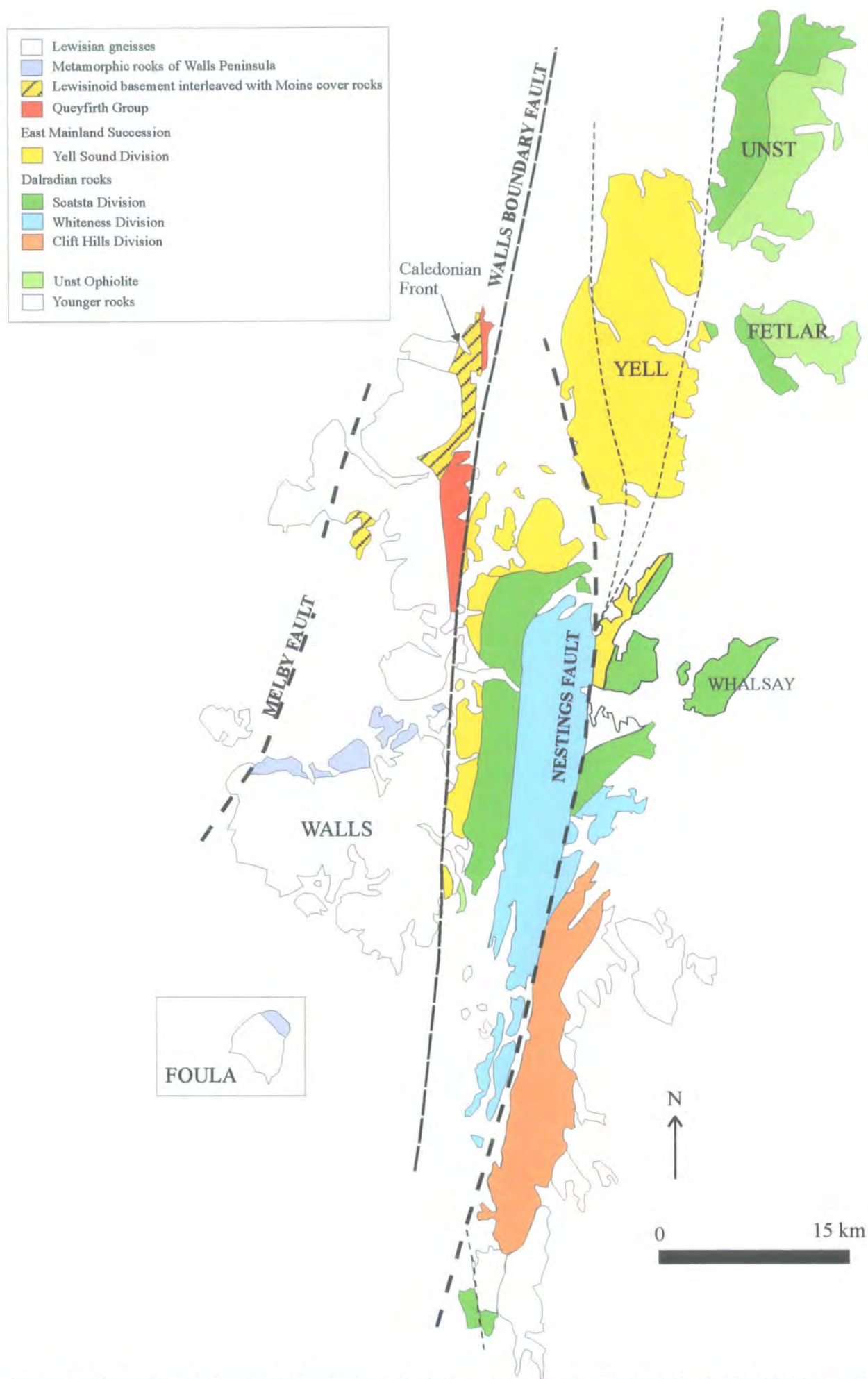


Figure 2.2 Map showing the location of Caledonian and older basement rocks of the Shetland Islands. NB. the Valayre and Skelldale gneiss mark the boundary between the Yell Sound and Scatsta Division.

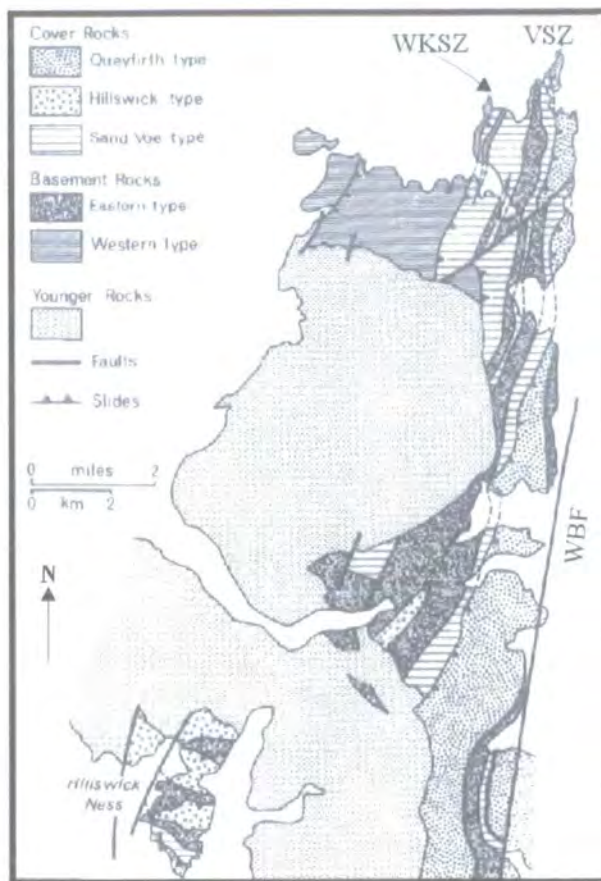


Figure 2.3 Geological map of the North Roe area (adapted from Flinn 1985).

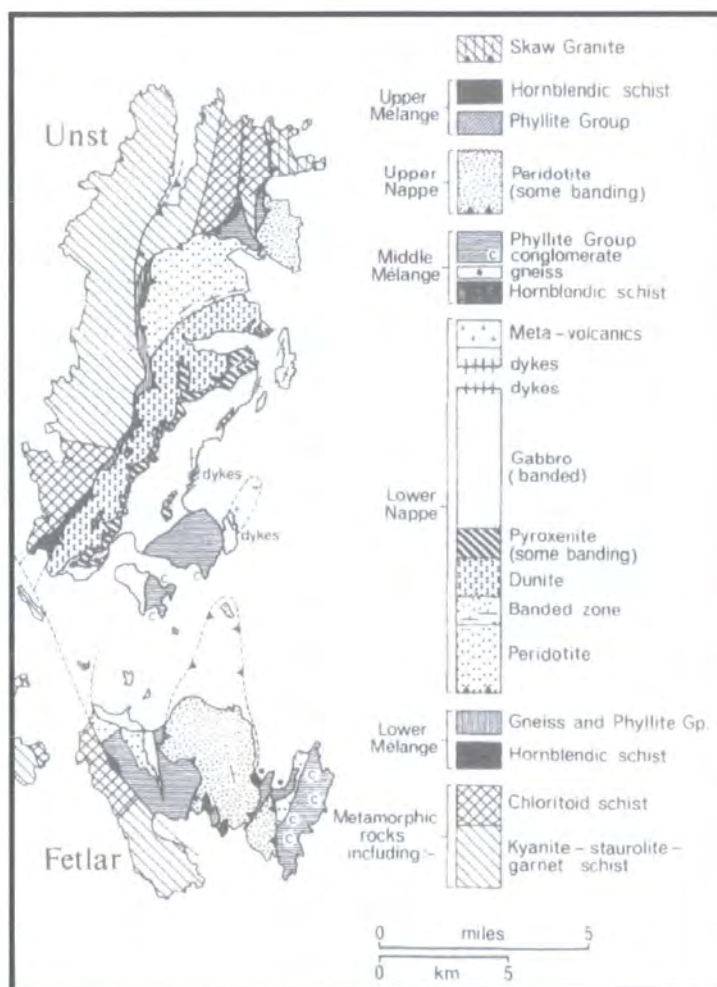


Figure 2.4 Geological map of the Ophiolite complex on the islands of Unst and Fetlar (adapted from Flinn 1985).

To the east of the psammites lies the main band of Eastern Gneiss, which is 250 metres thick. This unit is followed to the east by a 250m-thick garnet-mica schist of the Sand Voe Group. These units are then bounded by the Virdbeck shear zone (VSZ) (Figure 2.3), a ductile thrust that dips about 60° to the east showing evidence for top-W directed shear (Pringle 1970). This structure is overlain by the Queyfirth Group. The succession described below the VSZ is named the Sand Voe schuppen zone. Cover rocks within the schuppen zone (Sand Voe and Hillswick Groups) are both regarded as part of the Moine Supergroup (Pringle 1970; Flinn 1985).

2.1:1:2 Sand Voe Group

Sand Voe Group rocks are highly schistose, siliceous psammites with some garnet-mica psammites and pelitic units. These schistose rocks become very platy at their contacts with inliers of the basement gneisses. Cross bedding and conglomerate lenses have been identified (Flinn 1985). Pelitic garnet-mica schist also occurs adjacent to slivers of Eastern Gneisses. In general, the Sand Voe Group rocks show amphibolite-facies metamorphic parageneses.

2.1:1:3 Hillswick Group

The Hillswick Group is lithologically similar to the Sand Voe group. The group is composed mainly of amphibolite-facies siliceous psammites, garnet-mica psammites and garnet-mica schist. The Hillswick Group differs from the Sand Voe Group due to the presence of frequent 10-100m-thick units rich in pyrite and graphite.

2.1:1:4 Queyfirth Group

On the eastern side of the VSZ lies a sequence of calcareous and non-calcareous pelitic schists and volcanic rocks that are all affected by greenschist-facies metamorphism. This sequence is the Queyfirth Group (Pringle 1970) which has been tentatively correlated with the Dalradian Supergroup of Scotland (Flinn 1988).

2:1:1:5 Metamorphic rocks of the Walls Peninsula

Basement rocks of uncertain origin form a 2-3km-wide E-W-trending outcrop, that extends along the north coast of the Walls Peninsula and the adjoining islands to the northeast, where it is truncated by the WBF (Figure 2.2). Foliation strikes NE-SW and dips 40-70° to the SE and is parallel to the bedding of the overlying Devonian sedimentary rocks belonging to the Walls Formation. In the north, hornblende schists and amphibolites, intercalated with quartzo-feldspathic semi-pelites, are followed to the south by muscovite and biotite schists that are interbedded with thin bands of marble (Mykura and Phemister 1976). The most southerly unit comprises tremolite and mica schists that are commonly interbanded with marbles, hornblende schists and amphibolite (Mykura 1976). These rocks are cut by numerous faults and shear zones that strike NNE-SSW.

2:1:2 East Mainland Succession

The East Mainland Succession underlies most of Shetland east of the WBF (Figure 2.3). It is a 20km-thick sequence of Moine-Dalradian type metasedimentary rocks that strikes NNE-SSW. The sequence has been divided into four, main, lithologically different divisions (Figure 2.2; Flinn et al. 1972).

2:1:2:1 Yell Sound Division

The Yell Sound Division is the westernmost unit and contains the oldest rocks of the East Mainland Succession. The division is 9-14km in thickness and is bounded to the west by the WBF (Figure 2.2). Well-laminated psammites, interbanded with garnet-hornblende schists typify the division. Psammites vary in texture from schistose to granular. In places, the pelitic horizons contain staurolite and kyanite porphyroblasts suggesting that the rocks are generally amphibolite-facies units. Gneissose units are locally common and several generations of strongly tectonised pegmatites and aplites

cross-cut the psammites. The Yell Sound Division has been correlated with the Moine (Flinn et al. 1972), possibly the Glenfinnan Group (Flinn 1985). Flinn et al. (1991) defined the eastern boundary of the Yell Sound Division at the Valayre Gneiss, although this does not necessarily correspond to the Moine-Dalradian boundary (Flinn 1988). It was selected because the Valayre gneiss is a good marker and can be traced 80km along strike until it is cut out by the WBF to the southwest.

2.1:2:2 Moine-Dalradian boundary zone.

A 1km-thick zone of rocks of uncertain affinity occurs east of the Valayre Gneiss and are bounded to the east by the Skelladale gneiss, another continuous gneiss band running parallel to the Valayre Gneiss. The rocks that occur between the two gneiss bands are termed the Boundary Zone, with Moine rocks lying to the west and Dalradian rocks presently to the east of the Skelladale Gneiss. The contact between the Moine and the Dalradian must lie within the Boundary Zone and is thought to be tectonic (Flinn 1985). Outcrops of blastomylonitised hornblende gneiss are quite common in this unit and are interleaved with brown hornblende schists not found elsewhere on Shetland.

2.1:2:3 The Scatsta Division

The Scatsta Division lies to the east of the Yell Sound Division and is 4km thick (Figure 2.2). It comprises the Scatsta Pelitic Group and the Scatsta Quartzitic Group. The westernmost part of the division is composed of garnet-biotite-muscovite granulites and gneisses, crystalline limestone and calc-silicate units (Flinn 1985). Impure quartzites interbanded with staurolite-kyanite pelitic schists dominate the upper part. Most units within the division have been metamorphosed to upper greenschist/ lower amphibolite facies. The Scatsta Division has been correlated with the Appin Group of the Lower Dalradian Supergroup (Harris et al. 1994). Rocks correlated with the Scatsta Division outcrop on Unst and Fetlar (Figure 2.3) where they are structurally overlain by the Unst ophiolite complex (section 2:1:3).

2:1:2:4 The Whiteness Division

The Whiteness Division (Figure 2.2) consists mainly of flaggy micaceous quartz-feldspar psammite and is 6km thick. At its base lies the Weisdale Limestone, which has been correlated with the Ballachulish Limestone of the Appin Group of the Dalradian Supergroup in Scotland (Flinn et al. 1972). Above the limestone is the Collafirth Group which comprises semipelites and psammites interbedded with mica schists, calc-silicate granulites, thin marbles and hornblende schists. On top of the Collafirth Group is the Girlsta Limestone. The rocks between the Whiteness and Girlsta Limestone have been migmatized and are sometimes known as the Colla Firth permeation belt (Flinn 1954). The upper part of the Whiteness Division contains the Wadbister Ness Group and the Laxfirth Limestone. The Wadbister Ness Group consists of flaggy micaceous psammites, pelites, calc-silicate bands and hornblende schist. The Laxfirth Limestone marks the top of the Whiteness Division and has been correlated with the Tayvallich Limestone of the Argyll Group of the Dalradian Supergroup (Harris et al. 1994).

2:1:2:5 The Clift Hills Division

The Clift Hills Division follows conformably east of the Laxfirth Limestone (Figure 2.2). The base is defined by a metavolcanic unit which is locally spilitic. This unit is followed by a 3km-thick succession of semipelitic phyllites which, in places, are very fine-grained rocks with centimetre-scale graded bedding typical of distal turbidites (Flinn 1985). Impure limestones and quartzites are interbedded with the phyllites and some exhibit crude sole markings. The easternmost and youngest unit is composed of volcanoclastics, lavas, pillow lavas and serpentinitised ultrabasic rocks. Miller and Flinn (1966) and Harris et al. (1994) correlated the Clift Hills Division with the Southern Highland Group of the Dalradian Supergroup of Scotland.

2:1:3 The Unst Ophiolite

In Northeast Shetland, an ophiolite complex is exposed on the islands of Unst and Fetlar (Figure 2.2). The total reassembled thickness of this complex, which now occurs as at least two thrust sheets (Flinn 1958), is estimated to be about 8km (Spray 1988).

2:1:3:1 Metamorphic Rocks

Pelitic schists of the East Mainland succession crop out structurally below the ophiolite (Figure 2.4). They are mainly garnet-mica schists containing kyanite, staurolite and chloritoid porphyroblasts, suggesting that the rocks were metamorphosed at amphibolite facies. However, the succession has locally been intensely reworked at greenschist facies, an event that was interpreted by Flinn (1985) to be related to ophiolite emplacement.

2:1:3:2 Lower Nappe

The Lower Nappe comprises the main ophiolite unit and has been thrust upon the East Mainland succession lying to the west (Figure 2.4). It is a slice of rock 6km wide and over 20km long composed of peridotite, dunite, pyroxenite, gabbro, a sheeted dyke complex and a metavolcanic unit at the top (Figure 2.4; Flinn 1958). This corresponds well with a standard ophiolite assemblage (Flinn 1985). Zircons extracted from plagiogranite within the gabbro yielded an age of 492 ± 3 Ma (U/Pb), which constrains the crystallisation age of the ophiolite (Spray et al. 1991). The ophiolite sequence is deformed by open folds (e.g., on Fetlar; Figure 2.4) and cut by greenschist-facies shear zones, which relate to nappe emplacement. The more ultramafic units near the base of the Lower Nappe are cut by several generations of serpentinite veins and are heavily brecciated (Flinn 1985).

2:1:3:3 Mélange Zones

Zones of *mélange* occur below the Lower Nappe and at the top of both nappe sequences. The *mélange* zones comprise blocks of metasediments belonging to the Phyllite Group (see below), exotic masses of hornblende schist and slices of metasediments belonging to the East Mainland succession. The thrusts that carried the ophiolite slices into place occur at the top of the *mélange* units and are closely associated with the development of amphibolite-facies hornblende schists (Flinn 1985). These are thought to represent metamorphosed ocean floor, which is considered to relate to the early stages of obduction (Flinn et al. 1991).

2:1:3:4 Upper Nappe

Serpentinised peridotite lies above the middle *mélange* unit on Fetlar. It is underlain by a thrust dipping at 30° to the west on the east side and by the same angle to the east on the west side, as shown in Figure 2.4 (Flinn 1985).

2:1:3:5 The Phyllite Group

Rocks of the Phyllite Group commonly occur as a series of tectonic lenses in the *mélange* so that no primary succession has been established (Figure 2.4; Flinn 1985). The rocks have been intensely deformed and metamorphosed to greenschist facies. They were originally finely laminated graphitic and micaceous mudstones, alternating with clastic sandstones, and include lenses of polymictic conglomerates probably of turbiditic origin (Flinn 1958). Most conglomerates are only a few metres thick, but the Funzie conglomerate on the eastern side of Fetlar is several kilometres thick. It is mainly composed of quartzite pebbles but also contains some clasts of ophiolite affinity (Flinn 1958). All rocks within the group lie unconformably upon the upper surface of the main ophiolite unit. The rocks were affected by greenschist-facies metamorphism as a result of burial due to further ophiolite obduction, although the overlying rocks have subsequently been eroded (Flinn 1985).

2:1:3:6 Skaw Granite

The Skaw Granite is separated from the underlying ophiolite and metasediments by a top-W shear zone (Figure 2.4; Flinn 1985). Its relationship to the other rock units in Shetland is unknown (Mykura 1976). The age of the shear zone relative to the emplacement of the ophiolite complex is not known (Flinn 1985). Miller and Flinn (1966) recorded a K-Ar age of 354Ma for the biotite within the granite.

2:1:4 Regional Synthesis of Caledonian and Older Basement

Shetland forms a large exposure of Caledonian rocks lying close to the Late Silurian triple junction of Laurentia, Baltica and Gondwana. Correlations with the Lewisian, Moine and Dalradian rocks of Scotland have all been recognised in Shetland (Pringle 1970; Flinn 1985; Harris et al. 1994; Holdsworth et al. 1994), confirming that the basement rocks of Shetland are of Laurentian affinity.

In Northeast Shetland, the Dalradian rocks underlie a thrust contact with an ophiolite complex in the hangingwall. The gabbro within the ophiolite crystallised at 492 \pm 2Ma (U/Pb) and this is similar to other ages of felsic rocks in ophiolite fragments within the Scandinavian Caledonides, Canadian Appalachians and to the Ballantrae ophiolite in Scotland (Spray et al. 1991). The early stages of obduction are thought to have occurred after c.490Ma ago synchronous with the peak of metamorphism and formation of hornblende schists within the mélangé (Flinn et al. 1991).

The Caledonian front in Shetland differs from that of Scotland as there are no Cambro-Ordovician or Torridonian rocks preserved, unlike in the Moine Thrust Zone and along the adjacent foreland of Scotland. The ductile thrusts in Shetland are associated with blastomylonites and widespread crystallisation of garnet. This is broadly similar to the western Moine Nappe in Scotland (Holdsworth 1989). A discordant pegmatite within the Sand Voe Group has been dated at c.499Ma (Rb-Sr) and is affected by a foliation related to the WKSZ (Flinn 1985). Flinn (1979) and Watson (1984) believed that the Shetland nappes were emplaced during or after pegmatite emplacement with movement continuing to 400Ma, based on a spread of K-

Ar mineral ages within the Caledonian front in Shetland. An important change in the kinematic regime, coinciding with the closure of the Iapetus Ocean, was recorded by the onset of sinistral transcurrent movements on faults and shear zones parallel to the Caledonian orogenic belt (Watson 1984). On Shetland, this is recorded by the formation of the N-S striking WBF and associated fault rocks that are the subject of the present study.

2:1:4 Devonian Sandstones

The Devonian sandstones in Shetland are mostly unmetamorphosed rocks that regionally unconformably overlie the basement. They are divided into three main groups based on their geographical location and lithology (Figure 2.5; Mykura 1976).

2:1:4:1 Central Group

The Central Group contains the oldest Devonian rocks on Shetland and outcrops between the Melby Fault (MF) and the WBF on the Walls Peninsula (Figure 2.5). The group comprises the Walls and Sandness Formations, and has been equated with the Fair Isle Devonian succession east of the WBF (Mykura and Phemister 1976). The Sandness Formation is located north of the Sulma Water Fault (SWF) and east of the MF (Figure 2.5). The formation onlaps eastwards onto the basement and is composed of a succession of cross-bedded, finely laminated sandstones and silts (Mykura and Phemister 1976). At, or near the unconformity, conglomerates and breccias are common. Basic and intermediate lavas, tuffs, agglomerates, ignimbrites and felsite intrusions occur interleaved with the sandstones. The Walls Formation to the south of the SWF contains cross-bedded, laminated sandstones interbedded with silts and shales. Poorly preserved fossil fish and plant remains have been described (Mykura 1976). A Lower Devonian age has been given to plant material from the Sandness Formation and a Middle Devonian age for fish remains in the Walls Formation. Mykura (1976) correlated the Walls and Sandness Formations with the Lower-Middle Devonian of Orkney and Caithness. The rocks of both formations have been subjected to two phases of open to tight folding (Mykura 1976), or a continuous

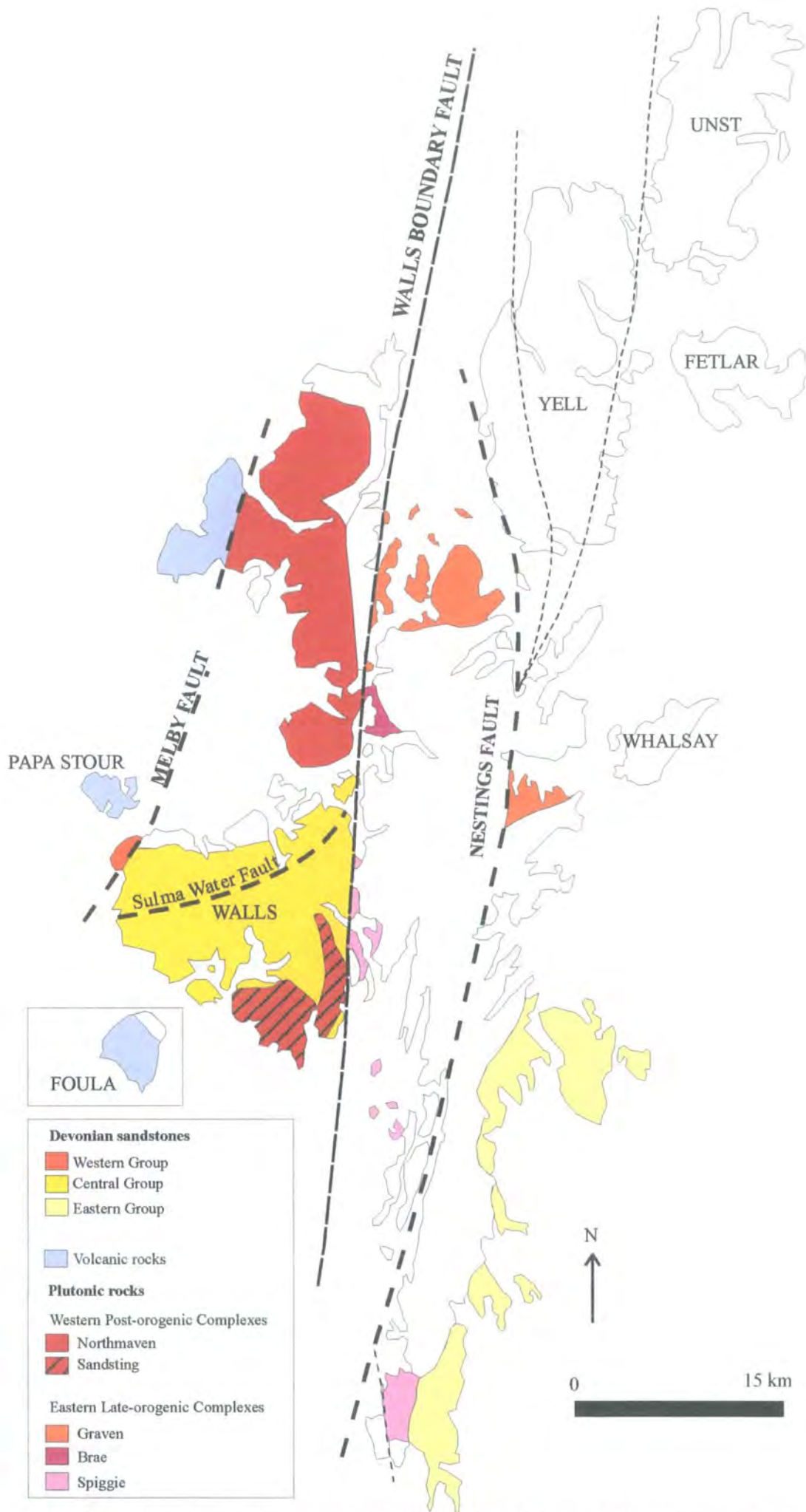


Figure 2.5 Geological map to show the location of Devonian sedimentary rocks and plutonic complexes on Shetland.

phase of syndepositional folding associated with the development of local unconformities, and left-lateral shearing along with local detachment faulting along the SWF (Séranne 1992a). Sandstones of the Walls Formation have been intruded by the Sandsting Granite Complex (Figure 2.5) which produced a contact aureole of hornblende-hornfels metamorphic facies (Mykura 1976). Folding on a kilometre scale and sinistral strike-slip movement on the SWF post-dated intrusion of the Sandsting Granite and was therefore later than 370 to 360Ma.

2:1:4:2 Western Group

The Western Group crops out west of the MF on the mainland, on Papa Stour and on Foula (Figure 2.5). The group comprises red sandstones and volcanic rocks of Middle Devonian age. The Melby Formation outcrops west of the MF on the mainland. Near the base of the formation, there are two beds of grey siltstone with shale containing carbonate nodules. The beds contain fish and plant remains and have been correlated with the Middle Devonian Sandwick fish beds of Orkney (Mykura 1976). Red sandstones, conglomerates and siltstones dominate the formation above the fish beds. Donovan et al. (1976) correlated the Melby Formation with the Middle Devonian of Orkney using fossil plant spores. The sandstones pass upwards into rhyolites and ignimbrites near to the top of the formation. The rocks of Eshaness occur west of the northern extension of the MF, where the sequence consists of sandstones that pass up into lavas, tuffs, agglomerates and ignimbrite. This sequence is folded into a N-S-trending open syncline. On Papa Stour, the rocks comprise rhyolites, basalts, tuffs and sandstones which are similar to the lower part of the Eshaness sequence. The sandstones of Foula lie unconformably on metamorphic rocks similar to those of the Walls Peninsula (see section. 2:1:1:5). The Devonian rocks here are cross-bedded and in places, conglomeratic or silty, and are folded into a N-S-trending open anticline.

2:1:4:3 Eastern Group

The Eastern Group crops out east of the Nestings fault as a narrow strip extending from Lerwick to Sumburgh Head in the south (Figure 2.5). The group onlaps metamorphic rocks to the west, with breccias at the base above the unconformity. It is composed mainly of flaggy sandstones that are commonly pebbly, with lenses of conglomerate and localised calcareous units containing fish remains. The age of the fish beds ranges from Middle to Upper Devonian (Mykura 1976). Sandstones of the Eastern and Western groups are more lithologically similar to the Old Red Sandstones of Orkney and Caithness than the Central Group (Flinn 1985).

2:1:5 Plutonic rocks

There are two groups of Caledonian plutonic complexes in Shetland, lying east and west of the WBF (Figure 2.5). The eastern complexes have given ages of about 400Ma and all plutons are cut by the WBF and NF (K-Ar and Rb-Sr, Flinn 1985). The plutons are foliated in places, and they are thought to have been emplaced before Caledonian deformation had ceased (Flinn 1985). There are no cross-cutting relationships with the Devonian sequence of the Eastern Group. The western complexes have yielded ages nearer to 350Ma (K-Ar and Rb-Sr), with associated dykes and granites cutting the sandstones of the Walls Formation of the Central Group.

2:1:5:1 Eastern Late-orogenic Complexes

2:1:5:1a Graven Complex

This magmatic complex comprises a wide range of plutonic rock types from ultrabasic to aplo-granophyric (Figure 2.5; Mykura 1976). The dominant components are granite, diorite and gabbro, all of which contain numerous hornblende diorite veins and pegmatites. Mykura (1976) described the complex as having formed by the superimposition of two separate vein complexes. The pegmatites, together with sheet-like bodies of granite, were intruded first into country rocks of the Yell Sound

Division, followed by locally hornblende-rich granites and diorites. Xenoliths and enclaves of psammite belonging to the Yell Sound Division are common. The contact aureole affects pelites and calcareous schists belonging to the Yell Sound Division, which contain sillimanite and diopside, respectively. The Graven Complex has yielded K-Ar ages ranging from 400Ma for the granites and pegmatites to approximately 385Ma for the dioritic phase (Miller and Flinn 1966), both of which were interpreted to date intrusion.

2:1:5:1b Brae Complex

The Brae Complex outcrops south of the Graven Complex (Figure 2.5). It consists of a series of intrusions varying from pyroxene-mica dolerite to ultramafic rocks and granite (Flinn 1985). The complex is cut by sheets of granodiorite and tonalite, followed by pegmatites similar to those of the Graven Complex and finally by lamprophyres (Mykura 1976). Intrusion of the Brae Complex has been dated to 385 +/-6Ma (Miller and Flinn 1966, K-Ar whole rock).

2:1:5:1c Spiggie Complex

The Spiggie Complex extends from Aith Voe, where it is cut by the WBF, to the islands of Hamnavoe and Hildasay (Figure 2.5). The majority of the complex consists of granodiorite and porphyritic adamallite. Other rock types present include hornblende diorite, monzonite and serpentinite. The complex also crops out near Quensdals Bay east of the NF. There, it is unconformably overlain by Devonian sandstones of the Eastern Group. Miller and Flinn (1966) dated the intrusion of the complex using the K-Ar whole-rock technique and recorded an age of 385 +/-8Ma.

2:1:5:2 Western Post-orogenic Complexes

2:1:5:2a Northmaven Complex

The Northmaven Complex (Figure 2.5) is composed of the Ronas Hill and Muckle Roe granites which are connected by a dioritic vein complex (Phemister 1979). The complex otherwise consists of granite, diorite and gabbro belonging to essentially one

period of magmatic activity. There are no cross-cutting relationships with Devonian sandstones. However, the granites are cut by a series of dykes, including a rare riebeckite porphyry, which also cuts the sedimentary rocks of the Walls Formation to the south (Flinn 1985). The complex is characterised by a series of randomly orientated and structureless sheet-like intrusions. The K-Ar age of the Ronas Hill granite is 358 ± 8 Ma (Miller and Flinn 1966), which was interpreted by these authors to date emplacement. Mykura and Phemister (1976) describe xenoliths of andesite which are very similar to the Eshaness andesites. These have been dated (K-Ar) at 373 ± 2 Ma (Flinn et al. 1968), suggesting that the Ronas Hill granite is younger than this age.

2:1:5:2b Sandsting Complex

The Sandsting Complex lies to the south of the Northmaven Complex and is cut by the WBF at its eastern margin (Figure 2.5). It is composed of sheet-like bodies of granite, granodiorite, granophyre and diorite. The granite and associated dykes cross-cut and metamorphose sedimentary rocks of the Walls Formation (Mykura and Phemister 1976). Biotites have yielded K-Ar ages of 334 Ma (Miller and Flinn 1966) and 360 Ma (Mykura and Phemister 1976), whilst hornblendes extracted from diorite gave an age of 369 Ma (Mykura and Phemister 1976). All these K-Ar dates were interpreted as intrusive ages.

2:1:6 Regional Synthesis of Devonian

In Scotland and Ireland, during the Early Devonian, faults and shear zones parallel to the Caledonian orogenic belt were active with sinistral transcurrent movements occurring along them, which is considered to have led to the intrusion of late orogenic granites (Hutton and McErlean 1991). On Shetland, the plutons are foliated in places and have no cross-cutting relationships with the Devonian sequence of the Eastern Group. The plutons are similar in age to the Newer Granites of Scotland (Harris et al. 1991). The thick Devonian sedimentary rocks of Shetland unconformably overlie deeply eroded Caledonian basement and are believed to represent remnants of the Devonian Orcadian Basin. The Orcadian Basin extended from northern Scotland and

possibly as far as western Norway. The basin consists of distinct half-graben sub-basins controlled by separate, closely spaced, sub-parallel, arcuate extensional faults (Norton et al. 1987). In Norway, the Devonian successions are very thick (>8km) and the individual basins are bound by widely spaced and larger extensional structures (Norton et al. 1987). In the Orcadian Basin, extensional structures dip to the E / SE whereas in Norway and East Greenland most extensional structures dip to the W / SW (Norton et al. 1987).

The Shetland Devonian is similar to the Middle Devonian sequence of Orkney and Caithness (Mykura and Phemister 1976). Alluvial fan deposits, which formed in shallow lakes and as beach ridges, dominate the Central Group of Shetland. Basaltic and andesitic lavas, rhyolitic ignimbrites, tuffs and concordant felsite intrusions are all commonly interbedded. The Central Group is tightly folded, with localised sinistral shear along steeply dipping faults and low-angle detachment faulting (Séranne 1992a), preceded by emplacement of the 360 \pm 11 Ma Sandsting plutonic complex. West of the MF, sandstones that are locally pebbly were deposited by rivers flowing to the ESE; they are intercalated with two lacustrine fish-bearing beds that are correlated to the Sandwich fish bed horizons of Orkney (Mykura 1991). The sedimentary rocks pass up into a thick sequence of volcanic rocks comprising basalts, andesite, mugearite, ignimbrites and agglomerates. These volcanic rocks have chemical characteristics transitional between those of calc-alkaline and tholeiitic types (Thirlwall 1979). The Devonian of East Shetland comprises alluvial fans that infill a basin situated to the east, braided stream deposits and lacustrine deposits. This assemblage can be regarded as broadly contemporaneous with that of the Eday Flags of the Orcadian province, but faunal differences suggest their development in a separate unconnected basin (Mykura 1991). Post-orogenic granite complexes were intruded at the end of the Devonian. They cut the sedimentary rocks of the Central Group, and represent the youngest rocks exposed on Shetland.

2:2 Offshore Geology

The Shetland Isles rise out of the northern North Sea forming part of the Shetland platform. To the west of the platform lie the West Shetland and Faroe-Shetland Basins, and to the east lies the Viking Graben (Figure 2.6).

2:2:1 Shetland Platform

The areas immediately offshore Shetland are located on the Shetland Platform (Figure 2.6). Caledonian basement rocks and remnants of the Devonian Orcadian Basin succession are exposed on the sea floor of the platform (Hitchie and Ritchen 1987). These rocks are dissected by Permo-Triassic half-grabens that are dominantly bounded by N-S-striking faults (Figure 2.6). The platform is locally covered by thin deposits of Tertiary sedimentary rocks. The platform was uplifted and eroded during the Late Jurassic.

To the east, the platform is separated from the East Shetland Basin (ESB) and Viking Graben (VG) by E-dipping normal faults (Figure 2.7). Therefore, the platform lies in the uplifted footwalls of basin-bounding faults that were active during the Late Jurassic (see section 2:2:2). Further uplift and erosion took place during Early Tertiary time possibly due to magmatic underplating related to the opening of the North Atlantic. As a result, the Shetland Platform is mostly free of Mesozoic sedimentary rocks (Johnson et al. 1993) and represents a high-standing horst.

2:2:1:1 West Fair Isle Basin

The West Fair Isle Basin is an elongate N-S-trending basin that extends from the east of Orkney to Southwest Shetland (Figure 2.6). The western margin of the basin is unfaulted, and is defined by the sea-bed limit of Permo-Triassic red beds drilled in the basin (Evans et al. 1981). The eastern margin of the basin is bounded by the WBF (McGeary 1989). Interpretation of seismic reflection data indicates that Permo-Triassic rocks attain a maximum thickness of 2.5 km and there is no evidence of any thickening of stratigraphic units towards the fault. The basin-bounding WBF is therefore thought to be post-Triassic (McGeary 1989; Johnson et al. 1993).

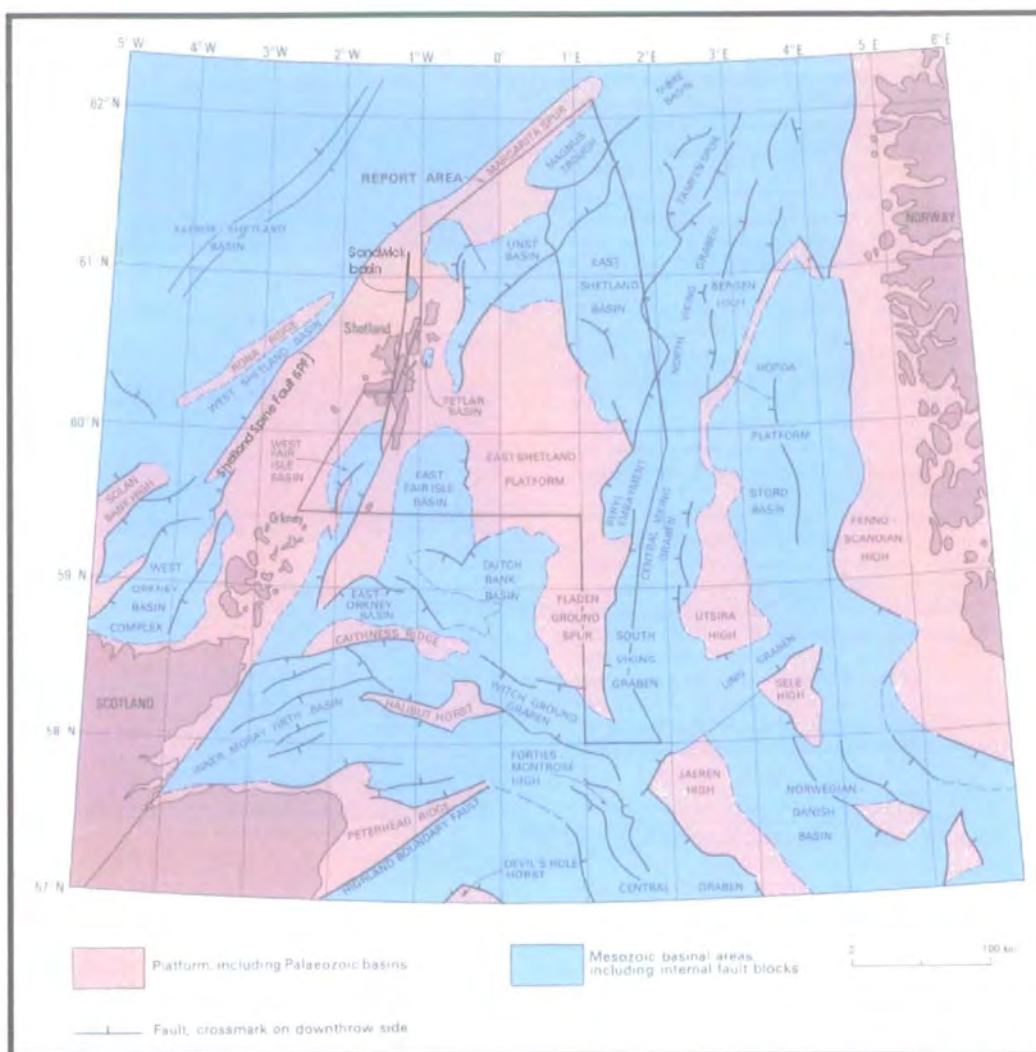


Figure 2.6 Map showing the location of the offshore basins and structures adjacent to the Shetland Isles (adapted from Johnson et al. 1993).

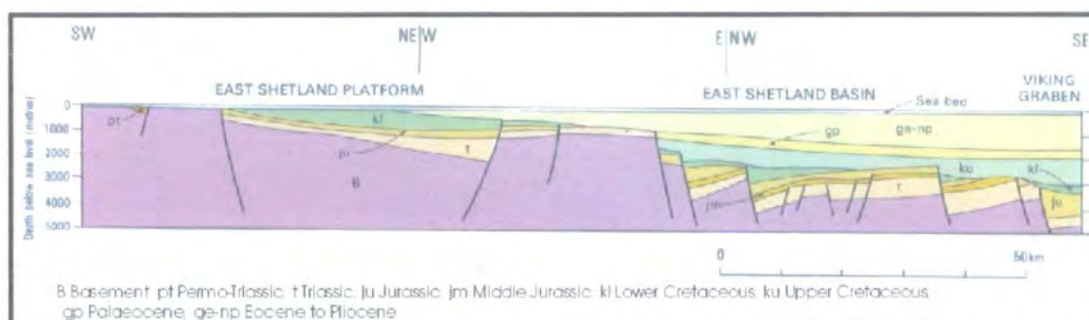


Figure 2.7 Structural cross section through the Shetland Platform, ESB and VG (adapted from Johnson et al. 1993).

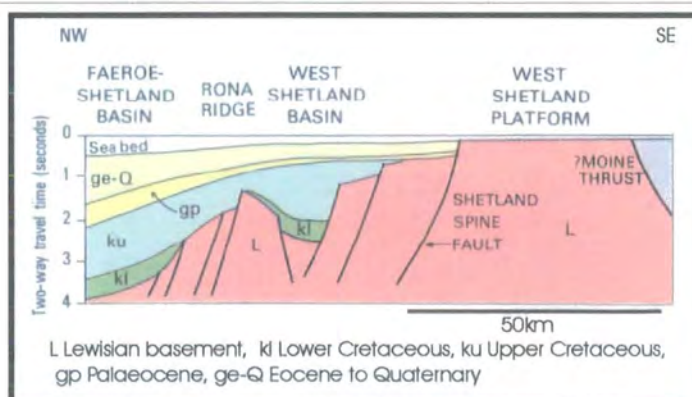


Figure 2.8 Structural cross section through the Shetland Platform, WSB and FSB (adapted from Johnson et al. 1993).

2:2:1:2 East Fair Isle basin

This basin contains a 2km thick sequence of Permo-Triassic strata and is located east of Fair Isle within the East Shetland Platform (Figure 2.6; Andrews et al. 1990). The western margin of the basin is unfaulted and limited by the sea bed outcrop of Permo-Triassic red beds. The eastern margin is bound by a sinuous N-S-striking fault. Within the southern part of the basin, thin Jurassic, Cretaceous and Tertiary sedimentary rocks onlap onto the Permo-Triassic stratigraphy (Andrews et al. 1990).

2:2:1:3 Unst and Fetlar basins

The Unst Basin lies between the Shetland Isles and the East Shetland Basin. It is a three-armed, fault-controlled basin containing up to 3600m of Permo-Triassic red beds, overlain by 800m of Jurassic and 400m of Lower Cretaceous sedimentary rocks (Johns and Andrews 1985). The basin initiated during the Early Permian, with syndepositional movements occurring on the faults throughout the Permo-Triassic (Johnson et al. 1993). Basin inversion occurred from the latest Cretaceous to mid Palaeocene times, and was associated with the opening of the North Atlantic, resulting in major erosion followed by Tertiary deposition (Johns and Andrews 1985). The small Fetlar Basin lies west of the Unst basin and adjacent to the east coast of Shetland (Figure 2.6). The basin is bounded to the east by a normal fault and is probably filled with Permo-Triassic sedimentary rocks (Johnson et al. 1993).

2:2:1:4 Sandwich Basin

The Sandwich Basin lies to the north of Shetland and is bound to the west by the WBF (Figure 2.6). At its eastern margin, sedimentary rocks lie unconformably upon Caledonian basement (McGeary 1989). Hitchen and Ritchie (1987) suggested that the basin fill was 2km thick and probably Devonian in age, although the possibility that it may be Permo-Triassic cannot be ruled out.

2:2:2 Viking Graben (VG) and East Shetland Basin (ESB)

The ESB and VG lie east of the Shetland platform (Figures 2.6, 2.7). Both are predominantly Mesozoic structural features and contain thick accumulations (up to 11km) of Triassic to Quaternary sedimentary rocks. Both basins are asymmetric with the larger faults and thicker syn-rift deposits developed along the western margins (Figure 2.7; Johnson et al. 1993). Rifting initiated in the Triassic (Ziegler 1982). Within the ESB there are variable thicknesses of Triassic stratigraphy. These variations have been attributed to intra-Triassic faulting (Steel and Ryseth 1990). During the Jurassic, the ESB and VG underwent major structural development. Lower-Middle Jurassic sequences thicken towards the axis of the VG (Richards 1990), representing a time of relative tectonic quiescence (Badley et al. 1988). The Upper Jurassic sequences in the ESB and VG thicken towards the basin margins and intra-basinal faults (Figure 2.7), suggesting that the faults were active during this time interval. Thick sequences of post-rift Cretaceous and Tertiary sedimentary rocks unconformably overlie the Upper Jurassic successions (Figure 2.7).

2:2:2:1 West Shetland Basin (WSB)

The WSB is a half-graben structure that initiated in the Early Permian or earlier, and is located to the west of the Shetland Platform (Figure 2.6; Hitchen and Ritchie 1987). It is bound to the east by the W-dipping Shetland Spine fault (SPF) (Figures 2.6, 2.8) that has a 6km normal displacement. In the southern part of the WSB, up to 6km of Permo-Triassic stratigraphy is present adjacent to the SPF. Towards the centre of the basin, a thin Mesozoic and Tertiary sequence unconformably overlies the Permo-Triassic succession.

2:2:2:2 Faroe-Shetland Basin (FSB)

The FSB lies to the west of the Rona Ridge (Figure 2.8) and possesses has a similar structural history to the WSB (Figure 2.6; Hitchen and Ritchie 1987). The basin contains a sequence of volcanic and sedimentary rocks up to 8km in thickness (Figure 2.8). A 3km-thick Upper Cretaceous to Palaeocene sedimentary succession has been recognised that is capped by a major phase of Palaeocene to Early Eocene igneous activity producing acidic and basic, intrusive and extrusive rocks. This phase is associated with the opening of the North Atlantic (Duindam and Van Hoorn 1987).

2:2:3 Regional Synthesis of Offshore Geology

The Shetland Platform exposes Caledonian basement and remnants of the Devonian Orcadian Basin at the sea floor. Rifting in the WSB, FSB, VG and ESB began in the Permo-Triassic. The Shetland Platform contains a number of Permo-Triassic basins that were formed as a result of extension normal to N-S-striking faults. The platform is mostly free of Mesozoic sedimentary rocks. During the Late Jurassic a major structural development affected the VG and ESB, resulting in the deposition of thick syn-rift deposits adjacent to the major faults. Footwall uplift associated with rifting led to Late Jurassic uplift and erosion of the Shetland Platform. Thick sequences of post-rift Cretaceous and Tertiary sedimentary rocks unconformably overlie the Jurassic stratigraphy of the ESB and VG. Brodie and White (1994) suggested that the basins offshore northern Scotland and Shetland were underplated by basaltic melt during the Early Tertiary opening of the North Atlantic. This led to uplift and erosion of the Shetland Platform during the Early Tertiary. The FSB contains a 3km succession of Upper Cretaceous to Palaeocene sedimentary rocks capped by a major phase of Palaeocene to Early Eocene igneous activity associated with the opening of the North Atlantic. The FSB is thought to be the equivalent to the Møre Basin further to the northeast.

2:3 Walls Boundary Fault System

The Shetland Isles are cut by three main faults, the Walls Boundary Fault (WBF), Nestings Fault (NF) and the Melby Fault (MF) (Figures 2.2, 2.5), which together constitute the Walls Boundary Fault System.

2:3:1 Melby Fault (MF)

The MF displays planar, polished, E-dipping surfaces arranged in an en-echelon fashion and with slickensides indicating reverse movement (Flinn 1977). Donovan et al. (1976) and Mykura (1991) interpreted a dextral displacement along the fault based on a matching of the paleogeography of the Devonian basins.

2:3:2 Nestings Fault (NF)

The NF is a steeply dipping strike-slip fault (Figure 2.9) along which a 16km dextral displacement has been suggested based on the observation of units offset on geological maps (Figure 2.5; Flinn 1977). It splays off the WBF and appears to have accommodated some displacement as the WBF changed strike (Flinn 1977, 1992). The fault zone, including its subsidiary faulting and folding is approximately 200-300m wide. In general, cataclasis is only strongly developed up to 30m from the fault (Flinn 1977).

2:3:3 Walls Boundary Fault

The WBF is a near-vertical, N-S-striking, multiply reactivated strike-slip fault. Offshore and to the south of Shetland, it has been suggested that the WBF is a continuation of the Great Glen Fault (GGF) in Scotland (Figure 2.1; Flinn 1961).

2:3:3:1 Onshore

Onshore, Flinn (1977) mapped a gouge-filled fracture containing sub-horizontal slickensides, which he took to represent the latest movement on the WBF. The WBF lies within broad zones of cataclasis, subsidiary faulting and localised folding (Figure 2.9; Flinn 1977) up to 2km in width. Crumple folds, shatter folds and kink bands commonly display a consistent sense of dextral vergence (Flinn 1977). Flinn (1977) also recognised slices of mylonite exposed sporadically along the trace of the WBF (Figure 2.9), and he related the mylonites to an earlier fault, possibly the GGF, which was active before the WBF, along the same line. The lack of matching rocks on either side of the WBF led Flinn (1969) instead to correlate aeromagnetic anomalies occurring to the east and west of the fault, giving rise to a 65km dextral offset. Flinn (1977) concluded that the WBF was a dextral transcurrent fault of Mesozoic age. Pringle (1970) mapped the North Roe area (Figure 2.3) in detail and showed that the Sand Voe Schuppen zone was bounded to the west by a ductile thrust (WKSZ, section 2:1:1:1) thought to be the along-strike equivalent of the Moine Thrust. In northern Shetland, this structure crops out about 1km west of the WBF trace and must intersect the WBF at depth. The Moine Thrust does not pass through the islands or farther to the south on the eastern side of the WBF. This indicates that the WBF must have had a sinistral displacement of 100-200km pre-dating the dextral displacement (65km) (Flinn 1992). Various authors have added their support to a post-Devonian dextral displacement on the WBF (see section 2:3:4)

2:3:3:2 Offshore

Deep seismic profiles across the WBF, both to the north and south of Shetland, show a steeply dipping structure that extends through the entire crust and offsets the Moho (McGeary 1989; McBride 1994b). It has long been thought that the WBF is a continuation of the GGF (Flinn 1961). McBride (1994a) mapped a 35km-wide step-over structure between the southern end of the WBF and the northern end of the GGF based on an interpretation of seismic data.

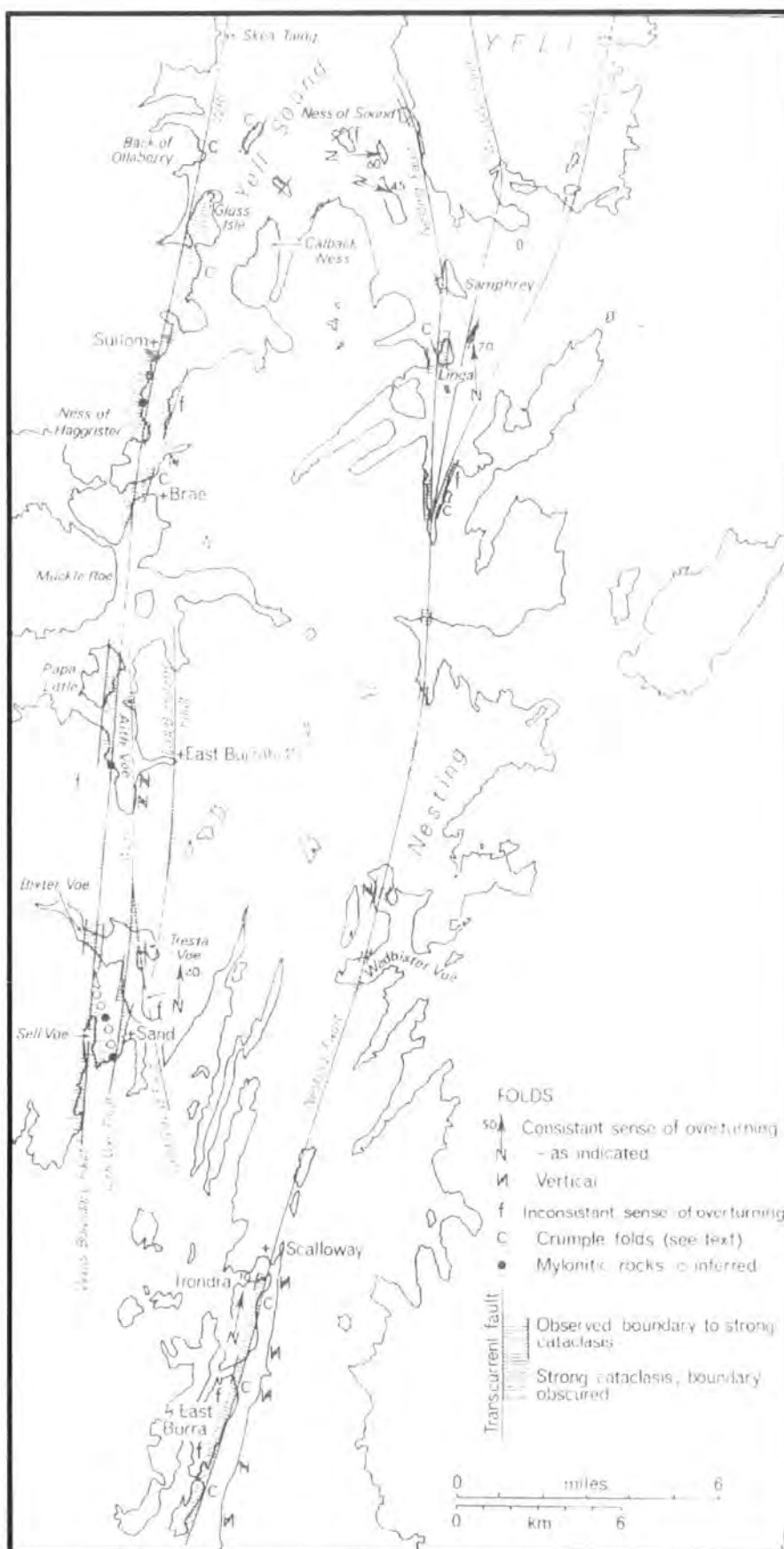


Figure 2.9 Map showing location of faults and associated cataclasis (after from Flinn 1977).

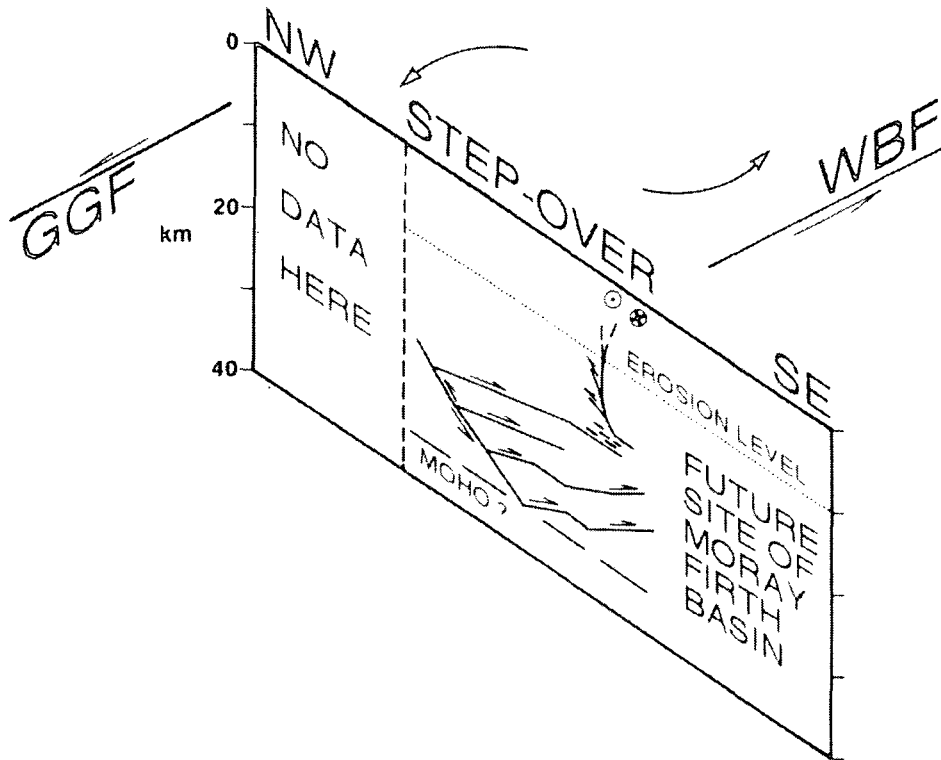


Figure 2.10 Interpretation of a cross section through the step-over structure for Early Devonian time and adjusted to crustal thickness of 30-35km (adapted from McBride 1994a).

A series of low-angle compressional structures are present at depth within the step-over zone (Figure 2.10). McBride (1994a) concluded that the observed direction of stepover implies that a zone of contraction would have formed within the stepover during Caledonian, sinistral, strike-slip movements along the WBF and GGF (Figure 2.10).

The WBF bounds the Sandwich and West Fair Isle sedimentary basins of the Shetland Platform. The fault clearly cuts Devonian and possibly Permo-Triassic sedimentary rocks in the Sandwich Basin (McGeary 1989). Permo-Triassic stratigraphical successions infill the West Fair Isle Basin and show no evidence of thickening towards the WBF; therefore, the WBF is post-Triassic (McGeary 1989). In the Moray Firth, movements on the GGF have affected sedimentary rocks as young as Lower Cretaceous and possibly Tertiary (Underhill 1991).

2:3:4 Regional Synthesis of WBF

Flinn (1977) concluded that the WBF was a dextral transcurrent fault of Mesozoic age with an offset of 65km based on matching aeromagnetic anomalies on either side of the fault (Flinn 1969). Flinn (1992) argued that the WBF must have had a sinistral displacement of the order of 100-200km pre-dating the dextral displacement. This was based on the fact that the WBF must intersect the Moine Thrust at depth in northern Shetland (Pringle 1970), and that this structure does not pass through the islands or farther to the south on the east side of the WBF. Other authors have supported the notion of a post-Devonian dextral displacement on the WBF. Mykura and Phemister (1976) concluded that the Fair Isle Old Red Sandstones and the Walls Sandstones were more similar to each other than to the Western and Eastern Devonian groups. Scapolite veining occurs along the west coast of Fair Isle, east of the WBF, and on the western side of the WBF along the east coast of the Walls Peninsula farther north. Rogers et al. (1989) recorded a post-Devonian offset of 95km based on restoring palaeogeography of the Devonian basins and the distribution of later sedimentary rocks on the Shetland Platform. Donovan et al. (1976) also proposed a dextral displacement of 65-80km on the WBF and 30km along the GGF near Inverness, both post-Devonian. Roddom et al. (1989) inferred a Carboniferous / Permian age for the formation of mylonites along the WBF, based on ^{40}Ar - ^{39}Ar (whole-rock) step heating. A multiphase kinematic history was suggested by Conroy (1996), comprising dextral strike-slip (450Ma), sinistral strike-slip (400-430Ma), dextral strike-slip (Late Devonian / Early Carboniferous and Mesozoic) and finally sinistral strike-slip of uncertain age.

Offshore, deep seismic profiles north and south of Shetland show the steeply-dipping WBF to penetrate the entire crust and offset the Moho (McGeary 1989; McBride 1994b). Flinn (1961) suggested that offshore, the WBF is a continuation of the GGF, although McBride (1994a) mapped a 35km-wide stepover structure between the WBF and GGF based on an interpretation of seismic data (section 2:1:3:3b). Permo-Triassic successions infill the basins bounded by the WBF and show no evidence of thickening towards the fault, suggesting post-Triassic movements (McGeary 1989). Farther south, movements on the GGF have affected sedimentary rocks as young as

Lower Cretaceous and possibly Tertiary (Underhill 1991). Several authors have extrapolated the WBF offshore to join the Møre-Trøndelag Fault Complex (MTFC) (Norton et al. 1987; Ziegler 1987; Grønlie and Roberts 1989; Séranne 1992b; Blystad 1995), suggesting that these faults were linked at some stage during their development and subsequent reactivation. If applied to pre-Devonian times (e.g., Conroy 1996), this correlation would conflict with traditional Caledonian models, since it would require linkage of shears intersecting Baltican and Laurentian basement complexes that were originally on opposite sides of the Iapetus Ocean (Doré et al. 1997a). It therefore seems more reasonable to argue that these structures could have become linked during the Mesozoic, or, at earliest, Devonian time (e.g., Grønlie and Roberts 1989), or that the correlation could be based upon chance alignment of structures.

Chapter 3. Walls Boundary Fault System, Shetland

The Walls Boundary Fault System comprises the Walls Boundary Fault (WBF), the Nesting Fault (NF) and the Melby Fault (MF) (Figure 3.1). The aim of this chapter is to describe the kinematic and structural evolution of the Walls Boundary Fault System. In the following sections, fault rock distribution and field relationships will be described. In this chapter, the major faults of the Walls Boundary Fault System are dealt with in the order of their known magnitude of displacement. Fault rock microstructures and textures are described in Chapter 4.

3:1 The Walls Boundary Fault Zone: locality descriptions and structure

The Walls Boundary Fault Zone (WBFZ) refers to a zone of rocks that are intensely deformed as a result of movement along the WBF. The WBFZ is exposed partially or fully at fourteen coastal sections along the trace of the fault zone (Figure 3.1). These localities are described from north to south in order to illustrate the along-strike variation in the geometry, cross-cutting relationships, spatial distribution and kinematic history exhibited by fault rocks within the WBFZ.

3:1:1 Ollaberry

Ollaberry forms an E-W headland in Yell Sound (locality a; Figure 3.1). Most of the fault zone is exposed on the northern and southern coastal sections of the headland. The northern section is known as Back Sand, a sandy bay surrounded by 50m high cliffs. The southern, Moo Wick section is composed of a rocky shoreline with mainly inlets and low cliffs (5-20m high; Plate 3.1). To the west of the WBF are schists (Figure 3.2) belonging to the Dalradian Queyfirth Group (section 2:1:1:4). East of the fault is a red, pegmatite-rich granite of the Devonian Graven complex (section 2:1:5:1a). A recumbent fold marks the beginning of the Moo Wick section described here (Plate 3.1).

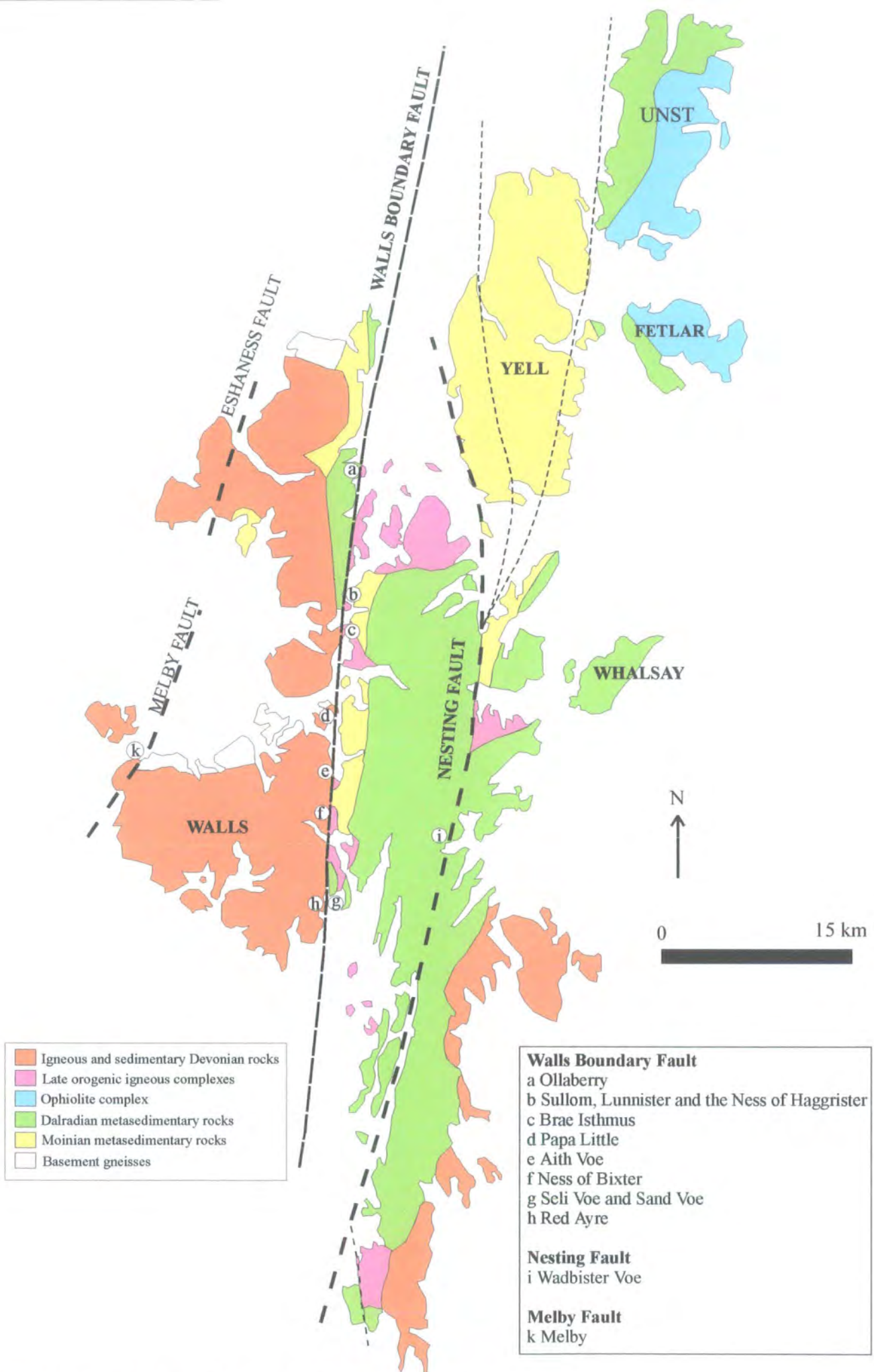


Figure 3.1 Geological map of Walls Boundary Fault System localities.
(NB Some localities along the WBF display more than one section through the fault zone.)

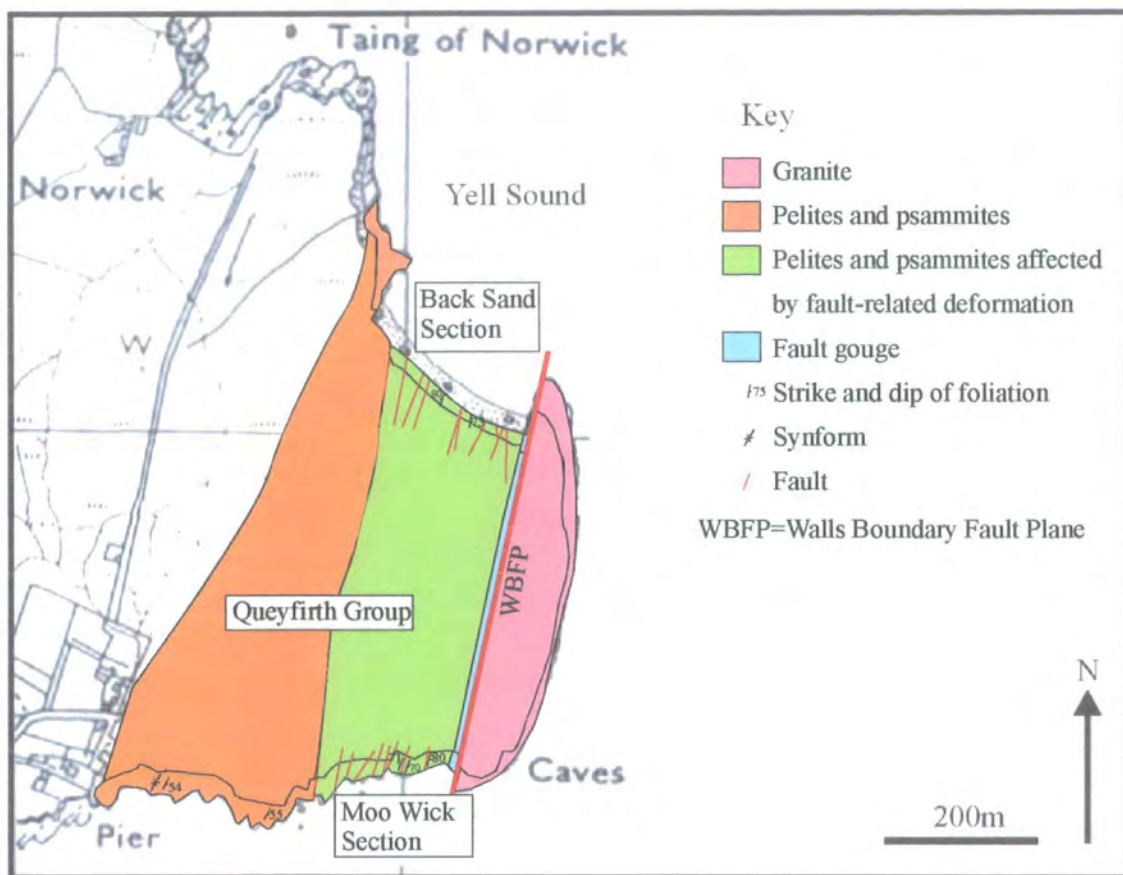


Figure 3.2 Geological map of Ollaberry.

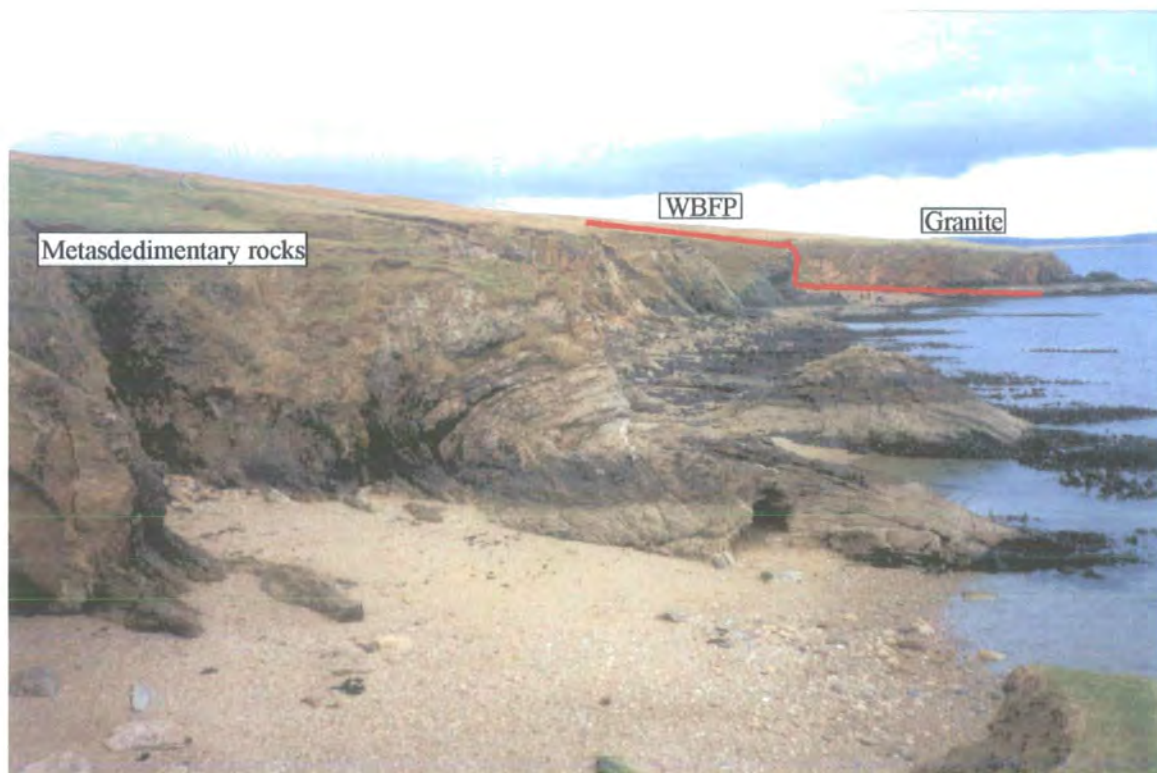


Plate 3.1 Photograph looking east along the Moo Wick section, Ollaberry. In the foreground are grey schistose rock and in the distance is the red / orange granite, thus marking the location of the WBFP.

The fault zone at this locality is approximately 300m wide with the majority of fault rocks having recognisable protoliths. Exotic slices of limestone and quartzite occur in places within the fault zone which have no obvious equivalents in the immediately adjacent country rocks.

Conroy (1996) described Ollaberry as the 'type' locality for the WBFZ and produced 1:2,000 scale structural maps of the fault zone along the Moo Wick and Back Sand sections in order to elucidate the structure and kinematic history of the WBF.

3:1:1:1 Protolith lithologies

3:1:1:1a Queyfirth Group

To the west of the WBF at Ollaberry, rocks belonging to the Queyfirth Group are exposed (Figure 3.2; Plate 3.1). Due to the sheared and fault-bounded nature of these rocks, a true stratigraphic succession through the group is not known at this locality. At Ollaberry the rocks comprise interbanded semipelites and impure flaggy psammities. Compositional layers are generally 15-70cm in thickness, and probably represent the original sedimentary horizons. The psammities are finely laminated, comprising 70% quartz, 15% orthoclase; 10% plagioclase, 5% muscovite with minor amounts of calcite. The pelites are composed predominantly of quartz and muscovite, along with chlorite, magnetite and minor amounts of plagioclase. Garnet porphyroblasts containing inclusion trails of quartz and magnetite are locally well developed, suggesting that the rocks have been metamorphosed to at least garnet-grade. The margins and tails of the garnet porphyroblasts have been strongly retrogressed to chlorite, suggesting a lower greenschist facies overprint.

3:1:1:1b Graven plutonic rocks

To the east of the WBF at Ollaberry, pegmatitic granite belonging to the Late Devonian Graven plutonic complex (section 2:1:5:1 a) is exposed (Figure 3.2; Plate 3.1). The granite is red in colour and coarse to medium grained with phenocrysts up to 1cm in length. It is composed of approximately 50% orthoclase, 25% quartz, 15% plagioclase and 10% chlorite, with some green biotite. The rock is equigranular with

randomly orientated phenocrysts forming an interlocking mosaic. No magmatic or solid-state fabric was observed in the field. The granite weathers locally to a green colour and is strongly retrogressed where feldspars have a speckled appearance and have broken down to aggregates of sericite. Xenoliths of basic material occur locally and appear to be aligned N-S. Randomly orientated, late-stage, pegmatite veins cross-cut the main granite intrusion.

3:1:1:2 Fault rocks

In this section, fault rocks are described in the order of their relative age (oldest to youngest; see section 3:1:2:3)

3:1:1:2a Cataclasites east of the WBF

Cataclastic series rocks east of the WBF at Ollaberry are derived entirely from granite. The cataclasites are usually green in colour, comprising finely comminuted clasts of granite, orthoclase, plagioclase, quartz, chlorite, epidote and white mica set within a fine-grained cataclastic matrix. Randomly orientated clasts are angular to sub-angular, ranging from 5mm to less than 0.5mm in size. The cataclasites possess no internal fabric and appear to be isotropic in the field on all scales of observation. Epidote and quartz veins transect the cataclasites and occur locally as clasts within the cataclasite matrix. The proportion of matrix varies from approximately 10% to 90%, so that the rocks can be subdivided into protocataclasites, cataclasites and ultracataclasites based upon the proportion of matrix present. Ultracataclasites are, in places, red in colour due to the effects of iron mineralisation.

3:1:1:2b Cataclastic rocks west of the WBF.

Cataclasite series rocks west of the WBF at Ollaberry are mainly derived from rocks belonging to the Queyfirih Group (section 2:1:1:4). Cataclasites and breccias are commonly derived from quartzite, psammite and, in a few cases, pelitic units. The cataclasites are grey in colour, containing angular-subangular clasts of comminuted host rock, quartz, muscovite, chlorite and calcite set in a fine cataclastic matrix.

Calcite mineralisation within the matrix is common, occurring mostly in veins but also as cement. The cataclasites contain no foliation or apparent banding.

3:1:1:2c Fault gouges

There are two types of gouge present at Ollaberry; a hard red gouge and a soft blue gouge.

The red gouge is derived from the granite. It is very fine grained and appears to be indurated (hardened by cementation or the effects of pressure and temperature (recrystallisation)); iron staining is ubiquitous. In thin-section and in the field, it appears to be a clay-rich isotropic paste with a centimetre-scale colour banding defined by variations in the clast-to-matrix ratio. The matrix has been pervasively cemented by hematite. It contains sub-rounded to sub-angular clasts (5mm to <0.1mm) of host rock, cataclasite, quartz and analcite. Feldspar clasts within the gouge have been partially pseudomorphed by calcite.

The blue gouge is derived from the pelites and psammities of the Queyfirth Group. It is incohesive and clay-like in appearance. It is very fine-grained with no clasts visible in the field. The gouge has a strong vertical foliation defined by aligned clay particles with a sub-horizontal lineation defined by the long axes of aligned clay minerals. XRD analyses (carried out by Sarah Sherlock, Open University, UK) show the gouge to be composed of quartz, albite, smectite, clinocllore, kaolinite, illite and orthoclase.

3:1:1:3 Fault rock distribution and age relationships

The distribution of fault rocks within the fault core, east and west of the WBF plane (WBFP) at Ollaberry is illustrated in Figure 3.3. The earliest fault-related deformation is found to the west of the WBFP. These structures are overprinted by cataclastic deformation, which generally increases towards the fault core. Fault gouge within the fault core cross-cuts all other fault rocks. In this section the earliest fault rocks are described first. These are usually found in the wall rocks on either side of the WBF core.

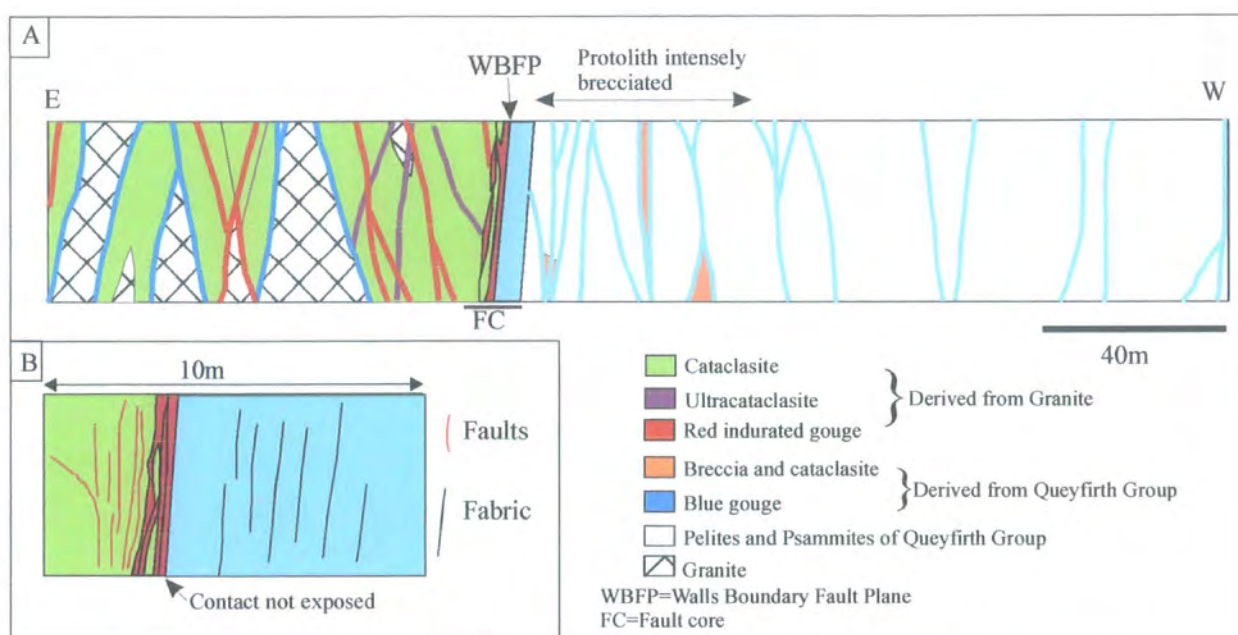


Figure 3.3 Schematic diagram to illustrate fault rock distribution (A) within the WBFP and, (B) within the fault core at Ollaberry. (A) and (B) are not to scale vertically.

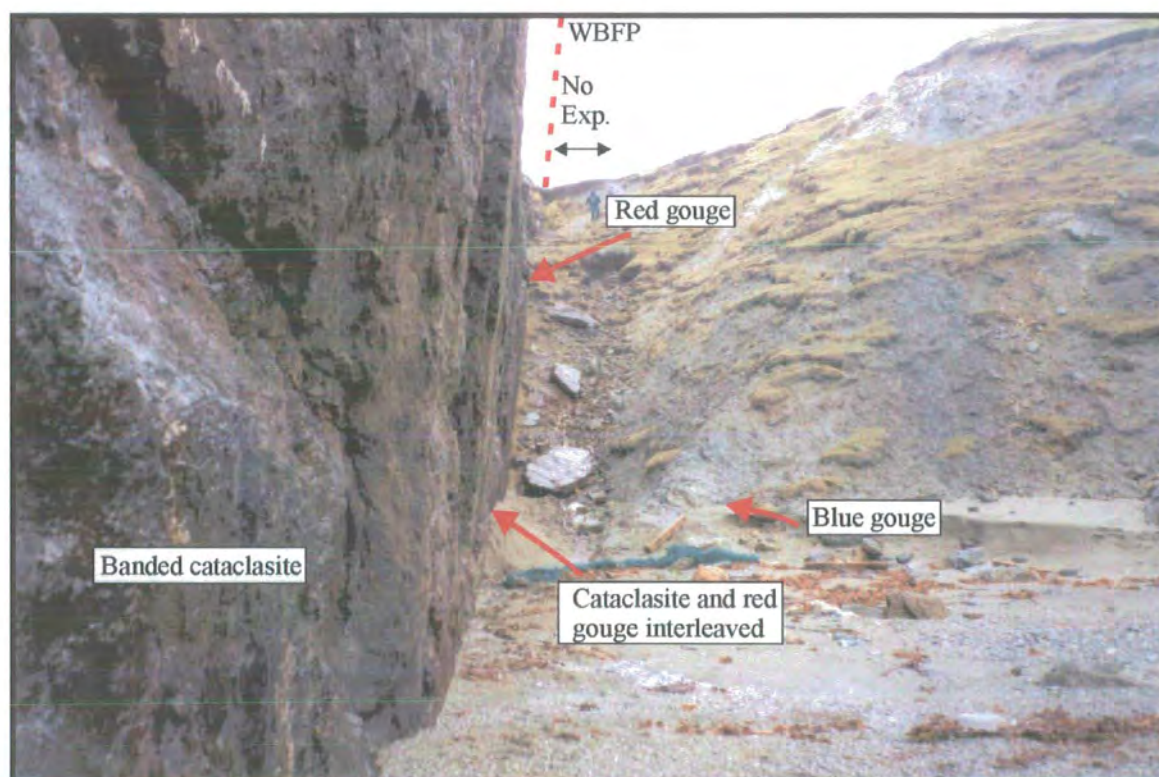


Plate 3.2 Photograph looking south along Walls Boundary Fault Plane (WBFP), Back Sand section, Ollaberry.

3:1:1:3a West of the WBF core

Breccias and (rare) cataclasites (section 3:1:1:2b) are exposed west of the WBF core (Figure 3.3). Both overprint the regional fabrics and dextral S-C' fabrics present within retrograde sheared pelites belonging to the Queyfirth Group. They form slivers bounded by later gouge-filled faults. Blue gouges are commonly present along subsidiary faults over a distance of 160m west of the fault plane (Figure 3.3; section 3:1:1:5). The blue gouges appear to be the youngest fault rocks west of the WBFP.

3:1:1:3b East of WBF core

A 100m zone of cataclasite series rocks is exposed east of the fault core (Figures 3.2, 3.3). The cataclastic deformation is irregularly developed, but generally increases towards the fault core. Cataclasites are isotropic and generally show no fabric in the field, although within 5m of the WBFP, an apparent banding defined by aligned clasts, grain size variation and iron-rich bands can be seen (Plate 3.2). Broad anastomosing zones of cataclasis are cut by N-S-striking ultracataclasite seams and later gouge-filled faults. Slivers of intensely fractured protolith are common and are usually bounded by gouge-filled faults. Blue / green and red fault gouges transect all the cataclastic fabrics (Figure 3.3). The relative age relationship between the red and blue/ green fault gouge is unclear.

3:1:1:3c WBF Core

The fault core is located in the central part of the WBFZ. It corresponds to the region of most intense fault-related deformation. The most obvious movement plane of the WBFZ is exposed within the fault core at the Back Sand section, Ollaberry (Plate 3.2). The fault plane (WBFP) is orientated 012/84E and defines a 40m-high vertical rock face. Here the fault core is approximately 10m wide. It is defined by a continuous sequence of fault rocks that extend from the wall rocks on either side and across the WBFP (the most obvious movement plane within the WBFZ). Green cataclasites (3:1:1:2a) crop out east of the WBFP and are cut by an indurated red fault gouge (section 3:1:1:2c; Figure 3.3; Plate 3.2). The red gouge and cataclasite are interleaved over an interval 1m in width. Cataclasites adjacent to the red gouge display a fault-parallel banding defined by grain-size variation with iron staining following the

banding. Clasts of cataclasite and vein material (calcite and analcite) commonly occur as clasts within the red gouge, suggesting that the gouge is younger than the cataclasite. The contact between the cataclasite and the red gouge is sharp and irregular. The fault plane forming the cliff that appears to separate the red gouge from the blue gouge to the west contains large-scale, horizontal, groove marks and slickenside lineations, which plunge shallowly to the S. However, the actual contact between the red and blue gouges is not exposed in cross-section. The blue gouge (section 3:1:1:2c) has a vertical N-S-striking fabric associated with a sub-horizontal lineation, both defined by aligned clay particles. The blue gouge zone cross-cuts retrograde sheared pelites west of the fault core.

The WBF separates fault rocks derived from granite belonging to the Devonian Graven Complex to the east from those derived from pelites and psammites belonging to the Queyfirth Group to the west. The WBF is the main structural boundary within the WBFZ and is associated with the fault core (area of most intense fault-related deformation). It is likely to correspond to the surface along which the last regionally significant movement occurred.

3:1:1:4 Protolith structure outside the WBFZ

As first recognised by Pringle (1970), west of the WBFZ, the garnetiferous psammites and pelites of the Queyfirth Group are regionally folded by two sets of structures (e.g., Plate 3.1). D1 structures are metre-scale upright folds that plunge shallowly to the SSE (Figure 3.4A). D1 axial planes strike NNW-SSE and dip steeply to the W. D2 structures refold D1 structures, and are open-to-tight, upright folds (metre-scale), plunging both to the N and S (Figure 3.4B). D2 axial planes strike NNE-SSW and dip steeply to the E. Upright D1 and D2 folds show no consistent vergence direction at Ollaberry. Associated with D2 folds is an axial planar fabric that contains a sub-horizontal, mineral stretching lineation which is parallel to the D2 fold axes (Figure 3.4C).

The granite exposed to the east of the WBF was undeformed prior to faulting.

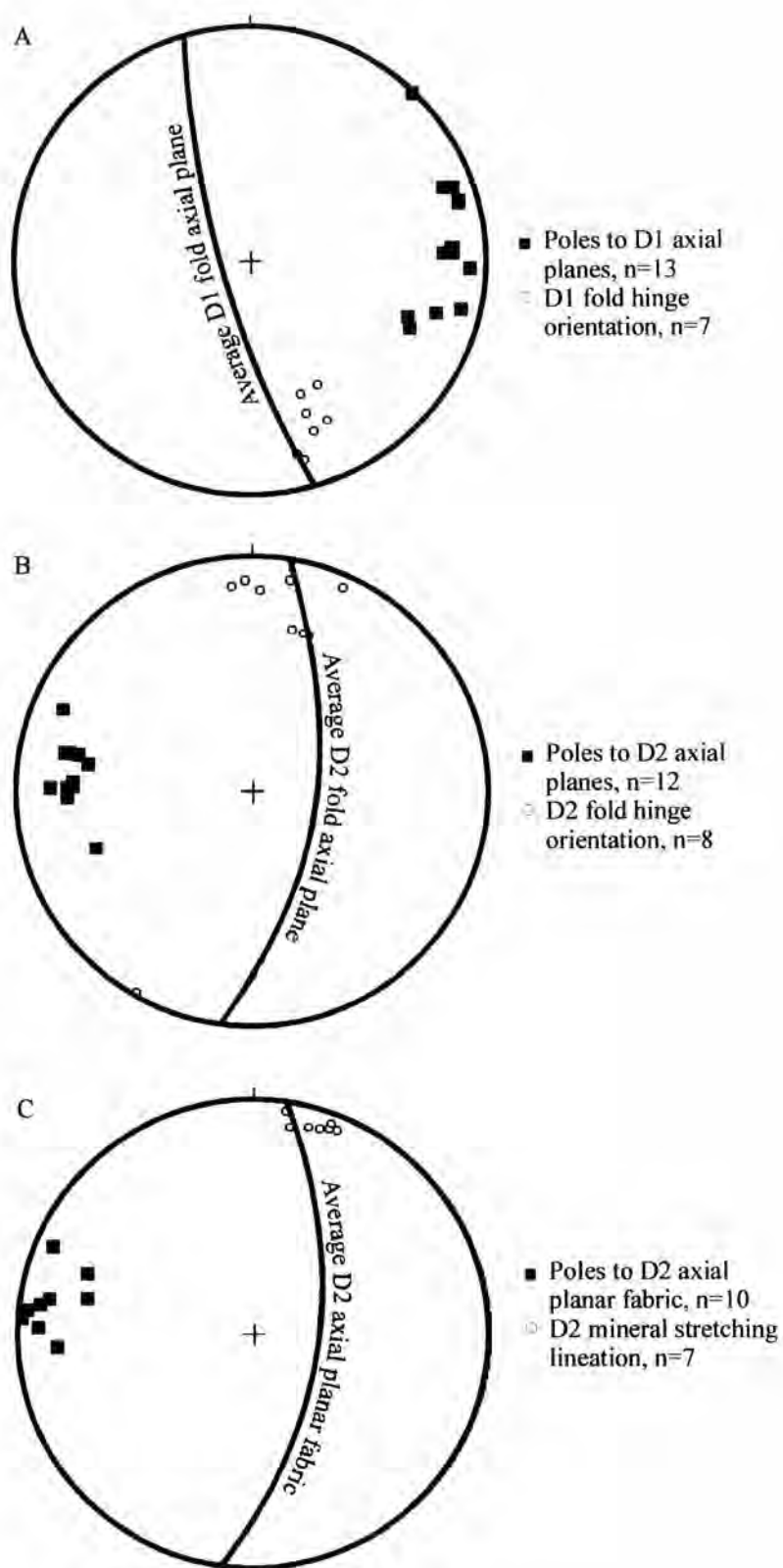


Figure 3.4 Stereographic projections of structural data from the Queyfirth Group (outside WBFZ), Ollaberry. (A) D1 fold data. (B) D2 fold data. (C) D2 axial planar fabric and mineral stretching lineations.

3:1:1: 5 Fault zone structure west of the WBFP

The fault zone at Ollaberry is at least 300m wide. To the east of the WBFP, 100m of cataclastic series rocks are preserved interleaved with granite (Figures 3.2, 3.3). West of the WBFP, intense deformation associated with the WBF extends for 150-160m into the Queyfirth Group rocks exposed along both the Back Sand and the Moo Wick sections (Figure 3.2). The eastern margin of both sections is bounded by the WBFP, and the western margin is marked by reverse faults containing 1m and 30cm of blue fault gouge within the Moo Wick and Back Sand sections, respectively (Figures 3.5, 3.6).

West of the WBFP, three structural domains have been recognised (Figures 3.5, 3.6) that are each characterised by differences in structure that are thought to reflect strain partitioning within the WBFZ.

3:1:1:5a Domain A (160-130m west of the WBFP)

The first gouge fault appears 135m west of the WBFP along the Back Sand section (Figures 3.6). The fault gouge is blue, incohesive and foliated, defined by aligned clay particles. The fault exhibits a reverse shear sense indicated by fold vergence and dip-slip shear bands within the gouge. Minor fractures parallel to the reverse fault contain sub-horizontal, sinistral, slickenside fibres defined by the stepping of quartz fibres. Subsidiary faults containing centimetre-thick blue gouge increase in frequency towards the east within Domain A (Figures 3.5, 3.6). Faults strike N-S to NE-SW and are mostly steeply-dipping to the E and WNW (Figure 3.7B). Slickenside lineations within exposed fault planes range from sub-horizontal to vertical (Figure 3.7B). Gouge-filled faults with sub-horizontal slickenside lineations usually display dextral shear senses defined by shear bands and fold vergence (Figures 3.5, 3.6). Dip-slip faults are usually reverse, although normal faults occur locally. The majority of faults are contractional within Domain A. Faults tend to localise along pelitic horizons and along the steep limbs of regional folds. In cross-section, the faults display anastomosing geometries and link together to form larger structures. This braided geometry occurs at all scales throughout the entire fault zone.

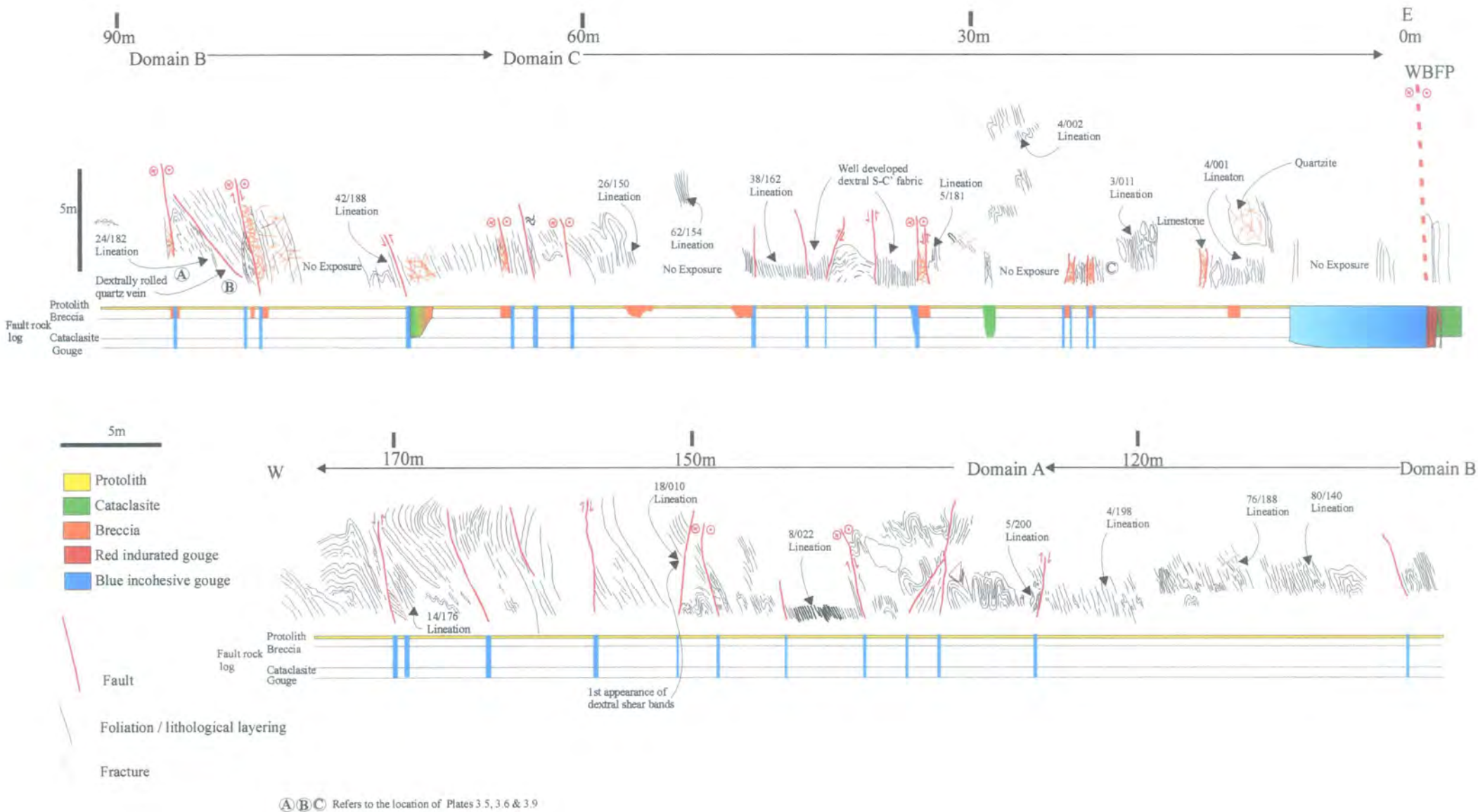


Figure 3.5 Cross section through the WBFPZ, west of the WBFP along the Moo Wick coastal section to illustrate the structure and fault rock distribution.

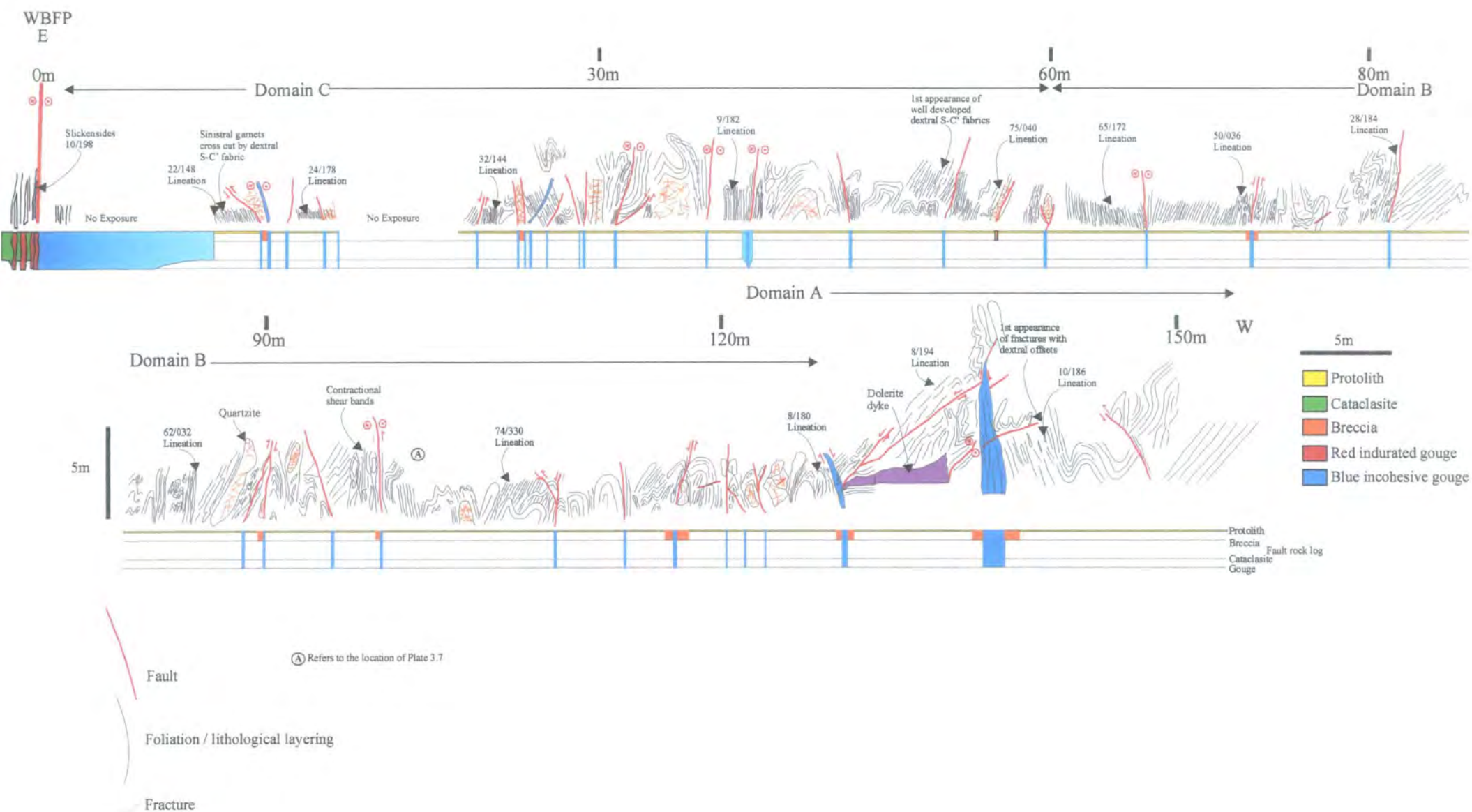


Figure 3.6 Cross section through the WBFZ, west of the WBFP along the Back Sand coastal section to illustrate the structure and fault rock distribution.

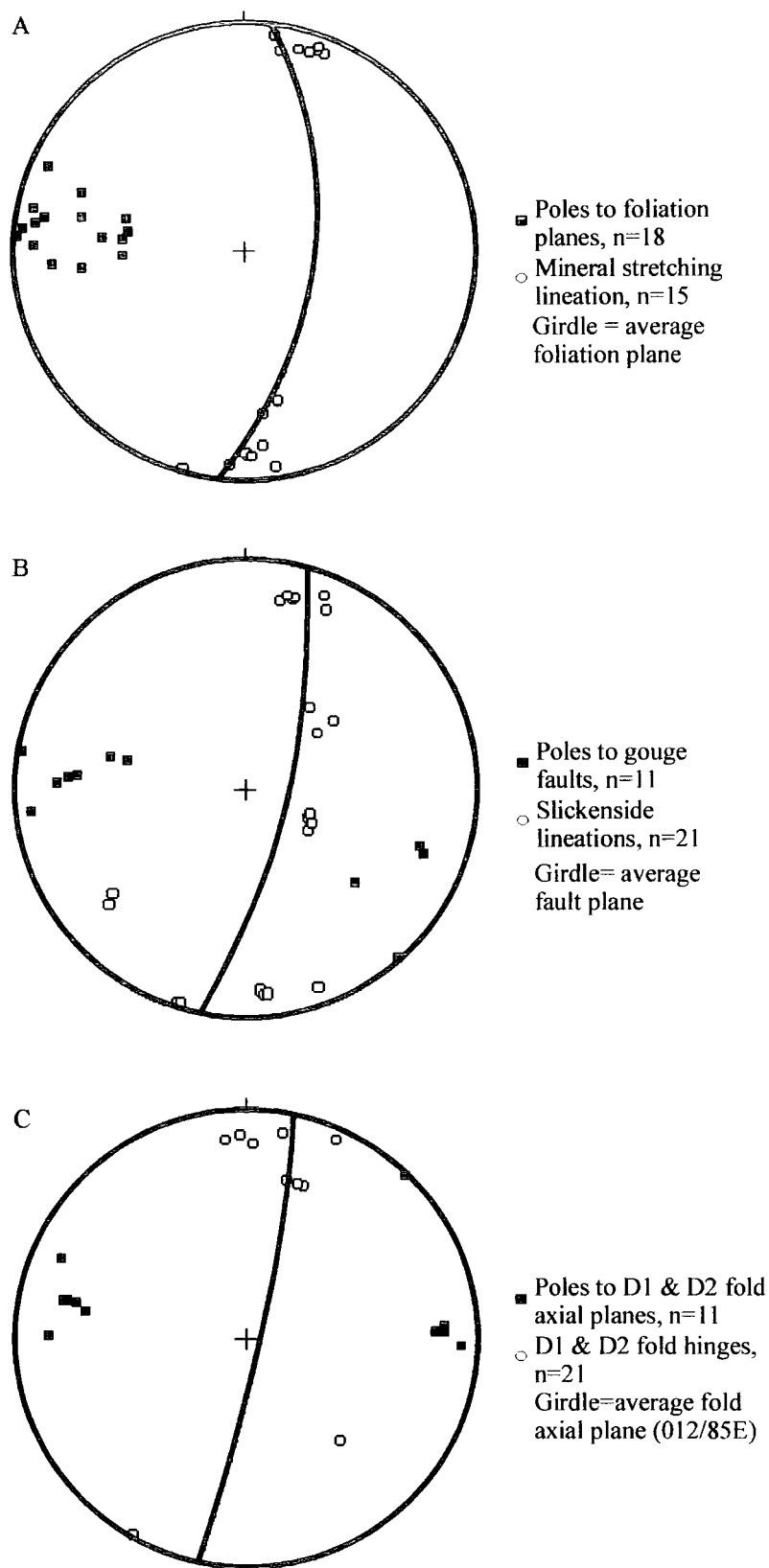


Figure 3.7 Stereographic projections of structural data collected from Domain A. (A) Foliation and mineral stretching lineation. (B) Gouge faults and slickenside lineations. (C) D1 & D2 fold data.

The fabric that is axial planar to D1 and D2 folds (Plate 3.3) is more penetrative within Domain A than outside the WBFZ and is associated with sub-horizontal lineations defined by elongate quartz and mica grains (Figure 3.7A). D1 and D2 structures within the WBFZ are difficult to distinguish from each other due to the sheared and faulted nature of the rocks. D1 and D2 folds strike N-S to NE-SW and plunge mainly to the N (Figure 3.7C). Foliation planes within Domain A strike N-S and dip steeply to the E (Figure 3.7A). In thin-sections viewed parallel to the mineral stretching lineation, garnets display σ -type geometries defined by asymmetric chlorite overgrowths that are consistent with sinistral shear. The garnets contain inclusion trails of a pre-D2 fabric. At distances of 140m west of the WBFP, D2 folds have interlimb angles $<20^\circ$ and are commonly isoclinal with no overall vergence direction. Axial planar faults and fractures are common along folds that have tightened up from open to tight outside the WBFZ to become almost isoclinal.

3:1:1:5b Domain B (130-60m west of the WBFP)

In Domain B, complex switches in the orientation of the mineral stretching lineation occur close to the domain boundaries (Figures 3.5, 3.6). The penetrative foliation within Domain B strikes N-S, dipping steeply either to the E or to the W (Figure 3.8A). Mineral stretching lineations defined by aligned quartz and mica grains form two main clusters (Figure 3.8A). On surfaces normal to fault planes and viewed parallel to sub-horizontal lineations, shear bands are consistent with dextral shear. Surfaces normal to fault planes and viewed parallel to dip-slip lineations contain shear bands indicating contractional movements. Both contractional and dextral shear bands are developed within pelitic protoliths. Iron oxide occurs in foliation-parallel seams.

D2 and D1 regional fold axial planes are sub-vertical striking N-S in Domain B. Fold plunges are highly variable and appear to lie on a girdle that strikes N-S and dips steeply to the E (Figure 3.8C), sub-parallel to the mean foliation (Figure 3.8A). Highly curvilinear D3 folds re-fold D2 folds and associated mineral lineations (Plate 3.4). The recumbent fold at the start of the Moo Wick section (Plate 3.1) is an example of a D3 fold structure. The hinges of the D3 folds plunge either to the N or to the S, lying along a N-S-trending steeply-dipping girdle that corresponds to the



Plate 3.3 Photograph looking south to show axial planar fabric associated with D2 folds (Domain A).

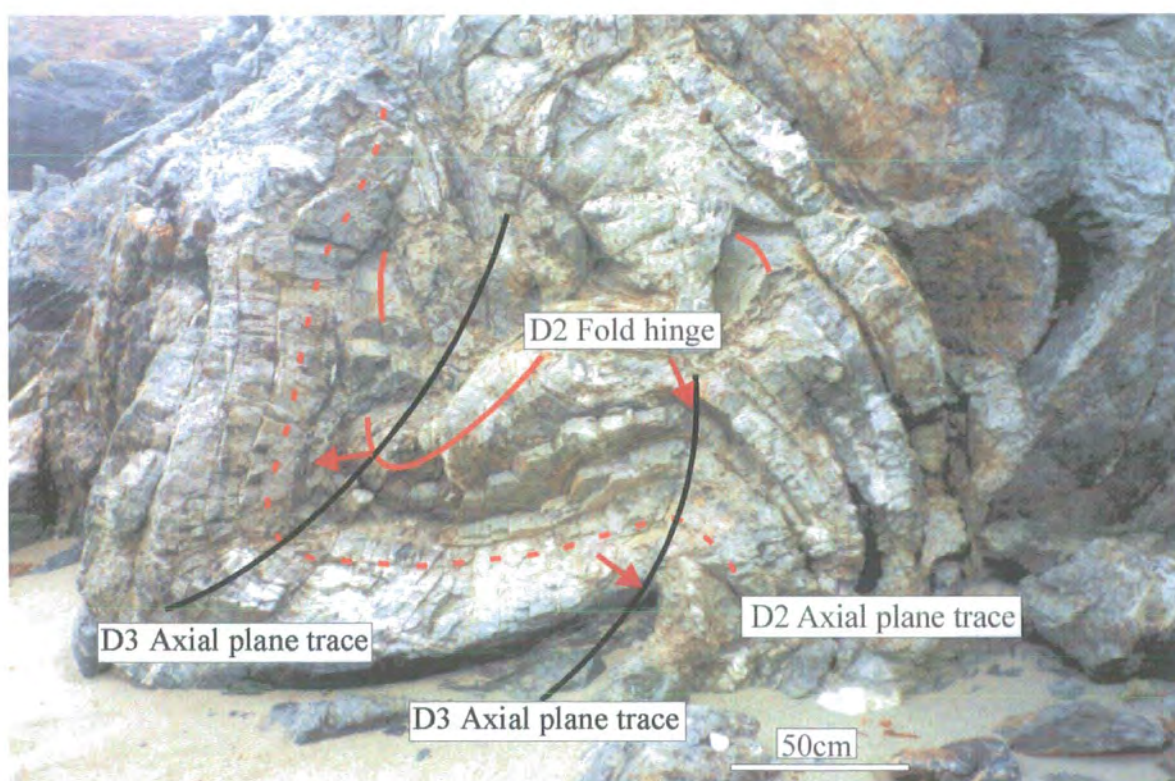


Plate 3.4 Photograph looking east to show geometry of D3 folds (Domain B). D2 structures are folded by highly curvilinear D3 folds with N-S-trending sub-vertical axial planes. Arrows illustrate D3 fold plunge variation.

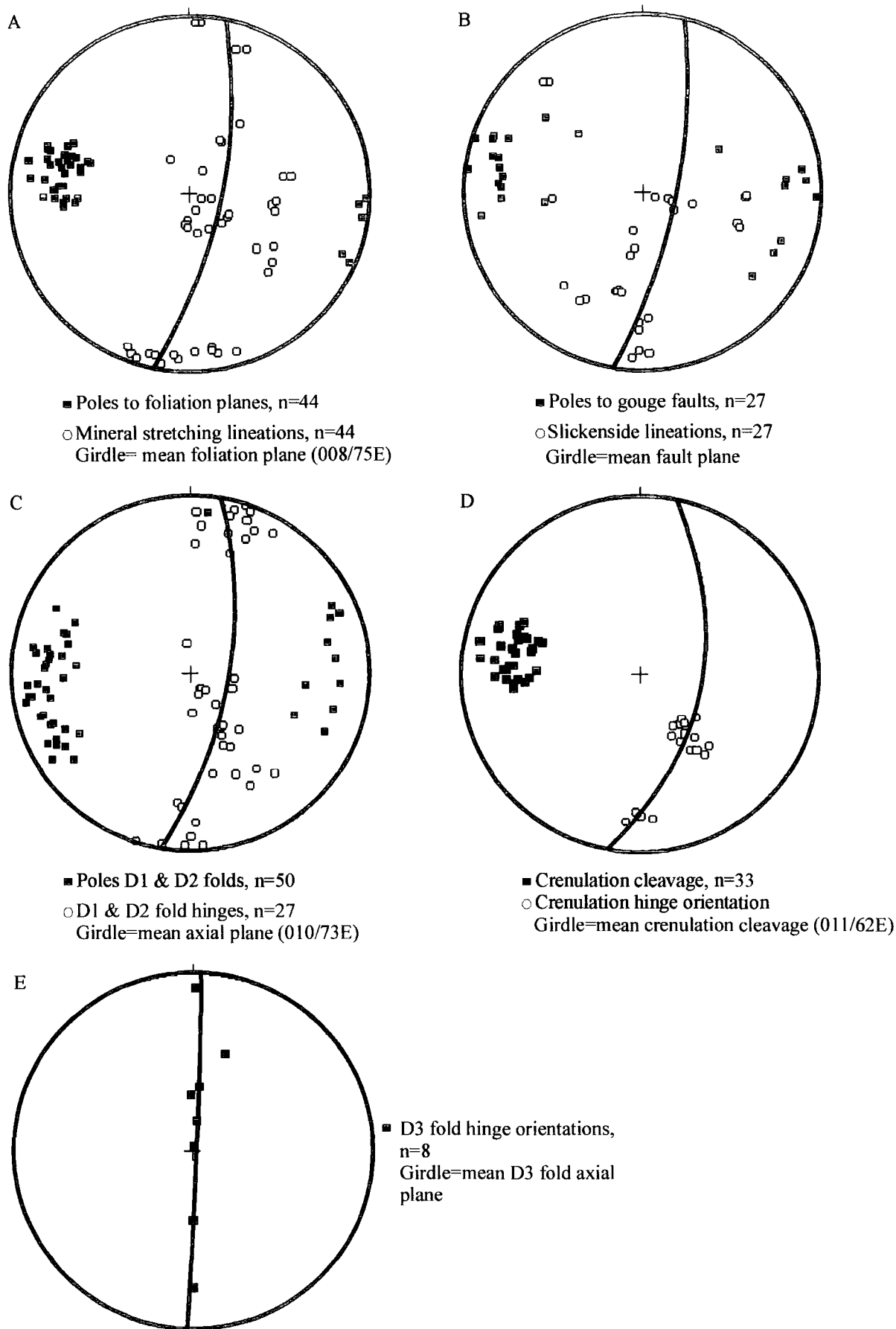


Figure 3.8 Stereographic projections of structural data collected from Domain B. (A) Foliation and mineral stretching lineation. (B) Gouge faults and slickenside lineations. (C) D1 & D2 fold data. (D) Crenulation cleavage and hinge orientation of dextral verging crenulations. (E) Hinge orientations of D3 folds.

mean fold axial plane (Figure 3.8E). Steeply-plunging D3 folds consistently exhibit 'S' vergence patterns. It is possible that these folds are related to an early phase of ductile shear along the fault, as they are not recognised within the Queyfirth Group outside the fault zone. The pattern of D3 fold hinge curvature and consistent sense of vergence of the steeply-plunging structures seem to be consistent with a sinistral sense of movement.

Dextral-verging kink bands and crenulations associated with a weak crenulation cleavage are common within iron-stained pelitic horizons of Domain B (Plate 3.5), and commonly exhibit axial-planar fractures. Crenulations along both coastal sections show a consistent dextral sense of vergence and are best developed within Domain B. The crenulation hinge orientations vary in plunge from shallow to steep, towards the S-SE (Figure 3.8D), and lie along a girdle (011/62E) that represents the average crenulation cleavage plane which is orientated sub-parallel to the WBFP (Figure 3.8D).

Late-stage, fault-related folds first appear within Domain B adjacent to units with crenulations and kink bands. The folds vary in style from sharply kinked to rounded closures with straight limbs. The folds occur on a centimetre- to metre-scale and mainly show a dextral sense of vergence. Dextral-verging folds plunge mainly steeply to the S with axial planes striking N-S (Figure 3.9A). Folds with a sinistral sense of vergence occur less frequently and appear to be conjugate to the dextral-verging folds. The sinistral-verging folds plunge steeply to the N with axial planes trending NW-SE (Figure 3.9B). Dextral verging folds refold D2 folds and their axial planar fabric. No examples were observed to refold D3 fold structures. Dextral- and sinistral-verging folds mainly occur adjacent to pelitic rocks with sub-horizontal lineations, dextral shear bands and dextral strike-slip faults. It is inferred that conjugate kink folds and shear bands accommodated N-S-directed shortening and shear across anisotropic metamorphic rocks (pelites and psammities). A 'stick-slip' model (Figure 3.10; cf. Williams 1987) is suggested, whereby kink folds accommodated layer-parallel shortening, whilst shear bands formed as a result of foliation-parallel shear. Differential slip rates along foliation planes cause local variations in shear strain to develop. Adjacent to areas of relatively slow strain rate (e.g. 'stick'), zones of relative compression (kink folds) and tension (shear bands) are

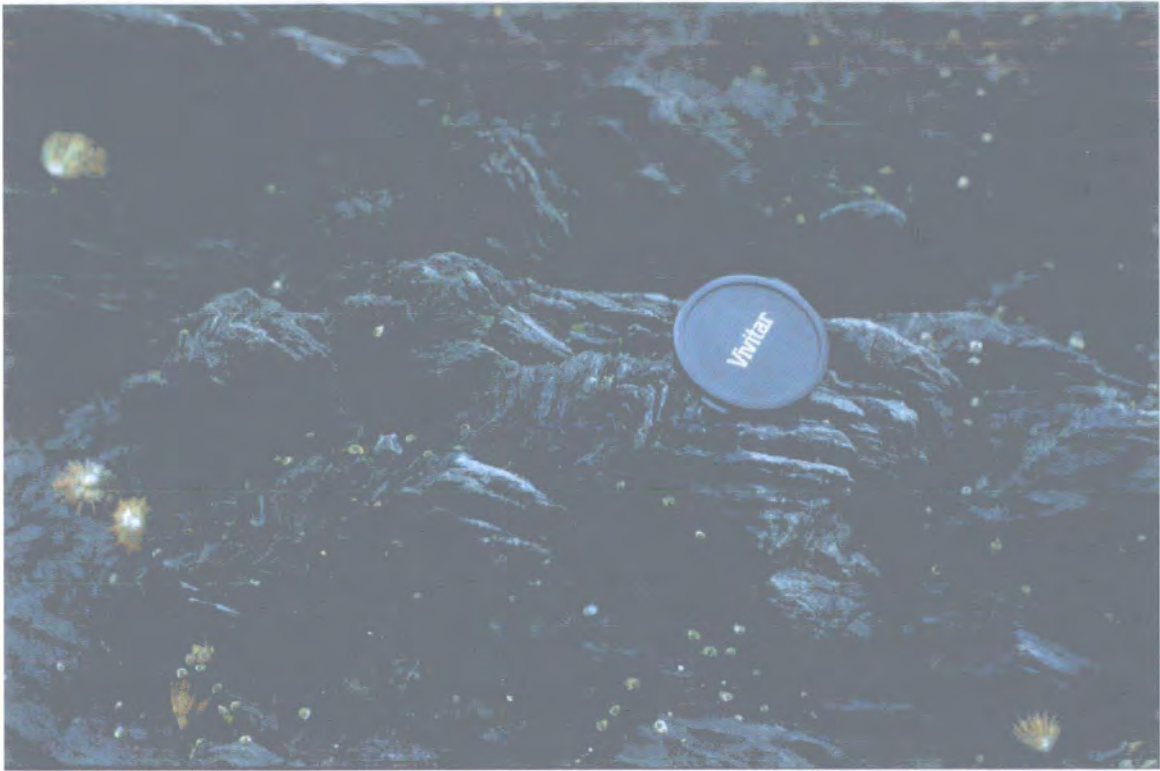


Plate 3.5 Photograph of steeply-dipping kink bands showing a dextral sense of vergence, Domain B, Moo Wick section.



Plate 3.6 Plan view photograph of dextrally folded quartz vein within a pelitic high strain zone, Domain B, Moo Wick section.

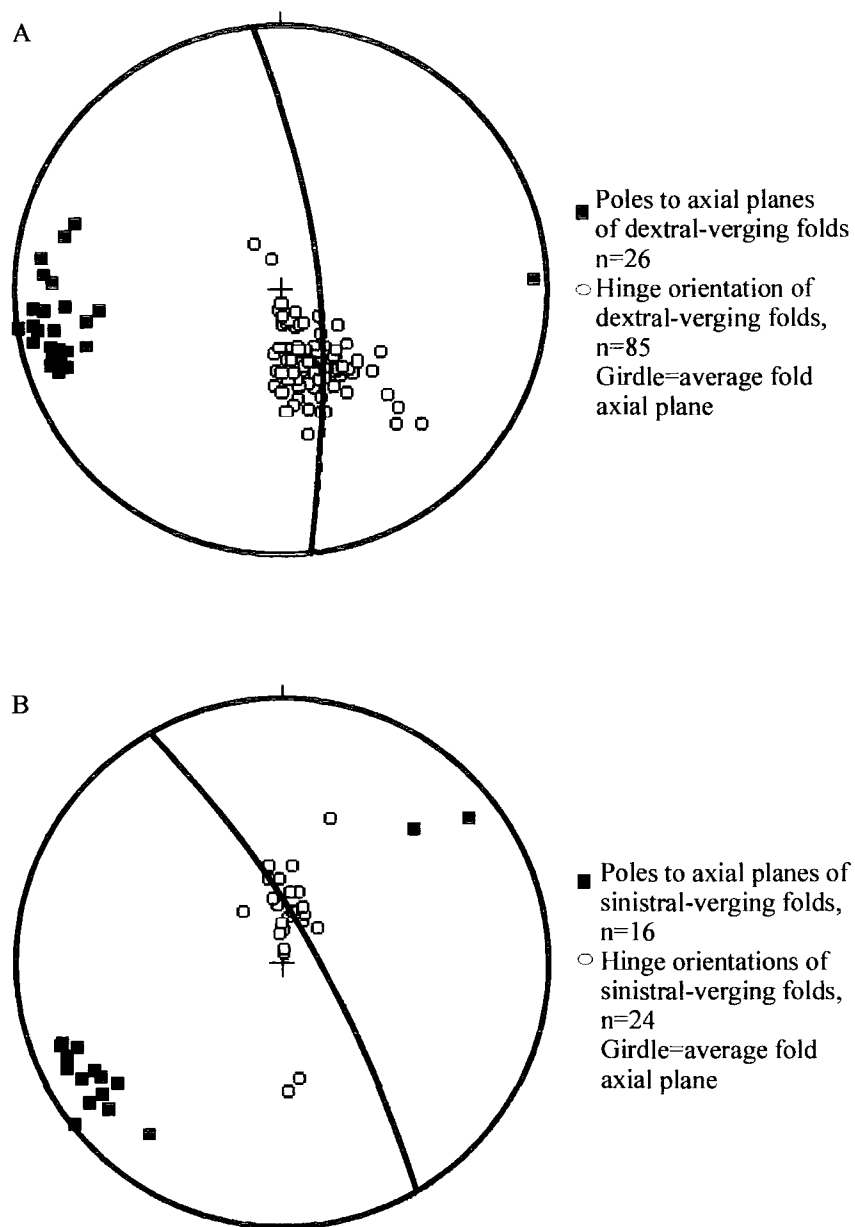


Figure 3.9 Stereographic projections to show (A) fold axial planes and hinge orientations of dextral-verging folds, and (B) fold axial planes and hinge orientations of sinistral-verging folds (Domain B).

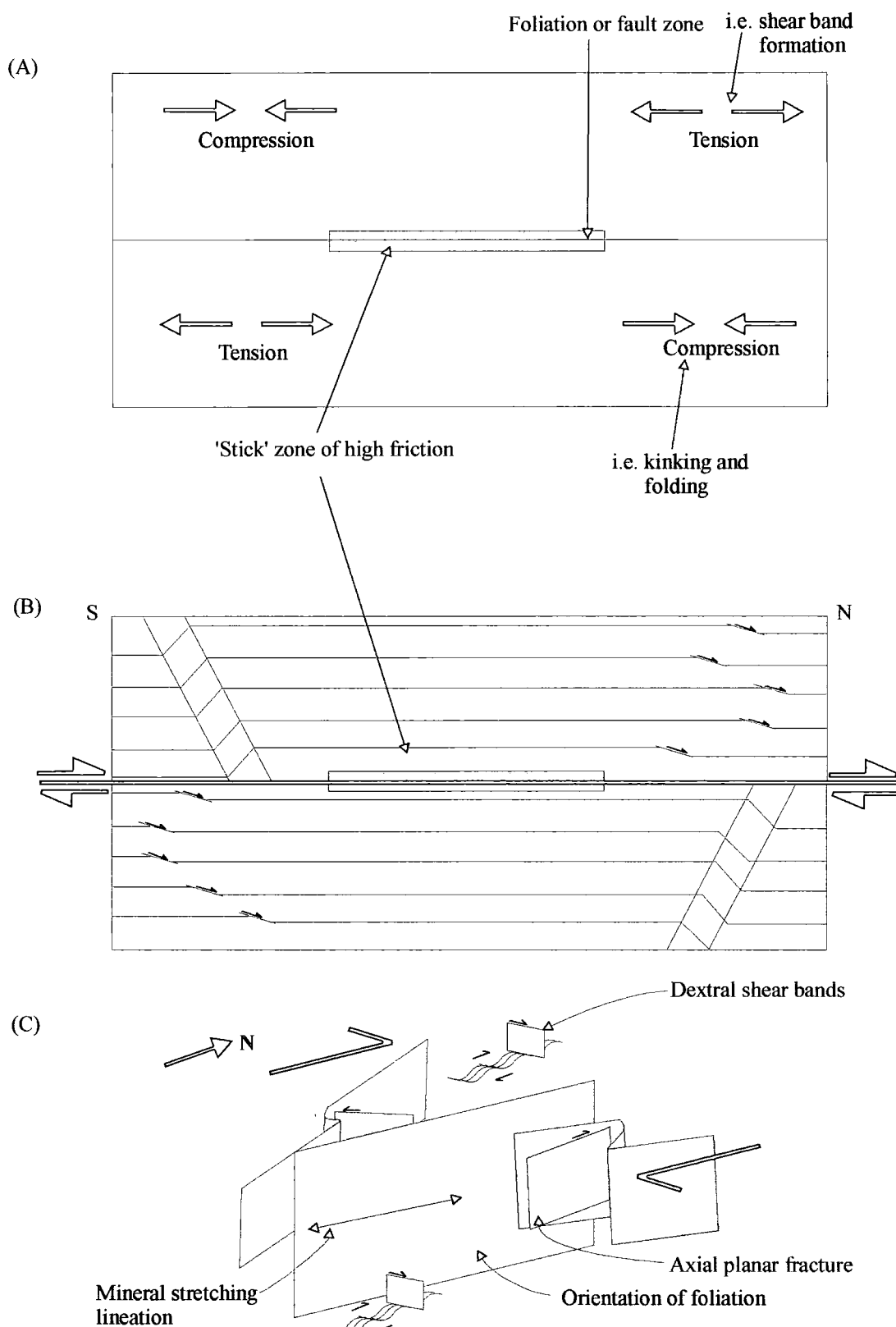


Figure 3.10 (A) Stick-slip model illustrating how compressional and extensional structures can form on the opposite sides of a 'stick zone' of high friction (adapted from Williams 1987). (B) Shows the model in (A) adapted for the structures observed in Domain B (where sub-horizontal lineations are present, i.e. not zones of contractional deformation). (C) 3-D summary of conjugate folds and shear band structures within Domain B, Ollaberry. Conjugate folds develop along with axial planar fractures in zones of N-S compression with dextral shear bands developed in areas of extension as a result of 'stick' slip deformation.

expected to form (Figure 3.10). The geometry of conjugate kink folds and their association with pelites containing shear bands within parts of Domain B is consistent with this model.

Dextrally folded quartz veins first appear 100m west of the WBFP along the Moo Wick section (Figure 3.5; Plate 3.6). The tightly folded veins occur in high-strain zones within pelitic units that contain sub-horizontal mineral stretching lineations (Plate 3.6). The veins are associated with dextral shear bands and dextrally-verging folds in adjacent psammite units (Plate 3.6).

Subsidiary gouge faults cross-cut pelitic rocks that contain dextral and contractional shear-band fabrics. The gouge faults become less planar and more anastomosing features at distances less than 100m west of the WBFP, commonly occurring in broad zones of intensely fractured pelite. Gouge-filled faults strike N-S and are steeply-dipping. Slickenside lineations vary from strike-slip to dip-slip (Figures 3.5, 3.6 and 3.8B). Shear bands within the gouge-filled faults are consistent with dextral strike-slip and contractional movements, respectively. Braided networks of sub-vertical fractures that strike between 030° and 060° are common in Domain B (Plate 3.7; Figure 3.11) increasing in frequency towards the WBFP. The fractures contain sub-horizontal slickenside lineations and form networks along which dextral displacements of millimetre- to centimetre-scale can be measured (Plate 3.7). The fractures are interpreted as R-type Riedel shears formed as a result of dextral shear along the WBF, and are commonly associated with dextral-verging folds that refold D2 axial planes (Plate 3.7).

3:1:1:5c Domain C (fault core to 60m west of WBFP)

In Domain C, high-strain zones are localised along pelitic units. The dextral shear-band fabric observed in Domain B intensifies and develops into a millimetre-scale, dextral S-C' foliation. In thin-section, this fabric cross-cuts retrograde garnets (Plate 3.8) which display well preserved σ -type geometries consistent with sinistral shear within Domain A. Thus, the dextral fabric clearly post-dates an earlier sinistral fabric. Fine-grained chlorite and white mica are concentrated along the shear planes, and in pressure-solution seams with bands of oxides, suggesting that shearing took place at

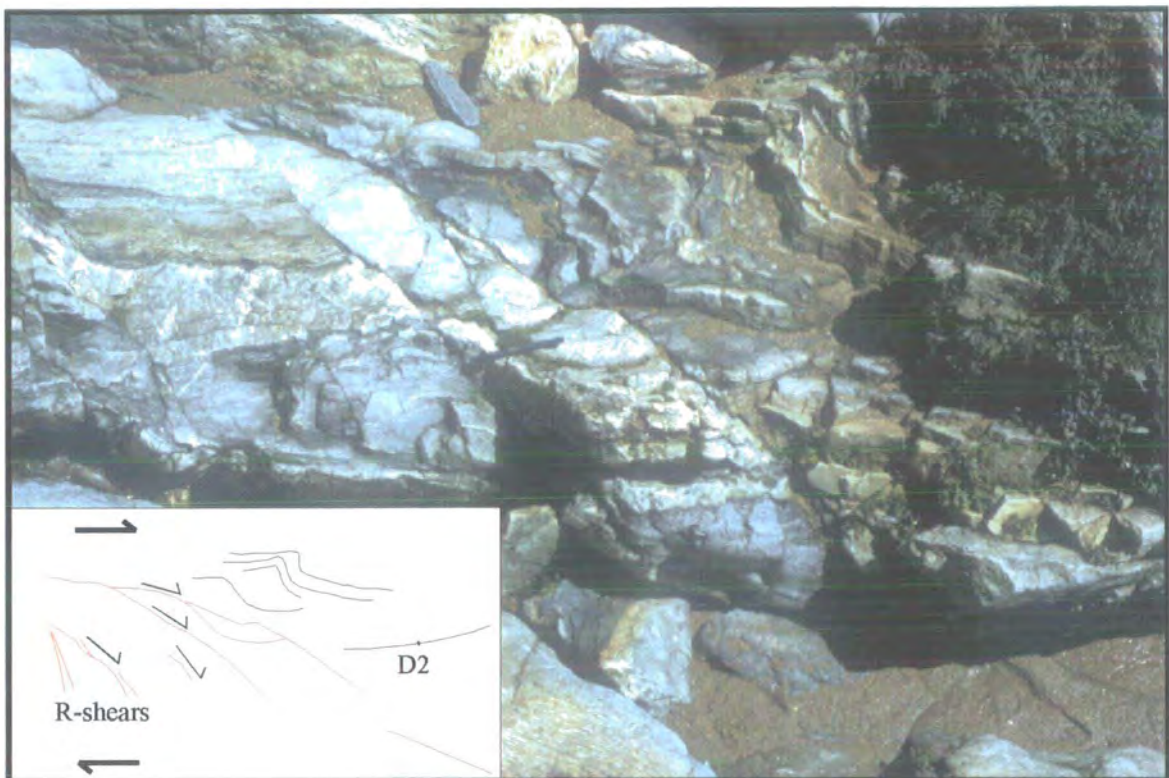


Plate 3.7 Photograph showing anastomosing geometry of dextral R-type Riedel shears and dextral verging folds refolding D2 axial planes (Domain B, Back Sand section).

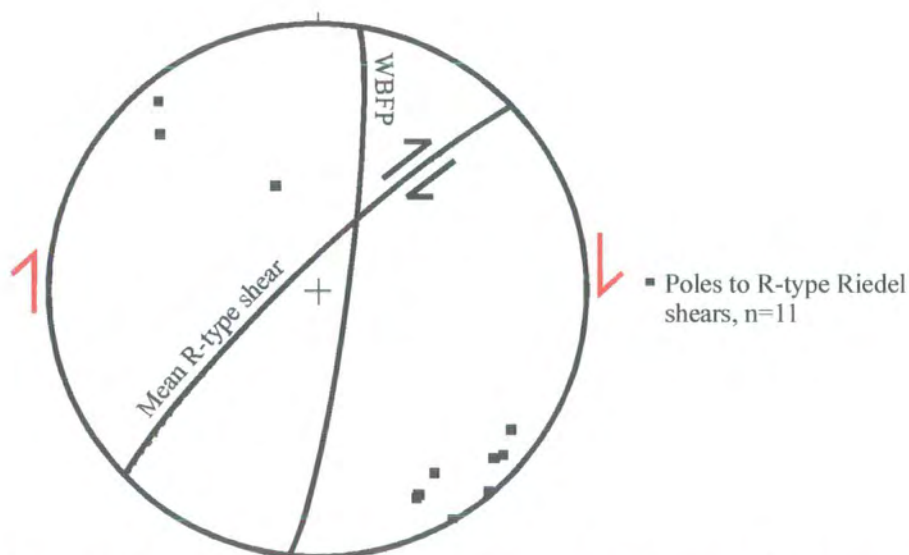


Figure 3.11 Stereographic projection showing the orientation of dextral R-type Riedel shears (within Domain B), indicating a dextral sense of shear for the WBF.

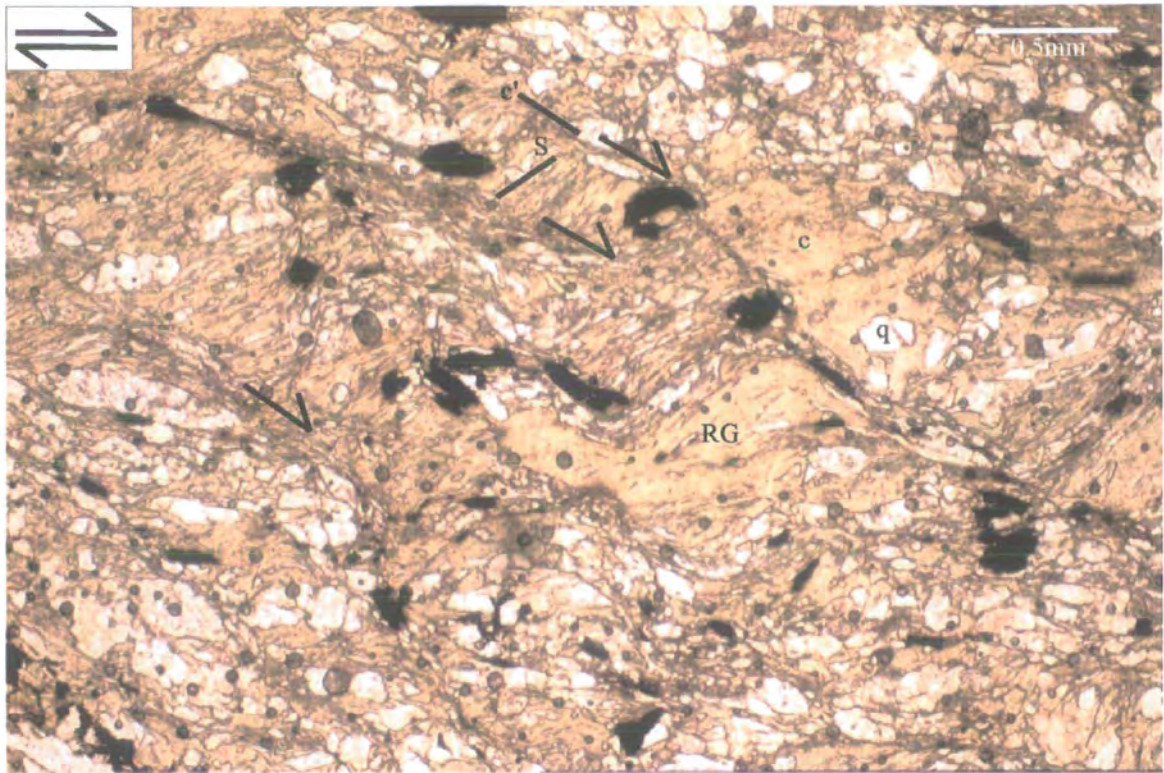


Plate 3.8 Photomicrograph of sheared pelite containing millimetre-scale s-c' fabric cross-cutting relict garnet (RG), which has been replaced by chlorite (c). NB the concentration of oxides along shear planes. Split arrows indicate shear sense parallel to the lineation. q - quartz. 25m west of the WBFP, Moo Wick section.

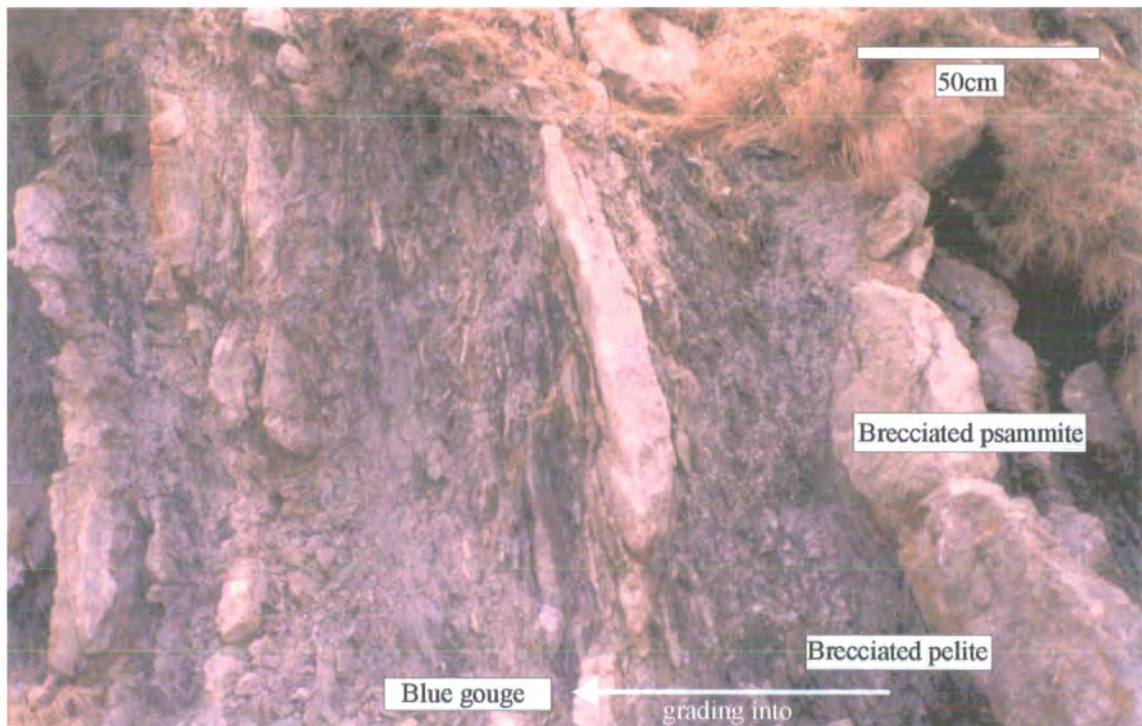


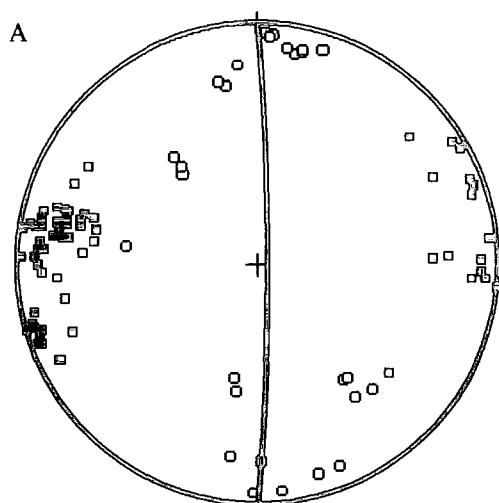
Plate 3.9 Photograph looking north to illustrate the development of blue gouge zone within a broad zone of intensely brecciated pelite and psammite, 25m west of WBFP, Domain C, Moo Wick section.

lower greenschist-facies metamorphic conditions. Steeply-dipping foliation planes strike N-S, and contain mainly sub-horizontal lineations defined by aligned micas (Figure 3.12A).

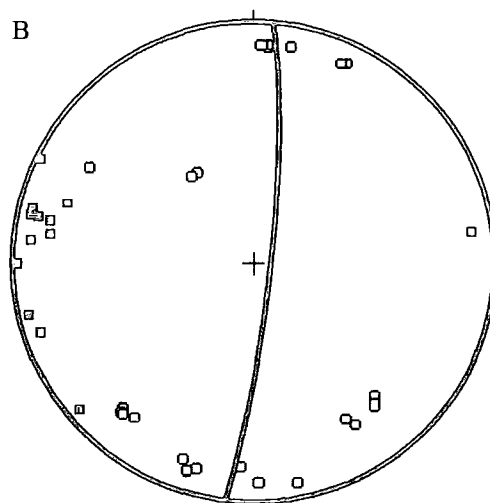
Dextral-verging crenulations associated with a weak crenulation cleavage (Figure 3.12D) and kink bands are abundant in most pelite units within Domain C. Crenulation hinges plunge shallowly and steeply to the S and N, lying along a girdle (006/84E) parallel to the WBFP (Figure 3.12D).

Subsidiary faults increase in frequency towards the WBFP, with gouges developing within zones of brecciated pelite several metres wide (Plate 3.9). Slices of intensely deformed psammite appear to 'float' in a cataclastically deformed pelite matrix that contains fault-parallel gouge zones (Plate 3.9). Near-vertical, gouge-filled faults within Domain C strike N-S and contain mainly sub-horizontal slickenside lineations (Figure 3.12B). Quartz mineral fibres together with centimetre-scale shear bands are consistent with dextral shear. Fault breccias occur as slices adjacent to gouge faults, and are locally folded by dextrally-verging minor folds.

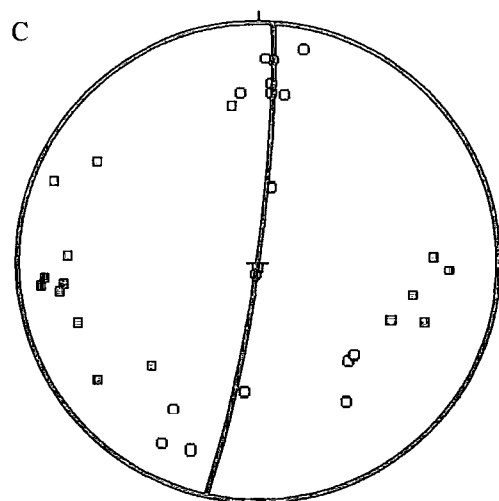
D1 and D2 regional folds strike roughly N-S, with hinges plunging shallowly and steeply (Figure 3.12C). The folds appear to be mis-orientated relative to fold axial planes within Domains A and B, due to faulting and are boudinaged in a N-S trend in breccia zones parallel to the WBFP. Chalcopyrite and pyrite mineralisation is abundant within brecciated rocks of Domain C. Sheared pelite containing a dextral S-C' fabric together with psammite is heavily brecciated, grading into 6-8m of foliated blue gouge (within the WBF core). Minor faults containing centimetre-scale shear bands, which indicate dextral shear, link into the main blue gouge. The incohesive gouge has a strong, vertical, N-S-striking fabric along with sub-horizontal lineations defined by aligned clay particles. Surfaces viewed parallel to the lineation display centimetre-scale shear bands and 'z' shaped microfolds that are consistent with dextral shear. The WBFP itself contains sub-horizontal slickenside lineations that plunge shallowly to the S.



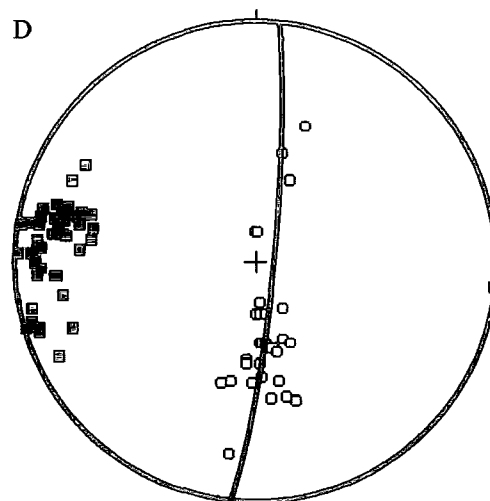
- ▣ Poles to foliation planes, n=69
- Mineral stretching lineation, n=30
- Girdle=average foliation plane



- ▣ Poles to gouge faults, n=14
- Slickenside lineations, n=21
- Girdle=average fault plane



- ▣ Poles to D1 & D2 axial planes, n=16
- D1 & D2 folds hinges, n=17
- Girdle=average axial plane



- ▣ Crenulation cleavage, n=51
- Crenulation hinge orientations, n=31
- Girdle=average crenulation cleavage (006/84E)

Figure 3.12 Stereographic projections of structural data collected from Domain C. (A) Foliation and mineral stretching lineation. (B) Gouge faults and slickenside lineations. (C) D1 & D2 fold data. (D) Crenulation cleavage and crenulation hinge orientations.

3:1:1:6 Fault zone structure east of the WBFP.

East of the WBFP, 100m of protolith granite and cataclasites are interleaved, forming the eastern end of the Ollaberry Peninsula (Figures 3.2, 3.3).

100m to the east of the WBFP, cataclasites possess no internal fabric and appear to be isotropic. Cataclasis is irregular, but generally increases towards the west. Cataclasites form irregular N-S-striking (Figure 3.13A) zones anastomosing around enclaves of protolith granite (10cm to 2m in width) (Plate 3.10). Gouge-filled faults transect the protolith granite and cataclasite (Plate 3.10). The protolith granite is extremely brecciated and is cut by quartz, epidote and chlorite veins with no consistent orientation.

Steeply-dipping, N-S-striking ultracataclasites (Figure 3.13B) cross-cut the cataclastic fabric (Plate 3.11). The ultracataclasites are typically several centimetres thick and contain sub-horizontal slickenside lineations. Associated with the ultracataclasites, secondary Riedel-type shears show both sinistral and dextral strike-slip offsets (Plate 3.11). The mean orientation of the dextral strike-slip fractures is 054/76NW, whilst the sinistral strike-slip fractures are orientated 125/77S. These fractures appear to be symmetrical to, and are bisected by the mean trend of the fault zone and associated ultracataclasites (Figure 3.13C). The main fault illustrated in Plate 3.11 contains 8cm of red-coloured (iron-stained) ultracataclasite and sub-horizontal dextral slickenfibres defined by the stepping of quartz fibres. The overall geometry is consistent with dextral strike-slip movements along the N-S master faults with a component of E-W-directed shortening (Figure 3.14). Fault-parallel epidote and quartz veining occurs adjacent to the N-S ultracataclasites (Plate 3.11).

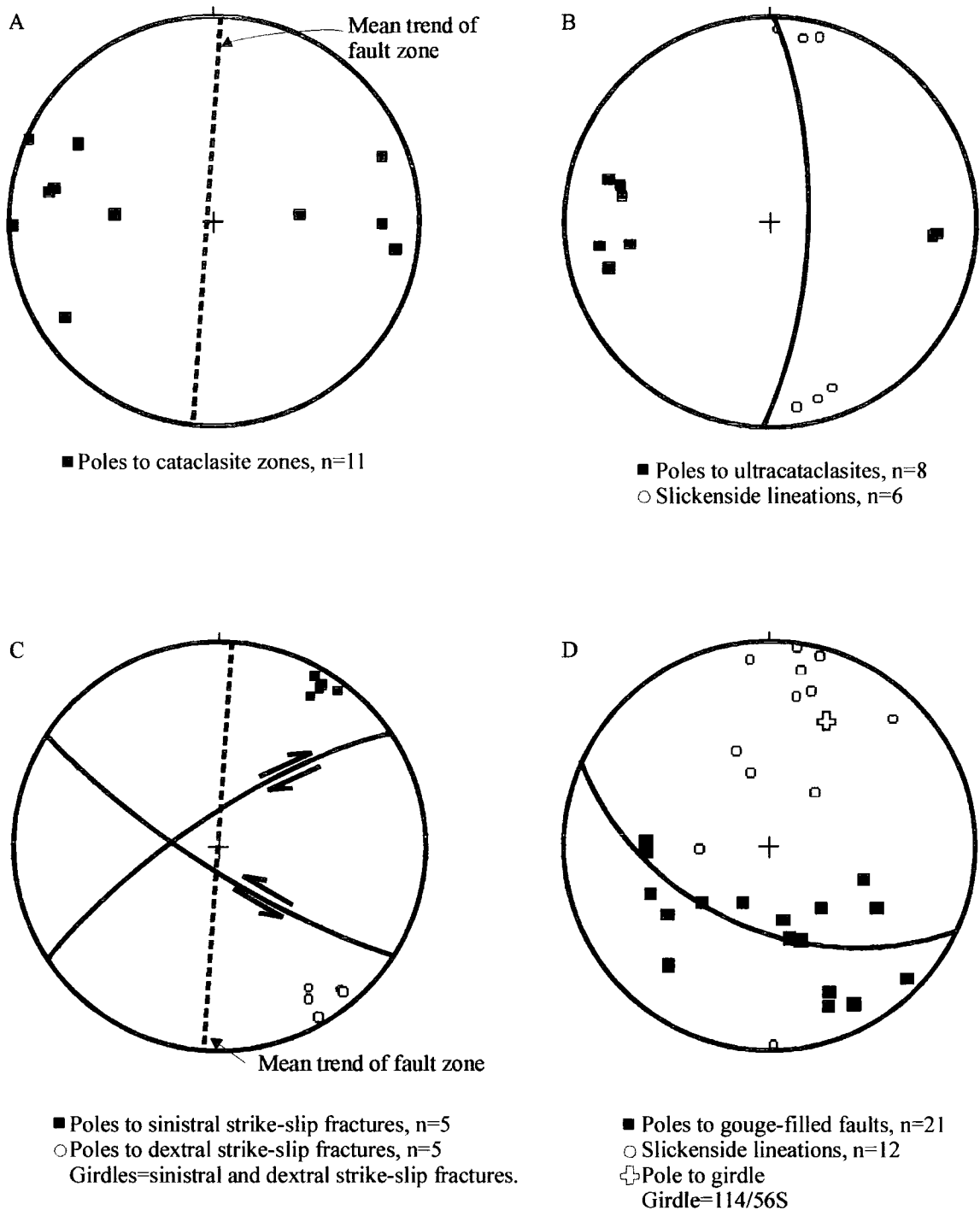


Figure 3.13 Stereographic projections of structural data collected east of the WBFP at Ollaberry. (A) Anastomosing cataclasite zones. (B) Ultracataclasites and slickenside lineations. (C) Dextral and sinistral strike-slip fractures adjacent to N-S-striking ultracataclasites (Plate 3.11). (D) Gouge-filled faults and slickenside lineations.



Plate 3.10 Photograph looking north showing anastomosing green cataclasite (c) surrounding enclaves of intensely fractured orange granite (gr) which are both cut by a thin gouge (g) with an apparent reverse offset, 100m east of the WBFP (HU 3720 8080).

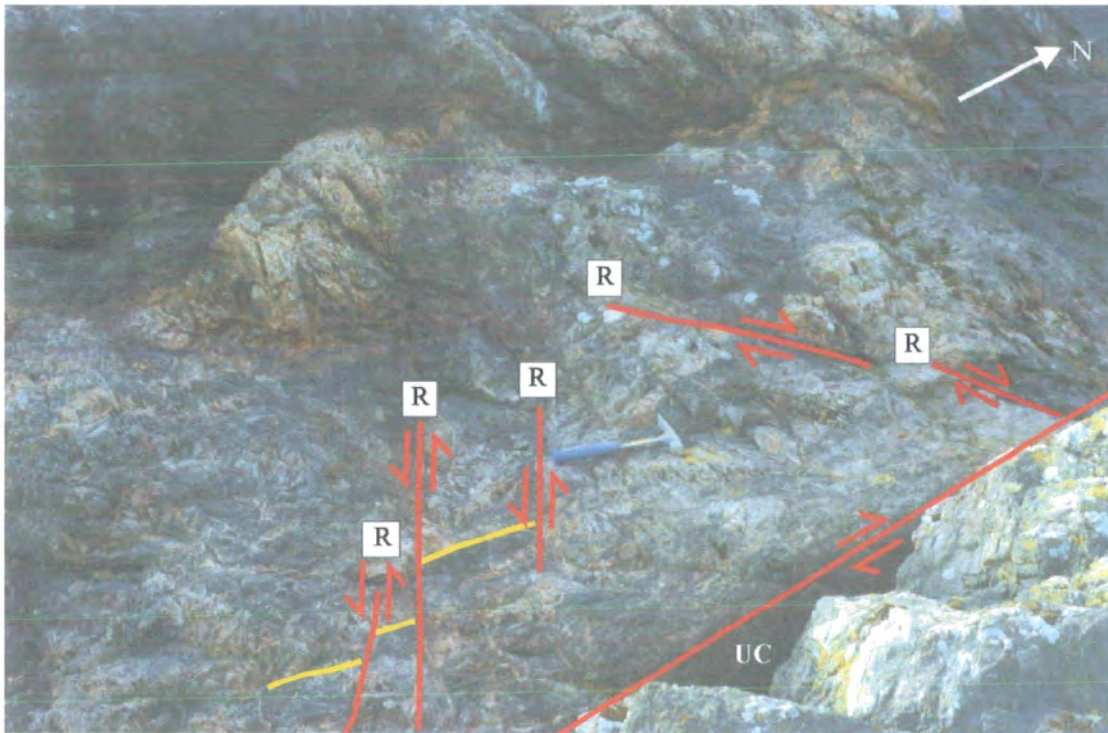


Plate 3.11 Photograph to show the kinematics of a N-S-striking ultracataclasite (UC) and symmetrical Riedel-type shears, 85m east of WBFP (HU 3719 8080).

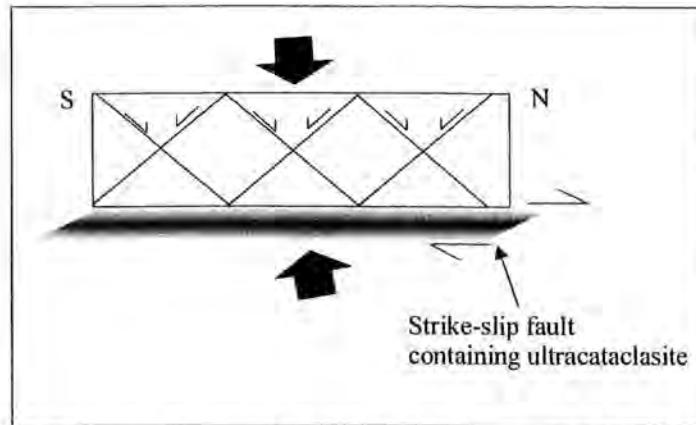


Figure 3.14 Plan view. Schematic diagram to illustrate the development of Riedel-type shears adjacent to a dextral strike-slip fault as a result of E-W (fault normal) directed compression.

At distances of less than 75m from the WBFP, gouge-filled faults are very common. Faults containing red and blue gouge cross-cut all the cataclastic fabrics, and usually bound slices of relatively undeformed pegmatitic granite that vary from 1m to 35m in thickness. The orientation and associated kinematics of gouge faults are highly variable. Slickenside lineations on polished fault surfaces and fabrics within the gouges are often not recognisable. However, the few faults that strike N-S tend to show either reverse or dextral strike-slip kinematic indicators (where slickenside lineations are present). The poles to gouge-filled fault planes lie along a girdle orientated 114/56S. Slickenside lineations cluster near to the pole of this girdle (34/015; Figure 3.13D), which represents the mean orientation of the fault plane intersections. Thus, the pole to the girdle corresponds to the mean transport direction indicating strike-slip faulting. Cataclasis becomes more intense with an apparent banding developed at distances of 5m from the WBFP (see section 3:1:1:3c). Hematite mineralisation along N-S seams is a common feature within the gouges and earlier cataclasites, becoming more frequent towards the WBFP.

3:1:1:7 Kinematic summary and discussion

The kinematic evolution of the WBFZ at Ollaberry is summarised in Table 3.1.

Kinematic Regime	Fault rocks / structures
3. Dextral transpression (youngest)	<ul style="list-style-type: none"> ◦ Fabrics within gouge ◦ Brittle faults (dextral strike-slip and contractional) ◦ R- and R'-type Riedel shears ◦ Folds, kink bands and crenulations ◦ Cataclasites
2. Dextral transpression	<ul style="list-style-type: none"> ◦ S-C' fabric of lower greenschist facies grade ◦ Contractional fabrics of lower greenschist facies grade ◦ Shear bands ◦ Cataclasites
1. Sinistral strike-slip? (oldest)	<ul style="list-style-type: none"> ◦ Sinistraly sheared garnets with chlorite tails? ◦ D3 folds?

Table 3.1 Table summarising the kinematic evolution of the WBFZ at Ollaberry.

The rocks on either side of the WBF at Ollaberry record different kinematic events. Those to the west record all the events summarised in Table 3.1. Here, the deformation related to phases 2 and 3 (Table 3.1) is strongly partitioned into three structural domains (Figures 3.15, 3.5, 3.6). Phase 2 and 3 structures and fabrics relating to dextral strike-slip and reverse movements are thought to be part of the same system and do not reflect distinct kinematic events. Thus, contractional and dextral strike-slip faults (phase 3) link together and are interpreted to be the same age. Both contractional and dextral strike-slip faults contain the same generation of fault rocks and structures, and display similar overprinting relationships. Ductile fabrics related to phase 2 are strongly partitioned with dextral shear bands and S-C' fabrics interpreted to be the same age as contractional fabrics (phase 2). Both contractional and strike-slip fabrics exhibit the same cross-cutting relationships and are texturally and microstructurally similar to each other.

Domain A (160-130m west of WBF) contains structures that indicate dextral strike-slip deformation with some contraction (Figure 3.15). Domain B (130-60m west of the WBF) comprises structures that indicate a mainly contractional deformation with some dextral strike-slip. Finally, dextral strike-slip kinematics dominate in Domain C (in zones up to 60m west of the WBF). The partitioning described for both the ductile and the brittle events is consistent with a dextral transpressional deformation.

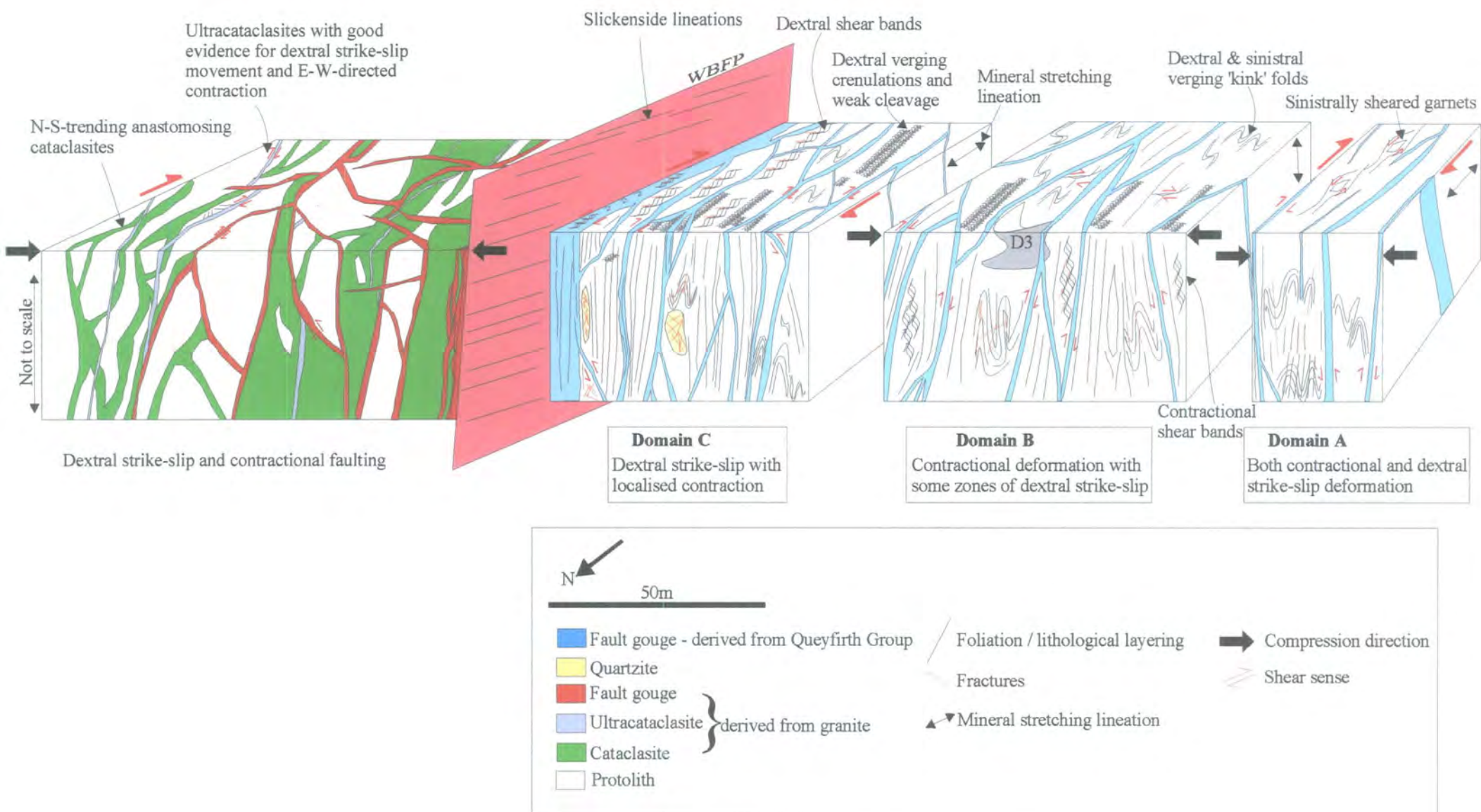


Figure 3.15 Schematic diagram to illustrate fault rock distribution, structures and strain partitioning within the WBFP at Ollaberry.

Although the ductile and brittle structures are described as separate kinematic phases, it is possible that they formed during the same event as the fault zone was being exhumed. East of the WBFP, the rocks preserve evidence of only the phase 3 deformation (dextral transpression; Table 3.1). The granite may not have been adjacent to the WBF during phases 1 and 2 or possibly had not been intruded at that time.

Conroy (1996) concluded that the earliest phase of movement along the WBF was related to the formation of the D1 folds, although these folds are recognised widely outside the WBFZ and are here interpreted to be regional structures pre-dating the WBFZ. Conroy (1996) refers to a sinistral phase followed by two phases of dextral strike-slip. The sinistral phase was recognised based on the presence of σ -type garnet porphyroblasts (c.f. Table 3.1). The dextral phases were recognised based on (a) dextral-verging crenulations, broken garnets and reverse-slip crenulations and, (b) cross-cutting crenulations, kink bands and a fabric within the blue gouge. Although the dextral phases seem to correspond well with the findings of the present study, the evidence described by Conroy (1996) could be explained by a single phase of dextral strike-slip (cf. phase 3; Table 3.1). A final phase of sinistral strike-slip was described by Conroy (1996) who referred to N-S-striking fractures with sinistral strike-slip offsets. These very minor structures are found only in Domain A (Figure 3.6) and are not found in the fault core. This suggests that the structures described by Conroy (1996) are not related to a regional phase of movement along the WBF and are probably small accommodation structures with little or no regional significance within the WBFZ.

3:1:2 Sullom, Lunnister and the Ness of Haggrister.

Sullom, Lunnister and the Ness of Haggrister form a mainly NNE-SSW coastal section of low cliffs (<5m), beaches and narrow inlets, along the west side of Sullom Voe (locality b; Figures 3.1; 3.16). E-W-trending coastal sections expose the WBFZ along the southern side of the Ness of Haggrister, more poorly on the north side of this peninsula and at Sullom. East of the WBF, granodiorite belonging to the Devonian Graven Complex (section 2:1:5:1a) is exposed. West of the WBF,



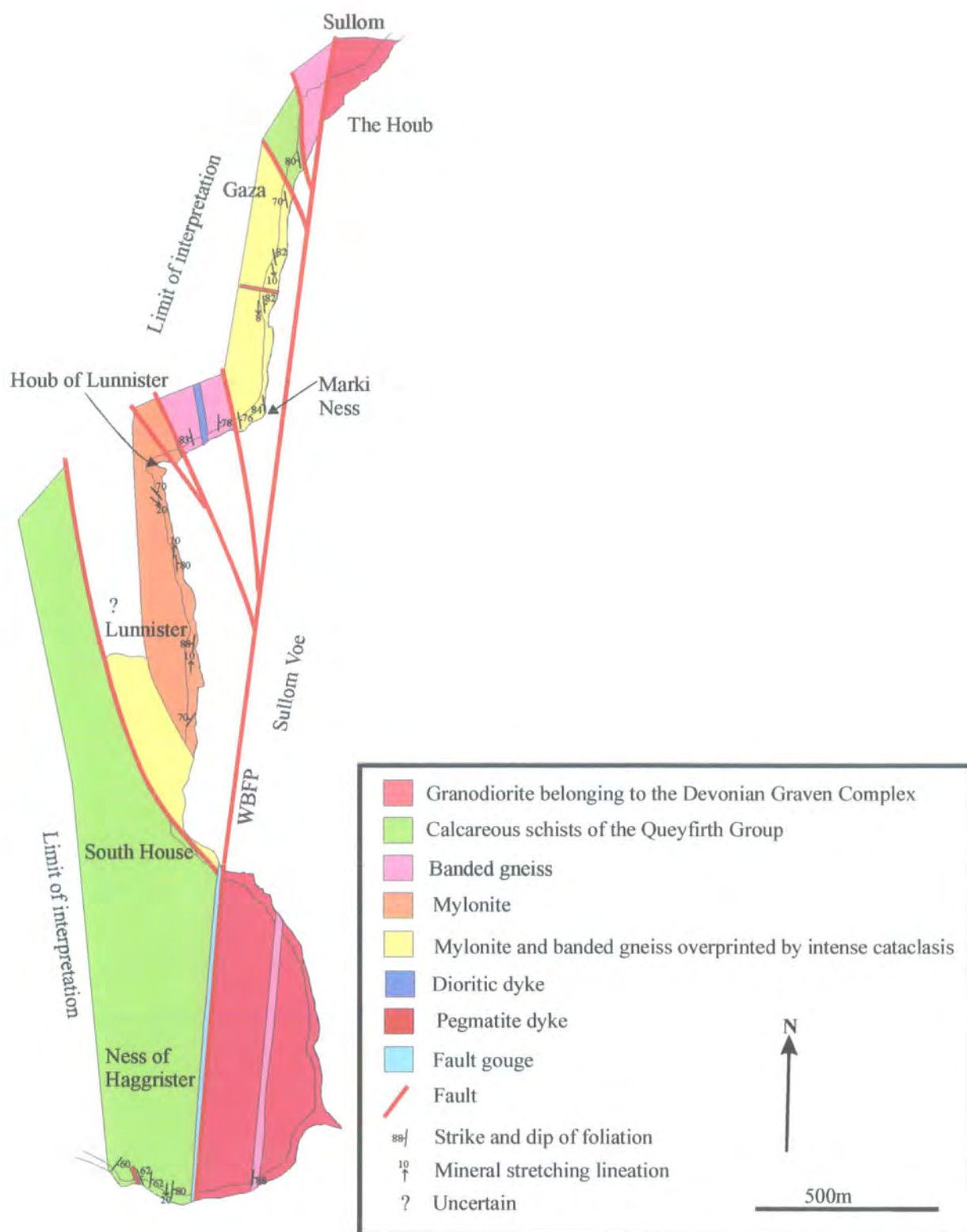


Figure 3.16 Geological map of Sullom, Lunnister and the Ness of Haggrister.

metasedimentary rocks of the Queyfirth Group occur (section 2:1:1:4), whilst banded gneiss, mylonite and cataclasite are exposed within fault-bounded slices (Figure 3.16). At Sullom, Lunnister and the Ness of Haggrister, the WBFZ varies in width from 300m to at least 500m wide (Figure 3.16). The WBF enters the Ness of Haggrister in the south trending 010° and bifurcates into several fault strands to the north of the Ness of Haggrister (Figure 3.16). The main fault strand continues to the NNE to intersect the coast at Sullom (Figure 3.16). There, the fault separates granodiorite belonging to the Graven Complex from a slice of banded gneiss (Figure 3.16). Inland exposure of the WBFZ and associated fault rocks is very poor.

Flinn (1977) noted the sporadic occurrence of cataclastically deformed mylonite over a distance of 2km along the coast north of the Ness of Haggrister. The mylonites were considered to be part of the Great Glen Fault, representing an earlier ductile phase of movement; pre-dating brittle faulting which led to extensive cataclasis together with the formation of fault gouge. Roddom et al. (1989) attempted to date the mylonites at Lunnister using K-Ar and Ar-Ar step-heating techniques on whole-rock samples. They assumed that the mylonites were derived from granodiorite of the Graven Complex and produced dates between 290 and 320Ma. Conroy (1996) mapped Sullom, Lunnister and the Ness of Haggrister at 1:10,000 scale. Cataclastically deformed mylonites exposed at Lunnister were interpreted to represent the earliest phase of movement along the WBF, although the shear sense was described as unclear. Shear bands were described in soft blue gouge adjacent to the WBFZ, indicating dextral shear. Conroy (1996) described the most recent phase of movement as sinistral strike-slip. This was suggested based on the presence of NE-SW-trending dolerite dykes that were interpreted to have been intruded into a NW-SE extensional setting, consistent with sinistral shear along the WBF.

3:1:2:1 Protolith lithologies

3:1:2:1a Granodiorite

Granodiorite belonging to the Devonian Graven Complex (Plate 3.12; section 2:1:5:1a) is exposed east of the WBF at Sullom and the Ness of Haggrister (Figure



Plate 3.12 Plan view. Protolith granodiorite belonging to the Devonian Graven Complex (G) 300m east of the WBFP on the southern side of the Ness of Haggrister. Granodiorite (G) contains N-S-orientated gneissose xenolith (X) and is cross-cut by pegmatite dyke (P).



Plate 3.13 Plan view. Calcareous schists belonging to the Queyfirth Group 300m west of the WBFP on the southern side of the Ness of Haggrister (Figure 3.16). The schists display moderately S-plunging open folds.

3.16). The granodiorite is pink / green in colour; and coarse to medium grained with phenocrysts of feldspar up to 0.75cm in length. It is composed of approximately 60% feldspar, 20% quartz, 10% hornblende, 5% chlorite and 5% epidote. The rock is equigranular with crystals forming a holocrystalline texture. The granodiorite contains a weak magmatic fabric defined by the alignment of feldspar and quartz phenocrysts. Locally, the granodiorite weathers to a green colour and is strongly retrogressed. Hornblende is replaced by chlorite, and feldspars have a speckled appearance due to their breakdown to aggregates of sericite. Xenoliths of psammitic and hornblende gneiss range in size from 30cm to several tens of metres across. The xenoliths strike N-S and in places contain a fabric defined by flattened quartz and feldspar aggregates. Randomly orientated pegmatite dykes cross-cut the granodiorite and xenoliths. The pegmatite dykes are usually 30cm to 1m thick and are coarse-grained with no magmatic or solid-state fabric.

3:1:2:1b Metasedimentary rocks

To the west of the WBF on the southern side of the Ness of Haggrister, rocks belonging to the Dalradian Queyfirch Group (section 2:1:1:4) are exposed (Figure 3.16). The rocks comprise calcareous schists, crystalline limestones and quartz-mica schists (Plate 3.13). Thick intervals (several metres) of finely layered calcareous schist are interbanded with 15 to 50cm thick limestone horizons and locally quartz-mica schists.

3:1:2:1c Gneissose rocks

Compositionally banded gneisses of uncertain origin are exposed west of the WBF at Sullom and north of the Houb of Lunnister (Figure 3.16). The gneisses are pink / green in colour, fine to medium grained and equigranular with crystals up to 0.5cm in length. Green-coloured gneiss comprises 80% hornblende and 20% feldspar that is interbanded on a metre-scale with pink-coloured gneiss comprising 70% feldspar, 20% quartz and 10% hornblende. Hornblende-rich gneisses in places contain centimetre-scale epidote-rich bands. The gneisses contain a N-S trending, sub-vertical, L-S tectonite fabric defined by flattened aggregates of quartz, feldspar and

hornblende with a sub-horizontal lineation defined by aligned crystals of hornblende, feldspar and quartz.

Mykura and Phemister (1976) described the banded gneiss at Sullom, Lunnister and the Ness of Haggrister and confidently inferred a direct correlation with the Lewisianoid Eastern Gneisses associated with the Caledonian front (see section 2:1:1:1). The Lewisianoid Eastern Gneisses form inliers of schistose, hornblende-rich gneisses intercalated with Moine cover rocks. In places the gneisses are feldspar-rich and contain fine bands of hornblende-rich units.

3:1:2:2 Fault rocks

In this section, fault rocks of the WBFZ are described in the order of their relative age relationships (oldest to youngest; see section 3:1:2:3).

3:1:2:2a Mylonites

Mylonitic rocks derived from compositionally banded gneiss (section 3:1:2:1c) are exposed west of the WBF. The mylonites occur interleaved with compositionally banded gneisses (section 3:1:3:1c) defining a fault-bounded block at least 300m wide (Figure 3.16). There are two types of mylonite. Pink / grey quartzo-feldspathic mylonites contain approximately 50% feldspar, 25% quartz, 20% muscovite and 5% chlorite and epidote with minor amounts of sphene. Millimetre-scale bands of fine-grained feldspar and muscovite aggregates are interlayered with quartz-rich bands. The fine-grained matrix wraps around orthoclase and plagioclase porphyroclasts, which are typically 2mm to 1cm in length. Blue / grey mafic mylonites are composed of approximately 35% hornblende, 30% feldspar and muscovite, 15% quartz, 15% green biotite and 5% epidote. Millimetre-scale bands of fine-grained feldspar + muscovite, hornblende + green biotite, and quartz are interlayered. The fine-grained matrix wraps around plagioclase, orthoclase and hornblende porphyroclasts, which range from 2mm to 1cm in length. All mylonites contain a strong foliation defined by stretched and flattened aggregates of quartz, feldspar, hornblende and mica. The proportion of matrix varies from 10 to almost 100%, so that the rocks can be

subdivided into protomylonites, mylonites and ultramylonites. The sub-vertical mylonitic foliation trends N-S with a sub-horizontal lineation defined by stretched quartz, feldspar, hornblende and mica grains. In surfaces and thin-sections viewed perpendicular to the mylonite foliation and parallel to the stretching lineation, σ and δ -type porphyroclasts consistently indicate sinistral shear.

3:1:2:2b Cataclasites west of WBFP

Cataclasites derived from mylonite and gneiss are exposed within a fault-bounded block west of the WBF along the coast near Lunnister (Figure 3.16). There are two types of cataclasite, here described as 'early' and 'late'.

'Early' cataclasites develop parallel to the mylonitic foliation and range in thickness from 0.5mm to up to 1m. 'Early' cataclasites comprise finely comminuted fragments of feldspar, quartz, hornblende, mica, mylonite and gneiss set within a fine-grained cataclastic matrix of the same. The fragments are angular to sub-angular, 1cm to less than a millimetre in size and randomly orientated. Millimetre-thick epidote, chlorite, quartz and albite veins commonly cross-cut and occur as fragments within the matrix.

'Later' cataclasites transect and contain fragments of 'early' cataclasites. The 'later' cataclasites comprise finely comminuted fragments of mylonite, banded gneiss, cataclasite, quartz, feldspar and scapolite set within a fine-grained cataclastic matrix that has been altered to a clay-rich paste. The cataclasites display millimetre-scale colour banding due to variations in the clast-to-matrix ratio. Finer-grained clay-rich layers display a foliation defined by aligned clay particles. N-S-trending cross-cutting hematite veins range from 1mm to 2cm in thickness and commonly form networks, locally acting as cement within the finer grained portions. In thin-section, scapolite, analcite and calcite vein fragments are present within the banded clay-rich matrix.

3:1:2:2c Cataclasites east of the WBFP derived from granodiorite

Cataclastic rocks east of the WBF at Sullom and the Ness of Haggrister (Figure 3.16) are derived entirely from granodiorite. There are two types of cataclasite: non-

foliated and foliated. The age relationship of the foliated and non-foliated cataclasites is unclear.

Non-foliated cataclasites are pale red / brown to green in colour, comprising finely comminuted clasts of granodiorite, orthoclase, plagioclase, quartz, chlorite, epidote and muscovite set within a fine-grained, epidote-rich, cataclastic matrix of the same, which has been partially altered to a clay-rich paste. Randomly orientated clasts are angular to sub-angular, ranging from 5mm to less than 0.5mm in size. Disseminated oxides are common and hematite mineralisation has partially cemented the finer-grained parts of the matrix. The cataclasites possess no internal fabric and appear to be isotropic in the field on all scales of observation. The proportion of matrix varies from 10 to 60%, so that the rocks can be subdivided into protocataclasites and cataclasites based upon the proportion of matrix.

Foliated cataclasites are green or red in colour, comprising finely comminuted clasts of granodiorite, orthoclase, plagioclase, quartz, chlorite, muscovite and epidote set within a fine-grained cataclastic matrix of the same. Clasts are sub-angular to sub-rounded, ranging from 5mm to less than 0.5mm in size. The cataclasites contain a foliation defined by aligned clasts and mica grains. In places, foliated cataclasites are red in colour due to the effects of iron mineralisation.

3:1:2:2d Cataclasites west of WBF derived from schists

Cataclastically deformed rocks west of the WBF on the southern side of the Ness of Haggrister are derived from calcareous schists belonging to the Dalradian Queyfirch Group (Figure 3.16). The cataclastic rocks are pale grey in colour and comprise finely comminuted fragments of calcite, quartz, mica and calcareous schist set within a fine-grained cataclastic matrix of the same. Randomly orientated fragments are angular to sub-angular, ranging from 0.5cm to less than a millimetre in size. The proportion of matrix varies from 10 to almost 70%, so that the rocks can be subdivided into breccias, protocataclasites and cataclasites. Fault-parallel stylolites defined by irregular iron-stained surfaces are common. The cataclasites are isotropic on all scales of observation in the field and possess no fabric. Calcite veins cross-cut

the cataclastic fabric and are also present as fragments within the matrix, suggesting that veining was broadly coeval with cataclasis.

3:1:2:2e Fault gouges

There are two types of gouge present at Sullom, Lunnister and the Ness of Haggrister, a hard red and a soft blue gouge.

The red gouge is derived from granodiorite belonging to the Devonian Graven Complex (section 3:1:3:1a). It is fine grained, clay-rich, cohesive and displays a fine colour banding defined by variations in grain size and clast-to-matrix ratios. In-thin section and in the field the gouge appears to be a clay-rich isotropic paste that has been cemented by hematite. Randomly orientated clasts (5mm to <0.5mm) of granodiorite, cataclasite, quartz, calcite and analcite are sub-angular to sub-rounded. Thin calcite veins transect the fine colour banding of the red gouge.

The blue gouge is derived from schists belonging to the Queyfirth Group (section 3:1:3:1b). It is incohesive, fine grained and clay-like in appearance. Bulk XRD analyses show the gouge to be composed of quartz, albite and smectite. The gouge fraction with a grain size of < 6µm comprises smectite, kaolinite, illite, clinocllore, quartz, albite and orthoclase. The gouge has a sub-vertical N-S-trending fabric (parallel to the WBF and other bounding fault surfaces) defined by aligned clay particles. The blue and red gouges are broadly the same age although enclaves of red gouge lie within the blue gouge (see section 3:1:2:3c) near the contact between them, suggesting that the blue gouge is the younger fault rock.

3:1:2:3 Fault rock distribution and age relationships, south side of the Ness of Haggrister

Along the south side of the Ness of Haggrister early fault rocks are preserved within the wall rocks west of WBF core. The earliest recognised fault rocks are overprinted by cataclastic deformation, which generally increases towards the WBF core. Fault gouges within the WBF core cross-cut all other fault rocks and structures within the

WBFZ. In the following section, the earlier fault rocks are described first. These are found in the wall rocks on either side of the fault core.

3:1:2:3a West of the WBF core

Sheared pelites, cataclasite and blue gouge are exposed west of the WBF core on the southern side of the Ness of Haggrister (Figure 3.16). Metre-scale ductile shear zones containing S-C' fabrics consistent with dextral shear have localised within pelitic protoliths and overprint regional structures and fabrics of the Queyfirth Group. Cataclasites cross-cut the regional fabrics and ductile shear zones within these retrograde pelites and are isotropic with no fabric visible in the field. Blue, incohesive, fault gouges transect all the cataclastic, sheared pelite and regional fabrics to the west of the WBFP.

3:1:2:3b East of the WBF core

Cataclasites and fault gouge are exposed east of the WBF core. Millimetre- to centimetre-thick, foliated cataclasites cross-cut the granodiorite and associated pegmatite dykes. A broad zone of non-foliated cataclasite overprints the granodiorite and associated pegmatite dykes. The cataclasites are isotropic on all scales with cataclastic deformation generally increasing towards the fault core. The mutual age relationship between the non-foliated and foliated cataclasite is unclear. Red, indurated, fault gouge cross-cuts and contains comminuted fragments of the non-foliated cataclasite.

3:1:2:3c WBF core

The fault core is located in the central part of the WBFZ and corresponds to the region of most intense fault-related deformation. The most obvious movement plane of the WBFZ is exposed on the southern side of the Ness of Haggrister (Figure 3.16). The fault plane (WBFP) is orientated 004/87W and defines a narrow inlet. Here, the fault core is approximately 10m wide (Figure 3.17) and is defined by a continuous sequence of fault rocks that extends from the wall rocks on either side and across the WBFP. West of the WBFP, a 5m wide zone of pale grey cataclasites overprints calcareous schists that contain shear bands consistent with dextral shear (Figure 3.17).

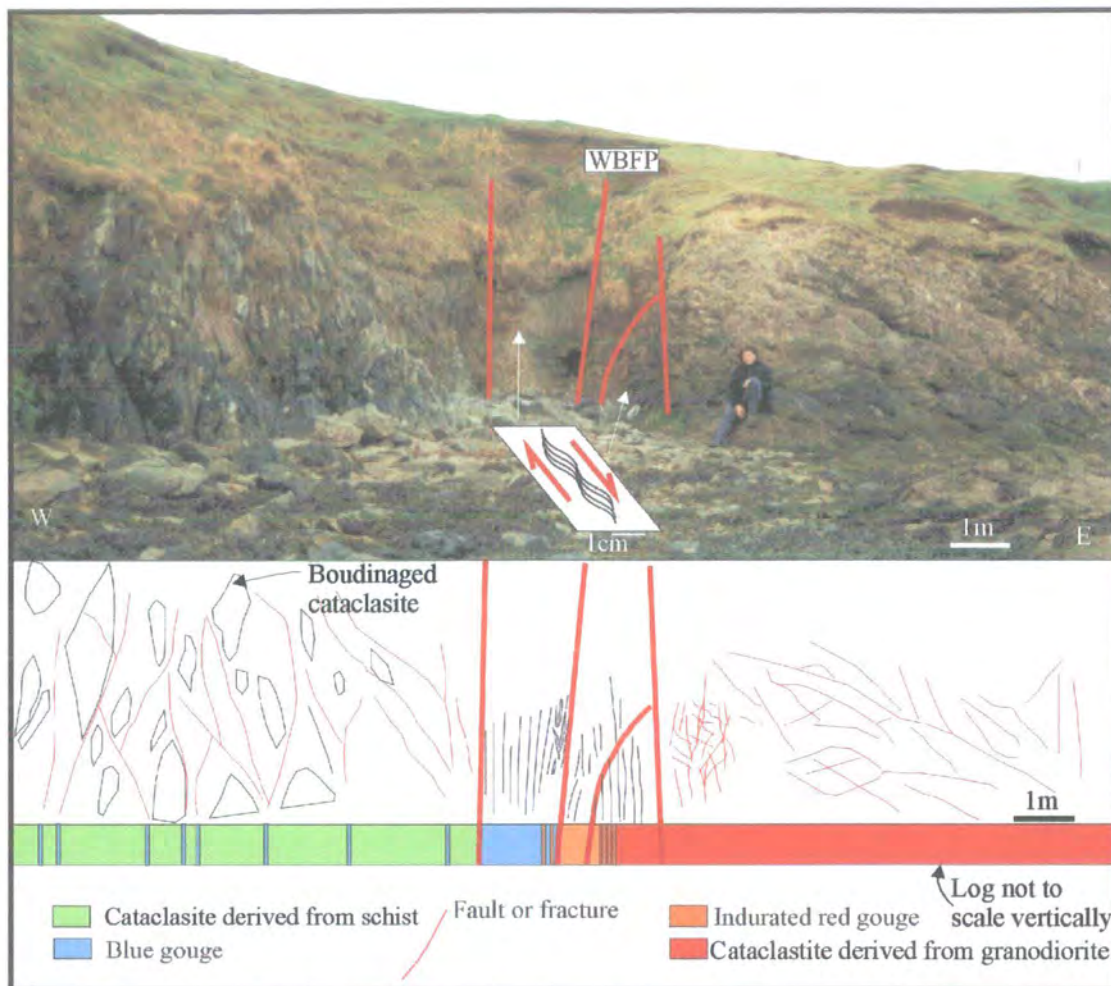


Figure 3.17 Photograph and sketch log of the WBF core to illustrate fault rock distribution, on the southern side of the Ness of Haggister (HU 3521 6989).

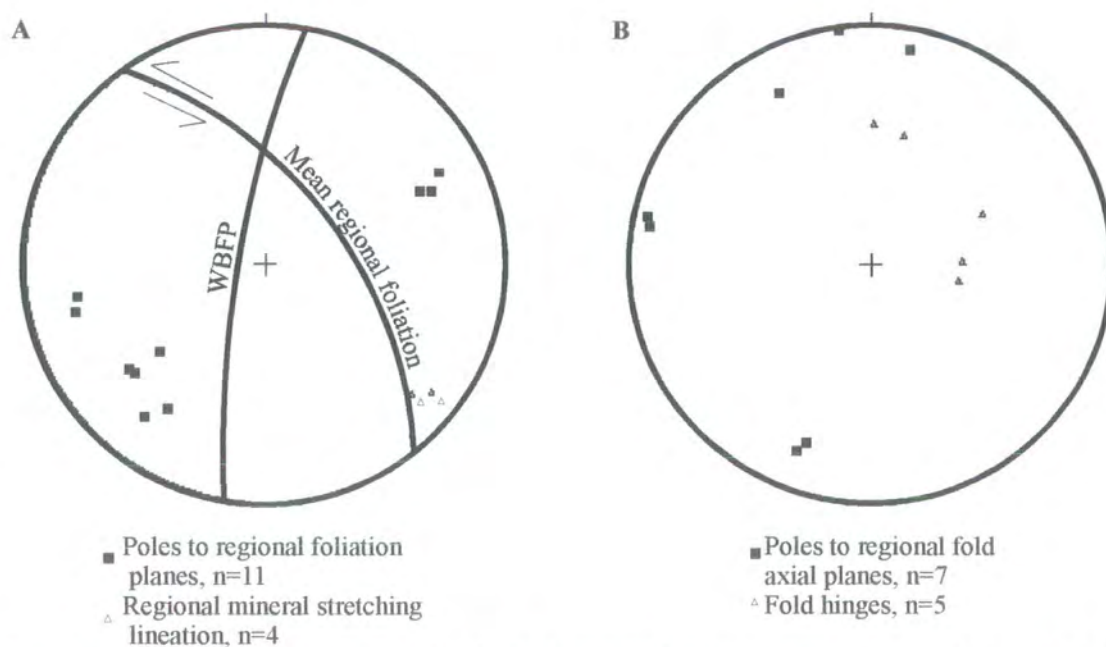


Figure 3.18 Stereographic projections showing (A) regional foliation and lineations and (B) regional fold axial plane and hinge orientations. Data collected from the Queyfir Group west of the WBFZ.

The cataclasites west of the WBF are rich in calcite, strongly recrystallised and appear to be isotropic on all scales of observation in the field. Centimetre-thick gouges cross-cut the pale grey cataclasites displaying anastomosing geometries around enclaves (10cm to 1m wide) of cataclasite and schist (Figure 3.17). Fragments of cataclasite, calcite and analcite (zeolite) vein material commonly occur as clasts within the blue gouge, suggesting that the gouge is the younger fault rock. The pale grey cataclasites and the main unit of blue gouge are separated by a steep W-dipping fault plane. The blue gouge is 2m thick and contains a steeply dipping fabric defined by aligned clay particles with sub-horizontal lineations, also defined by aligned clay particles. The fabric within the gouge wraps aligned clasts of country rock (Plate 3.14). W-dipping shears cross-cut the main foliation within the blue gouge (Plate 3.14). The eastern side of the blue gouge comprises a 40cm thick zone that contains N-S-orientated enclaves of red gouge (Plate 3.15). The contact between the interleaved gouge zone and the indurated red gouge to the east is sharp and polished (Plate 3.15). This polished surface is the WBFP (Figure 3.17). The indurated red gouge occurs to the east of the WBFP and is 1m thick (Figure 3.17). The indurated red gouge overprints iron-stained cataclasite derived from the granodiorite. East of the WBFP, the red gouge and red / brown cataclasite are interleaved over 1m. Cataclasite east of the WBFP is approximately 10m thick. The cataclasite has no fabric and is isotropic on all scales of observation in the field. Cataclasis decreases eastwards and grades into intensely fractured granodiorite. The age relationships of fault rocks within the WBF core are summarised in Table 3.2.

Relative age	Fault rock / structures
Youngest	Quartz slickenfibres on WBFP
	W-dipping shears in blue gouge
	Red and blue gouges
Oldest	Cataclasites west and east of WBFP

Table 3.2 Summary of fault rock relative age within the WBF core on the southern side of the Ness of Haggrister.



Plate 3.14 Photograph looking north of cross-section across blue gouge within the WBF core to show fabric associated with dextral shear cross-cut by W-dipping, dip-slip shears (A). Dashed lines mark main foliation which wraps around clasts of country rock (C).

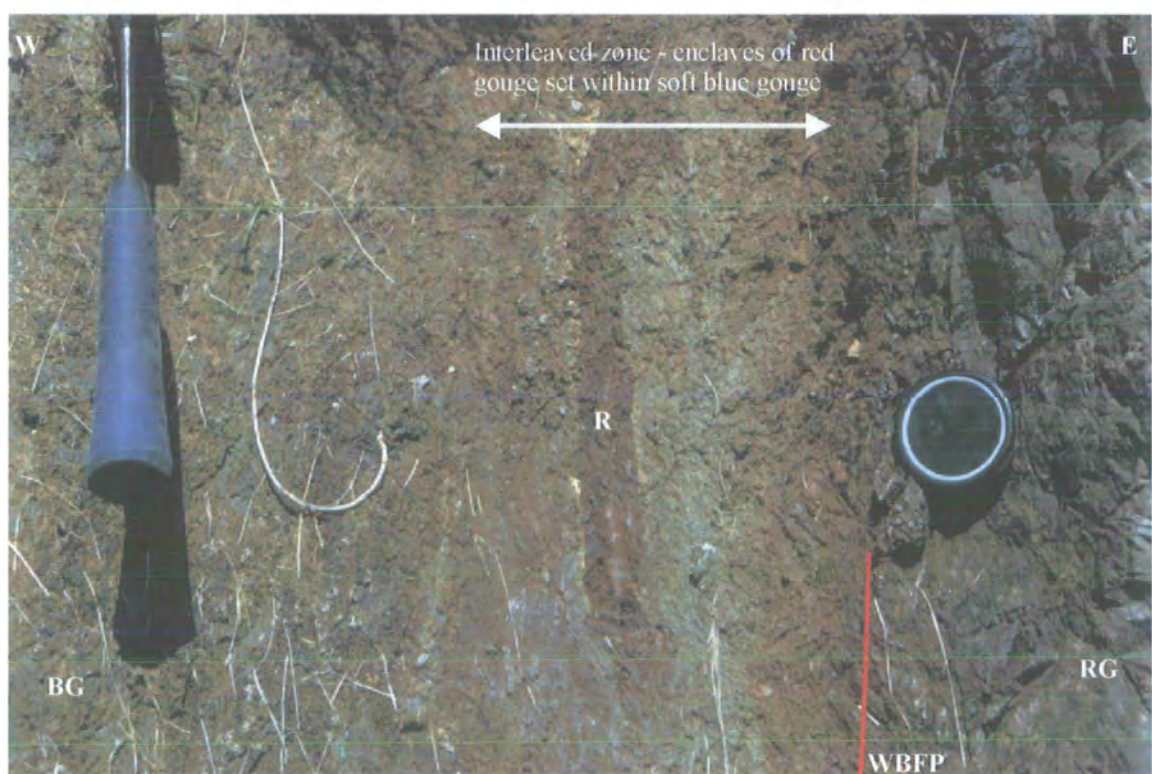


Plate 3.15 Photograph looking north to show the sub-vertical contact (WBFP) between the indurated red gouge (RG) to the right and incohesive blue gouge (BG) to the left. Note - the enclave of red gouge (R) within the soft blue gouge. The soft blue gouge is brown in places due to the effects of iron mineralisation.

3:1:2:4 Protolith Structure outside WBFZ

The foliation in the schists belonging to the Queyfirth Group is defined by flattened aggregates of calcite, quartz and mica. It strikes NW-SE and dips steeply to the NE (Figure 3.18A). The lineation is defined by the alignment of elongate calcite, quartz and mica crystals, and plunges shallowly to the SE. In surfaces viewed parallel to the lineation, sheared quartz lenses surrounded by a schistose fabric display σ -type geometries consistent with sinistral shear. At least two orientations of folding can be recognised at the Ness of Haggrister. Firstly, open folds with axial planes striking E-W and axes plunging moderately to the E (Figure 3.18B). Secondly, open folds with axial planes striking N-S and fold hinges plunge moderately to the N (Figure 3.18B). The relationship between the two fold orientations is unclear.

The granodiorite exposed to the east of the WBF was undeformed prior to faulting.

3:1:2:5 Fault zone structure southern side of the Ness of Haggrister

3:1:2:5a West of the WBF core

West of the WBFP, intense deformation associated with the WBFZ extends for approximately 150m into the Queyfirth Group rocks on the southern side of the Ness of Haggrister (Figure 3.16). At distances less than 150m west of the WBFP, the sub-vertical regional foliation is reoriented to strike almost N-S (Figure 3.19A) from NW-SE outside the WBFZ (Figure 3.18A). Regional fold axes appear to be aligned N-S (Figure 19B) and have tightened from open-tight outside the WBFZ to become locally isoclinal. Late-stage centimetre- to metre-scale folds first appear 140m west of the WBFP, and vary in style from sharply kinked to rounded closures with straight limbs. The fold axial planes strike NE-SW with hinges plunging moderately to the NE (Figure 3.19C). They consistently show a dextral sense of vergence.

Subsidiary faults containing centimetre-thick soft blue gouge and incohesive breccia first appear 120m west of the WBFP. The near-vertical gouge-filled faults strike N-S

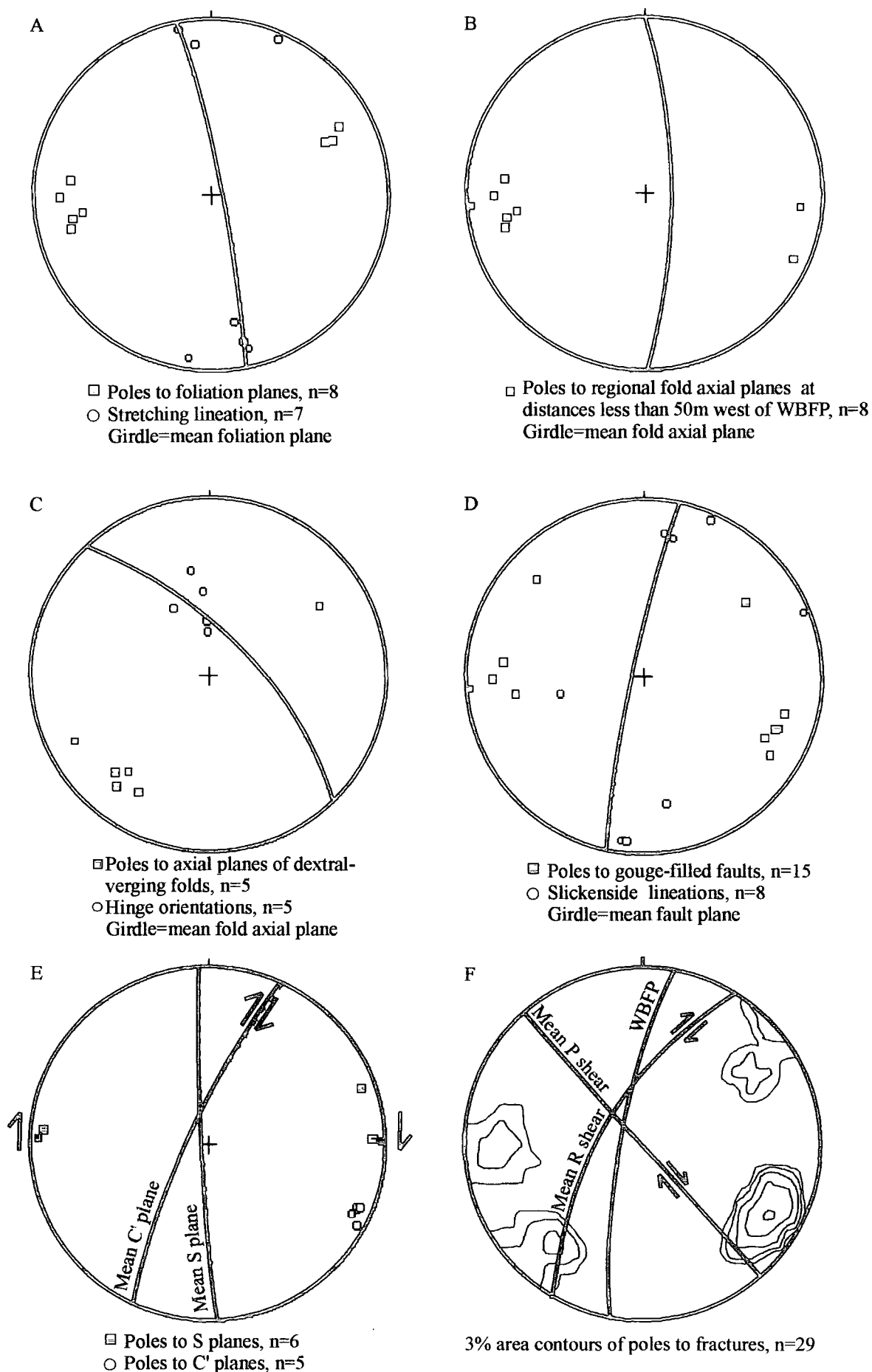


Figure 3.19 Stereonets of structural data collected within the WBFZ, west of the WBF core. (A) foliation and lineation within Queyfir Group rocks. (B) Regional fold axial planes. (C) Dextral-verging folds (D) Gouge-filled faults and slickenside lineations. (E) S-C' dextral shear fabrics from high strain zones. (F) Fractures with sub-horizontal slickenside lineations associated with N-S sub-vertical faults.

and contain mainly sub-horizontal slickenside lineations and fibres (Figure 3.19D). Sub-horizontal slickenfibres indicate dextral movements defined by the stepping of quartz fibres. The faults tend to localise within the more pelitic units and also along the steep limbs of rarely exposed regional folds. The mean spacing of the gouge-filled faults is approximately 5-10m where they sometimes form clusters or anastomosing networks. The faults generally increase in frequency to the east.

N-S-trending, brittle-ductile, high-strain zones develop within the pelitic-schists at distances less than 100m west of the WBFP (Plates 3.16, 3.17). Regional folds and foliation steepen into these high-strain zones which are typically 0.5m wide (Plate 3.16). Limestone- and quartz-rich units are boudinaged in a N-S trend and appear to 'float' in an anastomosing network of sheared pelite (Plate 3.16). In plan view, the regional foliation consistently swings into the shear zone in a clockwise direction (Plate 3.17). The high-strain zones comprise 25-50cm-thick, mica-rich shear zones that display well-developed S-C' fabrics consistent with dextral shear (Plate 3.17; Figure 3.19E). The shear zones are irregularly distributed between distances of 50m to 100m west of the WBFP, where they are cross-cut by gouge-filled faults and broad zones of brecciation.

At distances of less than 50m west of the WBFP, faulting and cataclasis is so intense that earlier shear zones and structures are largely unrecognisable. Foliation parallel (N-S) faults commonly branch into networks of sub-vertical fractures that contain sub-horizontal slickenside lineations. The fractures form three main clusters (Figure 3.19F), NW-SE, NE-SW and N-S. NE-SW-striking fractures display dextral strike-slip offsets of 5-30cm and are interpreted as R-type Riedel shears. NW-SE-trending fractures develop along the axial planes of dextral verging kink folds and display dextral strike-slip displacements of 5-30cm. These fractures are interpreted as P-type Riedel shears. The geometric configuration of R- and P-type Riedel shears is consistent with an overall dextral sense of shear for the WBF (Figure 3.20).

10 m west of the WBFP, intensely fractured and brecciated schists and limestones grade into a zone of cataclasites adjacent to the WBF core. The pale grey cataclasites are isotropic on all scales of observation in the field, although N-S-trending calcite veins are very common. In thin-sections cut parallel to sub-horizontal slickenside



Plate 3.16 Photograph looking north into high-strain zone (arrow) 90m west of the WBFP on the south side of the Ness of Hagggrister.

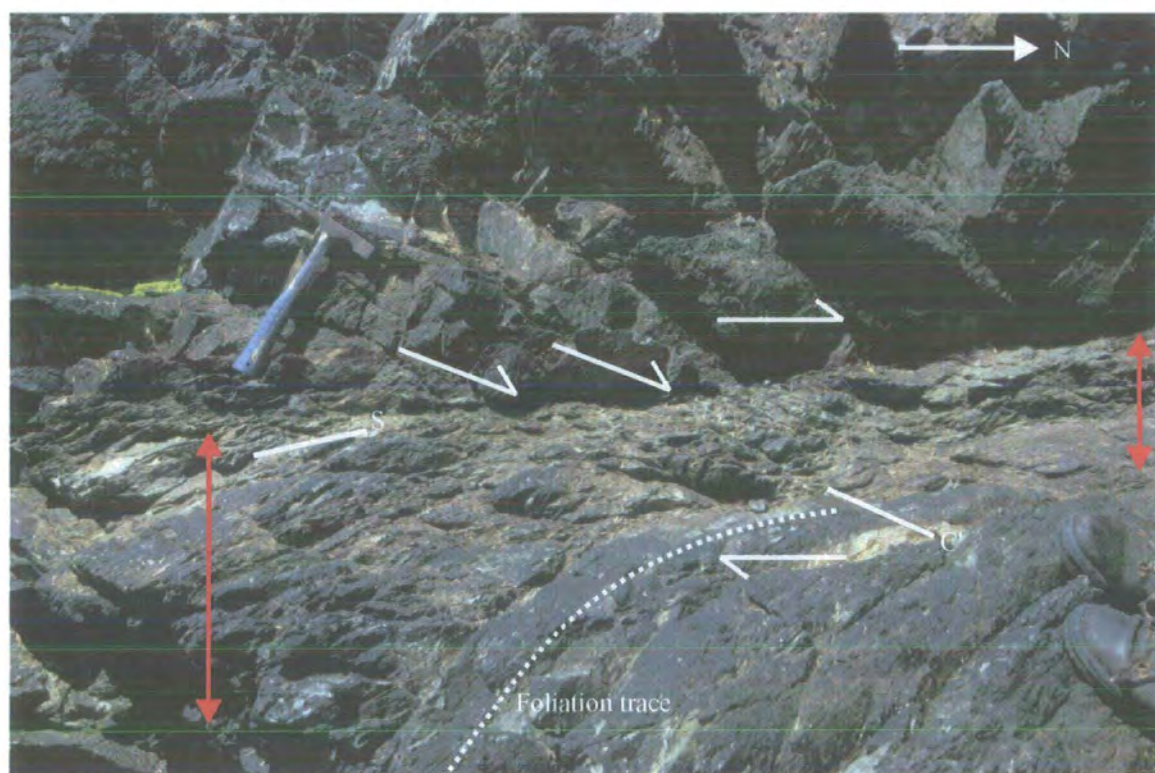


Plate 3.17 Plan view photograph of shear zone 90m west of the WBFP on the south side of the Ness of Hagggrister. Note - the clockwise rotation of the foliation into the shear zone indicating a dextral sense of shear and the dextral shear bands within the 30cm-wide shear zone (split arrows). Red arrows mark the width of the shear zone. S - S-plane, C' - C'-plane.

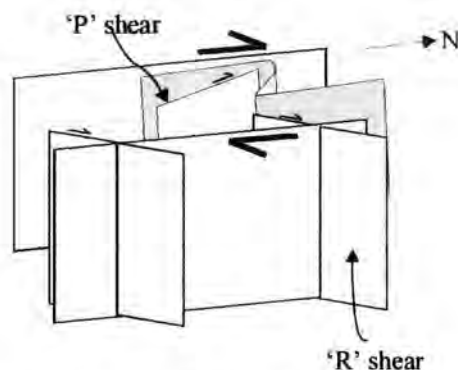


Figure 3.20 Schematic diagram to illustrate the geometrical configuration of P- and R-type Riedel shears (Figure 3.19F), which is consistent with an overall dextral sense of shear for the WBFZ.

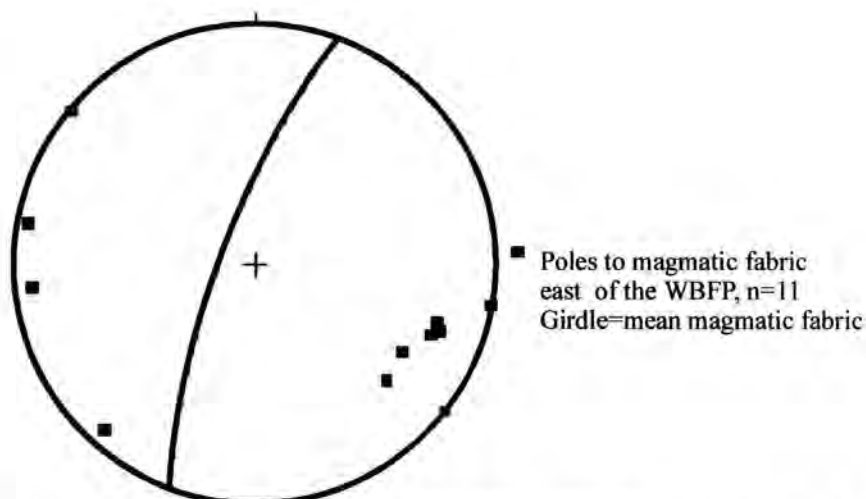


Figure 3.21 Stereographic projection to show the magmatic fabric within the granodiorite east of the WBFZ on the south side of the Ness of Haggister.

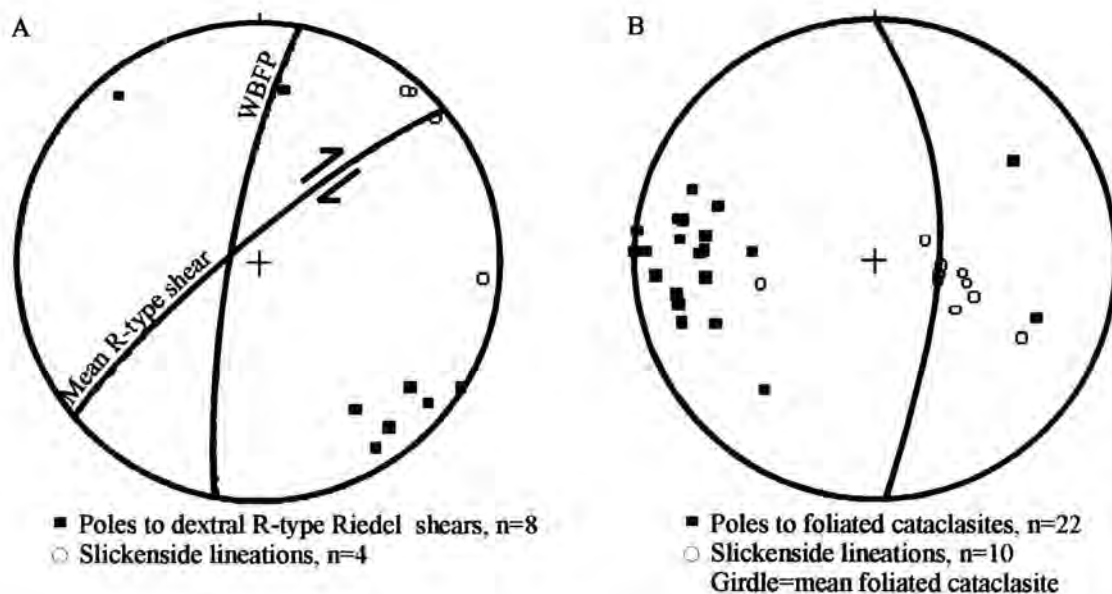


Figure 3.22 Stereographic projections of structural data collected east of the WBF core on the south side of the Ness of Haggister. (A) R-type Riedel shears which displace pegmatites dextrally. (B) Anastomosing foliated cataclasites.

lineations and perpendicular to the WBFP, N-S-trending fractures show apparent, dextral, millimetre-scale offsets of iron-stained stylolites.

3:1:2:5b East of the WBF core

Fault-related deformation extends for at least 300m east of the WBFP into the poorly exposed granodiorite of the Devonian Graven Complex. 250m east of the WBFP (HU 3549 7004), epidote, quartz and chlorite veins several millimetres thick cross-cut the weak N-S-striking magmatic fabric (Figure 3.21) defined by aligned feldspar phenocrysts. Here the granodiorite is moderately fractured. Sub-vertical, NE-SW-trending fractures with sub-horizontal slickenside lineations (Figure 3.22A) display dextral strike-slip offsets of pegmatite sheets of 2-30cm, and are interpreted as R-type Riedel shears (Plate 3.18). Less common WNW-ENE-trending fractures display sinistral strike-slip offsets of pegmatite veins of 2-10cm, and are interpreted as R'-type Riedel shears. The fractures are filled by millimetre-thick crystalline aggregates of epidote and quartz.

At distances between 100m and 40m east of the WBFP, cataclasites range from 2mm to 3cm in thickness. The cataclasites strike N-S and dip steeply to the E (Figure 3.22B) with slickenside lineations that plunge steeply to the E. Quartz and epidote slickenfibres step down-dip, indicating dip-slip normal movements. Green cataclasites are mica-rich with millimetre-scale quartz and epidote veins nucleating off the cataclasites. The cataclasites contain a N-S-trending foliation defined by aligned mica grains and are stained red in places due to the effects of iron mineralisation (Plate 3.19). Centimetre-scale cataclasites bifurcate into several strands surrounding enclaves of relatively undeformed granodiorite up to 30cm in length (Plate 3.19). It is unclear how many or how closely spaced the foliated cataclasites are, due to the poor level of exposure.

At distances less than 40m west of the WBFP, cataclasis is intense. Intensely fractured granodiorite grades into green/ brown-coloured cataclasite, which attains a thickness of 10m adjacent to the red gouge within the fault core. Cataclasite is isotropic on all scales of observation in the field.

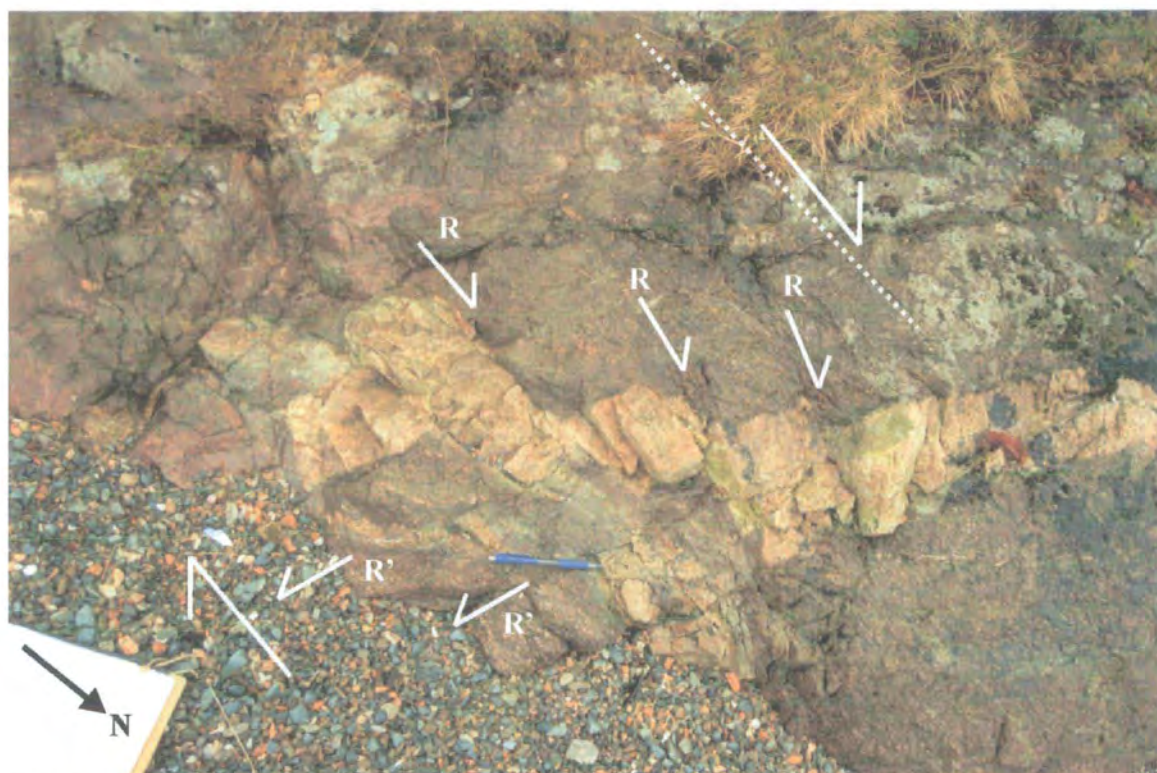


Plate 3.18 Plan view. Pegmatite dyke (HU 3549 7004) cross-cut by R- and R'-type Riedel shears with dextral and sinistral strike-slip offsets, suggesting an overall dextral sense of shear. Dashed line is the trend of the WBFP.

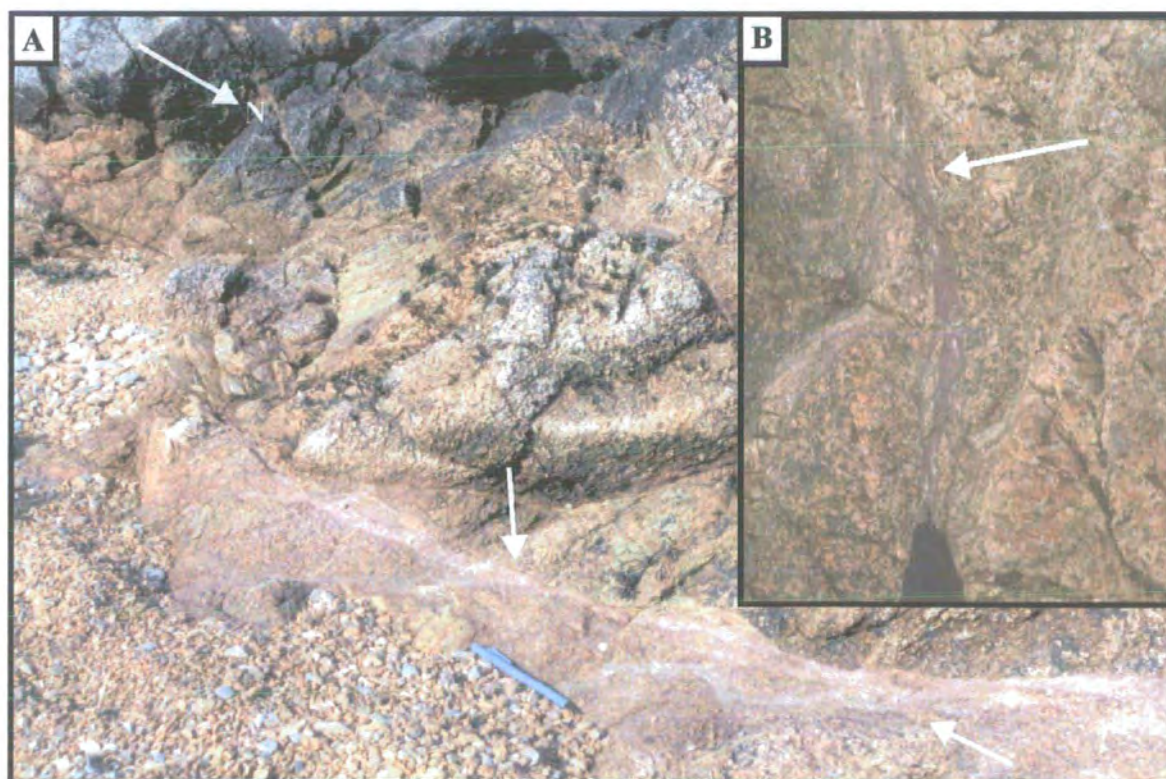


Plate 3.19 (A) Photograph of horizontal surface to show a network of red-coloured foliated cataclasites (HU 3527 6990). Arrows indicate where cataclasites bifurcate. (B) Photograph looking north to show foliated cataclasite geometry in cross-section. Arrow indicates where cataclasites link together.

3:1:2:5c WBF Core

Cataclasites overprint the calcareous schists (west of the WBFP) that contain a well-developed dextral shear fabric. Fault-parallel veins of calcite 1mm to 1cm thick are common and consistently show dextral strike-slip displacements across them. Anastomosing centimetre-thick gouges cross-cut the cataclasites (Figure 3.17; see section 3:1:2:3c). The gouges commonly lie adjacent to polished fault surfaces that contain sub-horizontal quartz slickenfibres, which consistently show a dextral sense of shear. Braided networks of sub-vertical fractures strike NE-SW and dip steeply to the NW (Figure 3.23A). The fractures contain sub-horizontal slickenside lineations and form networks along which dextral offsets of 1cm to 30cm can be measured. The fractures lie clockwise to the WBFP and are interpreted as R-type Riedel shears formed as a result of dextral strike-slip movement along the WBF.

Cataclasites derived from Queyfirth Group schists (west of WBFP) are cut by a soft blue gouge that lies in a zone adjacent to the WBFP. The blue gouge contains a sub-vertical N-S-trending foliation with lineations defined by aligned clay particles, which plunge shallowly to the S (Figure 3.23B). In surfaces viewed perpendicular to the WBFP and parallel to the lineation centimetre-scale shear bands within the blue gouge indicate dextral shear. In cross-section, W-dipping shears containing dip-slip lineations (Plate 3.14; Figure 3.23C) defined by the alignment of clay particles cross-cut the dextral shear band fabric. East of the WBFP, the banded red gouge contains sub-horizontal lineations. In thin-sections cut parallel to the lineation and perpendicular to the WBFP, millimetre-scale shear bands, together with anastomosing fractures within the red gouge, display a dextral sense of shear. The shear bands are cut by ENE-WSW tensional fractures (filled with calcite) and discrete NW-SE fractures showing an apparent sinistral shear (Figure 3.23E).

The actual WBFP appears to separate fault rocks derived from Queyfirth Group calcareous schists from those derived from granodiorite (Figure 3.17). Sub-horizontal quartz slickenfibres, which plunge shallowly to the N (Figure 3.23D), indicate sinistral strike-slip movements based upon the stepping direction of the quartz mineral fibres. The WBFP is the main structural boundary within the WBFZ and appears to correspond to the surface along which the last regionally significant movement took

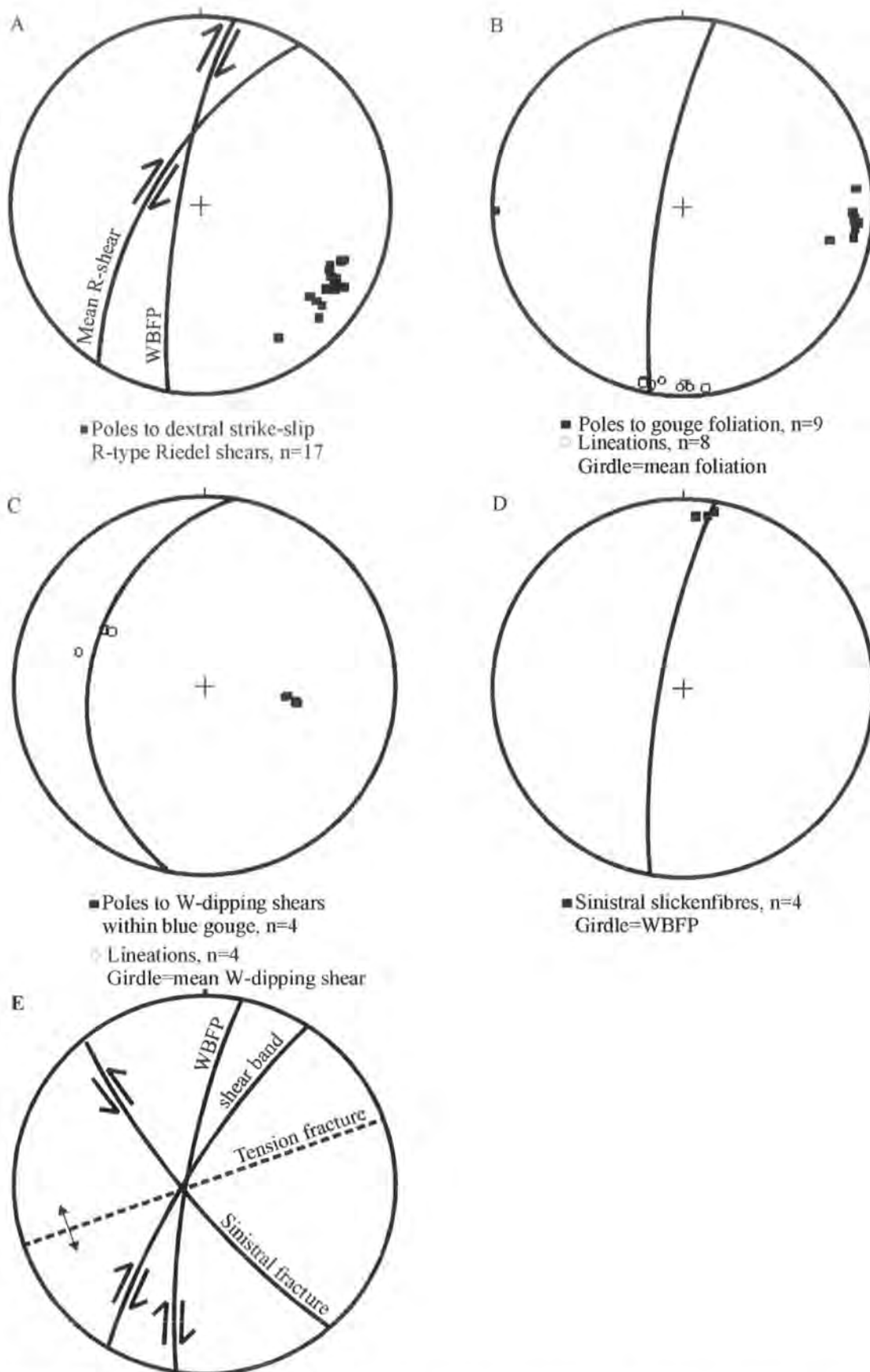


Figure 3.23 Stereographic projections showing (A) Dextral strike-slip fractures interpreted as R-type Riedel shears. (B) Blue gouge foliation and lineation. (C) W-dipping shear fabric within blue gouge. (D) Sinistral quartz slickenfibres on WBFP. Data collected from the WBF core on the south side of the Ness of Hagggrister. (E) The geometrical arrangement of shear bands, tension fractures and NW-SE fractures (R'-type Riedel shear) with apparent sinistral offsets within the banded red gouge, which is consistent with dextral shear.

place. The red gouge cross-cuts red / brown cataclasite (east of the WBFP) derived from granodiorite (see section 3:1:2:3c). The red / brown cataclasites are isotropic and show no fabric on all scales of observation in the field.

3:1:2:6 Fault rock distribution and age relationships, north of the Ness of Haggrister

North of the Ness of Haggrister, the WBFZ and associated fault rocks are commonly poorly exposed. The WBFP separates granodiorite of the Devonian Graven Complex to the east from slivers of cataclasite, mylonite, hornblende gneiss, albitic gneiss and schists (Figure 3.16). The exposures west of the WBFP are important, as they preserve mylonites not generally found elsewhere within the WBFZ.

3:1:2:6a West of the WBFP

West of the WBFP, mylonites crop out along the coast on the west side of Sullom Voe from South House (HU 3524 6997) to the Houb of Lunnister (HU 3523 7193) and from Marki Ness (HU 3549 7205) to Gaza (HU 3552 7262) within fault-bounded blocks up to 300m wide (Figure 3.16). Mylonitic series rocks are best exposed at Lunnister (HU 3530 7140). To the south, mylonites (section 3:1:2:2a) are intercalated with compositionally banded gneiss (section 3:1:2:1c). The mylonites and gneisses are variably affected by later cataclasis and folding and are cross-cut by extensive vein networks. To the north, mylonites are poorly exposed at Marki Ness and farther north where they are interleaved with gneiss and are intensely deformed by cataclasis.

At Lunnister (HU 3530 7140), the rocks comprise alternating layers of mylonite and ultramylonite 5-75cm thick (Figure 3.24). Quartzo-feldspathic mylonites (pink / grey) are locally interbanded with hornblende-rich mylonites (blue / grey) (Figure 3.24). Mylonites further to the south and north of Lunnister are interlayered on a metre-scale with compositionally banded gneiss (hornblende-rich and quartzo-feldspathic). Locally, the rocks display a gradation from gneissose to protomylonitic textures, suggesting that the protoliths to the two types of mylonite were the compositionally banded gneisses comprising hornblende-rich and quartzo-feldspathic units (see

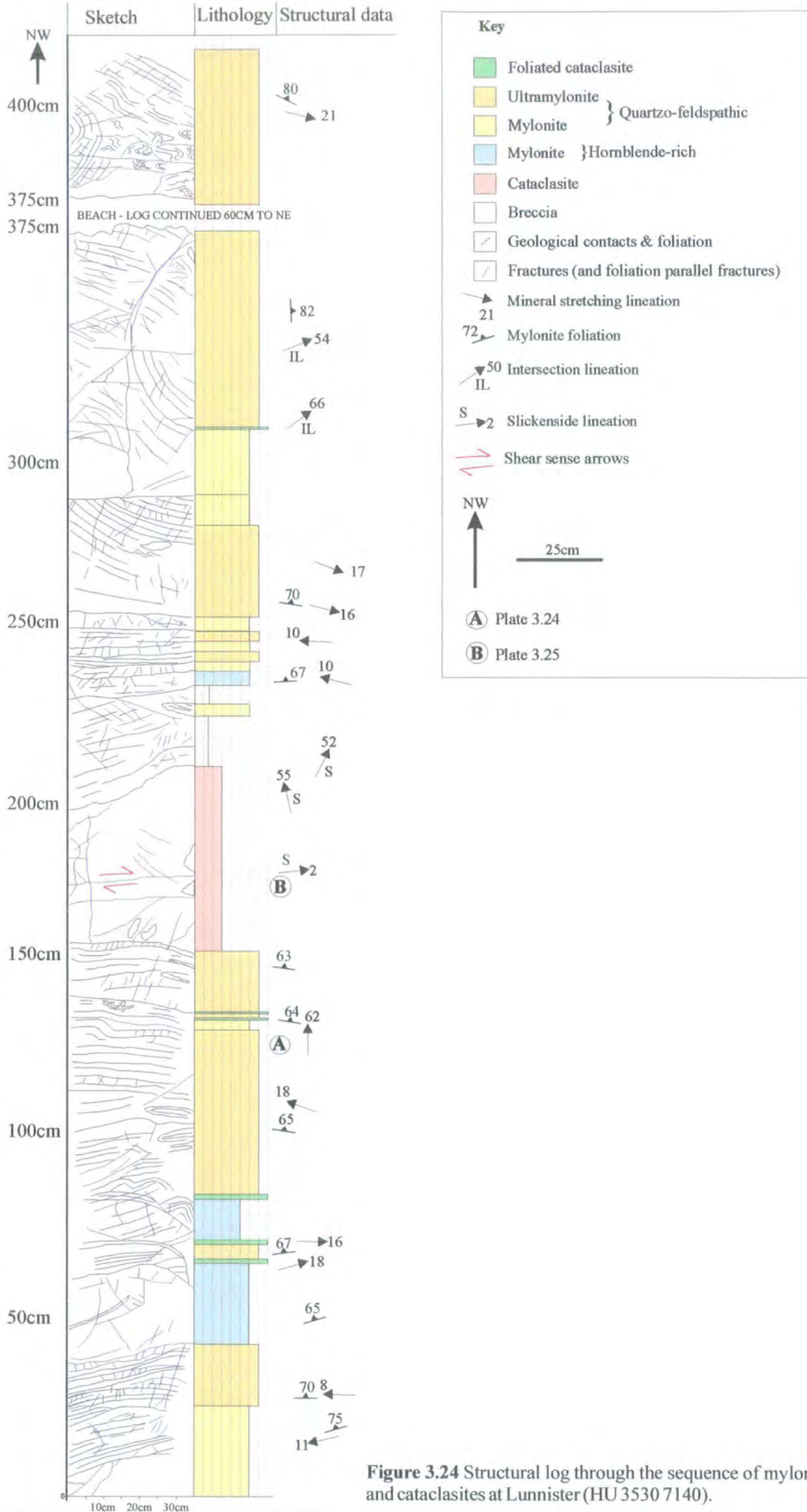


Figure 3.24 Structural log through the sequence of mylonites and cataclasites at Lunnister (HU 3530 7140).

section 3:1:2:1c). Green-coloured, mica-rich cataclasites 1mm to 1cm thick occur at the contacts between ultramylonites and mylonites (Figure 3.24). The cataclasites contain a foliation defined by aligned aggregates of mica. In thin-section, at some of the ultramylonite / mylonite contacts, millimetre-thick and highly altered pseudotachylite veins are present.

Cataclastically deformed rocks cross-cut and develop along the mylonitic foliation. The rocks comprise an outer zone of intensely fractured mylonite and breccia, which grades into a central unit of cataclasite ranging from 1mm to 75cm in thickness (Figure 3.24). The cataclasites contain randomly orientated clasts (0.1mm to 10cm in size) of mylonite, quartz, feldspar, hornblende and mica set within a fine-grained cataclastic matrix of the same. NNE-SSW- to NE-SW-orientated fractures containing millimetre-thick gouges transect the cataclasites and mylonites.

To the south of Lunnister, exposure is poor. Mylonites are interleaved on a metre-scale with compositionally banded gneiss. The rocks are intensely fractured and cut by centimetre- to millimetre-thick veins composed of calcite, quartz, epidote, albite and scapolite. Vein networks develop that are so intense that they form a matrix to breccias. Cataclasites again form sub-parallel and parallel to the mylonitic foliation and, in places, to the gneissose foliation. Pale grey cataclasites contain a N-S-orientated colour banding defined by variations in the clast-to-matrix ratio and hematite-rich bands, which locally acts as a cement. The pale grey cataclasites cross-cut mylonites and 'earlier' cataclasites. These cataclasites range in thickness from 1mm to 50cm. There are no cross-cutting relationships preserved between the 'later' cataclasites and gouge-filled faults. Both locally contain hematite cement and appear to have been formed under the same kinematic regime (see below), suggesting that they are broadly the same age.

To the north of Lunnister, exposure is very poor. Extensive cataclasis, N-S gouge-filled faults together with quartz, calcite, epidote and scapolite veining overprint slivers of banded gneiss, mylonite and calcareous schist.

3:1:2:6b East of the WBFP

East of the WBFP trace on the north side of the Ness of Haggriester and at Sullom, exposure is very poor. Along the north side of the Ness of Haggriester near the WBFP trace (HU 3535 7077), extensive cataclasis and gouge overprint the protolith granodiorite. At Sullom, patchy exposures of intensely fractured granodiorite are present along the coast (HU 3571 7298).

3:1:2:7 Fault zone structure north of the Ness of Haggriester

3:1:3:6a West of WBFP

To the west of the WBFP and along the western side of Sullom Voe mylonites, banded gneiss and calcareous schists occur within fault-bounded slices. Banded gneiss is cross-cut by rarely exposed, N-S-trending dolerite dykes (Figure 3.16). Mylonites are best preserved at Lunnister and to the south and north along the coast (Figure 3.16). The sub-vertical mylonite foliation is defined by stretched and flattened quartz, feldspar, mica and hornblende and appears to change orientation on a scale of tens of metres. Poles to the mylonite foliation planes lie along a girdle (047/23S) with the pole to the girdle or β axis plunging 67° towards 317° (Figure 3.25A). This suggests that the mylonitic foliation is folded by NW-SE-trending structures on a scale of tens of metres, with the mean hinge orientation plunging steeply to the NW ($67/317$) (Figure 3.25B). Centimetre to metre-scale folds with this orientation are present, with sharply-kinked to rounded closures and straight limbs. They consistently show a dextral sense of vergence (Plate 3.20). Fold axial planes strike NW-SE and dip steeply to the NE (Figure 3.25B). The fold hinge orientations of the centimetre to metre-scale dextral-verging folds are almost parallel to the β axis of the structures that fold the mylonitic foliation, and it is therefore suggested that the mylonite foliation is folded by a series of sub-vertical NW-SE-trending centimetre to tens of metre-scale folds, with dextral vergence and steep NW plunges. Mylonite lineations defined by stretched quartz, feldspar, hornblende and mica are sub-horizontal and vary in orientation due to the effects of later folding (Figure 3.25A).

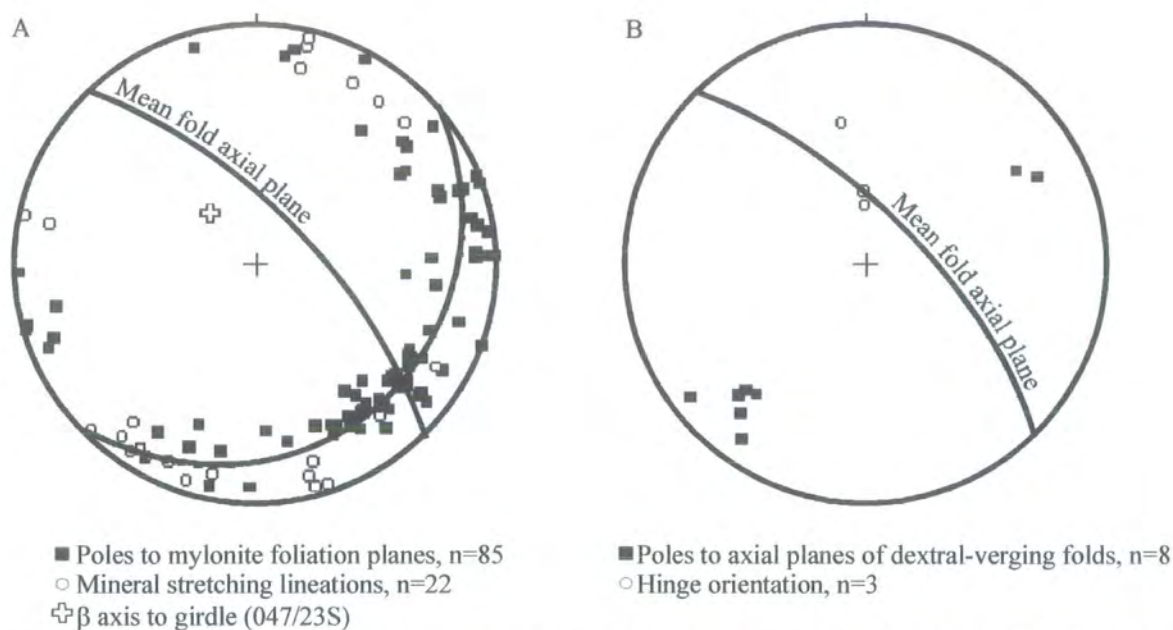


Figure 3.25 Stereographic projections showing (A) mylonitic foliation and mineral stretching lineation and (B) dextral-verging folds. Data collected from South House (HU 3524 6997) to the Houb of Lunnister (HU 3523 7193) and from Marki Ness (HU 3549 7205) to Gaza (HU 3552 7262).

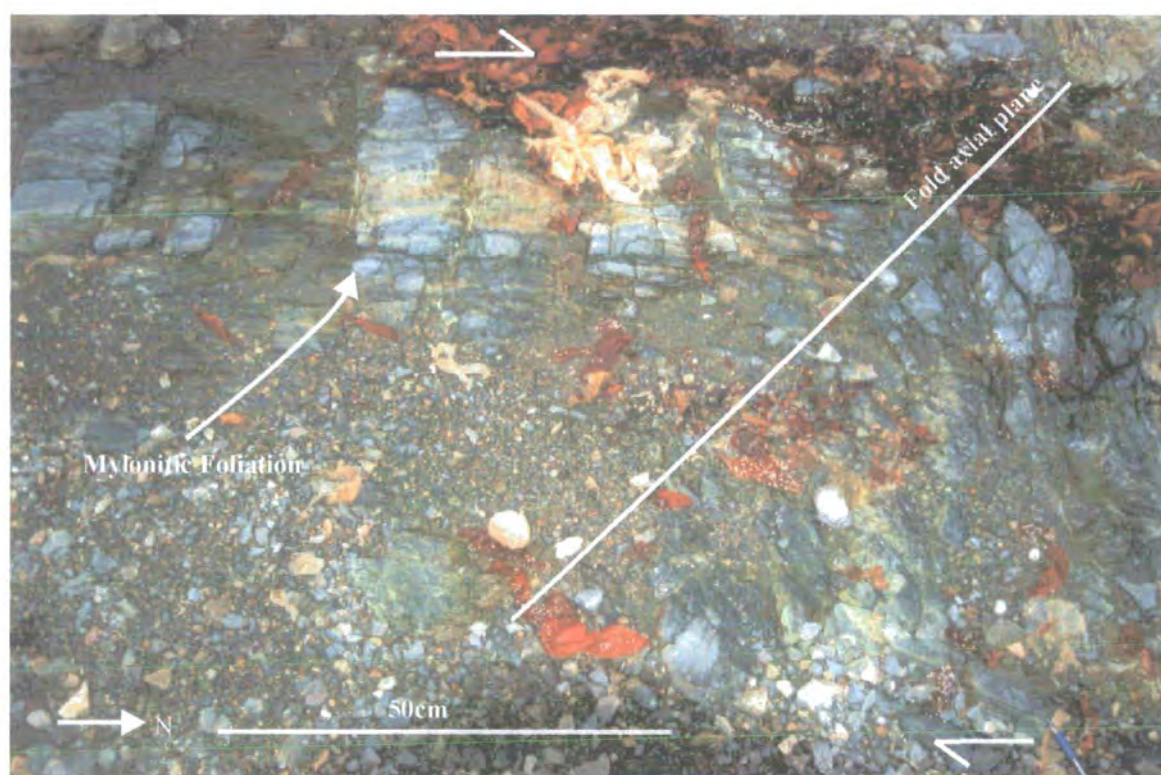


Plate 3.20 Plan view. Photograph to show the style of a dextral-verging kink fold, south of Lunnister (HU 3528 7134).

To the south of Lunnister, the rocks are poorly exposed, but display an increase in cataclasis to the south. Centimetre- to metre-scale cataclasites are developed parallel to the mylonitic and, in places, gneissose foliation. Once again, the mylonites, cataclasites and gneisses are transected by NE-SW-trending, steeply-plunging centimetre to tens of metre-scale folds (Figure 3.25B), which consistently show dextral vergence. Tension gashes infilled with calcite strike 070° , suggesting a NNW-SSE to NW-SE extension direction and an overall dextral sense of shear. N-S-trending, pale cataclasites cross-cut mylonites, 'early' cataclasites and gneisses. In thin-section, the pale cataclasites comprise comminuted fragments of mylonite, gneiss, cataclasite, feldspar and quartz together with scapolite and calcite vein material set within a fine-grained cataclastic matrix that has been altered to a clay-rich isotropic paste. The cataclasites show a centimetre-scale colour banding defined by variations in the proportion of clast-to-matrix ratio (Plate 3.21). N-S-trending millimetre- to centimetre-thick hematite veins locally act as cement. The iron-stained cataclasite zones widen with the development of braided networks of sub-vertical Riedel-type fractures, which strike NE-SW and contain sub-horizontal slickenside lineations (Figure 3.26). The fractures are interpreted as R-type Riedel shears with dextral strike-slip offsets of the mylonitic foliation of between 2 to 20cm (Plate 3.22). This configuration is consistent with dextral shear along the N-S-trending WBF. Millimetre-scale vein networks of calcite, epidote and quartz generally nucleate off the cataclasite seams. Carbonate veining is locally intense and is commonly associated with zones of cataclasis (Plate 3.23). In places, the veins display a pull-apart geometry indicating a dextral sense of shear.

From Marki Ness (HU 3549 7205) and farther north (Figure 3.16), exposure is extremely poor. In the few exposures, broad zones of intense cataclasis overprint mylonites and gneiss. The cataclasites are structureless and contain no fabric or banding on all scales of observation in the field.

The best-exposed mylonites and cataclasites are at Lunnister (HU 3530 7140). There, the mylonitic foliation, defined by flattened and stretched aggregates of quartz, feldspar, mica and hornblende, is well-developed. The foliation strikes NE-SW and dips steeply to the NW (Figure 3.27A) with mineral stretching lineations defined by stretched and elongate grains plunging shallowly to the NE and SW (Figure 3.27A).

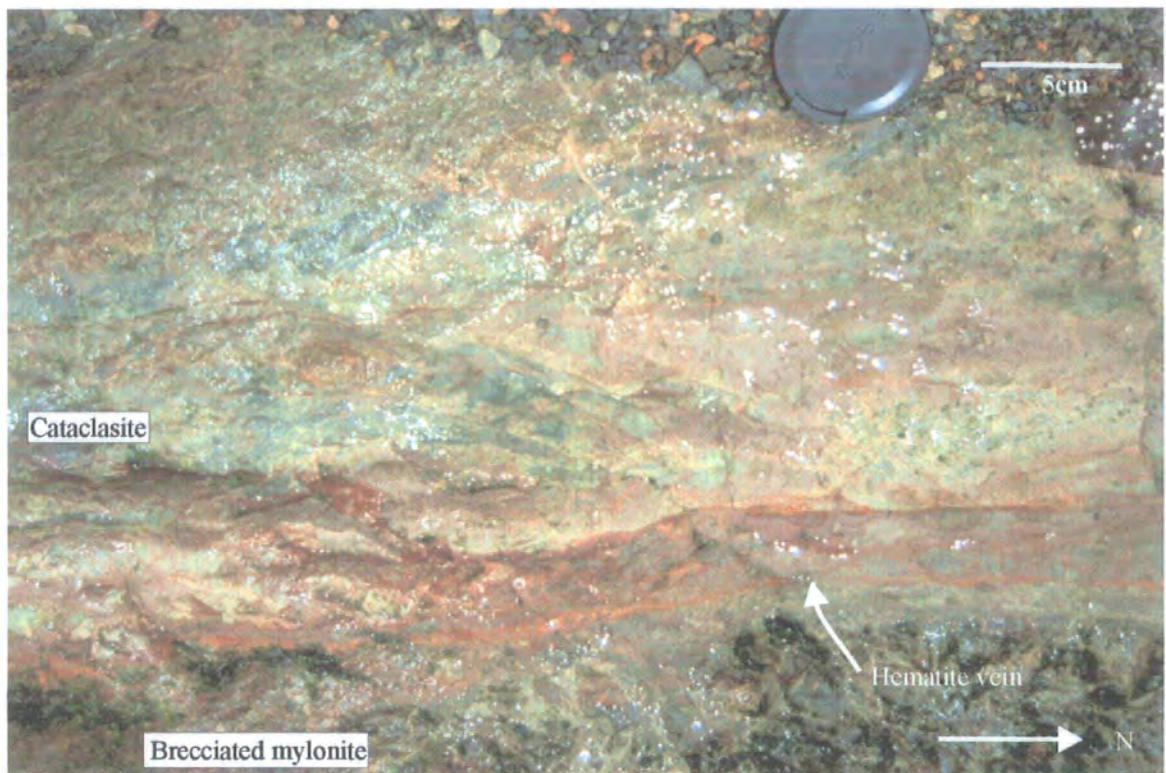


Plate 3.21 Plan view. N-S-orientated pale cataclasite containing bands of hematite which, in places, form small-scale vein networks (HU 3528 7132).

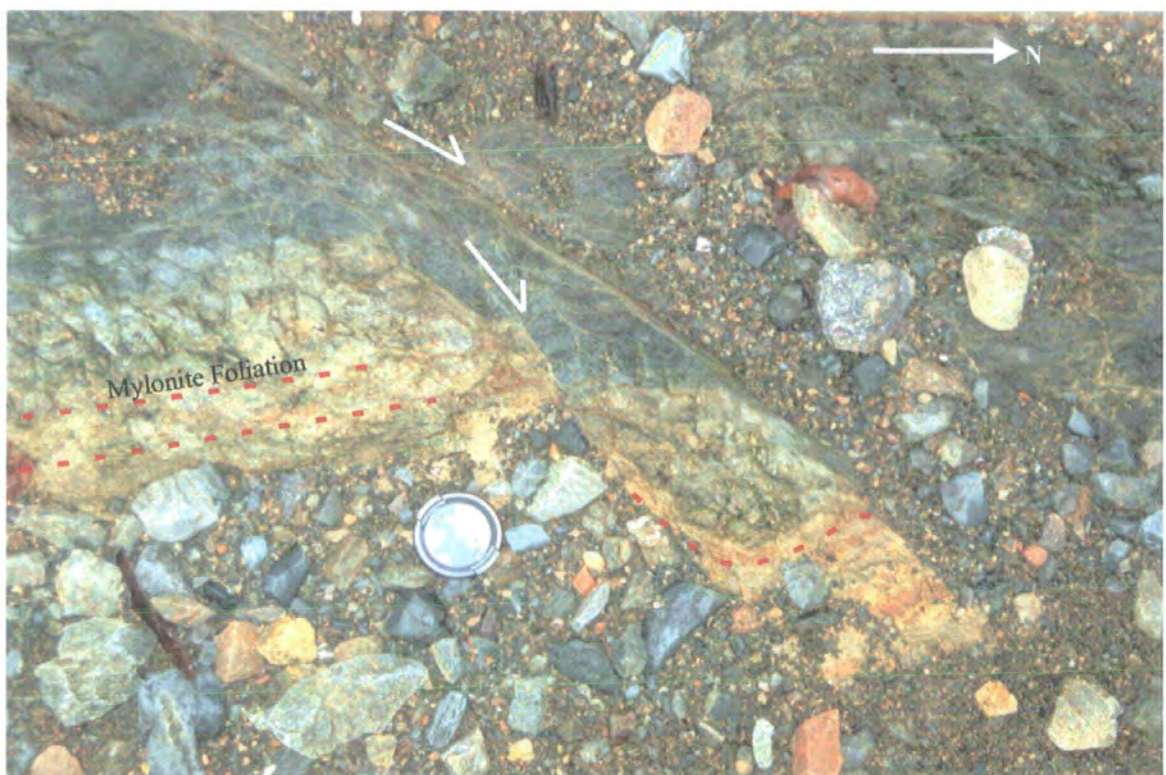


Plate 3.22 Plan view. Brecciated mylonite cross-cut by dextral strike-slip R-type Riedel shears containing pale grey cataclasite and hematite mineralisation (HU 3528 7132).

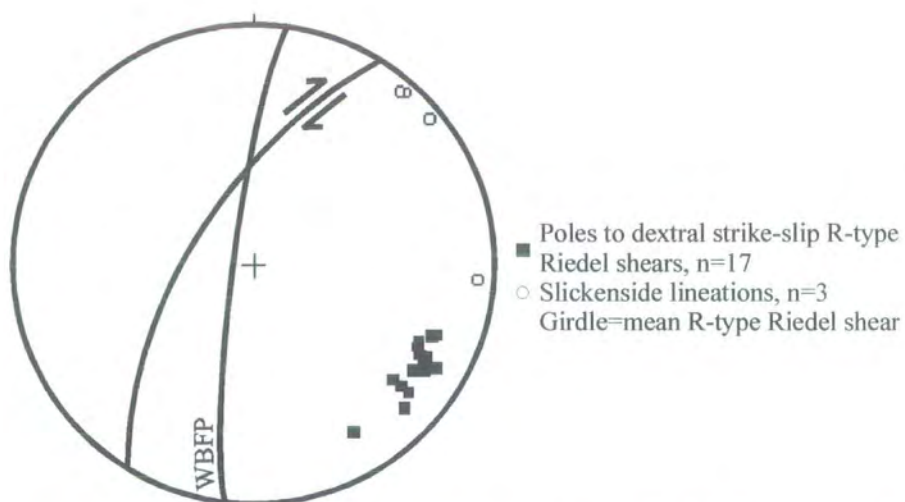


Figure 3.26 Stereographic projection to show the orientation of R-type Riedel shears containing pale, hematite-mineralised cataclasites with sub-horizontal slickenside lineations.



Plate 3.23 Plan view. Carbonate vein networks overprinting a gneissose fabric with the local development of cataclasis (C) (HU3523 7100).

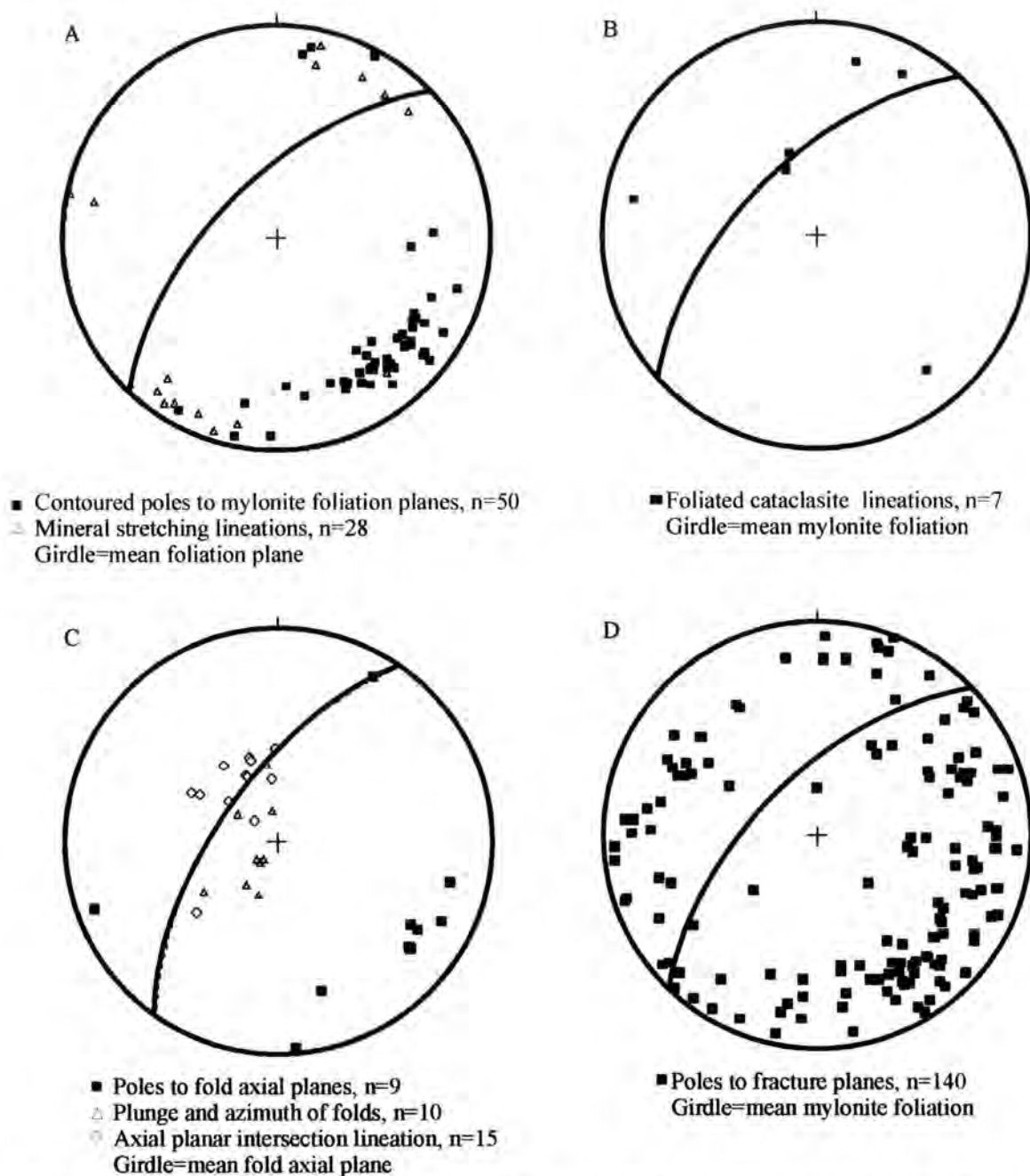


Figure 3.27 Stereographic projections showing of structural data from Lunnister. (A) Mylonitic foliation and mineral stretching lineations, (B) Mineral lineations within foliated cataclasites, (C) Fold axial planes and hinge orientations of folds with a dextral sense of vergence, along with intersection lineations of axial planar fabric on foliation planes, (D) Fracture planes.

The mylonite foliation wraps around porphyroclasts of feldspar and hornblende typically 1mm to 5mm in length. Porphyroclasts display well-developed σ - and δ -type geometries, which indicate consistently a sinistral sense of shear on outcrop surfaces and in thin-sections viewed normal to the foliation and parallel to the mineral lineation (Plate 3.24). Locally, within the more micaceous units, a well-developed S-C' fabric indicates a sinistral sense of shear when viewed in thin-sections cut parallel to the lineation and normal to the foliation (Plate 3.25). Rare σ - and δ -type porphyroclasts are present which suggest a dextral sense of shear. These are much less common and occur near boundaries between ultramylonite and mylonite, suggesting that they may develop due to relative differences in strain rate or perhaps a component of coaxial flow. In places, the mylonites are isoclinally folded on a centimetre-scale with axial planes parallel to the ultramylonite and mylonite foliation (Plate 3.26).

Green-coloured, micaceous-rich cataclasites 1mm to 1cm thick occur at the contacts between ultramylonites and mylonites (Figure 3.24). They are foliated and contain a range of lineations from sub-horizontal to dip-slip (Figure 3.27B). Cataclasites (1mm to 75cm thick) cross-cut (Figure 3.24) and also develop parallel to the mylonite foliation. The cataclasites contain randomly orientated clasts of mylonite, quartz, feldspar and hornblende set within a cataclastic matrix of the same. The cataclasites form linked zones of foliation-parallel faults and cross-cutting linking structures. Surfaces containing slickenside lineations and other kinematic indicators within the cataclasite are rare. N-S-orientated fractures containing millimetre-thick gouges cross-cut all other structures within the damage zones and adjacent mylonites. The surfaces of the fractures contain sub-horizontal slickenside lineations, along which dextral strike-slip offsets of cataclasites up to 30cm can be measured (Plate 3.27).

A metre-scale fold (Figure 3.24, above 250cm) that displays a dextral sense of vergence has deformed the whole sequence of mylonites and foliation-parallel cataclasites at Lunnister. The fold is cut by N-S fractures containing fault gouge. Axial planes of the dextrally verging folds strike NE-SW and dip steeply to the NW, with their fold hinges plunging steeply to the NW (Figure 3.27C). The dextral folding has led to the development of a weak axial planar fabric and intersection lineation on the surface of foliation planes.

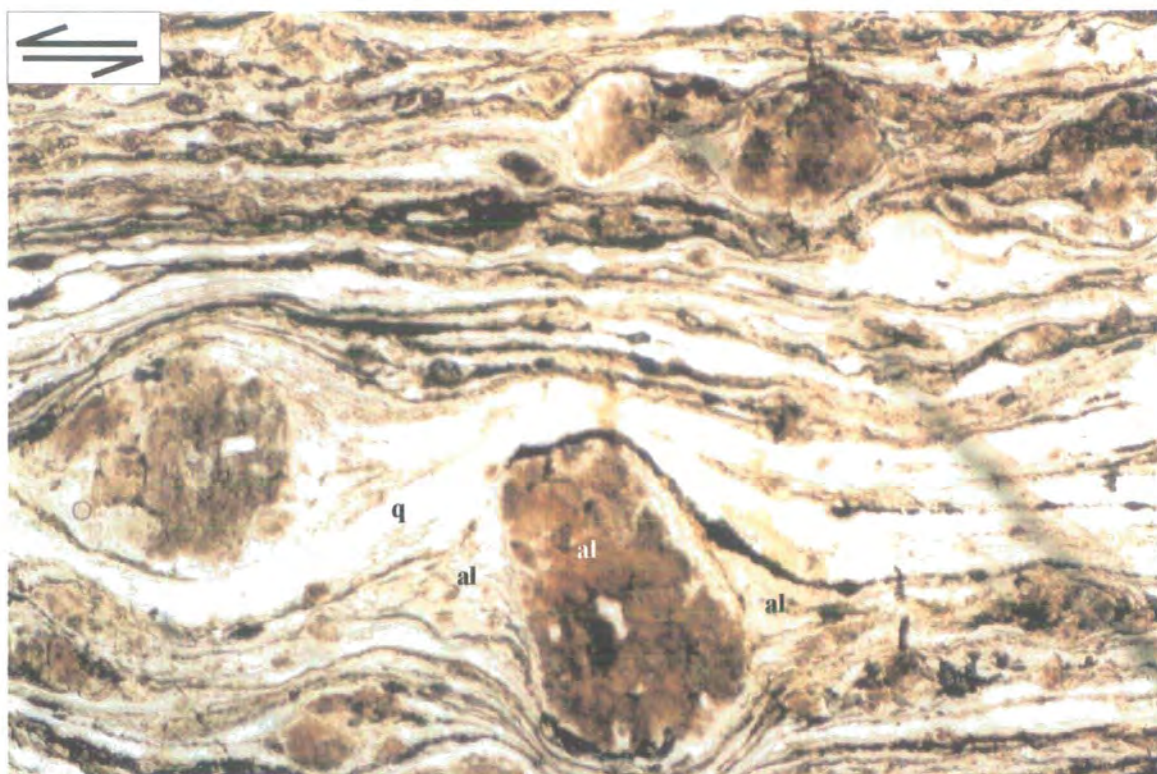


Plate 3.24 Photomicrograph to show mylonite from Lunnister containing albite (al) porphyroclast displaying a σ -type geometry with tails of fine-grained recrystallised albite (al), quartz (q) and sericite indicating sinistral shear. Split arrows indicate shear sense parallel to the lineation. Field of view 3.6 x 2.4mm, plane-polarised light.

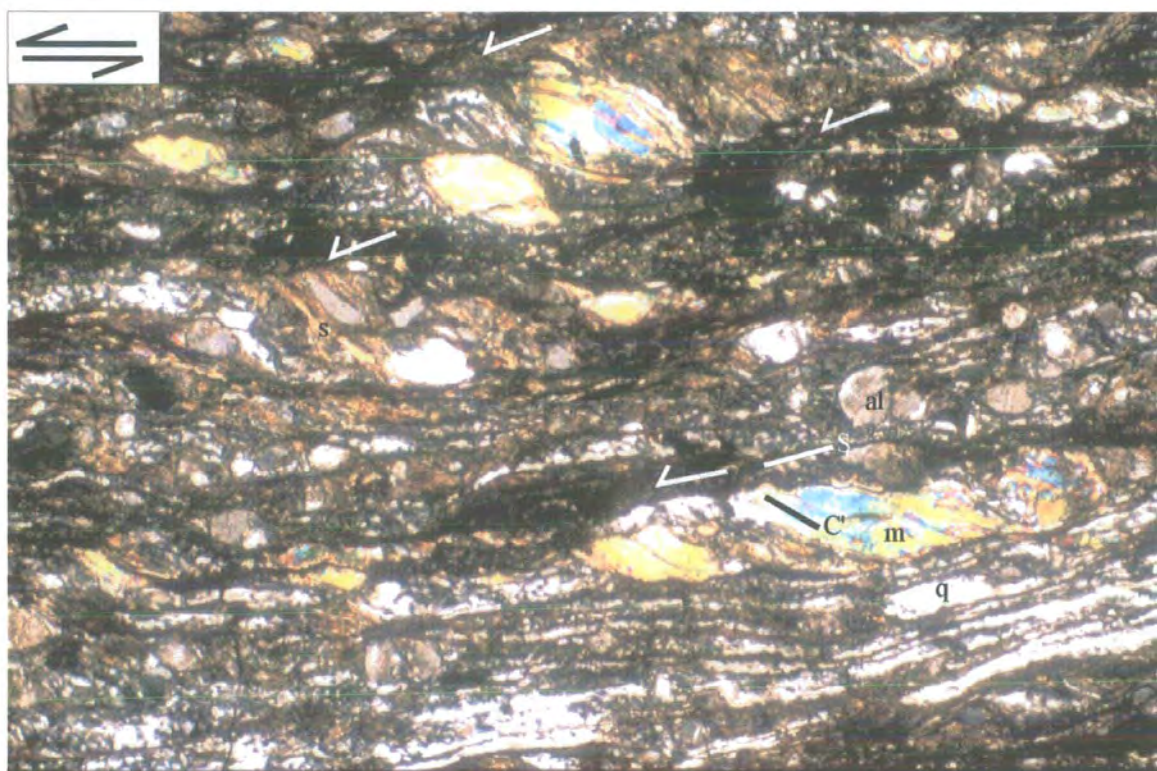


Plate 3.25 Photomicrograph of mica-rich mylonite from Lunnister displaying millimetre-scale S-C' fabrics indicating a sinistral sense of shear. m-muscovite, q-quartz, al -albite, s-fine-grained sericite. Split arrows indicate shear sense parallel to the lineation. Field of view 3.6 x 2.4mm, crossed polars.

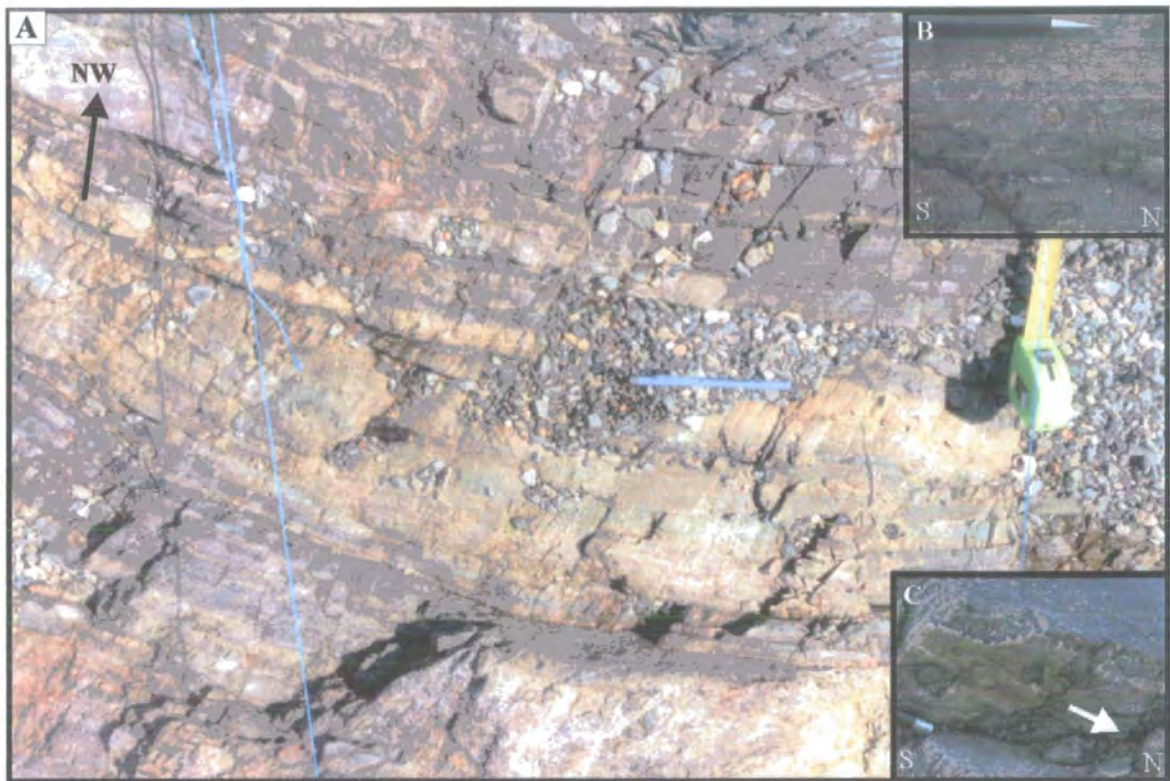


Plate 3.26 Photograph (A) showing ultramylonite fabric (A on Figure 3.24) and inset, (B) showing mylonite fabric with feldspar porphyroclasts, and (C) mineral stretching lineation defined by quartz plunging shallowly to the N.

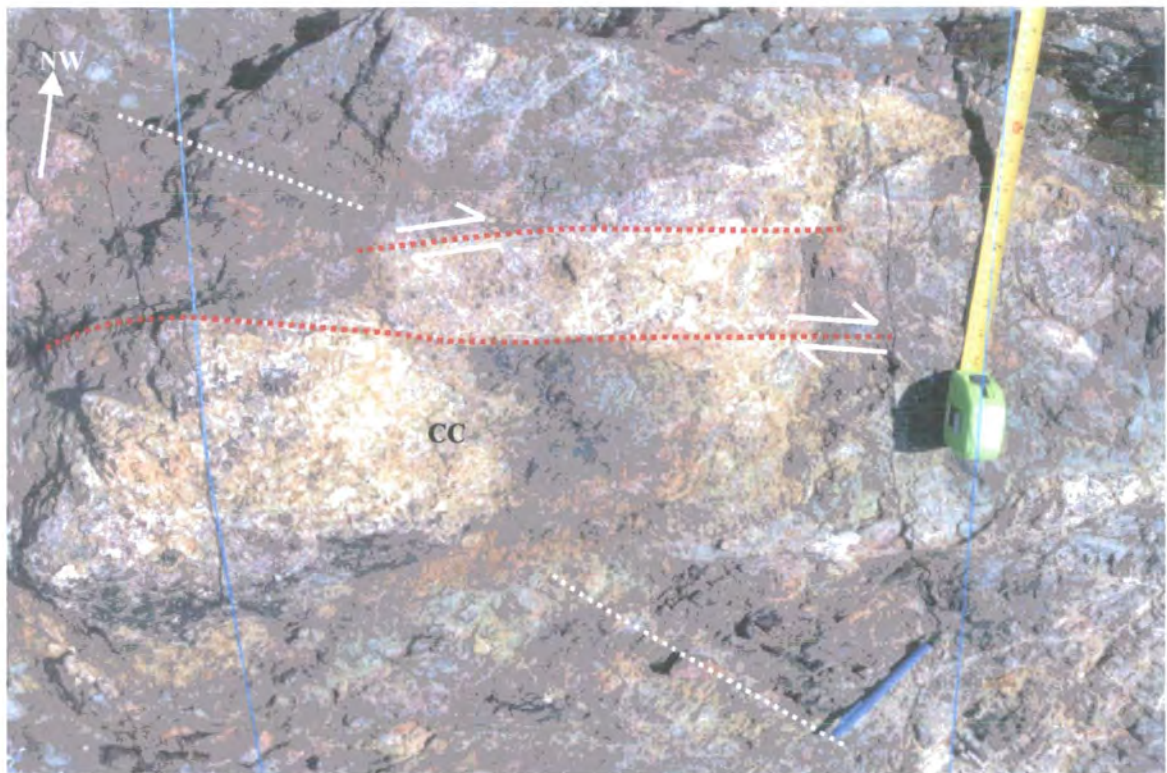


Plate 3.27 Photograph (B on Figure 3.24) N-S-orientated gouge-filled fractures (red dashed lines) cross-cutting cataclasite (CC), displaying a dextral strike-slip (shear arrows) displacement of 25cm. White dashed lines represent the mylonite foliation, which is cut by cataclasite.

The intersection lineations are best developed close to the fold closures where the axial planes are at a higher angle to the mylonitic foliation. Intersection lineations are parallel to the fold hinge and plunge steeply to the NW (Figure 3.27C). The intersection lineations clearly overprint the sub-horizontal lineation associated with the development of the mylonites. Mylonitic foliation at Lunnister generally strikes NE-SW (Figure 3.27A). This is close to the intersection between the mean fold axial plane and the girdle along which all the poles to mylonite foliation lie (Figure 3.25A). It is inferred that the mylonites and cataclasites of Lunnister lie close to the hinge of a large-scale dextral-verging fold, which explains the local presence of an axial planar fabric and associated intersection lineation. The whole sequence is intensely fractured. Fractures show a large scatter in their orientation (Figure 3.27D), but the most dominant set lies parallel to the mylonite foliation.

3:1:2:7b East of WBFP

To the east of the WBFP at Sullom and along the north side of the Ness of Haggrister, exposure is poor. Intense cataclasis with the local development of gouge overprints protolith granodiorite. The cataclasites are isotropic on all scales of observation in the field. At distances of 250m east of the WBFP, N-S-trending gneissose xenoliths occur and range in size from 50 cm to several metres. In thin-section, several of the smaller (~50cm in length) xenoliths display an annealed protomylonitic fabric, suggesting that the mylonites may have pre-dated the intrusion of the granodiorite.

3:1:2:7 Kinematic summary and discussion

The kinematic evolution of the WBFZ at Sullom, Lunnister and the Ness of Haggrister is summarised in Table 3.3.

Kinematic Regime	Fault rocks / structures
5. Sinistral strike-slip (Youngest)	<ul style="list-style-type: none"> Quartz slickenfibres on the WBFP
4. Dip slip, E-side down	<ul style="list-style-type: none"> W-dipping shears within the blue gouge of the WBF core cross-cut the dextral shear fabric
3. Dextral strike-slip	<ul style="list-style-type: none"> Fabric within blue and red gouges, WBF core Gouge-filled faults Riedel-type shears filled with gouge, cataclasites and hematite mineralisation. Dextral-verging folds 'Later cataclasites'
2. Dextral strike-slip – maybe same age as 3.	<ul style="list-style-type: none"> Shear zones within calcareous schists Foliated cataclasites? Dextral-verging folds
1. Sinistral strike-slip (Oldest)	<ul style="list-style-type: none"> Mylonites with σ and δ-type porphyroclasts S-C' fabrics and shear bands within mylonites 'Early' cataclasites

Table 3.3 Summary table of kinematic events at Sullom, Lunnister and the Ness of Haggrister.

The WBFZ at Sullom, Lunnister and the Ness of Haggrister comprises a kilometre-scale braided network of sub-vertical faults associated with cataclasis and the development of fault gouge (Figures 3.28, 3.29). The arrangement of these faults is similar to that of a positive flower structure (Figure 3.29B).

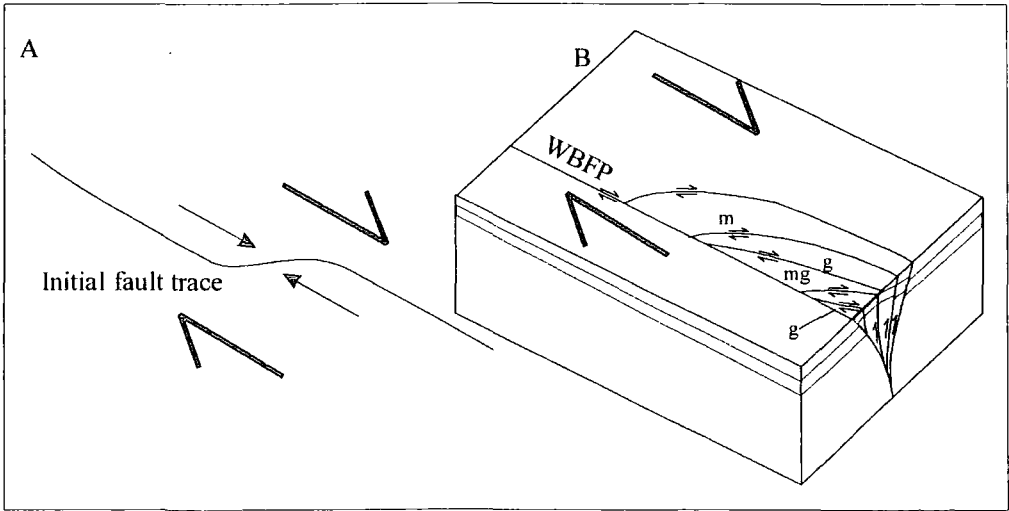


Figure 3.29B A model for the formation of a 'positive' flower structure at Sullom, Lunnister and the Ness of Haggrister. Large split arrows indicate the dominant sense of shear; small split arrows indicate the sense of strike-slip and reverse motion on the fault splays. m - mylonite, g - gneiss, mg - mylonite and gneiss. (A) Restraining bend on a dextral strike-slip fault. (B) A block diagram showing reverse, or positive, flower structure in 3-d for the WBFZ at Sullom, Lunnister and the Ness of Haggrister.

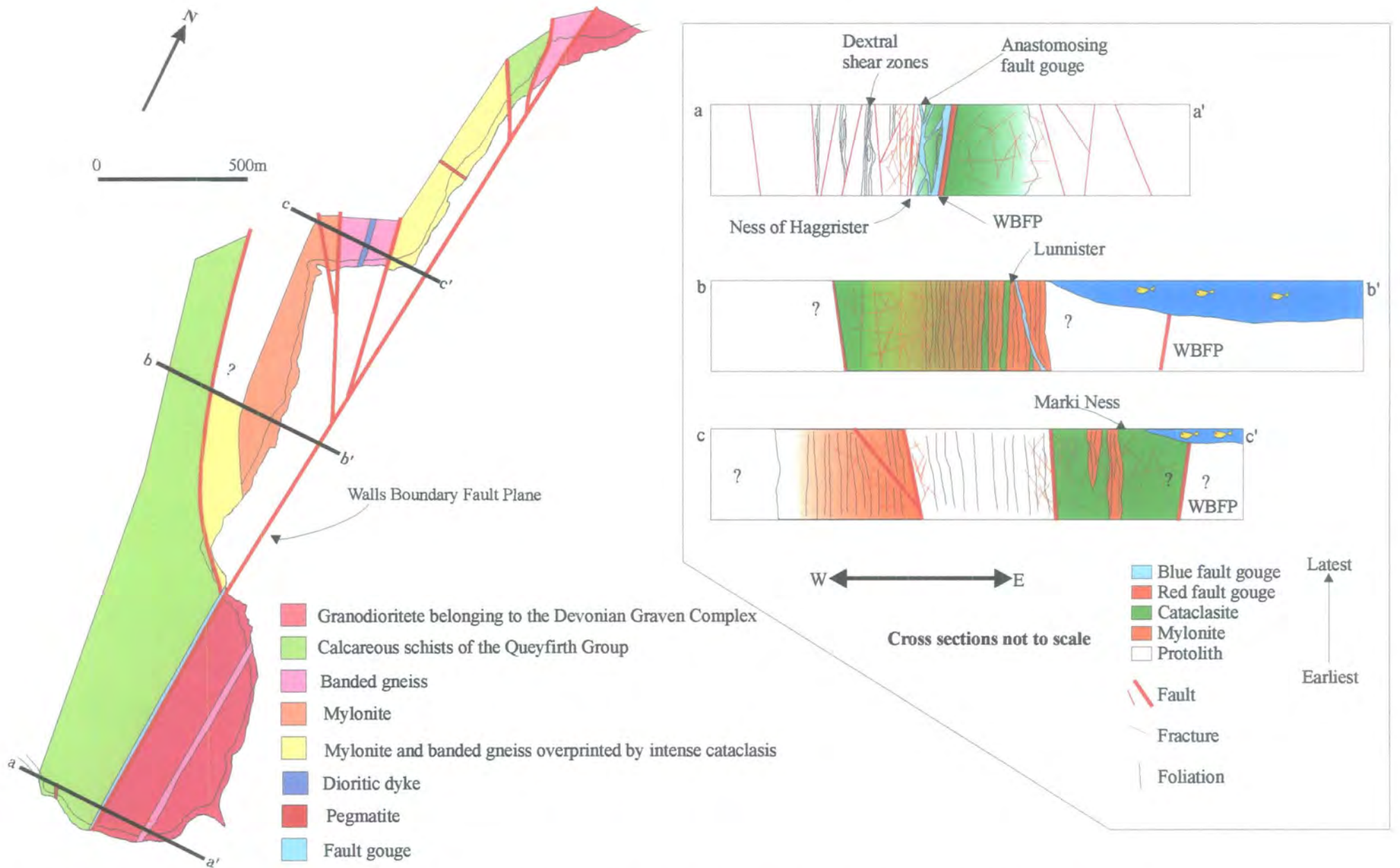


Figure 3.28 Summary map and schematic cross-sections to illustrate fault rock distribution and structure at Sullom, Lunnister and the Ness of Hagggrister.

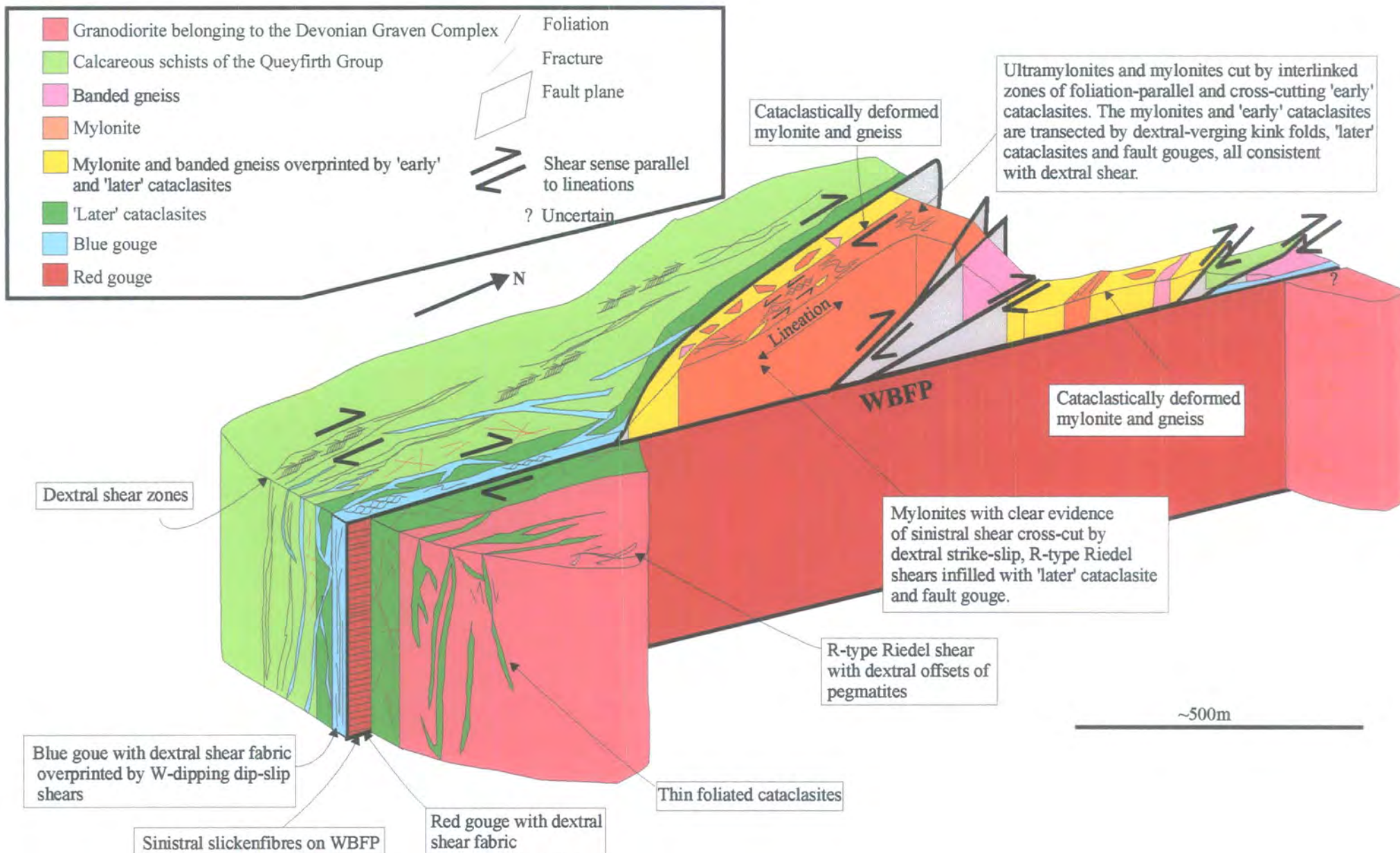


Figure 3.29 Schematic diagram to illustrate fault rock distribution, structure and geometry of the WBFZ at Sullom, Lunnister and the Ness of Haggrister. Not to scale vertically.

The flower structure formed as a result of dextral strike-slip movement along the WBF. An initial curve in the WBF trace may have led to the formation of a braided network of sub-vertical faults adjacent to a left-stepping restraining bend and a local region of transpression (Figure 3.29B). A component of reverse movement along the faults is inferred, due to the presence of deeply exhumed mylonitic fault rocks and basement rocks within the fault-bounded blocks. The main faults, which define the flower structure, are filled with fault gouge, suggesting that the broad network of faults formed during phase 3 (Table 3.3).

The rocks on either side of the WBFP at Sullom, Lunnister and the Ness of Haggrister record different kinematic events. The rocks west of the WBFP record all the kinematic events summarised in Table 3.3, whilst those to the east record only a dextral strike-slip event, suggesting that the granodiorite may not have been adjacent to the WBF during phases 1 and 2 (Table 3.3) or may not have been intruded at that time. In thin-section, several of the smaller (~50cm in length) gneissose xenoliths display an annealed protomylonitic fabric, suggesting that the mylonites formed during phase 1 (Table 3.3) may have pre-dated the intrusion of granodiorite. The most recent movement on the WBFP was sinistral strike-slip, post-dating a minor dip-slip event.

A major phase of dextral strike-slip brittle faulting (phase 3; Table 3.3) overprints a dextral strike-slip ductile event (phase 2; Table 3.3). In the absence of direct fault-rock dating, it is possible that the kinematically similar ductile and brittle fault rocks (phase 2 and 3) formed during the same event as the fault zone was being exhumed rather than in the separate kinematic phases described in Table 3.3. Brittle faulting led to the development of widespread cataclasites and gouges resulting in the present-day geometry of the fault network. Mylonites and 'early' cataclasites are the earliest recognised fault rocks at Sullom, Lunnister and the Ness of Haggrister. The mylonites and 'early' cataclasites are overprinted by all other structures and fault rocks within the WBFZ and were formed during a phase of sinistral strike-slip movement. These early fault rocks are preserved within an uplifted fault block to the west of the WBFP (Figures 3.28, 3.29). At Sullom, Lunnister and the Ness of Haggrister, the distribution of fault rocks is strongly controlled by the presence of pre-existing structures. 'Early' cataclasites commonly form interlinking zones of foliation-parallel

and cross-cutting structures. Later fault rocks appear to localise along anisotropic zones formed by earlier fault rocks and foliated pelitic horizons.

The kinematic evolution summarised in Table 3.3 is broadly similar to that proposed by Conroy (1996). Conroy (1996) concluded that the earliest phase of movement led to the formation of mylonites and that the shear sense was unclear. Roddom et al. (1989) dated the mylonites to between 290 and 320Ma using the K-Ar whole-rock method. The protolith was assumed to be granodiorite of the Devonian Graven Complex. It is clear from the present study that the mylonites were derived from compositionally banded gneiss and formed during an early phase of sinistral strike-slip movement. Gneissose xenoliths within the granodiorite display protomylonitic textures. No evidence of sinistral strike-slip movements have been found within the granodiorites belonging to the Devonian Graven Complex within the present study, suggesting that the granodiorite may not have been adjacent to the WBF or may not have been intruded at that time. The subsequent phase of dextral strike-slip was recognised by Conroy (1996) based upon dextral shear fabrics within the blue fault gouge and also on fold vergence. The most recent phase of movement, according to Conroy (1996), was sinistral strike-slip, recognised and based upon the intrusion of NW-SE-trending dolerite dykes into a NE-SW extensional regime. In the present study, the rarely exposed dolerite dykes were found to be N-S-trending, and not NE-SW-trending as described by Conroy (1996). The dykes transect banded gneiss. The relationship between these intrusions and fault rocks of the WBFZ is unknown.

3.1:3 Brae Isthmus

The Brae Isthmus (locality c; Figure 3.1) stretches 500m across in an E-W direction (Figure 3.30). The northern and southern sides of the isthmus form two E-W-trending coastal sections of beaches and low cliffs (<5m high), which partially expose the N-S-trending WBFZ. West of the WBFP hornblende-rich schists of the Dalradian Queyfirth Group are exposed (Figure 3.30). East of the WBFP, a fault-bounded sliver of crystalline limestone of uncertain origin and granodiorite belonging to the Devonian Brae Complex are exposed (Figure 3.30). The WBFP intersects the north side of the isthmus (HU 3503 6840) at a trend of 006° from the south side of the Ness of Haggrister.

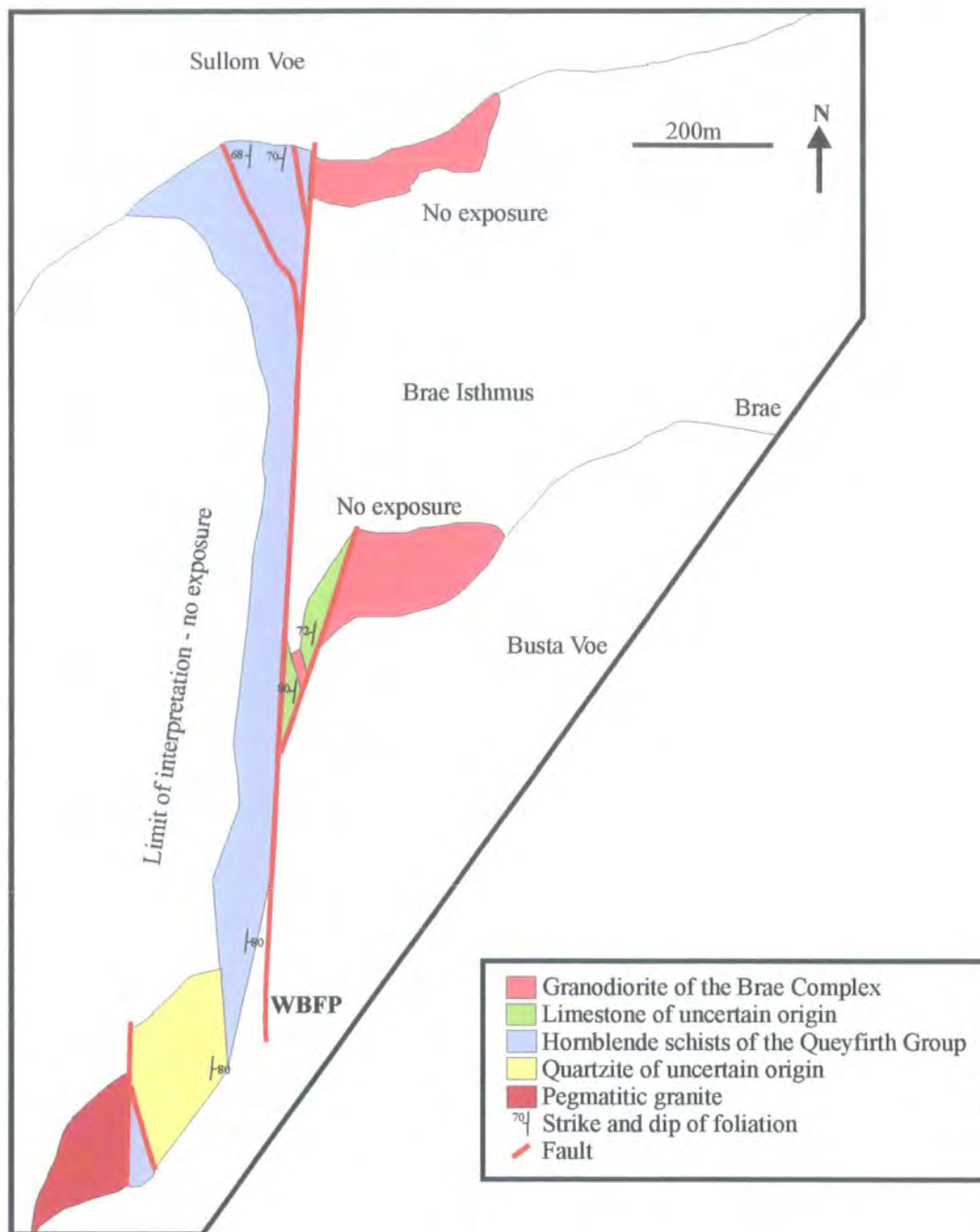


Figure 3.30 Geological map of Brae Isthmus.

It can be traced to the southern side of the isthmus (HU 3499 6757) and 200m farther south along the beach on the west side of Busta Voe. At Brae isthmus, the WBFZ comprises several fault strands, which enclose slivers of limestone and granodiorite (Figure 3.30).

Conroy (1996) described extensive outcrops showing extreme cataclasis and veining. Dextral shear bands were described within the gouge zone on the south side of Brae Isthmus.

3:1:3:1 Protolith lithologies

3:1:3:1a Granodiorite

To the east of the WBFP at Brae Isthmus, granodiorite belonging to the Devonian Brae Complex (section 2:1:5:1b) is exposed (Figure 3.30). The granodiorite is pink / green in colour and coarse grained, with phenocrysts up to 1cm in length. It is composed of approximately 65% feldspar (90% plagioclase, 10% orthoclase), 15% quartz, 15% hornblende and 5% chlorite. Locally, the granodiorite weathers to a green colour and is strongly retrogressed. Hornblende has broken down to chlorite and feldspars have broken down to aggregates of sericite and chlorite giving rise to a speckled appearance. The rock is equigranular with phenocrysts forming a holocrystalline texture. The rocks contain a weak N-S-trending magmatic fabric defined by an alignment of hornblende and feldspar phenocrysts. Xenoliths of dolerite and ultramafic rocks occur locally. The xenoliths range from 2cm to 25cm in length and appear to be aligned N-S. Enclaves of microdiorite range from 10cm to 50cm in length and appear to be orientated sub-parallel to the magmatic fabric. Randomly orientated pegmatite dykes cross-cut the granodiorite. The pegmatite dykes are 10cm to 1m thick, coarse grained and contain no magmatic or solid-state fabric.

3:1:3:1b Limestone

Crystalline limestone of uncertain origin is exposed within a fault-bounded slice east of the WBFP (Figure 3.30). The limestone is grey in colour, fine-grained, comprising

90% calcite and 10% quartz, and intensely deformed by the effects of cataclasis. The cataclastic matrix appears to be strongly recrystallised with the original fabrics and structures almost unrecognisable.

3:1:3:1c Hornblende schists

To the west of the WBF at Brae Isthmus, rocks belonging to the Dalradian Queyfirth Group (section 2:1:1:4) are exposed (Figure 3.30). They comprise green / grey-coloured, coarse- to medium-grained, hornblende-rich schists. The schists are finely laminated and in places contain epidote-rich layers along with subordinate bands of micaceous pelite. The schists contain a near-vertical N-S-trending foliation defined by flattened aggregates of hornblende and quartz, with sub-horizontal lineations defined by elongate hornblende, mica and quartz grains.

3:1:3:2 Fault rocks

In this section, fault rocks are described in the order of their relative age (oldest to youngest; see section 3:1:3:3).

3:1:3:2a Cataclasite derived from hornblende schist

Cataclasites west of the WBFP are derived mainly from hornblende-rich schists and in some cases from pelites. The cataclasites are grey / green in colour, comprising finely comminuted fragments of schist, hornblende, epidote and feldspar set within a fine-grained, epidote-rich, cataclastic matrix of the same. Randomly orientated fragments are angular to sub-angular, ranging from 1mm to almost 5cm in length. The cataclasites are isotropic on all scales of observation in the field.

3:1:3:2b Foliated cataclasites

Foliated cataclasites are exposed east of the WBF and are derived from granodiorite and cataclasite. The foliated cataclasites are dark green in colour comprising comminuted fragments (0.5cm to <0.1mm) of granodiorite, hornblende, feldspar, quartz, chlorite and muscovite set within a fine-grained (<3µm) cataclastic matrix of

sericite, chlorite, actinolite, epidote, albite, orthoclase and quartz. The fragments are sub-angular to sub-rounded and appear to be aligned along a N-S trend. The matrix contains a N-S-striking foliation defined by aligned mica grains, which wraps around porphyroclasts comprising plagioclase, orthoclase, quartz and cataclasite. Locally, pale green cataclasite with no fabric grades into foliated cataclasite near the margins.

3:1:3:2c Cataclasite derived from limestone

Pale grey cataclasites derived from crystalline limestone are exposed east of the WBF. The cataclasites comprise finely comminuted fragments of calcite, limestone and, in places, quartz set within a fine-grained cataclastic matrix of the same. Randomly orientated sub-angular clasts range from 1mm to 2cm in size. The matrix appears to be an interlocking mosaic of fine-grained calcite due to the effects of static recrystallisation. The cataclasites possess no internal structure and are isotropic on all scales of observation in the field. Millimetre-scale N-S orientated stylolites cross-cut the cataclastic fabric and commonly contain bands of iron oxide.

3:1:3:2d Fault gouges

The red and blue fault gouges developed at Brae isthmus are lithologically the same as those described at the Ness of Haggrister (see section 3:1:2:2e).

3:1:3:3 Fault rock distribution and age relationships

Early cataclasites are found east of the WBFP at Brae Isthmus. These are overprinted by extensive cataclasis and fault gouge exposed within the WBF core.

3:1:3:3a East of the WBF core

To the east of the WBF core, dark green-coloured cataclasites cross-cut granodiorite. Pale green cataclasites with no fabric appear to grade into dark green mica-rich cataclasites, which contain a near-vertical, N-S-trending foliation defined by aligned aggregates of mica. Centimetre-thick blue / green fault gouges tend to localise along the foliated cataclasites. Pale grey cataclasites cross-cut crystalline limestone. The

pale grey cataclasites are isotropic on all scales of observation in the field and are cut by red fault gouge within the fault core to the west (see section 3:1:4:3a).

3:1:3:3b West of the WBF core

To the west of the WBF core, cataclasites overprint hornblende-rich schists and pelites belonging to the Queyfirth Group. The cataclasites appear to be heavily altered, strongly retrogressed and are transected by calcite, quartz and epidote veins (1mm to 3cm thick). Hematite mineralisation occurs in N-S-orientated bands (centimetre-scale) within the cataclasite. The cataclasites are cross-cut by the soft blue gouge of the WBF core. Fragments (0.5 to 5cm) of cataclasite derived from hornblende-rich schist lie within the blue gouge.

3:1:3:3c WBF core

The fault core at Brae is located in the central part of the WBFZ and corresponds to the region of most intense fault-related deformation. The most obvious movement plane of the WBFZ is exposed along the beach to the south of Brae Isthmus (Figure 3.30). Here, the fault core is approximately 4-5m wide and is defined by the occurrence of 100% fault rock that extends from the wall rocks across the WBFP. The fault core of the WBFZ is poorly exposed at Brae Isthmus. A 1.5m thick zone of blue and red gouge is exposed on the south side of the isthmus (HU 3499 6757) and partially for 200m south along the beach on the western side of Busta Voe (Figure 3.30). The east side of the fault core contains a 3m wide zone of pale grey cataclasite derived from crystalline limestones. To the west, a 50cm-thick red coloured gouge cross-cuts pale grey cataclasites. The red gouge is cohesive, clay-like in appearance and displays a colour banding defined by variations in the clast-to-matrix ratio. In thin-section, the red gouge appears to be a clay-rich isotropic paste with a hematite cement. To the west of the red gouge, a 1m thick blue gouge is exposed. The blue gouge is clay-like in appearance and incohesive with a strong, N-S, sub-vertical foliation and sub-horizontal lineation, both defined by aligned clay particles. On outcrop surfaces viewed parallel to the lineation and perpendicular to the WBFP, centimetre-scale shear bands indicate a dextral sense of shear. The contact between the two gouges is very planar and represents the WBFP (cf. the Ness of Haggrister;

section 3:1:2:3c and Ollaberry; section 3:1:1:3c). Both gouges contain N-S-aligned clasts of cataclasite, foliated cataclasite and breccia ranging from 0.5cm to 30cm in length. The blue gouge overprints and contains clasts of cataclasite derived from hornblende schists west of the WBFP. The contact between the blue gouge and a 5m wide zone of cataclasites to the west is sharp. Cataclasites to the west are isotropic on all scales of observation in the field. Millimetre-scale epidote veins cross-cut the cataclastic fabric and in places form intense networks.

3:1:3:4 Fault zone structure

3:1:3:4a East of the WBFP

Fault-related deformation extends for approximately 150m east of the WBFP through a sliver of limestone and into poorly exposed granodiorite belonging to the Devonian Brae Complex. 140m east of the WBFP along the south coast of Brae Isthmus (HU 3515 6778), dark green-coloured cataclasites overprint the granodiorite. The cataclasites are mica-rich, displaying a N-S-trending sub-vertical foliation defined by aligned mica grains. Pale green cataclasites with no fabric appear to grade into dark green foliated cataclasites at their margins. The foliated cataclasites strike N-S and dip steeply to the E and W (Figure 3.31). Lineations defined by elongate chlorite and muscovite grains form two main clusters (sub-horizontal and dip-slip; Figure 3.31). Foliated cataclasites with sub-horizontal lineations viewed in thin-sections and outcrop surfaces parallel to the lineation contain centimetre- to millimetre-scale S-C' fabrics consistent with sinistral shear (Plate 3.28). Foliated cataclasites with dip-slip lineations display millimetre-scale S-C' fabrics and shear bands consistent with a normal (W-side down) sense of shear, when viewed in thin-sections parallel to the lineation. The foliated cataclasites vary in thickness from 1 to 50cm. They tend to bifurcate into several strands surrounding enclaves of granodiorite and unfoliated cataclasite, giving rise to a braided geometry. Foliated cataclasites are irregular in their distribution and do not appear to increase in frequency towards the fault core. Foliation-parallel veins (~1mm thick) of calcite, albite, epidote, chlorite and quartz are common within the cataclasites.

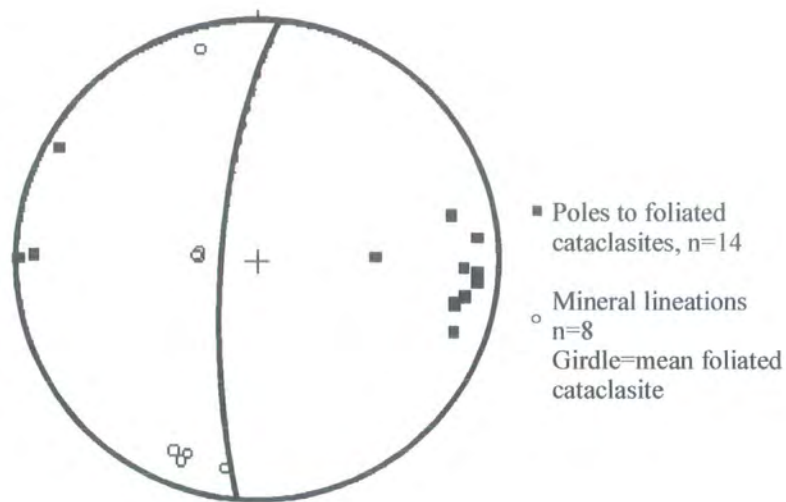


Figure 3.31 Stereographic projection to show foliated cataclasite structural data, Brae Isthmus.



Plate 3.28 Plan view. Foliated cataclasite, Brae Isthmus (HU 3515 6778). Shear arrows indicate C' planes of sinistral S-C' fabric within cataclasite. Shear arrow labelled G indicates foliation-parallel gouge vein with a dextral strike-slip displacement of 2cm. (Shear arrows parallel to lineations).

The adjacent granodiorite wall rocks are strongly retrogressed. Chlorite and actinolite fibres pseudomorph hornblende phenocrysts and feldspars are partially replaced by aggregates of chlorite and sericite, giving rise to a speckled appearance of the feldspar phenocrysts. Randomly-orientated, millimetre-thick veins of epidote, chlorite, albite, calcite and quartz commonly nucleate from the cataclasites and transect the granodiorite. Later gouges tend to localise along the foliated cataclasites (Plate 3.28). The gouges contain lineations defined by aligned clay particles, which plunge shallowly to the S. In plan view, dextral strike-slip displacements of 1 to 15cm along the gouges can be measured (Plate 3.28).

At distances of 40m east of the WBFP, fracturing within the granodiorite is very intense with randomly-orientated millimetre- to centimetre-thick quartz and epidote veins commonly forming networks and, in places, breccias. Farther to the west, a fault-bounded sliver of cataclased limestone is exposed. The fault separating cataclased limestone and granodiorite is not exposed (Figure 3.30). A 5m-wide zone of pale grey cataclasites derived from limestones is cross-cut by red gouge of the fault core (see section 3:1:3:3c). The cataclasites are isotropic in most places, but locally display a N-S-orientated colour banding defined by grain-size variations. N-S-striking stylolite surfaces are abundant within the cataclasite with a mean spacing of 1cm. The cataclasites display a red coloration in places due to the effects of iron mineralisation.

3:1:3:4b West of the WBFP

West of the WBFP along the western side of Busta Voe (HU 3499 6757), isotropic cataclasites that overprint hornblende-rich schists with pelites are poorly exposed. Cataclasis is irregularly developed but generally increases towards the fault core. The rocks are strongly retrogressed and cut by randomly-orientated calcite, quartz and epidote veins (1mm to 3cm thick). Iron mineralisation occurs in N-S-orientated bands within the cataclasite. Centimetre-thick pegmatite veins cross-cut the schists and are cut by N-S fractures along which dextral strike-slip displacements up to 30cm can be measured. Both the cataclasites and the schists are cut by soft blue gouge of the fault

core. The contact between the blue gouge of the fault core and cataclasites to the west is a sharp, N-S-orientated, vertical fault plane. Clasts of cataclasite derived from hornblende schist are present within the gouge.

3:1:3:5 Kinematic summary and discussion

The kinematic evolution of the WBFZ at Brae Isthmus is summarised in Table 3.4.

Kinematic Regime	Fault rocks / structures
3. ? (Youngest)	<ul style="list-style-type: none"> • WBFP containing slickenfibres (later than gouge)
2. Dextral strike-slip	<ul style="list-style-type: none"> • Dextral fabrics within gouges • Displacements along gouge-filled fractures cross-cutting foliated cataclasites
1. Sinistral strike-slip (oldest)	<ul style="list-style-type: none"> • Foliated cataclasites, sinistral S-C' fabrics, σ-type porphyroclasts

Table 3.4 Table summarising the kinematic evolution of the WBFZ at Brae Isthmus.

The WBFZ at Brae isthmus comprises a braided network of N-S-trending faults associated with the development of fault gouge and broad zones of cataclasis (Figure 3.32). The earliest recognised fault rocks at Brae Isthmus are exposed east of the WBFP and display evidence of sinistral strike-slip with localised dip-slip normal movements. A later phase of dextral strike-slip faulting led to the development of fault gouges and cataclasites. The most recent fault movement produced quartz slickenfibres, although the displacement sense is unclear. The only phase of faulting described by Conroy (1996) at this locality was dextral strike-slip (cf. phase 2; Table 3.4) associated with the development of fault gouge and intense cataclasis.

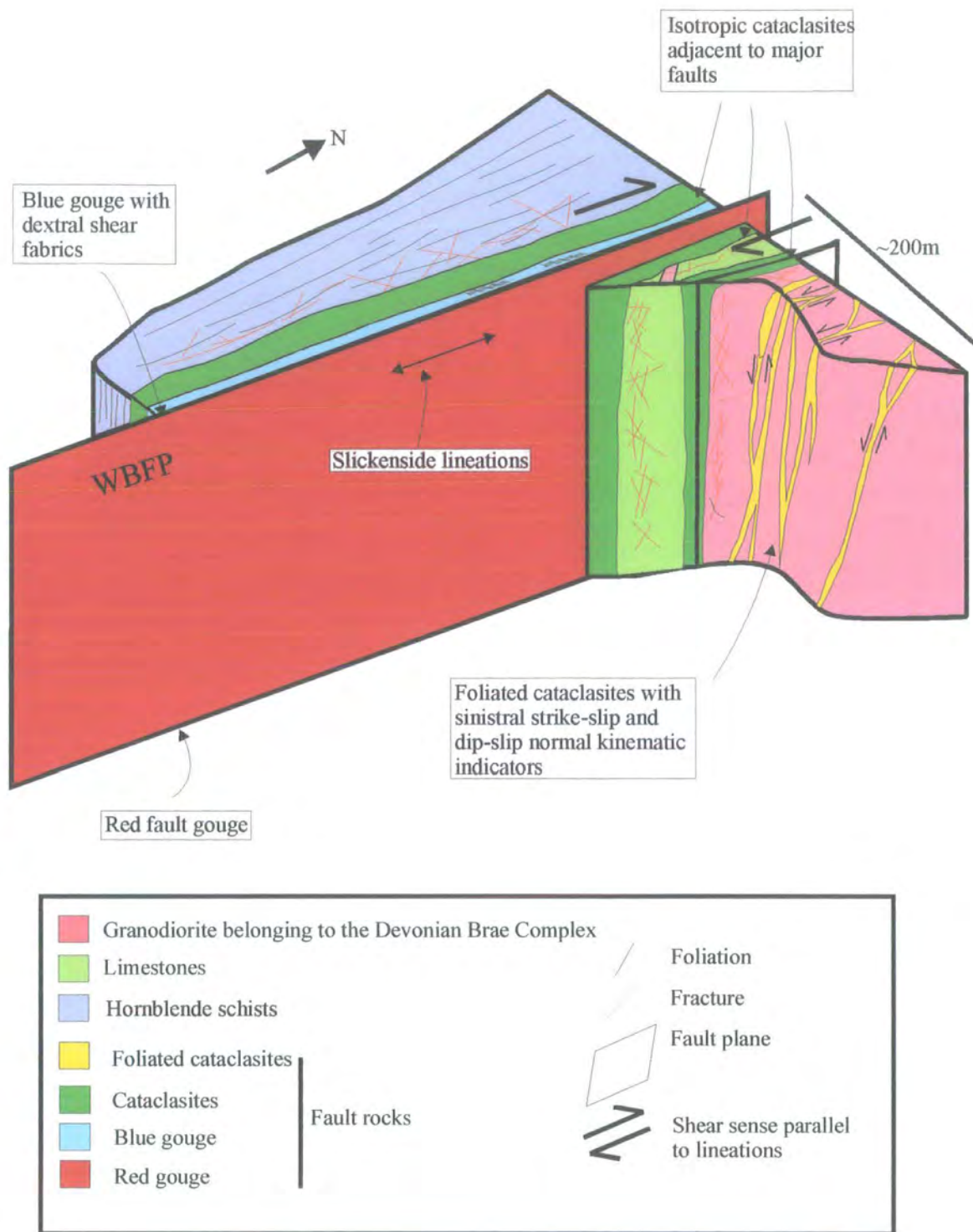


Figure 3.32 Schematic diagram to illustrate fault rock distribution and structures at Brae Isthmus.

3:1:4 Papa Little

Papa Little is an uninhabited island situated at the northernmost end of Aith Voe (locality d: Figure 3.1). The island stretches 2.5km from north to south and is 1.2km across at its widest point. The WBFP comes onshore into the northern cliffs of the Ayre of Papa Little (HU 3449 6177) at a bearing of 005° from Brae Isthmus, and passes to the south of the Ayre of Papa Little (HU 3445 6134) and out through the Bight of Warwick (Figure 3.33). West of the WBF, there is a banded gneiss of uncertain affinity, together with limestones, cataclasites and Late Devonian pegmatitic granites of the Northmaven Complex (Figure 3.33). East of the WBF, psammitic gneisses and hornblende schists belonging to the Moinian Yell Sound Division (section 2:1:2:1) are exposed (Figure 3.33). The WBFZ on Papa Little is at least 500m wide.

Conroy (1996) described extensive cataclasis on the north side of the island together with chloritic alteration and extensive epidote veining. Dextral S-C' fabrics were observed at the eastern edge of the fault zone. Flinn (1977) noted that on Papa Little and farther north, movement along the WBF appeared to have taken place on a single surface adjacent to 0.5m of red or green fault gouge.

3:1:4:1 Protolith lithologies

3:1:4:1a Gneissose rocks west of the WBF

Compositionally banded gneisses of uncertain origin are exposed west of the WBFP on Papa Little (Figure 3.33; Plate 3.29). The gneisses are pink / green in colour, fine to medium grained and equigranular. Pink-coloured gneiss comprises 65% feldspar, 20% quartz, 10% hornblende and 10% chlorite and epidote. Green-coloured gneiss is composed of approximately 70% hornblende, 20% quartz and 10% epidote and chlorite. The feldspar, quartz and hornblende form stretched and flattened equigranular aggregates, which define a sub-vertical foliation with sub-horizontal lineations defined by aligned quartz, feldspar and hornblende grains. The polygonal

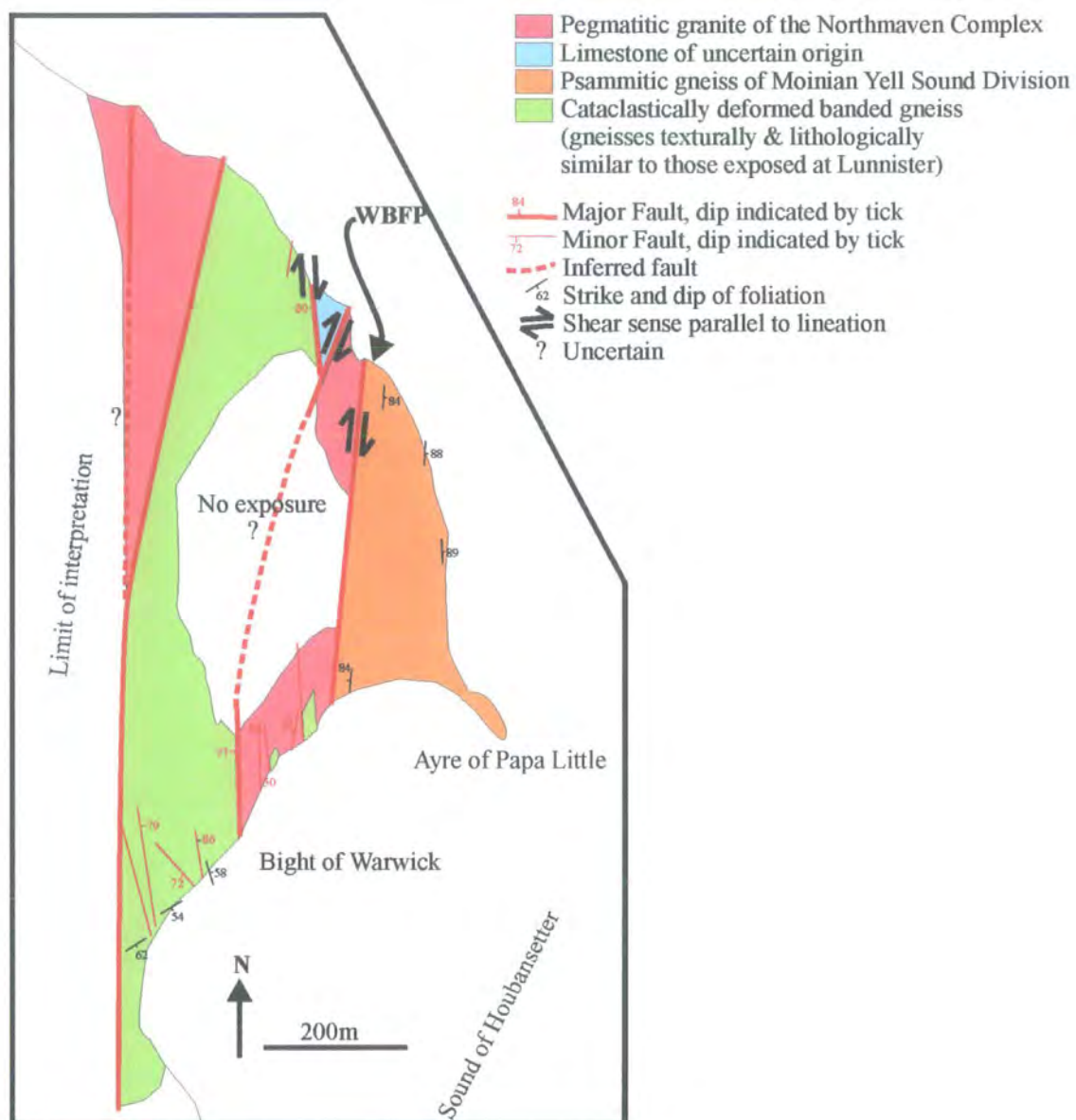


Figure 3.33 Geological map of the northeast part of Papa Little.



Plate 3.29 Cross-section through compositionally banded gneiss with NE-SW foliation cross-cut by millimetre-thick epidote veins, west of the WBFP.

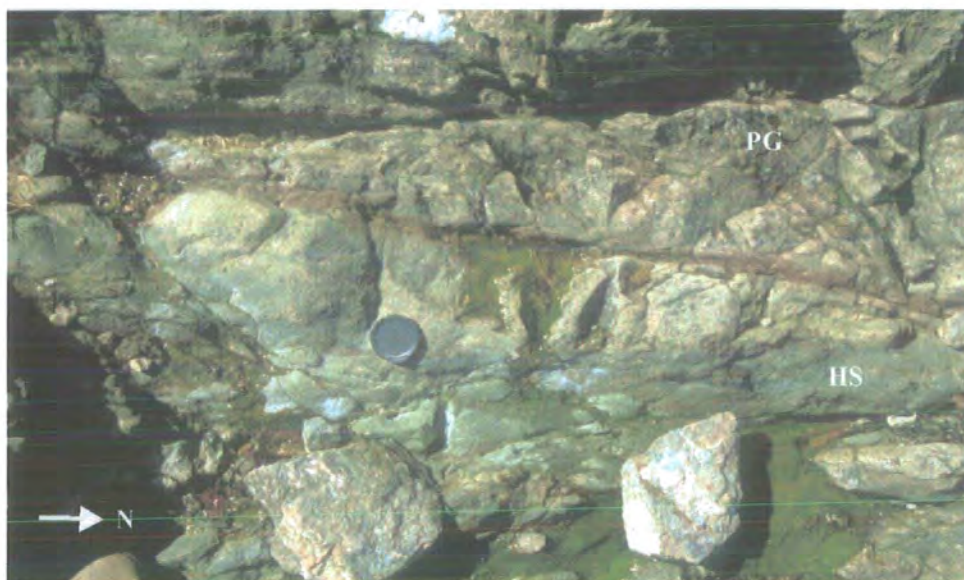


Plate 3.30 Plan View. Psammitic gneiss (PG) interlayered with hornblende schist (HS) belonging to the Yell Sound Division, east of the WBFP. Note: NW-SE-trending fracture filled with hematite stained fault gouge.

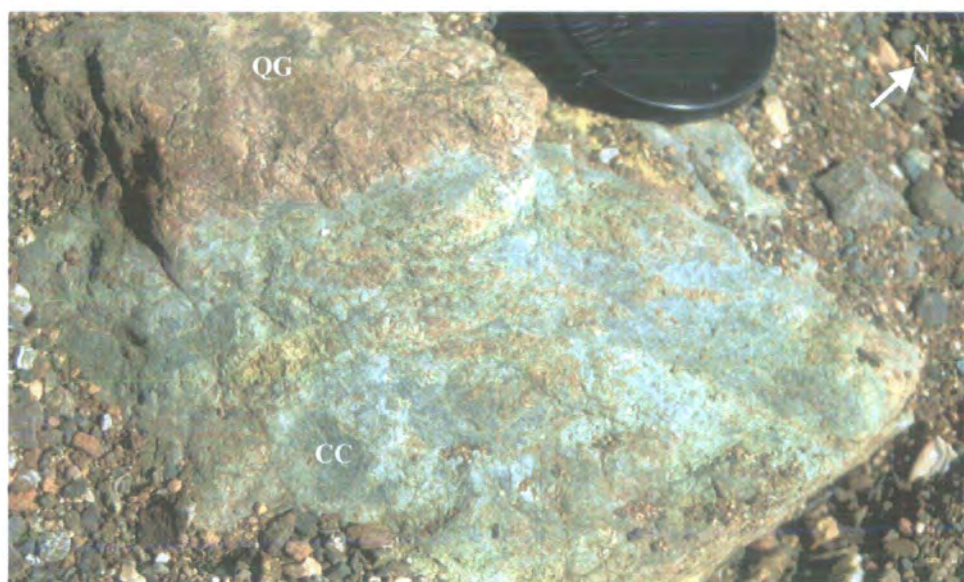


Plate 3.31 Plan View. Green-coloured cataclasite (CC) derived from quartzo-feldspathic gneiss (QG), west of the WBFP.

aggregates surround pockets of chlorite and epidote. The gneisses are texturally and compositionally similar to those exposed west of the WBFP at Sullom, Lunnister and the Ness of Haggrister (section 3:1:2:1c)

3:1:4:1b Pegmatitic granite

To the west of the WBFP on Papa Little, pegmatitic granites belonging to the Late Devonian Northmaven Complex (section 2:1:5:2a) are exposed as fault-bounded slivers within the gneissose and cataclastic rocks (Figure 3.33). The granites are orange in colour and medium- to coarse-grained crystalline rocks comprising orthoclase (50%), plagioclase (20%) and quartz (20%) with minor amounts of white mica and chlorite. The rock is equigranular with phenocrysts forming a holocrystalline texture. The granite contains no solid-state or magmatic fabric.

3:1:4:1c Limestone

Crystalline limestone of uncertain origin is exposed in a fault-bounded slice west of the WBF (Figure 3.33). Intense fracturing and cataclasis has obliterated any early fabrics or structures.

3:1:4:1d Yell Sound Division rocks

Gneissose rocks belonging to the Moinian Yell Sound Division crop out east of the WBFP on Papa Little (Figure 3.33; Plate 3.30). The rocks comprise psammitic gneiss interlayered with hornblende schists. The psammitic gneisses are pink, medium-grained, crystalline rocks comprising quartz (~65%) and feldspar (~35%). Feldspar porphyroblasts are surrounded by flattened polygonal aggregates of quartz crystals, which define a gneissose foliation. Hornblende-rich schists are medium- to coarse-grained rocks comprising hornblende (65%), chlorite (15%), feldspar (15%) and quartz (5%). Sheared polygonal aggregates of quartz and feldspar are surrounded by a matrix of aligned hornblende and chlorite laths, which define a schistosity. These rocks are compositionally and texturally different to the banded gneisses west of the WBFP (section 3:1:4:1a).

3:1:4:2 Fault rocks

In this section, the fault rocks are described in the order of relative age (oldest to youngest; see section 3:1:4:3).

3:1:4:2a Cataclasites west of the WBFP

West of the WBFP, cataclasites are interleaved with banded quartzo-feldspathic and hornblende-rich gneiss (Plate 3.31). The cataclasites are green in colour, comprising finely comminuted fragments of gneiss, feldspar, quartz, hornblende, epidote and chlorite set within a fine-grained cataclastic matrix of the same. Randomly-orientated clasts range from 0.5mm to 2cm in size. The cataclasites are isotropic on all scales of observation in the field. Millimetre-scale epidote and chlorite veins commonly nucleate from and cross-cut cataclasites. Iron staining occurs in N-S bands, which transect the cataclastic fabric.

3:1:4:2c Cataclasites east of the WBF

There are two types of cataclasite exposed east of the WBFP, unfoliated and foliated. The mutual age relationships between the cataclasites is unclear.

Unfoliated cataclasites are grey / green in colour, comprising finely comminuted fragments of gneiss, feldspar, quartz, hornblende and mica set within a fine-grained cataclastic matrix of the same. Sub-angular clasts (0.5mm to 2cm in size) are randomly orientated within an isotropic matrix.

Foliated cataclasites are green in colour, 2mm to 3cm thick, comprising finely comminuted clasts of gneiss, feldspar, quartz, hornblende and mica set within a fine-grained mica-rich cataclastic matrix. The cataclasites contain a N-S-orientated foliation defined by aligned aggregates of mica which wraps around aligned porphyroclasts.

3:1:4:2c Fault gouges

There are two types of fault gouge present on Papa Little, a red/brown gouge and a blue/grey gouge.

Red / brown gouge is derived from pegmatitic granite. It is very fine grained, incohesive and clay-like in appearance. The gouge displays a centimetre-scale colour banding defined by variations in grain size. Locally, the gouge is indurated due to the presence of an iron-rich cement. Aligned clay particles define a N-S-trending, sub-vertical foliation with sub-horizontal lineations.

The blue / grey gouge is derived from the psammitic gneiss and schists belonging to the Yell Sound Division. It is incohesive, fine-grained and clay-like in appearance. Aligned clay particles define a strong, N-S-orientated, sub-vertical foliation with sub-horizontal lineations.

3:1:4:3 Fault rock distribution and age relationships

On Papa Little, early cataclasites truncated by pegmatite veins are exposed west of the WBF core. Later cataclasites, incohesive breccias and fault gouge cross-cut earlier cataclasites and pegmatites, with cataclasis generally increasing towards the WBF core.

3:1:4:3a East of the WBF core

To the east of the WBF core on Papa Little, N-S-trending, hematite-mineralised, gouge veins (Plate 3.30) and foliated cataclasites overprint gneisses and schists belonging to the Moinian Yell Sound Division. The relationship between the mineralised gouge veins and foliated cataclasites is unclear. Anastomosing, centimetre-thick, blue gouges overprint intensely fractured gneiss.

3:1:4:3c West of the WBF core

To the west of the WBF core, green-coloured cataclasites overprint quartzofeldspathic and hornblende-rich gneisses (Plate 3.31). The cataclasites are isotropic

on all scales of observation in the field and are cross-cut by centimetre-thick pegmatite veins belonging to the Northmaven Complex, suggesting that some cataclasis pre-dated intrusion of the granites. Faults filled with brown-coloured fault gouge and incohesive breccias cross-cut the earlier cataclasites and pegmatitic granites.

3:1:4:3c WBF core

The most obvious movement plane of the WBFZ is exposed on the northern and southern coasts of the Ayre of Papa Little (HU 3449 6177 and HU 3443 6134 respectively). The fault plane (WBFP) is orientated 005/85E and is marked by narrow inlets. The fault core here is 25m wide (Plate 3.32).

Green / brown-coloured cataclasites and breccias derived from pegmatitic granite crop out west of the WBFP and are cross-cut by a red / brown-coloured incohesive breccia. The breccia contains randomly orientated blocks of granite ranging from 1cm to 50cm in length set within a clay-rich incohesive matrix. Locally, the matrix appears to be cemented by hematite mineralisation. The breccia is isotropic on all scales of observation in the field. Towards the WBFP, the 10m-wide breccia grades into a 1m thick brown / red coloured fault gouge (Plate 3.32). The gouge has a strong fabric parallel to the WBFP with lineations that plunge shallowly to the S; both defined by aligned clay particles. The eastern margin of the brown gouge contains narrow slivers of blue gouge (5-30cm in length). The blue gouge is separated from red / brown gouge (with slivers of blue gouge) by the WBFP (Plate 3.32). Here, the WBFP contains poorly preserved sub-horizontal quartz slickenfibres.

East of the WBFP a 1m thick blue gouge grades into an 8m wide zone of incohesive breccia eastwards (Plate 3.32). The blue gouge displays a strong, steeply-dipping fabric orientated N-S with sub-horizontal lineations, both defined by aligned clay particles (Plate 3.32). The incohesive breccia overprints psammitic gneiss and epidote-rich cataclasite, which occurs as clasts within the breccia and blue gouge. To the east of the blue gouge and breccia zone (12m east of the WBFP), a network of anastomosing shear zones containing blue gouge surrounds lenses of gneiss (Plate 3.33).

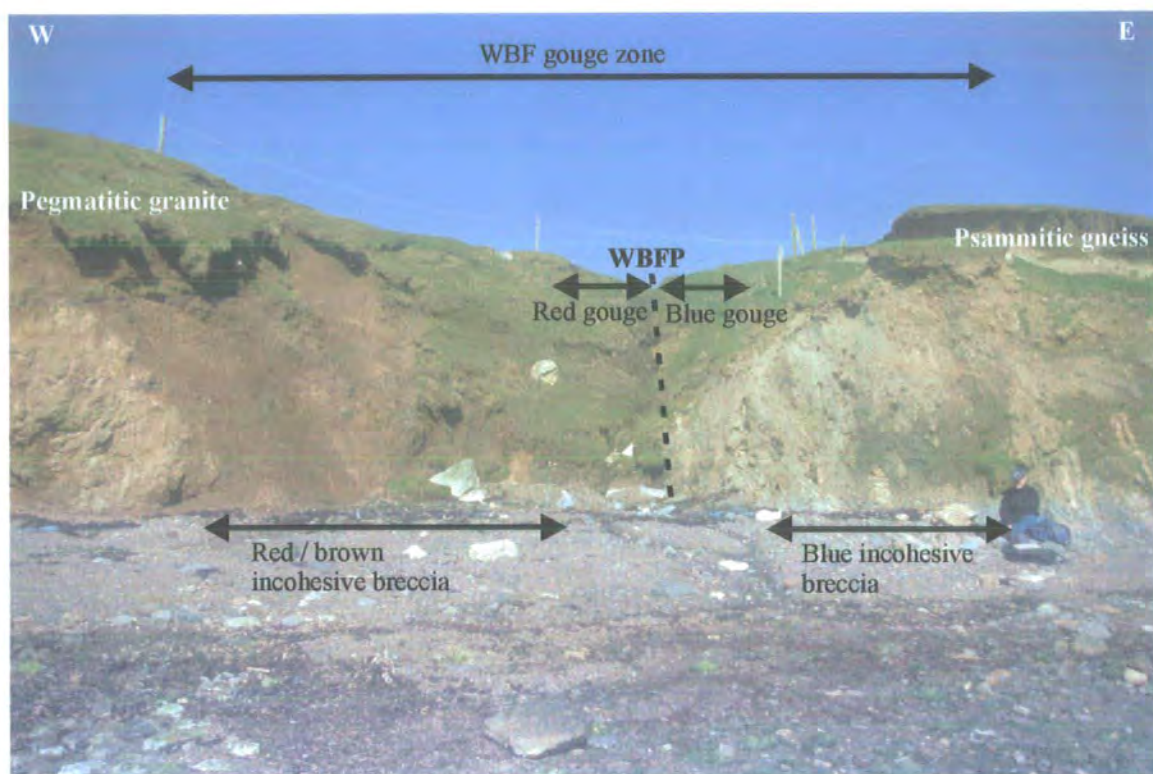


Plate 3.32 Cross-section through WBF core, south coast of the Ayre of Papa Little (HU 3443 6134).

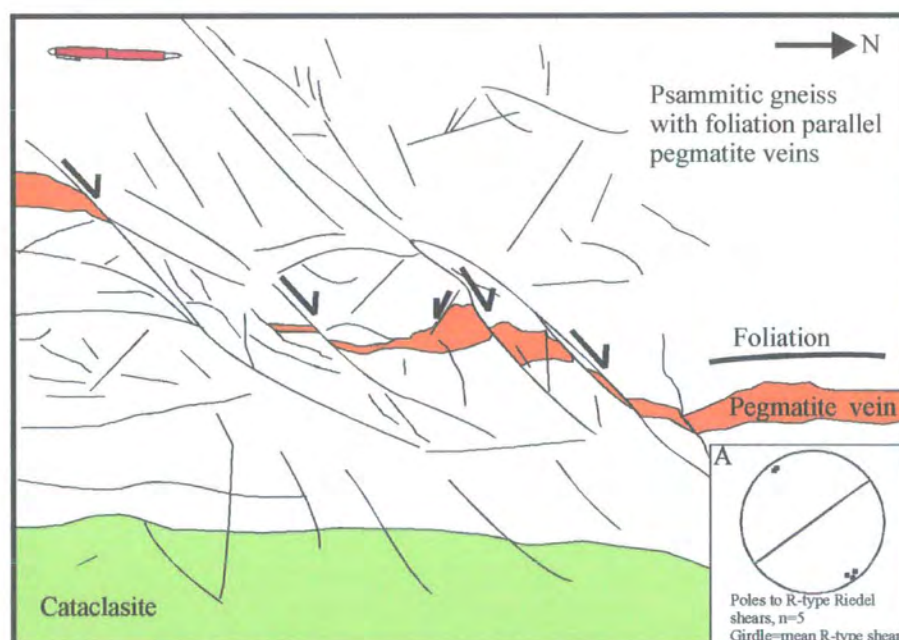


Figure 3.34 Plan View. Field sketch of centimetre-scale fault zone comprising R-type Riedel shears along which dextral displacements (2-20cm) of granite veins (foliation parallel) can be measured. Note: fractures contain sub-horizontal slickenside lineations. Inset (A) stereographic projection of R-type Riedel shears. 20m east of WBFP, south coast of Ayre of Papa Little (HU 3445 6134).

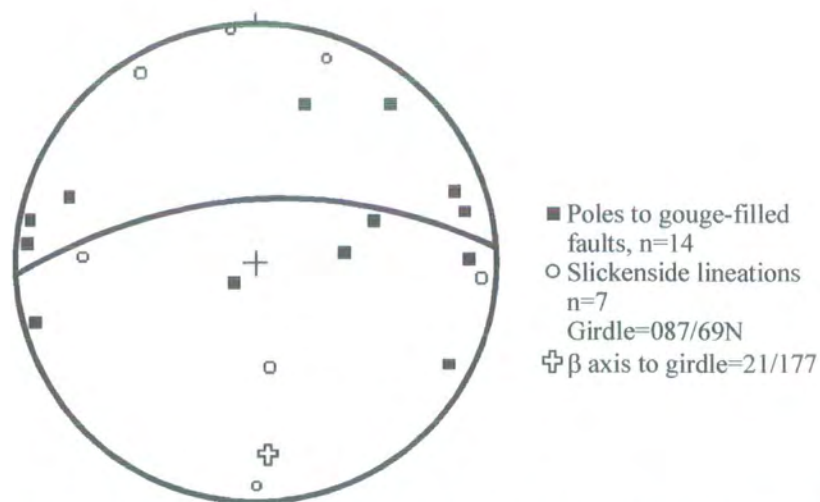


Figure 3.35 Stereographic projection of gouge-filled faults and slickenside lineations west of the WBFP on Papa Little.

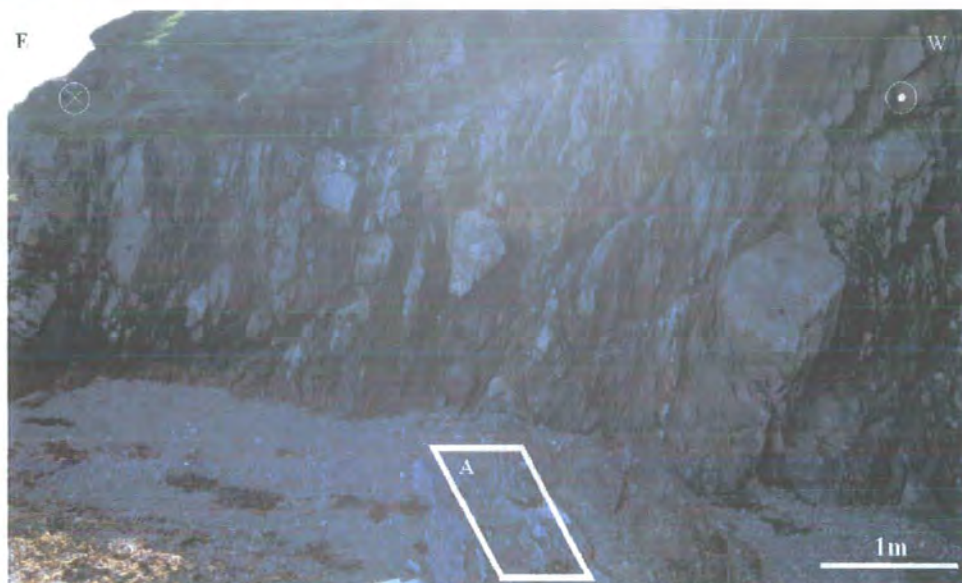


Plate 3.33 E-W-orientated cross-section to show intensely boudinaged psammitic gneiss cut by anastomosing networks of soft blue fault gouge, 12m east of WBFP, north coast of Ayre of Papa Little (HU 3450 6177). Note: box marked A shows location of Plate 3.34.

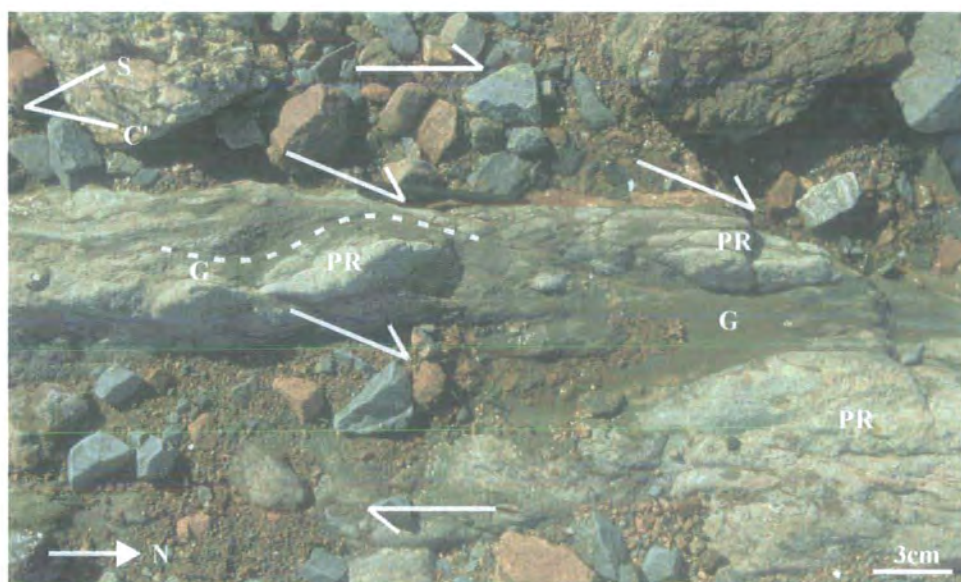


Plate 3.34 Plan View. Anastomosing blue gouge-filled shears (G) surrounding enclaves of intensely fractured protolith (PR) (psammitic gneiss). Dashed lines indicate centimetre-scale S-C' type fabric with split arrows indicating a dextral sense of shear along C' planes. Plate located as A on Plate3.33 (HU 3450 6177).

3:1:4:4 Fault zone structure

3:1:4:4a East of the WBF core

Fault-related deformation extends for at least 120m east of the WBFP into poorly exposed psammitic gneiss and hornblende schists of the Yell Sound Division. At distances of 110m east of the WBFP, psammitic gneiss is interlayered with hornblende-rich schists. Fracture intensity is low and there is little evidence for fault-related deformation. N-S-striking, iron mineralised, millimetre-thick gouge veins are widely spaced. The veins rarely contain slickenside lineations. Hornblende-rich schists display a N-S-orientated sub-vertical foliation defined by flattened and stretched hornblende, feldspar and quartz grains with sub-horizontal lineations defined by elongate hornblende laths. The schists appear to contain millimetre-scale shear bands, which indicate sinistral shear in thin-sections viewed parallel to the mineral stretching lineation. In thin-section, the shear bands are defined by aligned chlorite and actinolite needles together with concentrations of iron oxide.

At distances of 40m east of the WBFP, fracturing is more intense with thin, N-S-trending cataclasites cross-cutting the gneissose fabric. The cataclasites are 1mm to 2cm thick and contain a N-S-trending sub-vertical foliation defined by aligned aggregates of mica. The cataclasites are spaced approximately 1m apart and do not appear to contain any lineations or kinematic indicators.

Both fracturing and veining increase towards the WBFP. Randomly orientated veins of epidote, quartz, calcite and, in places, chlorite are 1mm to 5mm thick. The veins form intense networks and may constitute a matrix to localised breccias. At distances of less than 30m east of the WBFP, braided zones of sub-vertical, NE-SW-trending fractures contain sub-horizontal slickenside lineations. The fractures displace granite veins right-laterally by 1cm to 30cm and are interpreted as R-type Riedel shears, which suggest an overall dextral sense of shear for the WBF (Figure 3.34). Intense fracturing leads to the development of local breccia zones at distances less than 25m east of the WBFP. 20m east of the WBFP brecciated gneiss passes into a 12m-thick zone of anastomosing, centimetre-thick, blue gouges surrounding lenses of intensely

fractured gneiss (see section 3:1:4:3c). On outcrop surfaces viewed parallel to the sub-horizontal lineation (defined by aligned clay particles), centimetre-spaced shear bands are consistent with dextral shear.

3:1:4:4b West of the WBF core

Fault-related deformation extends approximately 300m west of the WBFP through fault-bounded slivers of pegmatitic granite into compositionally banded gneisses. 300m west of the WBFP (HU 3415 6093), cataclasites overprint quartzo-feldspathic and hornblende-rich banded gneiss. The cataclasites are isotropic on all scales of observation in the field and are cross-cut by centimetre-thick pegmatitic veins belonging to the Late Devonian Northmaven Complex, suggesting that these cataclasites pre-date intrusion of the pegmatite veins and associated granites. Cataclastic deformation is irregularly developed and appears to decrease to the east.

250m west of the WBFP, intensely fractured gneissose rocks are exposed. The gneisses contain a foliation defined by flattened aggregates of quartz, feldspar and hornblende, strikes NE-SW, dips moderately to the SE. Millimetre-thick, epidote-rich cataclasites commonly occur parallel to the foliation with randomly orientated epidote veins nucleating from them.

At 240m west of the WBF, the first gouge-filled fault appears. The brown-coloured fault gouge is 30cm thick and is orientated 165/84E, with slickenside lineations plunging shallowly to the N. A 10cm-thick calcite breccia is present within the centre of the fault gouge. Farther into the WBFZ, subsidiary gouge-filled faults increase in frequency and their poles lie along a girdle orientated 087/67N with the mean intersection of the fault planes parallel to the β axis to the girdle (21/177) (Figure 3.35). Slickenside lineations are sub-horizontal and show a vague clustering close to the pole to the girdle, which represents the mean fault plane intersection. Therefore, the mean fault plane intersection is interpreted to be sub-parallel to the overall transport direction of the WBFZ at this time of movement (cf. section 3:1:1:6).

200m west of the WBFP (HU 3429 6107) exposure is poor. Early cataclasites interleaved with compositionally banded gneiss are cut by several low-angle normal faults containing centimetre-thick brown coloured gouge.

At distances of 150m to 40m west of the WBFP, slivers of pegmatitic granite and gneiss (with cataclasite) are bounded by N-S faults containing centimetre-thick brown fault gouges. The gouges show dip-slip normal and dextral strike-slip movements, based upon shear bands and fold vergence within the gouge fabrics. 40m west of the WBFP, intensely fractured pegmatitic granite passes into breccia and locally cataclasite. Incohesive breccia overprints the cataclastically deformed granite 10m west of the WBFP (see section 3:1:4:3c)

3:1:4:4c WBF core

At the east side of the WBF core, a network of anastomosing shear zones containing blue gouge surrounds lenses of gneiss (3cm to 1m in length) boudinaged in a N-S trend (Plate 3.33). The gouges range in thickness from 2cm to 25cm, containing a sub-vertical N-S-trending foliation and sub-horizontal lineations, both defined by aligned clay particles. In plan view, the gouge contains a centimetre-scale S-C' type fabric indicating a dextral sense of shear (Plate 3.34). In thin-section, the gouge fabric is sinistrally displaced by later, NW-SE-trending fractures filled with carbonate and zeolite.

To the west, an 8m-wide zone of incohesive breccia grades into a 1m-thick blue gouge bounded to the west by the WBFP (Plate 3.32). The incohesive breccia zone overprints psammitic gneiss and epidote-rich cataclasite, which are present as clasts within the breccia and gouge. The blue gouge is 1m thick and contains a strong vertical N-S trending foliation (Plate 3.32) with sub-horizontal lineations; both defined by aligned clay particles. On outcrop surfaces viewed parallel to the lineation and normal to the WBFP, centimetre-scale shear bands signify a dextral sense of shear. The WBFP is orientated 005/85E and contains quartz slickenfibres that plunge gently to the S. To the west of the WBFP a metre-thick red / brown gouge is exposed. Near the WBFP the red / brown gouge contains centimetre-scale slivers of blue-coloured gouge. The gouge has a strong colour banding parallel to the WBFP defined by grain-size variations. Lineations defined by aligned clay particles plunge shallowly to the S. The gouge grades into a 10m wide incohesive breccia, which overprints an intensely fractured pegmatitic granite. The incohesive breccia is isotropic on all scales of observation in the field.

3:1:4:5 Kinematic summary and discussion

The kinematic evolution of the WBFZ on Papa Little is shown in Table 3.5.

Kinematic Regime	Fault rocks / structures
3. Sinistral strike-slip (youngest)	<ul style="list-style-type: none"> ◦ NW-SE-trending fractures infilled with carbonate and zeolite sinistrally displace dextral shear fabric within gouge
2. Dextral strike-slip	<ul style="list-style-type: none"> ◦ S-C' type fabric within blue fault gouge ◦ R-type Riedel shears offsetting granite veins ◦ Red gouge ◦ Incohesive breccias ◦ Cataclasites
1. Sinistral strike-slip (oldest)	<ul style="list-style-type: none"> ◦ Cataclasites cross-cut by pegmatitic granite veins, west of WBFP ◦ Sinistral shear bands overprinting regional fabric of hornblende schists, east of WBFP

Table 3.5 Table showing the kinematic evolution of the WBFZ on Papa Little.

On Papa Little, the rocks on both sides of the WBFP record all the kinematic phases summarised in Table 3.5. There, the WBFZ is an anastomosing network of roughly N-S-trending sub-vertical faults with a narrow fault core comprising fault gouge, breccia and the WBFP (Figure 3.36). The WBFP is the main structural boundary within the WBFZ. It separates fault rocks derived from, and protoliths comprising compositionally banded gneisses of uncertain origin, with pegmatitic granite of the Northmaven Complex to the west from fault rocks derived from and protolith rocks belonging to the Yell Sound Division to the east. Wide zones to the west and east of the fault core contain subsidiary faulting, strong cataclasis and several fault-bounded slivers of protolith.

The only phase of faulting described by Conroy (1996) on Papa Little was dextral strike-slip (cf. phase 2: Table 3.5), based on the recognition of dextral-shear fabrics within fault gouge along the eastern side of the fault zone.

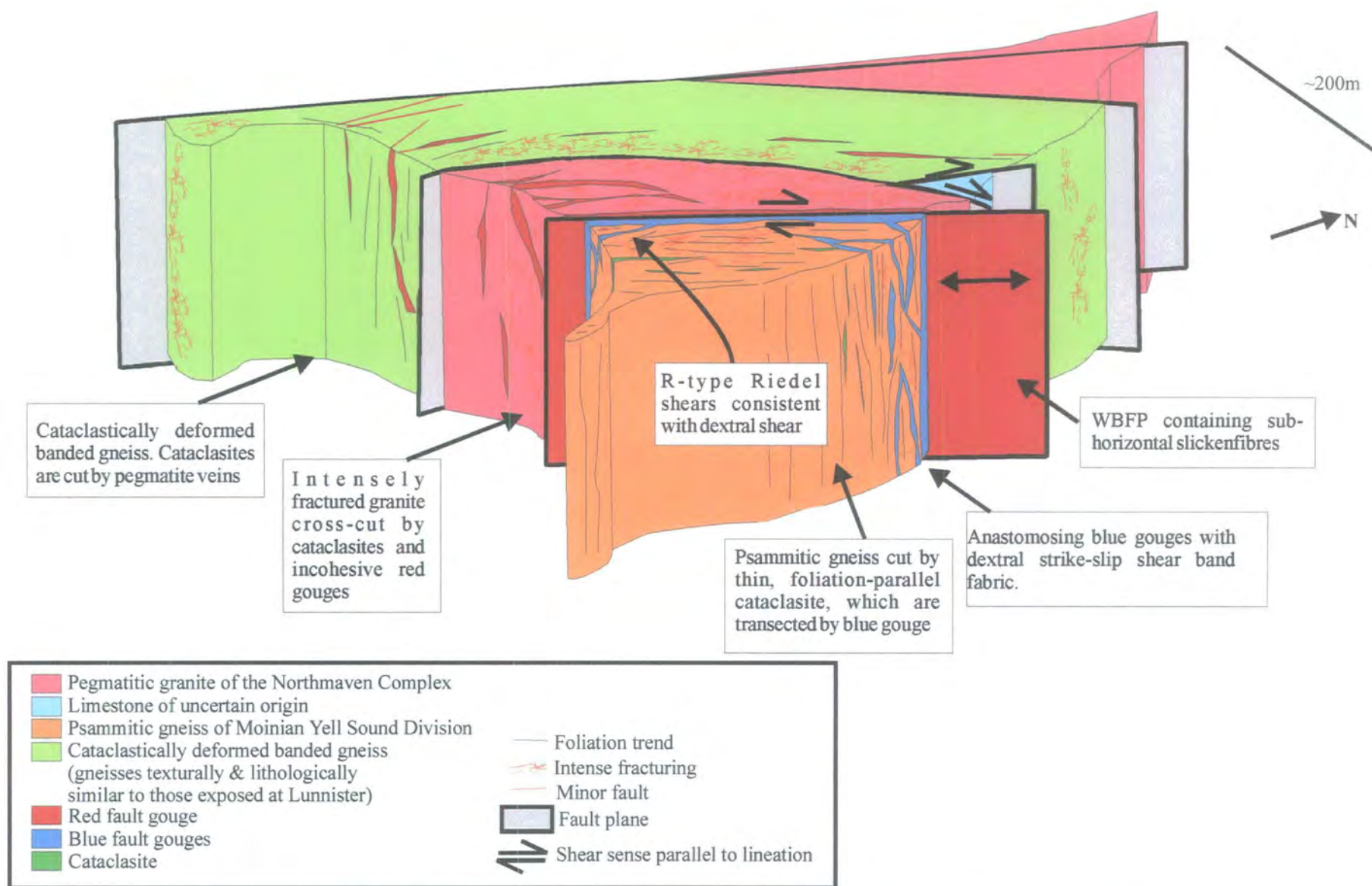


Figure 3.36 Schematic diagram to illustrate the fault rock distribution and the structure of the WBZ on Papa Little. Not to scale vertically.

3:1:5 Aith Voe

The western side of Aith Voe is a mainly NNW-SSE-trending coastal section of low cliffs (<5m high), beaches and narrow inlets from Point of Ayres (HU 3447 5723) to Keen Point (HU 3360 5926) (locality e, Figure 3.1). The WBFP intersects the coast at Waari Geo (HU 3409 5760) on a trend of 003° from Papa Little. The WBFZ at Aith Voe is 1 to 1.5km wide comprising an anastomosing network of NNE-SSW-trending sub-vertical faults (Figure 3.37). At Keen Point (HU 3360 5926), sandstones and volcanic rocks belonging to the Middle Devonian Sandness Formation are faulted against gneisses and schists belonging to the Moine-Dalradian boundary zone (Figure 3.37). To the east (near Waari Geo; Figure 3.37), the schists and gneisses are separated from a cataclastically deformed sliver of Devonian sandstone by a N-S-trending fault. The east side of the cataclastically deformed sandstone is bounded by the WBFP. To the east of the WBFP, fault-bounded slivers of mylonitic marble, hornblende schist and granite of the Spiggie Complex are exposed (Figure 3.37).

3:1:5:1 Protolith lithologies

3:1:5:1a Gneisses and schists

Compositionally banded gneisses and schists belonging to the Moine-Dalradian boundary zone (section 2:1:2:2) are exposed both west and east of the WBFP (Figure 3.37).

The rocks west of the WBFP comprise garnet-mica schist, kyanite-biotite schist, quartzo-feldspathic and hornblende-rich banded gneiss. Coarse-grained garnet-mica schists comprise garnet porphyroblasts (up to 1cm in size) surrounded by flattened aggregates of chlorite, muscovite, quartz and feldspar. Kyanite-biotite schists are medium grained comprising kyanite porphyroblasts surrounded by flattened aggregates of quartz and feldspar together with laths of biotite and muscovite. The compositionally banded gneisses are pink / green in colour and medium-grained with grains up to 0.5cm in length. The pink gneisses comprise equigranular aggregates of

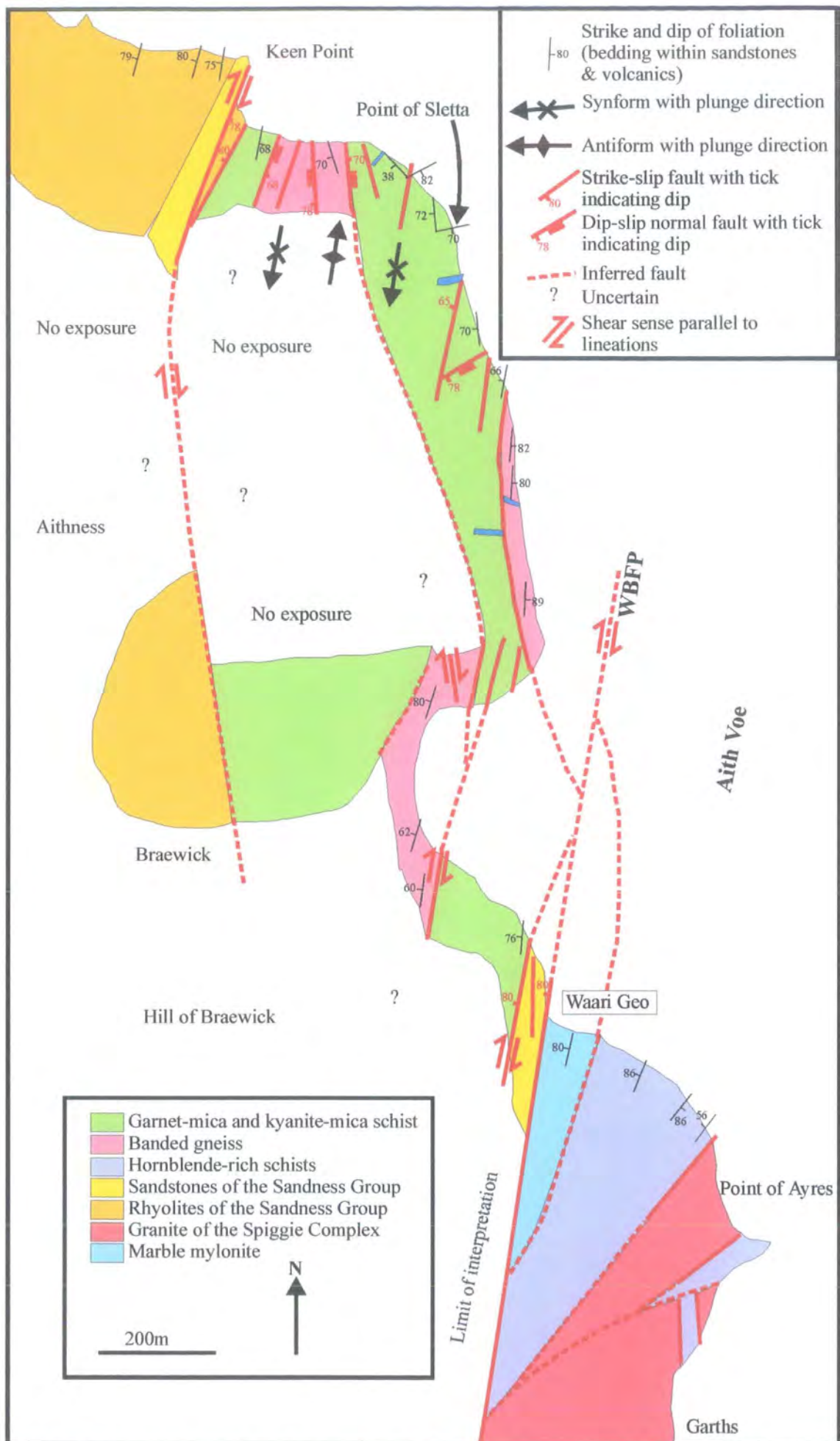


Figure 3.37 Geological map along the western side of Aith Voe.

feldspar (60%), quartz (20%), hornblende (10%) surrounding aligned biotite (5%) and muscovite (5%) grains. Green-coloured gneiss is composed of approximately 70% hornblende, 20% quartz and 10% epidote and chlorite. The rock contains a strong foliation defined by flattened aggregates of feldspar, quartz and hornblende with a sub-horizontal lineation defined by elongate mica, feldspar, quartz and hornblende grains. The gneisses are texturally and compositionally similar to those exposed west of the WBFP at Sullom, Lunnister and the Ness of Haggrister (section 3:1:2:1c) and on the island of Papa Little (section 3:1:4:1a).

The rocks east of the WBFP comprise poorly exposed hornblende schists (Figure 3.37). These are medium- to coarse-grained rocks comprising hornblende (65%), chlorite (15%), feldspar (15%) and quartz (5%). Sheared polygonal aggregates of quartz and feldspar are surrounded by a matrix of aligned hornblende and chlorite grains, which define the schistosity.

3:1:5:1b Sandstones and Volcanic rocks

Sandstones belonging to the Middle Devonian Sandness Formation (section 2:1:1:6a) crop out west of the WBFP (Figure 3.37). The rocks comprise a succession of cross-bedded, finely laminated sandstones and silts. A sequence of fine-grained, flow-banded rhyolites interbanded with centimetre-thick ignimbrite horizons lies conformably above the sandstones (Figure 3.37).

3:1:5:1c Granite

Granite belonging to the Late Devonian Spiggie Complex (section 2:1:1:7a) is exposed east of the WBFP (Figure 3.37). The granite is red / orange in colour and medium to coarse grained, comprising feldspar (70%), quartz (15%), hornblende (10%) and mica (5%). The granite is inequigranular and displays a porphyritic texture with phenocrysts of K-feldspar (up to 3cm in length). The feldspar phenocrysts are randomly orientated within a fine-grained matrix of feldspar, quartz, hornblende and mica phenocrysts displaying a holocrystalline texture. No magmatic or solid-state fabric was observed in the field.

3:1:5:2 Fault rocks

In this section, fault rocks are described in the order of their relative age (oldest to youngest; see section 3:1:5:3).

3:1:5:2a Marble mylonite

Marble mylonite is exposed within a fault-bounded sliver east of the WBFP (Figure 3.37; Plate 3.35). The mylonite is pale grey in colour and fine-grained, and consists of calcite (75%), tremolite (10%), muscovite (5%), albite (5%) and quartz (5%). Millimetre-scale bands of aligned calcite and muscovite wrap around porphyroclasts (0.5 to 2cm) of tremolite, albite, quartz and kyanite-biotite schists. The mylonite displays a strong foliation defined by elongate calcite and muscovite grains.

3:1:5:2b Phyllonitic rocks

Dark brown-coloured, fine-grained, mica-rich fault rocks are exposed within metre-scale shear zones west of the WBFP. Aligned aggregates of fine-grained biotite and muscovite define a mylonitic foliation, which surrounds porphyroclasts (0.1mm to 2cm) of feldspar, quartz, kyanite and cataclastically deformed schist. The N-S-trending sub-vertical foliation contains sub-horizontal lineations defined by aligned mica grains.

3:1:5:2c Cataclasite

Cataclasite is present adjacent to the WBFP and along other N-S-trending subsidiary faults within the WBFZ along the west coast of Aith Voe (Figure 3.37). The cataclasites are green / brown in colour, comprising finely comminuted fragments of sandstone, schist, gneiss, quartz, feldspar, hornblende, epidote and micas set within a locally hematite-mineralised, fine-grained cataclastic matrix of the same. Randomly orientated fragments are sub-angular to angular, ranging from 2mm to 25cm in size. The cataclasites are isotropic on all scales of observation in the field.



Plate 3.35 Plan view. Marble mylonite with σ -type porphyroclasts (K) of kyanite-biotite schist. Split arrows indicate shear sense parallel to lineation.

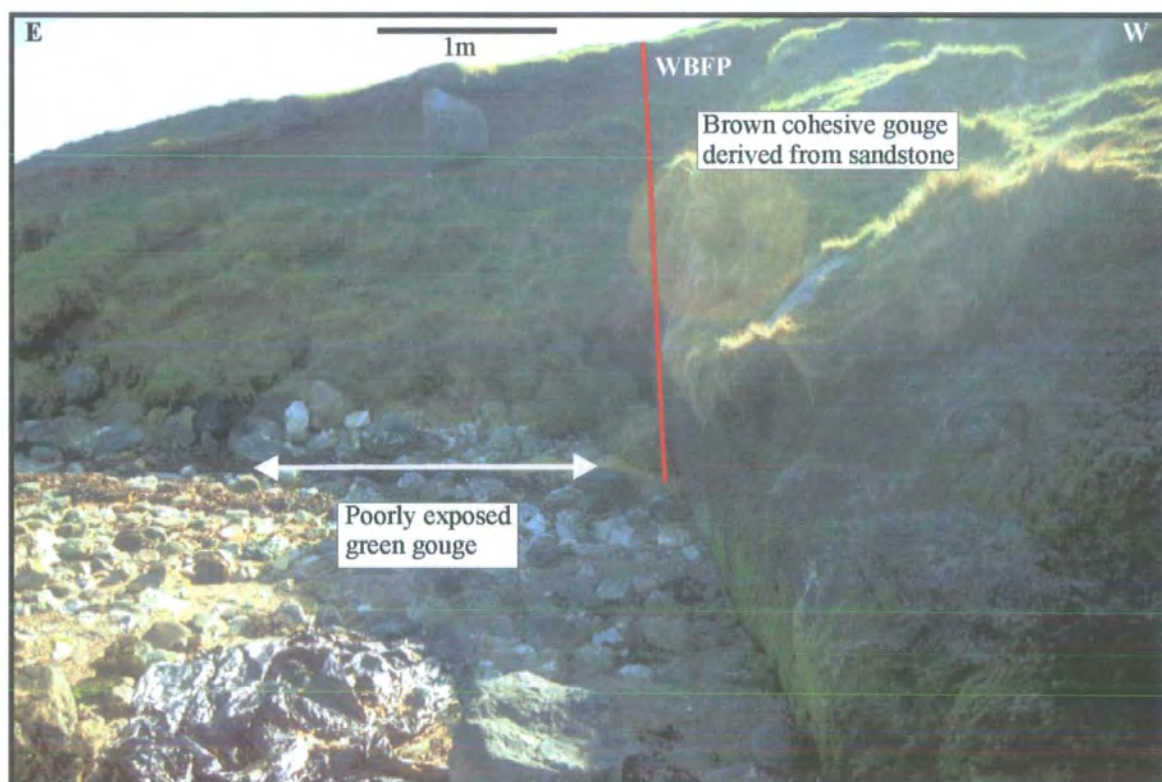


Plate 3.36 Cross-section across the WBFP and poorly exposed fault core at Waari Geo (HU 3409 5760).

3:1:5:2d Fault gouge

There are two fault gouges exposed within the WBFZ along the west coast of Aith Voe, a brown gouge and a green gouge. The brown gouge is clay-like in appearance, cohesive, well-banded and derived from sandstones belonging to the Sandness Formation. The brown gouge displays a colour banding defined by local variations in the clast-to-matrix ratio. N-S-trending, centimetre-thick hematite bands are common, locally acting as cement. The green fault gouge is incohesive and appears to be a clay-rich paste derived from marble mylonite. The green gouge contains a steeply dipping foliation with lineations that plunge shallowly to the N; both are defined by aligned clay particles.

3:1:5:3 Fault rock distribution and age relationships

The earliest fault rocks are generally found within wall rocks adjacent to and locally within the WBF core. Breccias, cataclasites and fault gouge of the WBF core transect all other structures and fault rocks.

3:1:5:3a West of the WBF core

The western side of the WBFZ is bounded by the Keen Point fault (HU 3360 5926) (Figure 3.37). This fault is filled with 0.5m of fault gouge and separates intensely fractured sandstones and rhyolites to the west from schists and gneisses to the east. Between Keen Point (HU 3360 5926) and the WBFP at Waari Geo (HU 3409 5760) exposure is poor. SSE of the Point of Sletta (HU 3389 5909; Figure 3.37) along the coast, schists and gneisses display a near-vertical, N-S-trending foliation defined by flattened aggregates of quartz, feldspar and mica, with sub-horizontal lineations defined by aligned mica grains. N-S-trending vertical shear zones infilled with phyllonitic rocks cross-cut schists and gneisses (HU 3402 5819). The phyllonitic rocks have lineations defined by aligned mica grains, which plunge gently to the N and a sub-vertical N-S-trending foliation defined by aligned aggregates of mica grains. N-S-trending subsidiary faults containing centimetre-thick gouge and breccia transect these shear zones. Broad zones of cataclasis are best-developed within wall rocks adjacent to the N-S-trending faults. Cataclasis and brecciation becomes very

intense at distances of less than 50m west of the WBFP and overprints all other structures and fabrics, with the rocks becoming almost unrecognisable.

3:1:5:3b East of the WBF core

East of the core of the WBF, exposure is very poor. Slivers of intensely fractured hornblende schist and granite appear to be overprinted by subsidiary faults, which are largely unexposed (Figure 3.37).

3:1:5:3 c WBF core

The fault core at Aith Voe is located in the central part of the WBFZ and corresponds to the region of most intense fault-related deformation. The most obvious and prominent fault plane (WBFP) within the WBFZ is exposed at Waari Geo (HU 3409 5760; Figure 3.37; Plate 3.36), forming a 1-2m-high vertical face and a narrow inlet. There, the poorly exposed fault core is approximately 20m wide and is defined by the occurrence of 100% fault rocks that extend from the wall rocks across the WBFP. To the west of the WBFP, a 10m-wide zone of breccia and cataclasite is present, derived from sandstones belonging to the Sandness Formation. The cataclasites display a brown coloration due to the presence of hematite cement. Locally, the cataclastic matrix appears to be altered to an isotropic clay-rich paste with disseminated iron oxide precipitate. To the east, a 50cm-thick brown coloured cohesive gouge overprints the cataclastic fabrics, and is bounded to the east by the WBFP. The gouge contains a colour banding defined by variations in grain size and hematite cement. A sub-vertical, N-S-trending foliation is present locally, defined by aligned clay particles. The WBFP is orientated 003/80W and contains quartz slickenfibres (16/005). To the east of the WBFP, a 1.5m-thick incohesive green gouge is present. The green gouge cross-cuts marble mylonite exposed to the east and contains a N-S-trending, sub-vertical foliation with sub-horizontal lineations; both are defined by aligned clay particles. East of the green gouge, a 10m-wide zone of anastomosing centimetre-thick soft green gouge surrounds blocks of boudinaged mylonite (10cm to 1m wide).

3:1:5:4 Fault zone structure

The WBFZ at Aith Voe is a 1.5km-wide zone of braided faults containing gouge and breccia. N-S trending fault strands bifurcate from the main WBFZ, encompassing slivers of protolith and earlier-formed fault rocks. This anastomosing geometry occurs on kilometre, metre and centimetre scales within the fault zone (Figure 3.37).

3:1:5:4a West of WBF core

The west side of the WBFZ is bounded by the Keen Point fault (HU 3360 5926) (Figure 3.37). This fault is filled with 0.5m of fault gouge and contains slickenside lineations, which plunge shallowly to the SW. On outcrop surfaces viewed parallel to slickenside lineation and normal to the fault plane, centimetre-spaced shear bands indicate dextral shear.

SSE of the Point of Sletta (HU 3389 5909) (Figure 3.37), open folds in schists and psammities tighten and steepen into a strongly foliated zone along the coast to the south. Foliation is near vertical and strikes N-S with lineations defined by aligned mica grains plunging shallowly to the S (Figure 3.38A). On outcrop and in thin-section surfaces viewed parallel to the lineation, millimetre-scale shear bands cross-cut the regional fabric and indicate sinistral shear. These rocks are cross-cut by N-S-trending, vertical shear zones (HU 3402 5819; Plate 3.37). The shear zones are typically 50cm wide. Schistosity planes in plan view swing into the high-strain zones in a clockwise direction, suggesting an overall dextral sense of shear (Plate 3.37). The shear zones contain semi-brittle phyllonitic rocks. Phyllonitic rocks have lineations defined by aligned mica grains, which consistently plunge shallowly to the N (Plate 3.37). Centimetre- to millimetre-scale, S-C' type fabrics indicate dextral shear on surfaces viewed parallel to the lineation and normal to the shear zone boundaries (Plate 3.37). In map view, the phyllonitic shears widen and bifurcate into several centimetre-thick strands. In cross-section, the shear zones locally shallow to near horizontal, commonly displaying shear fabrics indicating a top-N shear sense.

Subsidiary faults orientated N-S are common within the poorly exposed coastal sections. The faults cross-cut the dextral shear zones and contain centimetre-thick incohesive gouge and breccias.

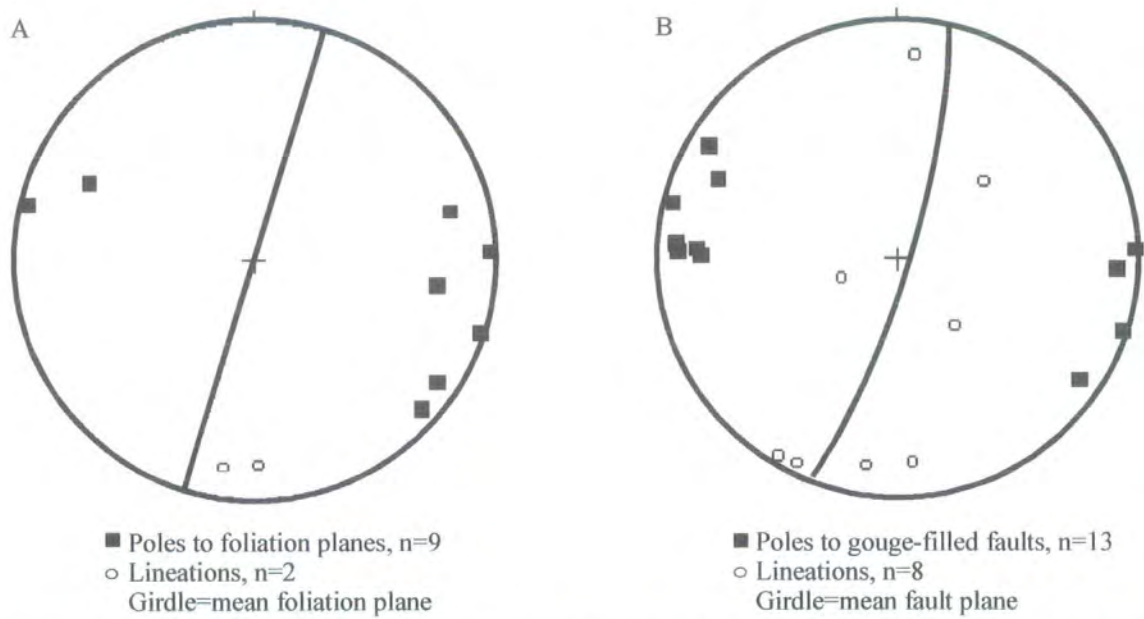


Figure 3.38 Stereographic projections to show (A) foliation and lineations within schists west of the WBFP, and (B) gouge-filled fault planes and slickenside lineations.

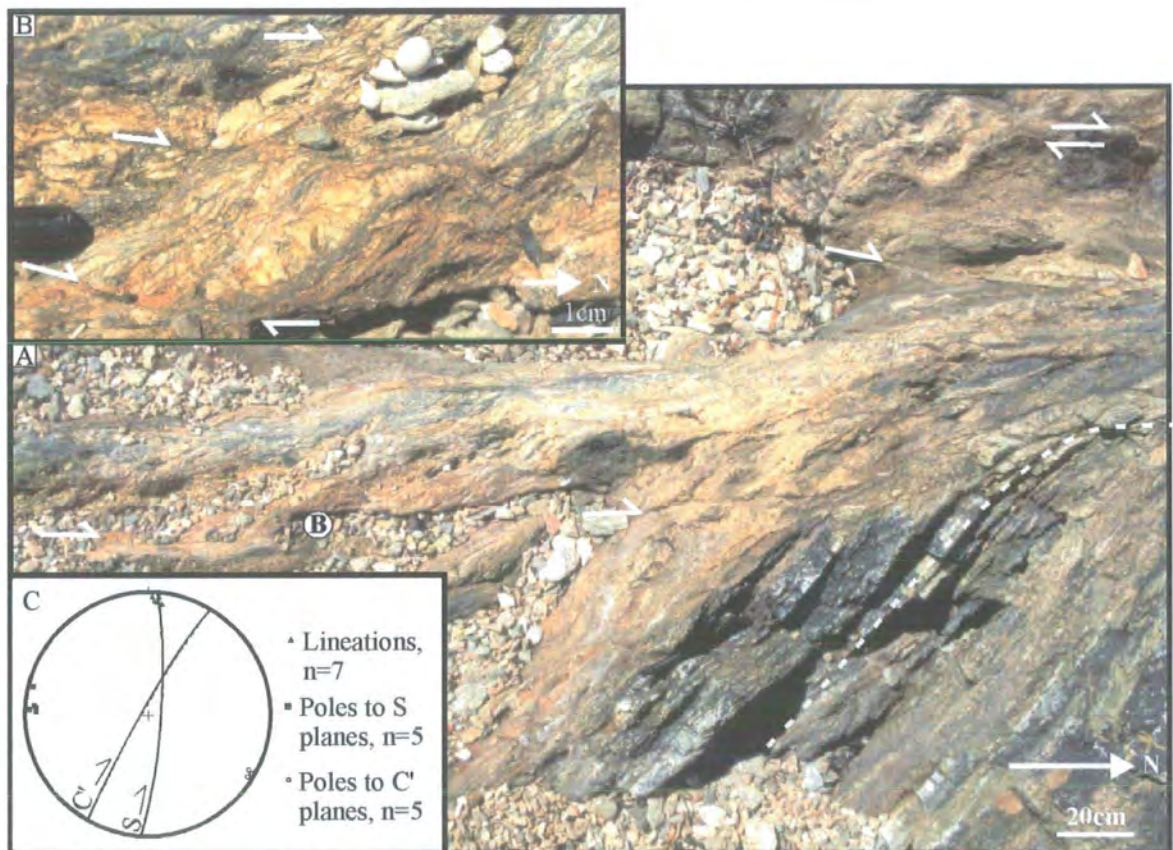


Plate 3.37 Plan View. (A) Semi-brittle shear zone cross-cutting kyanite- and biotite-rich schists, Aith Voe (HU 3402 5819). Schistose foliation swings into the shear zone in a clockwise direction. (B) Close up photograph of fabric located at B on the main photograph. Note: split arrows indicate shear sense parallel to lineation. (C) Stereographic projection to S and C' planes along with lineations (data collected from shear zone).

The gouge-filled faults strike NNE-SSW and dip steeply to the W and E. Slickenside lineations form two main clusters, dip-slip and sub-horizontal (Figure 3.38B). E-W-trending dolerite dykes (~1m thick) appear to cross-cut centimetre-scale, dextral shear zones (HU 3408 5823). The dolerite dykes are then offset dextrally along N-S sub-vertical fracture networks (Figure 3.39). Broad zones of cataclasis are most prominent within wall rocks adjacent to N-S-trending subsidiary faults containing gouge. Cataclasis is irregular and patchy, but generally increases towards the WBF. Green-coloured cataclasite injection veins orientated approximately 100° are perpendicular to dextral slickenfibres defined by the stepping direction of quartz fibres within NNE-SSW-trending centimetre-thick cataclasites (Figure 3.40), suggesting that they were formed as dilatational fractures during dextral strike-slip movements.

Centimetre- to metre-scale folds with sharply kinked closures and straight limbs first appear at distances of 120m west of the WBFP. The folds consistently show a dextral sense of vergence. Cataclasis and brecciation becomes very intense at distances of less than 50m west of the WBFP, with the rocks becoming almost unrecognisable. Epidote, quartz and calcite veins are usually a few millimetres thick. The randomly orientated veins commonly form interconnected networks.

3:1:5:4b East of the WBF core

East of the WBF core, poorly exposed slivers of intensely fractured hornblende schist and granite appear to be bounded by largely unexposed subsidiary faults (Figure 3.37), which are defined by breaks in slope.

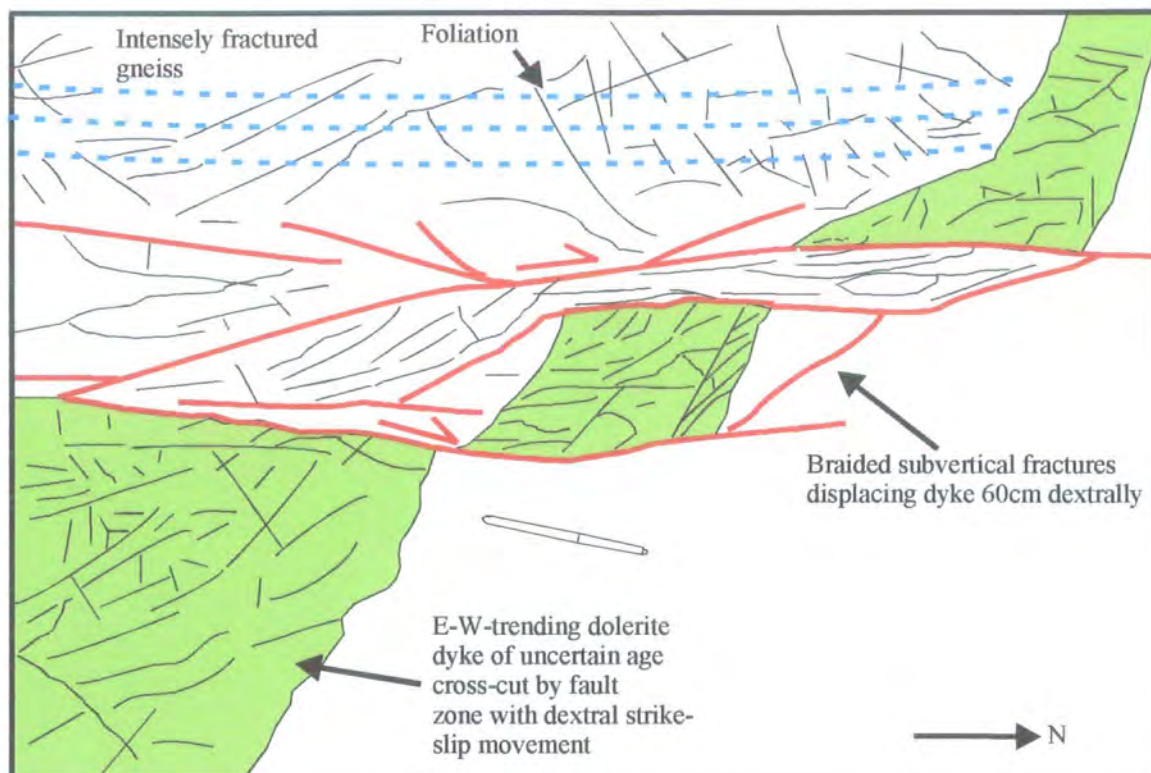


Figure 3.39 Plan View. Field sketch of E-W-trending dioritic dyke offset by sub-vertical dextral strike-slip fractures, west side of Aith Voe (HU 3408 5823).

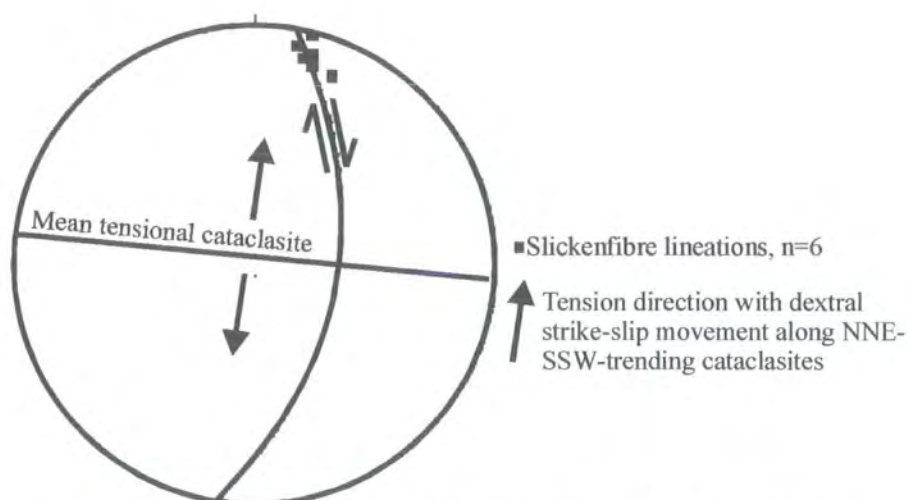


Figure 3.40 Stereographic projection showing the geometric relationship of NNE-SSW-trending centimetre-thick cataclasites, dextral slickenfibres and the mean orientation of tensional cataclasite injection veins.

3:1:5:5 Kinematic summary and discussion

The kinematic evolution of the WBFZ along the west coast of Aith Voe is summarised in Table 3.6.

Kinematic Regime	Fault rocks / structures
3. Dextral strike-slip	<ul style="list-style-type: none"> E-W dyke displaced by N-S fracture network Formation of fault gouge, cataclasis and breccias associated with the development of a kilometre-scale network of braided dextral strike-slip faults
2. Dextral strike-slip	<ul style="list-style-type: none"> N-S-orientated phyllonitic shear zones E-W-striking dyke cross-cutting dextral shear bands
1. Sinistral strike-slip	<ul style="list-style-type: none"> Sinistral shear bands overprinting regional fabrics? σ and δ-type porphyroclasts within marble mylonite

Table 3.6 Summary table of kinematic evolution of WBFZ along the west side of Aith Voe.

The structure and geometry of the WBFZ along the west side of Aith Voe is summarised in Figure 3.41. The rocks to the west of the WBFP are best-exposed and record all the kinematic events summarised in Table 3.6. The earliest event was sinistral strike-slip recorded by shear bands which overprint the regional schistose fabric west of the WBFP and σ and δ -type porphyroclasts within marble mylonite, both indicating sinistral shear. A ductile dextral phase is based on S-C'-type fabrics within phyllonites present along N-S-trending sub-vertical shear zone. A second cross-cutting phase of dextral strike-slip faulting led to the development of fault gouge, breccia and extensive cataclasis. During this event the present day geometry of faults was formed. The anastomosing network of N-S-trending faults resembles a positive 'flower' structure, whereby blocks of basement have been uplifted west of the WBFP (Figure 3.41; cf. section 3:1:2:7).

Conroy (1996) described the WBFZ at Aith Voe as a poorly exposed section dominated by intense cataclasis, with dextral shears trending 080-090°. It was also incorrectly stated that no outcrop of mylonite or fault gouge was present at this locality, contrasting with the findings of the present study and those of Flinn (1977).

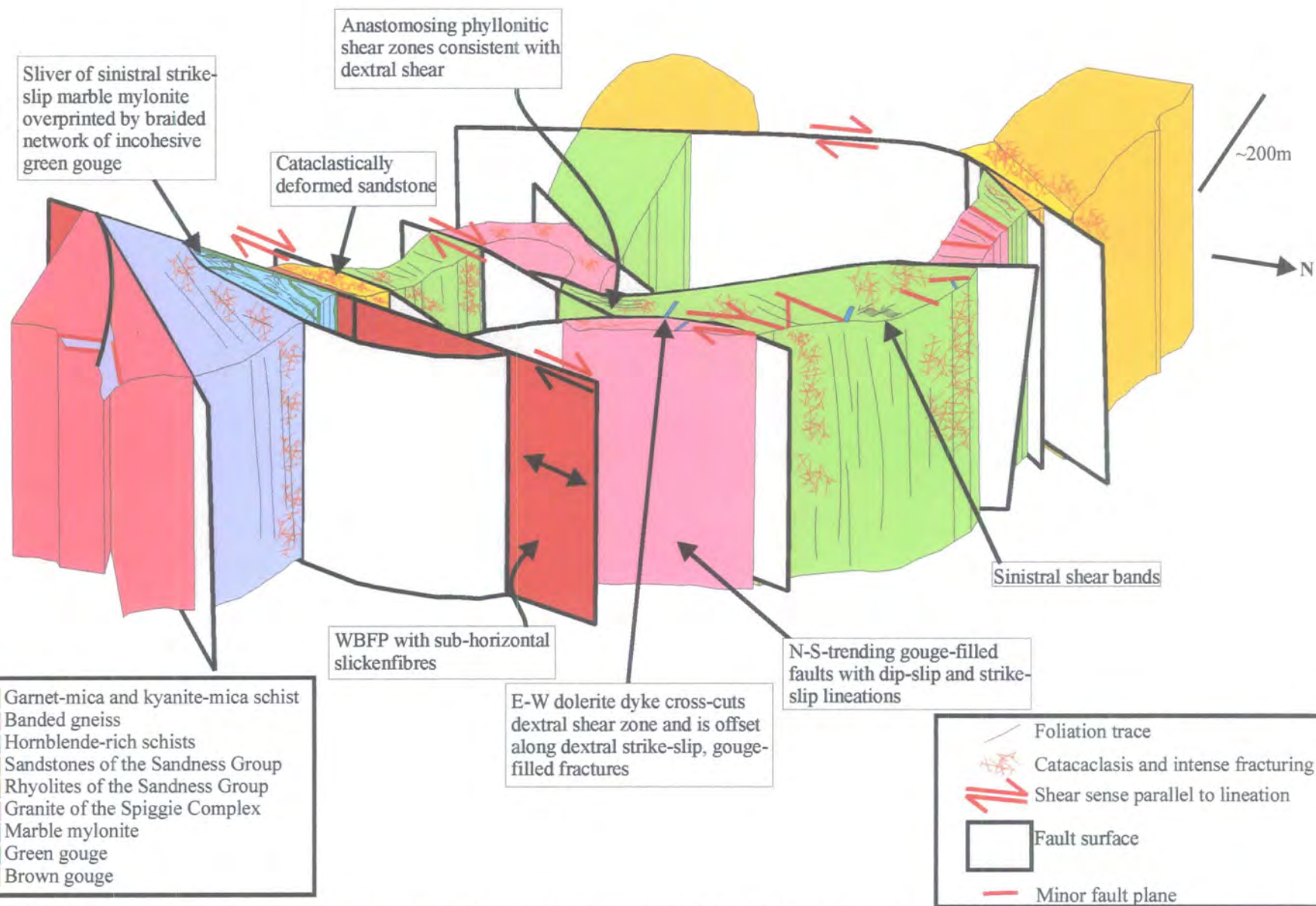


Figure 3.41 Schematic diagram to illustrate the structure of the WBFZ along the western side of Aith Voe. Not to scale vertically.

3:1:6 Ness of Bixter

The Ness of Bixter is a small headland extending into the firth of Sandasound Voe (locality f; Figure 3.1; Figure 3.42). An E-W-orientated coastal section on the south coast of the Ness of Bixter exposes the WBFZ. The WBFP intersects the south coast of the Ness of Bixter on a bearing of 004° from Aith Voe (locality e; Figure 3.1). To the west of the WBFP, sandstones belonging to the Middle Devonian Walls Formation (section 2:1:4:1) are exposed (Figure 3.42). East of the WBFP, fault-bounded slivers of cataclasite, calcareous schist (uncertain origin), granite (Spiggie Complex), calcareous schist (uncertain origin) and finally granite of the Late Devonian Spiggie Complex (section 2:1:5:1c) are exposed.

3:1:6:1 Protolith lithologies

3:1:6:1a Calcareous schists

Calcareous schists of uncertain origin occur in a fault-bounded slice east of the WBFP (Figure 3.42). The schists are grey in colour, medium grained and comprise calcite, quartz and mica. A N-S-striking sub-vertical foliation is defined by flattened aggregates of calcite and quartz with aligned mica grains defining sub-horizontal lineations. The calcareous schists exposed at the Ness of Bixter are similar in appearance to those belonging to the Queyfirth Group to the west of the WBFP at the Ness of Haggrister (see section 3:1:2:1b).

3:1:6:1b Sandstones

Sandstones belonging to the Middle Devonian Walls Formation are exposed west of the WBF (Figure 3.42). The rocks are grey in colour, fine to medium grained, and consist of a succession of cross-bedded, finely laminated sandstones and sporadic

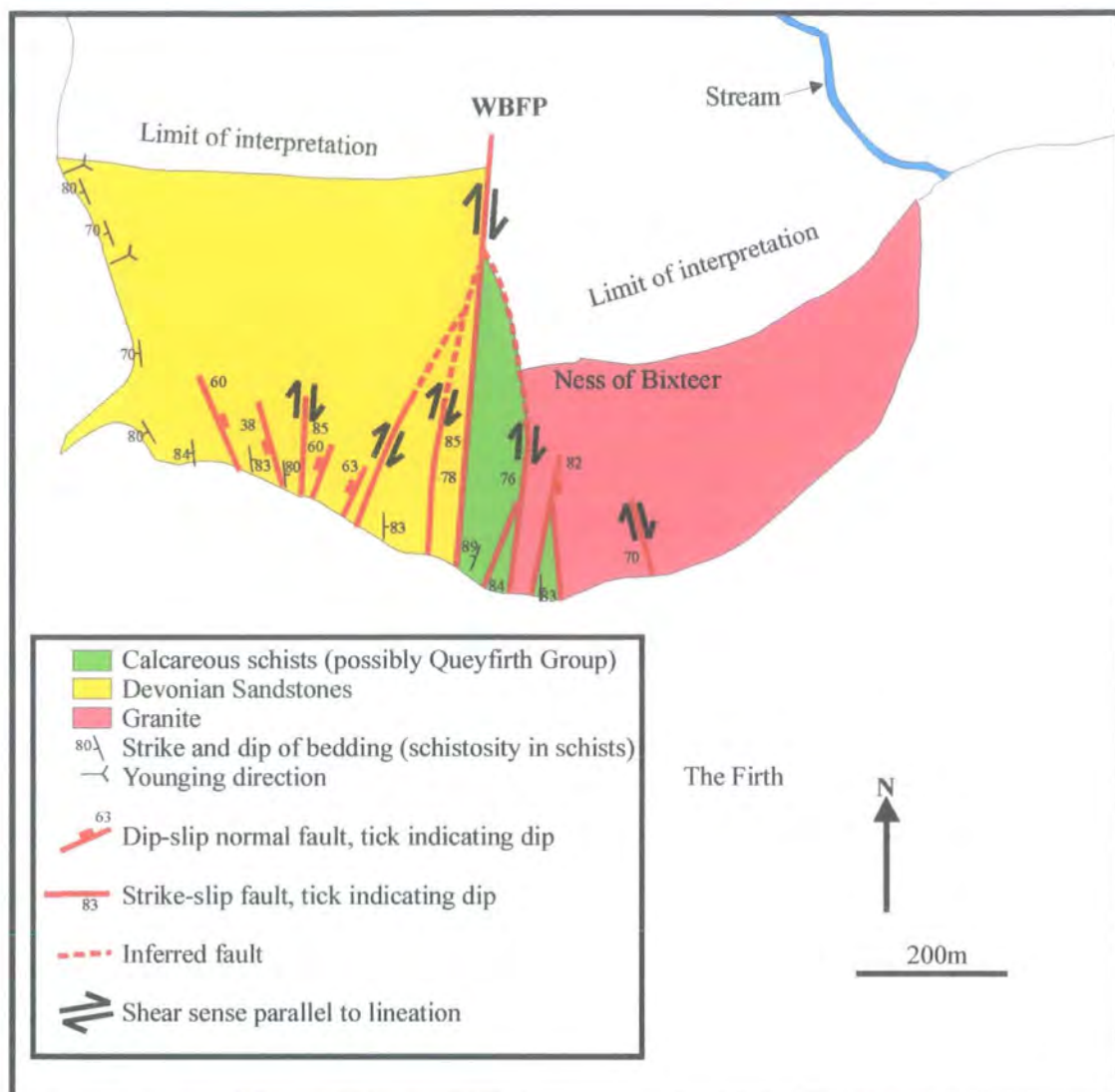


Figure 3.42 Geological map of the Ness of Bixter.

mudstones. The sandstones are pale grey in colour, fine to medium grained and well sorted. Outside the fault zone, bedding strikes NW-SE and dips moderately to the SW.

3:1:6:1c Granite

Granite belonging to the Late Devonian Spiggie Complex (section 2:1:5:1c) is exposed to the east of the WBFP (Figure 3.42). The granite is pink / orange in colour and medium to coarse grained with phenocrysts of feldspar up to 3cm in length. It is composed of approximately 40% orthoclase, 30% plagioclase, 20% quartz, 5% hornblende and 5% chlorite. The granite is inequigranular and displays a porphyritic texture. The randomly orientated orthoclase phenocrysts are surrounded by a coarse-grained matrix of plagioclase, orthoclase, quartz, hornblende and chlorite. Locally, the granite weathers to a green colour and is strongly retrogressed. Feldspars are replaced by aggregates of sericite, giving rise to a speckled appearance. Hornblende phenocrysts are partially broken down to fine-grained chlorite.

3:1:6:1d Pegmatite

The pegmatites are orange-coloured and coarse grained, comprising plagioclase (35%), orthoclase (35%), quartz (15%), biotite (5%) and muscovite (10%). The phenocrysts (~1cm in size) are equigranular and display a holocrystalline texture. The pegmatites cross-cut all the protoliths described in this section.

3:1:6:2 Fault rocks

In this section, fault rocks are described in the order of their relative age (oldest to youngest; see section 3:1:6:3).

3:1:6:2a Cataclasite

Cataclastically deformed rocks are exposed both west and east of the WBFP. Pale grey cataclasites comprise angular to sub-angular fragments (<2mm) of quartz, feldspar and sandstone set within a finely comminuted cataclastic matrix of the same.

Locally, pale grey cataclasites are cemented with calcite. Red cataclasites comprise finely comminuted fragments (<1cm in size) of feldspar, quartz, hornblende, mica and granite set within a fine-grained cataclastic matrix of the same. Randomly orientated clasts are angular to sub-angular. Hematite-cemented cataclasite bands transect the red cataclasites. The bands strike N-S and are 2mm to several centimetres thick. All types of cataclasite at the Ness of Bixter lack fabrics or apparent banding.

3:1:6:2b Breccia

Pale grey coloured incohesive breccias comprise comminuted fragments of sandstone, quartz and feldspar set within a fine-grained cataclastic matrix, which has been altered to a clay-rich paste. The breccias are isotropic on all scales of observation in the field. Millimetre-thick calcite veins are common within the breccia zone, locally acting as cement.

3:1:6:2c Fault gouge

Fault gouges at the Ness of Bixter vary from brown, yellow to green/blue in colour. The fault gouges are all incohesive, fine grained and clay-like in appearance. Bulk XRD analyses of the green/blue fault gouge within the WBF core at the Ness of Bixter show it to be composed of Ca-smectite, illite, clinochlore, tremolite, albite, muscovite and quartz (Conroy 1996).

3:1:6:3 Fault rock distribution and age relationships

The WBFZ at the Ness of Bixter is 500m wide, comprising a narrow fault core (~50m wide) flanked by wide zones of cataclasis. Fault-related deformation is strongly asymmetric, extending 350m west of the WBFP into Devonian sandstones and <150m east of the WBFP into calcareous schists and granite. Fault gouge, breccia and cataclasite increase in volume towards the WBF core and overprint Devonian sandstones, calcareous schists and granite. In this section, fault rock distributions within the rocks outside and adjacent to the fault core are described first, followed by a section describing fault rock distribution within the WBF core.

3:1:6:3a West of the WBF core

Gouge-filled faults first appear 350m west of the WBFP (HU 3434 5142). The faults contain 2 to 30cm of incohesive gouge flanked by zones of incohesive breccia and cataclasite, all of which overprint Devonian sandstones. At distances of less than 150m west of the WBFP (HU 3349 5134), 2-35cm-thick braided gouges, which locally contain calcite-mineralised breccias, are spaced approximately 5-6m apart. At distances between 40 to 100m west of the WBFP, cataclasis is intense with broad zones of incohesive breccia (~4m wide). Millimetre-scale calcite, scapolite and quartz veins occur within brecciated units, commonly forming networks. All fault rocks are interpreted to be roughly the same age, as no consistent cross-cutting relationships were observed in the field and all fault rocks could be apparently formed during the same kinematic regime (see section 3:1:6:4).

3:1:6:3b East of the WBF core

To the east of the WBFP, exposure is very poor. At distances of 140m east of the WBFP, the intensity of fracturing within the porphyritic granite is low. To the west, a 30m wide slice of calcareous schists is partially exposed (Figure 3.42). Fault rocks within the schists are absent. The west side of the calcareous schists is bounded by a fault containing 20cm of red fault gouge. West of this fault, a 20m-wide slice of porphyritic granite is exposed (Figure 3.42). The granite is moderately fractured and cross-cut by numerous, N-S-trending, millimetre- to centimetre-thick red gouge veins. The western side of the granite slice is bounded by a N-S-orientated fault, which contains 40cm of incohesive red fault gouge. Westwards to the core of the WBF, calcareous schists are poorly exposed. The schists are intensely fractured, and cross-cut by millimetre-thick calcite and gouge veins. In general, the volume of fault rocks east of the WBF core is much less than to the west of the WBF core.

3:1:6:3c The WBF core

The most obvious movement plane of the WBFZ is exposed on the southern side of the Ness of Bixter (Figures 3.42, 3.43). The WBFP is the main structural boundary within the WBFZ on the this side of the headland. It separates protoliths and fault rocks derived from Devonian sandstones to the west from those derived from calcareous schist and granite to the east. The fault plane (WBFP) is orientated 002/85W and defines a narrow inlet. Here, the fault core is approximately 50m wide (Figure 3.43), extending 40m west and 10m east of the WBFP. The fault core at the Ness of Bixter is located in the central part of the WBFZ and corresponds to the region of most intense fault-related deformation. Here, the fault core is defined by a continuous sequence of fault rocks that extends from the wall rocks (to the west and east) across the WBFP (the main structural boundary within the WBFZ) along an E-W trend.

The western side of the WBF core comprises intensely fractured and locally brecciated sandstones that are cross-cut by N-S-trending faults containing centimetre-thick gouge (Figure 3.43). At distances of 25 to 40m west of the WBFP, gouge-filled faults are spaced between 1 and 4m. Adjacent to the faults, the sandstones are overprinted by broad zones of incohesive breccia (Figure 3.43). At distances from 3 to 25m west of the WBFP, gouge-filled faults do not appear to increase in frequency. Broad zones of incohesive breccia (up to 4m wide) overprint patches of pale grey cataclasite. Millimetre-thick calcite veining is associated with brecciation and does not appear to increase in frequency towards the WBFP.

A 3m-wide zone containing blue / green fault gouge is bound to the east by the WBFP (Figure 3.43; Plate 3.38). The blue / green gouge overprints incohesive fault breccia and intensely fractured sandstones to the west. A 1.5m thick pegmatite cross-cuts and contains xenoliths of blue / green gouge (Figure 3.43; Plate 3.38). To the east of the pegmatite, 50cm of blue / green fault gouge contains a strong fabric with sub-horizontal lineations, both defined by aligned clay particles. The eastern side of the gouge is bounded by the WBFP, which is orientated 002/85W and contains sub-horizontal slickenside lineations (8/003).

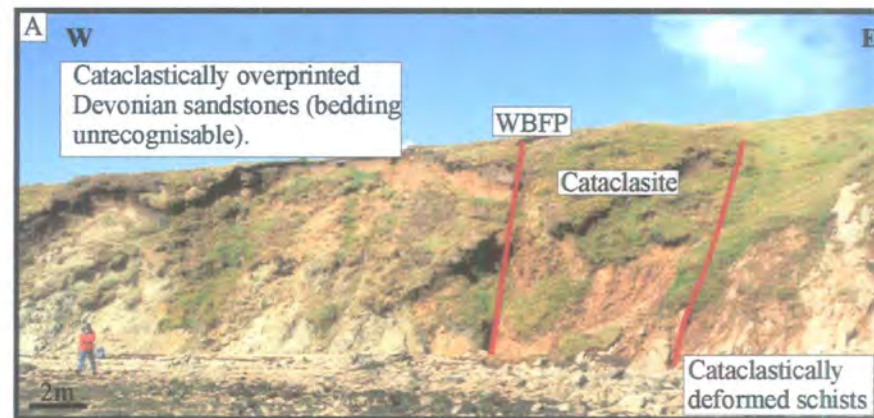


Figure 3.43 Structural log and cross-section through the WBF core on the south side of the Ness of Bixter (HU 3363 5123). Inset (A) Central part of core of the WBF showing the WBF.

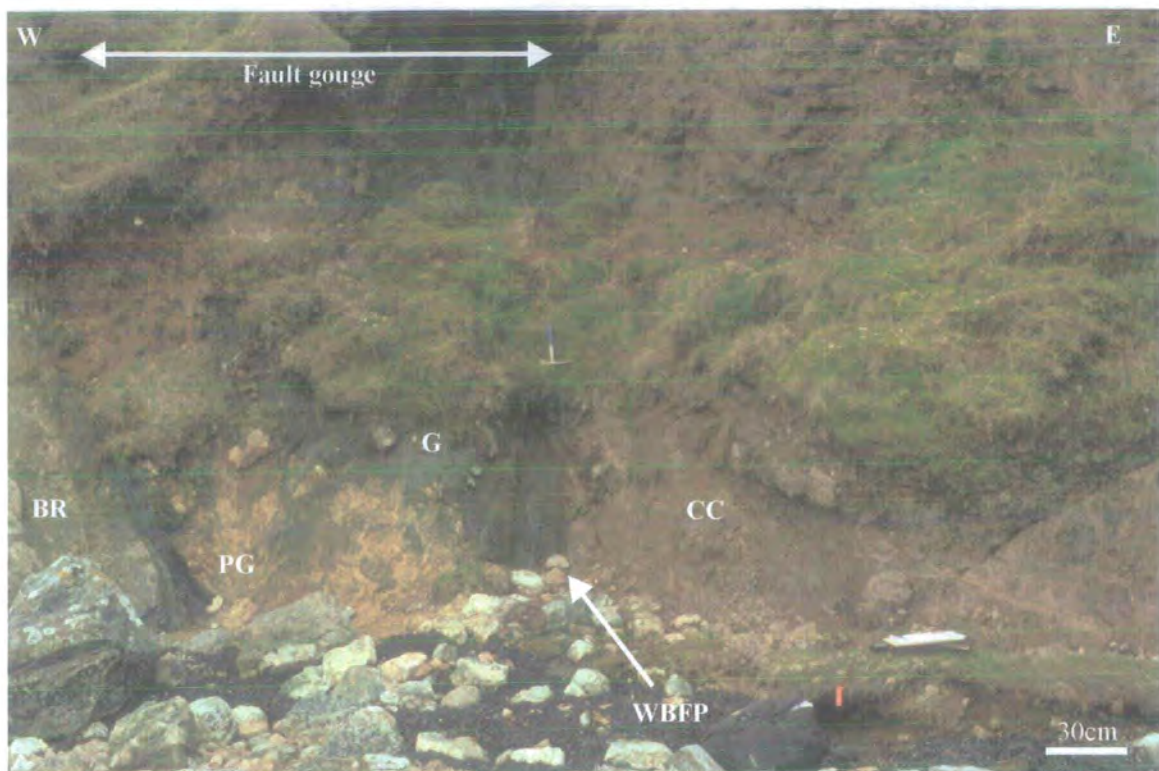


Plate 3.38 Plan view. Photograph to show fault rock distribution adjacent to the WBFP (HU 3363 5123. Located (A) on Figure 3.43. BR - Breccia PG - Pegmatite G - Gouge CC - Cataclasite.

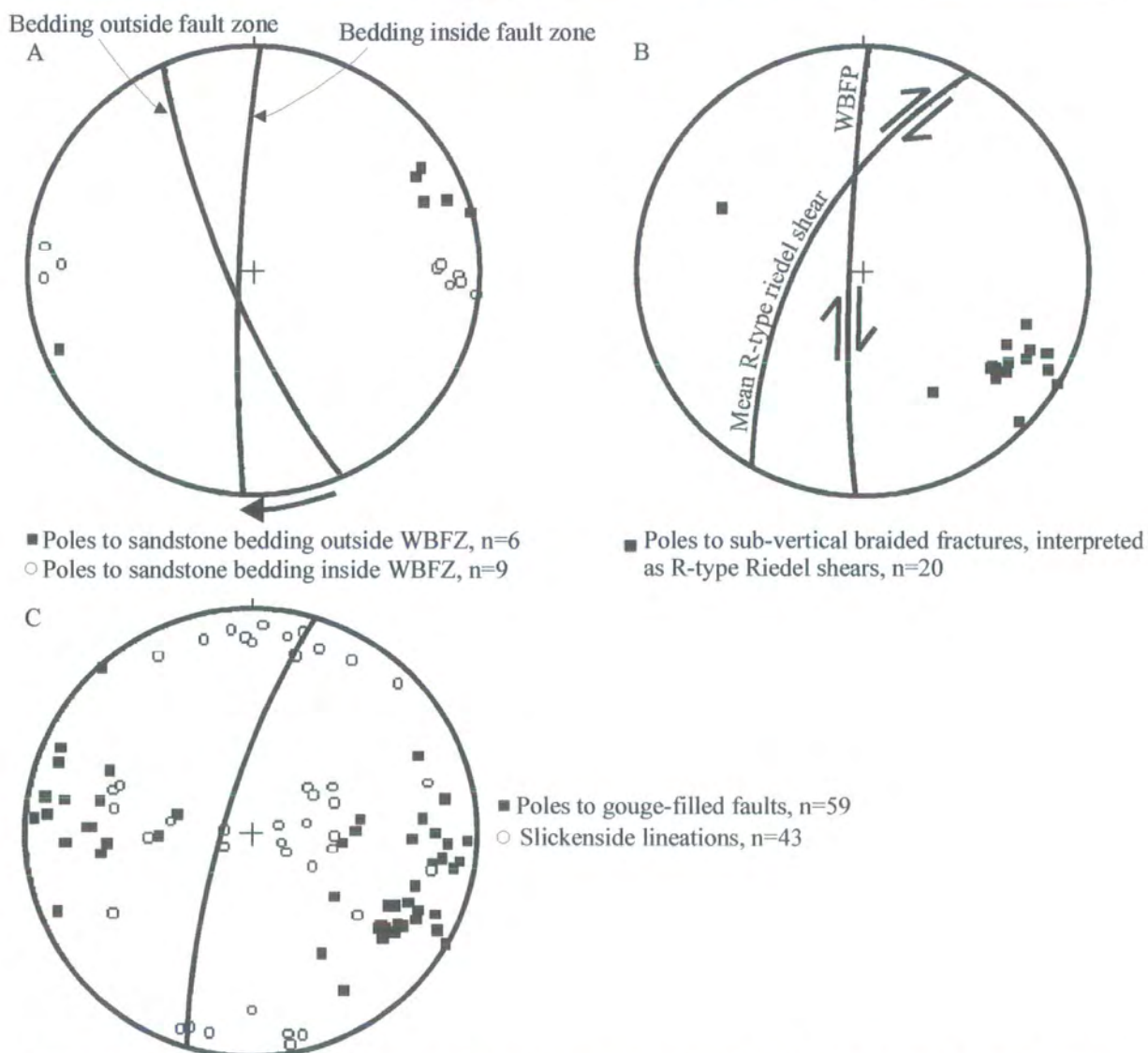


Figure 3.44 Stereographic projections to show (A) sandstone bedding, (B) R-type Riedel shears and (C) gouge-filled faults west of the WBF core.

To the east of the WBFP, a 4m-wide block of red-coloured cataclasite is exposed (Figure 3.43). The cataclasite is isotropic on all scales of observation in the field and is cross-cut by N-S-trending hematite-cemented cataclasites ranging from 2mm to several centimetres in thickness. To the west, the red cataclasite is cross-cut by blue / green gouge.

To the east of the cataclasite, a slice of calcareous schist of uncertain origin crops out (Figure 3.43). The schists are intensely fractured and locally brecciated, and are cross-cut by millimetre-thick gouge and calcite veins.

3:1:6:4 Fault zone structure

The WBFZ at the Ness of Bixter is 500m wide. Fault-related deformation is strongly asymmetric, extending 350m into Devonian sandstones west of the WBFP and <150m into fault-bounded slivers of calcareous schist and granite east of the WBFP. N-S-trending, gouge- and breccia-filled faults bifurcate and link together along their length to produce an anastomosing network (Figure 3.42).

3:1:6:4a West of the WBF core

Steeply-dipping bedding within the Devonian sandstones and mudstones changes orientation from NW-SE outside the fault zone to N-S within the fault zone (Figure 3.44A). The western boundary of the WBFZ is marked by a fault (HU 3434 5142) containing 2cm of yellow-coloured fault gouge. The N-S-trending, vertical fault plane contains dextral slickenfibres (12/346), defined by the stepping of quartz fibres. Here, fracturing within the adjacent wall rocks is moderate, and rarely exposed interbedded mudstone units are strongly sheared. Calcite-mineralised breccias occur within some N-S-orientated fault gouges. Sub-vertical, NE-SW-trending, braided fracture networks first appear 330m west of the WBFP (Figure 3.44B). The braided fracture networks offset the N-S-trending sandstone bedding by 2-35cm and are interpreted as R-type Riedel shears formed as a result of dextral shear along the WBF. Subsidiary faults containing centimetre-thick gouge are spaced approximately 10m apart until distances of <150m west of the WBFP. The faults strike N-S and dip

steeply to the E and W (Figure 3.44C). Slickenside lineations form two main clusters; strike-slip or dip-slip displacements. On outcrop surfaces viewed parallel to lineations and perpendicular to the fault planes, fold vergence, shear bands and, in places, stepping quartz slickenfibres indicate either dextral strike-slip or dip-slip normal movements.

150m west of the WBFP (HU 3349 5134), a dip-slip normal fault containing 30cm of yellow / brown fault gouge is exposed (Plate 3.39). Incohesive breccia occurs both sides of the main fault zone. The main fault zone is 1m wide and contains anastomosing fault gouge surrounding enclaves of intensely fractured sandstone (Plate 3.39). Anastomosing fault gouges link into the main gouge adjacent to the W-dipping polished fault plane. The fault plane contains quartz slickenfibres, which step down dip, indicating dip-slip normal movement.

To the east of the normal fault, sandstones are intensely fractured and contain frequently spaced (5-6m) gouge-filled faults. The faults transect intensely brecciated sandstones and contain 2-30cm thick zones of braided, N-S-trending, fault gouges (Figure 3.44C) adjacent to polished fault planes. Slickenside lineations form two main clusters, sub-horizontal and dip-slip. On outcrop surfaces normal to fault planes and parallel to lineations, shear bands and fold vergence indicate both dextral strike-slip and dip-slip normal movements. Metre-scale domains of dip-slip normal faults follow domains of dextral strike-slip faults. Strain partitioning into dextral strike-slip and an extensional component occurs on an outcrop scale (metre-scale) at distances <150m west of the WBFP. Both dextral strike-slip and normal faults are interpreted to be the same age based upon inconsistent overprinting relationships, fault-rock correlation and fault zone linkages. Centimetre-thick, calcite-mineralised breccias are common, especially along faults that display dextral shear criteria (Plate 3.40).

At distances between 40 and 100m west of the WBFP, cataclasis is intense with the development of local incohesive breccia zones (1 to 3m thick). Here, braided gouge-filled faults are spaced 4-5m apart and occur within zones of incohesive breccia. Randomly orientated, millimetre-thick calcite, scapolite and quartz veins occur within brecciated units, commonly forming interconnected networks. Centimetre-scale tension gashes orientated 070° and infilled with calcite occur within more coherent



Plate 3.39 Cross-section through dip-slip normal fault containing yellow / brown gouge (HU 3349 5134). BR- Incohesive breccia, G- Fault gouge S- Sandstone clasts. Note: arrows indicate sense of shear.



Plate 3.40 Cross-section through mineralised fault breccia developed along dextral strike-slip fault. Note: Intensely fractured sandstone (IFS).

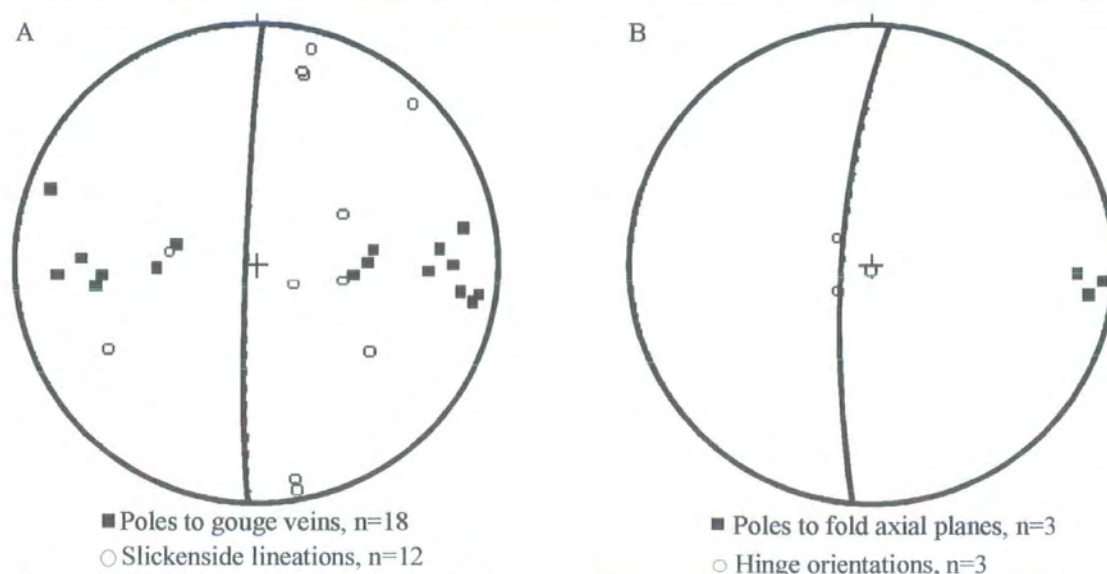


Figure 3.45 Stereographic projections of (A) gouge veins in granite and (B) dextral-verging folds within calcareous schists east of the WBF core.

units, implying a dextral sense of shear (see section 3:1:6:4c). Pale grey cataclasites occur locally within incohesive breccias and contain a calcite cement. Subsidiary gouge-filled faults, calcite-filled tension gashes, R-type Riedel shears, veining and breccias increase in frequency towards the fault core

3:1:6:4b East of the WBF core

At distances of up to 140m east of the WBFP, the intensity of fracturing within the porphyritic granite is very low. Sub-vertical fractures with a mean orientation of 040/70NW and sub-horizontal slickenside lineations offset granite veins by a few centimetres, and are interpreted as R-type Riedel shears. To the west, a 30m-wide slice of calcareous schists is partially exposed (Figure 3.43). Fault-related deformation within the schists is virtually absent. The western side of the calcareous schists is bounded by a fault orientated 010/82E (HU 3377 5124; Figure 3.43). The fault contains dip-slip slickenside lineations and 20cm of red fault gouge. On surfaces viewed parallel to the lineation and normal to the fault plane, down-dip verging folds infer a dip-slip normal movement. To the west, a 20m-wide slice of porphyritic granite is exposed (Figure 3.42). The granite is moderately fractured and cross-cut by numerous N-S-trending red gouge veins. Gouge veins show either dip-slip or strike-slip slickenside lineations (Figure 3.45A). Outcrop surfaces viewed normal to the fault planes and parallel to the lineations, display centimetre-scale shear bands indicating dextral strike-slip or dip-slip normal movement. The western side of the granite sliver is bounded by a fault orientated at 003/76W, which contains 40cm of incohesive red fault gouge, and with sub-horizontal lineations defined by aligned clay particles (HU 3371 5124; Figure 3.42). On surfaces viewed parallel to the lineation and normal to the fault plane, shear bands show dextral shear. Between the WBF core and the fault containing red gouge (70m to the east) calcareous schists are poorly exposed. The schists are intensely fractured and cross-cut by millimetre-thick calcite veins and N-S-trending gouge veins. Centimetre-scale folds with sharp closures and straight limbs are steeply-plunging structures with N-S-trending axial planes (Figure 3.45B). The folds show a dextral sense of vergence.

3:1:6:4c WBF core

The western side of the WBF core comprises intensely fractured and locally brecciated sandstones that are cross-cut by faults containing centimetre-thick gouge (Figure 3.43). The faults are orientated N-S and dip steeply to the E and W (Figure 3.46A). Slickenside lineations form two main clusters, sub-horizontal and down-dip. At distances of 25 to 40m west of the WBFP, gouge-filled faults are spaced between 1 and 4m and mainly contain dip-slip slickenside and slickenfibres lineations (Figure 3.43). Where slickenfibres are present they display dip-slip normal movement defined by the down-dip stepping of quartz fibres. Adjacent to the gouge-filled faults, sandstones are reduced to broad zones of incohesive breccia (Figure 3.43). Sub-vertical tension gash arrays infilled with calcite occur within intensely fractured units 40m west of the WBFP. The tension gashes are typically 1-3cm thick, 3-35cm long and are orientated 070°, suggesting a dextral sense of shear (Plate 3.41; Figure 3.46B). Sub-vertical, anastomosing, NE-SW-trending fractures dip steeply to the NW (Figure 3.46C). The fractures contain sub-horizontal slickenside lineations and display dextral strike-slip offsets. The fractures are interpreted as R-type Riedel shears formed as a result of dextral shear along the WBF.

At distances between 3 and 25m west of the WBFP, subsidiary faulting does not appear to increase in frequency. Here, the faults contain dextral-verging folds and shear bands on outcrop surfaces normal to fault planes and parallel to sub-horizontal slickenside lineations (Figure 3.43). Both extensional and strike-slip faults are inferred to be of the same age as they contain the same fault rocks and do not display any consistent cross-cutting relationships. The faults appear to represent strain partitioning on an outcrop scale.

A 3m-wide zone containing blue / green fault gouge is bounded to the east by the WBFP (Figure 3.43; Plate 3.38). The blue / green gouge overprints incohesive fault breccia and intensely fractured sandstones to the west. A 1.5m-thick pegmatite cross-cuts and contains xenoliths of blue / green gouge (Figure 3.43; Plate 3.38). To the east of the pegmatite, 50cm of blue / green fault gouge contains a strong fabric with sub-horizontal lineations, both defined by aligned clay particles. Centimetre-scale shear bands are present within outcrop surfaces viewed parallel to the lineation and normal to the WBFP, consistently indicating dextral shear.



Plate 3.41 Plan view. Calcite-filled tension gashes orientated 070° , suggesting an overall dextral sense of shear. Plate located as (B) on Figure 3.43.

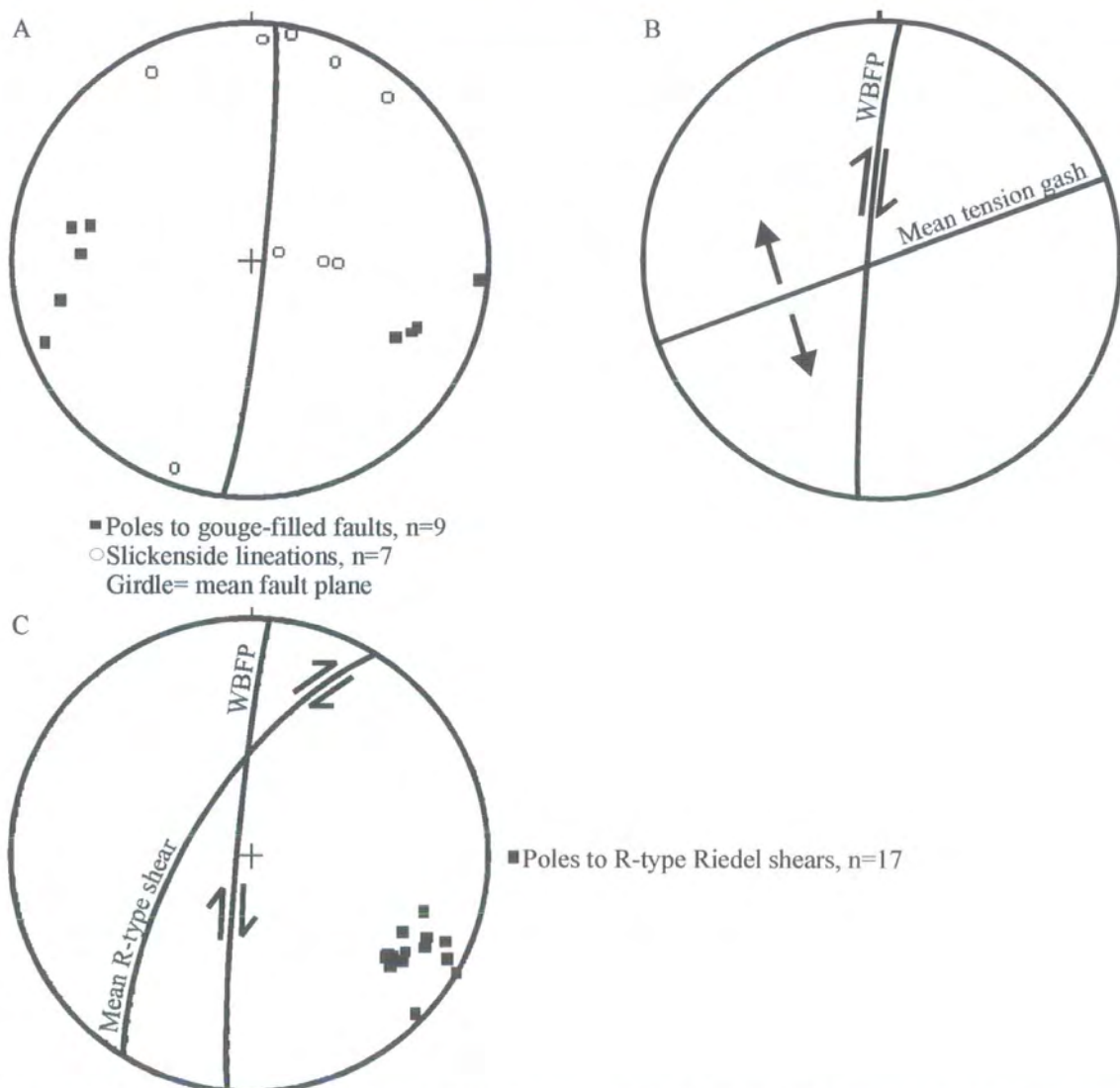


Figure 3.46 Stereographic projections to show (A) gouge-filled faults, (B) the geometrical configuration of calcite-filled tension gashes and (C) R-type Riedel shears.

The east side of the gouge is bound by the WBFP, which is orientated 002/85W and contains slickenside lineations plunging at 8/003.

To the east of the WBFP, a 4m-wide block of red-coloured cataclasite is exposed (Figure 3.43). The cataclasite is isotropic and is cut by N-S-trending hematite-cemented cataclasites ranging from 2mm to several centimetres thick (Figure 3.43). The red cataclasite is cut by blue / green gouge to the west.

To the east of the cataclasite, a slice of calcareous schist of uncertain origin crops out (Figure 3.43). The schists are intensely fractured and locally brecciated, with abundant millimetre-scale calcite and gouge veining. The calcareous schists are similar in appearance to those exposed west of the WBFP on the southern side of the Ness of Haggister, implying a minimum dextral strike-slip offset of 20km along the WBFP (see section 3:1:2:1b). Kink folds with a consistent dextral sense of vergence are common (see section 3:1:6:4b). Subsidiary faulting is infrequent within the schists.

3:1:6:5 Kinematic summary and discussion

The kinematic evolution of the WBFZ at the Ness of Bixter is summarised in Table 3.7.

Kinematic Regime	Fault rocks / structures
1. Dextral strike-slip	<ul style="list-style-type: none"> • Dextral shear bands within fault gouges • Slickenside and slickenfibres indicators • Dextral-verging folds with fault gouges • Sliver of calcareous schists east of the WBFP similar in appearance to those exposed west of the WBFP on the southern side of the Ness of Haggister, indicating a minimum dextral strike-slip offset of 20km along the WBFP • R-type Riedel shears • Tension gashes

Table 3.7 Summary table of the kinematic evolution of the WBFZ at the Ness of Bixter.

The WBFZ on the south side of the Ness of Bixter is 500m wide. The WBF is the main structural boundary within the WBFZ separating Devonian sandstones to the west from calcareous schists and granite to the east. It corresponds to the surface along which the most recent regionally significant took place along the WBF. The structure and distribution of fault rocks at the Ness of Bixter is summarised in Figure 3.47. Fault-related deformation is strongly asymmetric, with cataclastic deformation more intense to the west of the WBF. The WBFZ comprises a braided network of dextral strike-slip and dip-slip normal gouge-filled faults, which appear to bifurcate from the WBF core. The WBF core is 50m wide and comprises a narrow central zone containing fault gouge (2m wide) flanked by a zone of gouge, breccia and cataclasites. A dextral strike-slip phase of faulting is recognised within rocks on both sides of the WBF at the Ness of Bixter. Here, the geometry of the WBFZ defines a 'negative' flower structure. Anastomosing faults bounding slivers of fault rock and protolith display either dextral strike-slip or dip-slip normal kinematics and appear to root into the WBF core. The 'negative' flower structure developed due to continued dextral strike-slip movement along a releasing bend of the WBF. The presence of a 'negative' flower structure could explain why earlier fault rocks are not exposed at the Ness of Bixter (cf. Sullom, Lunnister and the Ness of Haggrister; section 3:1:2:7).

Conroy (1996) described the WBFZ on the south side of the Ness of Bixter to be a mass of cataclastic sandstones, calc-silicate schists and psammites shot through with red, feldspar-rich, granite material. No kinematic indicators were recorded by Conroy (1996) at this locality.

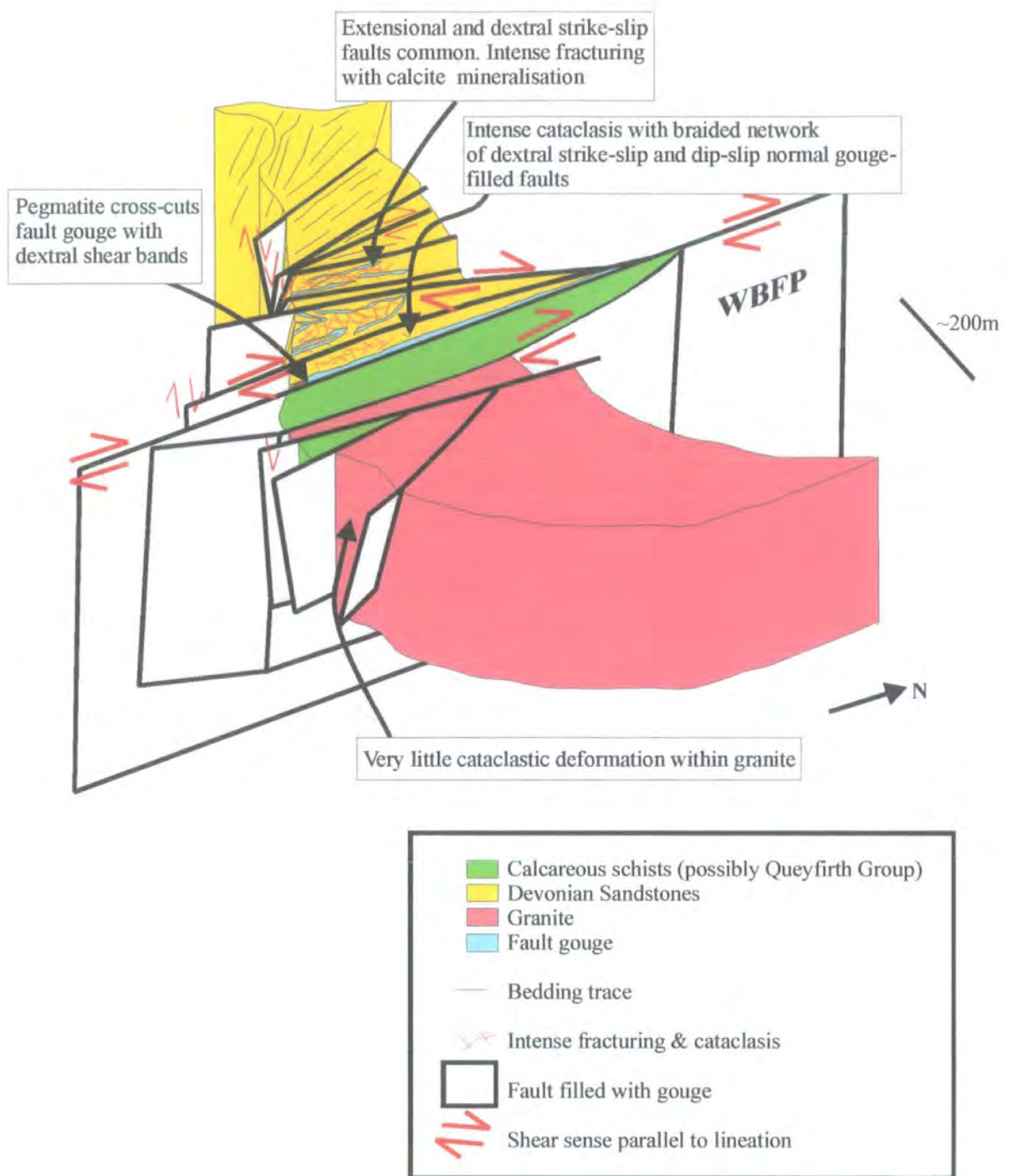


Figure 3.47 Schematic diagram to illustrate the structure of the WBFP at the Ness of Bixter. Not to scale vertically.

3:1:7 Seli Voe and Sand

The Seli Voe to Sand coastal section is dominated (locality g: Figure 3.1) by 5 to 40m-high cliffs, beaches and a rocky shoreline. Here, the WBFZ is 1.5km wide, extending from the west coast of Seli Voe to the west coast of Sand Voe. The actual WBFP is not exposed at Seli Voe but the fault trace is marked by a flat-bottomed valley, which can be traced from the south side of the Ness of Bixter to the head of Seli Voe along a bearing of 004°. At Seli Voe, the WBF separates sandstones of the Middle Devonian Walls Formation (section 2:1:4:1), cut by granite belonging to the Late Devonian Sandsting Complex to the west (section 2:1:5:2b), from a thin sliver of cataclasite, followed to the east by a succession of pelites and psammities (Figure 3.48). To the east of the pelites and psammities, a fault-bounded sliver of blastomylonite, cataclasite and foliated cataclasite is followed by granodiorite belonging to the Late Devonian Spiggie Complex (section 2:1:5:1c) (Figure 3.48).

Flinn (1977) briefly described the WBFZ at Seli Voe to Sand as a 1.5km-wide zone of cataclastic deformation with the local development of fault gouge. A minimum dextral strike-slip offset of 33km was suggested based upon a correlation between the pelites and psammities exposed to the east of the WBFP at Seli Voe and similar rocks belonging to the Queyfirth Group exposed to the west of the WBFP at Ollaberry. Conroy (1996) discounted this correlation and suggested that the schists at Seli Voe are more quartz rich, have not developed mullions and display more regular garnet growth than the rocks exposed at Ollaberry. Flinn (1977) briefly described a fault-bounded slice of mylonites on the coast between Seli Voe and Sand which can be traced inland. Conroy (1996) stated that no mylonites could be observed and briefly described cataclastically deformed rocks within the WBFZ at Seli Voe.

3:1:7:1 Protolith lithologies

3:1:7:1a Metasedimentary rocks

To the east of the WBFP, an 850m-thick succession of pelites, psammities and quartzites of uncertain origin is exposed (Figure 3.48).

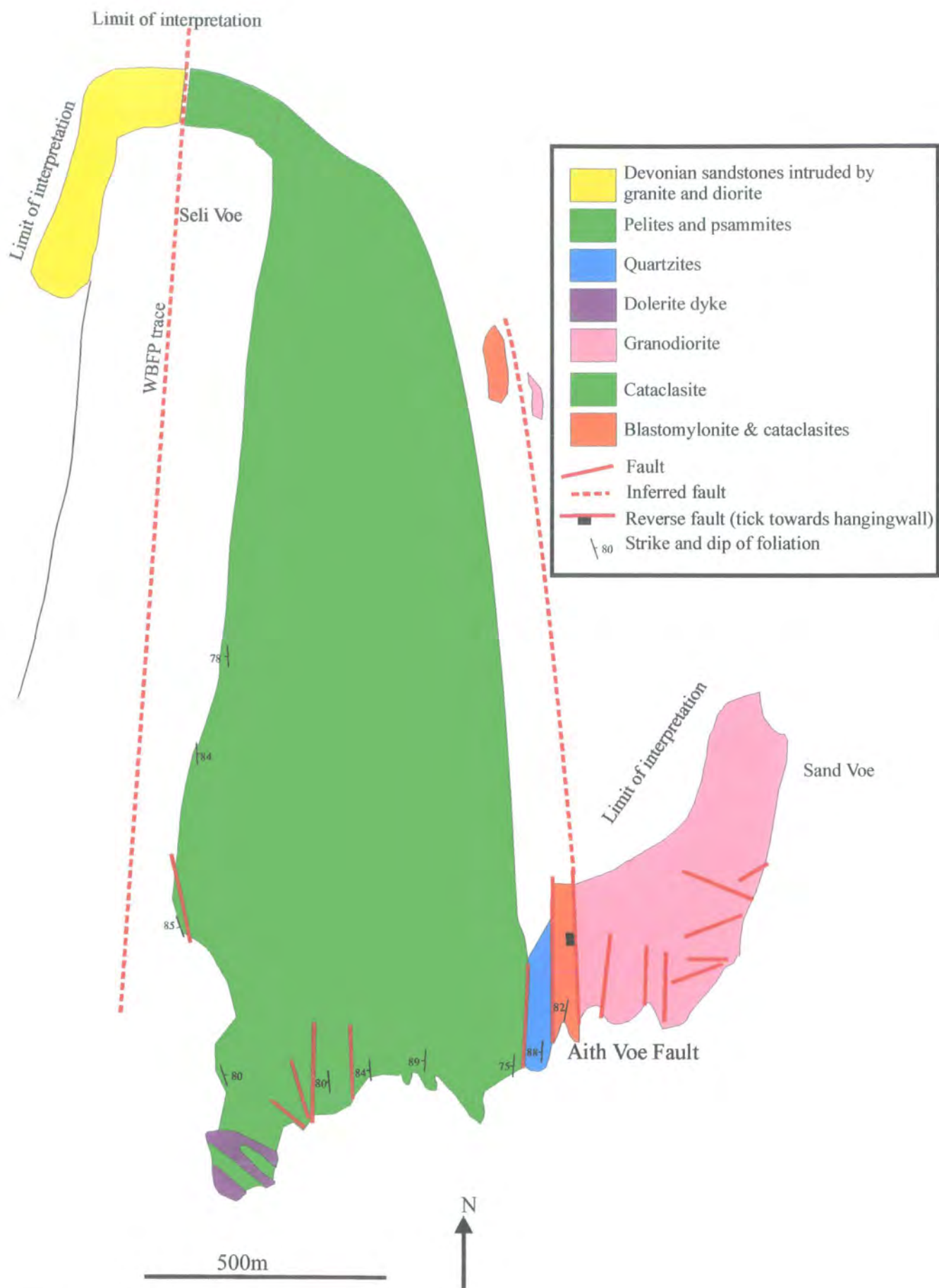


Figure 3.48 Geological map of Seli Voe to Sand.

The psammites are finely laminated, comprising 70 % quartz, 20% feldspar, 5% chlorite and 5% muscovite together with garnet porphyroblasts (up to 1cm in size). Garnet porphyroblasts are locally well developed suggesting that the rocks have been metamorphosed to at least garnet grade. The psammite layers are generally between 30-70cm in thickness, and probably represent the original sedimentary layering. The whole sequence is transected by a series of N-S-orientated upright open folds. A NW-SE-trending dolerite dyke some tens of metres thick cuts the metasedimentary rocks and is associated with a contact aureole containing andalusite and chloritoid porphyroblasts (Figure 3.48).

The psammites and pelites are lithologically and structurally similar to those exposed to the west of the WBFP at Ollaberry, which are interpreted to be part of the Dalradian Queyfirth Group. Flinn (1977) noted this similarity and also the fact that the dolerite dyke is lithologically similar to one found transecting psammites and pelites of the Queyfirth Group west of Ollaberry.

3:1:7:1b Granite west of WBFP

To the west of the WBFP, granite and diorite belonging to the Late Devonian Sandsting Complex intrude into sandstones belonging to the Middle Devonian Walls Formation (Figure 3.48). The granite is orange in colour and coarse grained with phenocrysts up to 1.5cm in length. It is composed of orthoclase (50%), plagioclase (20%), quartz (20%), chlorite (5%) and muscovite (5%). The phenocrysts are randomly aligned, equigranular and display a holocrystalline texture. Diorite sheets occur interleaved within the granite. The diorite is dark grey in colour and medium grained, comprising pyroxene (20%), hornblende (25%), plagioclase (40%) and biotite (10%). The rock is equigranular and displays a holocrystalline texture. Both the granite and the diorite lack any magmatic or solid-state fabrics in the field.

3:1:7:1c Sandstones

Sandstones belonging to the Middle Devonian Walls Formation are exposed west of the WBFP (Figure 3.48). The rocks are grey in colour, fine to medium grained and consist of a succession of finely laminated sandstones and in places mudstones.

3:1:7:1d Granodiorite east of WBFP

Granodiorite is exposed east of the WBFP between Seli Voe and Sand (Figure 3.48). The granodiorite is grey in colour, coarse grained and contains phenocrysts up to 1cm in length. It is composed of approximately 40% plagioclase (sericitised), 15% orthoclase, 20% quartz, 10% chlorite and 10% epidote together with minor amounts of hornblende and biotite. The rocks are strongly retrogressed and weather to a green colour. Hornblende and biotite have broken down to chlorite and epidote grains. Plagioclase phenocrysts have a speckled appearance due to their breakdown to muscovite laths, which appear to follow the twin or cleavage planes. Many of the plagioclase grains are almost completely replaced by aggregates of muscovite. In places, the rocks display a weakly developed magmatic fabric, which trends N-S and is defined by aligned phenocrysts. Locally, the granodiorite grades into patches of porphyritic granite, similar in appearance to those exposed east of the WBFP at the Ness of Bixter (see section 3:1:6:1c). The porphyritic granite displays a N-S-trending magmatic fabric defined by aligned feldspar phenocrysts. Xenoliths of randomly orientated hornblendite ranging from 5 to 50cm in length are common within the granodiorite.

3:1:7:2 Fault rocks

In this section, fault rocks are described in the order of their relative age (oldest to youngest; see section 3:1:7:3)

3:1:7:2a Blastomylonites

Blastomylonites are exposed within a fault-bounded sliver east of the WBFP (Figure 3.48). The blastomylonites are pink/ grey in colour and medium grained, comprising approximately 50% orthoclase, 25% quartz, 10% muscovite, 10% epidote and 5%

plagioclase (Plate 3.42). Millimetre-scale, orthoclase-rich bands are interlayered with quartz-rich bands. Medium-grained muscovite laths and epidote aggregates occur at the boundaries between quartz and feldspar. More mafic blastomylonites are blue / grey in colour, medium grained and consist of 30% hornblende, 30% epidote, 15% chlorite, 15% feldspar and 10% quartz. Millimetre-scale bands of hornblende and epidote are interlayered with chlorite, feldspar and quartz.

All mylonites display a strong foliation defined by stretched and flattened aggregates of quartz, feldspar, hornblende and mica. The sub-vertical foliation trends N-S with a sub-horizontal lineation defined by elongate feldspar, quartz, hornblende and muscovite grains. Mylonitic fabrics within more mafic blastomylonites are less well preserved and appear to be strongly retrograded. The medium-grained matrix wraps around orthoclase porphyroclasts up to 3cm in length. In the field, and in thin section the mylonites appear to be strongly annealed or recrystallised where quartz and feldspar within layers display holocrystalline textures and 120° triple junctions at grain boundaries. The proportion of matrix varies from 50% to almost 95%, so that the rocks can be subdivided into blastomylonites and blasto-ultramylonites.

3:1:7:2b Cataclasites

Cataclastic series rocks are exposed east and west of the WBFP, derived from sandstone, granite and blastomylonites. Pale grey-coloured cataclasites comprise fragments of quartz, feldspar, and sandstone set within a fine-grained cataclastic matrix of the same. Clasts are angular to sub-angular and range from 0.1mm to 1cm in size. The cataclasites appear to be isotropic on all scales of observation in the field. Green-coloured cataclasites comprise finely comminuted fragments of plagioclase, orthoclase, quartz, hornblende, chlorite, epidote, muscovite and granite or blastomylonite set within a fine-grained cataclastic matrix of the same (Plate 3.43). The cataclasites are isotropic on all scales of observation in the field. Randomly orientated millimetre- to centimetre-scale quartz, epidote and calcite veins commonly transect the cataclastic fabric and occur as clasts within the matrix.

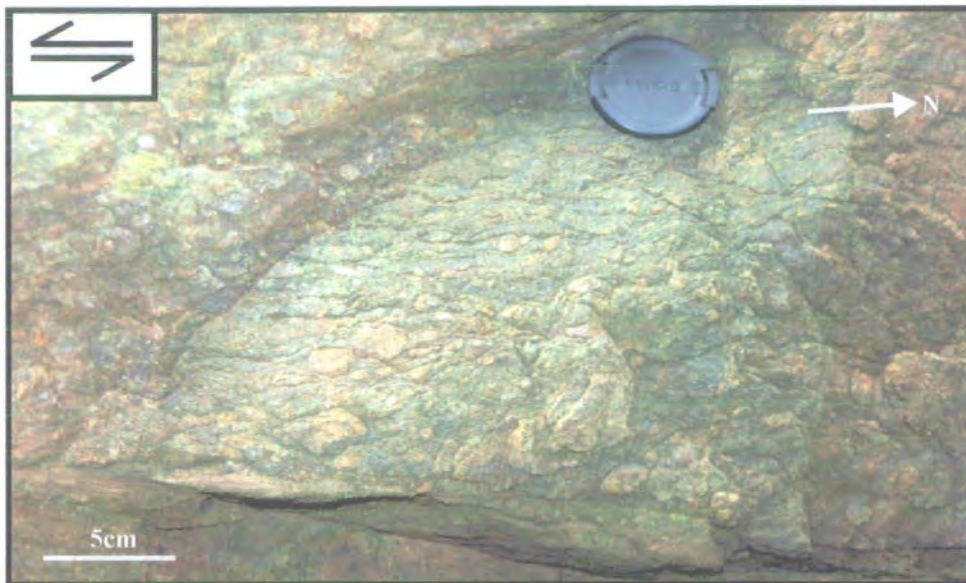


Plate 3.42 Plan view. Blastomylonite with N-S orientated fabric and σ -type orthoclase porphyroblasts (HU 3431 4666). Split arrows indicate shear sense parallel to the lineation.



Plate 3.43 Cross-sectional view. Green-coloured cataclasite containing angular fragments of blastomylonite (HU 3432 4666).



Plate 3.44 Cross-sectional view. Foliated cataclasite containing fragments of blastomylonite

3:1:7:2c Foliated cataclasites

Foliated cataclasites are exposed east of the WBFP within a fault-bounded sliver (Figure 3.48). The cataclasites are green/pink/grey in colour and coarse to finegrained (Plate 3.43). Cataclasites comprise finely comminuted fragments of blastomylonite, feldspar, quartz, epidote, muscovite and chlorite set within a fine-grained cataclastic matrix of the same. N-S-aligned fragments vary from less than 0.5mm to 3.5cm in length. The fragments are surrounded by anastomosing centimetre- to millimetre-scale bands defined by colour variations (Plate 3.44). The bands appear to vary in their length and distribution in the field. In thin-section, the bands are defined by compositional and grain-size variations together with the alignment of fragments and mica grains. The cataclasites display a N-S-trending, sub-horizontal lineation defined by aligned clasts and mica grains.

3:1:7:2d Fault gouge

There are two types of gouge present at Seli Voe and Sand, a hard red and a soft blue gouge.

The red gouge is derived from granodiorite belonging to the Devonian Spiggie Complex (section 3:1:7:1 d). It is fine grained, clay-rich, cohesive and displays a fine colour banding defined by variations in grain size and clast-to-matrix ratios. Randomly orientated clasts (5mm to <0.5mm) of granite, cataclasite, quartz and calcite are sub-angular to sub-rounded.

The blue gouge is derived from pelites and schists of uncertain origin (section 3:1:7:1 d). It is incohesive, fine-grained and clay-like in appearance. The gouge has a sub-vertical, N-S-trending fabric defined by aligned clay particles.

3:1:7:3 Fault rock distribution and age relationships

The WBFZ is 1.5km wide at Seli Voe and Sand. Fault-related deformation is strongly asymmetric extending 200m west of the WBFP into Devonian sandstones and granite, and approximately 1.3km to the east into pelites, psammites and Devonian

granodiorite. The earliest fault rocks, including blastomylonites, are exposed east of the WBFP within a fault-bounded block. Earlier formed fault rocks are overprinted by broad zones of cataclastic deformation, which generally increase towards the core of the WBF and other major faults within the fault zone. In this section, early fault rock distributions are described first and include blastomylonites not generally found elsewhere within the WBFZ.

3:1:7:3a East of WBF core

Blastomylonites are exposed along the coast between HU 3429 4665 and HU 3432 4667 within a fault-bounded block 30m wide (Figure 3.49). The blastomylonites are bounded to the west by a N-S-trending gouge-filled fault, which separates intensely fractured quartzites to the west. Here, the blastomylonite sequence is at least 8m thick. The blastomylonites are intensely deformed by the effects of cataclasis, folded and cross-cut by networks of centimetre-scale veins.

The rocks are best exposed at HU 3431 4666 (Figure 3.50). Here, the rocks comprise alternating layers of blastomylonite and blasto-ultramylonite 10 to 150cm thick. In places, quartzo-feldspathic blastomylonites are interbanded on a centimetre- to metre-scale with hornblende-rich blastomylonites and appear to be derived from a sheeted igneous complex of uncertain origin. Granite veins trending N-S cross-cut the blastomylonites (Figure 3.50) and in the field do not appear to contain any mylonitic foliation. N-S-orientated quartz and epidote veins up to 5cm thick transect the mylonitic foliation. Green-coloured, millimetre- to centimetre-thick cataclasites cross-cut and develop along the mylonitic foliation and appear to be coeval with the quartz and epidote veining (Figure 3.50).

To the east of the blastomylonites, a 4m-wide sliver of green-coloured cataclasite is exposed (Figure 3.49; Plate 3.43). In the field, the cataclasite contains fragments of blastomylonite and therefore appears to have formed later. The cataclasite appears to be isotropic on all scales of observation in the field. The contact between the cataclasite and the blastomylonite sequence is not exposed but is marked by a narrow N-S-trending inlet, probably due to the presence of a fault. A 2m-wide porphyritic granite intrusion cross-cuts the cataclasite (Figure 3.49). To the east, a 4m-wide foliated cataclasite (Plate 3.44) unit is exposed (Figure 3.49).

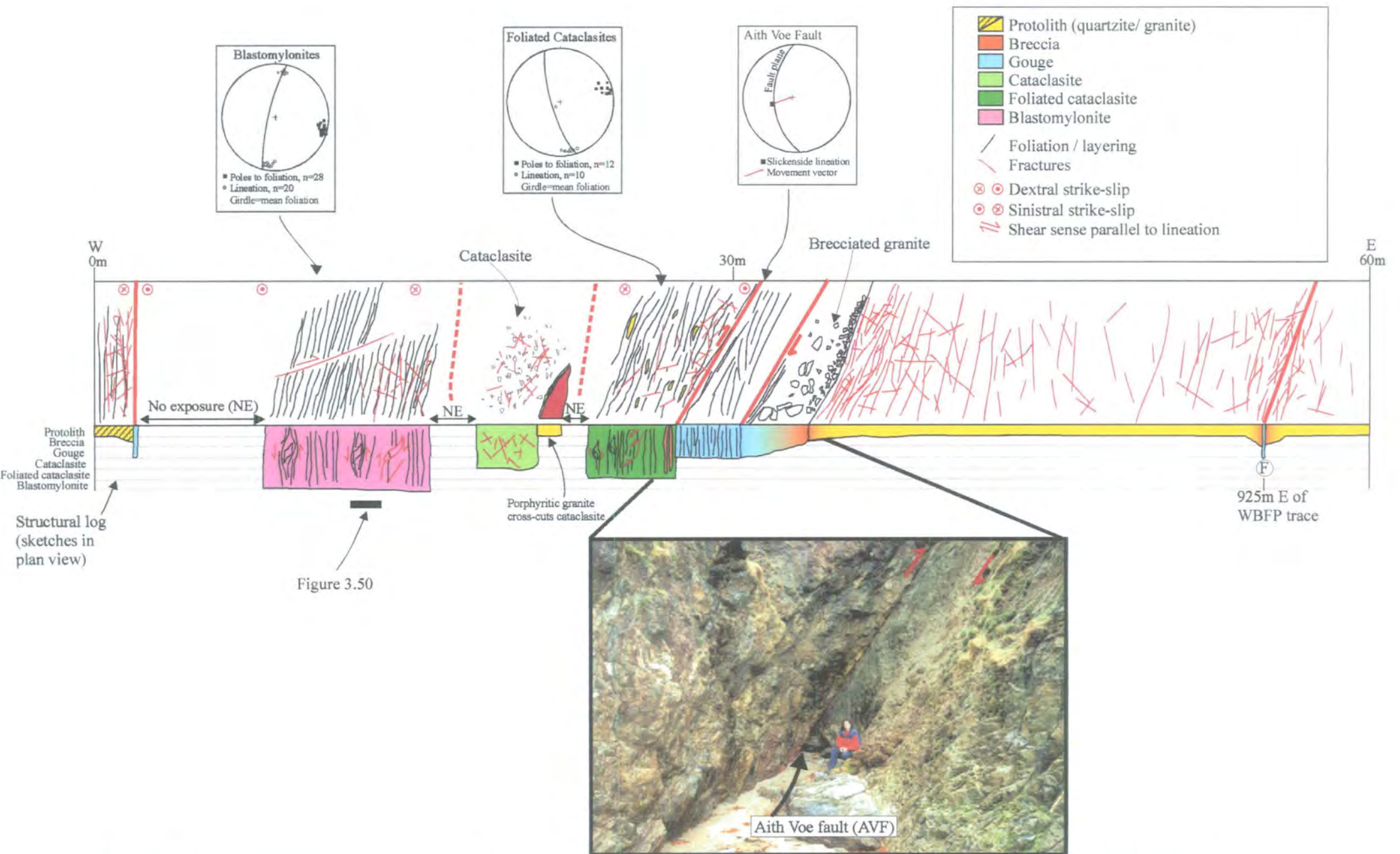


Figure 3.49 Structural log (above) and cross-section (below) through fault-bounded sliver of blastomylonite, cataclasite, foliated cataclasites and granodiorite.

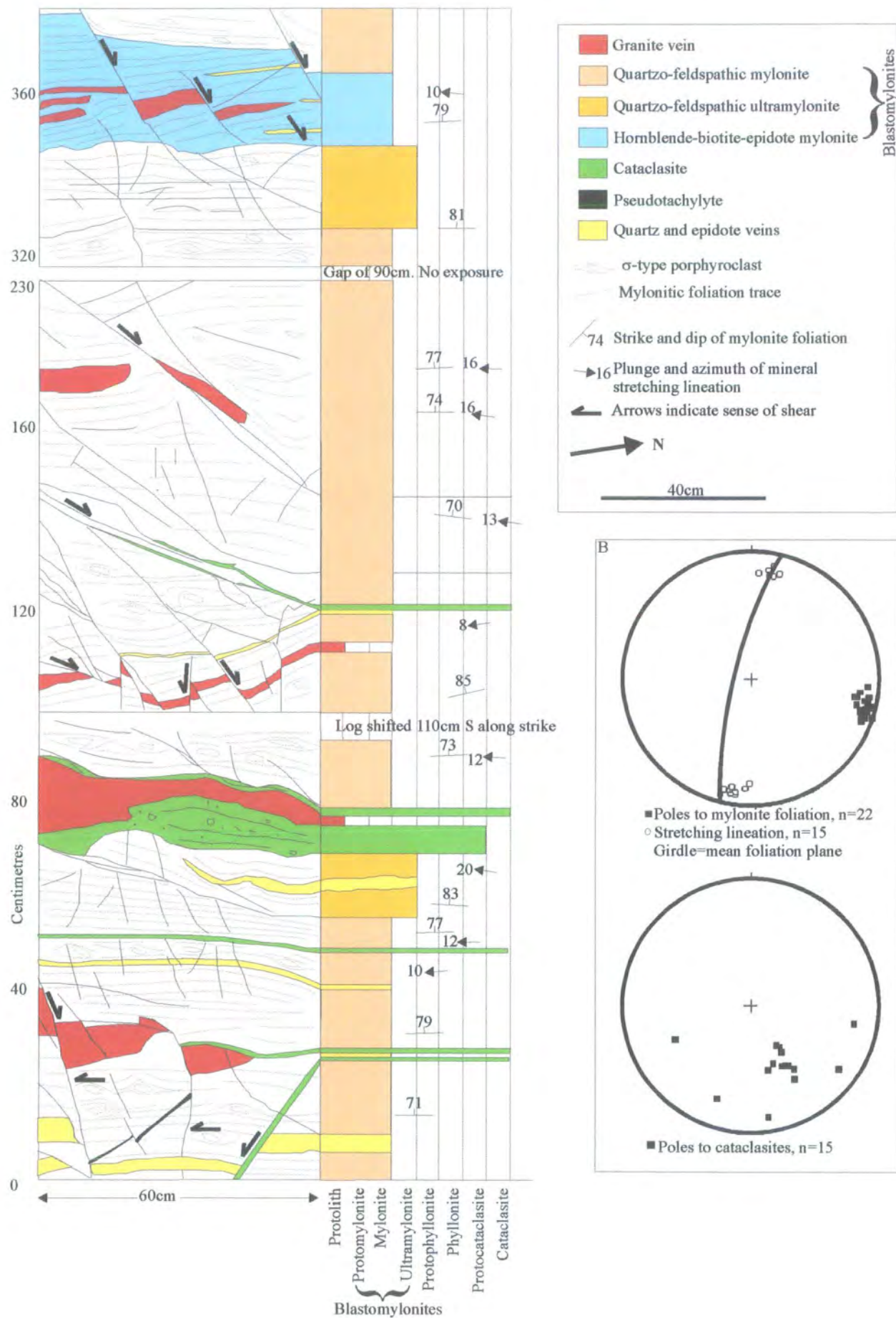


Figure 3.50 Structural log of blastomylonites and overprinting structures (HU 3431 4666, located on Figure 3.49). (B) Stereographic projections.

The foliated cataclasite appears to contain clasts of blastomylonite and isotropic cataclasite. Farther east, the foliated cataclasites are cut by a N-S-trending, 2m-wide soft blue gouge (Figure 3.49). In places, the gouge is cohesive and red coloured due to the affects of iron mineralisation which locally acts as cement. The contact between the foliated cataclasite and soft blue gouge is marked by the Aith Voe Fault (AVF; 177/55W). Foliated cataclasite near the soft blue gouge contains N-S-trending, sub-vertical, brown-coloured bands defined by iron mineralisation, which again, locally acts as cement. To the east, the fault gouge grades into incohesive breccia and intensely fractured granodiorite belonging to the Devonian Spiggie Complex.

To the west of the fault-bounded block of blastomylonites, cataclasites and foliated cataclasites, an 850m-thick succession of quartzites, pelites and psammities (Figure 3.48) is overprinted by broad zones of cataclastic deformation and locally by the development of gouge-filled faults. To the east of the fault-bounded block, faults containing soft blue gouge commonly cross-cut the granodiorite up to 250m east of the AVF (Figures 3.48, 3.49).

3:1:7:3b West of WBF core

West of the WBF core, sandstones of the Devonian Walls Formation and granite belonging to the Devonian Sandsting Complex (Figure 3.48) are overprinted by cataclastic deformation. Cataclastic deformation generally increases in intensity to the east, with the development of discrete gouge-filled faults within broad zones of breccia and intensely fractured protolith.

3:1:7:3c WBF core

The WBF core is poorly exposed along the beach at the head of Seli Voe. Farther north, a flat-bottomed, peat-filled valley marks the extrapolation of the WBF core from the Ness of Bixter. The fault core at the Ness of Bixter is located in the central part of the WBFZ and corresponds to the region of most intense fault-related deformation. It is defined by a continuous sequence of fault rocks that extends from the wall rocks across the WBFP, which is the main structural boundary within the WBFZ. A green-coloured cataclasite is exposed at the eastern side of the beach. The

cataclasite is isotropic on all scales of observation in the field. The WBFP or any other part of the WBF core is unexposed at the head of Seli Voe.

3:1:7:4 Fault zone structure

The fault zone comprises a 1.5km-wide zone of cataclastic deformation, which appears to increase in intensity towards the WBF core and other major faults within the WBFZ. These faults bound a series of blocks east of the WBF core (Figure 3.48).

3:1:7:4a East of WBF core

To the east of the WBF core, an 850m-thick sequence of psammites, pelites and quartzites is separated from a fault-bounded block of blastomylonite, cataclasite and foliated cataclasite across a N-S-trending near-vertical fault. To the east, the foliated cataclasite is separated from granodiorite by a N-S-trending, W-dipping fault (AVF) containing 2m of fault gouge.

Fault-related deformation extends approximately 1.3km to the east of the WBFP into granodiorite. 1.3km east of the WBFP (HU 3463 4701), epidote, quartz and chlorite veins several millimetres thick cross-cut the moderately fractured granodiorite. Sub-vertical, NE-SW- to almost E-W-trending fractures with sub-horizontal slickensides display dextral strike-slip offsets of pegmatite dykes of up to 1.5m, and are interpreted as R-type Riedel shears (Plate 3.45). The fractures are infilled by millimetre-thick soft blue gouge. In cross-section, pegmatite dykes display apparent reverse offsets of several centimetres. The geometrical configuration of these fractures resembles a small-scale positive 'flower' structure (Plate 3.46). In plan view, the NE-SW-trending fractures (e.g., those labelled C; Figure 3.51) are linked by ENE-WSW-trending fractures (e.g., those labelled R; Figure 3.51). Both sets of fractures contain sub-horizontal slickenside lineations and offset pegmatite veins by several centimetres. The fractures labelled R are interpreted to represent R-type Riedel shears relative to those labelled C (Figure 3.51).



Plate 3.45 Cross-sectional view. NW-SE trending pegmatite dyke offset by 1.5m along dextral strike-slip fracture containing 0.5cm of iron-stained cataclasite (HU 3463 4701).

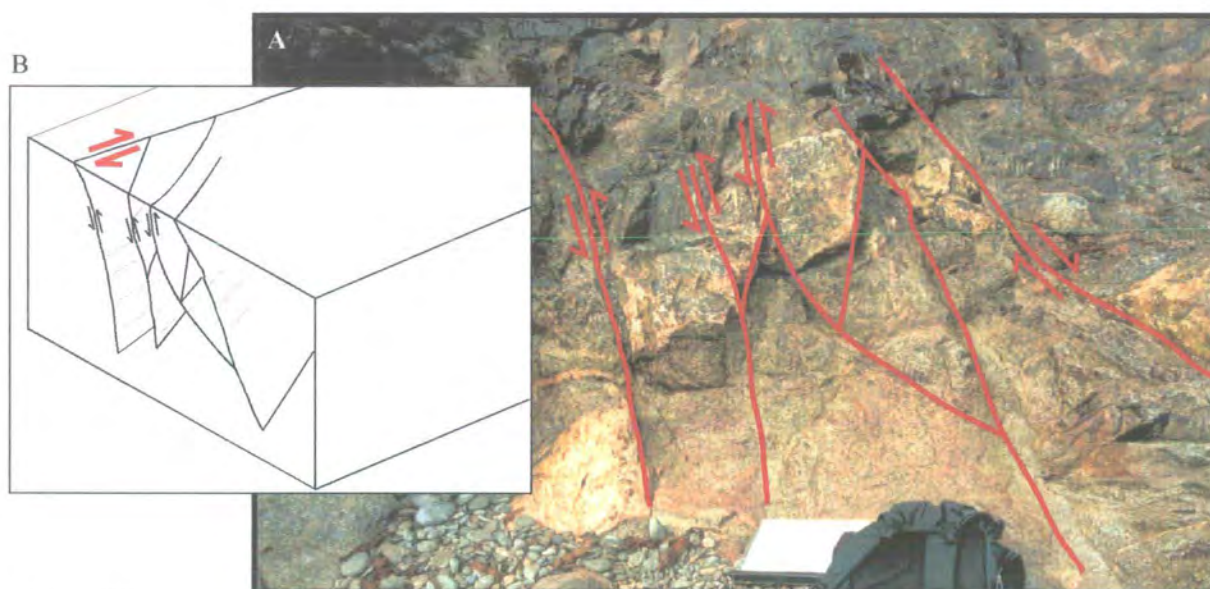


Plate 3.46 Cross-sectional view. (A) Apparent reverse offsets of pegmatite dyke across dextral strike-slip fractures containing millimetre-thick soft blue gouge. (B) Schematic diagram to show that the geometry of fractures in (A) resembles a 'positive' flower structure (HU 3463 4701). Red dashed lines represent slickenside lineations.

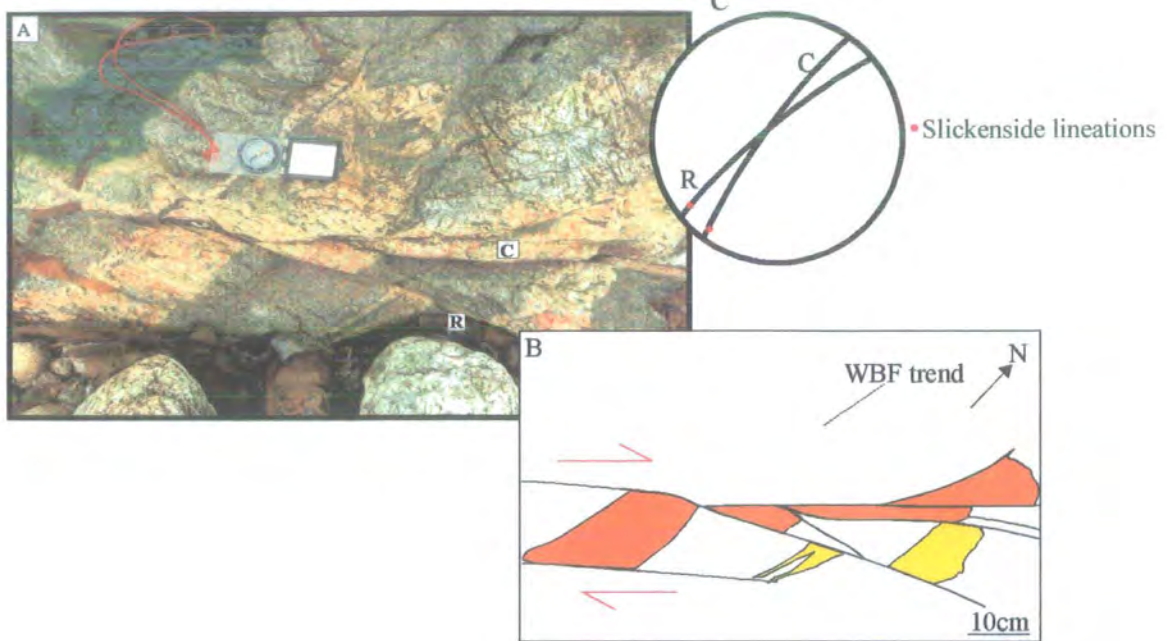


Figure 3.51 (A) Plan view of NE-SW-trending dextral strike-slip fractures offsetting pegmatite vein. (B) Summary sketch of fracture geometry shown in (A). (C) Stereographic projection to show orientation of fractures labelled C and R in (A).



Plate 3.47 Cross section through NE-SW orientated fault containing 50cm of soft blue gouge (HU 3461 4690).

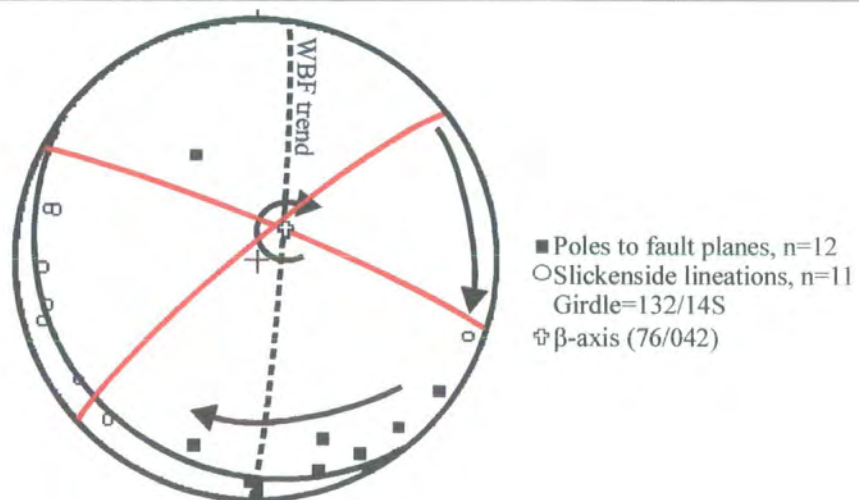


Figure 3.52 Stereographic projection to show gouge-filled (10-50cm thick) dextral strike-slip fault data. Red girdles represent end members of dextral strike-slip faults that were thought to have formed as R-type Riedel shears to the WBF. Some of these were rotated due to continued dextral movement along the WBFZ.

At distances of 1.14km east of the WBFP, NE-SW-orientated faults are common, spaced every 10-20m. The faults contain 10 to 50cm of soft blue fault gouge (Plate 3.47) that contains a strong foliation defined by aligned clay particles. The strike of the faults ranges from 030° to almost 090°, all with sub-horizontal slickenside lineations (Figure 3.52). On outcrop surfaces viewed normal to the fault planes and parallel to the lineation, centimetre-spaced shear bands consistently indicate dextral shear. The faults are interpreted as R-type Riedel shears to the N-S-trending WBF. Poles to fault planes lie along a girdle (132/14S) with a sub-vertical β -axis or pole to the girdle orientated 76/042 (Figure 3.52). The faults are interpreted to have formed as R-type Riedel shears with some of them rotated along the girdle (132/14S) in a clockwise direction about the β -axis due to continued dextral movement along the WBFZ. Farther to the southwest, at distances of 1.07km east of the WBFP the granodiorite is highly fractured with abundant iron staining present on fracture surfaces. From here to a distance of 925m east of the WBFP, the outcrops are inaccessible.

At 925m east of the WBFP, a fault containing 50cm of soft blue gouge is orientated at 007/70W (the most easterly fault (F) on Figure 3.49). To the west, the granodiorite is intensely fractured and contains abundant millimetre-thick quartz, epidote and gouge veins. Locally, the gouge veins display a N-S-trending, centimetre-scale, anastomosing geometry (Plate 3.48A). Steeply-dipping, N-S-trending gouge veins with dip-slip lineations commonly display reverse dip-slip offsets of hornblende xenoliths of up to 5cm (Plate 3.48B). Fracturing and iron staining increases markedly to the west. An incohesive breccia zone overprints the granodiorite and grades into a 2m-thick soft blue gouge adjacent to a fault plane orientated 177/55W (Aith Voe Fault; Figure 3.49). The gouge contains a strong fault-parallel foliation with a dip-slip lineation; both defined by aligned clay particles. Slickenfibres consistently show a reverse dip-slip sense of movement based upon the down-stepping of quartz mineral fibres up the dip of the fault plane. The fault gouge overprints a 4m-wide sequence of foliated cataclasites (Plate 3.44) to the west (Figure 3.49). In thin-section and in the field, the millimetre- to centimetre-scale colour banding is defined by compositional and grain-size variations, together with the alignment of fragments and mica grains; both forming a N-S-trending sub-vertical foliation (Figure 3.49). The alignment of clasts and mica grains defines a sub-horizontal lineation.

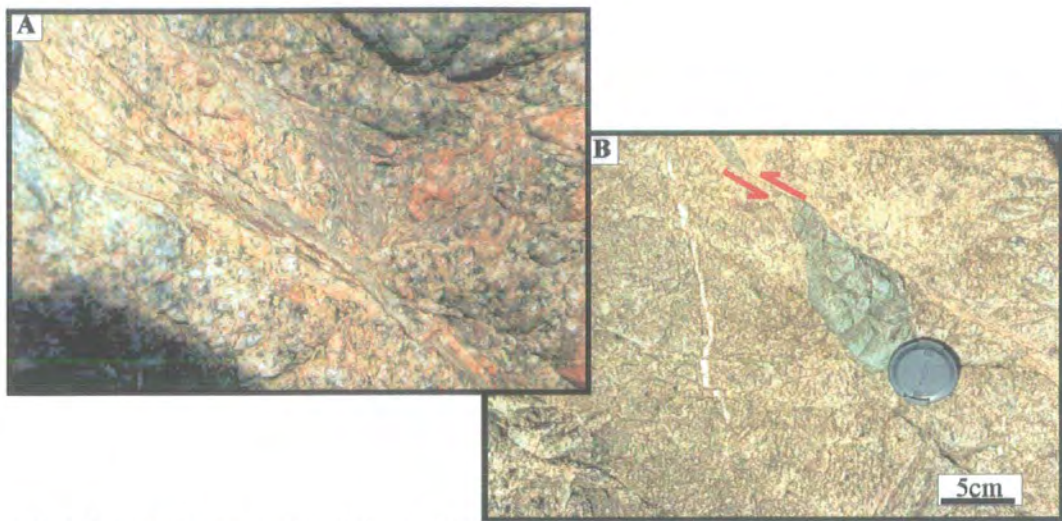


Plate 3.48 (A) Cross-sectional view to illustrate anastomosing geometry of millimetre- to centimetre-thick soft blue gouge veins. (B) Reverse dip-slip offset of hornblende xenolith by 5cm.

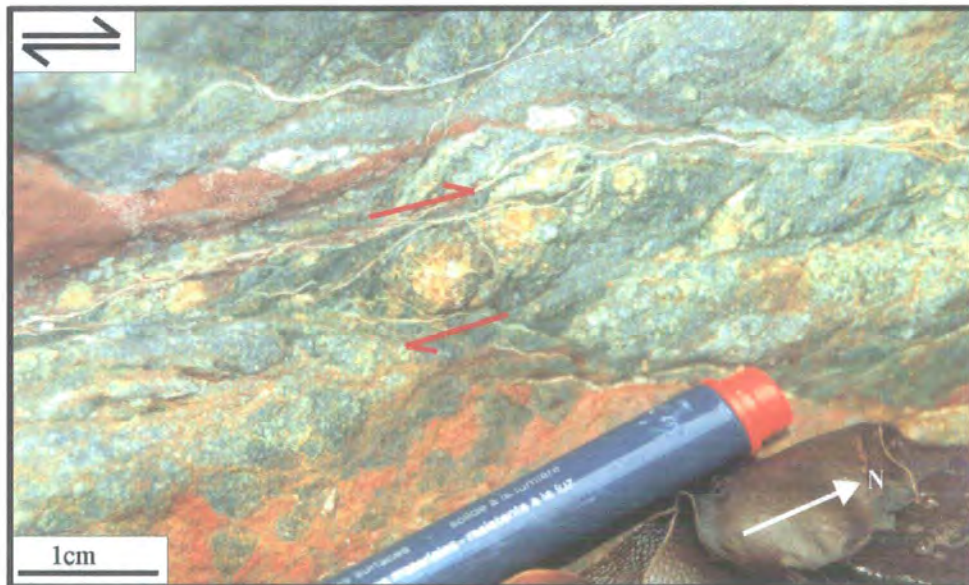


Plate 3.49 Plan view. Foliated cataclasite with σ -type porphyroblast indicating dextral shear. Split arrows indicate shear sense parallel to the lineation.

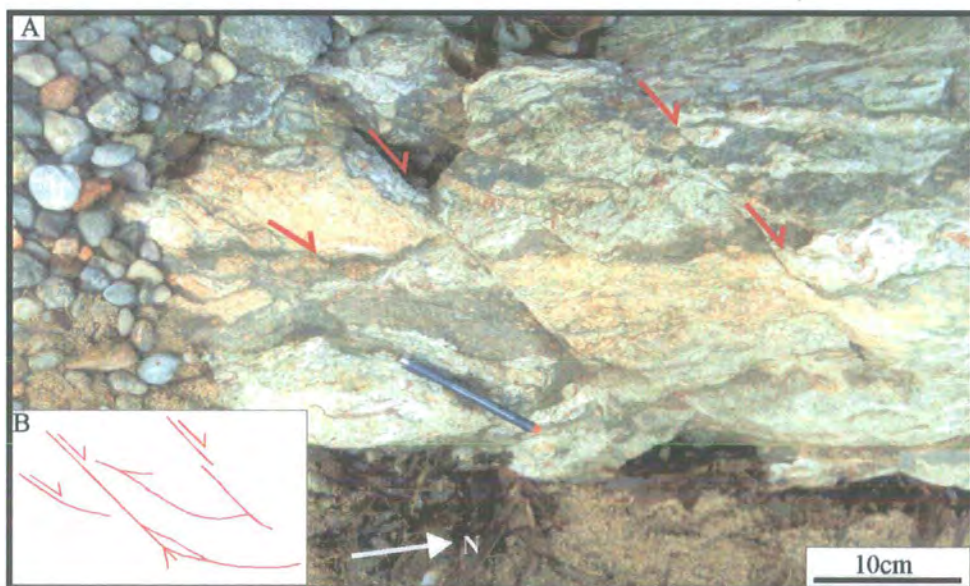


Plate 3.50 Plan view. (A) Colour banding within foliated cataclasite offset by 2-20cm along dextral strike-slip NE-SW trending fractures. (B) Sketch interpretation of fracture geometry. Fractures with larger offsets tend to curve and link into foliation parallel fractures. The NE-SW fractures are interpreted as R-type Riedel shears to the N-S trending foliation-parallel faults.

On outcrop surfaces viewed normal to the foliation and parallel to the lineation, σ -type porphyroclasts (fragments) consistently indicate dextral shear (Plate 3.49). The foliated cataclasites are cross-cut by a series of closely-spaced (1 to 30cm), NE-SW-trending, sub-vertical fractures. The fractures contain sub-horizontal slickenside lineations and offset colour banding by 2 to almost 40cm in a dextral sense (Plate 3.50). Fractures with larger offsets curve to link into foliation-parallel fracture zones. A few metres to the west, green-coloured cataclasites are exposed containing fragments of blastomylonite. Farther west, an 8m-thick sequence of blastomylonite is exposed (Figure 3.49), bounded to the west by a N-S-trending gouge-filled fault, which separates them from intensely fractured quartzites to the west. The fault contains sub-horizontal quartz slickenfibres indicating dextral strike-slip movement based upon the stepping of the quartz fibres.

The blastomylonites are best exposed at HU 3431 4666 (Figure 3.50). The rocks display a strong NNE-SSW, sub-vertical foliation defined by flattened and stretched aggregates of quartz and feldspar (Figures 3.49, 3.50B). A sub-horizontal lineation is defined by elongate quartz and feldspar and, in places, aligned mica grains. On outcrop surfaces viewed normal to the foliation and parallel to the lineation, σ -type porphyroblasts consistently indicate sinistral shear (Plate 3.51). In places, the rocks grade from protomylonitic textures into rocks that resemble a metamorphosed sheeted igneous complex. Green-coloured, millimetre- to centimetre-thick cataclasites cross-cut and develop along the mylonitic foliation. These appear to be coeval with quartz and epidote veins, which trend N-S and are up to 5cm thick. They vary in their orientation from N-S to almost E-W (Figure 3.50B). The cataclasites contain sub-horizontal slickenside lineations. N-S- to NE-SW-trending cataclasites offset the mylonitic foliation and granite veins by 1 to 20cm in a dextral sense and are interpreted as R-type Riedel shears. ENE-WSW-trending cataclasites offset the mylonite foliation, granite and epidote/quartz veins by 1 to 10cm in a sinistral sense, and are interpreted as R'-type Riedel shears. The geometrical configuration of R- and R'-type Riedel shears is consistent with dextral shear along the WBFZ. Quartz and epidote veins are both offset by and cross-cut the cataclasites (Figure 3.50), suggesting that veining was coeval with cataclasis. Centimetre-scale kink folds post-date the mylonitic foliation and NE-SW-trending cataclasites (Plate 3.51).

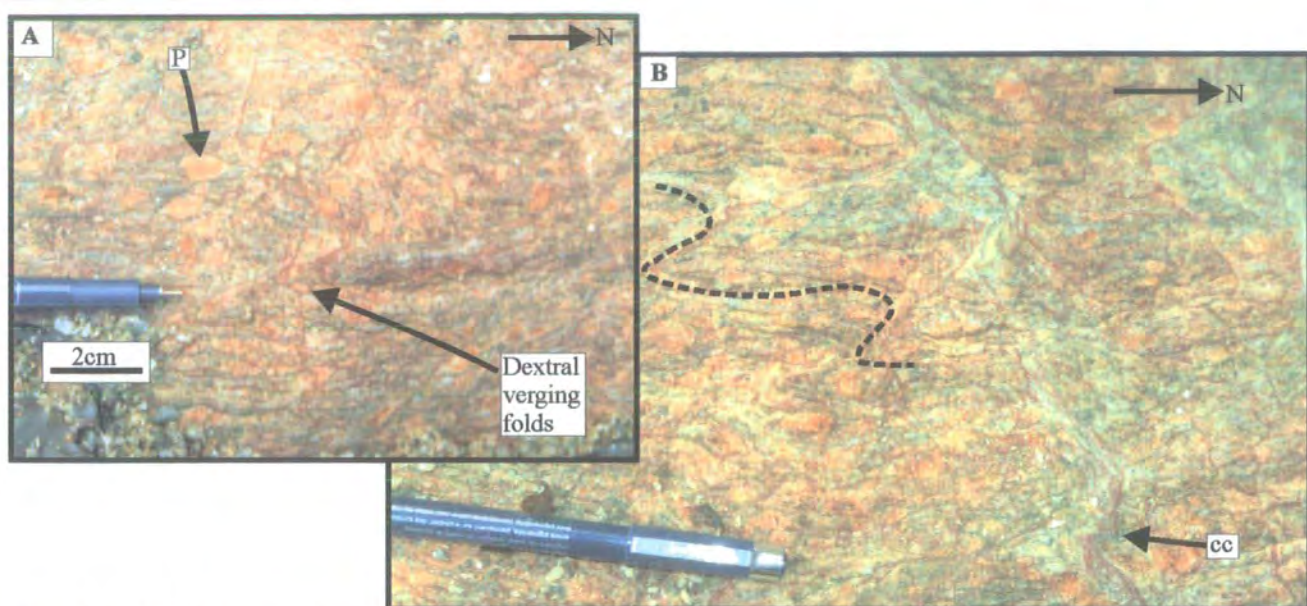


Plate 3.51 (A) Plan view. Blastomylonite with σ -type orthoclase porphyroclasts (P) indicating sinistral shear. Dextral-verging centimetre-scale folds overprint mylonitic fabric. (B) Plan view. Dextral-verging folds (dashed lines) post-date the mylonitic fabric and NE-SW-trending cataclasite(CC).

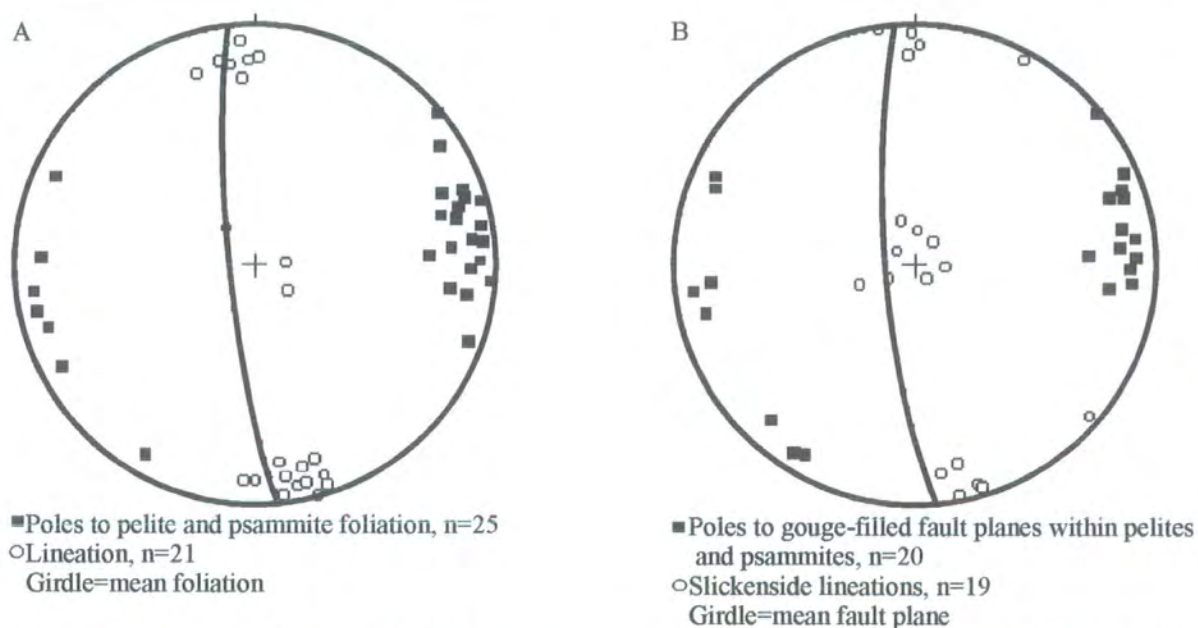


Figure 3.53 Stereographic projections for pelites and psammites east of the WBFP. (A) Foliation and lineation. (B) Gouge-filled faults and slickenside lineations.

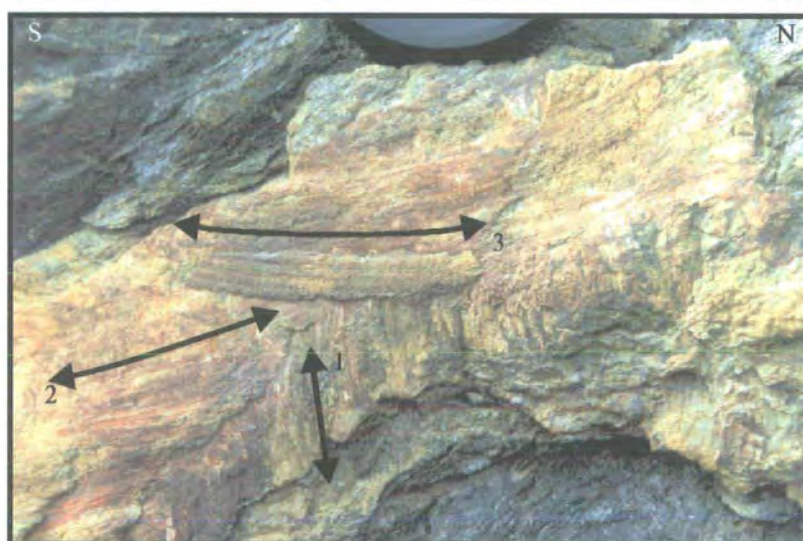


Plate 3.52 View to show the sequence of slickenside lineations on a N-S vertical fault plane. 1 is earliest, 2 and 3 are both later strike-slip slickenside lineations (HU3389 4650).

The folds consistently show a dextral sense of vergence. In cross-section, the blastomylonites are in places offset by up to 1m along moderately W-dipping reverse faults.

To the west of the fault-bounded block of blastomylonites, the succession of quartzites, pelites and psammites is overprinted by broad zones of cataclastic deformation and locally the development of gouge-filled faults. Interlayered pelites and psammites display a N-S-trending, near-vertical foliation defined by stretched and flattened aggregates of quartz, feldspar and mica (Figure 3.53A). Sub-horizontal lineations are defined by aligned mica grains. 700m east of the WBFP, centimetre-scale shear bands indicate dextral shear in surfaces viewed normal to the foliation and parallel to the lineation. Between 700m and 470 m east of the WBFP, exposure is very poor.

At 460m west of the WBFP, strongly retrograde brecciated pelites and psammites contain abundant iron staining. N-S-trending, near-vertical faults develop in the psammitic units (Figure 3.53B). The faults contain centimetre-thick soft blue gouge adjacent to slickensided fault planes. Dip-slip slickenside lineations are consistently overprinted by strike-slip slickenside lineations (Plate 3.52). 400m east of the WBFP, fracturing is intense. Centimetre-scale kink bands with a dextral sense of vergence are locally developed in more pelitic units. N-S-trending faults filled with centimetre-thick gouge increase in frequency towards the west, with a spacing ranging from 2 to 25m. At 310m east of the WBFP psammitic units are dominant over pelitic units. N-S-trending upright folds are almost isoclinal, with faults developed along the axial planes. Farther west, a NW-SE-trending dolerite dyke (50m wide) transects psammites and interbedded pelites (Figure 3.48). Several sub-vertical fractures orientated NW-SE offset thin granite veins by 1 to 20cm in a sinistral sense. These are interpreted as R'-type Riedel shears to N-S-trending gouge-filled faults formed during dextral strike-slip movements along the WBFZ. Millimetre- to centimetre-scale carbonate veins form networks and in places breccias.

To the northwest, along the east coast of Seli Voe 150m east of the WBFP, garnet-bearing psammites are cut by several, N-S-trending, vertical faults containing centimetre-thick gouge and breccia. Adjacent to the faults carbonate veins (up to

0.5cm thick) are present along N-S-trending fractures. Carbonate-filled tension gashes orientated 060° link into N-S-trending fractures, suggesting an overall dextral sense of shear.

3:1:7:4b West of WBF core

To the west of the WBF core, poorly exposed sandstones of the Devonian Walls Formation and granite belonging to the Devonian Sandsting Complex are strongly overprinted by cataclastic deformation. Cataclastic deformation generally increases to the east with the development of discrete, N-S-trending, gouge-filled faults within zones of breccia and intensely fractured protolith.

3:1:7:5 Kinematic summary and discussion

The kinematic evolution of the WBFZ at Seli Voe and Sand is summarised in Table 3.8.

Kinematic regime	Fault rocks / structures
3. Dextral strike-slip (youngest)	<ul style="list-style-type: none"> ◦ Reverse dip-slip movement along the AVF and the development of a 'positive' flower structure during dextral strike-slip along the WBF ◦ NE-SW-trending R-type Riedel shears ◦ N-S and NE-SW dextral strike-slip gouge-filled faults ◦ N-S- to almost E-W-trending cataclasites ◦ Dextral-verging folds ◦ Tension gashes ◦ 35km minimum dextral strike-slip offset along the WBF based upon a correlation of pelites and quartzites east of the WBF with similar rocks exposed west of the WBF at Ollaberry
2. Dextral strike-slip	<ul style="list-style-type: none"> ◦ Foliated cataclasites with σ-type porphyroclasts
1. Sinistral strike-slip (oldest)	<ul style="list-style-type: none"> ◦ Blastomylonites with σ-type porphyroblasts indicating sinistral shear ◦ Cataclasites?

Table 3.8 Summary table of the kinematic evolution of the WBFZ at Seli Voe and Sand.

The WBFZ at Seli Voe and Sand is 1.5km wide. Fault-related deformation is strongly asymmetric, extending 200m west of the WBFP and 1.3km to the east of the WBFP. The along-strike variation in fault-rock distribution and structure is illustrated in (Figure 3.54). The WBFZ at Seli Voe and Sand comprises a kilometre-scale braided network of sub-vertical faults associated with cataclasis and the development of fault gouge (Figures 3.54). The arrangement of these faults is similar to that of a 'positive' flower structure (Figure 3.54). The flower structure formed as a result of dextral strike-slip movement along the WBF. An initial curve in the WBF trace may have led to the formation of a braided network of sub-vertical faults adjacent to a left-stepping restraining bend and a local region of transpression (Figure 3.54). A large component of reverse movement along the AVF helped to exhume blastomylonites, cataclasites and foliated cataclasites within a fault-bounded block. The main faults, which define the flower structure, are filled with fault gouge, suggesting that the broad network of faults formed during phase 3 (Table 3.8).

The rocks on either side of the WBFP at Seli Voe and Sand record different kinematic events. The rocks to the east of the WBFP record all the kinematic events summarised in Table 3.8. West of the WBFP, the rocks record only cataclasis and gouge formation related to the most recent dextral strike-slip movement during phase 3. East of the WBFP, a major phase of dextral strike-slip faulting (phase 3; Table 3.8) appears to overprint structures relating to a ductile, dextral strike-slip ductile event (phase 2; Table 3.8). Although the ductile and brittle dextral strike-slip events are described as separate kinematic phases, it is possible that they formed during the same time as the fault zone was being exhumed. Blastomylonites are the earliest recognised fault rocks at Sand. The blastomylonites are overprinted by all other structures and faults rocks within the WBFZ, and were formed during an early phase of sinistral strike-slip movement. At Seli Voe and Sand, the distribution of fault rocks appears to be strongly controlled by the presence of pre-existing structures. Cataclasites commonly form interlinking zones of foliation-parallel and cross-cutting structures. Later fault rocks (gouges) appear to localise along anisotropic zones formed by earlier fault rocks and foliated pelitic horizons. Conroy (1996) and Flinn (1977) did not recognise any kinematic indicators at Sand and Seli Voe.

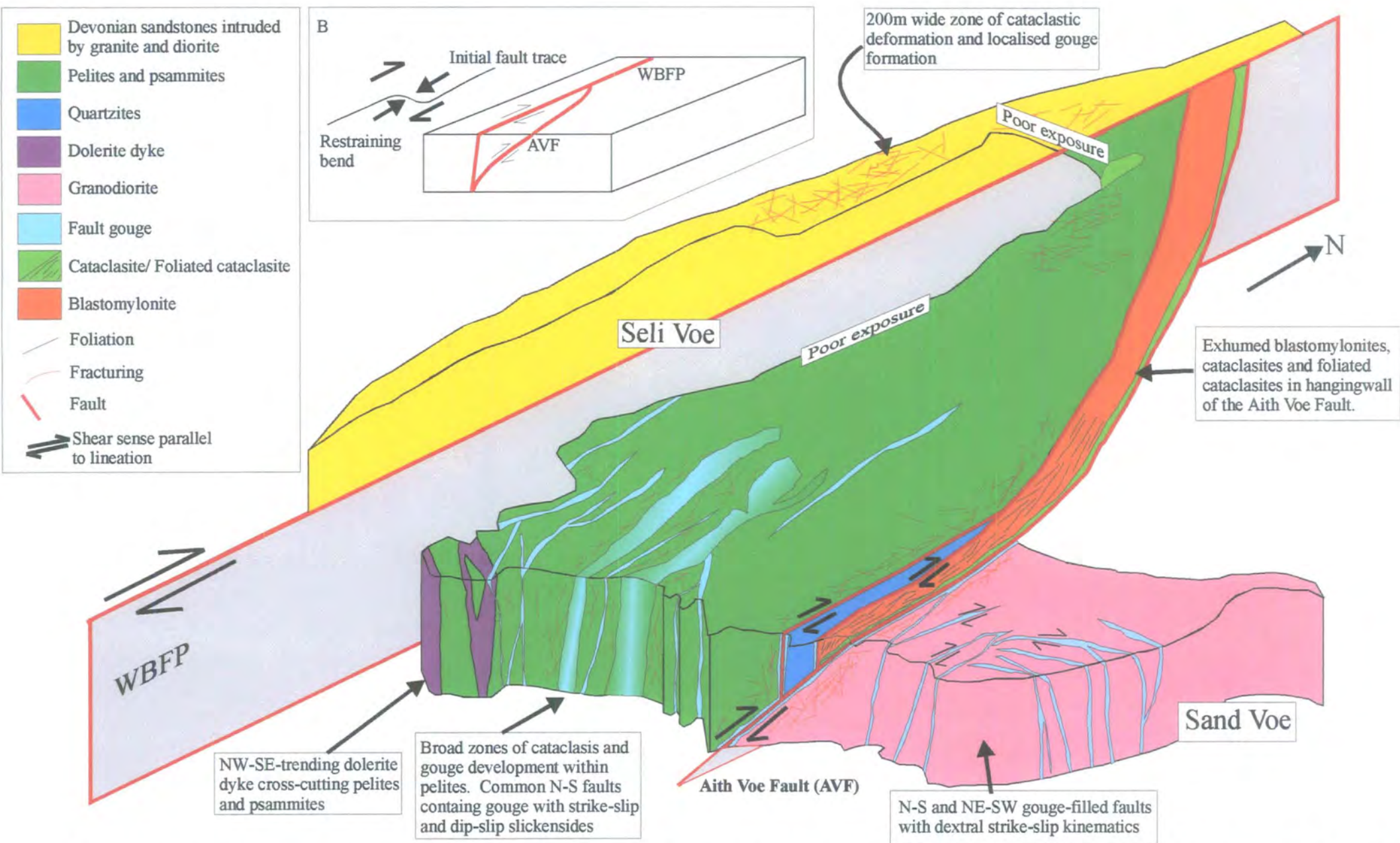


Figure 3.54 Schematic 3d diagram to illustrate fault rock distribution, structure and geometry of the WBFP at Sand and Seli Voe. Not to scale. (B) A model for the formation of a 'positive' flower structure at Sand and Seli Voe.

3:1:8 Red Ayre

The rocky shoreline and sandy beaches near Red Ayre lie along the west coast of Seli Voe, 350m to the west of the WBF trace (locality h; Figure 3.1). Granite belonging to the Devonian Sandsting Complex (section 2:1:5:2b) surrounds a N-S-trending xenolith of mylonite that is 60m across in an ENE-WSW trend and at least 300m long (Figure 3.55). Both the granite and the mylonite are affected by intense cataclasis associated with the WBFZ.

3:1:8:1 Protolith lithology

3:1:8:1a Granite

Granite and locally diorite belonging to the Late Devonian Sandsting Complex are intruded in this area into sandstones belonging to the Middle Devonian Walls Formation (Figure 3.55). The granite is orange in colour and coarse grained with phenocrysts up to 1.5cm in length. It is composed of approximately 50% orthoclase, 20% plagioclase, 20% quartz, 5% chlorite, and 5% muscovite. The phenocrysts are randomly aligned, equigranular and display a holocrystalline texture. No magmatic or solid state fabrics were observed in the field.

3:1:8:2 Fault rocks

In this section, fault rocks are described in the order of their relative age (oldest to youngest; see section 3:1:8:3).

3:1:8:2a Mylonites

Mylonites are exposed within a NW-SE-trending sliver within granite belonging to the Sandsting Complex (Figure 3.55). The mylonites are pink/ grey in colour and medium grained consists mainly of altered feldspar and quartz. Millimetre-scale feldspar-rich bands are interlayered with quartz-rich bands.

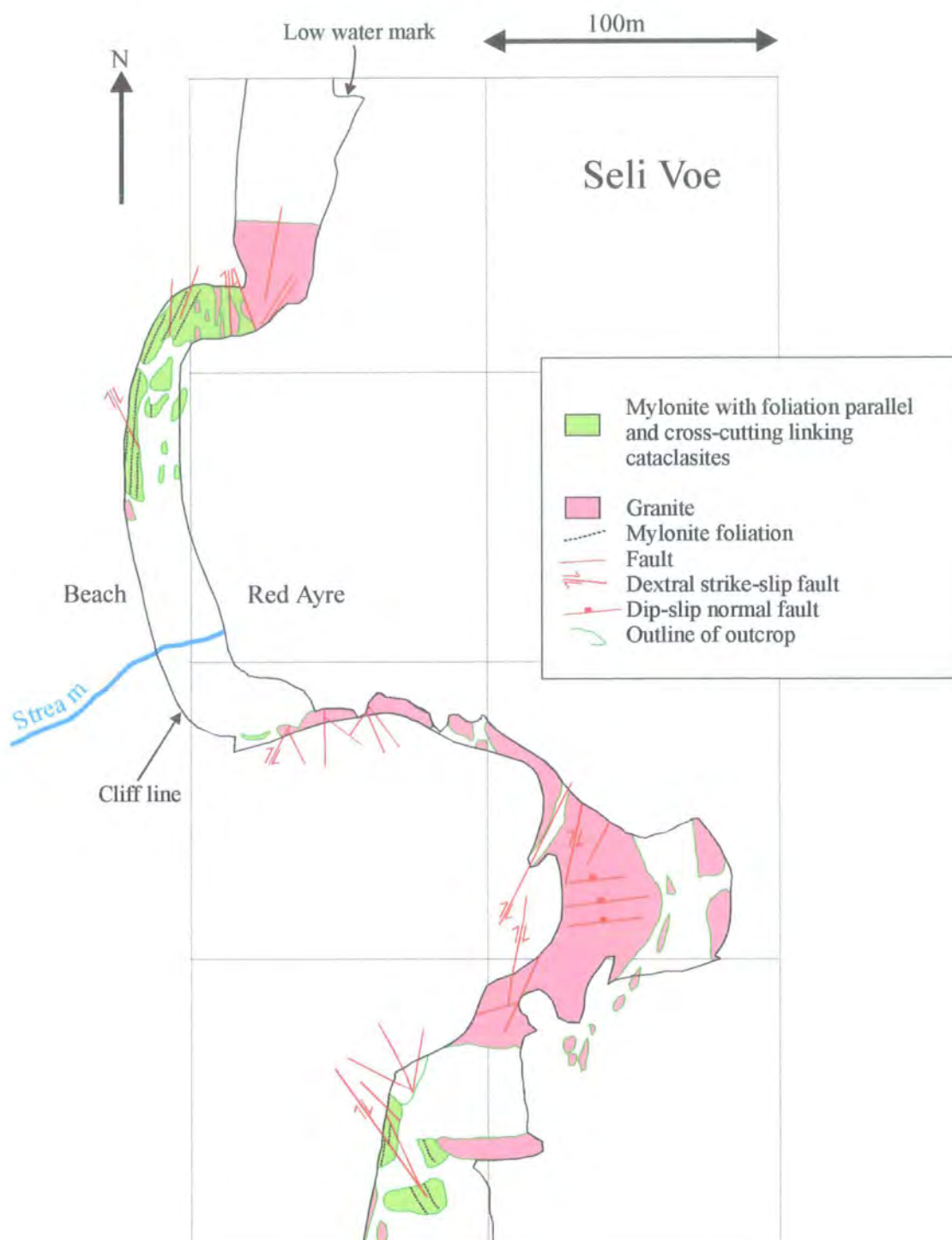


Figure 3.55 1:200 scale geological map of Red Ayre mylonites and surrounding granite.

The mylonites display a strong foliation defined by stretched and flattened aggregates of quartz and feldspar. The sub-vertical foliation trends N-S with a sub-horizontal lineation defined by elongate quartz and feldspar grains. The medium-grained matrix wraps around relict porphyroclasts up to 3mm in length. In the field and in thin-section, the mylonites appear to be strongly altered, cataclastically deformed and transected by extensive millimetre-scale networks of quartz and calcite. The mylonites appear to be lithologically similar and possibly equivalent to those exposed at Lunnister 30km to the north (see section 3:1:2:2a)

3:1:8:2b Cataclasites

There are two types of cataclasite exposed at Red Ayre, 'early' and 'late'.

'Early' cataclasites are found only within the mylonites. They mainly develop parallel to the mylonitic foliation and range in thickness from 0.5mm up to 3cm. They comprise finely comminuted fragments of feldspar, quartz and mica set within a fine-grained cataclastic matrix of the same. The fragments are angular to sub-angular, 0.5cm to less than a millimetre in size and randomly orientated. In thin-section, millimetre-scale injection veins filled with cataclasite nucleate off the foliation-parallel cataclasites into highly altered mylonitic wall rock.

'Later' cataclasites are exposed within the granite that surrounds the mylonites. The 'later' cataclasites comprise finely comminuted fragments of granite, quartz, feldspar and mica set within a fine-grained cataclastic matrix that has been altered to a clay-rich paste. Fault-parallel, cross-cutting, hematite veins (1mm to 2cm in thickness) overprint the cataclasites, locally acting as cement within the fine-grained portions. In thin-section, calcite vein fragments are present within the clay-rich matrix.

3:1:8:2c Fault gouge

Blue-coloured fault gouges are exposed within the sliver of mylonite. The gouge is incohesive, fine grained and clay-like in appearance. The gouges display a sub-vertical, fault-parallel fabric defined by aligned clay particles that is sub-parallel to the bounding fault surfaces. The blue gouges and 'later' cataclasites are interpreted to be

of broadly the same age based upon overprinting relationships observed in the field (see section 3:1:8:3).

3:1:8:3 Fault rock distribution and age relationships

The contact between the sliver of mylonite and host-rock granite is irregular with fragments of mylonite (1cm to 1m in length) present within the granite several metres away from the main contact (Plate 3.53). Centimetre-thick granite veins cross-cut the mylonitic fabric and 'early' cataclasites and appear to be coeval with millimetre-scale quartz and calcite veins. The sliver of mylonite is interpreted to be a large-scale xenolith within the granite. The WBFP trace lies only 350m to the east, in Seli Voe, suggesting that the mylonites represent an earlier phase of movement along the WBFZ, pre-dating emplacement of the granite.

The mylonites, 'early' cataclasites and granite are post-dated by cataclastic deformation, which generally increases towards later faults and contain centimetre-thick soft blue gouges (within mylonite) and 'later' cataclasites (within granite). Soft blue gouges cross-cut the mylonite, 'early' cataclasites and granite veins but do not appear to be present within the main granite unit. 'Later' clay-rich cataclasites overprint granite and do not appear to be developed within the mylonite. Blue gouges and 'later' cataclasites are kinematically similar (see section 3:1:8:4) and display identical overprinting relationships. They are interpreted to be of the same age with pre-existing structures and / or lithology controlling whether cataclasite or gouge is developed.

3:1:8:4 Structure

The mylonite foliation at Red Ayre trends N-S and dips steeply to the W (Figure 3.56A; Plate 3.54). Lineations defined by elongate quartz and feldspar grains plunge shallowly to the S. On surfaces viewed normal to the foliation and parallel to the lineation, the shear sense is unclear. 'Early' cataclasites with sub-horizontal slickenside lineations develop parallel to the foliation (Figure 3.56B).

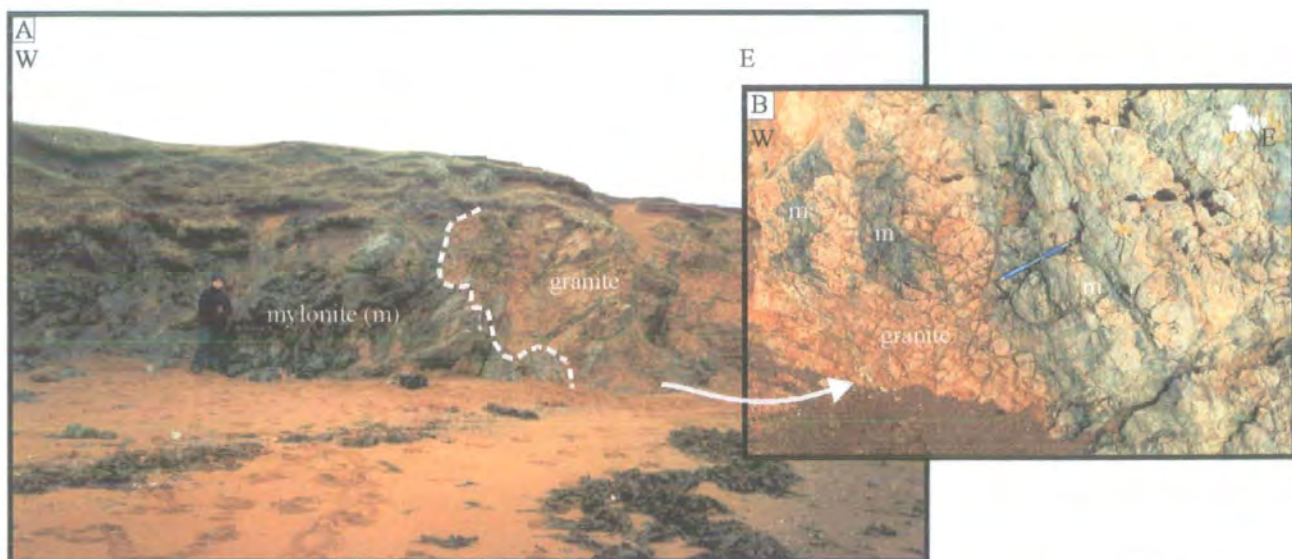


Plate 3.53 (A) Cross-sectional view. Irregular contact (dashed line) separating granite to the east from mylonite to the west. Note: the occurrence of mylonite xenoliths to the east of the contact and the cross-cutting granite veins to the west. (B) Plan view. Close up of mylonite xenoliths within granite (located on A).

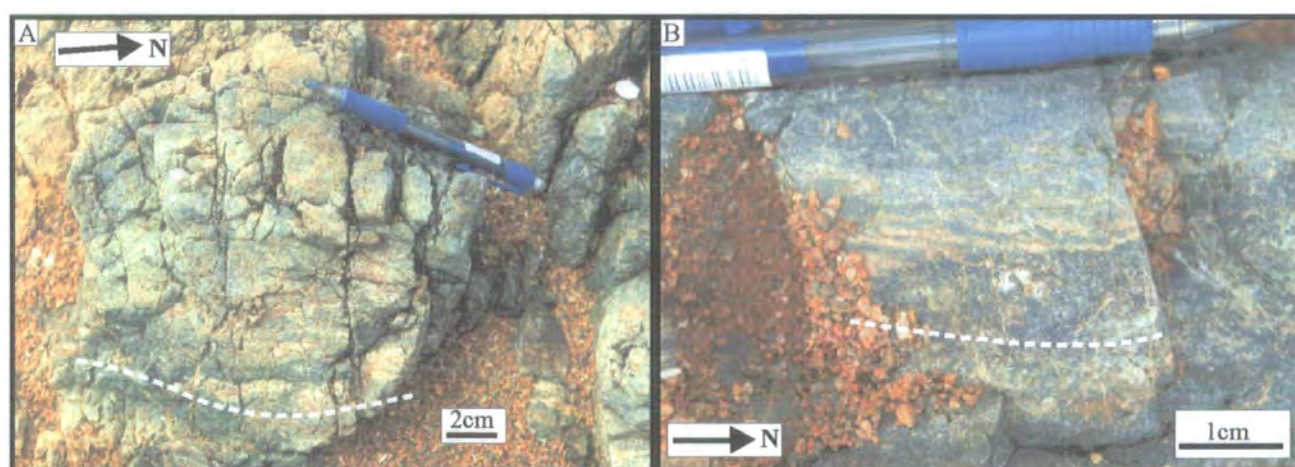


Plate 3.54 (A) Plan view. Typical outcrop of mylonite with N-S-trending foliation (dashed line) cut by millimetre-scale quartz, calcite and cataclasite veins. (B) Plan view. Close up image of mylonites to show millimetre-scale banding.



Plate 3.55 Cross-section through pale brown-coloured ENE-WSW-trending cataclasite within granite. Quartz slickenfibres indicate dip-slip normal movement.

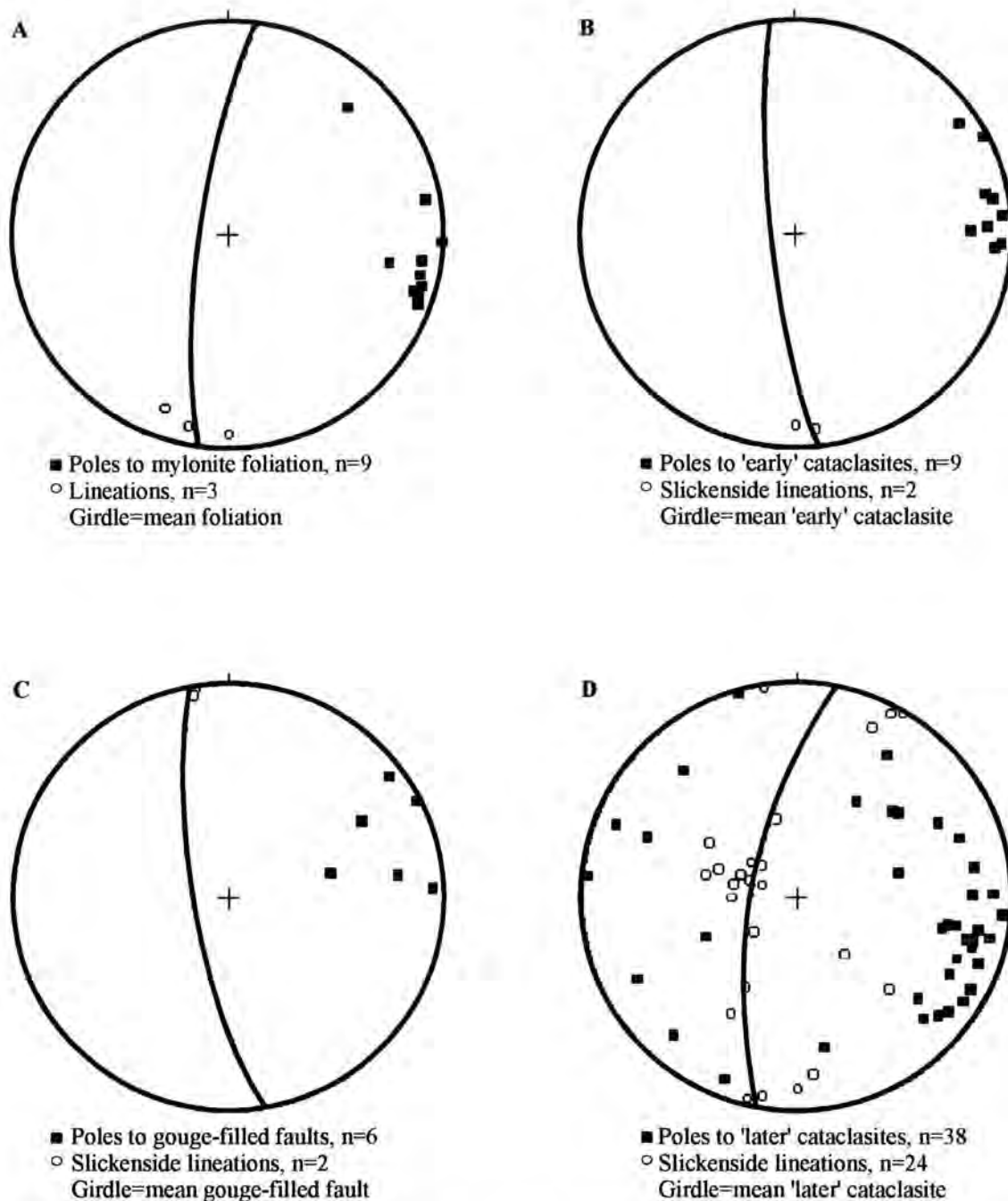


Figure 3.56 Stereographic projections to show structural data collected at Red Ayre. (A) Mylonite foliation and lineations. (B) 'Early' cataclasites overprinting mylonites. (C) Gouge-filled faults overprinting mylonites and 'early' cataclasites. (D) 'Later' cataclasites.

They locally cross-cut the mylonite foliation to form linking structures. The cataclasites are 0.5mm to 3cm thick and do not contain any fabric in the field. In thin-section, E-W-orientated injection veins filled with cataclasite nucleate from the foliation-parallel cataclasites. Millimetre-thick pseudotachylite veins locally bound some cataclasites. The pseudotachylites display well-developed flow banding and chaotic microfolds. Granite veins 3cm to 50cm thick cross-cut the mylonites and 'early' cataclasites (Plate 3.53). N-S trending, sub-vertical faults containing centimetre-thick gouge (Figure 3.56C) appear to form adjacent to 'early' cataclasites. The gouge-filled faults cut through the granite veins. Quartz slickenfibres indicate dextral strike-slip movement based upon the stepping direction of the fibres.

Outside the mylonite xenolith, NNW-NNE-trending faults containing pale brown 'later' cataclasites (5 to 10cm thick) overprint the granite and are spaced 1m to 30m apart. The faults contain both sub-horizontal and dip-slip slickenside lineations (Figure 3.56D). Faults that contain sub-horizontal slickenside lineations locally display quartz slickenfibres, which indicate dextral strike-slip movements, based upon the stepping direction of the mineral fibres. Locally, N-S-trending faults link into ENE-WSW-orientated faults (Plate 3.55) that contain dip-slip slickenfibres. The quartz slickenfibres step down the fault plane indicating dip-slip normal movement. This configuration of N-S- and ENE-WSW-trending faults is consistent with dextral shear.

3:1:8:5 Kinematic summary and discussion

The kinematic evolution of the rocks exposed at Red Ayre is summarised in Table 3.9.

Kinematic Regime	Fault rocks / structures
◦ Dextral strike-slip (youngest)	◦ Fault gouge and clay-rich 'later' cataclasites along mainly N-S-trending faults and linking into dip-slip normal structures
◦ ? (oldest)	<ul style="list-style-type: none"> ◦ Mylonites ◦ Foliation-parallel 'early' cataclasites and cross-cutting linking structures ◦ Millimetre-thick pseudotachylites ◦ Both mylonites and 'early' cataclasites pre-date emplacement of granite

Table 3.9 Summary table of the kinematic evolution of the rocks exposed at Red Ayre.

At Red Ayre, a N-S-trending xenolith of mylonite containing 'early' cataclasites and locally pseudotachylite is present within the granite. The mylonite and 'early' cataclasites are cross-cut by the granite, which belongs to the Devonian Sandsting Complex. Miller and Flinn (1966) recorded K-Ar biotite ages of 334Ma and 360Ma, whilst Mykura and Phemister (1976) dated hornblendes extracted from diorite at 369Ma (K-Ar), which were interpreted by these authors to date intrusion. The WBFP trace lies only 350m to the east of Red Ayre, suggesting that the mylonites represent an earlier phase of movement along the WBFZ pre-dating the emplacement of the granite. The mylonites resemble those exposed at Lunnister 30km to the north along the trace of the WBFP (see section 3:1:2:2a). The only other possible origin of the mylonites is that they are equivalent to those exposed within the Caledonian front to the west of the WBFP in the North Roe area (section 2:1:1). However, the mylonites within the Caledonian Front are a higher metamorphic grade than those exposed at Red Ayre. The rocks at the Caledonian front are cut by the WBF to the east and therefore would not be exposed to the west of the WBFP to the south of the North Roe area, assuming a dextral strike-slip offset along the WBFP. The mylonites, 'early' cataclasites and host-rock granite are affected by intense cataclasis, and are cross-cut by gouges and 'later' cataclasites associated with the WBFZ. The later fault rocks and associated structures are consistent with dextral strike-slip movement along the WBFP, which lies 350m to the east beneath Seli Voe.

3:1:9 Summary

The following table summarises the kinematic history of the WBFZ for sections 3:1:1 to 3:1:8, which will be discussed further in Chapter 8.

Kinematic Regime	Location
5. Sinistral strike-slip (Youngest)	<ul style="list-style-type: none"> • Ness of Haggrister • Brae Isthmus • Papa Little
4. Dip slip, E-side down	<ul style="list-style-type: none"> • Ness of Haggrister
3. Dextral strike-slip	<ul style="list-style-type: none"> • Ollaberry • Sullom, Lunnister and the Ness of Haggrister • Brae Isthmus • Papa Little • Aith Voe • Ness of Bixter • Sand to Seli Voe • Red Ayre
2. Dextral strike-slip –maybe same age as 3 at some localities.	<ul style="list-style-type: none"> • Ollaberry • Ness of Haggrister • Aith Voe • Sand to Seli Voe
1. Sinistral strike-slip (Oldest)	<ul style="list-style-type: none"> • Ollaberry? • Lunnister • Brae Isthmus • Papa Little • Aith Voe • Sand to Seli Voe • Red Ayre

Table 3.10 Summary table of the kinematic events recognised within the WBFZ and the locations where they were recognised.

3:2 The Nesting Fault: locality description and structure

Flinn (1977, 1992) described the Nesting Fault (NF) as a splay of the N-S-trending WBF, which accommodated some strike-slip displacement as the WBF changed strike. The NF splays from the WBF offshore to the south of Seli Voe and links back into the WBF offshore to the north of Ollaberry (Figure 3.1). A 16km dextral displacement has been suggested based upon the interpretation of units offset on geological maps (Figure 3.1). In the present study, the Nesting Fault Zone (NFZ) refers to a zone of rocks that are intensely deformed as a result of movement along the NF. It is partially or fully exposed along five coastal sections. In the following section, only the best of these is described, which is thought to be fully representative of the other partially exposed coastal sections.

3:2:1 Wadbister Voe

The north coast of Wadbister Voe provides the most complete and best-exposed section through the N-S-trending NFZ on Shetland (locality j; Figure 3.1). The E-W-trending coastal section comprises a rocky shoreline with many narrow inlets and low cliffs (<5m high). To the west of the NF are limestones, hornblende schists and calc-silicates belonging to the Whiteness Division (Figure 3.57). East of the NF, psammites and semi-pelites of the Whiteness Division are present which are older than the rocks exposed to the west (Sheet 128, Central Shetland, solid edition map). The fault zone at this locality is approximately 600m wide. Fault-related deformation is strongly asymmetric, extending 550m to the west of the Nesting Fault Plane (NFP) in Whiteness Division rocks compared to only 50m east of the NFP in psammites and pelites.

Flinn (1977) described the NF to be a 6m-wide zone of breccia and fault powder on the north side of Wadbister Voe. Flinn (1977) described strong cataclasis extending only 30m on either side of the fault, with common kink-folds displaying a dextral sense of vergence outside this zone. Conroy (1996) described the Nesting Fault as a dextral strike-slip fault, associated with intense cataclasis, gouge development and dextral-verging folds.

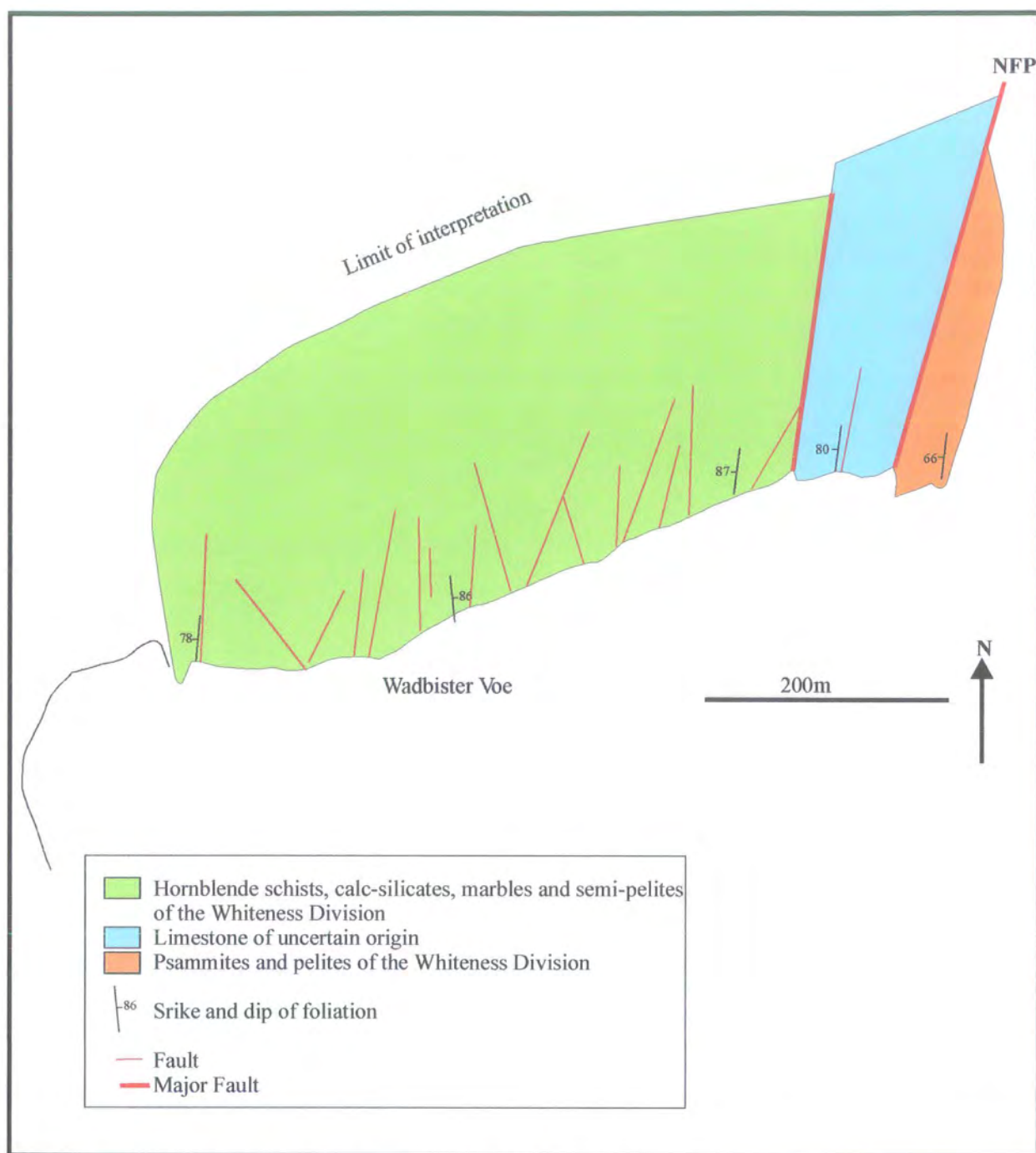


Figure 3.57 Geological map along the northern coast of Wadbister Voe.

3:2:1:1 Protolith lithologies

3:1:2:1a Whiteness Division rocks west of the NF

Rocks belonging to the Dalradian Whiteness Division (section 2:1:2:4) are exposed to the west of the NF, at Wadbister Voe (Figure 3.57). The rocks comprise mainly hornblende-rich schists interbanded with calc-silicates, marbles and semi-pelites. Compositional layers are generally between 15cm to 2m in thickness, and probably represent the original sedimentary horizons. The hornblende-rich schists are green / grey coloured, coarse to medium grained and finely laminated. Locally, the schists contain subordinate bands of semi-pelite, calc-silicate and marble. The schists contain a near-vertical, N-S-trending foliation defined by flattened aggregates of hornblende and quartz, with sub-horizontal lineations defined by elongate hornblende, mica and quartz grains.

A fault-bounded sliver of limestone lies to the east of the schists and adjacent to the NF (Figure 3.57). The limestone is grey in colour, fine grained and consists of 90% calcite and 10% quartz. It is also intensely deformed by the effects of cataclasis .

3:1:2:1b Whiteness Division rocks east of the NF

To the east of the NF, psammites and semi-pelites belonging to the Dalradian Whiteness Division are exposed (section 2:1:2:4; Figure 3.57). These are slightly older than the rocks west of the NF (Sheet 128, Central Shetland, solid edition map). The psammites are grey / pink in colour, medium grained and comprise approximately 60% quartz, 30% feldspar, 5% chlorite and 5% muscovite. Psammites 1-3m in thickness are interlayered with thin (~30cm thick), more pelitic units, and probably represent the original sedimentary horizons. The rocks display a N-S-trending, sub-vertical foliation defined by flattened aggregates of quartz and feldspar with sub-horizontal lineations defined by elongate quartz, feldspar and mica grains.

3:2:1:2 Fault Rocks

The fault rocks described in this section are interpreted to be of the same age based upon overprinting relationships (see section 3:2:1:3).

3:2:1:2a Breccia

Pale grey-/green-coloured incohesive breccias comprise finely comminuted fragments of schist, limestone, quartz, hornblende, feldspar and mica set within a fine-grained clay-rich matrix. The breccias are isotropic on all scales of observation in the field. Millimetre-thick calcite veins commonly occur within the breccia zones, locally acting as cement.

3:2:1:2b Fault gouge

Fault gouges at Wadbister Voe are green/blue in colour, incohesive, fine grained and clay-like in appearance. The soft blue/green gouge displays a strong foliation defined by aligned clay particles parallel to the bounding fault surfaces.

3:2:1:3 Fault rock distribution and age relationships

Cataclastic deformation, which generally increases towards the core of the NF, overprints the regional fabrics. In this section, the wall rocks are described first followed by a section on the NF core.

3:1:1:3a West of the NF core

Breccias and gouges are exposed west of the NF core. Both overprint the regional fabrics within rocks belonging to the Whiteness Division. Blue / green gouges are commonly present along subsidiary faults over a distance of 550m west of the fault plane.

3:2:1:3a East of the NF core

Gouge-filled faults overprint the regional fabrics of psammites and semi-pelites belonging to the Whiteness Division. Gouges are present up to 50m to the east of the NF core.

3:2:1:3c NF core

The most obvious movement plane of the NFZ defines a narrow inlet and is exposed at HU 4374 5065 on the north side of Wadbister Voe. The fault plane (NFP) is orientated 016/85E and is the main structural boundary within the NFZ on the north side of the Wadbister Voe. Here, the fault core is approximately 6m wide (Figure 3.58). The fault core corresponds to the region of most intense fault-related deformation. Here, the fault core is defined by a continuous sequence of fault rocks that extend from the wall rocks to the west and east, and across the NFP, which is the main structural boundary within the NFZ.

On the west side of the NF core, centimetre-spaced shear bands overprint the regional schistosity. To the east, a 5m-wide zone of incohesive breccia overprints the calcareous schists containing shear bands. N-S-orientated slices of limestone and schist appear to 'float' within the breccia. The eastern side of the breccia zone grades into a 50-60cm thick soft blue / green gouge, which is bounded to the east by the NFP. The gouge displays a strong fault-parallel foliation with a sub-horizontal lineation; both defined by aligned clay particles. The gouge cross-cuts intensely fractured psammites to the east.

3:2:1:4 Fault zone structure

3:2:1:4a West of the NF core

At distances of up to 550m west of the NFP, the regional foliation in the Whiteness Division is defined by flattened aggregates of quartz, hornblende, feldspar and calcite. The foliation is near-vertical and trends NNE-SSW, with sub-horizontal lineations defined by aligned mica, quartz, feldspar and hornblende grains (Figure 3.59A).

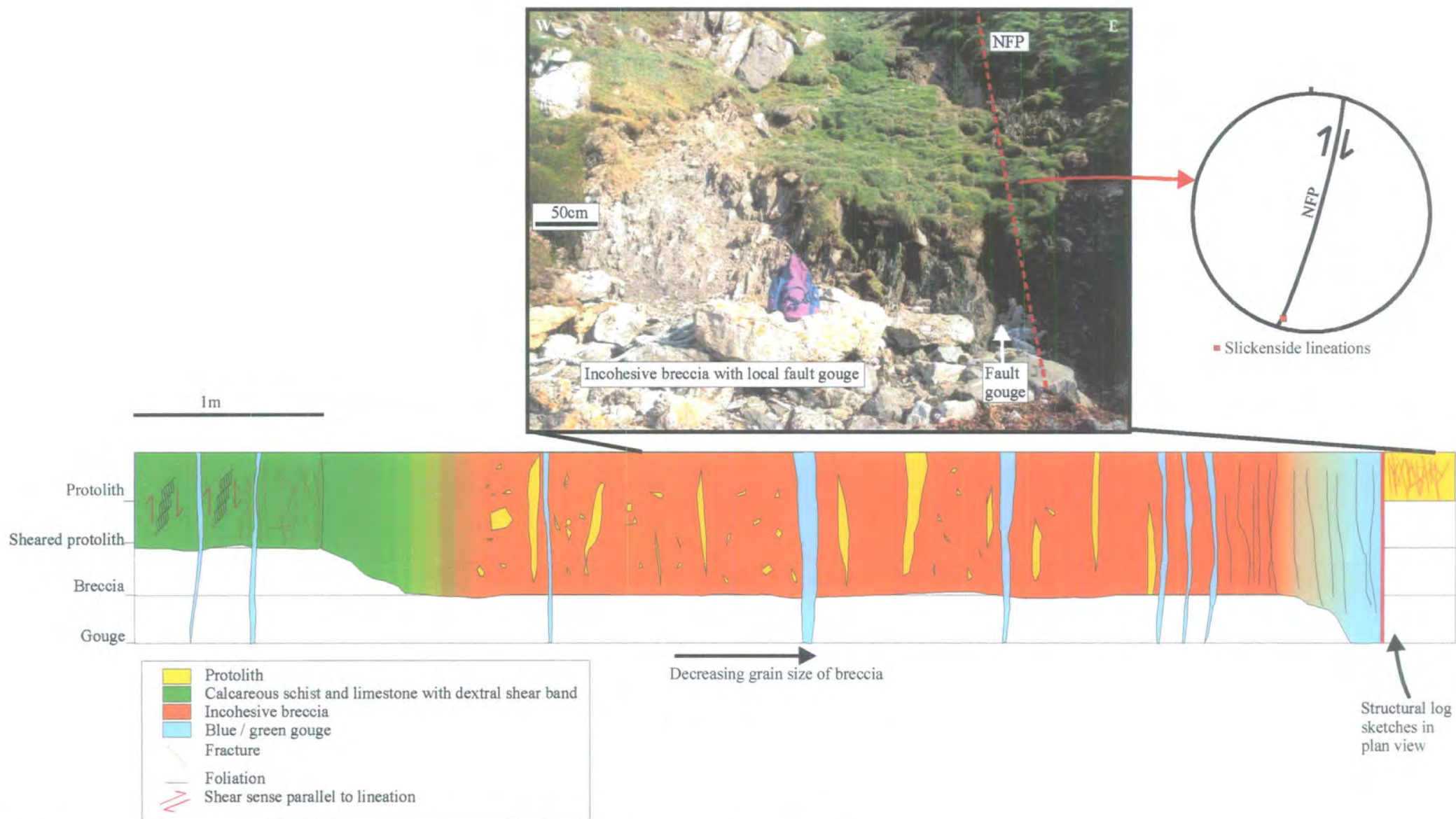
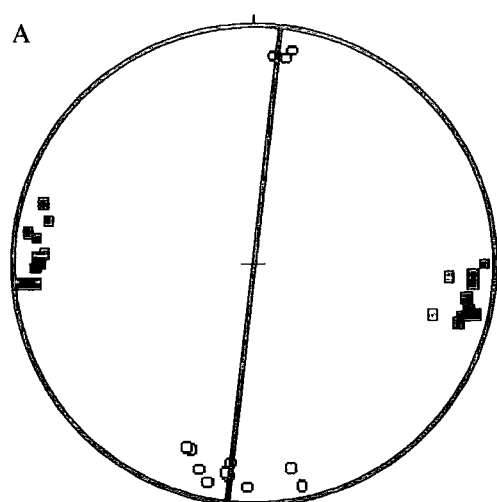
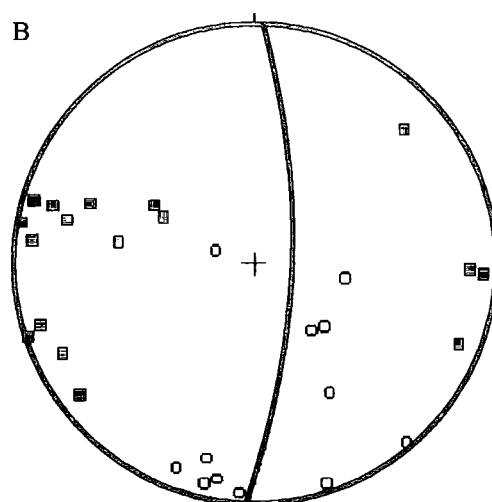


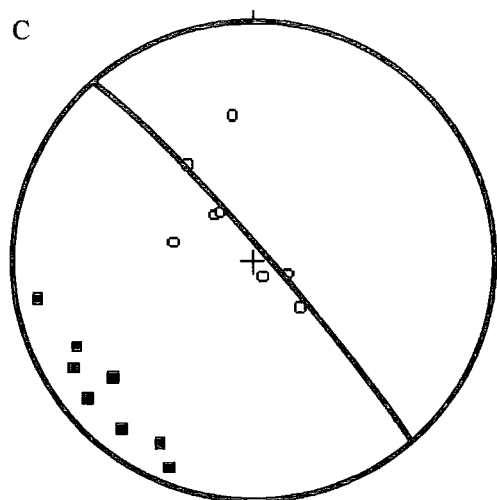
Figure 3.58 Structural log of the NF core to illustrate fault rock distribution and overprinting relationships.



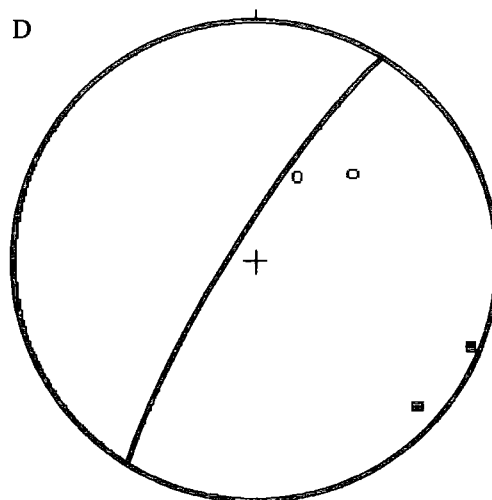
■ Poles to regional foliation planes, n=21
○ Stretching lineation, n=13
Girdle=mean regional foliation



■ Poles to gouge-filled fault planes, n=17
○ Slickenside lineations, n=12
Girdle=mean gouge-filled fault plane



■ Poles to axial planes of kink folds with a dextral sense of vergence, n=8
○ Hinge orientation, n=8
Girdle=mean axial plane



■ Poles to axial planes of kink folds with a sinistral sense of vergence, n=2
○ Hinge orientation, n=2
Girdle=mean axial plane

Figure 3.59 Stereographic projections of structural data west of the NF core. (A) Regional foliation and lineation. (B) Gouge-filled faults and slickenside lineations. (C) Dextral-verging kink folds. (D) Sinistral-verging kink folds.

The first fault appears at 550m west of the NFP and appears to have localised within a more pelitic unit. The fault is near-vertical, N-S-trending and contains 2cm of soft blue gouge with sub-horizontal slickenside lineations. At between 550m and 420m, gouge-filled faults are spaced every 10-20m apart. At 350m west of the NFP, centimetre-scale dextral shear bands overprint the regional foliation within pelitic units in surfaces viewed normal to the foliation and parallel to the lineation. Gouge-filled faults between 350m and 250m west of the NFP are commonly mineralised by calcite. At 250m west of the NFP, a sub-vertical, N-S-trending fault contains 5-10cm of gouge with sub-horizontal slickenside lineations. On outcrop surfaces viewed normal to the fault plane and parallel to the slickenside lineations, centimetre-scale shear bands within the gouge indicate a dextral sense of shear. To the east gouge-filled faults increase in frequency and commonly occur in clusters. The faults trend N-S and dip moderate-steeply to the E and W (Figure 3.59B). Slickenside lineations vary from sub-horizontal to dip-slip. Faults with dip-slip slickenside lineations are usually reverse, based upon shear bands and fold vergence within the gouge. Gouges adjacent to fault planes with sub-horizontal slickenside lineations display shear bands and dextral-verging folds, indicating right-lateral strike-slip movement.

Late-stage, fault-related folds first appear at 210m west of the NFP, and vary in style from sharply kinked to rounded closures with straight limbs. The folds occur on a centimetre to metre-scale and mainly show a dextral sense of vergence. Dextral-verging folds plunge mainly steeply to the N and S with axial planes striking NE-SW (Figure 3.59C). Folds with a sinistral sense of vergence occur less frequently and appear to be conjugate to the dextral-verging folds. The sinistral-verging folds plunge moderately to the N with axial planes trending NE-SW (Figure 3.59D). Dextral- and sinistral-verging folds mainly occur adjacent to pelitic rocks with sub-horizontal lineations, dextral shear bands and dextral strike-slip faults. It is inferred that the conjugate kink folds accommodated N-S directed shortening across the anisotropic metamorphic rocks (pelites and psammities) (cf. Folds in Domain B Ollaberry; section 3:1:1:5 b). At 180m west of the NFP, gouge-filled faults are spaced 2-6m apart.

At 90 m west of the NFP a N-S sub-vertical fault containing 20cm of fault gouge bounds a unit of crystalline limestones to the east. At 60m west of the NFP, fracturing is intense. Sub-vertical, NE-SW-trending fractures with sub-horizontal

slickenside lineations offset the lithological layering by 5cm to 30cm dextrally (Figure 3.60A; Plate 3.56). The fractures curve and link into foliation-parallel fracture zones and are interpreted as R-type Riedel shears to the NF. NW-SE, sub-vertical fractures with sub-horizontal slickenside lineations also offset the lithological layering by 5cm to 30cm in a dextral sense (Figure 3.60B; Plate 3.57) and link into foliation-parallel fracture zones. These are interpreted as P-type Riedel shears to the NF. The geometrical configuration and asymmetry of R- and P-type Riedel shears with respect to the trace of the NF is consistent with dextral shear along the NF (Figure 3.61). Kink folds that show a consistent dextral sense of vergence (Plate 3.58) are common within the limestone, and are similar to those described farther to the west. Centimetre-thick, calcite-filled, tension veins trend ENE-WSW indicating NNW-SSE orientated extension, which is also consistent with dextral shear along the NF (Figures 3.60C, 3.61; Plate 3.59).

3:2:1:4b East of the NF core

Fault related deformation extends only 50m to the east of the NFP into psammites and semi-pelites belonging to the Whiteness Division. Gouge-filled faults are rarely exposed to the east of the NFP. The rocks up to 50m east of the NFP are characterised by intense fracturing and millimetre-scale networks of calcite veins.

3:2:1:4c NF core

On the western side of the NF core, centimetre-spaced shear bands overprint calcareous schists and indicate a dextral sense of shear (Plate 3.60). The schists are overprinted by a 5m wide zone of incohesive breccia to the east (Figure 3.59). N-S-orientated slices of limestone and schist appear to 'float' within the breccia and display curvilinear folds. In cross-section, the slivers of limestone are transected by folds, which verge up to the W with sub-horizontal hinges. In plan view, the folds display a dextral sense of vergence. To the east, the breccia zone grades into a 50-60cm thick soft blue / green gouge, which is bounded to the east by the NFP (Figure 3.59). The gouge displays a strong fault-parallel (016/85E) foliation with a lineation, which plunges gently to the S (07/193); both are defined by aligned clay particles. On outcrop surfaces viewed normal to the fault plane and parallel to the lineation,

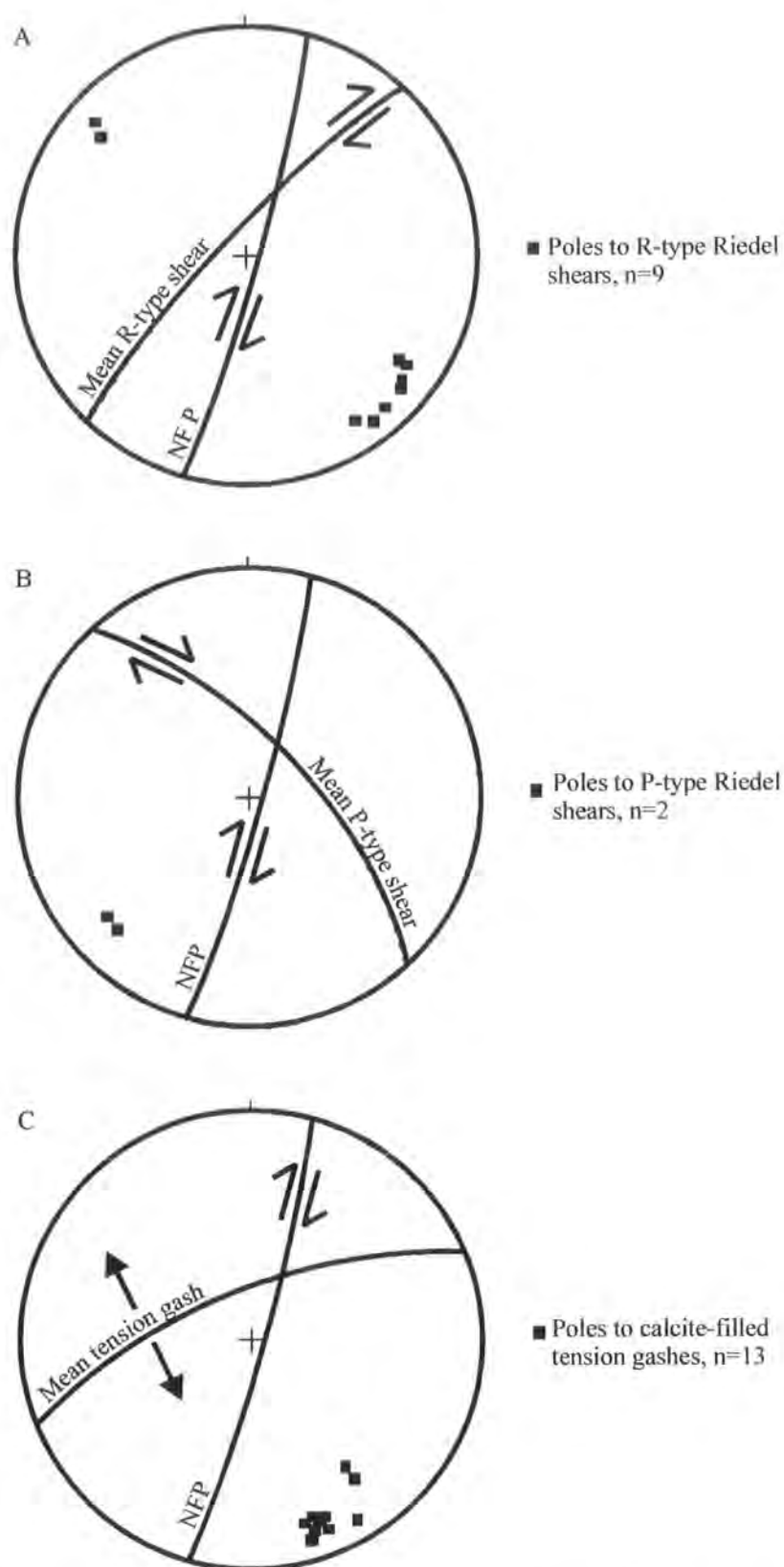


Figure 3.60 Stereographic projections to show (A) R-type Riedel shears, (B) P-type shears and (C) tension gashes (arrows indicate extension direction) from Wadbister Voe.

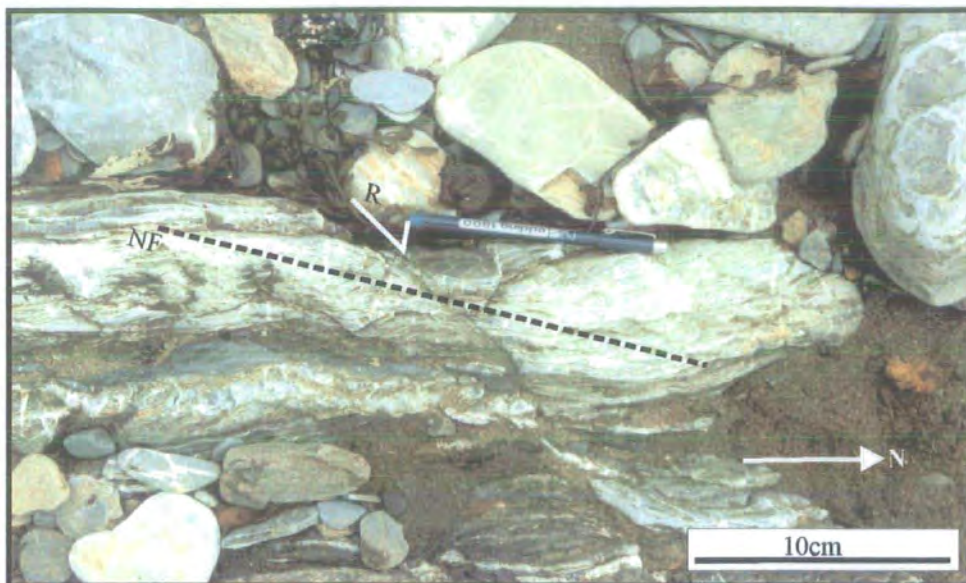


Plate 3.56 Plan view. R-type Riedel shear with sub-horizontal slickenside lineation offsetting lithological layering by 5cm (dashed line equals trace of NFP) (HU 4370 5064).

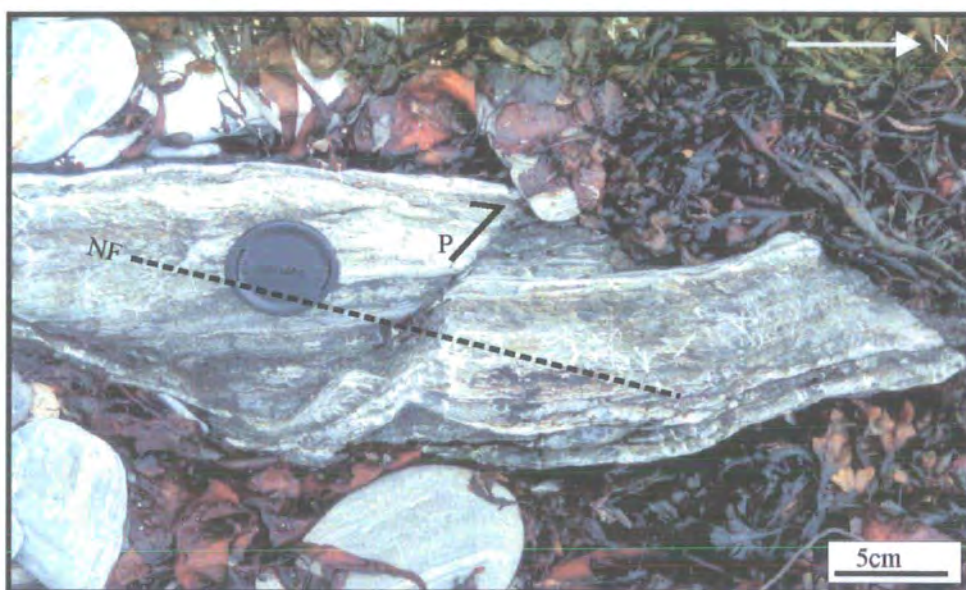


Plate 3.57 Plan view. P-type Riedel shears with sub-horizontal slickenside lineation offsetting lithological layering by 5cm (dashed line equals the trace of the NFP) (HU 4370 5064).

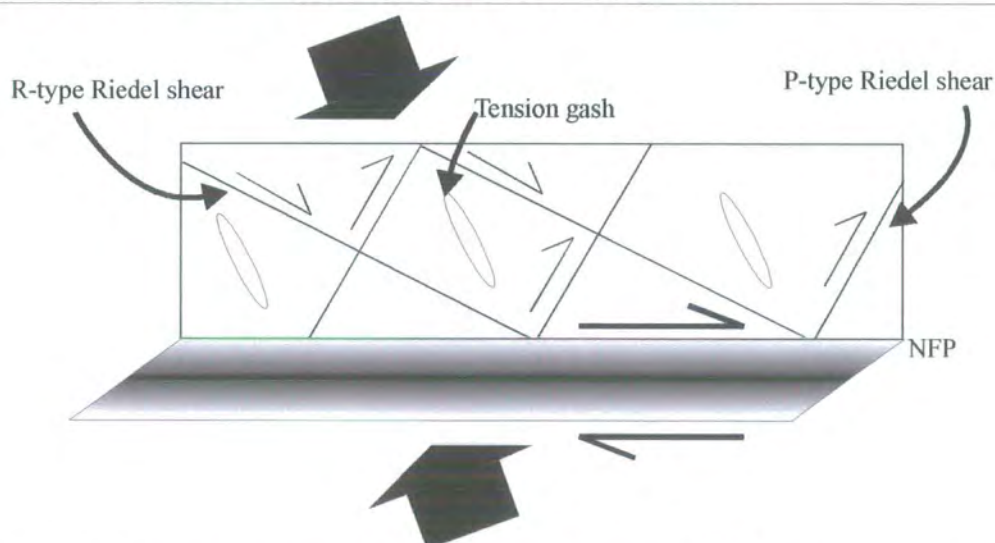


Figure 3.61 Schematic diagram to illustrate the development of Riedel-type shears as a result of E-W-directed compression to the west of the NFP. The shears show an asymmetry to the NFP with P-type shears at a higher angle to the NFP than R-type shears, which is consistent with dextral shear.

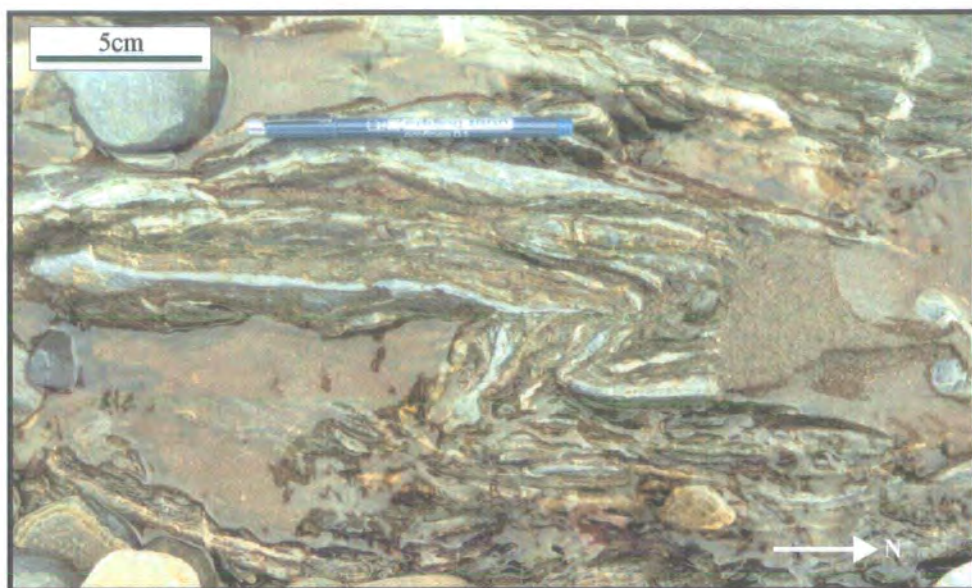


Plate 3.58 Plan view. Centimetre-scale kink fold with dextral sense of vergence (HU 4370 5064).



Plate 3.59 Plan view. Image to show the relationship between R-type riedel shears and calcite-filled tension gashes with respect to the NFP orientation (dashed white line) (HU 4370 5064).

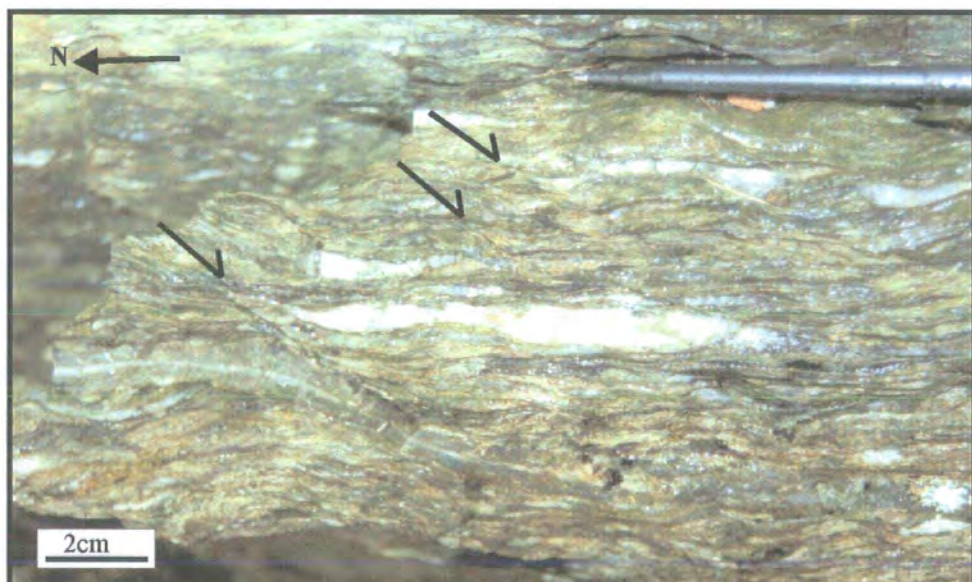


Plate 3.60 Plan view. Centimetre-spaced shear bands within calcareous schist on the west side of the NF core (HU 43745065). Split arrows indicate sense of shear parallel to the lineation.

centimetre-scale shear bands indicate dextral shear. Locally, millimetre- to centimetre-scale kink bands with a sinistral sense of vergence are present within the gouge. The gouge is bounded to the east by a polished fault plane (NFP) orientated 016/ 85E, with slickenside lineations orientated parallel to the lineation in the gouge. Intensely fractured psammites are exposed to the east of the NFP (Figure 3.59).

3.2:1:5 Kinematic summary and discussion

The kinematic evolution of the NFZ is summarised in Table 3.11.

Kinematic Regime	Fault rocks / structures
Dextral transpression	<ul style="list-style-type: none"> ◦ Dextral strike-slip and contractional gouge-filled faults ◦ Configuration of R- and P-type Riedel shears ◦ Dextral verging kink folds ◦ Calcite-filled tension gashes ◦ Dextral shear bands within calcareous schists ◦ Dextral shear bands within gouge of the fault core

Table 3.11 Summary table of kinematic regime and the fault rocks / structures exposed along the N side of Wadbister Voe.

Along the north side of Wadbister Voe, the NFZ is characterised by brecciation, a wide zone of subsidiary faulting, kink folding and the development of gouge, all consistent with dextral transpression. There is no evidence for more than one phase of movement along the NF at Wadbister Voe. The present study supports Flinn (1977) who interpreted the NF to have formed as a result of dextral strike-slip movement along a large-scale, left-stepping, restraining bend along the WBF, resulting in 16km of dextral displacement along the NF.

3:3 The Melby Fault: locality description and structure

The Melby Fault (MF) forms the other regionally significant fault (Figure 3.1) exposed on Shetland. It has long been considered to be a strike-slip fault despite there being no documented evidence of such movement within the literature (e.g. Mykura 1976; Mykura and Phemister 1976; Mykura 1991). Donovan et al. (1976) proposed a dextral strike-slip offset of a 'considerable amount' based upon reconstructing Devonian palaeogeography. Flinn (1977) described the MF as a series of polished SE-dipping surfaces arranged in an en echelon fashion with slickenfibres indicating reverse motion. Rogers et al. (1991) suggested that the fault is an inverted syn-depositional normal fault. A major, dextral strike-slip, displacement was implied by Séranne (1992a) based upon his maps and fold axes orientations within the Devonian sedimentary rocks, which were thought to have formed during Carboniferous inversion of the Orcadian Basin. Conroy (1996) interpreted the outcrops to the east of the MF trace to display evidence for dextral shear overprinted by strong cataclastic deformation. The Melby Fault Zone (MFZ) refers to a zone of rocks that are intensely deformed as a result of movement along the MF. The fault zone is accessible but poorly exposed in one coastal section and inaccessible, except by boat, along another.

3:3:1 Melby

The MF intersects high cliffs (~100-180m high) and forms a narrow inlet named Hesti Geo (HU 1742 5570). Here, the fault trace separates sandstone, conglomerates and rhyolites of the Middle Devonian Western Group (see section 2:1:4:2) to the northwest from conglomerates, sandstones and silts of the Devonian Sandness Formation (see section 2:1:4:1) to the southeast. The exposures are inaccessible except by boat. The MF trace can be traced inland to the northeast and is defined by a break in slope. Farther to the northeast, the MF trace cuts a 500m-wide sandy beach (HU 1940 5777; locality k; Figure 3.1) and extends offshore into St. Magnus Bay where it has been correlated with the equally poorly exposed Eshaness Fault (Figure 3.1; Flinn 1992). On the western side of the bay, a series of sandstones, conglomerates and rhyolites belonging to the Middle Devonian age Western Group are exposed (Figure 3.62).

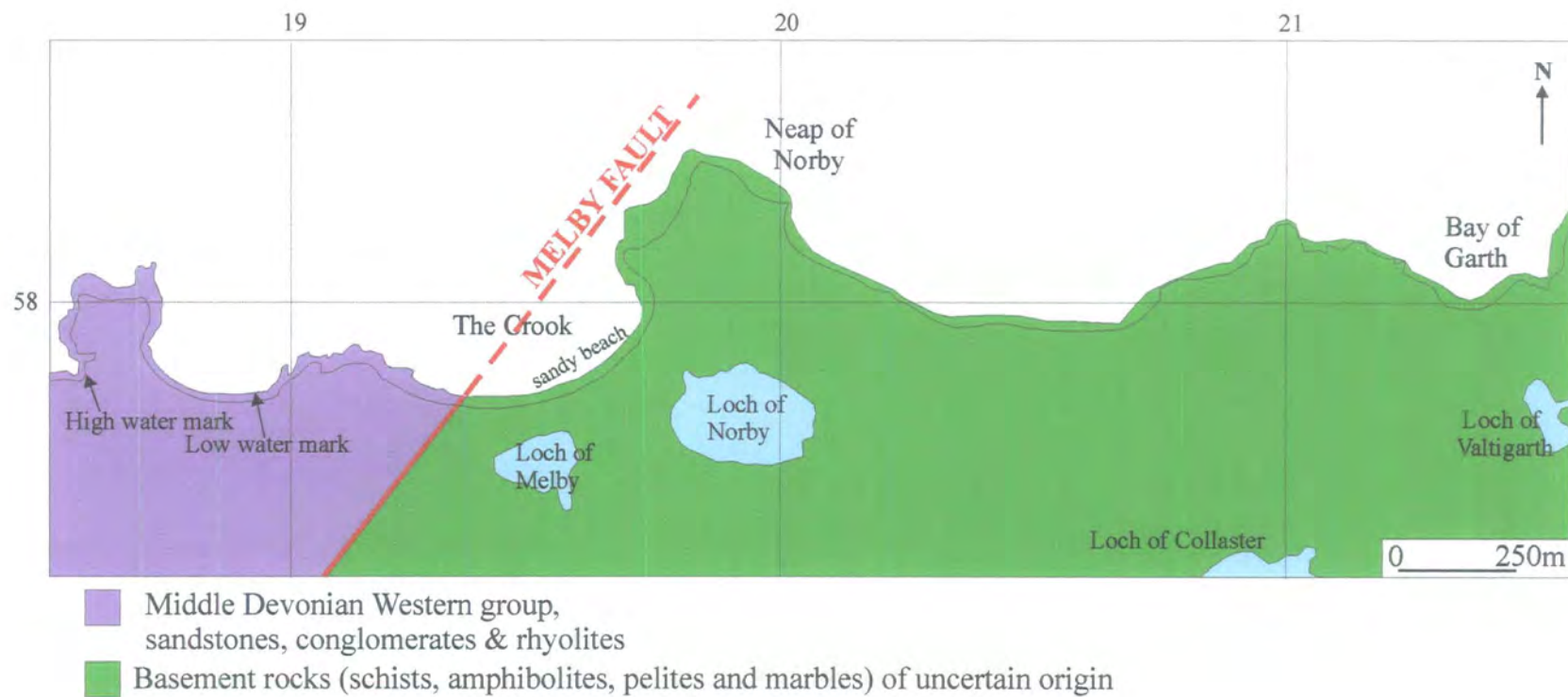


Figure 3.62 Geological map of Neap of Norby area.

To the east, across the MF trace, basement rocks of uncertain origin (section 2:1:1:5) comprising interlayered hornblende schists, amphibolites, quartzo-feldspathic semi-pelites and marbles are present. To the south, conglomerates, sandstones and silts belonging to the Devonian age Sandness Formation unconformably overlie the basement rocks.

3:3:1:1 Protolith lithologies

3:3:1:1a West of the MF trace

To the west of the MF trace, rocks belonging to the Middle Devonian age Melby Formation of the Western Group are exposed (Figure 3.62). Red coloured conglomerates, sandstones and silts are interbedded on a centimetre- to metre-scale. The sequence passes into cross-bedded sandstones, which are interlayered with rhyolite and ignimbrite horizons.

3:3:1:1b East of the MF trace

Hornblende schists, amphibolites, quartzo-feldspathic semi-pelites and marbles interlayered on a centimetre- to metre-scale are exposed east of the MF trace (Figure 3.62). The rocks contain a NE-SW foliation defined by flattened aggregates of quartz, feldspar, hornblende, mica and calcite, which dips approximately 50° to the SE. Aligned hornblende and mica grains define a sub-horizontal lineation. Randomly orientated pegmatite dykes (20 to 50cm thick) cross-cut the regional foliation.

3:3:1:2 Fault rocks

3:3:1:2a Phyllonites

Dark green / grey-coloured, fine-grained, mica-rich fault rocks are exposed within centimetre-scale shear zones 200m east of the MF trace. Aligned aggregates of fine-grained mica define a mylonitic foliation, which surrounds porphyroclasts (0.1mm to 4cm) of feldspar, quartz and cataclastically deformed schist (Plate 3.61).

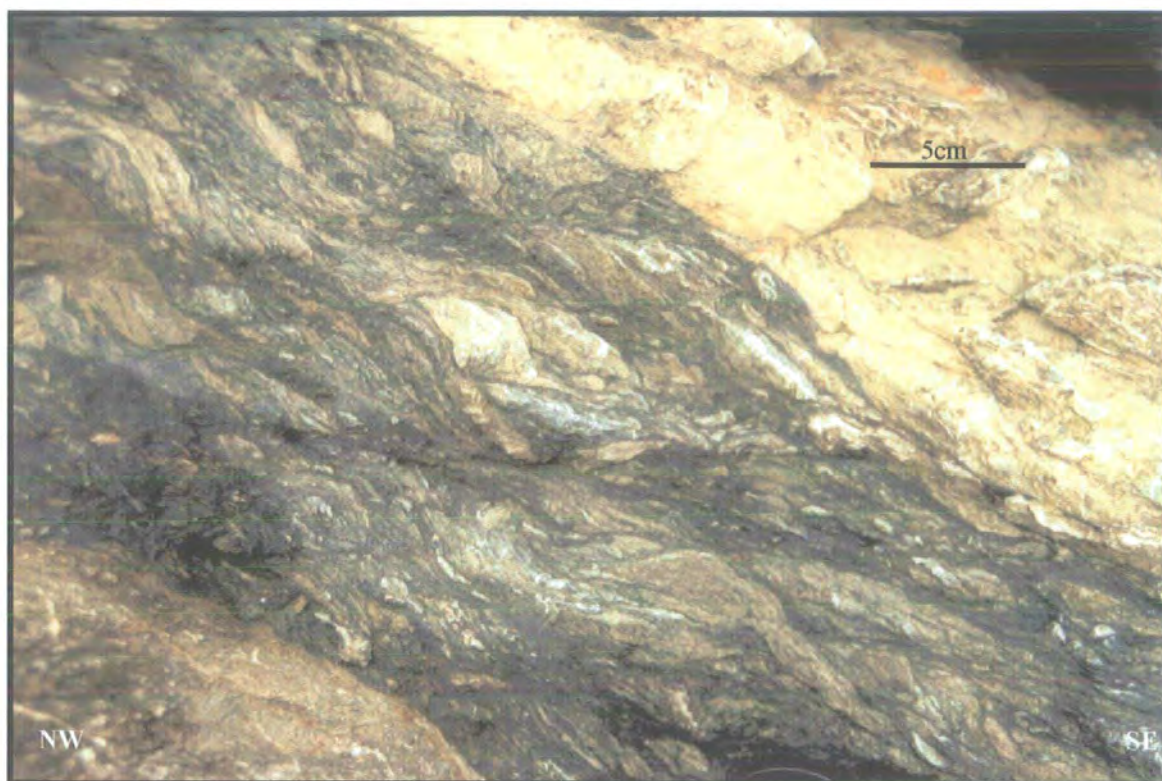


Plate 3.61 Cross-sectional view. Image of SE-dipping phyllonitic shear zone (029/36SE) with lineations orientated normal to the paper, i.e. 12/044 (HU 1975 5818).

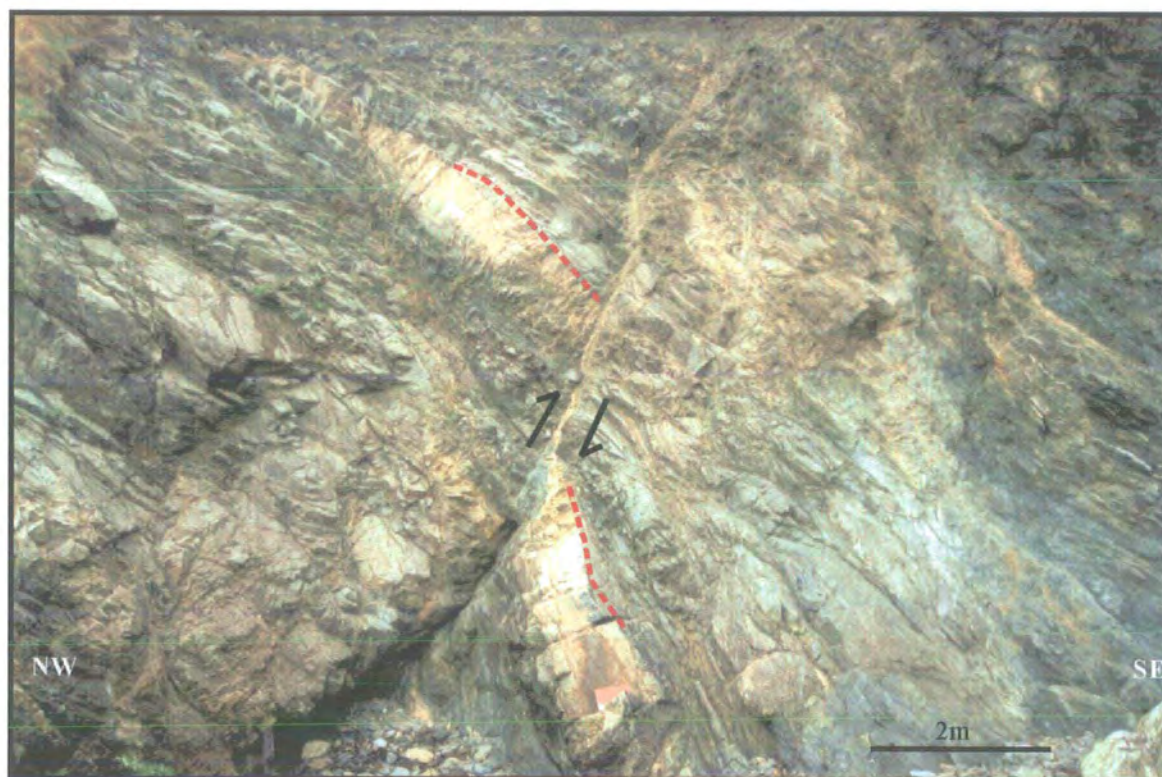


Plate 3.62 Cross-sectional view. NE-SW-trending, gouge-filled fault with dip-slip slickenside lineations and a reverse offset of 2m (HU 1974 5817).

The NE-SE-trending, SE-dipping foliation contains sub-horizontal lineations defined by aligned mica grains.

3:3:1:2b Fault gouge

Fault gouges at Melby are blue in colour, incohesive, fine-grained and clay-like in appearance. The soft blue gouge displays a foliation defined by aligned clay particles parallel to the bounding fault surfaces.

3:3:1:3 Fault rock distribution and age relationships

3:3:1:3a East of the MF trace

To the east of the MF trace, foliation (052/50SE) within the basement rocks is cross-cut by several, NE-SW-trending, phyllonitic shear zones (029/36SE; Plate 3.61) which dip shallowly to moderately to the SE (HU 1975 5818). At HU (HU 1975 5818) the basement rocks and pegmatites are overprinted by centimetre-thick gouge-filled faults.

3:3:1:3b West of the MF trace

To the west of the MF trace, the interbedded sedimentary rocks and rhyolites are intensely fractured. No faults were observed in the exposures to the west of the MF trace.

3:3:1:3 Fault zone structure

3:3:1:3a East of the MF trace

To the east of the MF trace, basement rocks display a foliation orientated at 052/50SE with sub-horizontal lineations. On outcrop surfaces viewed normal to the foliation and parallel to the lineation, σ -type feldspar porphyroclasts (up to 5cm in size) indicate dextral shear. These rocks are cross-cut by several poorly-exposed phyllonitic shear zones (~30cm thick; Plate 3.61) orientated 029/36SE with sub-

horizontal lineations (12/044) defined by aligned mica grains (HU 1975 5818). The shear sense could not be determined due to the lack of outcrop surfaces orientated normal to the shear zone and parallel to the lineation. At grid reference locality HU 1974 5817, the basement rocks and pegmatites are overprinted by centimetre-thick gouge-filled faults (Plate 3.62). The faults are orientated NNE-SSW (sub-parallel to the MF trace) and dip approximately 60° to the NW. The faults contain dip-slip slickenside lineations and are contractional, based upon offsets of the regional foliation (052/50SE) by up to 2m in a reverse sense.

3:3:1:3b West of the MF trace

To the west of the MF trace, the interbedded sedimentary rocks and rhyolites are intensely fractured. The bedding trends NE-SW and dips steeply to the NW. Along some of the bedding surfaces, sub-horizontal slickenside lineations are present.

3:3:1:4 Kinematic summary and discussion

The kinematic evolution of the rocks exposed at Melby is summarised in Table 3.12.

Kinematic regime	Fault rocks / structures
3. Reverse dip-slip (youngest)	<ul style="list-style-type: none"> NE-SW-trending gouge-filled faults, which dip moderately to steeply to the NW. The faults display reverse dip-slip offsets of up to 2m Intense fracturing
2. Strike-slip	<ul style="list-style-type: none"> Phyllonitic shear zones (029/36SE) (unclear if related to faulting along the MF)
1. Dextral shear (oldest)	<ul style="list-style-type: none"> σ-type feldspar porphyroclasts indicating dextral shear. (unclear if related to faulting along the MF)

Table 3.12 Summary table of kinematic regime, structures and fault rocks exposed at Melby.

Reverse dip-slip movement along gouge-filled faults (phase 3; Table 3.12) is consistent with the observations of Flinn (1977), who described the MF as a series of polished SE-dipping surfaces arranged in an en echelon fashion with slickenfibres

indicating reverse motion. Conroy (1996) interpreted the outcrops to the east of the MF trace to display evidence for dextral shear based on σ -type feldspar porphyroclasts. These were observed in the present study but it is unclear if they are related to early movements along the MF. Donovan et al. (1976) and Séranne (1992a) suggested dextral strike-slip movements along the MF based upon palaeogeography of the Devonian basins, and compressional directions during Carboniferous inversion, respectively. Conroy (1996) observed strong cataclastic deformation which overprinted all other rocks and structures (cf. phase 3; Table 3.12).

Chapter 4. Fault rock textures and microstructures: WBFZ

The aim of this chapter is to provide a comprehensive description of key fault rock microstructures and textures along the multiply reactivated WBFZ. Fault rock overprinting relationships (discussed in Chapter 3) combined with microstructural studies will be used to formulate the detailed textural and microstructural evolution (summarised in Chapter 8) exhibited by fault rocks along key fault zone strands, in order to assess the processes and factors that controlled deformation, localisation and reactivation along the WBFZ (discussed in Chapter 8).

Much of the WBFZ comprises a 500m to 2km-wide zone of braided sub-vertical faults associated with broad zones of cataclasis and the development of fault gouge formed during dextral strike-slip. Subsequent dip-slip and sinistral strike-slip (minor) reactivation of the WBFZ localised deformation within pre-existing fault gouges located within the central part of the WBFZ (fault core). The earliest recognised fault-related deformation comprises mylonitic fault rocks formed during sinistral shear. These fault rocks are only found within fault-bounded blocks that were exhumed in a series of 'positive' flower structures (see sections 3:1:2; 3:1:7) during dextral strike-slip movements along the WBFZ.

In the following sections, textures and microstructures of protolith and fault rock assemblages formed within the WBFZ will be described in the order of their age (oldest to youngest), deduced from the field relationships described in Chapter 3. The earliest fault rock assemblages formed during sinistral strike slip along the WBFZ and are referred to in this chapter as primary fault rocks. Later fault rocks formed during dextral strike-slip reactivation of the WBFZ are referred to as secondary fault rocks.

4:1 Protoliths

4:1:1 Banded gneiss

Compositionally banded felsic and mafic gneisses of uncertain origin are exposed west of the WBF at Sullom, Lunnister and the Ness of Haggrister (section 3:1:2).

Felsic gneisses comprise both fine- and coarse-grained gneisses. Fine-grained gneisses comprise 70% feldspar (K-feldspar and plagioclase An₄₀ with a ratio of 1:1), 20% quartz and less than 10% hornblende, epidote and micas. They contain equigranular-polygonal aggregates of feldspar and quartz grains (~0.1mm in size) which surround isolated pockets of hornblende, epidote and mica (Plate 4.1A&B). Both quartz and feldspar grains display aspect ratios of up to 3:1, a grain elongation which defines the macroscopic foliation. Feldspars are partially sericitised and display sweeping undulose extinction. Quartz grains also display sweeping undulose extinction together with deformation lamellae. Coarse-grained gneisses comprise 60% feldspar (K-feldspar and plagioclase An₃₅ with a ratio of 1:1), 30% quartz and 10% chlorite and muscovite. They contain equigranular-polygonal aggregates of feldspar and quartz grains (0.5 to 1mm in diameter) together with chlorite and muscovite grains (0.5mm in length), which are scattered through the rock (Plate 4.1C&D). Both the quartz and the feldspar grains display aspect ratios of up to 3:1 and together with aligned mica grains define a macroscopic foliation. Feldspar grains are partially sericitised and display sweeping undulose extinction. Quartz grains also display sweeping undulose extinction and deformation lamellae.

Mafic gneisses are fine to medium grained and comprise 65-80% hornblende and 20-30% feldspar together with minor amounts of epidote locally forming continuous bands. Mafic gneisses contain equigranular-polygonal aggregates of elongate hornblende and feldspar grains (~0.2-0.5mm in diameter) (Plate 4.1A&B). The long axes of both the hornblende and feldspar grains define a macroscopic foliation. Both hornblende and feldspar grains display sweeping undulose extinction.

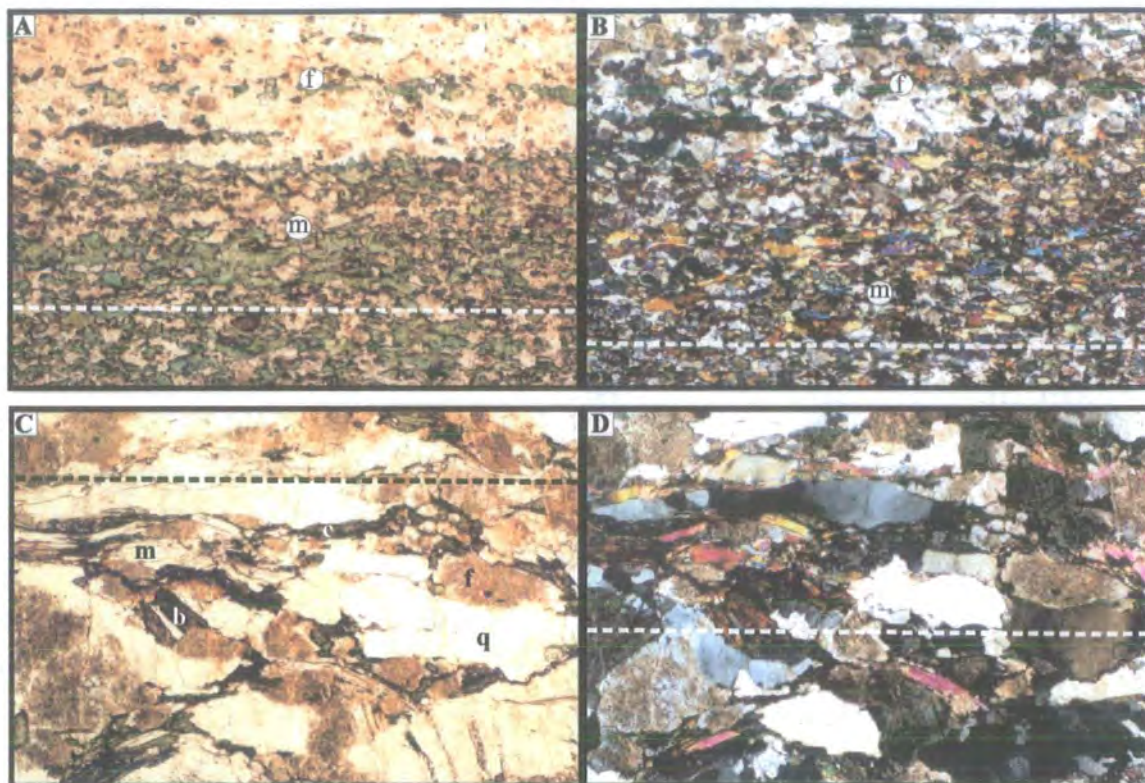


Plate 4.1 Gneisses at Sullom, Lunnister and the Ness of Haggrister. (A) & (B) Photomicrographs to show the fine-grained felsic (f) and mafic (m) gneiss together with the contact. Felsic gneiss comprises equigranular-polygonal aggregates of elongate feldspar and quartz. Mafic gneiss comprises equigranular-polygonal aggregates of elongate hornblende and feldspar. Dashed line represents gneissose foliation. (A) Plane-polarised light and (B) crossed polars. Field of view for (A) & (B) 3.6 x 2.4mm. (C) & (D) Coarse-grained felsic gneiss comprising elongate equigranular-polygonal aggregates of feldspar (f) and quartz (q) grains together with aligned biotite (b), chlorite (c) and muscovite (m) grains. Dashed line represents gneissose foliation. (C) Plane-polarised light and (D) crossed polars. Field of view for (C) & (D) 3.6 x 2.4mm.

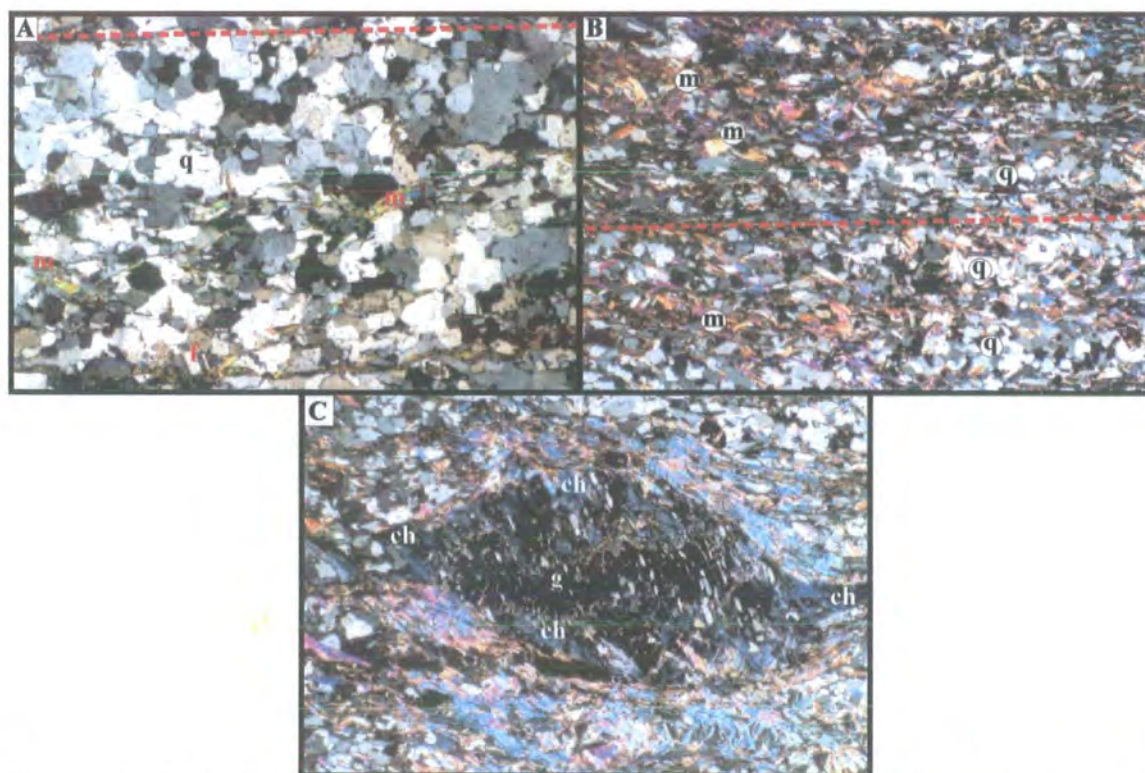


Plate 4.2 (A) Psammite belonging to the Queyfirth Group at Ollaberry. The rocks are mainly composed of inequigranular-polygonal aggregates of quartz grains (q) which surround isolated feldspar grains (f) and aligned muscovite (m) grains. Dashed line - layering. Field of view 3.6 x 2.4mm, crossed polars. (B) Pelite of the Queyfirth Group at Ollaberry. The rock comprises quartz ribbons (q) which are interlayered with bands of chlorite and muscovite (m). Dashed line - schistosity. Field of view 3.6 x 2.4mm, crossed polars. (C) Garnet porphyroblast within pelite at Ollaberry, displaying σ -type geometry consistent with sinistral shear. The margins and tails have been retrograded to chlorite (ch). Field of view 3.6 x 2.4mm, crossed polars.

The compositional banding and textures described in this section are typical of high-grade metamorphic rocks. The gneisses comprise a stable assemblage of plagioclase, K-feldspar, hornblende, quartz, epidote and micas indicating metamorphism under amphibolite-facies conditions.

4:1:2 Queyfirth Group

Much of the Queyfirth Group comprises interbanded psammites and pelites on a centimetre- to metre-scale (e.g., Ollaberry, section 3:1:1). Calcareous units are present locally (e.g., The Ness of Haggrister, section 3:1:2).

Psammites comprise 70% quartz, 15% K-feldspar, 10% plagioclase An_{15} and 5% muscovite (Plate 4.2A). They contain inequigranular-polygonal aggregates of quartz grains (0.1 to 0.4mm in size) which surround isolated pockets of feldspar and aligned muscovite grains. The psammites contain a layering defined by aligned mica grains. Quartz and feldspar grains both display sweeping undulose extinction. Protolith psammites within the WBFZ are commonly cut by a series of sub millimetre-scale calcite veins.

Pelite units consist of 50% quartz, 20% chlorite and 20% muscovite together with minor amounts of garnet and magnetite (Plate 4.2B). They also contain quartz ribbons which are interlayered on a sub millimetre-scale with bands of aligned chlorite and muscovite grains (0.1 to 0.3mm in size), both of which define a schistosity (Plate 4.2B). The quartz ribbons comprise aggregates of relatively strain-free, equigranular-polygonal, quartz grains (~0.1mm in size). Locally, well-developed garnet porphyroblasts (1mm to 1cm in size) which contain trails of quartz and magnetite are present (Plate 4.2C), suggesting that the rocks have been metamorphosed to at least garnet grade. The porphyroblasts commonly form σ -type geometries, which are consistent with sinistral shear during the garnet-grade metamorphism. The margins and tails of the garnet porphyroblasts have been strongly retrograded to chlorite (Plate 4.2C), suggesting a lower greenschist-facies overprint.

4:1:3 Devonian sandstones

Sandstones exposed at the Ness of Bixter (section 3:1:6) comprise 75% quartz, 10% plagioclase and ~15% calcite, chlorite and unidentified clay minerals together with minor amounts of magnetite and muscovite (Plate 4.3A&B). The rock is well sorted, clast supported and consists mainly of randomly orientated, sub-angular to angular, equigranular quartz grains (~0.2mm in size) (Plate 4.3A&B). The quartz grains are rimmed by ultrafine-grained clay material and the pore spaces are filled with diagenetic chlorite and calcite. The presence of chlorite indicates that the sandstones were sufficiently buried and weakly metamorphosed under low-grade conditions.

4:1:4 Plutonic rocks

4:1:4:1 Sullom and the Ness of Haggrister

Granodiorite is exposed to the east of the WBF at Sullom and the Ness of Haggrister (section 3:1:2) belonging to the Devonian Graven Complex (section 2:1:5:1a). The granite is medium grained and comprises 65% feldspar (80% albite and 20% K-feldspar), 20% quartz, 10% hornblende and 5% chlorite. Euhedral feldspar phenocrysts (1 to 4mm in diameter), hornblende phenocrysts (1 to 4mm in diameter) and interstitial, inequigranular-polygonal aggregates of quartz (1 to 4mm in diameter) form a holocrystalline texture (Plate 4.4A). Feldspars are partially sericitised while hornblende is partially replaced by chlorite fibres. Polygonal quartz grains commonly display sweeping undulose extinction. Locally, the granite contains a weak magmatic fabric defined by the alignment of feldspar phenocrysts. The texture and composition of the rock described in this section are consistent with an intrusive igneous rock of granodioritic composition.

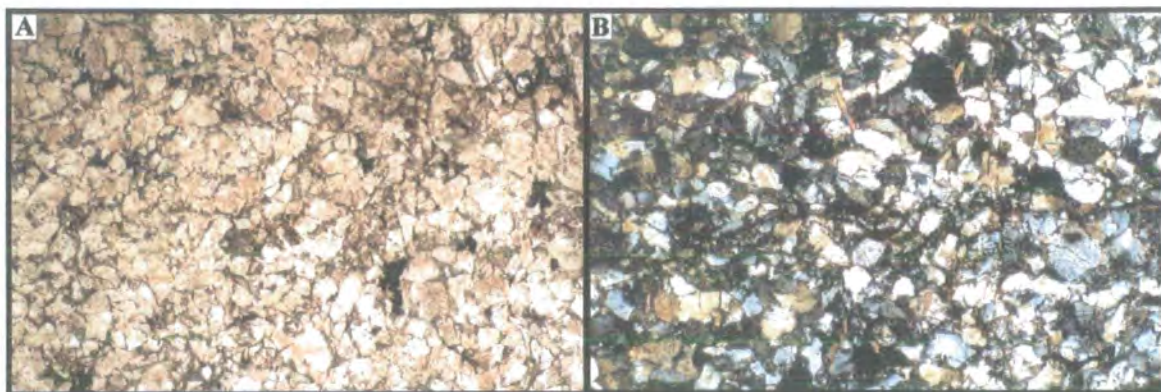


Plate 4.3 (A) & (B) Devonian sandstones from the Ness of Bixter (section 3:1:6). The sandstones are well sorted and are mainly composed of randomly orientated sub-angular to angular quartz (75%) grains together with 10% plagioclase clasts and ~15% calcite, chlorite and clay minerals that fill the pore spaces between grains. (A) Plane-polarised light, (B) crossed polars. Field of view for (A) & (B) is 3.6 x 2.4mm.

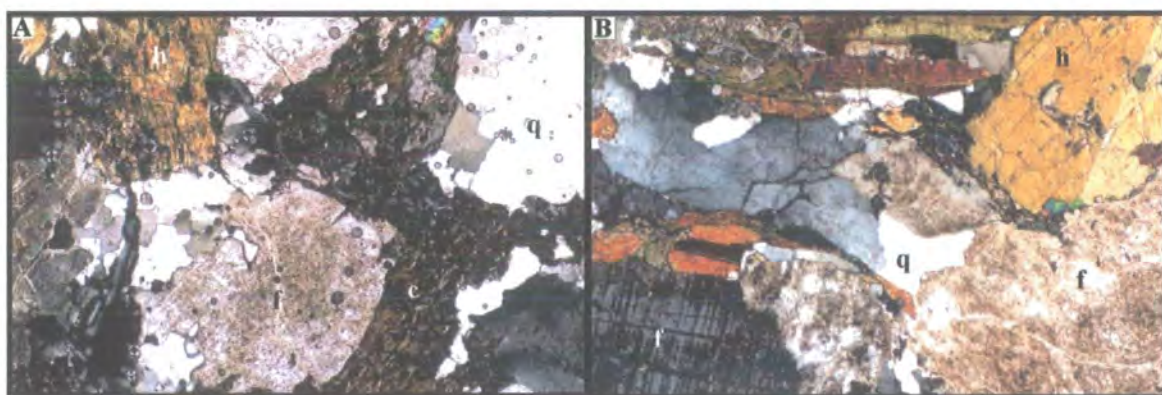


Plate 4.4 (A) Medium-grained granodiorite from east of the WBF at the Ness of Haggrister (section 3:1:2), comprising feldspar (f) and hornblende (h) phenocrysts together with interstitial quartz, forming a holocrystalline texture. Hornblende phenocrysts are commonly replaced by chlorite fibres (c). Field of view 3.6 x 2.4mm, crossed polars. (B) Granodiorite from east of the WBFZ at Brae Isthmus (section 3:1:3), comprising a holocrystalline texture of euhedral feldspar (f) and hornblende (h) phenocrysts together with interstitial quartz (q). Field of view 3.6 x 2.4mm, crossed polars.

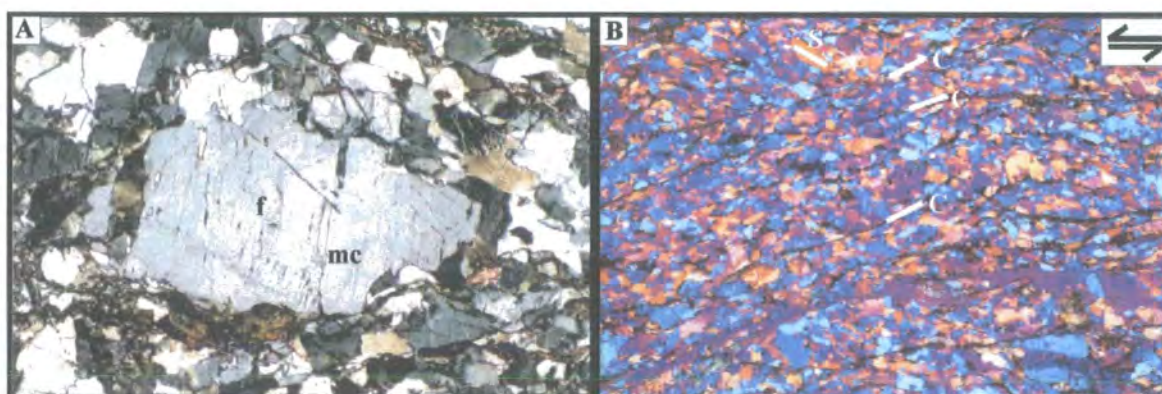


Plate 4.5 (A) Photomicrograph to show relict core and mantle structure within blastomylonite from Seli Voe to Sand (section 3:1:7). The feldspar porphyroblast (f), which contains healed microcracks (mc), is wrapped by strain-free equigranular-feldspar grains. Field of view 3.6 x 2.4mm, crossed polars. (B) Fine-grained blastomylonite with feldspar and quartz grains which show no preferred orientation. Relict S-C' fabrics are preserved with S-planes (s) defined by elongate quartz grains and C-planes (c) defined by fine-grained white mica. Field of view 3.6 x 2.4mm, crossed polars with sensitive tint plate.

4:1:4:2 Brae Isthmus

Granodiorite belonging to the Devonian Brae Complex (section 2:1:5:1b) is exposed to the west of the WBF at Brae Isthmus (section 3:1:3). The granodiorite is composed of approximately 60% feldspar (90% albite, 10% K-feldspar), 20% hornblende, 15% quartz and 5% chlorite. Euhedral feldspar (~4mm in diameter) and hornblende (1mm to 4mm in diameter) phenocrysts together with, interstitial inequigranular-polygonal, quartz aggregates (0.5 to 2mm in diameter) form a holocrystalline texture (Plate 4.4B). Locally, granodiorite contains a weak magmatic fabric defined by the alignment of hornblende and feldspar phenocrysts. Feldspar grains are partially sericitised, whilst hornblende grains are partially replaced by chlorite fibres. Feldspar grains display sweeping undulose extinction and are cut by intergranular fractures filled with quartz and calcite. Quartz grains display sweeping undulose extinction and deformation lamellae. The textures and relative abundance of minerals in the rocks described in this section are consistent with an intrusive igneous rock of a granodioritic composition.

<h4>4:2 Primary fault-rock assemblages</h4>
--

The earliest recognised fault-related deformation (sinistral strike-slip) along the WBFZ is preserved in two deeply-exhumed, fault-bounded blocks. These blocks are part of two, distinct, kilometre-scale, 'positive' flower structures, exposed at (a) Seli Voe to Sand (section 3:1:7) and (b) Sullom, Lunnister and the Ness of Haggrister (section 3:1:2), that were probably exhumed during later dextral strike-slip movement along the WBFZ.

4:2:1 Mylonitic rocks

4:2:1:1 Sand to Seli Voe blastomylonites

A sequence of deeply-exhumed quartzo-feldspathic blastomylonites (section 3:1:7) is exposed within the hangingwall of the Aith Voe Fault. These represent the only blastomylonites found within the extensive exposures of the WBFZ on Shetland. The protolith to these fault rocks is unknown.

Quartzo-feldspathic blastomylonites comprise feldspar (mainly K-feldspar) porphyroclasts up to 1cm in size, which are wrapped by interlayered aggregates of polygonal feldspar and quartz grains (Plate 4.5A).

The feldspar porphyroclasts display relict core and mantle structures (Plate 4.5A), where the porphyroclasts are wrapped by strain-free, equigranular feldspar grains which display no crystallographic preferred orientation and commonly form tails and continuous bands parallel to the macroscopic foliation. The equant-polygonal feldspar grains (typically 0.3 to 0.5mm in diameter) display curved to straight contacts and 120° triple junctions. The feldspar porphyroclasts display sweeping undulose extinction and commonly contain arrays of healed microcracks. Quartz ribbons interbanded with layers of feldspar also display equant-polygonal strain-free quartz grains (0.3 to 0.5mm in diameter).

Within finer-grained blastomylonites, thought to be originally ultramylonites, layers of white mica grains (<0.1mm in size) occur between the quartz and feldspar layers. The white mica grains appear to define a relict S-C' fabric consistent with sinistral shear (Plate 4.5B). Polygonal quartz and feldspar grains (~0.1mm in diameter) are elongate with the long axes parallel to the macroscopic foliation. Feldspar porphyroclasts appear to be absent within the finer-grained mylonites. In places, isolated quartz ribbons (~0.5mm thick) comprise coarser-grained, polygonal, strain-free quartz grains (0.5 to 1mm in diameter) than in the surrounding matrix. This may

be due to higher dislocation densities within isolated quartz ribbons than the surrounding matrix, which have enabled more pronounced grain growth during static recrystallisation (Passchier and Trouw 1996). Another explanation is that the distribution and size of micas and other mineral phases strongly controlled the grain size and shape of the quartz due to grain-boundary pinning (see Holdsworth and Grant 1990 for a more detailed explanation).

4:2:1:1a Metamorphic conditions and operative deformation mechanisms

Due to the quartzo-feldspathic nature of the rocks, and the absence of other mineral phases indicative of metamorphic grade, it is almost impossible to assign a metamorphic facies to the blastomylonite. Many of the deformation microstructures within the mylonite matrix have been destroyed due to post-tectonic recrystallisation processes. These processes include recovery, recrystallisation and grain-boundary area reduction (GBAR), and are collectively known as static recrystallisation (Passchier and Trouw 1996). Static recrystallisation occurs at relatively 'high' temperatures (>400 to 500°C), whereby dislocation tangles are removed, grain boundaries become straight and grains tend to grow in size due to GBAR processes.

4:2:1:2 Lunnister mylonites

Interbanded quartzo-feldspathic and hornblende-rich mylonites that are interpreted to be derived from banded felsic and mafic gneisses (see section 4:1:1) are well exposed at Lunnister (section 3:1:2). These represent the most extensive and best-preserved mylonites exposed within the WBFZ on Shetland.

4:2:1:2a Felsic mylonites

Felsic mylonites correspond to domains of quartzo-feldspathic mylonites and ultramylonites described in the field (section 3:1:2). Domains of mylonite comprise 'rigid' feldspar porphyroclasts, which are wrapped by a network of polycrystalline quartz ribbons and bands of ultrafine-grained feldspar, sericite and biotite (Plate

4.6A&B). When viewed under a sensitive tint plate, aggregates of fine-grained quartz and feldspar display strong crystallographic preferred orientations (Plate 4.6B).

Polycrystalline quartz ribbons with aspect ratios of between 20:1 and 100:1 display a variety of microstructures. The quartz ribbons comprise flattened quartz grains (~ 1 to $10\mu\text{m}$ in size) which display interlobate grain boundaries (Plate 4.6C). The quartz grains show aspect ratios between 3:1 and 10:1 and are dominantly equigranular. The long axes of the lobate grains are orientated either parallel to, or up to 50° (in more highly-strained quartz ribbons, e.g., Plate 4.6D) in a clockwise direction to the trace of the macroscopic foliation, which is consistent with sinistral shear. Larger quartz grains (10 to $20\mu\text{m}$ in size), which are mantled by equigranular-interlobate quartz grains (~ 1 to $10\mu\text{m}$ in size), giving rise to core and mantle structures, display a strong sweeping undulose extinction, deformation lamellae and well-developed subgrains. Subgrain boundaries generally pass laterally into lobate grain boundaries. The grain size of the subgrains ($\sim 1\mu\text{m}$) is similar to the adjacent lobate quartz grains, indicating subgrain rotation as a mechanism of recrystallisation.

Feldspar (albite and K-feldspar) porphyroclasts display Φ - (e.g., Plate 4.6G), δ - and σ -type (e.g., Plate 4.6A) geometries consistent with sinistral shear. The porphyroclasts are sub-rounded to well rounded, 5mm to less than 0.5mm in size and display aspect ratios of less than 5:1. Locally, feldspar clasts display δ - and σ -type geometries consistent with dextral shear (Plate 4.6B), possibly due to local variations in strain rate within the mylonites (the relative proportion of sinistral to dextral examples is 70%: 30%). The feldspar clasts commonly display a speckled appearance due to the partial breakdown to ultrafine-grained aggregates of sericite. The largest feldspar clasts (typically $>1\text{mm}$) are commonly cut by arrays of shear and tensile intergranular fractures, which are typically filled by aggregates of ultrafine-grained feldspar. Many of the shear fractures are antithetic fractures, which offset feldspar clasts dextrally, but clearly indicate an overall sinistral sense of shear (e.g., Plate 4.6E). Locally, fragments of cataclastically deformed feldspar lie in trails, parallel to the macroscopic foliation (Plate 4.6F), which are surrounded by ultrafine-grained feldspar and polycrystalline quartz ribbons. The cataclastically deformed feldspar trails are commonly cut by a series of R-type Riedel shears indicating an overall sinistral sense of shear (Plate 4.6F).

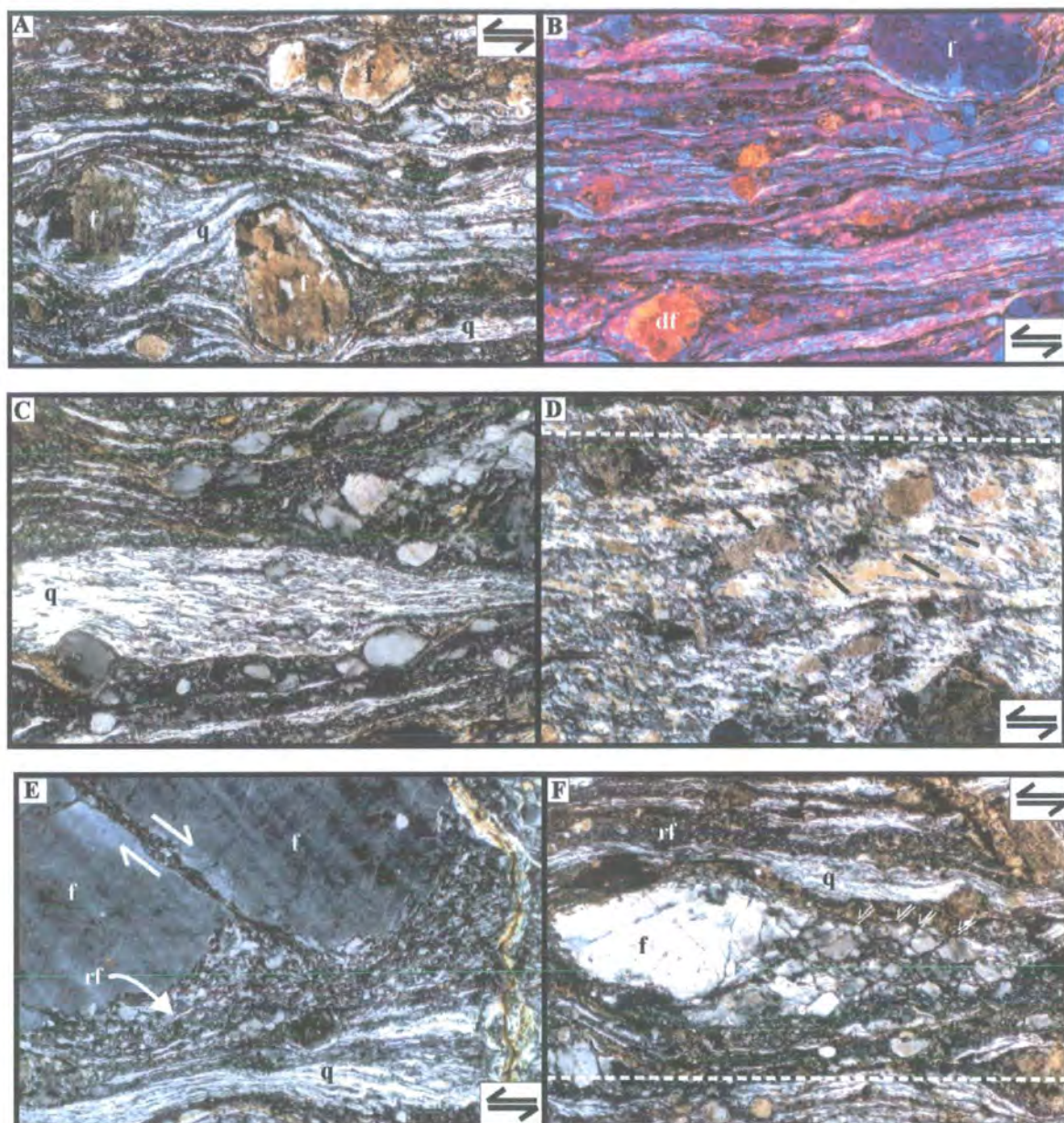


Plate 4.6 (A) Quartzo-feldspathic mylonite comprising relatively undeformed but altered asymmetric feldspar (f) porphyroclasts (σ -type), which are surrounded by polycrystalline quartz ribbons (q) interlayered with fine-grained feldspar, sericite and biotite. Field of view 3.6 x 2.4mm, crossed polars. (B) Quartzo-feldspathic mylonite viewed under a sensitive tint plate to show strong preferred crystallographic orientations of fine-grained quartz and feldspar aggregates. f=feldspar porphyroclasts, df=dextral porphyroclast. Field of view 3.6 x 2.4mm. (C) Close-up of polycrystalline quartz ribbons (q), which comprises aggregates of elongate quartz grains that display interlobate grain boundaries. Field of view 1.44 x 0.96mm, crossed polars. (D) Close-up of highly-strained quartz ribbons. The long axes of the lobate quartz grains (black lines) are orientated up to 50 degrees in a clockwise direction from the macroscopic foliation (dashed line), which is consistent with sinistral shear. Field of view 1.44 x 0.96mm, crossed polars. (E) Feldspar porphyroclast (f) cut by an antithetic intergranular fracture filled with ultrafine-grained feldspar. The fracture displays an apparent dextral shear indicating an overall sinistral sense of shear. The feldspar porphyroclast is also mantled by fine-grained, dynamically recrystallised feldspar grains (rf). Field of view 1.44 x 0.96mm, crossed polars. (F) Cataclastically deformed feldspar grain (f) surrounded by quartz ribbons (q) and fine-grained, dynamically recrystallised feldspar (rf). Angular fragments derived from the feldspar grain (f) are drawn out parallel with the macroscopic foliation (dashed line) and are cut by a series of sinistral, R-type, Riedel shears (white lines & split arrow). Field of view 3.6 x 2.4mm, crossed polars.

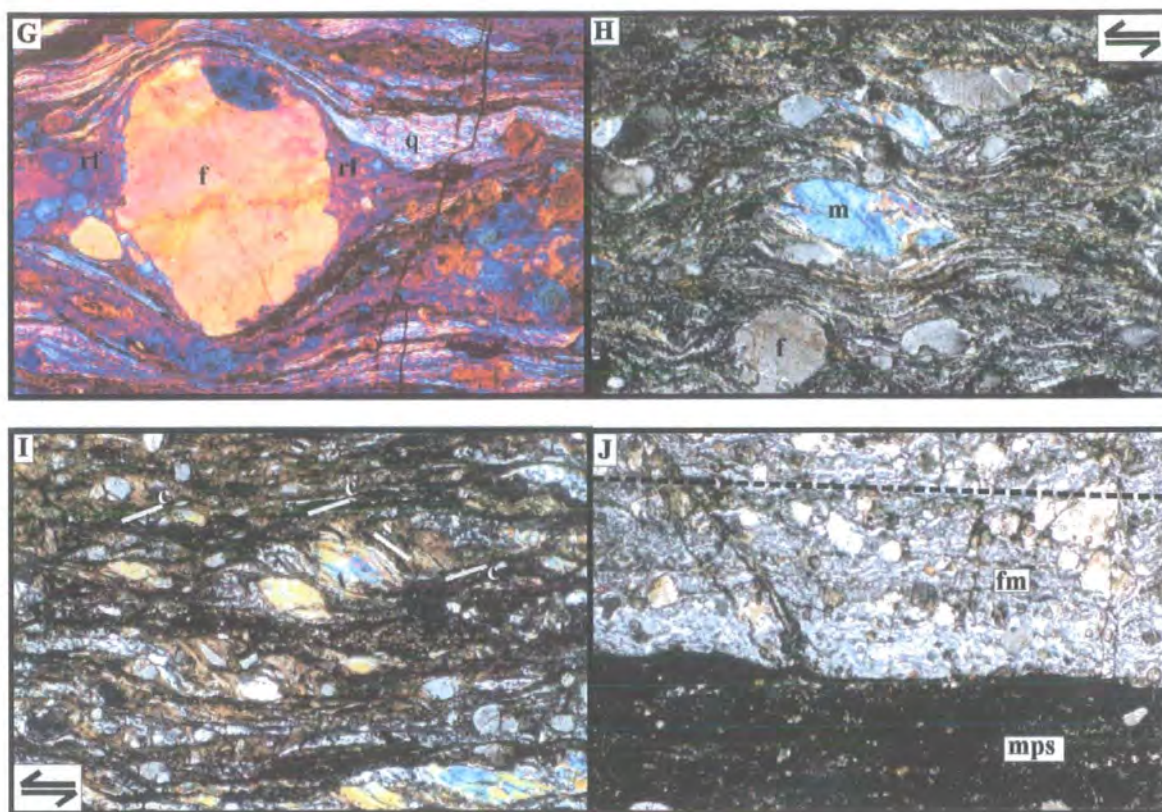


Plate 4.6 continued. (G) Feldspar porphyroblast (f) displaying ϕ -type geometry is mantled by ultrafine, equigranular-interlobate, feldspar grains, which are drawn out to form continuous tails or beards (rf) and display a strong preferred crystallographic orientation. Quartz ribbons (q) also display a strong preferred crystallographic orientation. Field of view 3.6 x 2.4mm, sensitive tint plate. (H) Ultramylonite with newly-formed muscovite grain (m), which displays mica-fish geometry consistent with sinistral shear. Field of view 3.6 x 2.4mm, crossed polars. (I) Well-developed S-C' fabric consistent with sinistral shear. c=c-planes and s=s-planes. Field of view 3.6 x 2.4mm, crossed polars. (J) Image to show mylonitised pseudotachylite vein (mps) within felsic mylonite (fm) developed parallel to the macroscopic foliation (dashed line). Field of view 3.6 x 2.4mm, crossed polars.

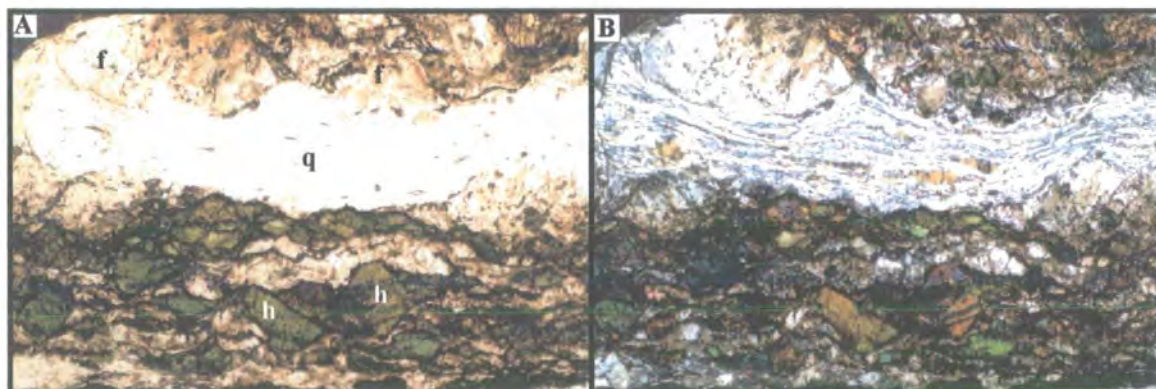


Plate 4.7 (A) & (B) Mafic protomylonites comprising 'rigid' hornblende (h) and feldspar (f) porphyroclasts which are wrapped by polycrystalline quartz ribbons (q) and layers of fine-grained feldspar, sericite, chlorite and biotite. Field of view for (A) & (B) 3.6 x 2.4mm. (A) Plane-polarised light & (B) crossed polars.

Feldspar clasts less than 1mm in size are rarely cut by intergranular fractures. The feldspar clasts display strong patchy extinction interpreted to be due to sub-microscopic cataclasis. Both albite and K-feldspar porphyroclasts are mantled by aggregates of ultrafine, equigranular-interlobate feldspar grains (individual grains ~0.005mm in size), which display a strong preferred orientation (Plate 4.6G). The mantles appear to be drawn out to form laterally continuous tails and bands, which are orientated parallel to the macroscopic foliation. In places, the mantles contain larger (~0.1 to 0.5mm in size) fragments of cataclastically deformed feldspar, which have broken away from the host clast.

Packages of ultramylonite (millimetre- to metre-thick) grade or show transitions from mylonite due to variations in strain rate and/ or protolith composition and grain size. Ultramylonites are finer grained and contain fewer and smaller porphyroclasts than the adjacent mylonites. They commonly contain white mica grains (5 μ m in size), which display mica-fish geometries consistent with sinistral shear (Plate 4.6H). Locally, the mylonites display well-developed, sub-millimetre-scale, S-C fabrics consistent with sinistral shear (Plate 4.6I). C-planes appear to be defined by ultrafine-grained aggregates of biotite, sericite and chlorite.

Within the felsic mylonites, dark-coloured, opaque bands of ultrafine-grained ultramylonite with very sharp and straight boundaries are developed parallel to the macroscopic mylonite foliation (Plate 4.6J). The dark mylonites contain rounded clasts of quartz but do not contain any feldspar clasts. In places, injection structures nucleate from the dark material and cut into the mylonite host rock. These dark-coloured mylonites are thought to be derived from foliation-parallel pseudotachylite veins formed during localised high strain rate events during mylonitisation (cf. Sibson 1980 and White et al. 1980). The pseudotachylite veins are strongly overprinted by mylonitic deformation. Many of these veins are now ultrafine-grained ultramylonites, and as a result do not preserve many pseudotachylite textures.

4:2:1:2b Mafic protomylonites

Mafic protomylonites correspond to the domains of hornblende-rich mylonites described from field localities (section 3:1:2) and are interpreted to be derived from

mafic gneiss. Domains of protomylonite comprise 'rigid' hornblende and feldspar porphyroclasts, which are locally wrapped by a network of polycrystalline quartz ribbons, bands of ultrafine-grained feldspar, sericite, chlorite and biotite (Plate 4.7A&B). When viewed under a sensitive tint plate, aggregates of fine-grained quartz and feldspar display strong crystallographic preferred orientations. The quartz ribbons (<0.1mm wide) display similar microstructures to those observed in domains of felsic mylonite (section 4:2:1:2a).

Sub-rounded feldspar porphyroclasts (K-feldspar and albite, 5mm to ~1mm in size) display strong, patchy, undulose extinction and are cross-cut by arrays of intergranular fractures which are commonly filled with ultrafine-grained feldspar. Mantles of ultrafine, equigranular-interlobate, feldspar grains (typically 0.005mm in size) are locally developed and are drawn out into tails and bands parallel to the macroscopic foliation.

Sub-angular hornblende porphyroclasts are characterised by strong, patchy, undulose extinction and twinning and are commonly cut by intergranular fractures. Mantles of fine-grained hornblende are not observed within the mafic mylonites. In places, fine-grained opaque material mantles the hornblende porphyroclasts and is drawn out into tails and bands parallel to the macroscopic foliation. Locally, the margins of hornblende porphyroclasts are replaced by retrograde biotite, actinolite and less commonly chlorite. Epidote grains also partially replace hornblende porphyroclasts.

4:2:1:2c Metamorphic conditions during mylonitisation

Felsic mylonites display an apparently stable mineral assemblage of albite, K-feldspar, quartz, sericite and biotite. Mafic mylonites display an apparently stable mineral assemblage of albite, K-feldspar, hornblende, quartz, biotite, actinolite and chlorite. The relative abundances of hydrous mineral phases (sericite, biotite, actinolite, epidote and rare chlorite) in comparison with the relatively unmodified gneisses, suggests that the hydrous minerals developed during localised retrograde metamorphism during mylonitisation. The coexistence of retrograde biotite, actinolite and hornblende and the relative absence of chlorite within mafic mylonites indicates mylonitisation in upper greenschist-facies conditions, which is consistent with the

deformation textures and operative deformation mechanisms summarised in the following section.

4:2:1:2d Operative deformation mechanisms

The observed microstructural similarities between felsic and mafic mylonites suggest that both fault rocks deformed under similar conditions.

Felsic and mafic mylonites comprise 'rigid' feldspar and or hornblende porphyroclasts, which are wrapped by a network of polycrystalline quartz ribbons and bands of ultrafine-grained feldspar, sericite and biotite. The porphyroclasts display relatively low aspect ratios ($<5:1$) and appear to be relatively undeformed internally. In contrast, the polycrystalline quartz ribbons and bands of ultrafine-grained feldspar, sericite and biotite display comparatively high aspect ratios ($<100:1$), appear to be very highly strained and form an interconnected weak-layer (IWL) microstructure (section 1:6:4). These observations suggest that the rheological behaviour of the highly strained mylonitic fault rocks was primarily controlled by the rheological behaviour of the quartz ribbons and ultrafine-grained feldspar (Handy 1990).

Highly-strained quartz ribbons display evidence for advanced dislocation creep and dynamic recrystallisation (e.g., subgrain rotation recrystallisation, section 1:6:2:2). Larger quartz grains (10 to 20 μm in size) display sweeping undulose extinction, deformation lamellae and subgrains, which pass into aggregates of lobate quartz grains (1 to 10 μm in size) that surround the larger quartz grains. Well-developed core and mantle structures suggest that deformation was accommodated by dislocation glide and subgrain rotation recrystallisation at lower strains (White 1976). However, more highly strained quartz ribbons contain lobate quartz grains where their long axes are orientated up to 20° to the macroscopic foliation defining an oblique foliation. This is consistent with the operation of grain boundary migration recrystallisation mechanisms (Passchier and Trouw 1996).

Large feldspar porphyroclasts ($>1\text{mm}$ in size) are cut by many fractures some of which are healed by ultrafine-grained aggregates of feldspar. Locally, fragments of cataclastically deformed feldspar have separated from the host clasts and have been

drawn out into the mylonitic matrix. No fractures were observed to contain fibrous vein infills, suggesting that fracture opening was not associated with localised pressure solution (section 1:6:2:1). As smaller (<1mm in size) porphyroclasts are rarely observed to be fractured, it is suggested that intergranular fracturing was an important mechanism of grain-size reduction within larger porphyroclasts, especially at the onset of mylonitisation. The larger feldspar porphyroclasts also display, strong irregular, undulose extinction due to the effects of sub-microscopic cataclasis.

Tails and mantles of ultrafine-grained, equigranular-interlobate feldspar grains, which display a strong crystallographic preferred orientation, surround the majority of feldspar porphyroclasts. These lobate feldspar grains are consistently finer than the lobate quartz grains described above. The feldspar microstructures indicate a combination of dislocation creep and grain boundary sliding processes (Tullis and Yund 1985).

Hornblende porphyroclasts mainly display strong, patchy, undulose extinction and commonly intergranular fractures. The dominant deformation mechanism within hornblende appears to have been cataclasis.

The quartz grains preserved in felsic and mafic mylonites displays evidence for widespread dynamic recrystallisation. These observations are consistent with deformation of quartz at temperatures of between 400°C and 700°C (see section 1:6:3; Passchier and Trouw 1996). The microstructures associated with feldspars suggest that deformation took place between 400°C and 500°C. Therefore, mylonitisation is postulated to have occurred at upper greenschist facies or temperatures of between 400°C and 500°C and depths of 13-16km (assuming an average geothermal gradient of 30°C/km). However, the geothermal gradient may have been elevated and therefore mylonitisation could have taken place at shallower depths, given the presence of late-Caledonian granitic intrusions along the trace of the WBFZ in Shetland (section 2:1:5). Granites to the west of the WBFZ are post-mylonitisation (see section 3:1:8), but the exact age relationships between intrusions east of the WBFZ, which are older than those to the west (section 2:1:5), and mylonitisation are unclear.

4:2:2 Cataclastic rocks

The cataclastic rocks described in this section are kinematically similar and were both formed during sinistral shear. Lunnister cataclasites are associated with the mylonites described in section 4:2:1:2, while the foliated cataclasites at Brae are derived from granodiorite (section 4:1:4:2).

4:2:2:1 Lunnister cataclasites

The Lunnister cataclasites ('early' cataclasites; section 3:1:2:2b) are associated with and derived from the mylonitic series rocks described in section 4:2:1:2. Cataclasites develop parallel to and cross-cut the mylonitic foliation and range in thickness from 0.5mm (Plate 4.8A) to up to 1m. Foliation-parallel cataclasites are bounded by sharp fracture or fault surfaces. In thin-section, injection veins nucleate from the sharp surfaces and cross-cut both the cataclasite and the adjacent mylonite (Plate 4.8B). The injection veins are composed of a brown-coloured isotropic material with an aphanitic or 'glassy' texture that sometimes appears to have been altered to a clay-rich isotropic paste. The veins are interpreted to be devitrified pseudotachylites. The cataclasites comprise finely comminuted fragments of feldspar, quartz, hornblende, mica and mylonite set within a fine-grained cataclastic matrix (Plate 4.8C&D). The fragments are randomly orientated, angular to sub-angular and range from 1cm to ~10µm in size. Both quartz and feldspar clasts are cut by extensive arrays of intergranular fractures. Feldspar clasts display strong, patchy, undulose extinction due to sub-microscopic cataclasis. Quartz clasts display sweeping undulose extinction and deformation lamellae. No fractures were observed to contain fibrous vein infills, suggesting that fracture opening was not associated with localised high pore-fluid pressures. A later phase of randomly orientated, sub-millimetre-thick, scapolite veins cross-cut both the mylonites and the cataclasites. Mykura and Phemister (1976) postulated that this veining was possibly related to intrusion of plutonic rocks belonging to the Graven Complex.

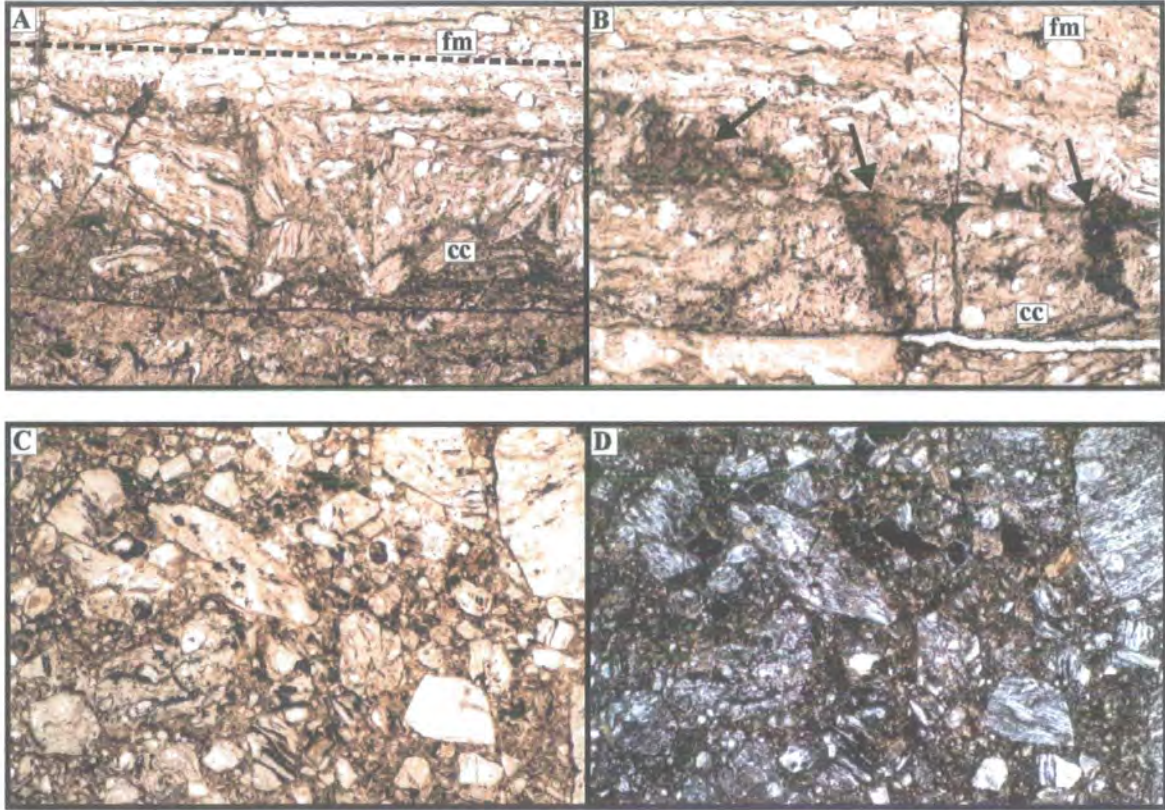


Plate 4.8 Cataclasites derived from mylonite at Lunnister (section 3:1:2). (A) Millimetre-thick cataclasite (cc) developed parallel to the mylonite foliation (dashed line) within felsic mylonite (fm). Field of view 3.6 x 2.5mm, plane-polarised light. (B) Foliation-parallel, millimetre-thick cataclasite (cc) bounded by sharp fracture surface. Pseudotachylite injection veins (arrowed) nucleate from the planar fracture surface into both the wall-rock felsic mylonite (fm) and the cataclasite (cc). Field of view 3.6 x 2.4mm, plane-polarised light. (C) & (D) Cataclasite comprising randomly orientated fragments of mylonite, feldspar and quartz set within a fine-grained cataclastic matrix of the same. Field of view for (C) & (D) 3.6 x 2.4mm. (C) Plane-polarised light and (D) crossed polars.

4:2:2:1a Operative deformation mechanisms and localisation

The dominant deformation mechanism is cataclastic flow (mechanical disaggregation and grain-size diminution) in and between grains and grain boundary sliding. Quartz and feldspar deform by cataclasis, indicating temperatures of less than 250°C and 300°C or depths of 8.5 to 10km (see section 1:6:3) (assuming an average geothermal gradient of 30°C/km). The Lunnister cataclasites are interpreted to have localised along the mylonite foliation during progressive exhumation of the fault zone during sinistral shear, which led to a switch from viscous to frictional deformation mechanisms. However, in the absence of direct fault-rock dating, it may be possible that the cataclasites formed during a later phase of sinistral strike-slip movement.

4:2:2:2 Brae Isthmus foliated cataclasites

The foliated cataclasites exposed at Brae Isthmus (section 3:1:3) are derived from granodiorite (section 4:1:4:2) of the Devonian Graven Complex and were formed during sinistral shear. Foliated cataclasites comprise sub-angular to rounded clasts (0.3mm to 0.01mm in size) of quartz, feldspar, epidote and cataclasite set within a brown-coloured, ultrafine-grained optically isotropic matrix (Plate 4.9A&B). The matrix displays an apparent foliation defined by aligned fragments and colour variations. Non-foliated cataclasites adjacent to wall rock appear to grade laterally into cataclasite with a foliated matrix. The foliated matrix displays an anastomosing geometry, which surrounds foliation-parallel lenses of cataclasite (Plate 4.9A&B). Cataclasite lenses with aspect ratios of up to 10:1 are drawn out and in places boudinaged parallel to the macroscopic foliation. The feldspars within the cataclasites are highly altered to aggregates of sericite and are commonly cut by intergranular fractures (Plate 4.9C). Quartz clasts display strong undulose extinction and deformation lamellae and are commonly cut by intergranular fractures. Hornblende clasts are almost completely replaced by aggregates of retrograde chlorite. The foliated cataclasites are cut by a series of sub-millimetre-scale shear bands consistent with sinistral shear (Plate 4.9A&B). The wall-rock granodiorite adjacent to the foliated cataclasites is commonly cut by extensive arrays of calcite-filled tension fractures (Plate 4.9D).

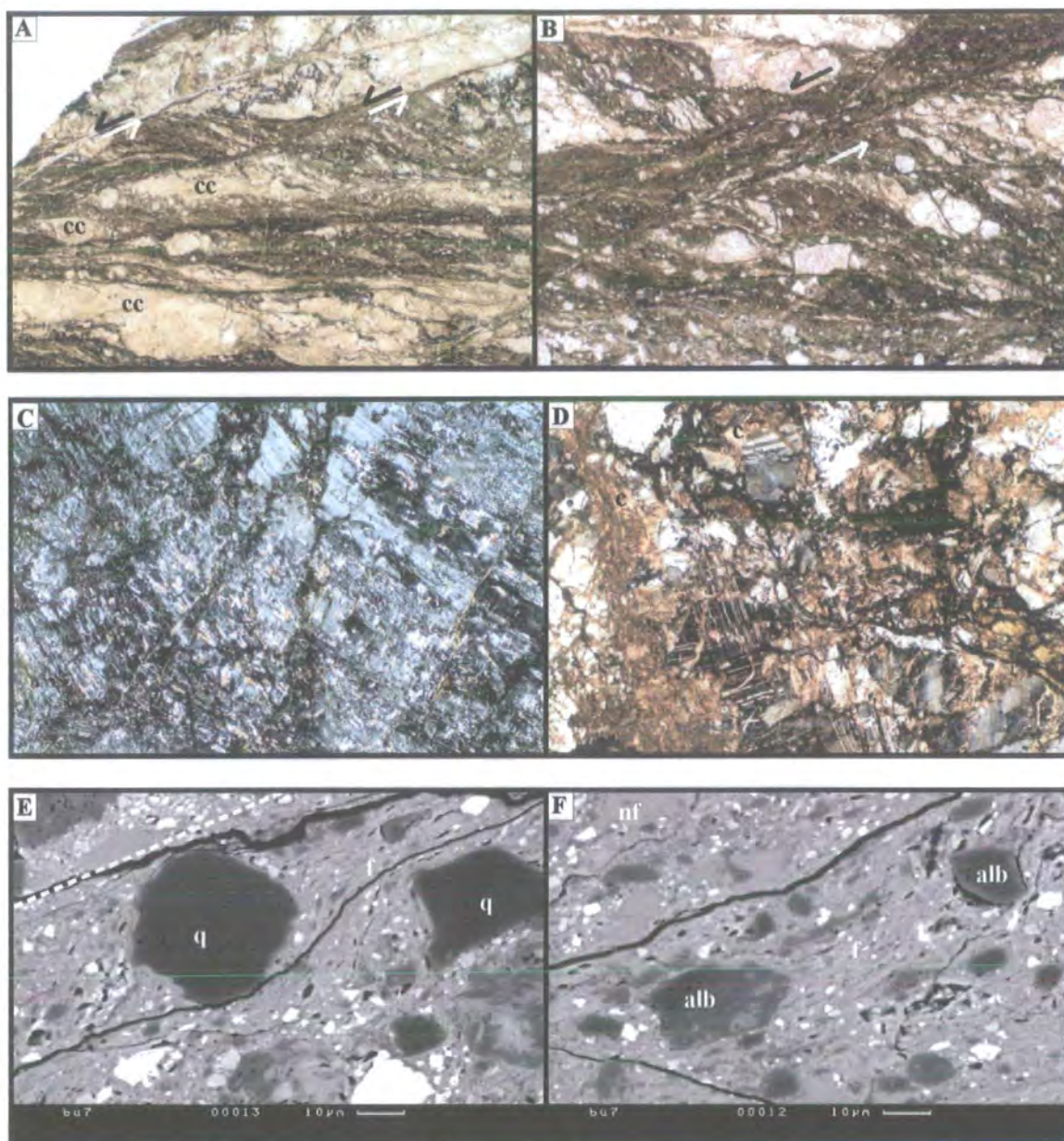


Plate 4.9 Foliated cataclasites from Brae Isthmus (section 3:1:3). (A) Large-scale image of foliated cataclasite comprising elongate slivers of cataclasite (cc) surrounded by a network of ultrafine-grained, brown-coloured cataclasite which displays an apparent foliation defined by colour variations and aligned clasts. The foliated cataclasite is cut by a series of shear bands consistent with sinistral shear (split arrows). Field of view 14.4 x 9.6mm, plane-polarised light. (B) Foliated cataclasite containing aligned fragments of cataclasite, feldspar and quartz set within a brown-coloured, foliated matrix containing sinistral shear bands (split arrows). Field of view 3.6 x 2.4mm, plane-polarised light. (C) Close-up of highly sericitised, cataclastically deformed, plagioclase fragment within foliated matrix. Field of view 1.44 x 0.96mm, crossed polars. (D) Wall-rock granodiorite cut by extensive calcite veining (c). Field of view 3.6 x 2.4mm, crossed polars. (E) Backscatter SEM image of rounded quartz clasts surrounded by matrix of aligned chlorite and sericite fibres (f), which form strain shadows parallel to the macroscopic foliation (dashed line). (F) Backscatter SEM image to show non-foliated cataclasite (top left; nf) grading into foliated cataclasite comprising albite fragments (alb) which are surrounded by intergrown sericite and chlorite fibres (f).

Backscatter SEM studies of the matrix show a gradation from non-foliated cataclasites to foliated cataclasites. Non-foliated cataclasites comprise randomly orientated sub-angular to sub-rounded fragments of K-feldspar, albite, quartz, actinolite, hornblende, epidote, sericite and chlorite, which show a gradation from 30 to 1µm in diameter. Foliated cataclasites comprise a matrix of aligned sericite and chlorite fibres (1 to 5µm in length), which surround sub-rounded to well-rounded clasts of quartz and less commonly albite (Plate 4.9E&F). The intergrown sericite and chlorite fibres commonly mantle clasts of quartz and albite to form strain shadows parallel to the macroscopic foliation. Quartz clasts also display quartz overgrowths parallel to the macroscopic foliation.

4:2:2:2a Metamorphic conditions during cataclasis

The foliated cataclasites comprise a stable assemblage of quartz, albite, chlorite, sericite and epidote. The original feldspar and hornblende grains have suffered intense alteration to aggregates of phyllosilicates (sericite and chlorite) and epidote. The retrograde minerals display a strong grain-shape preferred orientation and shear bands consistent with sinistral shear. The phyllosilicates commonly form strain shadows around the margins of quartz and less commonly albite porphyroclasts. These observations suggest that the sinistral strike-slip foliated cataclasites have experienced lower greenschist-facies metamorphism and hydration, synchronous with fault-related deformation. This is consistent with the observed deformation textures and the operative deformation mechanisms summarised in the following section.

4:2:2:2b Operative deformation mechanisms

Foliated cataclasites comprise isolated quartz, feldspar, hornblende and cataclasite slivers, which are wrapped by a network of intergrown sericite and chlorite, that appear to form an IWL microstructure (sections 1:6:3, 1:7:2:3a). These observations are consistent with the overall rheological behaviour of the foliated cataclasites having been controlled by deformation within the network of phyllosilicate grains (Handy 1990).

Sericitised feldspar grains are commonly observed within the lenticular cataclasite slivers. Chlorite grains appear to be derived from the breakdown of hornblende grains. Both sericitisation and chloritisation reactions involve a chemically active fluid phase and silica loss from the parent grains (Beach 1980). This suggests that feldspar and hornblende grains may have acted as diffusive mass transfer (DMT) sources for the development of the network of sericite and chlorite (DMT 'sinks'). Due to the fine grain size of the phyllosilicate grains, in the absence of TEM it is not possible to determine the operative deformation mechanisms, which are postulated to include intracrystalline slip and recrystallisation processes (Imber 1998).

4:3 Secondary fault-rock assemblages

Secondary fault rocks (cataclasites and fault gouges) overprint primary fault-rock assemblages, and were formed during dextral strike-slip reactivation of the WBFZ. Later reactivations along the WBFZ localised into pre-existing fault gouges and are therefore not characterised by the development of specific fault-rock assemblages.

4:3:1 Seli Voe to Sand banded cataclasites

Banded cataclasites (termed 'foliated cataclasites' in section 3:1:7) overprint a series of blastomylonites (section 4:2:1:1) exposed in the hangingwall of the Aith Voe Fault. The cataclasites comprise randomly orientated, sub-rounded to angular clasts (1 cm to 0.1 mm in size) of blastomylonite, feldspar and quartz set within a cataclastic matrix of quartz, feldspar, calcite and muscovite. The cataclasites contain a millimetre-scale banding defined by grain size and clast-to-matrix variations. Locally, blastomylonite fragments display fault-parallel strain shadows of fibrous muscovite (Plate 4.10A&B). It is uncertain whether the muscovite fibres grew during cataclasis or are part of the original blastomylonite texture. Fault-parallel veins (0.1 to 0.5 mm thick) of opaque grains are common. Feldspar grains display kinked twin planes, irregular undulose extinction and arrays of calcite-filled fractures. Quartz grains display sweeping undulose extinction and are commonly cut by intergranular fractures.

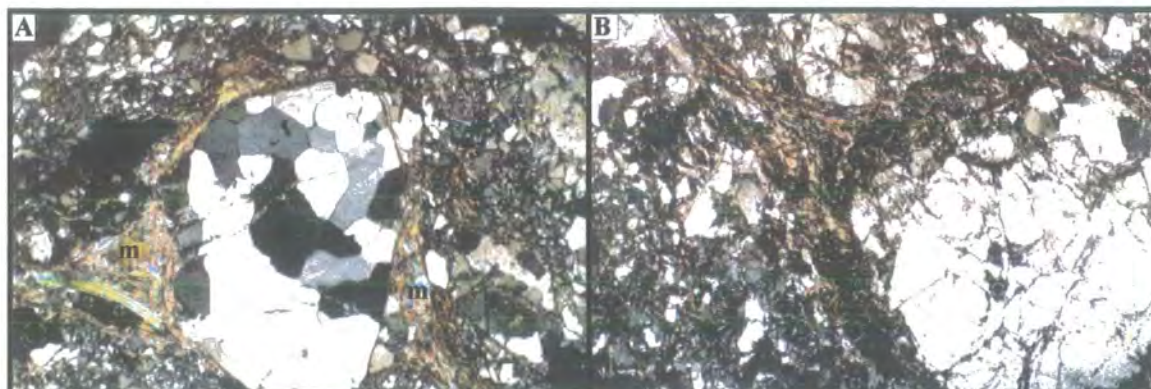


Plate 4.10 Banded cataclasites from Seli Voe to Sand (section 3:1:7). (A) & (B) Cataclasites comprise randomly orientated sub-rounded to angular clasts of blastomylonite, feldspar and quartz set within a fine-grained cataclastic matrix of the same +epidote and micas. In places, rounded blastomylonite and feldspar clasts which are mantled by tails of fine-grained muscovite (m). The cataclasites display an apparent banding defined by variations in the clast-to-matrix ratio. Field of view 3.6 x 2.4mm, crossed polars.

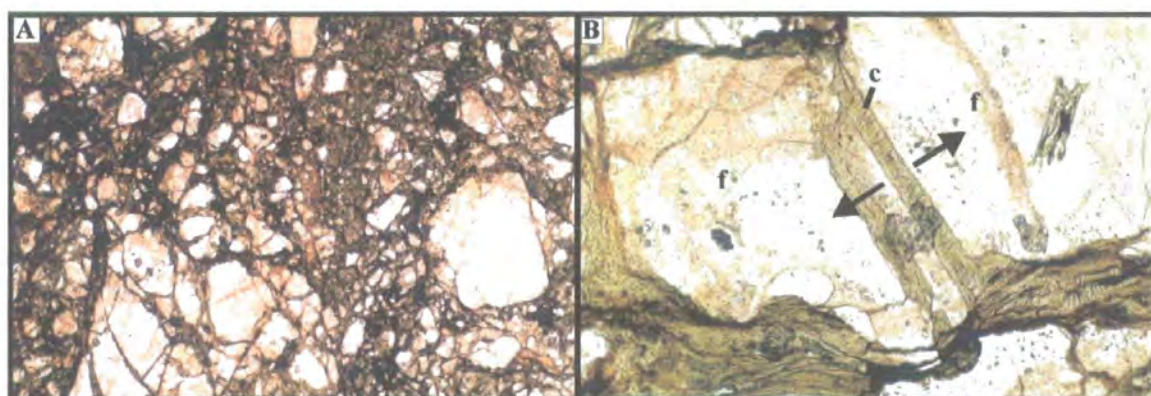


Plate 4.11 Cataclasites located east of the WBFZ at Ollaberry (section 3:1:1). (A) Cataclasite comprising randomly orientated fragments of feldspar and quartz set within a fine-grained matrix of chlorite, sericite, epidote, quartz and feldspar. Field of view 3.6 x 2.4mm, plane-polarised light. (B) Close-up of feldspar grain (f) cut by intergranular fracture filled with chlorite fibres (c) orientated normal to the fracture surface. Arrows indicate opening direction of fracture which is parallel to the chlorite fibres. Field of view 1.44 x 0.96mm, plane-polarised light.

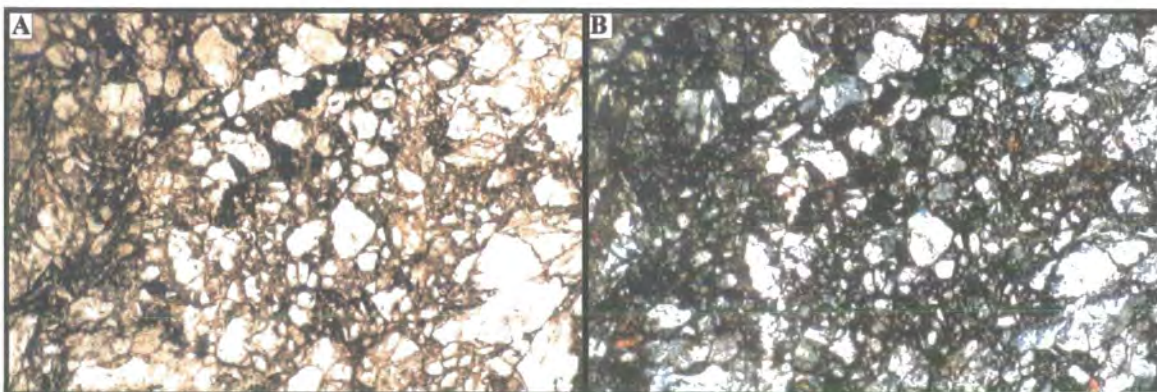


Plate 4.12 Cataclasites derived from granodiorite east of the WBFZ at the Ness of Haggrister (section 3:1:2). (A) & (B) Cataclasite comprising randomly orientated fragments of feldspar and quartz set within a fine-grained cataclastic matrix of chlorite, sericite, epidote, feldspar and quartz together with opaque material. (A) Plane-polarised light, (B) crossed polars. Field of view for (A) & (B) is 3.6 x 2.4mm.

4:3:1:1 Operative deformation mechanisms

The dominant deformation mechanism is cataclastic flow (mechanical disaggregation and grain-size diminution) in and between grains, grain boundary sliding and pressure solution. Feldspar and quartz deform by cataclasis, indicating temperatures of less than 250°C to 300°C (section 1:6:3) or depths shallower than 8.5 to 10km (assuming an average geothermal gradient of 30°C/km).

4:3:2 Ollaberry cataclasites

Cataclastic series rocks east of the WBF at Ollaberry are derived entirely from pegmatitic granite (section 3:1:1:1b) of the Devonian Graven Complex (section 2:1:5:1a). The cataclasites comprise randomly orientated, sub-angular to angular fragments of feldspar and quartz (5mm to less than 0.5mm in size) set within a fine-grained cataclastic matrix of chlorite, sericite, epidote, feldspar and quartz (Plate 4.11A). Partially sericitised feldspar clasts are cut by extensive arrays of intergranular fractures, which are filled with chlorite and green biotite fibres orientated normal to the fracture surfaces (Plate 4.11B). Intergranular fractures are locally filled with an iron oxide mineral. The feldspar clasts also display kinked twin planes, healed microcracks and strong, patchy, undulose extinction due to sub-microscopic cataclasis. Quartz displays strong, patchy, undulose extinction and extensive arrays of intergranular fractures. Millimetre-thick epidote and quartz veins both cross-cut the cataclasites and occur locally as clasts within the cataclasite matrix, suggesting that veining was coeval with cataclasis.

4:3:2:1 Operative deformation mechanisms

The dominant deformation mechanism is cataclastic flow (mechanical disaggregation and grain-size diminution) in and between grains, grain boundary sliding and pressure solution. Feldspar and quartz deform by cataclasis, indicating temperatures of less than 250°C to 300°C or depths of less than 8.5 to 10km (assuming an average geothermal gradient of 30°C/km). Elevated pore-fluid pressures are inferred, which

led to hydro-fracturing of feldspar grains and the precipitation of chlorite and green biotite fibres parallel to the opening direction of the fractures. The precipitation of chlorite and green biotite is consistent with cataclasis at temperatures between 250 and 300°C (Yardley 1994). Sericitised feldspar grains are commonly observed within the cataclasites. Sericitisation reactions involve a chemically active fluid phase and silica loss from the parent grains (Beach 1980). The cataclastic matrix is rich in hydrous minerals such as sericite, chlorite and epidote, which suggests fluid-assisted cataclasis. In other words, dilatancy due to cataclasis has promoted the influx of fluids, which has led to the breakdown of feldspar to sericite and the precipitation of new minerals (eg., epidote, chlorite and biotite) from solution.

4:3:3 Sullom, Lunnister and Ness of Haggrister cataclasites

Cataclasites derived from granodiorite (section 4:1:4:1) of the Devonian Graven Complex exposed to the east of the WBF are texturally and microstructurally identical to those exposed at Ollaberry (section 4:3:2), as shown in Plate 4.12, and are not described here.

To the west of the WBF, cataclasites developed during dextral shear (termed 'later' cataclasites in section 3:1:2), commonly cross-cut and are derived from primary fault-rock assemblages formed during sinistral shear (mylonites & cataclasites). The cataclasites comprise randomly orientated, sub-angular to sub-rounded clasts (0.5 to 0.01mm) of feldspar, quartz, mylonite, cataclasite and gneiss set within a fine-grained cataclastic matrix that has been altered to a clay-rich isotropic paste (Plate 4.13A&B). The cataclasites display a fault-parallel, sub-millimetre-scale, colour banding due to variations in the clast-to-matrix ratio. Within the finer-grained clay-rich layers, an apparent foliation is present, probably due to the alignment of clay particles. Fault-parallel hematite veins, 0.01 to 0.1mm thick, form braided networks within the finer-grained cataclasites (Plate 4.13B). Feldspar and quartz clasts display strong patchy undulose extinction and are cut by extensive arrays of intergranular fractures. In places, the cataclasites contain fragments (0.1 to 0.5mm in size) of scapolite veins (Plate 4.13A), which are thought to be the same generation of veins as those which cross-cut earlier formed mylonites and cataclasites (sections 4:2:1:2 & 4:2:2:1; primary fault rocks).

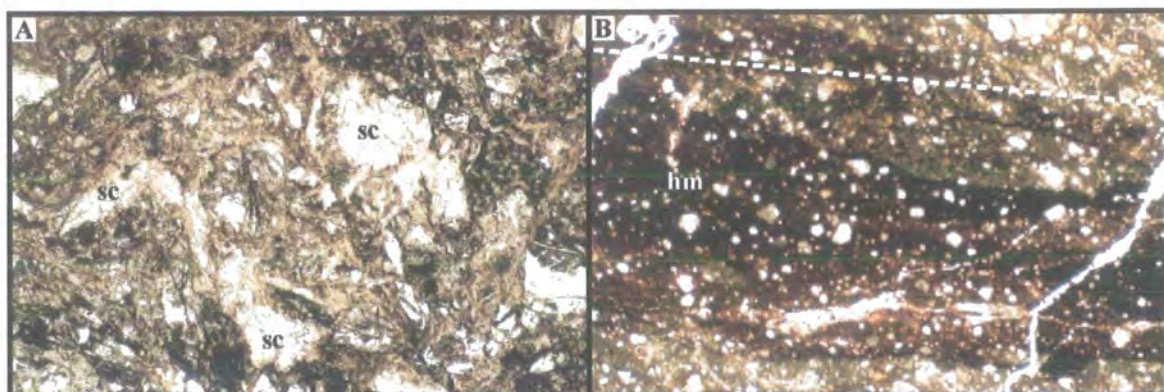


Plate 4.13 Cataclasites ('later' cataclasites, section 3:1:2) from Sullom, Lunnister and north of the Ness of Haggister derived from primary fault-rock assemblages (A) Cataclasite comprising randomly orientated fragments of mylonite, cataclasite, feldspar, quartz and scapolite veins (sc) set within a cataclastic matrix that is partially altered to a clay-rich paste. Field of view 3.6 x 2.4mm, plane-polarised light. (B) Clay-rich cataclasite (cc) cross-cut by fault-parallel hematite veins (hm). Dashed line-WBF trend. Field of view 3.6 x 2.4mm, plane-polarised light.

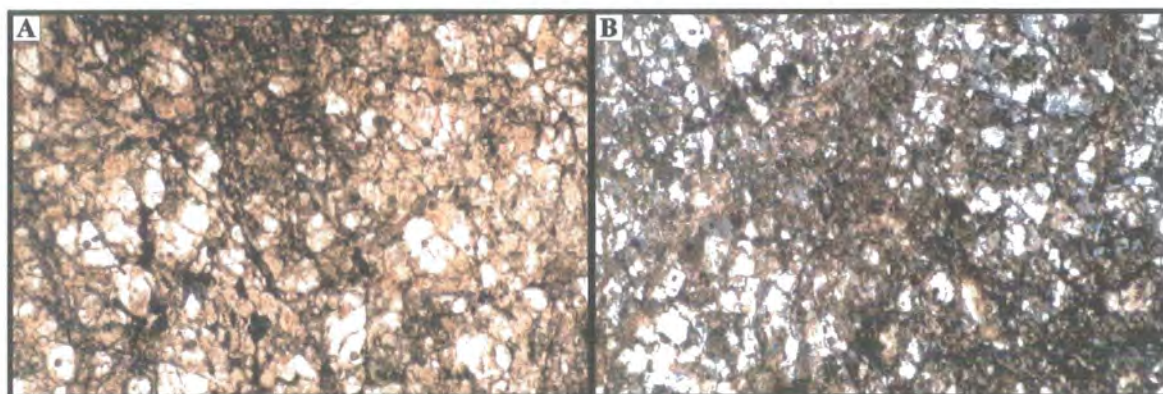


Plate 4.14 Cataclasite derived from Devonian sandstone west of the WBFZ at Bixter (section 3:1:6). (A) & (B) Field of view 3.6 x 2.4mm, plane-polarised light and crossed polars, respectively. Cataclasites comprise randomly orientated finely comminuted fragments of quartz and minor amounts of feldspar set within a fine-grained cataclastic matrix of quartz, calcite and chlorite, which has, in places, been altered to a clay-rich isotropic paste.

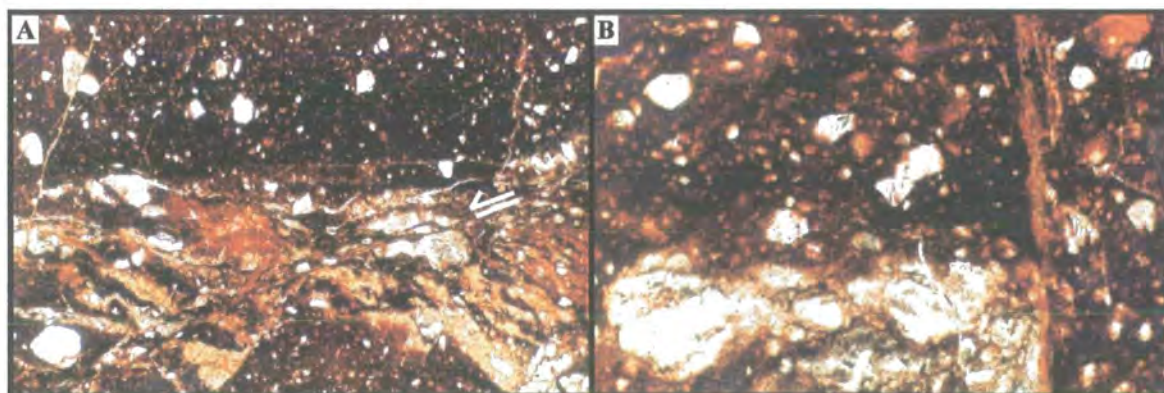


Plate 4.15 Red fault gouge from Ollaberry (section 3:1:1). (A) Image of cohesive fault gouge, which comprises sub-rounded to rounded clasts of cataclasite, quartz, epidote and feldspar set within a red to brown-coloured matrix, which appears to be an iron-rich isotropic paste. In places, the gouge is cut by a series of fractures which display sinistral strike-slip offsets (split arrow). Field of view 3.6 x 2.4mm, plane-polarised light. (B) Close-up of red to brown-coloured isotropic matrix. Field of view 1.44 x 0.96mm, plane-polarised light.

4:3:3:1 Operative deformation mechanisms

The dominant deformation mechanism is cataclastic flow (mechanical disaggregation and grain-size diminution) in and between grains, and grain boundary sliding. Feldspar and quartz deform by cataclasis, indicating temperatures of less than 250°C to 300°C or depths of less than 8.5 to 10km (assuming an average geothermal gradient of 30°C/km). The cataclasites matrix is commonly altered to a clay-rich paste. The clays form as a result of the infiltration of aqueous fluid during frictional deformation, inducing alteration of unstable minerals (such as feldspar) formed at higher temperatures and pressures (Warr et al. 2001). The presence of syn-tectonic clay alteration indicates temperatures of less than 200°C or depths less than 6km (assuming an average geothermal gradient of less than 30°C/km). Therefore cataclasites are interpreted to have formed at temperatures of less than 200°C and depths shallower than 6km.

4:3:4 Cataclasites derived from Devonian sandstones

Cataclasites derived from Devonian sandstones (section 4:1:3) are exposed to the west of the WBF at the Ness of Bixter (section 3:1:6). The cataclasites comprise randomly orientated, finely comminuted fragments of quartz (0.01 to 0.2mm in size) and minor amounts feldspar set within a fine-grained cataclastic matrix of quartz, calcite and chlorite, which appears to be altered to a clay-rich isotropic paste (Plate 4.14A&B). The cataclasites are isotropic on all scales of observation and do not display any banding or alignment of clasts. In places, the matrix appears to be mineralised by fine-grained calcite. Extensive networks of millimetre-thick calcite veins commonly cut the sandstones in the wall rocks adjacent to the cataclasite. Quartz and feldspar clasts display strong, patchy, undulose extinction and are cut by extensive arrays of intergranular fractures, which are commonly filled with calcite.

4:3:4:1 Operative deformation mechanisms

The dominant deformation mechanism is cataclastic flow (mechanical disaggregation and grain-size diminution) in and between grains, and grain boundary sliding. Quartz and feldspar deform by cataclasis, indicating temperatures of less than 250°C to 300°C or depths of less than 8.5 to 10km (assuming an average geothermal gradient of 30°C/km). Calcite mineralisation within parts of the cataclasite was probably precipitated by fluids which were drawn into the fault zone by dilatancy during cataclasis (see section 1:5:2). The presence of clay material which formed due to hydrothermal alteration during frictional deformation, indicates temperatures of less than 200°C or depths less than 6km (assuming an average geothermal gradient of less than 30°C/km) (Frey 1988). Therefore, the cataclasites are interpreted to have formed at temperatures of less than 200°C and depths shallower than 6km.

4:3:5 Fault gouge

4:3:5:1 Incohesive fault gouge

Optical microscopy of incohesive, blue-coloured, fault gouges exposed within the WBF core was impossible due to the difficulty involved in making thin sections.

XRD analyses carried out by Sarah Sherlock (Open University, UK) on samples collected from the Ness of Haggrister (section 3:1:2), show that the blue gouge is composed of quartz, plagioclase, chlorite, illite, smectite and kaolinite. Infiltration of aqueous fluid during frictional deformation induces alteration of unstable minerals formed at higher temperatures and pressures and leads to the formation of clays (Warr et al. 2001). The presence of smectite and mixed-layer clays suggests temperatures of approximately 200°C (Frey 1988). However, faulting may reduce the kinetic barriers to mineral changes (Vrolijk and Van der Pluijm 1999), therefore lowering the temperature estimates.

4:3:5:2 Cohesive fault gouge

Cohesive red to brown-coloured fault gouge is exposed within the WBF core. In thin-section, the gouge appears to be a red-brown, clay-rich, isotropic paste that has been cemented by hematite (Plate 4.15A&B). The gouge contains randomly orientated sub-rounded to rounded clasts (0.1mm to 0.5mm in size) of cataclasite, quartz and feldspar. The gouge displays a foliation, probably defined by aligned clay grains. In places, the gouge is cut by fractures which display sinistral strike-slip offsets (Plate 4.15A). Randomly orientated calcite and analcime (zeolite) veins (0.1 to 0.5mm thick) cross-cut and are present as fragments within the gouge. The presence of analcime indicates temperatures of less than 150°C or depths shallower than 5km (assuming an average geothermal gradient of 30°C/km) (Frey 1988).

4:4 Summary

- Primary, sinistral, strike-slip movements were associated with the development of blastomylonites, upper greenschist-facies mylonites and localised pseudotachylites.
- Mylonites deformed primarily by intracrystalline crystal-plastic mechanisms.
- Exhumation of the fault zone (maybe during continued sinistral strike-slip movements) promoted a transition from viscous creep to mainly frictional deformation mechanisms, leading to the localisation of cataclasites (consistent with sinistral shear) along the mylonite foliation.
- Locally, the influx of hydrous fluid led to the development of phyllosilicate-rich, foliated cataclasites, the textures of which are consistent with sinistral shear.
- Further fault-zone exhumation occurred during a period of tectonic quiescence due to erosion.
- Dextral strike-slip reactivation of the WBFZ led to the development of a sequence of extensive cataclasite and fault-gouge assemblages, which display evidence for a progressive, syn-tectonic shallowing of the fault zone.

Chapter 5. The Geology of the Fosen peninsula

The Fosen Peninsula is situated to the northwest of Trondheimsfjord and southeast of the Norwegian Sea between 63.5 and 64.5°N (Figures 5.1, 5.2).

The Fosen Peninsula exposes a series of top-ESE transported nappes that were emplaced during the Siluro-Devonian (Scandian) orogeny. The nappe rocks, which include extensively exposed Precambrian crystalline complexes, are cut by at least one, late-orogenic, top-SW extensional detachment fault zone (the Høybakken detachment, Figure 5.2). The formation of the Høybakken detachment was broadly coeval with the development of Devonian basins and the deposition of Devonian sedimentary rocks unconformably upon the Caledonian basement. The Devonian sedimentary rocks, Høybakken detachment and Scandian nappe units are deformed by a series of NE-SW-trending, regional-scale folds (Figure 5.2). The rocks of Fosen are also transected by the ENE-WSW-striking Møre-Trøndelag Fault Complex (MTFC) (Figure 5.2), formerly known as the Møre-Trøndelag Fault Zone (Grønlie and Roberts 1989).

5.1 The Scandinavian Caledonides

The Scandinavian Caledonides are roughly 300km wide (present day) and 1,800km long, extending from the Tornquist line in the North Sea to the Varanger Peninsula in northern Norway (Andersen 1998). This mountain chain is broadly comparable in dimensions to the Cenozoic Himalayan mountain belt.

The Scandinavian Caledonides were formed during the polyphase Caledonian orogeny which culminated in the closure of the Iapetus Ocean and the collision of the palaeocontinents Baltica (to the east) and Laurentia (to the west). The earliest stage of development, known as the Finnmarkian event, reflects a collision between Baltica and an arc complex, that took place in Late Cambrian to earliest Ordovician time. The climax of orogenic deformation, the Scandian event, occurred during the Middle Silurian to Early Devonian when Laurentia collided with Baltica.

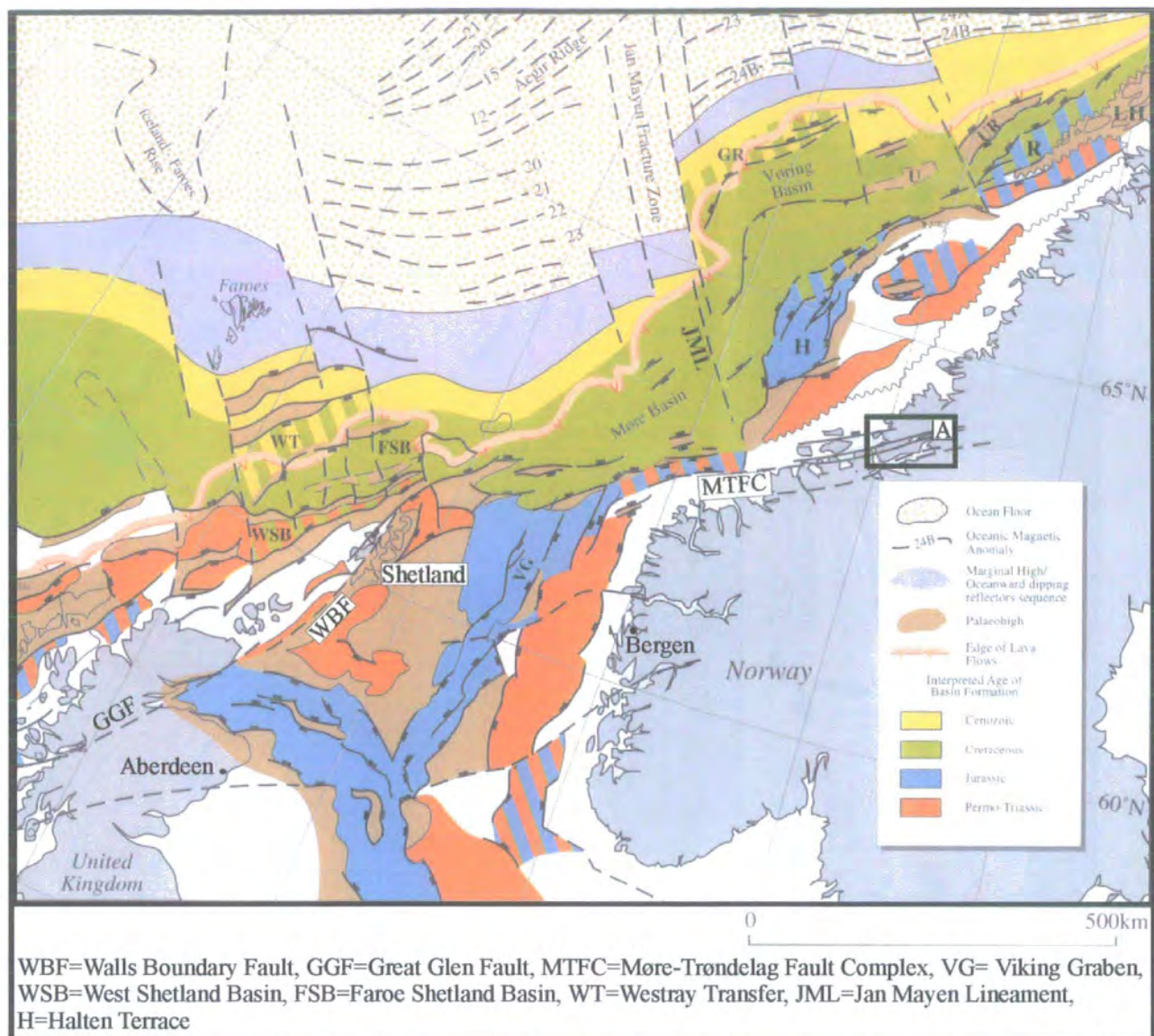


Figure 5.1 Map to show the location of the Fosen Peninsula (A) and the major offshore basins of the Northeast Atlantic margin (adapted from Doré et al. 1997b).

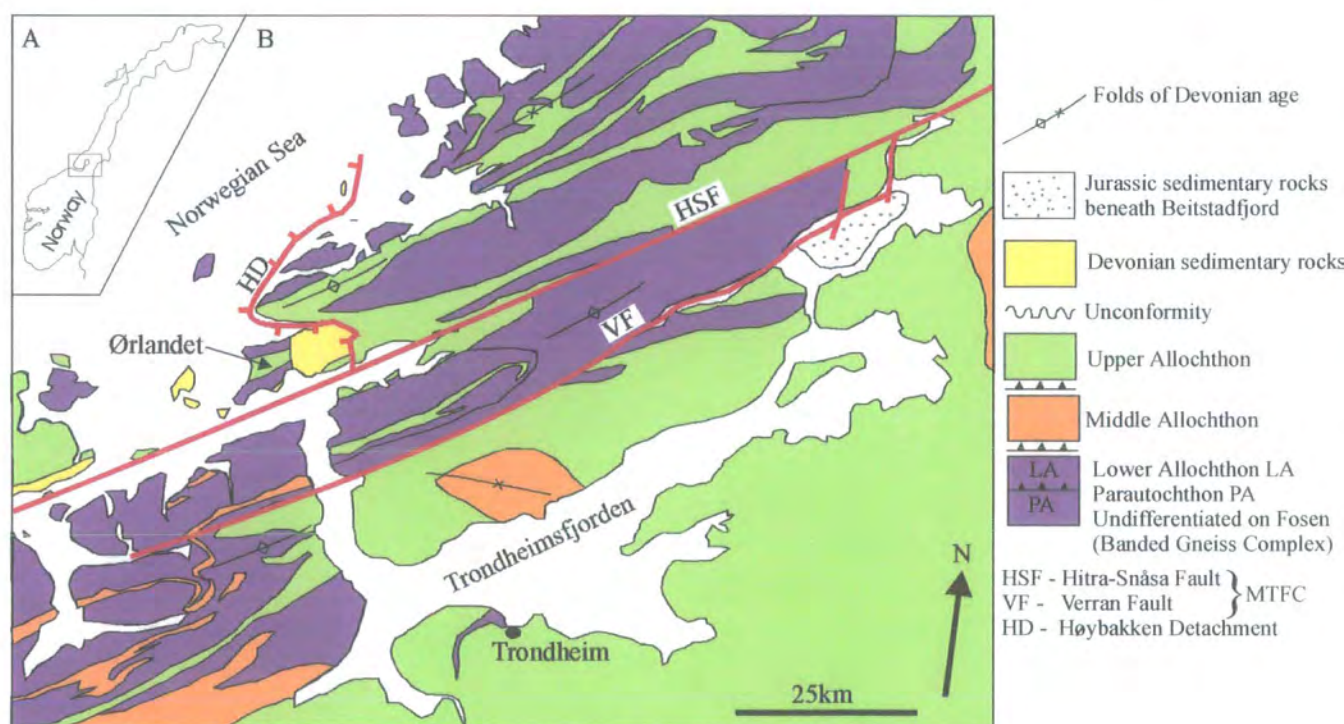


Figure 5.2 Simplified geological map of the Fosen area, Central Norway.

At this time, the margin of Baltica was partially subducted beneath the Laurentian plate down to depths of 125km or more, with ultra-high and high-pressure (UHP and HP) metamorphism at eclogite and granulite facies; broadly coeval with E-SE transport of the major nappes and thrust sheets.

The Fosen Peninsula forms part of the Western Gneiss Region (Figure 5.3), exposing some of the deepest levels of the Scandinavian Caledonides. The tectonostratigraphy of the Caledonides is divided into five main units (from base to top): the Autochthon / Parautochthon and four allochthons - Lower, Middle, Upper and Uppermost (Roberts and Gee 1985; Gee et al. 1985). The correlation of the main tectonic and stratigraphic units in the Central part of the Scandinavian Caledonides is summarised in Table 5.1.

5:1:1 Autochthon / Parautochthon

In Central Norway, an autochthonous sedimentary sequence comprising Cambrian age black shales locally underlain by sandstones and overlain by Ordovician limestones lies unconformably upon the Palaeoproterozoic gneisses (Roberts and Gee 1985). These black shales provided the décollement over which the Lower Allochthon was transported during the top-E-SE, Scandian thrusting (Roberts and Gee 1985).

On Fosen and elsewhere, the Parautochthon comprises penetratively foliated Palaeoproterozoic complexes that have been strongly reworked during the Scandian orogeny (Roberts 1998b). In the extreme west of Fosen, the gneisses are more heterogeneous in terms of composition, with a variety of gneisses intruded by granites and in places gabbroic units (Gee et al. 1985). The crystalline gneisses have been metamorphosed to amphibolite facies, and locally to granulite facies in the Roan district of Fosen (Gee et al. 1985). A high-pressure mafic granulite in the Roan igneous complex has been dated at 432 \pm 6 Ma (Dallmeyer et al. 1992), inferred to date peak metamorphic conditions in Roan. The gneisses locally contain pods of eclogite (Gee et al. 1985; Möller 1988) and are strongly foliated; they commonly show L-S tectonite fabrics and are extensively recrystallised / annealed (Gilotti and Hull 1993).

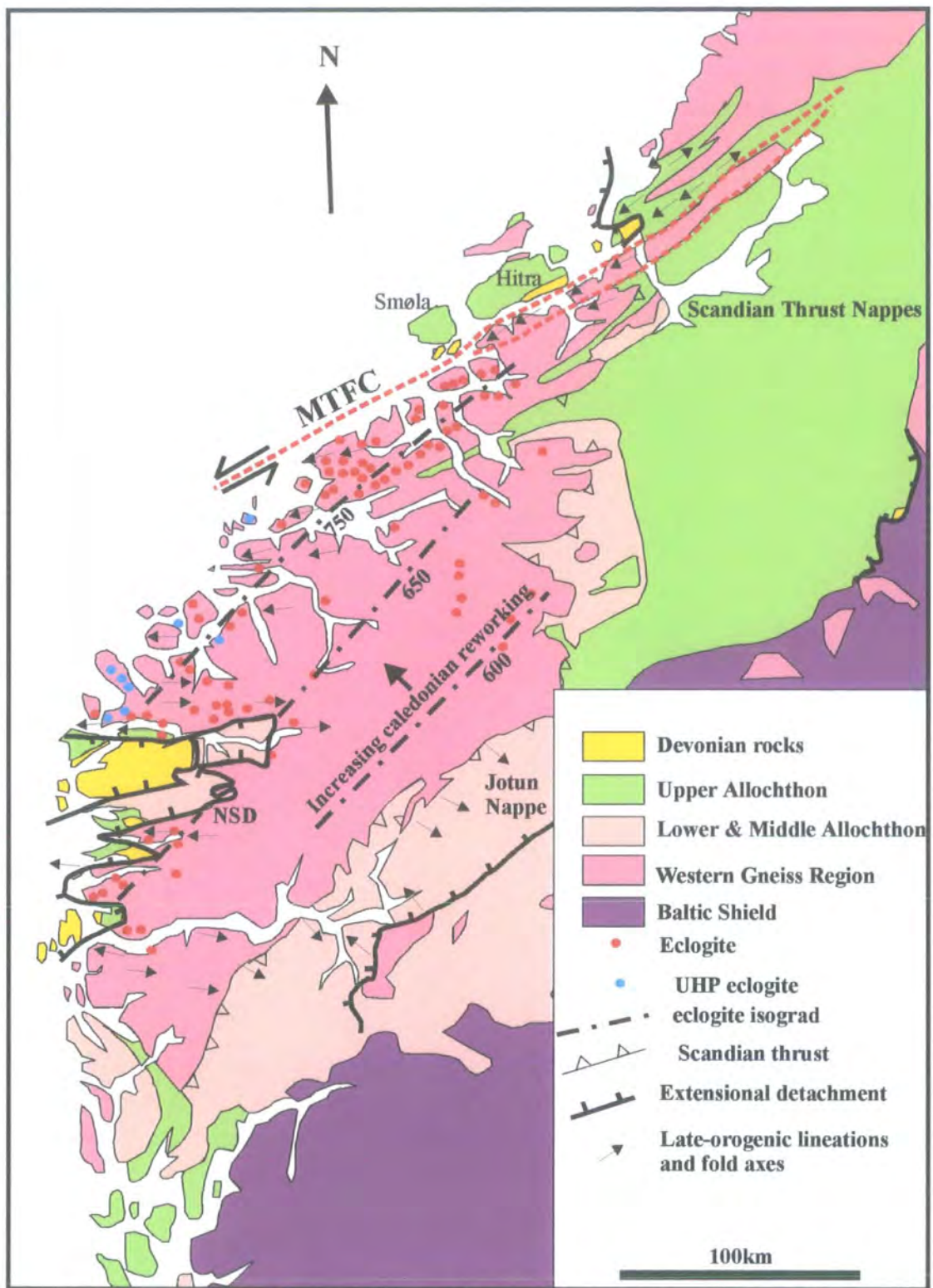


Figure 5.3 Geological map of Western and Central Norway together with the location of ultra-high and high-pressure metamorphic rocks and eclogite isograds (after Krabbendam and Dewey 1998).



	Southwestern areas			Central areas		North of Grong–Olden Culmination	Eastern Areas
Tectonic units	Dombås (Guezou 1978)	Oppdal (Krill 1980)	Trollheimen (Gee 1980)	Western Trøndelag (Wolff and Roberts 1980; Roberts and Wolff 1981)	Eastern	(Stephens <i>et al.</i> this volume)	Central and Southern Jämtland (Gee 1975a)
Late-orogenic sediments				Late Silurian(?) to Mid-Devonian	Early Devonian		
Uppermost Allochthon						Helgeland Nappe Complex	
Upper Allochthon	Trondheim Nappe Complex Fokstua Group Musadal group Skåkåhøi Group	Tronget unit		Støren Nappe Meråker Gula Nappe Complex Levanger Nappe Øyfjell		Gjersvik Nappe Leipik Nappe Gelvanakko Nappe Stikke Nappe Björkvattnet Nappe	Köli Nappes (Tännfors district) Seve–Köli Nappe Complex
	Botheim Group	Blåhø Unit		Skjøtingen Nappe Essandjø		Seve Nappes	
Middle Allochthon	Andbergshøi Complex Veslefjell Group	Sætra Nappe		Leksdal Nappe Dolerite- intruded Sandstone	Rensklepp Nappe For subdivision of this unit, see Sjöström (1983)	Särv Nappes (with Ottfjället Dolerites)	
		Risberget Unit	Indre Kam Formation (Hansen 1971) Augen gneiss	Sandstone without dolerite Hervola Nappe		Augen gneiss	Offerdal Nappe Tännäs Augen Gneiss Nappe
Lower Allochthon	Osen–Røa Nappe Complex (Nystuen 1981)	Not distinguished	Svarthammer unit (Hansen 1971) in part	Foliated granite and rhyolite; Bjørndalen Formation (Gee 1977)		Jämtland Supergroup in Jämtlandian Nappes	
Parautochthon and Autochthon	'sparagmite'	Åmotsdal Unit	Gjevilvatnet Group	Bjørndalen Formation	Quartzites and black phyllites	Tåsjön and Sjöutälven Groups	
	Precambrian gneiss and granite	Lønset Unit (gneiss)	Trollheimen Granite	Precambrian granite and rhyolite	Precambrian granite and rhyolite	Precambrian granite, gneiss, etc.	

Table 5.1 Correlation of main tectonic and stratigraphic units in the central southern part of the Scandinavian Caledonides (adapted from and bibliography in Gee *et al.* 1985).

On Fosen, it is almost impossible to distinguish parautochthonous basement from Precambrian crystalline rocks in the overlying Lower Allochthon without recourse to geochronology (Figure 5.2; Gee et al. 1985).

5:1:2 Lower Allochthon

The Lower Allochthon comprises Vendian to Lower Cambrian sedimentary rocks (e.g., Jämtland Supergroup, Table 5.1). On Fosen, the Jämtland Supergroup has been correlated with Caledonised units of granite and rhyolite, together with limestones and sandstones of the Bjørndalen Formation (Table 5.1). Above the gently W-dipping sole thrust of the Caledonian front, the rocks are telescoped by folds and reverse faults that shallow at depth to link into the underlying sole thrust (Roberts and Gee 1985). To the west, the Lower Allochthon contains increasing amounts of Precambrian gneiss. The gneisses are penetratively foliated, locally mylonitised, and recrystallised under greenschist facies and, in westernmost areas, amphibolite facies (Roberts and Gee 1985).

On Fosen, the Lower Allochthon (Figure 5.2) comprises laterally extensive sheets of strongly deformed Precambrian gneiss and locally subordinate quartzites, phyllites and limestones metamorphosed under greenschist facies conditions (Gee et al. 1985). The gneisses reach amphibolite and locally granulite metamorphic facies in the western part of Fosen (e.g., Roan Window; Möller 1988; Roberts 1998a).

5:1:2 1 Banded Gneiss Complex on Fosen Peninsula

In the area north of the Verran Fault (VF) (Figure 5.2), the amount of Precambrian gneiss within the Lower Allochthon makes it virtually impossible to distinguish this unit from the underlying parautochthonous gneisses (Gee et al. 1985). The gneisses north to northwest of the VF have been informally termed the Banded Gneiss Complex (BGC) of Fosen (Möller 1988) (also called the Vestranden Gneiss Complex by Gilotti and Hull (1993)). Scandian deformation and metamorphism are so intense that protolith granitic-tonalitic / orthogneisses and basic rocks have been highly

reworked into strongly banded L-S tectonites (Roberts 1998a). On Fosen, in view of the intense Scandian reworking, correlations of units with those in established, lower-grade allochthons further east are uncertain (Roberts 1998a).

There are three main units within the BGC; orthogneisses, paragneisses and amphibolites (Gilotti and Hull 1993). Orthogneisses are grey migmatitic and non-migmatitic quartzo-feldspathic gneisses. Paragneisses comprise granitoid orthogneisses surrounding enclaves of marble, calc-silicates, various schists and kyanite-bearing gneiss and amphibolites (Gilotti and Hull 1993). Roberts (1998a) described transitions over a few metres from homogeneous, coarsely foliated and migmatized orthogneiss with mafic sheets inside the lenses, into heterogeneous banded gneisses which typify the BGC. The protolith orthogneisses of Fosen have been dated between c. 1830 and 1640Ma (U-Pb zircon; Johansson 1986; Schouenborg et al. 1991; Johansson et al. 1993). Not all the Caledonised orthogneisses on Fosen are of Proterozoic age (Roberts 1998b). Ordovician to Early Silurian dioritic and granitic rocks have been traced from the islands of Smøla and Hitra to the Størnfjord-Ørlandet area of NW Fosen (Gautneb and Roberts 1989). An age of 460 \pm 5Ma has been obtained from the Follafoss tonalite (Figure 5.2), which forms part of the BGC and crops out between the VF and HSF (D. Roberts pers.comm., 2000). Variably deformed pegmatite dykes cross-cut Scandian fabrics within the BGC and their intrusion has been dated at c.400Ma (Roberts 1998b).

5:1:3 Middle Allochthon

The Middle Allochthon comprises thick successions of unfossiliferous, Neoproterozoic psammites, locally with Precambrian crystalline gneisses at the base (Gee et al. 1985). The rocks were intensely deformed during the Scandian event, with local mylonitisation and isoclinal folding within the psammites (Roberts and Gee 1985). In parts of Central Norway and Sweden, the psammites of the Middle Allochthon are quarried as flagstones. Metamorphic grade increases from greenschist facies in the east to amphibolite facies in the most western areas (Roberts and Gee 1985). A characteristic of the Middle Allochthon is the presence of pre-tectonic mafic

dykes. K-Ar and ^{40}Ar - ^{39}Ar dating of these dykes indicates an age of around 665Ma (Claesson and Roddick 1983).

The extent to which the Middle Allochthon is represented on Fosen (Figure 5.2) and in other western areas remains to be established due to the intense deformation, metamorphism and subsequent recrystallisation of the rocks (Gee et al. 1985). Locally, this Middle Allochthon level is considered to be present in the form of thin thrust sheets composed of arkosic flagstones and amphibolitised mafic dykes.

5:1:4 Upper Allochthon

The Upper Allochthon is the most varied and complex unit in the Scandinavian Caledonides. Scandian age metamorphism ranges from greenschist to granulite and eclogite facies conditions, with the highest grades occurring in the basal units (Roberts and Gee 1985). The successions belonging to the Upper Allochthon have been transported several hundred kilometres east to southeast of their original locations (Roberts and Gee 1985). The Upper Allochthon is divided into two parts (Table 5.1). The lower part is represented by the Seve nappes, which consist of high-grade schists, gneisses and amphibolites. On Fosen and in Central Norway as a whole, the Seve nappes is represented by the Skjøtingen Nappe (Table 5.1), which comprises psammitic schists, amphibolites with subordinate schists and marbles, and locally gneisses and migmatites (Gee et al. 1985). Detailed correlation of the Seve nappes into some parts of the Fosen district remains unclear (Gee et al. 1985).

The upper part of the Upper Allochthon is represented by the Köli nappes, which generally consist of volcano-sedimentary successions metamorphosed under greenschist- to amphibolite-facies conditions (Gee et al. 1985). Locally, these successions are lying unconformably upon obducted slices of deformed ophiolite. On Fosen, the Köli nappes are represented mainly by the Støren and Gula Nappes.

Evidence for the early, Finnmarkian phase of deformation has been reported from the Seve nappes of this region (Dallmeyer 1990). Ophiolite obduction occurred slightly earlier, in Arenig time (Roberts et al. in press). All these early structures are

overprinted by the main Scandian deformation (Roberts and Gee 1985). On the Fosen Peninsula, rocks of the Upper Allochthon crop out mainly south of the VF and to the north of the HSF (Figure 5.2).

5:1:5 Uppermost Allochthon

The Uppermost Allochthon comprises a series of nappes consisting of migmatitic gneisses, amphibolites, psammites, marbles, schists and, locally, ophiolite fragments, with zones of lower grade supracrustal rocks (Roberts and Gee 1985; Stephens et al. 1985). Caledonian granites, granodiorites and gabbros intruded the complex in Late Ordovician / Early Silurian time (Nordgulen et al. 1993), prior to Scandian thrust emplacement onto the underlying Köli nappes (Stephens et al. 1985). Rocks mapped as belonging to the Uppermost Allochthon occur to the northeast of the area described here and are not exposed on the Fosen Peninsula (Figure 5.2).

5:1:6 Regional synthesis of the Scandinavian Caledonides

Norway forms a large exposure of Caledonian rocks lying to the east and northeast of the East Greenland and Scottish portions of the Caledonian orogenic belt, which are separated by post-Caledonian basins that are presently mostly offshore. As noted in section 5:1, the closure of the Iapetus Ocean and eventual collision of Laurentia and Baltica (Figure 5.4) caused the polyphase Caledonian orogeny.

The rifted margin of Baltica is represented by the Lower and Middle Allochthons, and the Seve nappes of the Upper Allochthon. The various Köli nappes constitute a series of exotic, outboard terranes representing diverse locations within the Iapetus Ocean, and include ophiolites, volcanic arcs and marginal basin assemblages (Gale and Roberts 1974; Roberts et al. 1984; Stephens and Gee 1989; Smith 1995; Roberts et al. in press). The Uppermost Allochthon is inferred to represent exotic terranes of possible Laurentian affinity (Roberts et al. 1984; Stephens et al. 1985; Roberts 1988).

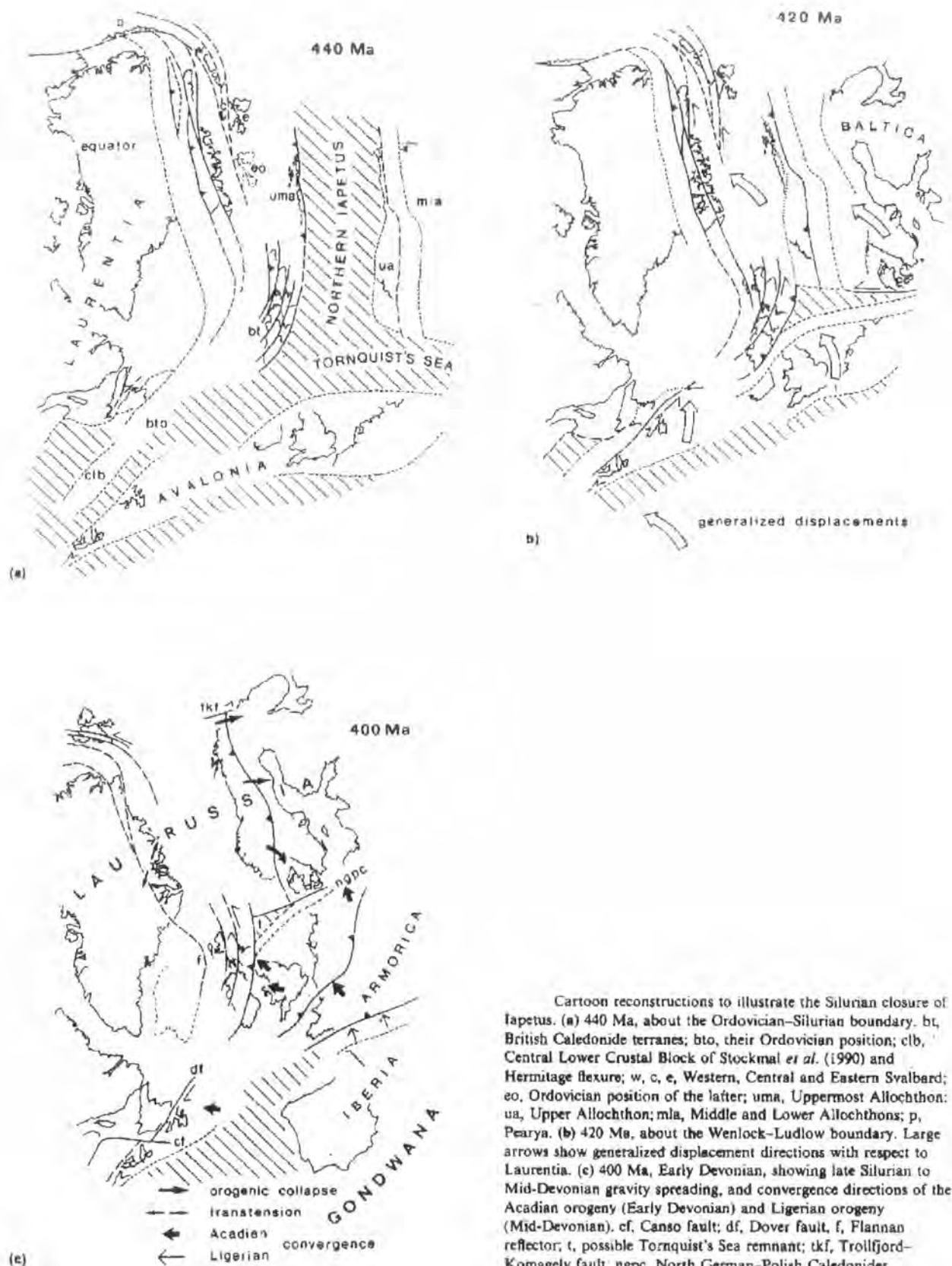


Figure 5.4 Cartoon sketches to illustrate the closure of the Iapetus Ocean from 440 to 400 Ma (after Soper et al. 1992)

The Iapetus Ocean is thought to have opened in Vendian to Early Cambrian times. The early, rifting phase (in latest Riphean to Vandian time) is marked by intrusion of dolerite dykes into metasedimentary rocks of the Middle Allochthon and Seve nappes, representing the margin of Baltica. The exact width of this ocean is unknown. Closure of the Iapetus Ocean is believed to have started in the Mid to Late Cambrian with the oceanward subduction of Baltican margin, leading to the development of an ensimatic island arc (Figure 5.5). Collision between Baltica and the arc in Late Cambrian time produced the Finnmarkian orogenic event, represented in the Seve nappes and Middle Allochthon. In the Köli nappes, 'early' ophiolites range in age from 497 ± 2 Ma (Leka) to 481 ± 5 Ma (Bymarka, Trondheim) (Roberts et al. in press). These ages are similar to those of the Shetland (493 ± 3 Ma), and Pipestone Pond (494 ± 3 Ma) and Betts Cove (489 ± 3 Ma) of the Canadian Appalachian oceanic fragments (U-Pb zircon; Spray et al. 1991). Obduction of ophiolites in the Trondheim region, eastward, upon rocks of the Gula Nappe, occurred in Arenig time (Roberts et al. in press). In Southwest Norway, obduction was later, in Mid Ordovician time, and emplacement onto Laurentia has been suggested (Dunning and Pedersen 1988).

Continuing subduction processes during the Ordovician led to the formation of ensialic island arcs and marginal basins ('later' ophiolites) (Figure 5.5). 'Later' ophiolites are dated at 437 ± 2 Ma (Sulitjelma ophiolite) (Pederson et al. 1991). Compilations of U/Pb age data for the Caledonian-Appalachian oceanic fragments show that there is a virtual continuous spread from 500 to 440 Ma with most generated between 500 and 480 Ma (Spray et al. 1991). The production of oceanic crust over a period of 60 Ma would have produced a sizeable ocean devoid of ocean margin geochemical signatures. Evidence suggests that several distinct oceanic basins were created and destroyed throughout this period (Spray et al. 1991).

During the final collision of the continents Laurentia and Baltica, producing the Scandian orogeny, thick nappe units developed which translated rocks originally belonging to the margin of Baltica and in some cases rocks with Laurentian affinity (Uppermost Allochthon), in an E / SE direction over Baltica (Figure 5.4). In the East Greenland and Scottish Caledonides, crustal imbrication was taking place broadly at the same time as the Scandian but with an opposite polarity (Figure 5.4).

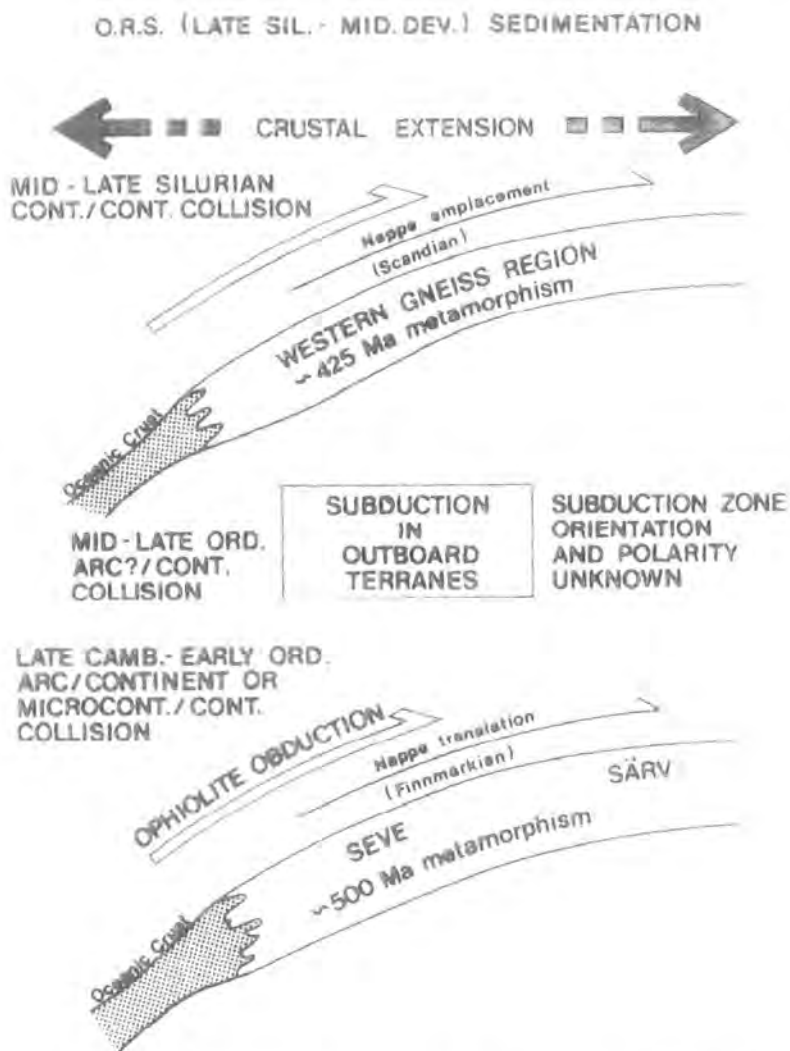


Figure 5.5 Subduction and tectonic history of the Scandinavian Caledonides (after Sturt and Roberts 1991).

5:2 Late-orogenic collapse and Devonian basins

Following the final development of the Scandinavian Caledonides, extensional collapse led to rapid tectonic denudation of the orogen and exhumation of high / ultra high-pressure (HP and UHP) metamorphic rocks, and provided the basis for the formation of the Devonian sedimentary basins. The direction of tectonic transport changed from top-E/SE during the Scandian orogeny, to a general top-W during Early- to Mid-Devonian extension (Andersen 1998).

On the Fosen Peninsula, Devonian sedimentary rocks are exposed in the Ørlandet area (Figure 5.2). The rocks are part of an elongate sedimentary basin that stretches 150km west-southwestwards to include a belt of skerries and islands (including Hitra and Smøla; Figure 5.3). On Fosen, the Devonian rocks occur in the Bjugn Basin (Steel et al. 1985), which is situated to the north of the ENE-WSW-striking MTFC, and is bounded to the east by the W-dipping Høybakken detachment (HD) (Figure 5.2).

5:2:1 Stratigraphy of the Bjugn basin

On Ørlandet, Devonian sedimentary rocks of the Bjugn Basin unconformably overlie metamorphic rocks belonging to the Lower and Upper Allochthons. The Devonian rocks are bounded to the east by a W-dipping extensional detachment (Høybakken Detachment; Figures 5.2, 5.6). The successions are dominated by coarse-grained conglomerates and sandstones of mainly fluvial origin (Siedlecka 1975; Bergfjord 1989). The rocks occur either unconformably upon or in extensional-tectonic contact above multiply deformed nappe rocks. The rocks are generally regarded as molasse deposits derived by erosion of the rapidly exhumed Scandian nappes (Steel et al. 1985).

Stratigraphy within the Bjugn Basin on Fosen attains a minimum thickness of 3km (Siedlecka 1975), and comprises two formations.

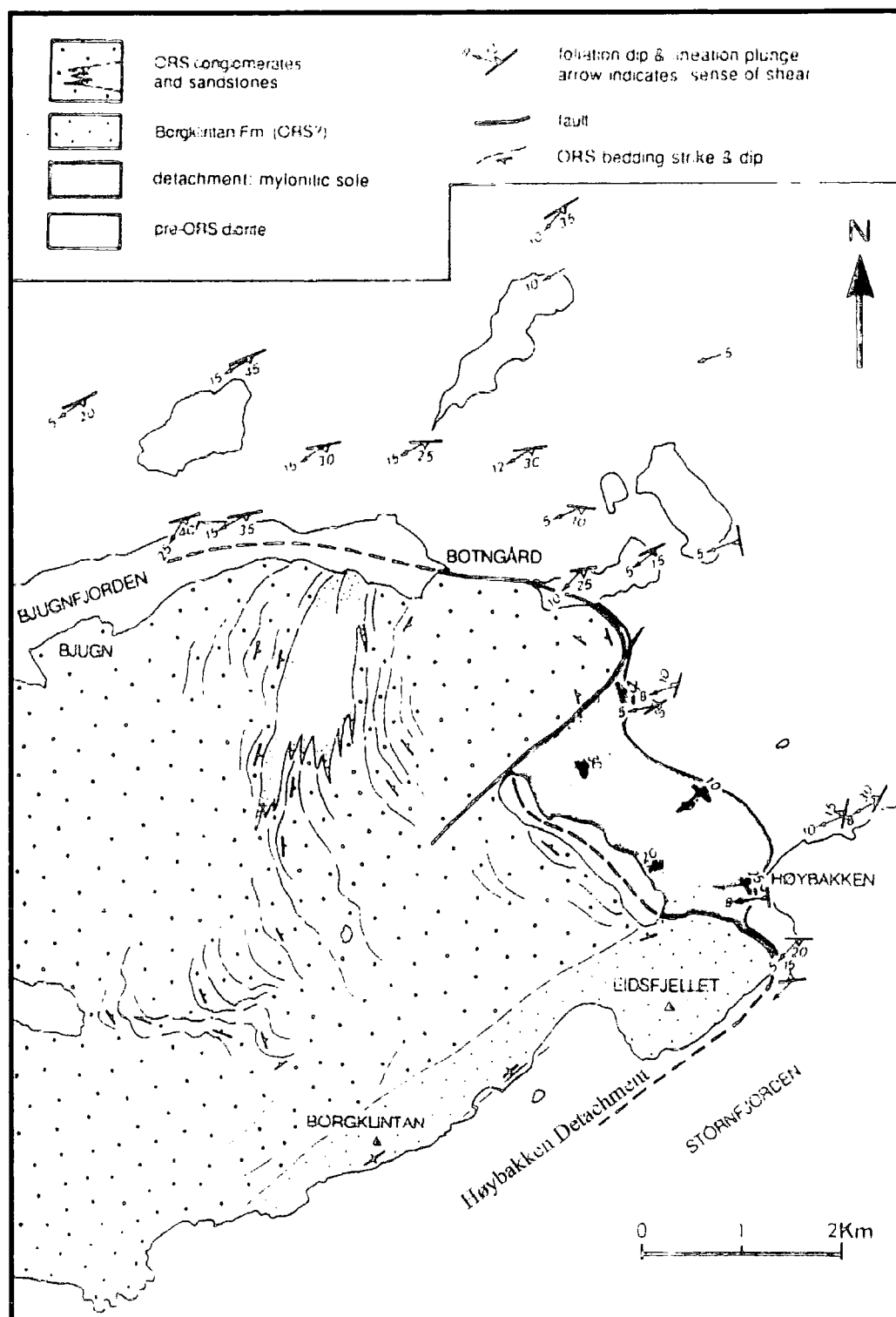


Figure 5.6 Geological map of the Høybakken detachment and the northeast side of the Bjugn Basin Northwest Fosen (after Séranne 1992b).

The 500m-thick Austrått Formation is the lowermost unit (Figure 5.7), consisting of coarse-grained, lithic or feldspathic sandstones which contain isolated pebbles and conglomerate horizons (Steel et al. 1985). The overlying Bjugn Conglomerate are thought to be the time equivalent of distal basinward mudstones interbedded with fine-grained sandstones and occasionally conglomerates belonging to the Hitra Formation on the island of Hitra (Siedlecka 1975; Steel et al. 1985;). The Hitra and Austrått formations are believed to be Downtonian age (Siedlecka 1975; Steel et al. 1985; Bøe et al. 1989). Séranne (1992b) suggested that the Austrått Formation is a deformed equivalent of the overlying Bjugn Conglomerate.

The contact between the Austrått Formation and the overlying Bjugn Conglomerate is not exposed but was believed to be an unconformity or possibly a NE-SW-trending fault (Siedlecka 1975). The Bjugn conglomerate (Figure 5.7) is c.2km thick and comprises thickly bedded polymict conglomerates interbedded with finer-grained laminated units (Steel et al. 1985). Subordinate sandstone and mudstone units are commonly several metres thick, displaying fining up sequences. Finely-laminated mudstones contain plant fossils of Early to possibly lower Mid Devonian age (Steel et al. 1985). Siedlecka (1975) described pebbles that were similar to the Downtonian sedimentary rocks of Hitra, suggesting reworking of sediments deposited in earlier basins.

Along the northwest coast of Störn fjorden to the west of Høybakken, the Borgklintan Formation is exposed (Figures 5.6, 5.7). The formation comprises highly brecciated rock metamorphosed under greenschist-facies conditions. The protoliths are thought to be acidic lavas interlayered with medium-grained, clastic sedimentary rocks (Siedlecka 1975). Séranne (1992b) described mylonitisation of the Borgklintan Formation into steeply dipping ENE-WSW high-strain zones, overprinted by cataclastic deformation, and gradually passing up into undeformed conglomerates (Figure 5.7). The origin of the Borgklintan Formation is uncertain.

Granitic dykes are a common feature within the Bjugn Basin. Intrusions have formed bodies several tens of metres thick and include xenoliths of country rock (Séranne 1992b). Intrusive bodies are continuous over several metres while others are offset by extensional faults (Séranne 1992b).

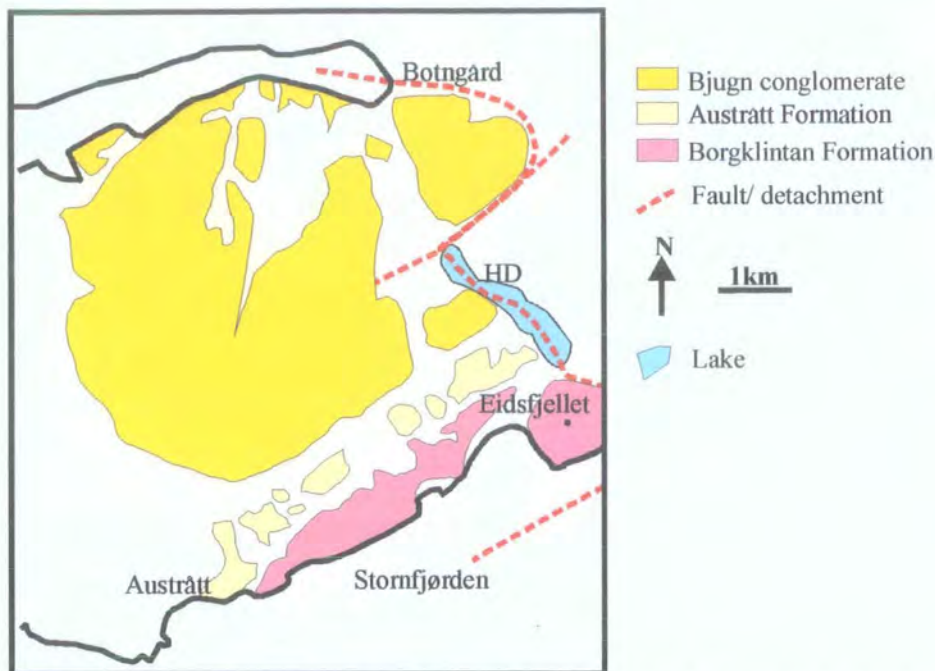


Figure 5.7 Geological map to show the location of Devonian rocks within the Bjugn basin, Southwest Fosen (adapted from Siedlecka 1975).

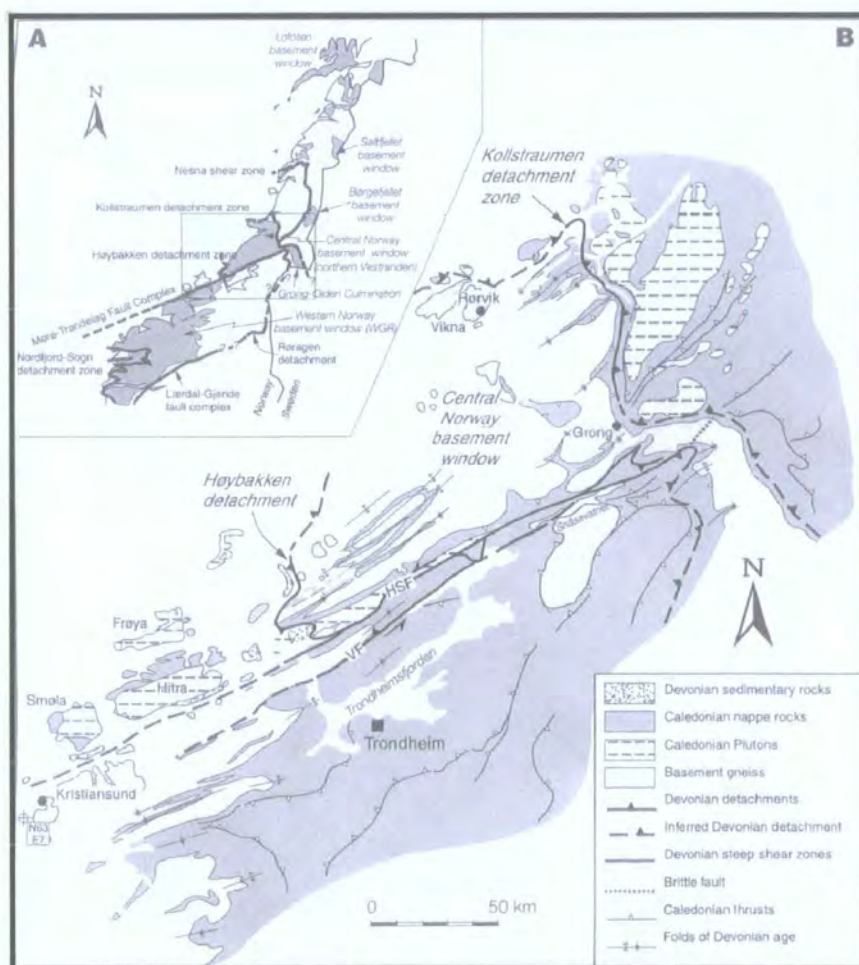


Figure 5.8 (A) Sketch map of central parts of Scandinavian Caledonides, highlighting basement windows and Early-Middle Devonian faults and shear zones. (B) Tectonic map of Trondheimsfjorden, locating MTFC, Høybakken and Kollstraumen detachment zone. HSF - Hitra-Snåsa Fault, VF - Verran Fault (After Braathen et al. 2000).

5:2:2 Structure within the Bjugn basin

The stratigraphy within the Bjugn basin on Fosen defines an open syncline with the fold axis plunging 20° to the ENE (Figure 5.6; Séranne 1992b; Roberts 1983). To the southwest of Fosen, on Hitra (Figure 5.3), folding is tighter with the development of an axial planar cleavage. Phengite along this cleavage is of Late Devonian to Early Carboniferous age (Bøe et al. 1989). In the northwest of the basin on Fosen, bedding is deflected in a clockwise sense, and in the southeast part of the basin in an anticlockwise sense (Figure 5.6; Séranne 1992b). Séranne (1992b) noted that, to the southeast, bedding is folded about steeply dipping axial planes with the development of progressive syntectonic unconformities, suggesting syn-sedimentary folding. N-S-trending faults and fractures displace sedimentary bedding by several centimetres and are mostly dip-slip normal (Séranne 1992b). Within the upper part of the stratigraphic sequence towards the northeast (Figures 5.6, 5.7), conglomerates contain a flat-lying foliation and were metamorphosed under greenschist-facies conditions (Séranne 1992b). However, the lowermost unit of the basin in the southwest is not deformed or metamorphosed. This suggests that the basal series in this area does not correspond to the base of the basin, and that the metamorphism is due not to burial but to proximity to a tectonic contact that defines the northeast margin of the basin (Séranne 1992b).

5:2:3 Høybakken detachment (HD)

A low-angle, W-dipping fault is exposed on the coast west of Høybakken (Figures 5.6, 5.7). The HD underlies the Borgklintan Formation and extends westwards beneath the Bjugn Basin (Figure 5.6). The HD is responsible for the strain gradient observed within the sedimentary rocks. Underlying the most recent movement plane of the detachment is a 2-3km-thick zone of mylonite series rock (Braathen et al. 2000). Séranne (1992b) described a weathered zone several decimetres thick underlying the contact between the hangingwall and footwall, a sole of well-foliated white mylonite 10-20m thick, and a very thick zone of mylonite / protomylonite (derived from diorite gneiss or diorite) within a section through the fault zone west of Høybakken (Figure 5.6). Overlying the detachment there are semi-brittle mylonites

derived from granitic rocks belonging to the Eidsfjellet intrusive rocks of the Borgklintan Formation (see section 5:2:1; Séranne 1992b). The fault plane separating the hangingwall and footwall contains grooves plunging W to WSW (Braathen et al. 2000). Mineral stretching lineations within the mylonitic sole consistently plunge shallowly to the SW (Séranne 1992b). σ - and δ -type porphyroclasts, microfolds and shear bands display top-SW shear criteria on surfaces viewed parallel to the mineral lineation (Séranne 1992b; Braathen et al. 2000). N-S-striking, dip-slip normal faults cross-cut the mylonitic sole and the detachment itself, tilting fault blocks to the ENE (Séranne 1992b). Banded cataclasites are more common towards the top of the fault zone, near the fault plane, commonly showing top-SW shear criteria (Braathen et al. 2000). Sheared and partly mylonitised granitic dykes dated (U-PB, zircon) between 404 to 401Ma are common within the HD (Braathen et al. 2000).

The HD, together with the overlying Devonian sedimentary rocks is folded into an open syncline plunging 10° to the SW (Figure 5.6). To the south, the HD surrounds Eidsfjellet (Figure 5.6), with a sub-vertical foliation in the overlying formation trending ENE-WSW (Séranne 1992b). Sinistral strike-slip shear criteria have been observed in surfaces parallel to the sub-horizontal stretching lineation (P.T. Osmundsen, pers.comm., 2000). To the north of the basin, foliation strikes NE-SW and dips to the SE, and shearing is oblique-dextral in surfaces viewed parallel to the mineral lineation (Séranne 1992b).

The break in strain and metamorphic grade that occurs across the HD must imply considerable displacement (Séranne 1992b). Roberts (1983) described syn-depositional normal faults on Hitra and inferred such faults in the Fosen area. Mineral stretching lineations within the mylonitic sole are not folded, suggesting that top-SW shear was either synchronous with or post-dating folding (Figure 5.6). Therefore, deposition of the Devonian sedimentary rocks was broadly coeval with extensional movements along the HD.

Top-SW fabrics overprint top-NE fabrics within basement gneisses located close to the basin margins of the Devonian sedimentary rocks (Séranne 1992). Gilotti and Hull (1993) described amphibolite facies L-S and L>S fabrics, NE-SW-trending folds

sub-parallel to the mineral lineation and small-scale (ductile) sinistral, strike-slip shear zones within the Vestranden Gneiss Complex, N of the VF (see section 5:1:2:1a; Figure 5.2). These structures indicate constrictional strain and are similar to those described from the Western Gneiss Region (WGR) within the footwall of the Nordfjord-Sogn Detachment (NSD) (Krabbendam and Dewey 1998). Piasecki and Cliff (1988) dated muscovite from pegmatites generated along mylonites from sinistral strike-slip shear zones in the Jøssund area, SW Fosen, at 389 ± 6 and 386 ± 6 Ma (Rb-Sr mineral ages). These dates correspond well to a Middle Devonian age for the deposition of the Bjugn Conglomerate, which contains syndepositional NE-SW-trending folds (Séranne 1992b; Siedlecka 1975).

5:2:4 Regional Synthesis of Late-orogenic collapse

Extensional collapse of the Scandinavian Caledonides led to the exhumation of HP and UHP metamorphic rocks (Western Gneiss Region; Figure 5.3), the formation of Devonian basins and a rapid tectonic denudation of the orogen (Andersen 1998). Whereas the Central and western portions of the Scandinavian Caledonides have been strongly affected by extensional deformation, the more eastern parts have not been significantly affected by this late-stage movement.

Peak HP and UHP metamorphism in the Western Gneiss Region (WGR) is dated at 420-400 Ma (Krabbendam and Dewey 1998). Exhumation was interpreted to have occurred directly after peak metamorphism at the end of the Scandian orogeny (Andersen 1998). Eclogites occur as close as 1 km below essentially unmetamorphosed Devonian sedimentary rocks (Figure 5.3), suggesting that exhumation had taken place by the time the sediments were deposited. However, in more recent studies of U-Th-Pb monazite geochronology, Terry et al. (2000) combined the new geochronology with previous P-T estimates, to illustrate that UHP metamorphic rocks (lower plate) were exhumed during syn-collisional exhumation (410 to 400 Ma), where they came in contact with HP metamorphic rocks (upper plate) at ~400 Ma (Figure 5.9). Both UHP and HP metamorphic rocks were then exhumed together during late- to post-orogenic collapse between 400 and 375 Ma.

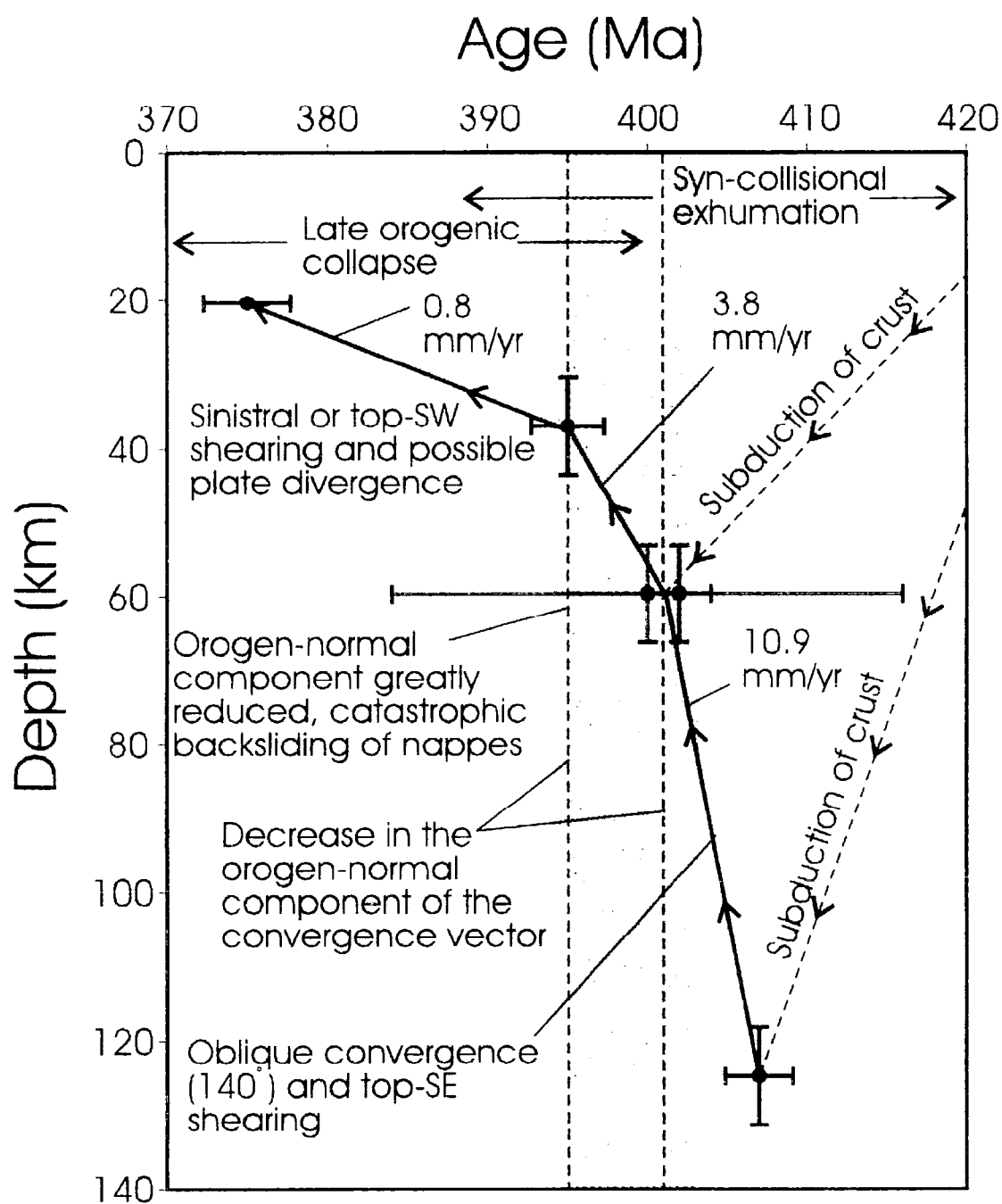


Figure 5.9 Exhumation rate diagram outlining local structural observations and regional (plate-scale) events. The time of extensional basin deposition (shaded) is for part of the Hirta Basin constrained to the late Emsian by the plant fossils of Allen (1976) and the revised time scale by Tucker et al. (1998). Full time of deposition in this and other basins was probably both earlier and later. (after Terry et al. 2000).

Therefore, the exhumation histories of UHP and HP metamorphic rocks record a change in mechanism from syn-collisional exhumation through late- to post-orogenic collapse (Terry et al. 2000). It is important to note that deposition of sediments in the Hitra extensional basin occurred in the Late Emsian from 403 to 394Ma, at the same time the Lower Plate was reaching peak metamorphic conditions at c.401Ma (Figure 5.9; Terry et al. 2000).

In western and Central Norway, Devonian sedimentary rocks lie unconformably upon Caledonised basement within large sedimentary basins bounded by W / SW-dipping extensional detachments (Figure 5.3) (Roberts 1983; Séranne and Seguret 1987; Osmundsen et al. 1998). The Nordfjord-Sogn Detachment (NSD; Figure 5.3) juxtaposes Caledonian eclogites (c. 420-400Ma) in the footwall against Middle Devonian sedimentary rocks (c. 390Ma) in the hangingwall. Mylonite zones within the NSD show clear evidence for top-W sense of shear (Séranne and Seguret 1987). The contrast in metamorphic grade between the hangingwall and footwall of the NSD requires the omission of between 35 to 50km of crustal section and infers large displacements along the detachment (Andersen 1998). Crustal thickness would have been halved in 40Ma following crustal thickening during the Scandian orogeny (Andersen 1998). Devonian basins are situated in the hangingwall of the NSD zone. The largest basin, the Hornelen Basin, contains 25km of Devonian stratigraphical succession comprising mainly sandstones and siltstones, but with a distinct basin-edge fringe of conglomerates (Osmundsen et al. 1998). The basin-bounding fault of the Hornelen basin is again a large-scale W-dipping extensional detachment.

Krabbendam and Dewey (1998) described many structures within the mylonitic sole and the underlying gneisses of the Nordfjord-Sogn detachment (NSD) similar to those found in the HD, indicating constrictional strain. The fault rocks within the NSD are similar to those found within the HD and show evidence for ductile top-W overprinted by brittle top-W kinematic indicators, inferring that the detachment was being exhumed (Krabbendam and Dewey 1998). The Devonian rocks as well as the underlying detachments and gneisses, are folded into open to tight, W-plunging folds. The exhumation of HP and UHP metamorphic rocks, movements along extensional detachments and deposition of Devonian sedimentary rocks was broadly coeval in western and Central Norway.

North of the MTFC, bi-directional opposed extension led to the exhumation of BGC whereas to the south unidirectional (top-W) extension dominated (Braathen et al. 2000). These authors also identified a top-NE detachment (Kollstraumen Detachment; Figure 5.8) to the northeast. Thus, movements along two extensional detachments (HD and the Kollstraumen Detachment; Figure 5.8), moving at the same time but in opposite directions, led to the exhumation of the BGC and the formation of the MTFC as a sinistral strike-slip transfer structure (Braathen et al. 2000).

Krabbendam and Dewey (1998) suggested that sinistral transtension was the dominant exhumation mechanism in the Western Gneiss Region and was partially partitioned with increasing transtensional angle towards the MTFC.

Extensional detachments and associated Early Devonian sedimentary basins have been identified in East Greenland (Strachan 1994), suggesting that orogenic collapse was occurring across the entire Caledonide orogen. In the Scottish Caledonides, Devonian sedimentary rocks in the Orcadian Basin lie in distinct, closely-spaced, arcuate half-grabens (Norton et al. 1987). An unconformity at the base of the Middle Devonian was formed due to a rapid increase in extension in the Orcadian Basin. No such unconformity occurs in Norway, suggesting a constant rate of extension in western Norway. In Norway, the basins contain thick stratigraphical successions (>8km) and are bounded by widely spaced and larger extensional structures (Norton et al. 1987). These differences are probably due to the greater crustal thickening that took place in Norway during the Scandian orogeny (Norton et al. 1987). In Scotland, extensional structures dip to the E/SE whereas in Norway and Greenland most extensional structures dip to the W/SW (Norton et al. 1987).

5: 3 The Møre-Trøndelag Fault Complex

The Møre-Trøndelag Fault Complex (MTFC), formerly designated fault zone, was defined by satellite imagery analysis (Gabrielsen and Ramberg 1979), and comprises strong lineaments following the Caledonian structural grain. The lineaments extend from the Grong-Olden Culmination (GOC) near Grong (Figure 5.8) in the northeast, through the Fosen Peninsula (Figure 5.2) to the southwest and offshore (Gabrielsen and Ramberg 1979).

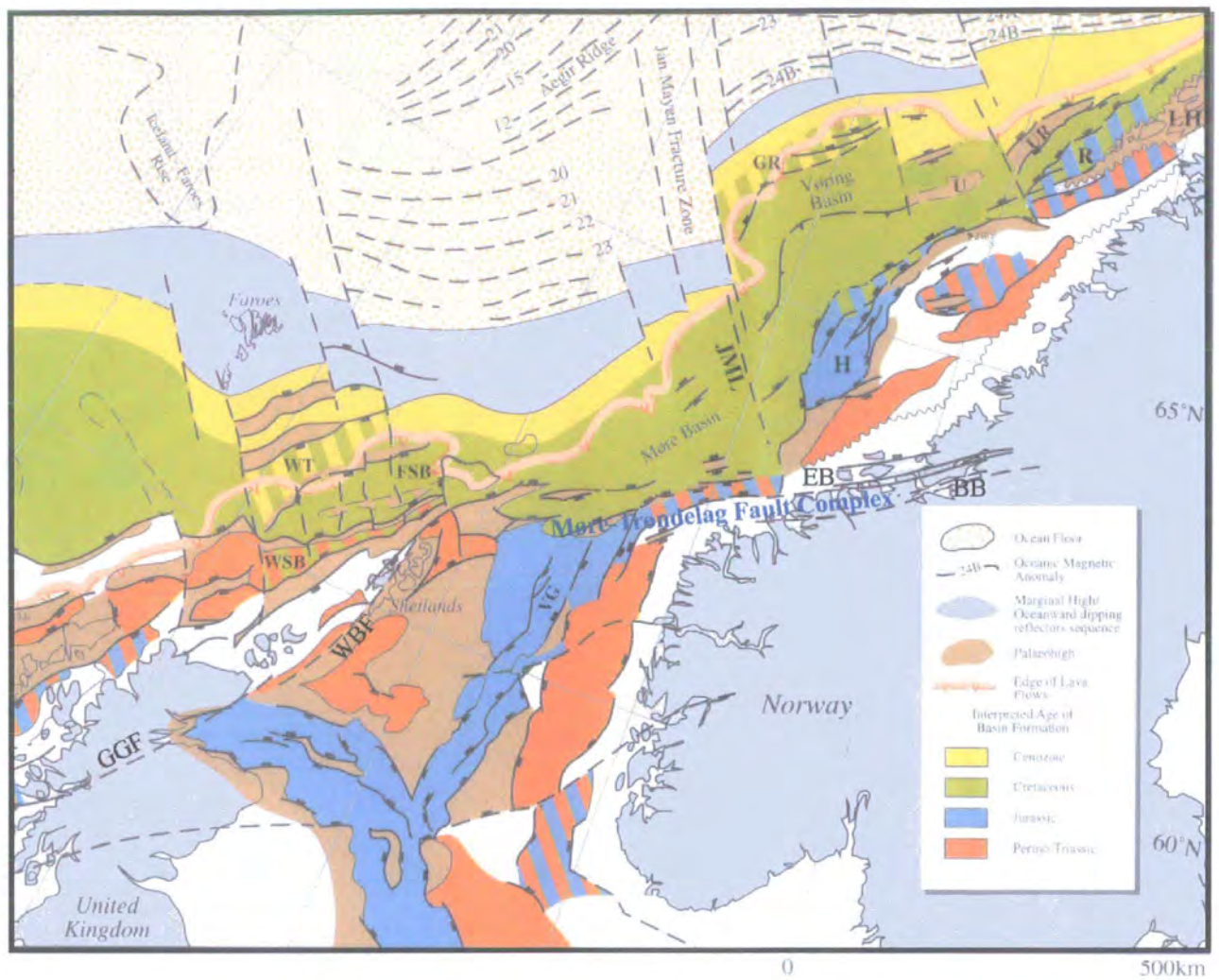
The MTFC approximately defines the coastline of Central Norway between Hitra and Romsdal and extends offshore to define the southern margin of the Møre Basin and the northern margin of the Viking Graben (Figure 5.10; Séranne 1992b; Grunnaleite and Gabrielsen 1995; Doré et al. 1997b; Gabrielsen et al. 1999). Several authors have extrapolated the MTFC to join the Walls Boundary Fault of Shetland and the Great Glen Fault of Scotland (Norton et al. 1987; Ziegler 1987; Grønlie and Roberts 1989; Séranne 1992b; Blystad 1995).

5:3:1 The MTFC onshore

The MTFC is a 10-20km-wide, crustal-scale zone of fault-related deformation, extending from the GOC in the northeast, through the Fosen Peninsula to the south coast of Hitra (Figures 5.2, 5.8)

On the Fosen Peninsula, the MTFC cuts through a series of E-SE transported Scandian nappes, and Devonian sedimentary rocks (Figure 5.2). The MTFC has a prolonged history of polyphase deformation varying from strike-slip through oblique-slip to dip-slip at different structural levels (Grønlie and Roberts 1989; Bøe and Bjerkli 1989; Grønlie and Torsvik 1989; Grønlie et al. 1991, 1994; Bering 1992; Séranne 1992b). Towards the northeast, in the county of Nord-Trøndelag, the bulk lateral displacement along the MTFC on the southern flank of the GOC is no more than 4-5km based upon units offset on geological maps (Roberts 1998a). The displacement appears to diminish eastwards, with the development of a horsetail splay with many minor E-W faults involved (Roberts 1998a).

Many conflicting accounts of the kinematic history of the MTFC have appeared in the literature (Table 5.2). The earliest movement recognised in the field is believed to be Devonian age, ductile, sinistral strike-slip (Grønlie and Roberts 1989; Torsvik et al. 1989; Grønlie et al. 1991; Séranne 1992b; Roberts 1998a). Several authors have suggested that a precursor fault in the basement may have caused deflections (to the NE) in the regional E- to SE-directed thrust transport during the Scandian orogeny (Grønlie and Roberts 1989; Séranne 1992b).



WSB=W Shetland Basin, FSB=Faroe Shetland Basin, JML=Jan Mayen Lineament, H=Halten Terrace, EB=Edøysfjorden Basin, BB=Beitstadfjorden Basin, VG= Viking Graben, WBF=Walls Boundary Fault, GGF=Great Glen Fault

Figure 5.10 Map of basins along the Northeast Atlantic Margin (adapted from Doré et al. 1997b).

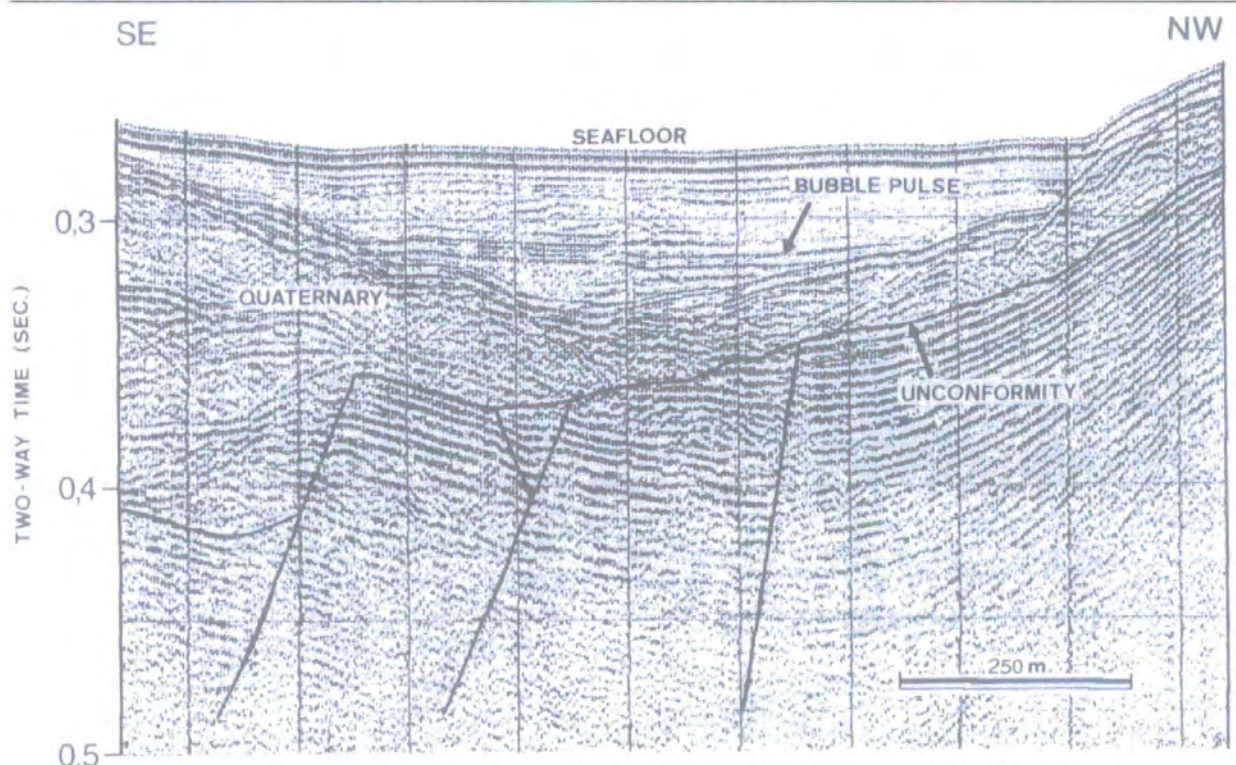
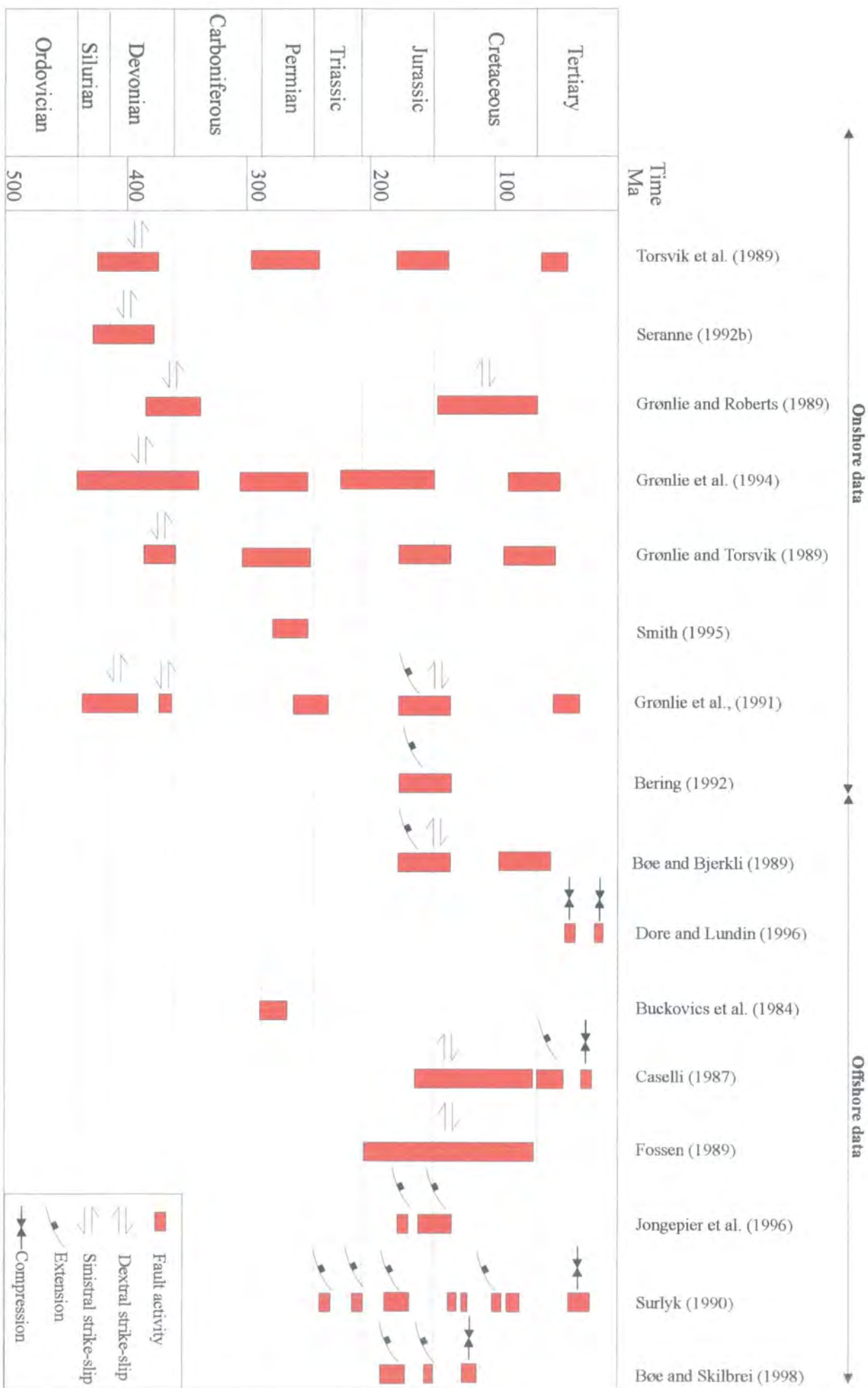


Figure 5.11 Seismic section through northwest margin of Beitstadfjorden (after Bøe and Bjørkli 1989). VF is situated to the right.

Table 5.2 Summary of kinematic events suggested for the MTFC, taken from onshore and offshore publications.



Gilotti and Hull (1993) disagreed with published geological maps and observed the same rock type on either side of the HSF, suggesting that displacements could not be large along the HSF. Sinistral strike-slip, ductile shear zones in the BGC of SW Fosen are dated at 389 ± 6 and 386 ± 6 Ma (Rb-Sr, muscovite), which are thought to be broadly contemporaneous with early movements along the MTFC and late-orogenic extensional collapse (Piasecki and Cliff 1988; Séranne 1992b; Roberts 1998a). Krabbendam and Dewey (1998) suggested that sinistral transtension was partially partitioned within the WGR with increasing transtensional angle towards the MTFC, invoking a purely sinistral strike-slip component along the MTFC during Early-Mid Devonian times. Braathen et al. (2000) suggested that north of the MTFC, bi-directional, opposed extension led to exhumation of the BGC whereas to the south unidirectional (top-W) extension dominated. As a result, Braathen et al. (2000) inferred that the MTFC formed as a sinistral strike-slip transfer structure between the W-dipping Høybakken and NE-dipping Kollstraumen extensional detachments to the southwest and northeast respectively (Figure 5.8). Séranne (1992b) suggested that during sinistral strike-slip movements, Devonian basins formed in extensional detachments within the releasing bends of the MTFC.

Later brittle deformations have been described as Late Devonian / Early Carboniferous, Permian, Late Jurassic / Early Cretaceous and Late Cretaceous / Early Tertiary based upon isotopic (Sm-Nd, K-Ar), fission track dating and palaeomagnetic studies (Table 5.2; Torsvik et al. 1989; Grønlie and Torsvik 1989; Grønlie et al. 1994; Smith 1995).

Grønlie and Roberts (1989) and Grønlie et al. (1991) have carried out the only detailed field studies to date along the MTFC. Landsat™ interpretation of lineaments combined with analysis of aerial photographs and geological maps suggested a complex array of anastomosing faults, which display a geometric configuration of a dextral strike-slip fault zone (Grønlie and Roberts 1989). Doré et al. (1997a) argued that the mapped geometry is consistent with sinistral strike-slip movements along the MTFC. Grønlie and Roberts (1989) and Grønlie et al. (1991) recognised an initial, ductile, sinistral strike-slip event overprinted by brittle sinistral strike-slip structures. It has been assumed that the brittle sinistral event is roughly of the same age as ENE-

WSW trending faults that cut lithified Devonian sedimentary rocks N of the MTFC within the Bjugn Basin (Séranne 1992b; Roberts 1998a).

There are two main fault strands of the MTFC, the Verran Fault (VF) to the south and the Hitra-Snåsa Fault (HSF) to the north (Figure 5.2). Both structures trend ENE-WSW and are sub-vertical (Grønlie and Roberts 1989; Grønlie et al. 1991; Séranne 1992b; Roberts 1998a). Fault rocks along the HSF comprise mylonites overprinted by small-scale recrystallised breccias with quartz and epidote veining (Grønlie and Roberts 1989). Along the VF 'crush zone', quartz-epidote breccias are cut by prehnite-matrixed cataclasites which, in turn, are cut by extensive zeolite and calcite veining associated with brecciation (Grønlie and Roberts 1989). Grønlie et al. (1991) described clasts of mylonite within cataclasites and N-S-trending pseudotachylites along the VF, while Séranne (1992b) described extensive mylonites along the VF (SW Fosen) indicating a dextral sense of shear.

5:3:2 The MTFC offshore

The MTFC defines the coastline of Central Norway between 64 and 62° N and extends offshore to define the southern margin of the Møre Basin and the northern margin of the Viking Graben, suggesting that the MTFC played an important role in the architecture of these Mesozoic basins (Figure 5.10).

5:3:2:1 Beitstadfjorden Basin

The Beitstadfjorden Basin (BB) is located in the hangingwall of the SE-dipping VF on the Fosen Peninsula (Figures 5.2; 5.10). Coal fragments found on the north side of Beitstadfjorden yield a Middle Jurassic age and are thought to be derived from the floor of Beitstadfjorden during Quaternary glaciation (Kjerulf 1870; Vigran 1970). Based on seismic reflection and refraction profiles Oftedahl (1972, 1975) inferred a 600-700m-thick Jurassic sequence unconformably overlain by 200-300m of sedimentary rocks interpreted to be Cretaceous-Tertiary. Bøe and Bjerkli (1989) interpreted the upper unit to be Quaternary glacial deposits lying unconformably upon a 250m-thick Jurassic sequence (Figure 5.11). No Cretaceous or Tertiary fragments

have been found along the shores of Beitstadfjorden (Bøe and Bjerkli 1989). There are two main fault orientations, ENE-WSW and NNE-SSW (Figure 5.11). To the northwest, the ENE-WSW basin-bounding fault is the VF (Figure 5.12). Up to 250m of Jurassic strata are present adjacent to the VF, which downthrows to the SE (Figure 5.11; Bøe and Bjerkli 1989). There is no thickening of strata towards the fault, suggesting that fault movement is post-Middle Jurassic (Figure 5.11). The NNE-SSW striking faults appear to transect the VF (Figure 5.12). A fault offsetting the VF near Follafooss, extends to the north where a 200m sinistral strike-slip displacement has been recognised (Bøe and Bjerkli 1989). In the north of the basin, open to gentle folds strike N-S to NE-SW and appear to be truncated by the VF (Figure 5.12; Bøe and Bjerkli 1989). Along the western, southeastern and eastern margins of the Beitstadfjorden basin, the Jurassic sequence lies unconformably upon basement rocks (Figure 5.12). Bøe and Bjerkli (1989) suggested that Late Jurassic to Early Cretaceous, dip-slip normal faulting was followed by dextral strike-slip faulting, evidenced by N-S- to NE-SW-trending open folds together with sinistral strike-slip movements along NNE-SSW trending faults. Bøe and Bjerkli (1989) stated that the folds were cut by the VF and suggested the possibility of Cretaceous to Early Tertiary faulting.

5:3:2:2 Edøyfjorden Basin

The Edøyfjorden Basin is situated to the south of Smøla along the north side of the MTFC (Figure 5.10). Mesozoic rocks in the Edøyfjorden basin are separated from the overlying Quaternary sequence by an angular unconformity. The thickness of the Quaternary sequence varies from several metres to c. 150m. On the southeast side of Edøyfjorden, the Mesozoic sequence is downthrown along a NE-SW-trending fault with an orientation c. 060/60N, which may be the offshore continuation of the HSF (Figures 5.13, 5.14; Bøe and Bjerkli 1989). 500m to the southeast, another fault with a similar orientation is present, possibly the offshore continuation of the VF (Bøe and Bjerkli 1989). A dip-slip normal throw on the HSF could be 1km or more, but the exact amount cannot be determined due to limited seismic penetration. A similar displacement is observed on the bounding fault to the southeast (possibly VF) (Figure 5.14; Bøe and Bjerkli 1989). The maximum thickness of the Mesozoic sequence is c.800-1000m within the axis of the basin.

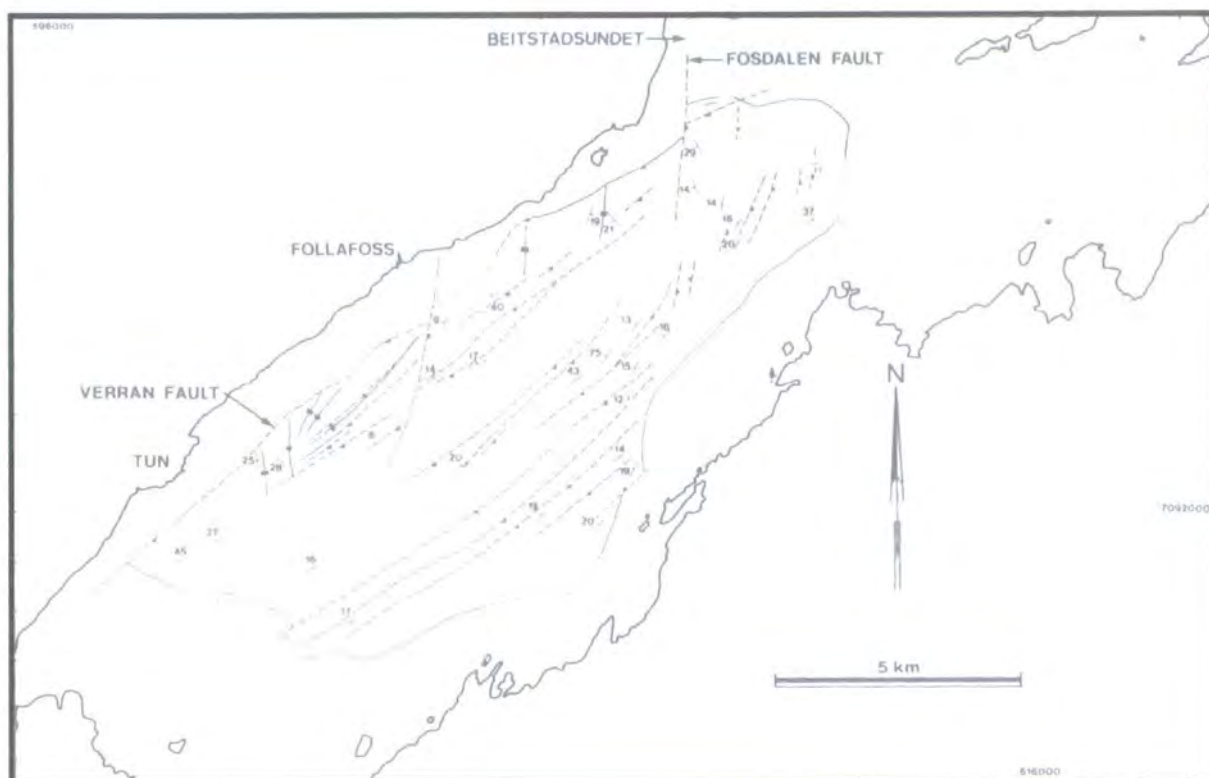


Figure 5.12 Structural map of the top Mesozoic within Beitstadsfjorden (after Bøe and Bjerkli 1989).

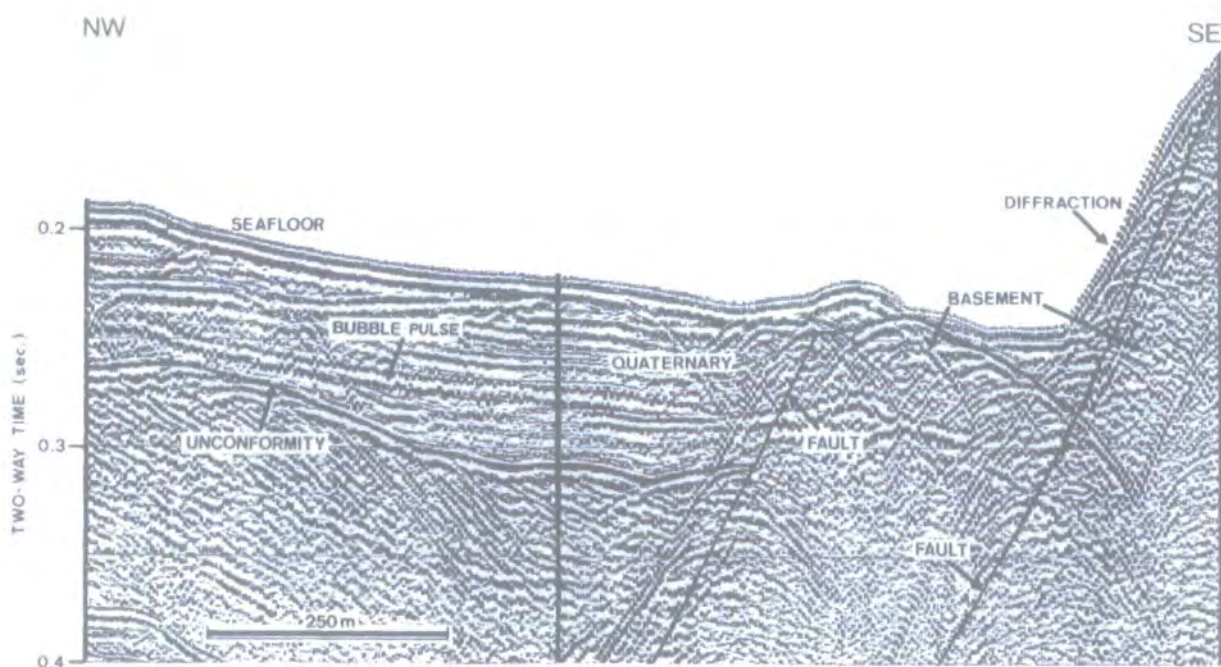


Figure 5.13 Seismic section through the southeast margin Edøyfjorden basin (after Bøe and Bjerkli 1989).

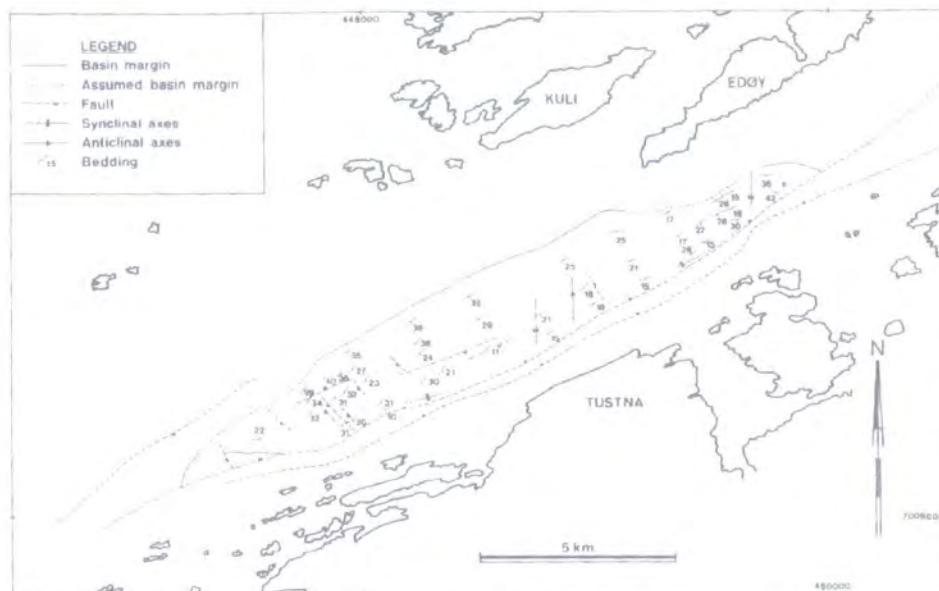


Figure 5.14 Structural map of top Mesozoic within Edøysfjorden (after Bøe and Bjerkli 1989).

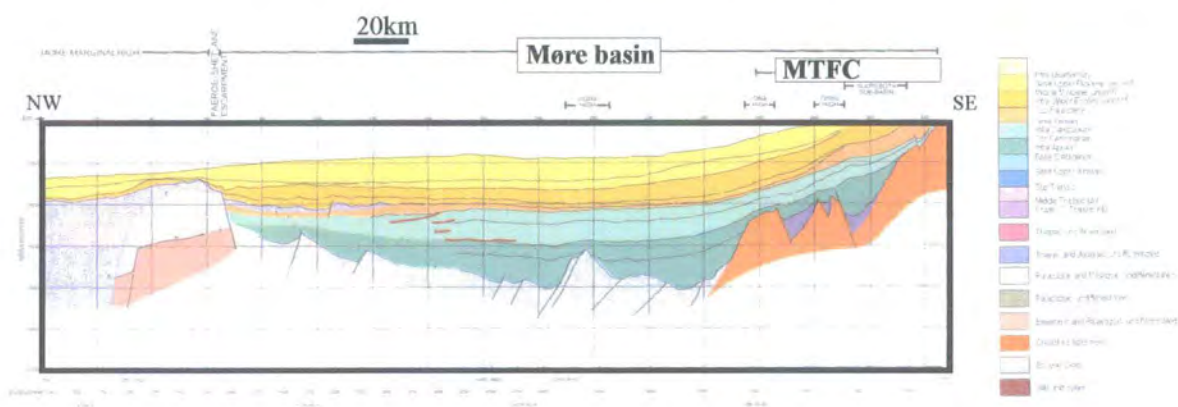


Figure 5.15 NW-SE cross-section through the Møre Basin (after Brekke 2000).

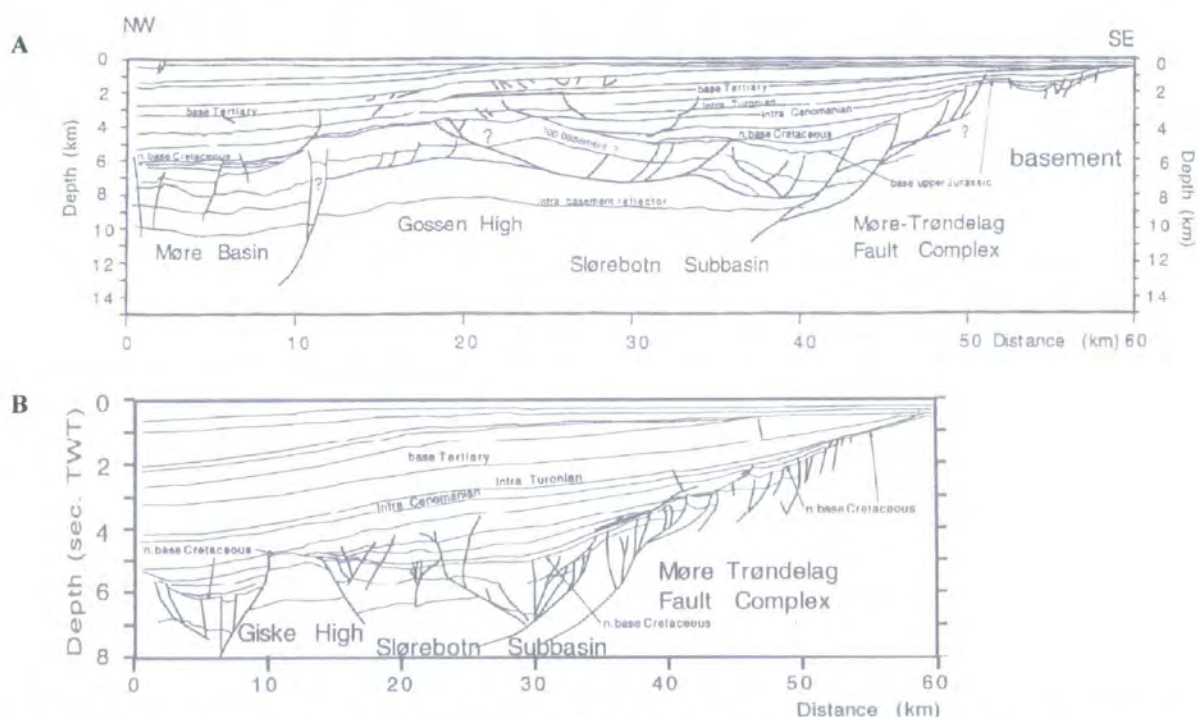


Figure 5.16 NW-SE sections through (A) MTFC, Slørebotn Subbasin, Gossen High and southeast margin of MB and (B) MTFC, Slørebotn Subbasin and Giske High (after Grunnaleite and Gabrielsen 1995).

The Mesozoic rocks contain gentle to open N-S-to ENE-WSW-trending folds (Figure 5.14; cf. Figure 5.12). Close to the basin-bounding faults, fold axes are rotated from N-S to ENE-WSW (Figure 5.14). There is no thickening of strata or soft sedimentary structures close to the major faults, suggesting that fault movements were not syndepositional (Bøe and Bjerkli 1989). Bøe and Bjerkli (1989) suggested that dip-slip normal displacements occurred, with a maximum downthrow near the centre of the basin, followed by dextral strike-slip movement.

5:3:2:3 Møre Basin

The Møre Basin (MB) is an elongate, NE-SW-striking Cretaceous basin (Figure 5.10). The MB is bounded to the southeast by the MTFC (Figure 5.10). Its northern boundary is diffuse and is separated from the Vøring Basin at the Jan Mayen lineament. To the west, the MB terminates against the Møre Marginal High, the oceanward margin which corresponds to the Faroe-Shetland Escarpment (Figure 5.15). To the south, the northernmost part of the Viking Graben delimits the MB (Figure 5.10; Grunnaleite and Gabrielsen 1995).

The MB is defined at its base by the base Cretaceous unconformity and contains up to 6km of Cretaceous stratigraphy in the axial parts of the basin (Brekke 2000). The base Cretaceous unconformity truncates a topography of rotated fault blocks formed during Late Middle-Jurassic to Early Cretaceous rifting, which define sub-basins and intra-basinal highs (Figure 5.15; Grunnaleite and Gabrielsen 1995). Cretaceous sediments onlap the base Cretaceous unconformity along the western and eastern margins of the basin, suggesting that the MB was formed by thermal subsidence or downwarping of its flanks after the Late Middle Jurassic to Early Cretaceous rifting event (Figure 5.15; Brekke 2000). The greater dip of strata along the eastern margin is a combination of downflexing in Early Cretaceous times and Late Tertiary uplift of the adjacent mainland (Brekke 2000). The deepest parts of the MB were highly elevated and subject to erosion during the Mid Jurassic (Brekke 2000). Minor faulting related to Late Cretaceous-Palaeocene extension has been recognised in the MB (Doré et al. 1997a). The Paleocene section thickens to the west before being obscured by thick flow basalts associated with the opening of the North Atlantic (Doré et al. 1997a). The Cretaceous and Tertiary strata are affected by reverse faults

and gentle folding related to two phases of compression during the Tertiary (e.g., Eocene-Early Oligocene, Miocene-Pliocene; Doré et al. 1997a, 1997b).

The MTFC bounds the southeast margin of the MB and acts as a transitional zone between the narrow, shallow, basement platform parallel to the Møre coast, and the deep MB (Figure 5.16). The MTFC comprises a broad, NE-SW- to ENE-WSW-trending system of fault-controlled ridges, highs and minor basins (Brekke 2000). Wells drilled into the highs (e.g., Gossen and Giske; Figure 5.16) show crystalline basement overlain by a thin Middle Jurassic sequence beneath post-Middle Cretaceous rocks (Brekke 2000). Thin Jurassic and possibly Triassic strata are consistent with there being a shallow basement beneath the Late Jurassic and Early Cretaceous basin fill of the MB (Brekke 2000). This set of basement highs and minor basins possibly originated as a system of half-grabens in Triassic times (Brekke 2000). Post-Caledonian subsidence probably occurred during Permo-Triassic and Late Jurassic-Early Cretaceous times (Table 5.2; Grunnaleite and Gabrielsen 1995).

The MTFC is thought to comprise one or two listric main faults with many synthetic faults branching up into the hangingwall (Figure 5.16). The listric faults or detachments are thought to sole out at depths of 15km (Grunnaleite and Gabrielsen 1995). The vertical throw of the near base Cretaceous is c.5km with the relief of the basin margin exaggerated by post-tectonic differential subsidence and rotation (Grunnaleite and Gabrielsen 1995). This displacement corresponds to late Mid Jurassic to Early Cretaceous rifting, as post-Lower Cretaceous sedimentary rocks onlap onto truncated fault blocks (Figure 5.16). Antithetic normal faults, which strike sub-parallel to the main MTFC, formed marginal platform highs during late Middle Jurassic to Early Cretaceous rifting (e.g., Gossen and Giske Highs, Figure 5.16).

Inversion occurred during the Early Cretaceous (Grunnaleite and Gabrielsen 1995; Bøe and Bjerkli 1998) as indicated by reactivated normal faults, folding and stratigraphic relationships across the faults. Minor offsets are seen in the Upper Cretaceous sequence with the youngest reflector to be cut being the intra-Turonian (Figure 5.16). Rotated extensional faults in the Lower Tertiary (Palaeocene) sequence are common above the MTFC (Grunnaleite and Gabrielsen 1995). The entire Upper Cretaceous and Lower Tertiary section is tilted above the MTFC, related to Mid

Tertiary inversion (Eocene-Early Oligocene, Miocene-Pliocene) (Caselli 1987; Surlykk 1990; Grunnaleite and Gabrielsen 1995; Doré and Lundin 1996; Doré et al. 1997b; Bøe and Skilbrei 1998). Some faults cross-cut the entire Cretaceous-Tertiary and Quaternary sequences with some vertical offsets of the seabed found above the inner part of the MTFC (Grunnaleite and Gabrielsen 1995). Several authors have stated that the MTFC is still tectonically active offshore (Ringdal 1983; Bungum et al. 1991; Lindholm et al 1995), with a concentration of earthquakes along the southern margin of the MB.

Chapter 6. The Møre-Trøndelag Fault Complex

As noted in Chapter 5, the ENE-WSW-trending Møre-Trøndelag Fault Complex (MTFC) is a 10-20km-wide, steeply dipping zone of fault-related deformation on the Fosen Peninsula, Central Norway (Grønlie and Roberts 1989; Grønlie et al. 1991, 1994). The MTFC comprises two major fault strands, the Hitra-Snåsa Fault (HSF) to the north and the Verran Fault (VF) to the south. Both are sub-vertical structures striking ENE-WSW. The principal faults are well exposed north of Verrasundet, with several cross-sections through key parts of the fault zone (Figure 6.1). The aim of this chapter is to describe the kinematic and structural evolution of the MTFC. In the following sections, Landsat™ image interpretation, regional structure, fault rock distribution and field relationships will be described. Fault rock microstructures, textures and dating are described in Chapter 7.

6.1 Landsat™ interpretation of the Møre-Trøndelag Fault Complex (MTFC)

The Landsat™ image of the Fosen Peninsula (Figure 6.2) illustrates the kilometre-scale geometry of the MTFC. The two major, bounding lineaments, the HSF and the VF are approximately 11km apart in the southwest and 5km apart in the northeast on the Fosen Peninsula. Both to the north and to the south of the MTFC, the orientation of major lineaments is different than within the complex itself (Figure 6.2). Within the MTFC, the major lineaments strike ENE-WSW, NNE-SSW and NE-SW (Figures 6.2, 6.3). ENE-WSW lineaments are parallel to the main bounding structures (HSF, VF) and are linked by a series of en-échelon NNE-SSW and NE-SW lineaments (Figures 6.2; 6.3), although no single structure links the VF and HSF directly. The MTFC is transected by several NNW-SSE lineaments along which no offsets are observed (Figures 6.2, 6.3).

The HSF is defined by a strong ENE-WSW-trending lineament that links into many equally spaced, NE-SW-trending lineaments which die out several kilometres to the SW (Figures 6.2, 6.3).

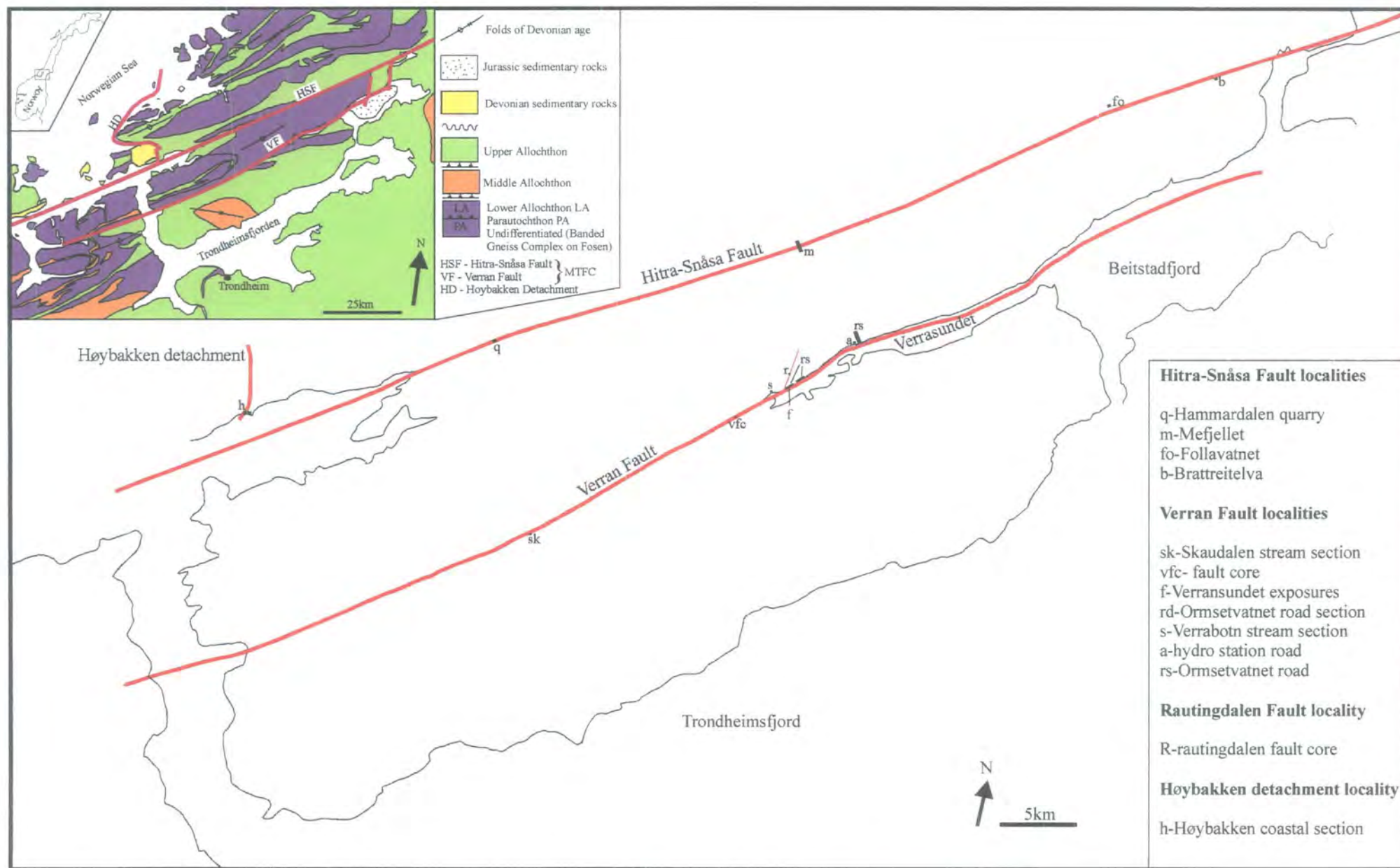


Figure 6.1 Map to show position of localities used during this study. Inset - simplified geological map of the Fosen Peninsula.

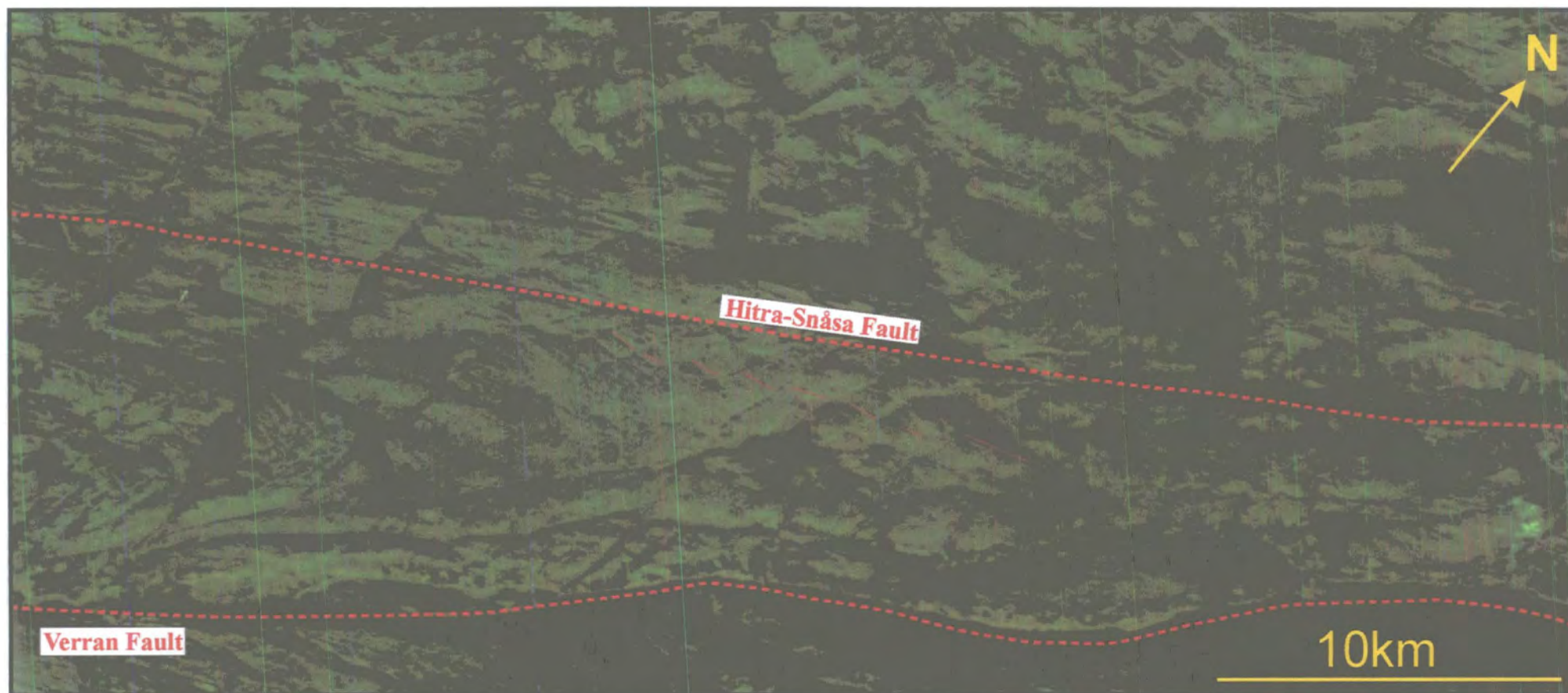


Figure 6.2 Landsat™ image of the Møre-Trøndelag Fault Complex on the Fosen Peninsula, Central Norway. Fine solid red lines represent rotated foliation trends on the northwest side of NE-SW-orientated lineaments splaying from the HSF.

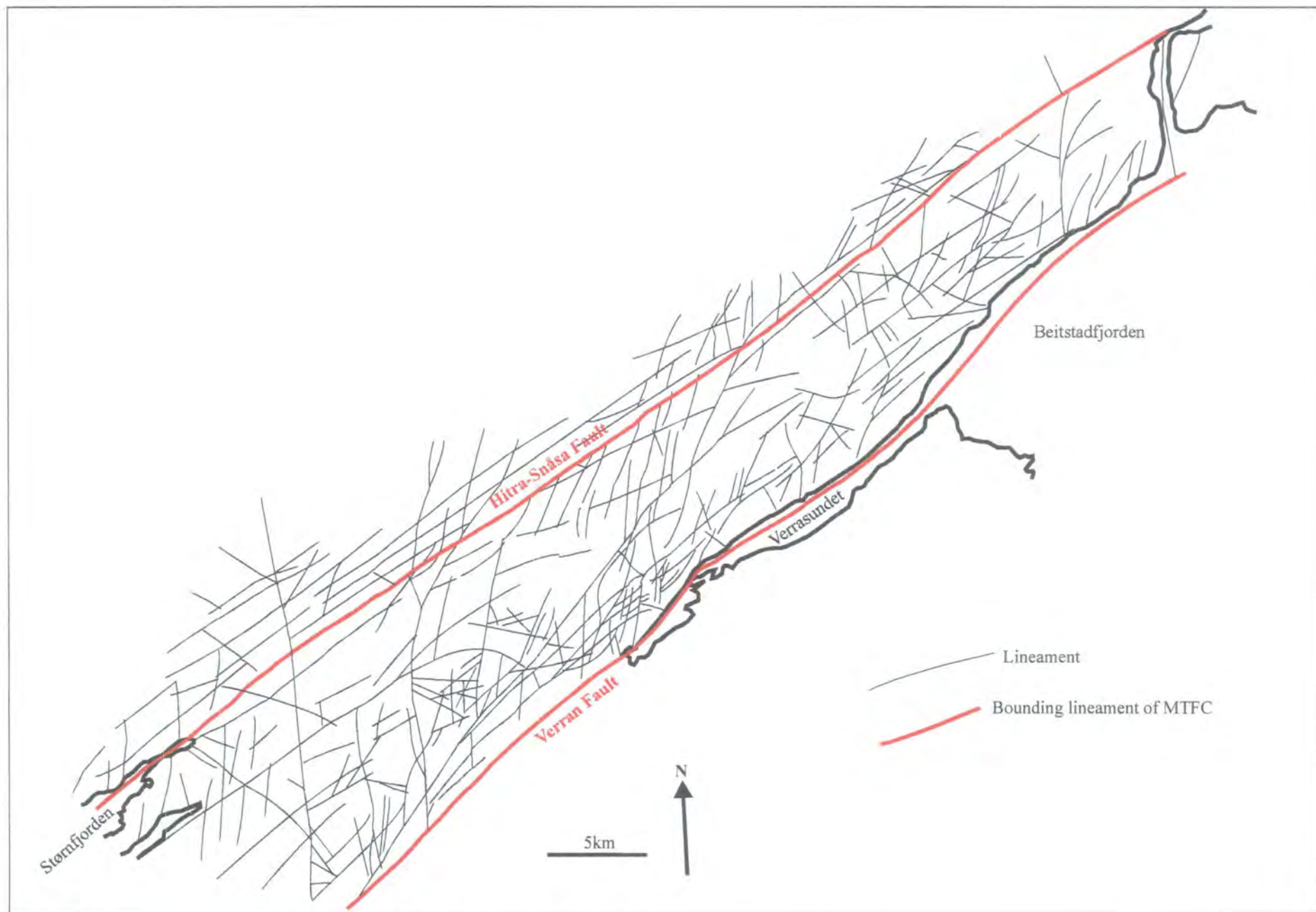


Figure 6.3 Landsat interpretation of the MTFC on the Fosen Peninsula, northwest of Trondheimsfjord.

Near the central part of the HSF between Størnfjorden and Beitstadfjorden, the ENE-WSW-trending fabric has been rotated clockwise to E-W on the NW side of NE-SW-trending lineaments, which link into the main structure (fine red lines; Figure 6.2). This geometry is consistent with an apparent sinistral sense of shear.

The VF comprises an ENE-WSW-trending lineament that defines the coastline of Beitstadfjorden and Verransundet (Figure 6.3). NNE-SSW-trending lineaments splay from the VF and curve into a series of ENE-WSW lineaments farther north (Figures 6.2, 6.3). Both the VF and the parallel lineaments to the north display an anastomosing geometry resembling a strike-slip duplex (Figure 6.2).

6:2 Regional structure across the MTFC

The aim of this section is to describe briefly the regional structure of the study area to illustrate how fault-related deformation can be distinguished from regional deformation and metamorphism. Protolith fabrics are strongly annealed and are differentiated from fault-related fabrics using thin-section observations.

6:2:1 Protolith lithology

Compositionally banded gneisses of the Banded Gneiss Complex of Fosen are exposed to the north of the VF (Figure 6.1; section 5:1:2:1). The gneisses in the study area are derived from Proterozoic granitic-tonalitic orthogneisses which were intruded by a series of Ordovician to Early Silurian diorites and granites. Both the orthogneisses and the intrusions have been highly reworked into strongly banded L-S tectonites (Roberts 1998a) during Scandian deformation and metamorphism. Due to the intense deformation and metamorphism it is generally impossible to tell the protolith orthogneisses, granites and diorites apart.

The gneisses are pink / grey in colour, fine to coarse grained and equigranular with a grain size ranging from 0.5 to 1cm in length. The gneisses comprise potassium feldspar, plagioclase feldspar and quartz as the main constituents, accounting for

approximately 70 to 80% of the rock. Grains of plagioclase are albitic, while K-feldspar occurs as microcline and perthitic orthoclase. K-feldspar appears to be more abundant than plagioclase, although this may be due to the fact that throughout the rock plagioclase is preferentially replaced by retrograde epidote. Epidote, chlorite, biotite, muscovite, hornblende and sphene make up approximately 20 to 30% of the rock together with accessory magnetite and pyrite. The relative abundance of the minerals varies spatially and reflects chemical variations in protolith composition and metamorphic grade. Quartz-rich layers are interlayered on a millimetre-scale with feldspar-rich bands. The gneisses contain an ENE-WSW-trending, sub-vertical fabric defined by flattened aggregates of quartz and feldspar with a well-developed, sub-horizontal lineation defined by aligned grains of feldspar and quartz.

It is unclear which tectonostratigraphic unit the gneisses belong to. This is because the abundance of Precambrian gneiss within the Lower Allochthon in the Fosen area makes it virtually impossible to distinguish this unit from the underlying parautochthonous gneisses, due to the intense, overprinting, Scandian deformation and metamorphism in the study area (Figure 6.1; see section 5:1:2:1).

6:2:2 Mefjellet to Trong Sundet traverse

The Mefjellet to Trong Sundet traverse (located in Figure 6.4) is orientated perpendicular to the VF and HSF to show the variation in gneissose fabrics and regional structure. In plan view, the gneissose foliation trend swings from ENE-WSW on the north side of Trong Sundet to NW-SE on the southern shores of Ormsetvatnet. To the north, the foliation swings from NW-SE to an ENE-WSW orientation over a distance of 3.5km (Figure 6.4). Over the whole traverse the lineation, defined by elongate quartz and feldspar grains, plunges shallowly to the ENE. A cross-section orientated NW-SE demonstrates the regional folding of the gneissose foliation into an antiform (Figure 6.5). The poles to the foliation planes lie along a girdle with the β -axis representing the fold hinge orientation. The orientation of the fold hinge is sub-parallel to the mineral stretching lineation, which plunges shallowly to the ENE.

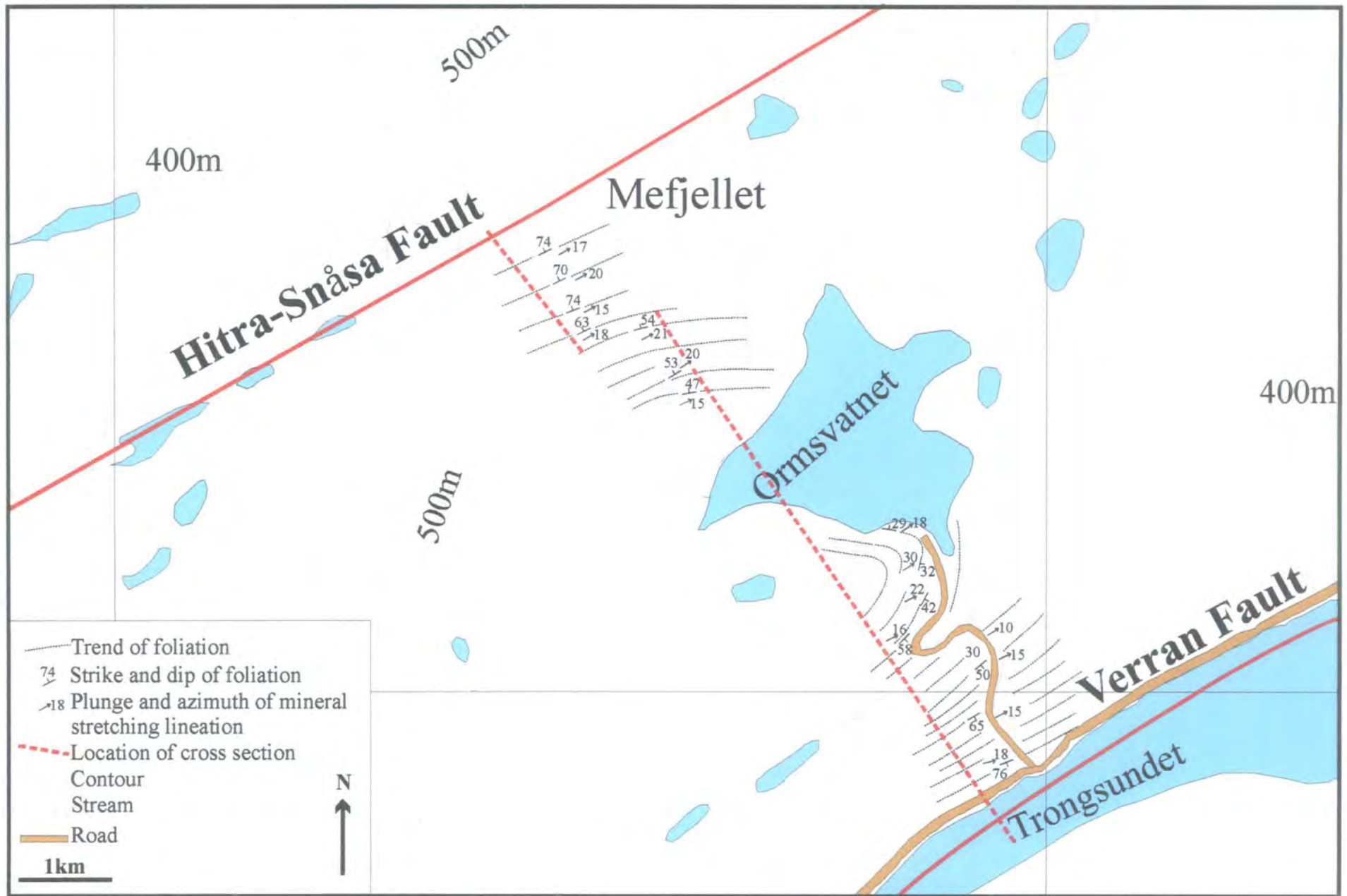


Figure 6.4 Map to show the location of cross-section (Figure 6.5), foliation and lineation between Trongsundet and Mefjellet.

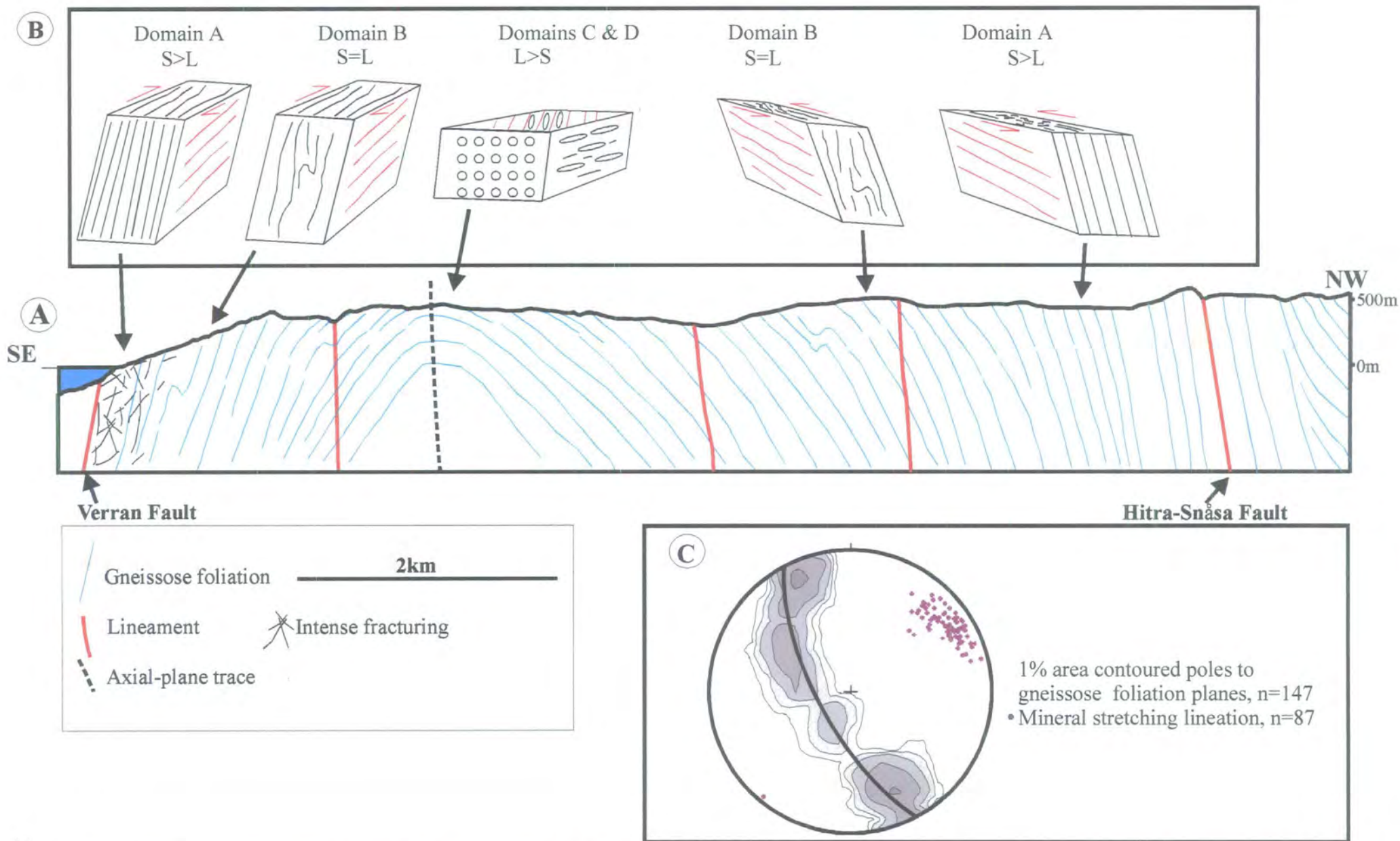


Figure 6.5 (A) Cross-section across the MTFC from Trongsundet to Meffjellet (Figure 6.4). (B) Schematic diagrams to illustrate tectonite fabrics in structural domains around fold. (C) Stereographic projection to show gneissose foliation and mineral stretching lineation.

Four main structural domains have been recognised through the fold (Figure 6.6). The domains are each characterised by differences in structure, fabrics and metamorphic grade.

6:2:2:1 Domain A

Domain A is characterised by strongly foliated gneisses displaying S>L tectonite fabrics on both the NW and the SE limb of the fold (Figure 6.6; Plate 6.1). The gneisses in Domain A comprise feldspar (50%), quartz (20%), chlorite (10%), epidote (10%), muscovite (5%) and sphene (<5%), together with accessory magnetite and pyrite. The gneisses within Domain A comprise quartz-rich bands interlayered on a millimetre-scale with feldspar-rich bands. Disseminated grains of epidote and aligned mica are present throughout the rock. The foliation is defined by flattened aggregates of feldspar and quartz and trends ENE-WSW, dipping steeply to the NW and SE, respectively, on each fold limb (Figure 6.7). Within domain A on both fold limbs, the lineation defined by elongate quartz and feldspar grains is orientated parallel to the fold hinge which plunges shallowly to the ENE (Figure 6.7). Centimetre-scale kink folds display a dextral sense of vergence on the SE limb and a sinistral sense of vergence on the NW limb. On surfaces viewed parallel to the sub-horizontal lineation defined by elongate quartz and feldspar grains and normal to foliation planes, feldspar augen are locally developed. On the NW limb, augen show σ -type geometries consistent with sinistral shear and on the SE limb σ -type augen are consistent with dextral shear (Figure 6.6). Centimetre- to metre-thick amphibolite sheets occur locally, and lie parallel to the gneissose foliation.

6:2:2:2 Domain B

Domain B is characterised by layered gneisses which display S=L tectonite fabrics (Figure 6.6; Plate 6.2). The gneisses in Domain B comprise feldspar (50%), quartz (20%), epidote & clinozoisite (10%), chlorite (5%), muscovite (5%), hornblende (5%) and sphene (<5%), together with accessory magnetite and pyrite. On a millimetre-scale the gneisses consist of interlayered quartz-rich and feldspar-rich bands. Aligned mica, hornblende and sphene grains, together with epidote and clinozoisite, are disseminated throughout the rock.

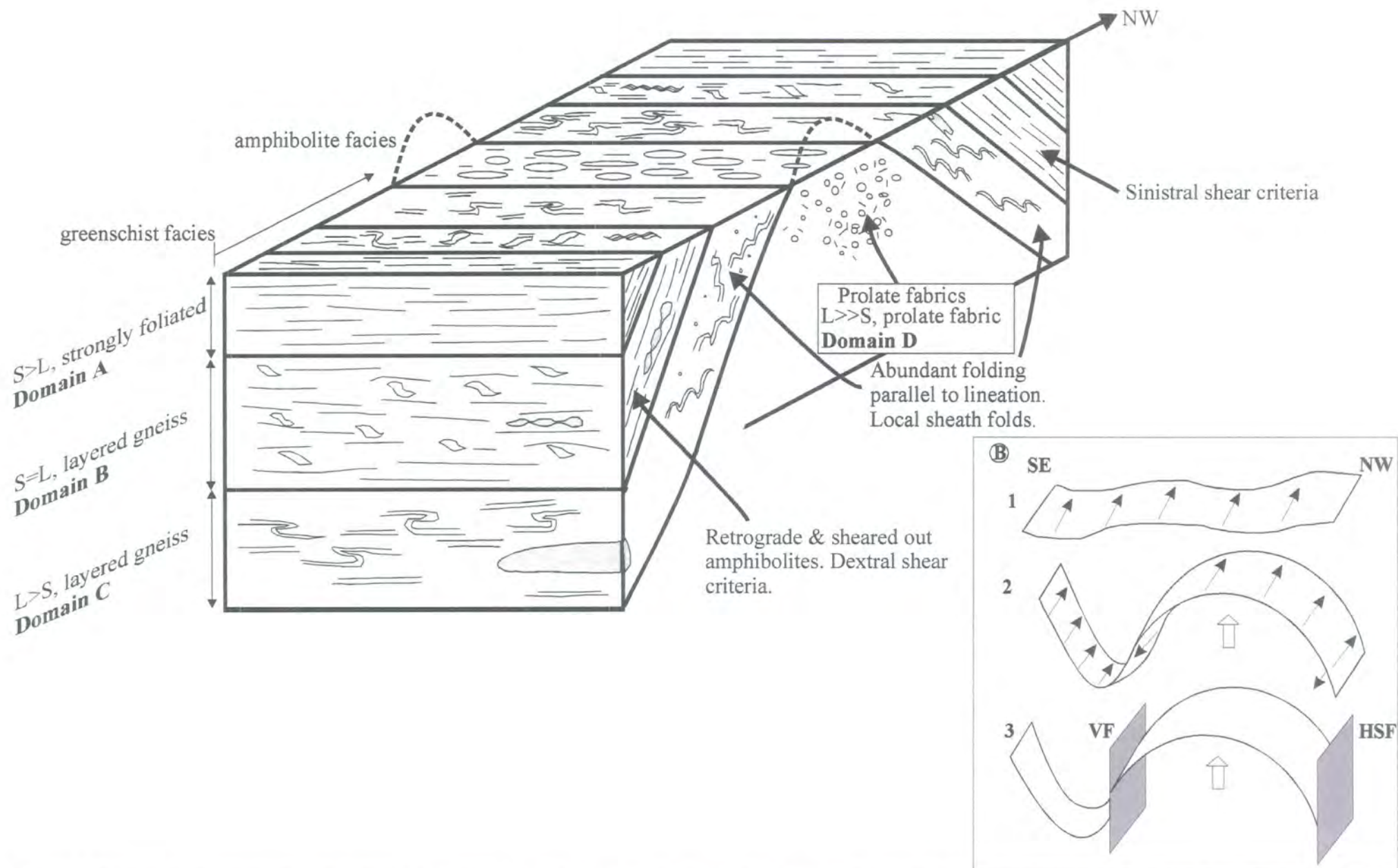


Figure 6.6 Not to scale. Schematic diagram to show the gneissose fabrics and structures associated with the regional-scale antiform between Trongsundet and Mefjellet. (B) Inset. Schematic diagram to show the evolution and development of the fold. 1. low-angle top-SW shear. 2. constrictional strain during sinistral transtension leads to upright folding parallel to the transport direction. 3. the HSF and VF are superimposed on the regional structure.



Plate 6.1 (A) Cross-sectional view to show strong gneissose foliation viewed in XY plane within Domain A on SE fold limb. (B) Plan view to show strong linear fabric with feldspar augen consistent with dextral shear in XZ plane (Domain A, SE fold limb).

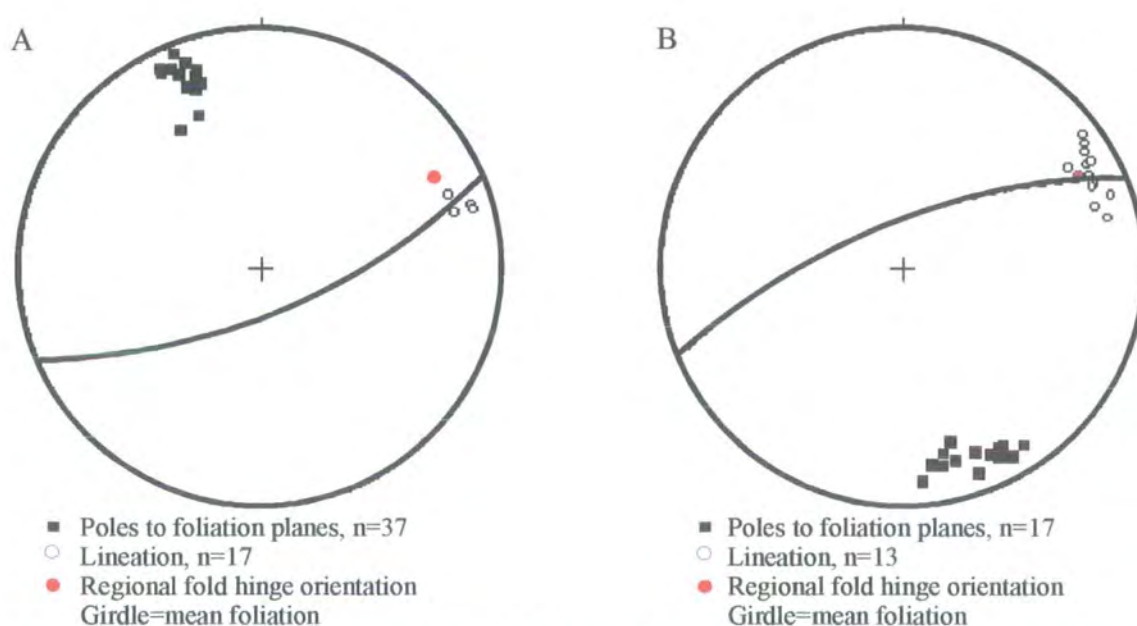


Figure 6.7 Stereographic projections to show foliation and lineation within Domain A from (A) SE fold limb and (B) NW fold limb.

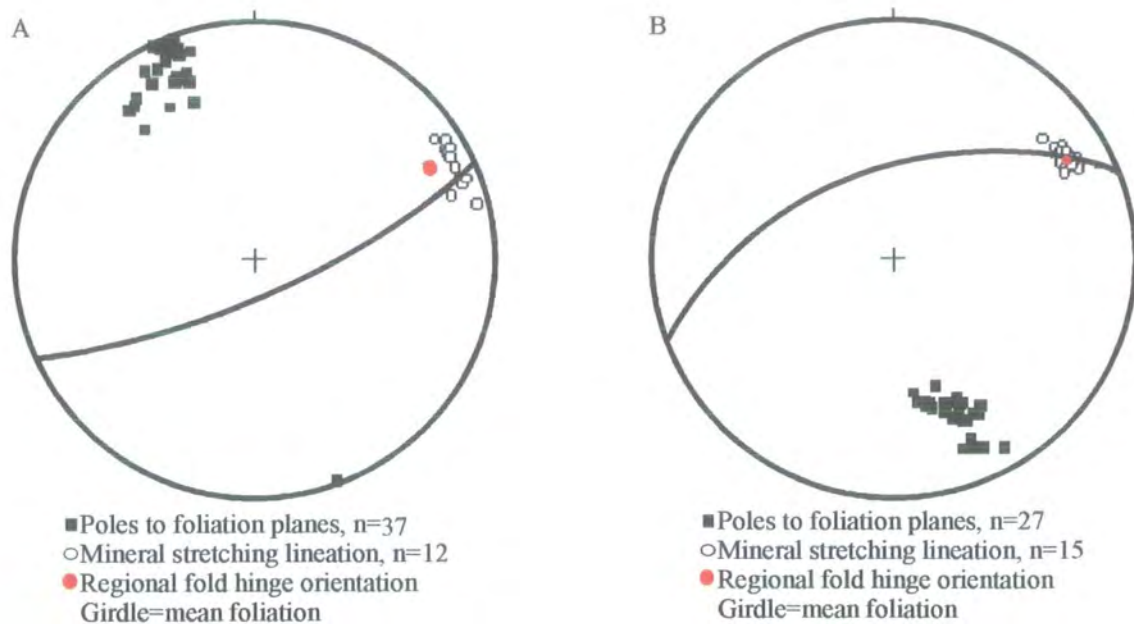


Figure 6.8 Stereographic projections to show gneissose foliation and lineation from Domain B. (A) SE fold limb and (B) NW fold limb.

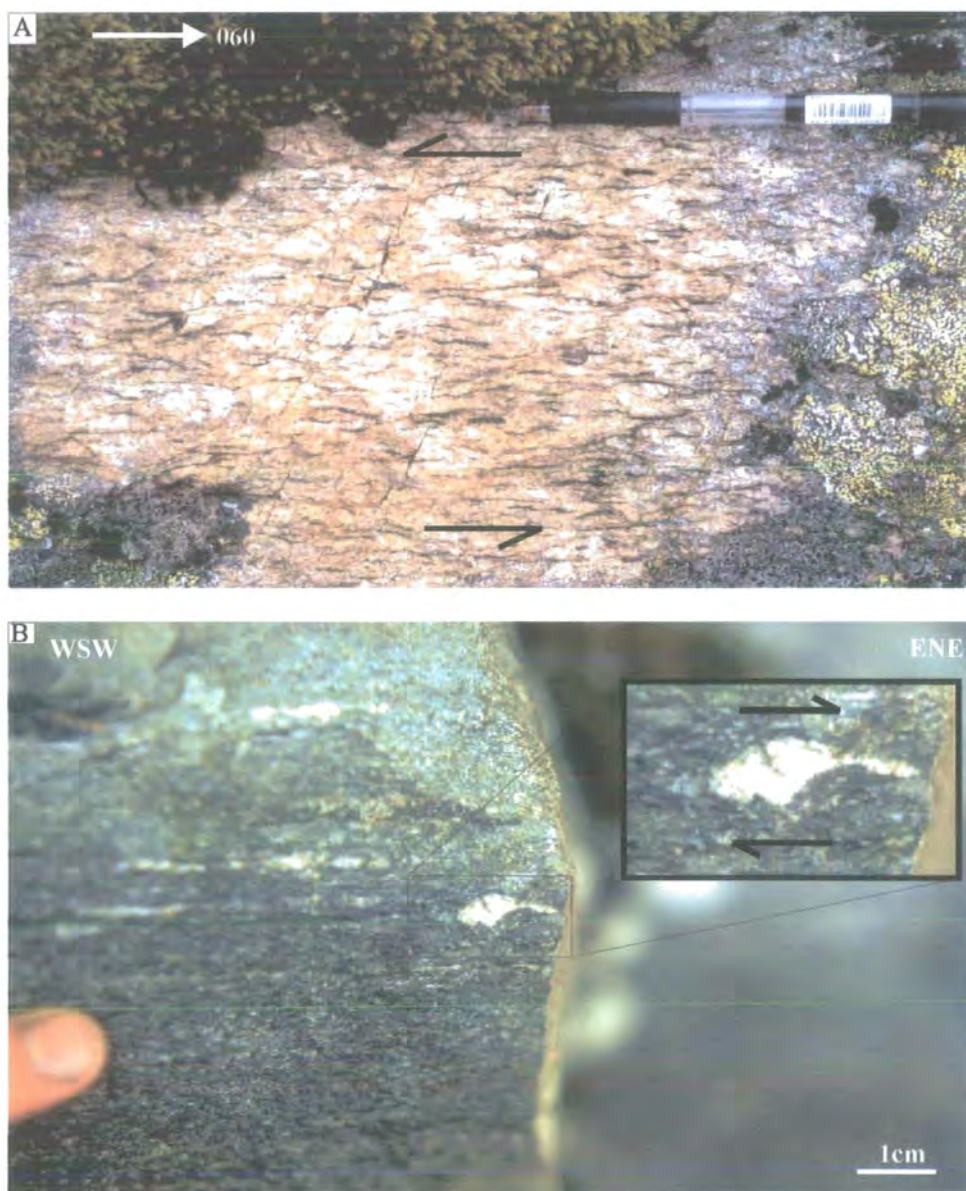


Plate 6.2 Plan view images parallel to lineation to show gneissose fabric in Domain B. (A) Coarse-grained gneissose fabric with some shear bands indicating sinistral shear, NW fold limb. (B) Fine-grained gneissose fabric with σ -type feldspar porphyroclast consistent with dextral shear, SE fold limb.

Foliation defined by flattened aggregates of feldspar and quartz trends ENE-WSW and dips steeply to the NW and SE, respectively, on each fold limb (Figure 6.8). Lineations defined by elongate quartz and feldspar are parallel to the fold hinge, which plunges shallowly to the ENE (20/062). On the NW fold limb, outcrop surfaces viewed parallel to the lineation and normal to the foliation (XZ plane) display poorly developed, centimetre-scale, shear bands, consistent with sinistral shear within coarse-grained layered gneiss (Plate 6.2A). On the SE fold limb, outcrop surfaces viewed parallel to the lineation and normal to the foliation (XZ plane) display σ -type feldspar porphyroclasts consistent with dextral shear (Plate 6.2B). Amphibolite sheets have been retrograded and sheared to aggregates of chlorite, biotite, epidote and quartz. The sheared amphibolites are typically 10-30cm thick and display well-developed, centimetre-scale, S-C' fabrics which are consistent with dextral shear. The shear bands are defined by fine-grained chlorite, suggesting that shearing took place under greenschist-facies conditions. Thus, the pattern of opposed dextral and sinistral shear on opposite limbs is the same as in Domain A.

6:2:2:3 Domain C

Domain C is characterised by layered gneiss which displays L>S tectonite fabrics (Plate 6.3). The gneisses in domain C comprise feldspar (50%), quartz (20%), biotite (10%), epidote (10%), muscovite (5%), sphene (<5%) and minor amounts of clinozoisite, garnet and kyanite. Millimetre-thick alternating bands rich in feldspar, quartz and hornblende define a foliation, with the lineation defined by quartz and feldspar rods. In thin-sections cut parallel to the lineation and normal to the foliation, garnet grains are boudinaged in an ENE-WSW trend and overgrown by chlorite fibres. ENE-WSW-trending muscovite fibres overgrow clinozoisite grains. Myrmekite textures are also common within Domain C. The foliation displays upright folding with the poles to foliation lying along a girdle (Figure 6.9). Lineations plunge shallowly to the NE (mean=20/050) and appear to be anticlockwise of the mean fold hinge orientation (20/062). Centimetre- to metre-scale, tight to isoclinal folds are common within Domain C. The fold axes appear to be parallel to the lineation. Fold structures on the SE fold limb display 'Z' vergence patterns within cross-sectional surfaces viewed normal to the foliation and lineation, indicating an antiformal structure to the northwest.

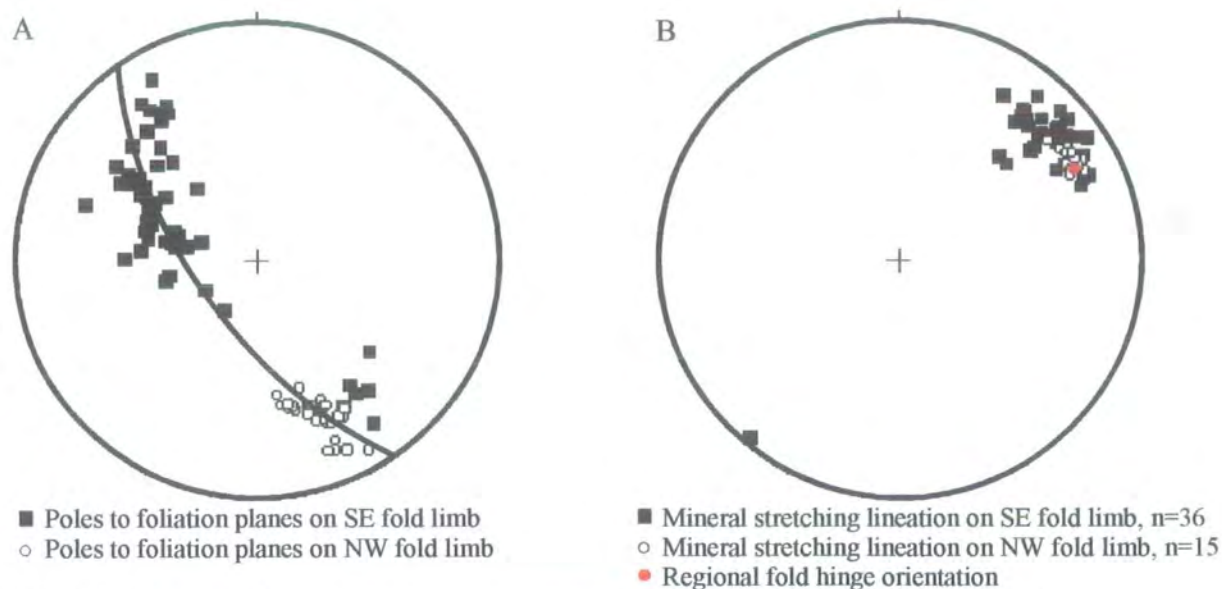


Figure 6.9 Stereographic projections to show gneissose foliation and lineation within Domain C.

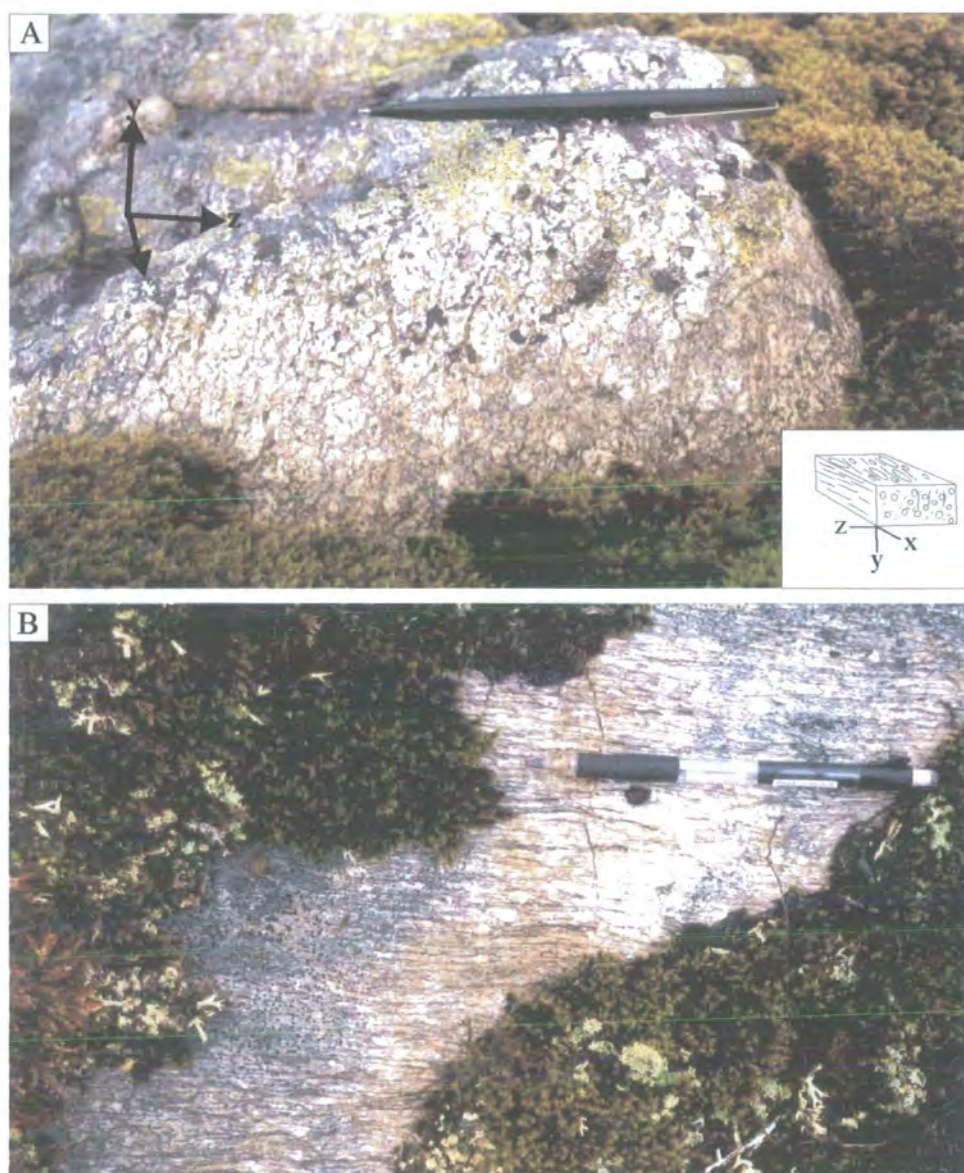


Plate 6.3 (A) Cross-sectional view (YZ plane) to show virtually no fabric elements in this section. Prolate feldspars display circular shapes in cross-section, Domain C, NW fold limb.. (B) View parallel to lineation to show strong L-fabric of feldspar augen within gneiss, Domain C, NW fold limb. (A) & (B) illustrate a layered gneiss with an L>S tectonite fabric.

On the NW fold limb, centimetre-scale folds display 'S' vergence patterns indicating an antiform to the southeast, when viewed in cross-sectional surfaces normal to the foliation and lineation. No axial planar fabric was observed associated with these structures in the field.

6:2:2:4 Domain D

Domain D is characterised by augen gneiss with $L \gg S$ tectonite fabrics and represents the core of the antiform (Figure 6.6; Plate 6.4). Orthoclase, plagioclase feldspar and polymineralic quartzo-feldspathic augen (1cm to 10cm long) occur in a medium-grained matrix of quartz, biotite and muscovite with minor garnet, kyanite and epidote. In thin-section, myrmekite textures are common. The augen are strongly prolate, defining an almost perfect L-fabric. Quartz and feldspar rods together with aligned mica grains define the lineation. The lineation plunges shallowly to the NE (mean 22/045) and is anticlockwise of the fold hinge orientation (20/062) (Figure 6.10). When viewed normal to the lineation, the foliation is absent or extremely poorly defined (Plate 6.4B). Locally, a poorly developed foliation defined by flattened feldspar and quartz augen (Plate 6.4) strikes WNW-ESE and dips shallowly to the NE (Figure 6.10). No axial planar fabrics were observed in the field within Domain D. The textures within Domain D are indicative of an almost purely constrictional strain regime.

6:2:2:5 Summary of structural domains

Linear augen gneisses of Domain D are overlain by layered gneisses of Domain C, which display $L > S$ tectonite fabrics and abundant lineation-parallel folds (Figure 6.6). These structures are interpreted to have formed during constrictional strain under amphibolite to upper greenschist-facies conditions. Within the overlying Domains A and B, mylonitic gneisses display $S=L$ and $S > L$ tectonite fabrics (Figure 6.6) generated under greenschist-facies conditions, and are interpreted as being formed under a non-coaxial strain regime.

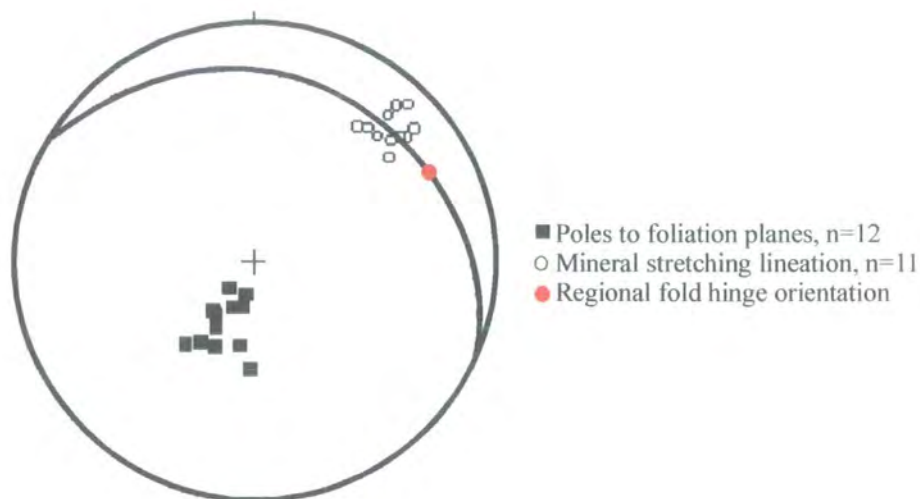


Figure 6.10 Stereographic projection to show gneissose foliation and lineation from Domain D.

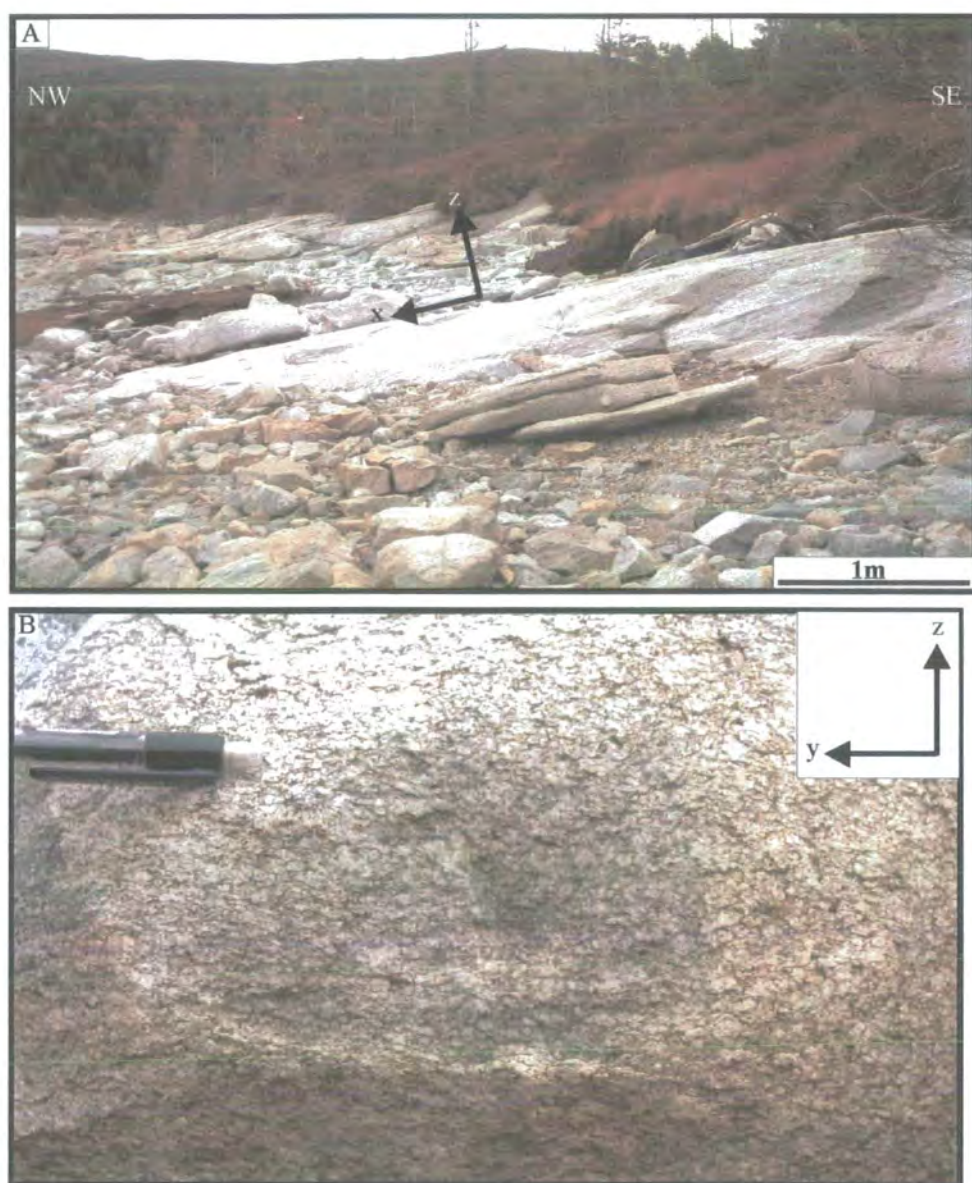


Plate 6.4 (A) View parallel to lineation to show strong L-fabric within augen gneiss, Domain D. (B) Cross-sectional view normal to lineation (XY plane) to show virtually no fabric elements in this section. Strongly prolate feldspars show circular shapes in this section (XY plane). (A) & (B) illustrate an augen gneiss with an $L \gg S$ fabric.

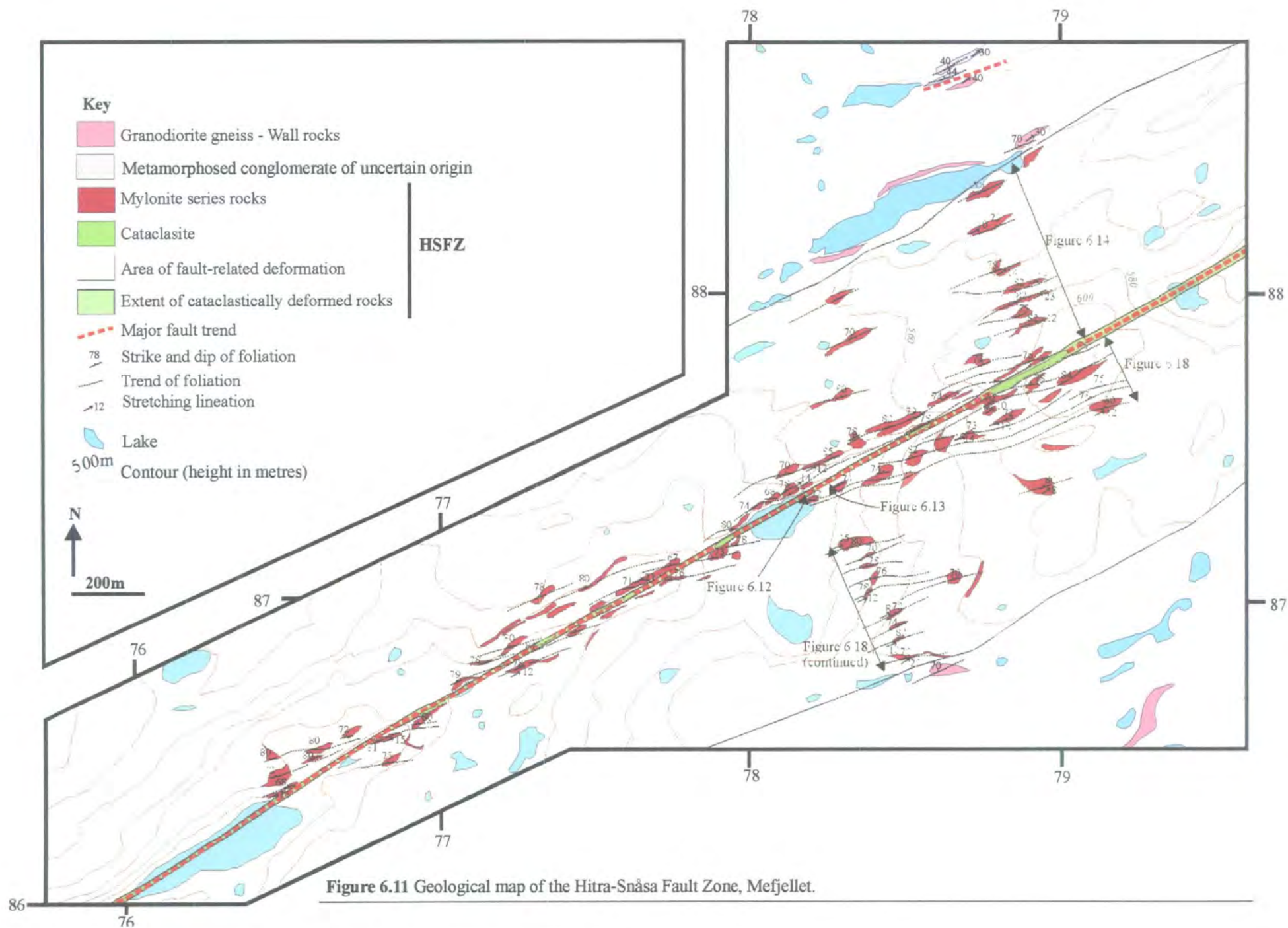
The distribution of structures associated with the different domains around the fold is explained by the model summarised in Figure 6.6B (c.f. Krabbendam and Dewey 1998). A low-angle, top-WSW shear accompanied by constrictional strain produces a series of upright folds with hinges parallel to the transport direction, leading to a larger degree of exhumation of the gneisses within the fold core (i.e., higher grade fabrics in the fold core). This results in a sinistral shear sense on the NW fold limb and a dextral shear sense on the SE fold limb (e.g., Domains A & B).

6:3 The Hitra-Snåsa Fault Zone: locality descriptions and structure

The designation Hitra-Snåsa Fault Zone (HSFZ) refers to a zone in which the country rocks are intensely deformed as a result of movement along the Hitra-Snåsa Fault (HSF). The HSFZ is exposed partially or fully at four sections along the trace of the fault zone on the Fosen Peninsula (Figure 6.1). These localities are described in the order of their relative importance (i.e., localities with better exposure are described first) to illustrate the along-strike variation in the geometry, cross-cutting relationships, spatial distribution and kinematic history exhibited by fault rocks within the HSFZ.

6:3:1 Mefjellet section

The best exposures of the Hitra-Snåsa Fault Zone (HSFZ) on Fosen are found in the Mefjellet area (locality m; Figure 6.1). Mefjellet is a hilly area (400-650m high) to the north of the Ormsetvatnet reservoir. The terrain is characterised by rocky exposures, crags, scrubby moorland and lakes. The central part of the HSFZ defines an ENE-WSW-orientated linear valley with an alignment of lakes surrounded by cliffs and rocky crags. Both to the northwest and to the southeast of the HSFZ, gneisses belonging to the Banded Gneiss Complex of Fosen (see section 5:1:2 1) are exposed (Figure 6.11).



Grønlie and Roberts (1989) described the HSF as a nearly straight lineament between Størnfjorden and Hjøllbotn associated with mylonites, small-scale recrystallised breccias and pseudotachylites (Grønlie et al. 1991). Mylonitic rocks are described as being dominant over the more brittle fault-rock products. This was interpreted to represent a fairly deep crustal section exhibiting mainly crystal-plastic deformation with a later, comparatively small-scale, brittle overprint (Grønlie and Roberts 1989).

6:3:1:1 Fault rocks

In this section, fault rocks are described in the order of their relative age (oldest to youngest; see section 6:3:1:2).

6:3:1:1a Mylonite

Mylonitic series rocks derived from quartzo-feldspathic banded gneisses (see section 6:2:1) are well exposed on Mefjellet. The grey-coloured, quartzo-feldspathic mylonites contain approximately 50% feldspar, 25% quartz, 10% muscovite, 10% epidote and 5% chlorite and biotite with minor amounts of sphene. The relative abundances of minerals vary with distance to the fault core, due to differences in strain intensity which have induced retrograde metamorphic reactions within the mylonites. Millimetre-scale bands of fine-grained feldspar and muscovite aggregates are interlayered with quartz-rich bands. The fine-grained matrix wraps around plagioclase, orthoclase and epidote / quartz aggregate porphyroclasts, which are typically 2mm to 3cm in length. The mylonites contain a strong foliation defined by stretched and flattened aggregates of quartz, feldspar and mica. The proportion of matrix varies from 10 to almost 100%, so that the rocks can be subdivided into protomylonites, mylonites and ultramylonites. The sub-vertical mylonitic foliation trends ENE-WSW with a sub-horizontal lineation defined by elongate quartz and feldspar together with aligned mica grains. In surfaces and thin-sections viewed perpendicular to the mylonite foliation and parallel to the stretching lineation, σ - and δ -type porphyroclast geometries are well developed.

6:3:1:1b Cataclasite

Cataclastic series rocks exposed on Mefjellet are derived entirely from quartzo-feldspathic mylonites. The cataclasites are usually pale green in colour, comprising finely comminuted clasts of mylonite, pseudotachylite, orthoclase, plagioclase, quartz, chlorite, epidote, muscovite and sphene set within a fine-grained cataclastic matrix. Randomly orientated clasts are angular to sub-angular, ranging from 5mm to less than 0.5mm in size. The cataclasites possess no internal fabric and appear to be isotropic in the field on all scales of observation. Epidote and quartz veins cross-cut the cataclasites and occur locally as clasts within the cataclasite matrix. The proportion of matrix varies from approximately 10% to 90%, so that the rocks can be subdivided into protocataclasites, cataclasites and ultracataclasites based upon the proportion of matrix.

6:3:1:1c Pseudotachylite

Black- to dark brown-coloured pseudotachylites derived from quartzo-feldspathic mylonites are well exposed within the HSFZ on Mefjellet. The pseudotachylites are cohesive, glassy and very fine grained. Rounded to sub-rounded clasts (~30%) of feldspar, quartz and mylonite ranging from 20µm to 3cm in diameter are set within a reddish brown to black glassy matrix (~70%). The matrix is completely free of mica, epidote and amphibole, and displays a millimetre-scale colour banding which probably reflects variations in composition. In thin-section and in the field, pseudotachylite veins display very straight boundaries, flow textures and injection structures. The pseudotachylites commonly occur adjacent to distinct slip surfaces and grade into a marginal cataclasite zone adjacent to the mylonitic host rock.

6:3:1:2 Fault rock distribution and age relationships

Within the Mefjellet area (Figure 6.11), the earliest recognised fault rocks within the HSFZ are mylonite series rocks that overprint banded gneisses (section 6:2:1) exposed both to the northwest and southeast of the HSFZ (Figure 6.11). Towards the fault core, ENE-WSW- to NW-SE- and N-S-trending epidote veins, cataclasites and pseudotachylites cross-cut the mylonite series rocks. Locally, millimetre-thick calcite

and zeolite veins transect the cataclasites, and appear to localise along pre-existing fractures.

6:3:1:2a Hitra Snåsa Fault core

In the Mefjellet area, the fault core is located in the central part of the HSFZ and corresponds to the 20m-wide region of most intense cataclastic deformation overprinting mylonites.

The HSF core is well exposed at grid-reference locality 7796 8719 and is illustrated by a structural log (Figure 6.12). Here, the rocks comprise strongly foliated quartzo-feldspathic mylonites, which are overprinted by 2 to 40cm-thick zones of breccia. The breccia zones increase in frequency towards the HSFP (Hitra Snåsa Fault Plane; Figure 6.12) and appear to localise along the pre-existing mylonite foliation. Centimetre-thick, epidote-rich cataclasites overprint the mylonite and commonly bound zones of brecciated mylonite. These cataclasites are spaced 3cm to 2m apart towards the outer parts of the fault core. The cataclasites increase in frequency towards the fault core and are spaced on a millimetre to centimetre scale. Millimetre- to centimetre-thick pseudotachylites commonly occur within the fault core. Pseudotachylite veins both cross-cut and are present as clasts within the cataclasite matrix, suggesting that cataclasite and pseudotachylite development was broadly coeval. Minor zeolite veins (millimetre-thick) overprint epidote-rich cataclasites. Within the centre of the HSF core, brecciated mylonite grades into a 2m-thick epidote-rich cataclasite (Plate 6.5) and locally ultracataclasite.

The best-exposed overprinting and fault rock distribution relationships within the HSF core are exposed at locality 7829 8741. Here, quartzo-feldspathic mylonites are cross-cut by N-S- and NE-SW- to ENE-WSW-trending epidote-rich cataclasites (Figure 6.13; Plate 6.6). The millimetre- to centimetre-thick cataclasites are spaced ~1mm to 40cm apart and commonly form braided geometries. Millimetre-thick epidote veins appear to have nucleated from the cataclasites. Centimetre-thick N-S- and NE-SW- to ENE-WSW-trending pseudotachylite veins are locally developed (Plate 6.6). The pseudotachylite veins have nucleated from discrete slip surfaces and are flanked by thin cataclasite seams.

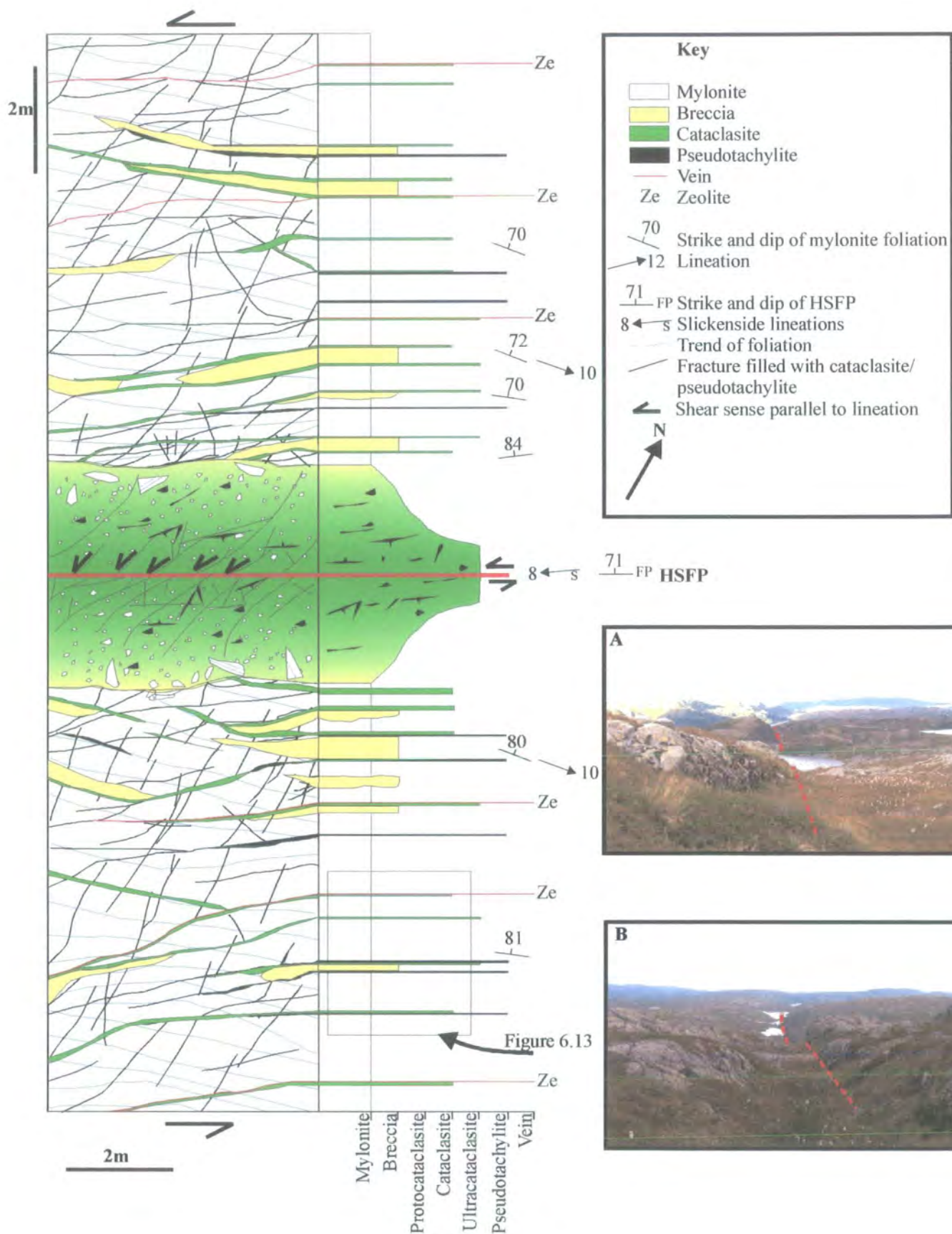


Figure 6.12 Schematic structural log to illustrate overprinting relationships, fault rock distribution and structure within the core of the HSFZ (7796 8719). (A) and (B) Photographs looking ENE and WSW along the HSFP.

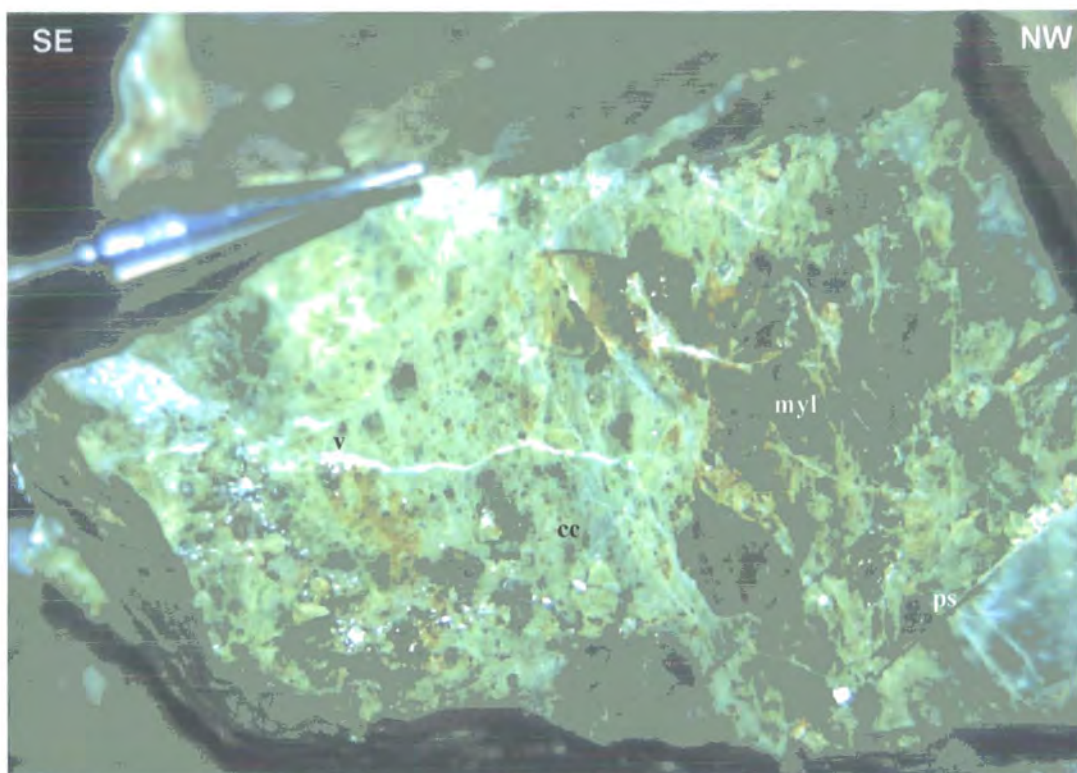


Plate 6.5 Cross-section view looking southwest. Green-coloured cataclasite from within the HSF core (7796 8719), Mefjellet. Randomly orientated sub-angular to angular clasts (<1mm to 3cm in size) of mylonite (myl), feldspar, quartz, epidote, mica and pseudotachylite (ps) are set within a fine-grained cataclastic matrix. Calcite veins (v) cross-cut cataclasite.

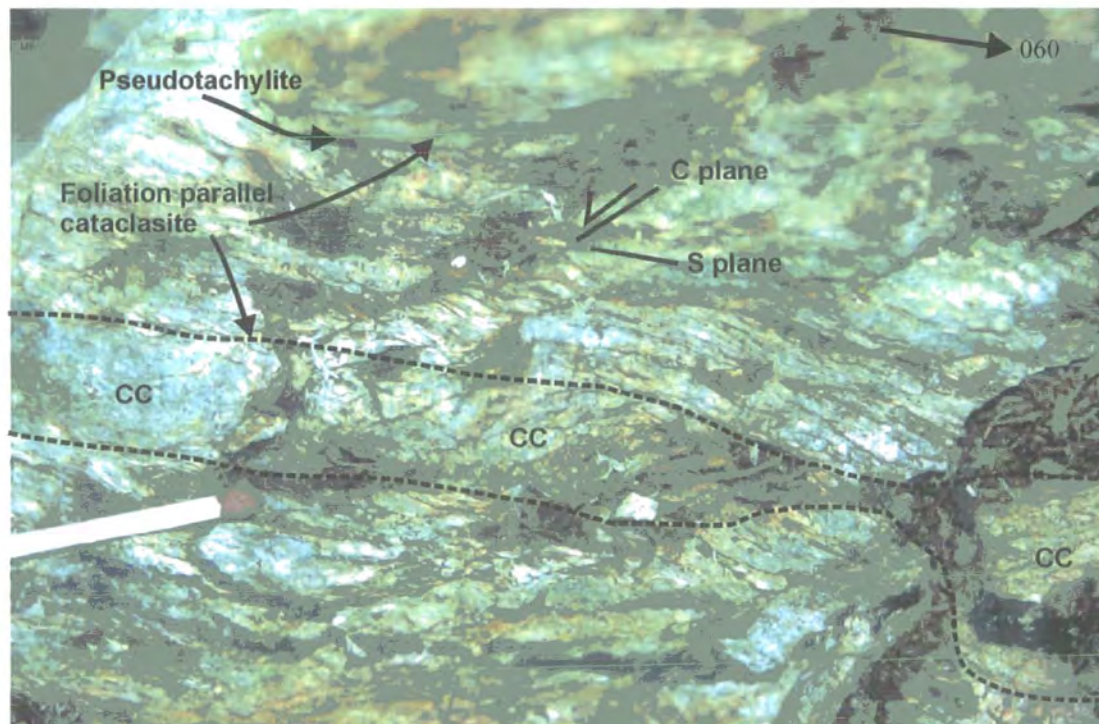


Plate 6.6 Plan view. Image to illustrate mylonite with overprinting cataclasite (CC) and pseudotachylite of part of Figure 6.13 (7829 8741).

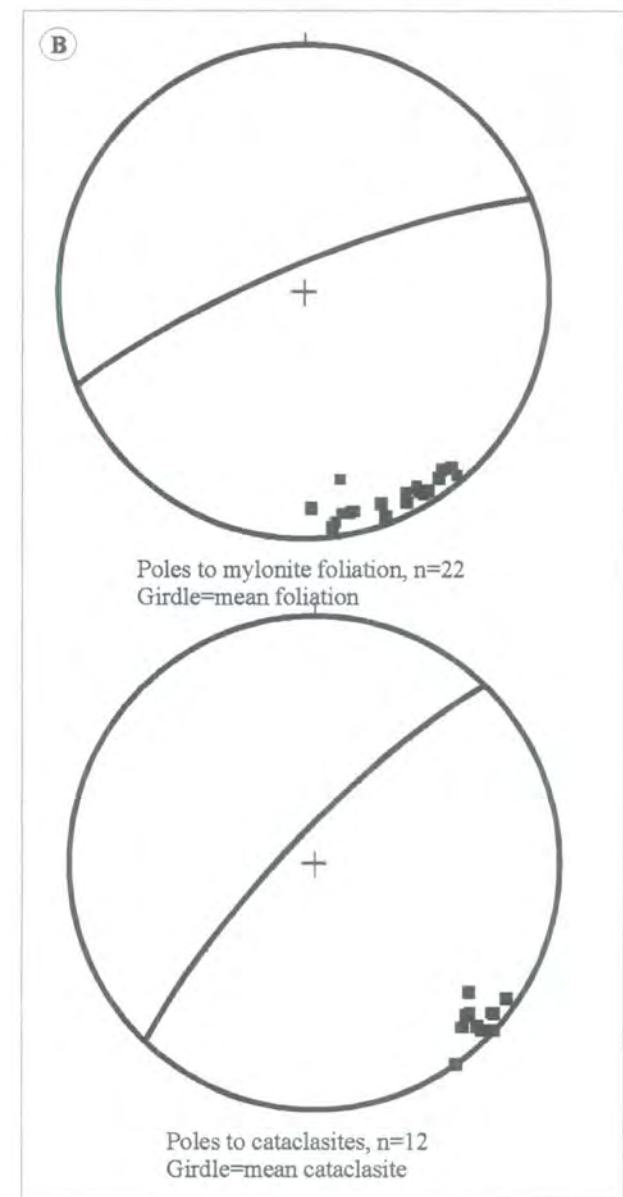
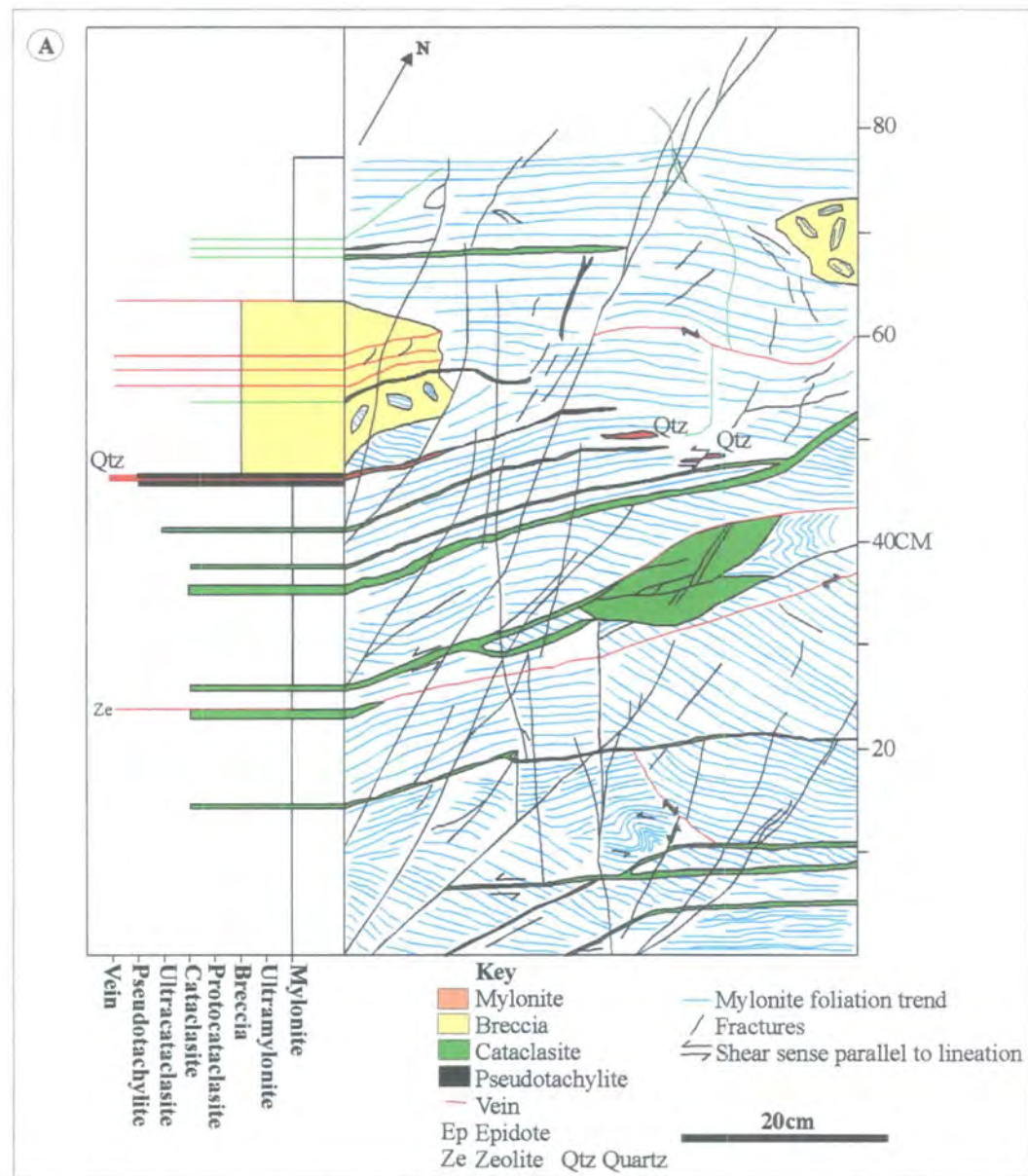


Figure 6.13 (A) Detailed structural log located 6m south of HSFP (located on Figure 6.12) to show fault rock distribution, overprinting relationships and structure. (B) Stereographic projections to show mylonite foliation and cross-cutting cataclasites (7829 8741).

Zones of breccia, 20cm to 40cm thick, are bounded by cataclasite and pseudotachylite veins that overprint intensely fractured mylonite. Millimetre-thick zeolite veins overprint and appear to localise along pre-existing cataclasites.

6:3:1:3 Fault zone structure

In the Mefjellet area, the HSFZ is approximately 1km wide. It comprises a 1km-wide ductile shear zone containing mylonite series rocks with a narrow central fault core containing cataclasite and pseudotachylite. Both to the northwest and to the southeast of the fault zone, gneisses belonging to the Banded Gneiss Complex of Fosen (section 5:1:2:1) are exposed.

6:3:1:3a NW of Hitra Snåsa Fault core

Northwest of the HSFP, fault-related deformation extends for approximately 500m into compositionally banded gneisses exposed in the Mefjellet area (Figure 6.11). To the northwest of the HSFP, the trend of the mylonite foliation appears to switch from 060° to almost 085° over a scale of tens of metres, both parallel and normal to the trend of the fault zone (Figure 6.11). This swinging of the foliation strike resembles the geometry of an S-C' fabric, but on a larger, tens of metres scale. At distances of 500m northwest of the HSFP, a protomylonitic fabric overprints granitic/ granodiorite gneiss (Figure 6.14). This is interpreted to represent the northwest limit of fault-related deformation. Over a decreasing distance to the HSFP, mylonites become dominant over protomylonitic fabrics (Plate 6.7A-G). The intensity of the mylonitic fabrics varies in an ENE-WSW trend together with variations normal to the HSFP (Figure 6.14; Plate 6.7A-H). The fabric varies in intensity from protomylonite to mylonite normal to the HSFP over distances between 2m and 50m, reflecting varied strain rates and protolith grain size within the HSFZ. This variation in intensity may be ascribed to alternating mylonite zones 2m to 50m thick with different strain rates, or anastomosing zones of high strain surrounding low-strain mylonites. This geometry may also explain the regular swings in the trend of the foliation both laterally and normal to the HSFP.

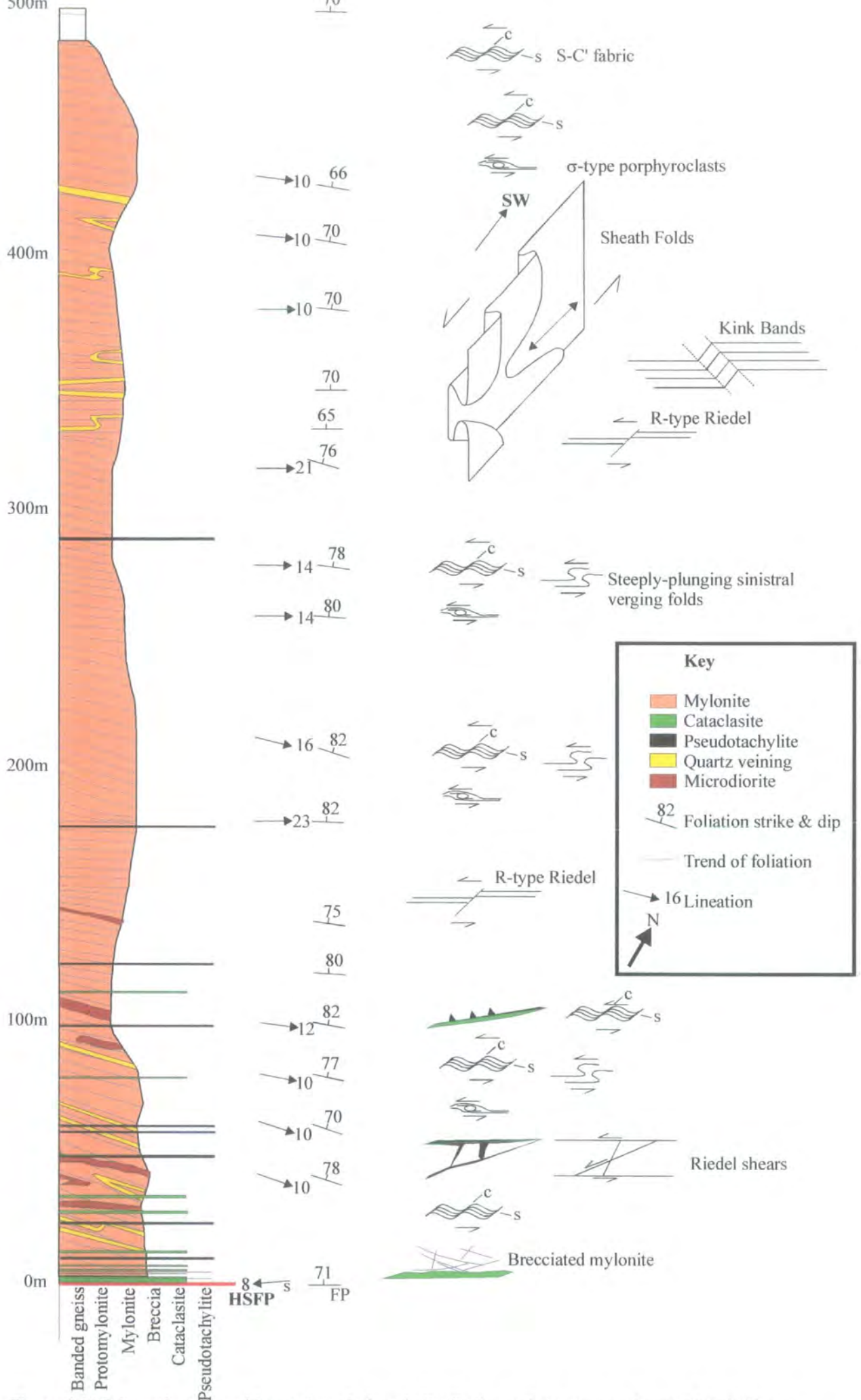


Figure 6.14 Schematic structural log to show fault rock distribution and structure northwest of the HSF core. Located on Figure 6.11.

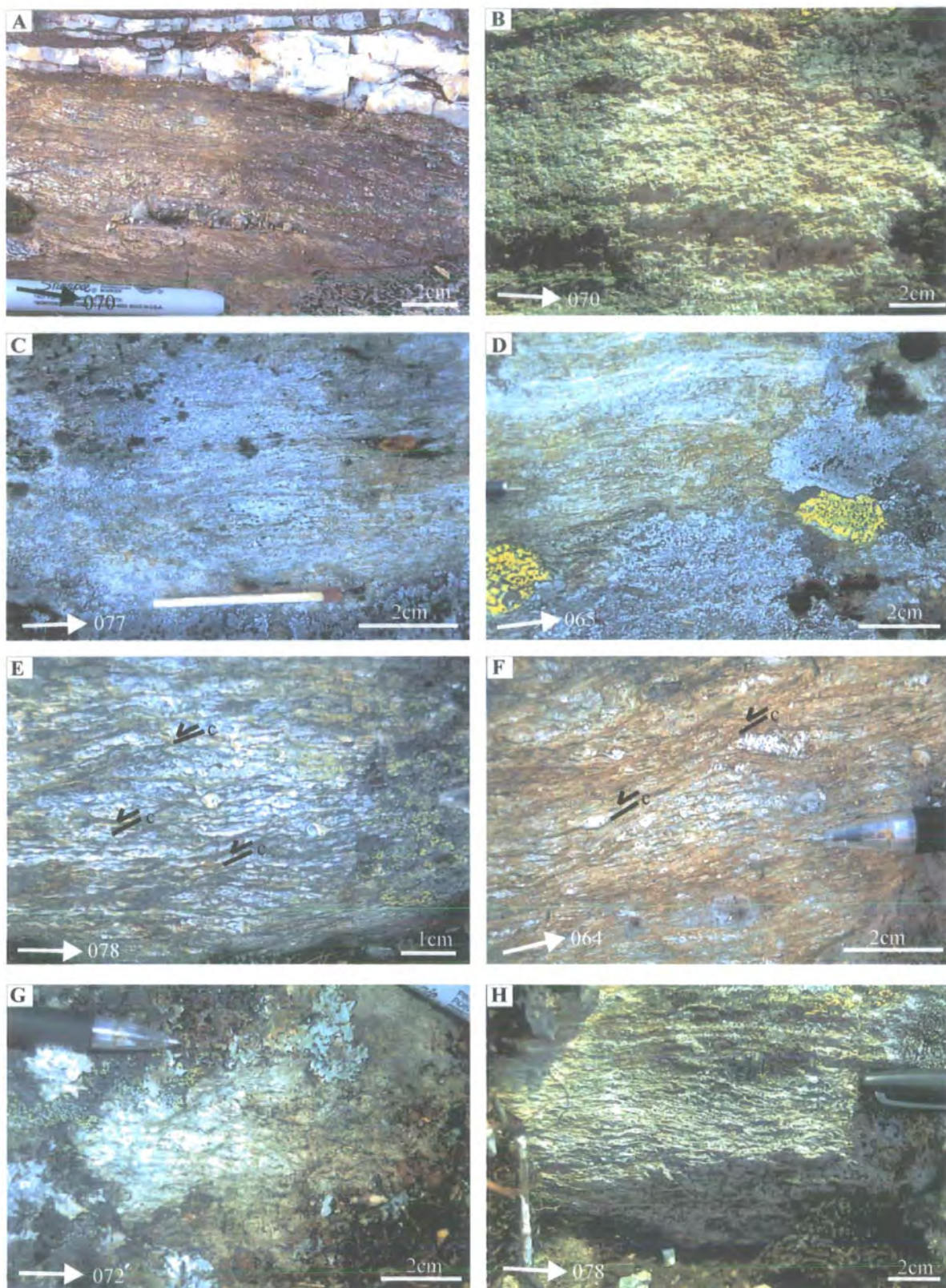


Plate 6.7 Plan view images to show fabrics viewed parallel to the lineation and normal to the foliation, at decreasing distances to HSFP along a NW-SE traverse (Figure 6.14). (A) Mylonite 430m. (B) 410m Protolith / weak protomylonite fabric. (C) Protomylonite 320m. (D) Protomylonite/ mylonite 260m. (E) Mylonite 210m. (F) Mylonite 180m. (G) Protomylonite 100m. (H) Mylonite 40m.

The mylonite foliation defined by flattened and stretched aggregates of quartz and feldspar trends ENE-WSW and dips steeply to the NW (Figure 6.15A). Lineations defined by elongate quartz and feldspar plunge shallowly to the ENE. Centimetre-spaced S-C' fabrics (Figure 6.15A) are locally developed and increase in frequency towards the HSFP (Figure 6.14), indicating a sinistral shear when viewed on outcrop surfaces parallel to the lineation and normal to the foliation. Feldspar porphyroclasts ranging from <0.5mm to 1cm in size commonly display σ -type geometries consistent with sinistral shear on outcrop surfaces and in thin-sections viewed parallel to the lineation and normal to the foliation (Plate 6.7E&F). Towards the HSFP, the mylonites are finer grained and have a platy appearance (Plate 6.7E-H). The mylonites locally display sinistral-verging, millimetre- to centimetre-scale folds (Figure 6.14) on outcrop surfaces viewed parallel to the lineation and normal to the foliation, which fold the S-C' fabrics. The folds display steeply-dipping fold hinges and E-W-trending axial planes (Figure 6.15B) and vary in style from sharply kinked to sub-rounded closures with straight limbs.

Foliation-parallel quartz veins (2cm to 50cm thick) are common within the HSFZ and increase in thickness and frequency towards the HSFP (Figure 6.14). In thin-sections viewed normal to the foliation and parallel to the lineation, the quartz veins display mylonite and ultramylonite fabrics. The preferred orientation of the quartz grains is consistent with sinistral shear.

At distances of up to 420m northwest of the HSFP (Figure 6.14) the quartz veins are folded by centimetre- to metre-scale curvilinear folds. The folds are common between 420 and 300m northwest of the HSFP. Axial planes strike ENE-WSW to NE-SW and dip steeply to the NW (Figure 6.15C). The fold hinge orientations lie along a girdle sub-parallel to the mean axial plane and the mylonite foliation (Figure 6.15C). When the fold hinge is sub-horizontal, the folds are asymmetric and verge upwards to the SE or NW (Plate 6.8A). When the folds plunge sub-vertically, they consistently display sinistral vergence in plan view (Plate 6.8B). Surfaces of the quartz veins display a strong lineation, defined by elongate quartz grains, parallel to the mylonite lineation. The folds are interpreted as sheath folds. Sheath folds develop as a result of passive amplification of initial perturbations in a layer subject to layer-parallel shear (Cobbold and Quinquis 1980) and are common in natural shear zones.

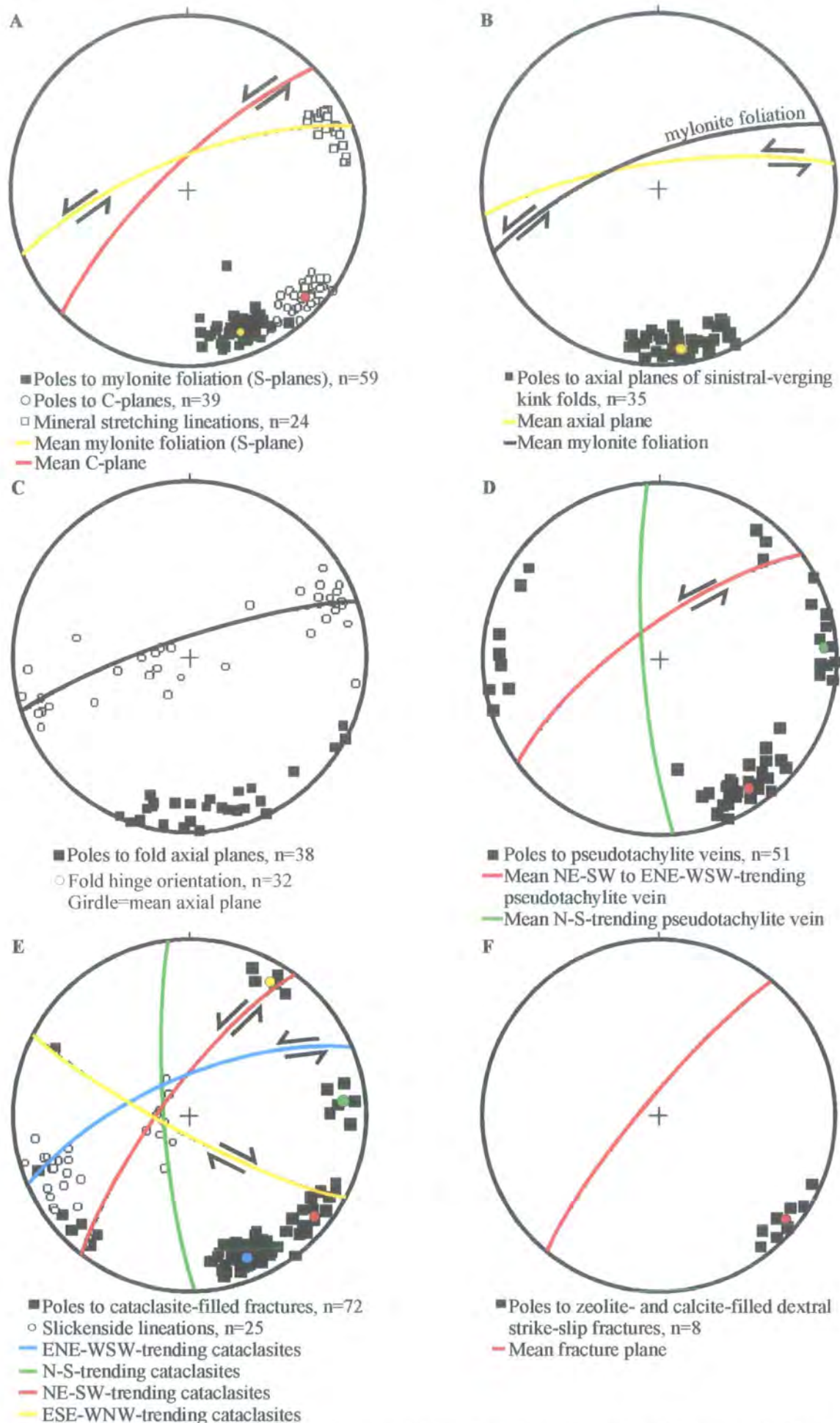


Figure 6.15 Stereographic projections of structural data collected northwest of the HSF core. (A) Poles to mylonite foliation, C-planes and lineations. (B) Poles to axial planes of sinistral-verging folds. (C) Sheath fold axial planes and hinge orientation. (D) Poles to pseudotachylite veins. (E) Poles to cataclasite-filled fractures and slickenside lineations. (F) Zeolite and calcite-filled dextral strike-slip fractures.

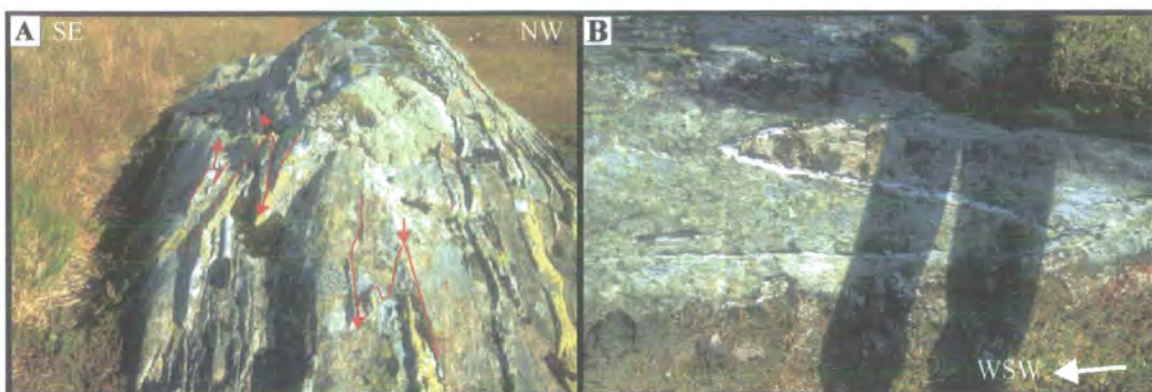


Plate 6.8 (A) Image to show folded quartz veins in cross-section and in plan view. Red arrows represent fold plunge. When folds plunge steeply they show sinistral vergence in plan view. Folds with sub-horizontal fold hinges verge to the NW in (A). (B) Image of steeply-plunging fold displaying a sinistral sense of vergence.



Figure 6.16 Schematic diagram illustrating geometry of curvilinear (sheath) folds consistent with sinistral shear. Dashed arrow represents the sub-horizontal lineation.

The geometry of the sheath folds and the vergence direction are consistent with sinistral shear (Figure 6.16).

At distances of less than 150m from the HSFP, 20cm to 1m-thick dykes of microdiorite are commonly exposed and increase in frequency towards the HSFP (Figure 6.14). The dykes are cross-cut by the mylonite foliation, suggesting that they pre-date the mylonitisation (although no such dykes are exposed outside the fault zone). In thin-sections viewed parallel to the lineation and normal to the foliation, millimetre-scale S-C' fabrics are consistent with sinistral shear.

Brittle deformation is most intense between 0m and 100m northwest of the HSFP, although thin, ENE-WSW-trending, sub-vertical pseudotachylite veins have been recognised up to 280m northwest of the HSFP (Figure 6.14). Centimetre-thick pseudotachylite veins are common at distances of less than 50m northwest of the HSFP. The near-vertical pseudotachylites trend NE-SW to ENE-WSW and N-S (Figure 6.15D). The ENE-WSW- to NE-SW-trending pseudotachylite veins overprint and appear to localise along the pre-existing mylonite foliation. The pseudotachylites commonly occur adjacent to distinct slip surfaces and pass into a marginal cataclasite zone adjacent to the mylonitic host rock. The pseudotachylite veins also contain (millimetre- to centimetre-scale) injection structures which branch from the planar surface into the mylonite wall rock (Plate 6.9). NNE-SSW-trending fractures containing thin (<1mm) pseudotachylite offset quartz veins by 1cm to 15cm, giving an apparent sinistral sense of shear (Plate 6.10). The pseudotachylites form networks bound by ENE-WSW- to NE-SW-trending slip surfaces. Discordant NNW-SSE- to N-S-trending injection veins form centimetre- to metre-scale networks which nucleate off NE-SW to ENE-WSW slip surfaces and link into other sub-parallel slip surfaces (Plates 6.11, 6.12). In plan view, the NE-SW- to ENE-WSW-trending pseudotachylites display millimetre-scale colour banding, which probably reflects compositional variations, parallel to the pseudotachylite boundaries. ENE-WSW- to NE-SW- trending pseudotachylites link into R-type Riedel shears filled with thin pseudotachylite or cataclasite which offset the mylonite foliation by 1cm to 5cm in an apparent sinistral sense, indicating an overall sinistral sense of movement along the HSFP (Plate 6.13). Locally, pseudotachylite injection veins overprint the R-type Riedel shears suggesting a multiple generation of pseudotachylite during sinistral



Plate 6.9 Plan view. Millimetre-scale cataclasite adjacent to a planar slip surface with pseudotachylite and injection veins (arrowed, iv) nucleating from the planar surface (7860 8758).



Plate 6.10 Plan view. NNE-SSW-trending sub-vertical hairline fractures filled with pseudotachylite offsetting the mylonite foliation and quartz veins by 1mm to 10cm sinistrally (7863 8762).



Plate 6.11 Plan View. Image to show geometrical arrangement of centimetre-scale pseudotachylites (7859 8758).

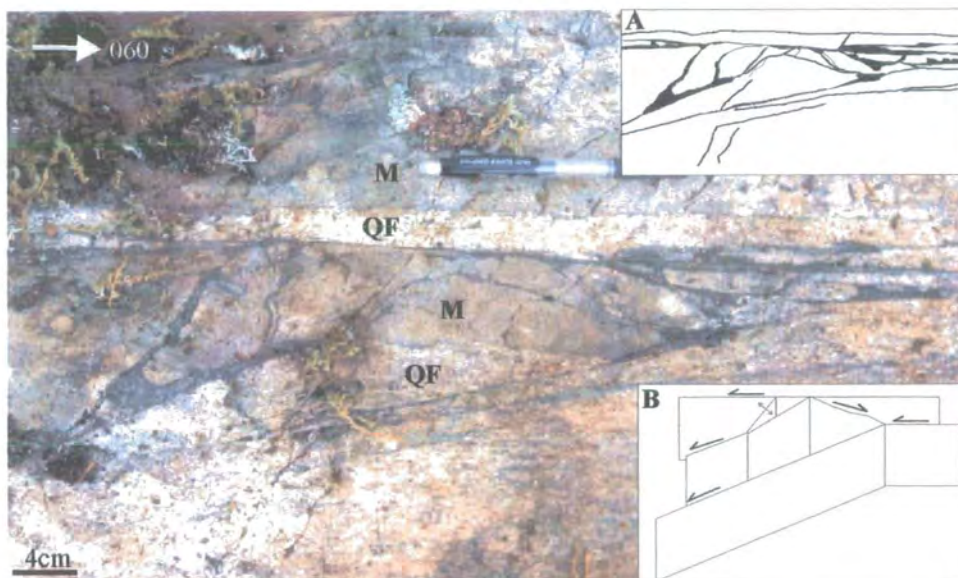


Plate 6.12 Plan view, located as A on Plate 6.11. Close up of centimetre-thick pseudotachylite to show geometrical configuration. M=Mylonitised mafic intrusion and QF= quartzo-feldspathic mylonite. (A) Sketch of pseudotachylites. (B) 3D geometry of pseudotachylites (7859 8758).



Plate 6.13 Plan view. Image to show pseudotachylites linking into NNE-SSW to NE-SW, R-type Riedel shears (R) with sinistral strike-slip offsets of 0.5cm to 3cm. R-type Riedel shears are cut by a N-S-trending injection vein (I) containing flow banding, suggesting multiple generation of pseudotachylite during sinistral strike-slip movement along the HSFP (7859 8758).

movement. In thin-sections cut parallel to sub-horizontal slickenside lineations in cataclasites exposed along strike of pseudotachylites, σ -type host-rock porphyroclasts and sub millimetre-scale folds within flow banding are consistent with sinistral shear (Plate 6.14).

At distances of less than 50m northwest of the HSFP, foliation-parallel (ENE-WSW) faults containing centimetre-thick cataclasites commonly branch into networks of sub-vertical fractures. The cataclasite-filled fractures form three main clusters (Figure 6.15E), ENE-WSW to NE-SW, N-S and WNW-ESE. ENE-WSW- to NE-SW-striking fractures contain sub-horizontal slickenside lineations and display sinistral strike-slip offsets of 5-30cm. These fractures are interpreted as R-type Riedel shears. N-S-trending extensional fractures link into ENE-WSW to NE-SW-trending structures. The geometric configuration of R-type Riedel shears and extensional fractures is consistent with sinistral transtension along the HSFZ (Figure 6.17).

Locally, NE-SW-orientated, sub-vertical fractures (Figure 6.15F) display dextral strike-slip offsets of the mylonite foliation of 1cm to 5cm. The fractures are associated with centimetre-scale folds, which display a dextral sense of vergence, located beyond the tip zones of the fractures. Millimetre-thick zeolite and calcite fill the fractures, which consistently overprint pre-existing cataclasites. It is unclear whether these fractures represent a different kinematic event or reflect local strain-rate variations within the HSFZ during sinistral transtension, and were then filled by later zeolite and calcite mineralisation.

Centimetre-thick cataclasites and pseudotachylites overprint intensely fractured mylonites 20 m northwest of the HSFP. These locally grade into zones of brecciated mylonite interleaved with intensely fractured mylonite with centimetre-thick cataclasites and pseudotachylites adjacent to the WBF core.

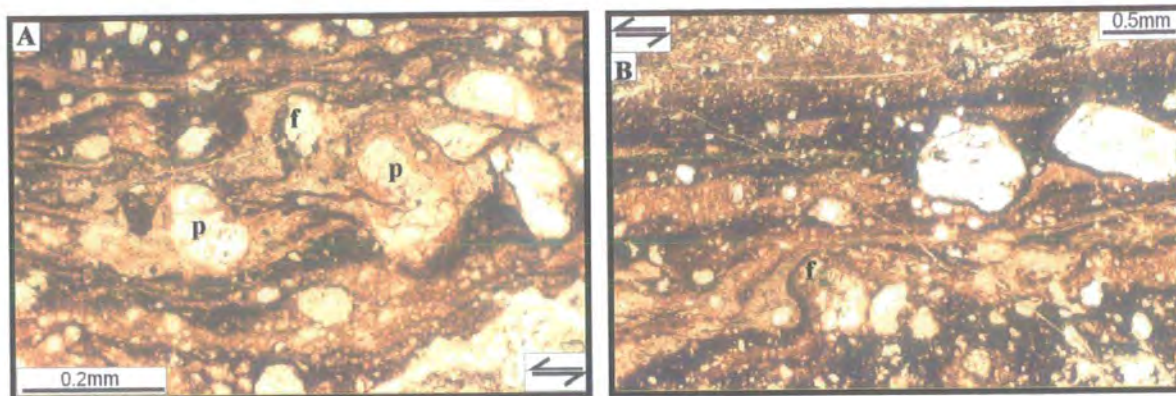


Plate 6.14 Photomicrographs of pseudotachylites exposed at 7859 8755 viewed parallel to sub-horizontal slickensides within thin cataclasites exposed along strike of the pseudotachylites. (A) and (B) show sub millimetre-scale colour banding defined by compositional variations in the melt material. Millimetre-scale folds (f) are present together with host-rock σ -type porphyroclasts (p), both of which are consistent with sinistral shear.

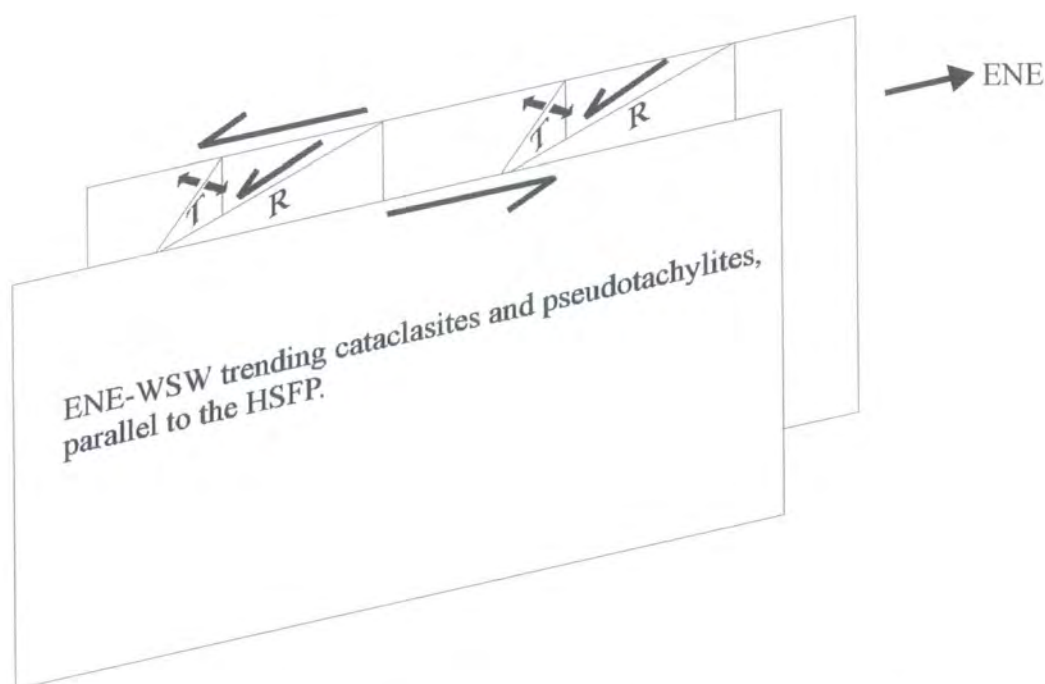


Figure 6.17 Schematic diagram to illustrate the geometry of sub-vertical R- type Riedel shears (R) and extensional fractures (T) with respect to ENE-WSW trending fractures, cataclasites and/ or pseudotachylites, which is consistent with sinistral strike-slip movements along the HSFP.

6:3:1:3b SE of Hitra-Snåsa Fault core

Fault-related deformation extends for approximately 500m into banded gneisses exposed in the Mefjellet area (Figure 6.11). To the southeast of the HSFP, the trend of the mylonite foliation changes from 060° to almost 085° over a tens of metres scale, both parallel and normal to the trend of the fault zone (Figure 6.11). This swinging of the foliation strike is similar to the swing in foliation to the northwest of the HSFP and resembles the geometry of an S-C-type fabric, but on a larger scale. As well as to the northwest of the HSFP, the intensity of mylonitic fabrics appears to vary along an ENE-WSW trend together with variations normal to the HSFP (Figure 6.18; Plate 6.15A-H). The fabric intensity varies from mylonite to protomylonite over distances between 2m and 50m. This variation in intensity maybe ascribed to variations in strain rate within the shear zone leading to the generation of alternating mylonite zones 2m to 50m thick commonly forming anastomosing zones of high-strain mylonites surrounding low-strain protomylonites. This geometry is consistent with swings in the trend of the foliation both laterally and normal to the HSFP.

At distances of up to 600m southeast of the HSFP, a weak protomylonite fabric overprints gneisses (Figure 6.18). This is interpreted to represent the southeast limit of fault-related deformation. The mylonite foliation defined by stretched and flattened aggregates of quartz and feldspar trends ENE-WSW and dips steeply to the NW (Figure 6.19A). Lineations defined by elongate quartz and feldspar grains together with aligned mica plunge shallowly to the ENE. Centimetre- to millimetre-scale, S-C' fabrics are locally developed and increase in frequency towards the HSFP (Figure 6.18). The S-C' fabrics consistently indicate sinistral shear when viewed on outcrop surfaces parallel to the sub-horizontal lineation and normal to the foliation (Plate 6.15BDE). S-planes trend ENE-WSW (070/78N) and the C-planes NE-SW (044/78NW), with approximately 25° between the strikes of these surfaces (Figure 6.19A). Feldspar porphyroclasts ranging from 1mm to 1cm in length commonly display σ - and δ -type geometries consistent with sinistral shear (Plate 6.15ABCE) when viewed on outcrop surfaces parallel to the lineation and normal to the foliation. At decreasing distances to the HSFP, feldspar porphyroclasts are commonly completely replaced by fine-grained aggregates of retrograde epidote.

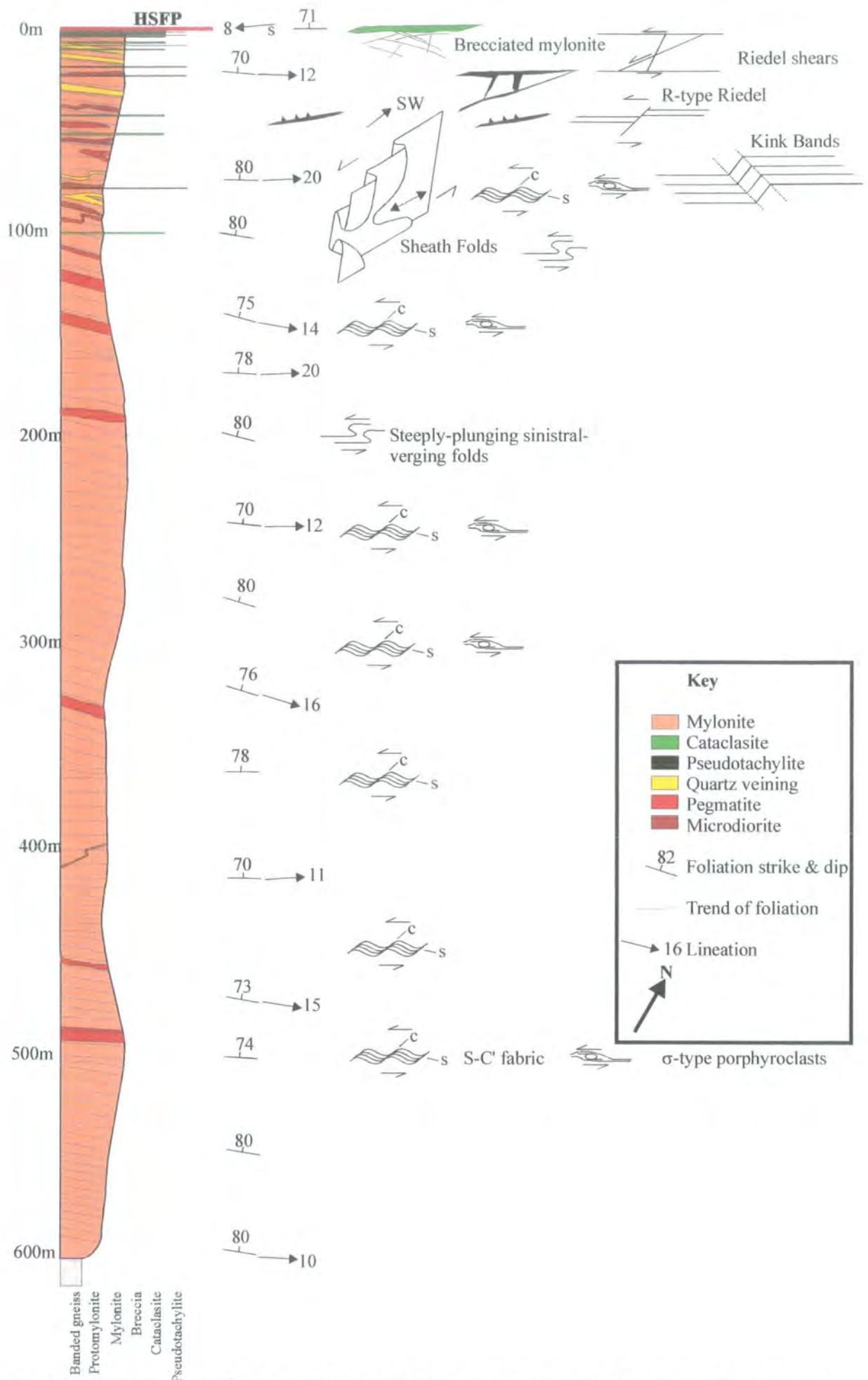


Figure 6.18 Schematic structural log to show fault rock distribution southeast of the HSF core. For location, see Figure 6.11.

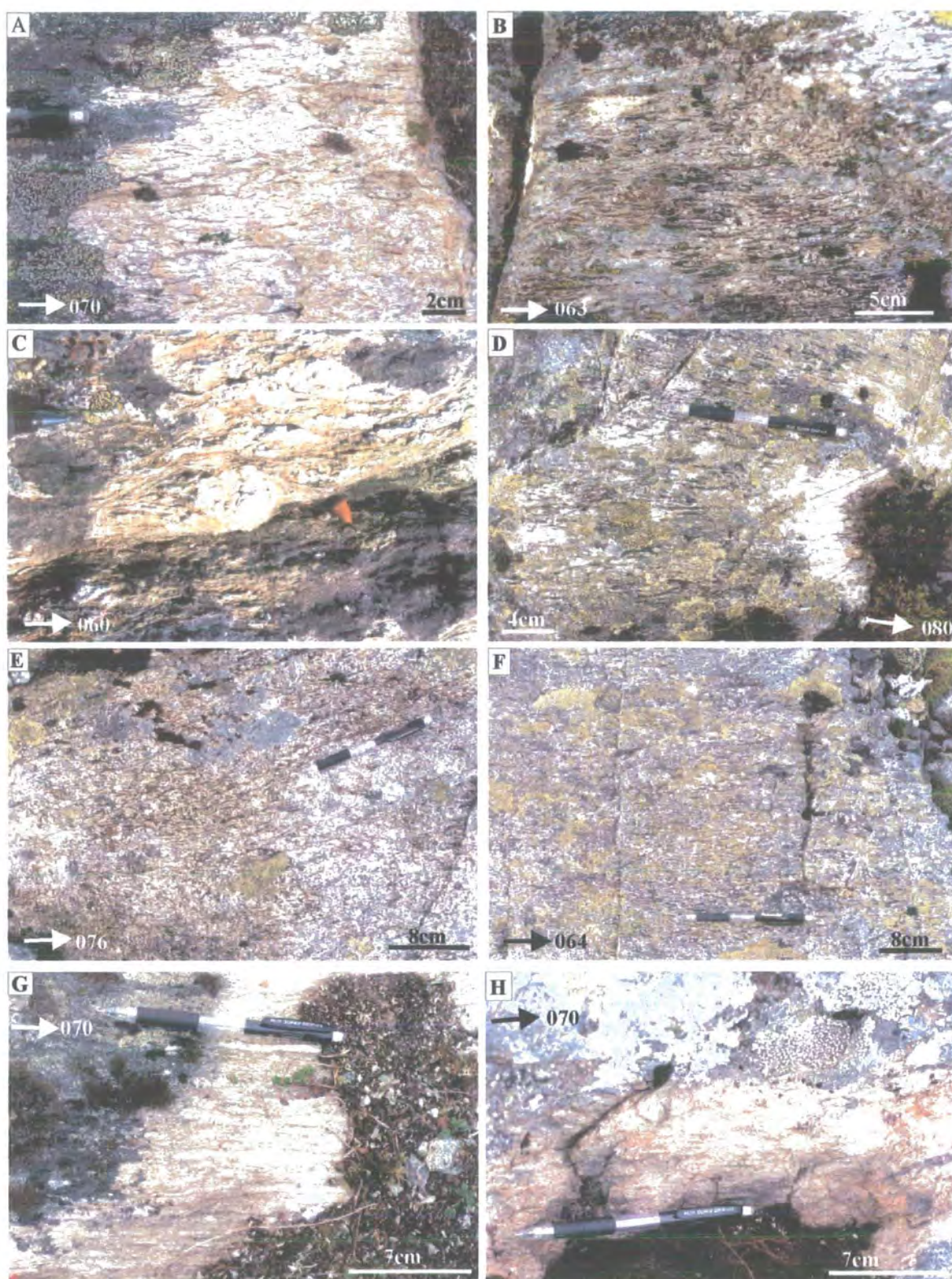


Plate 6.15 Plan view images to show fabrics viewed parallel to the lineation and normal to the foliation, at decreasing distances to the HSFP along a NW-SE traverse, southeast of the HSFP (Figure 6.18). (A) Protomylonite, 600m. (B) Mylonite, 500m. (C) Protomylonite, 430m. (D) Protomylonite, 330m. (E) Mylonite, 280m. (F) Mylonite, 180m. (G) Protomylonite, 75m. (H) Mylonite, 15m.

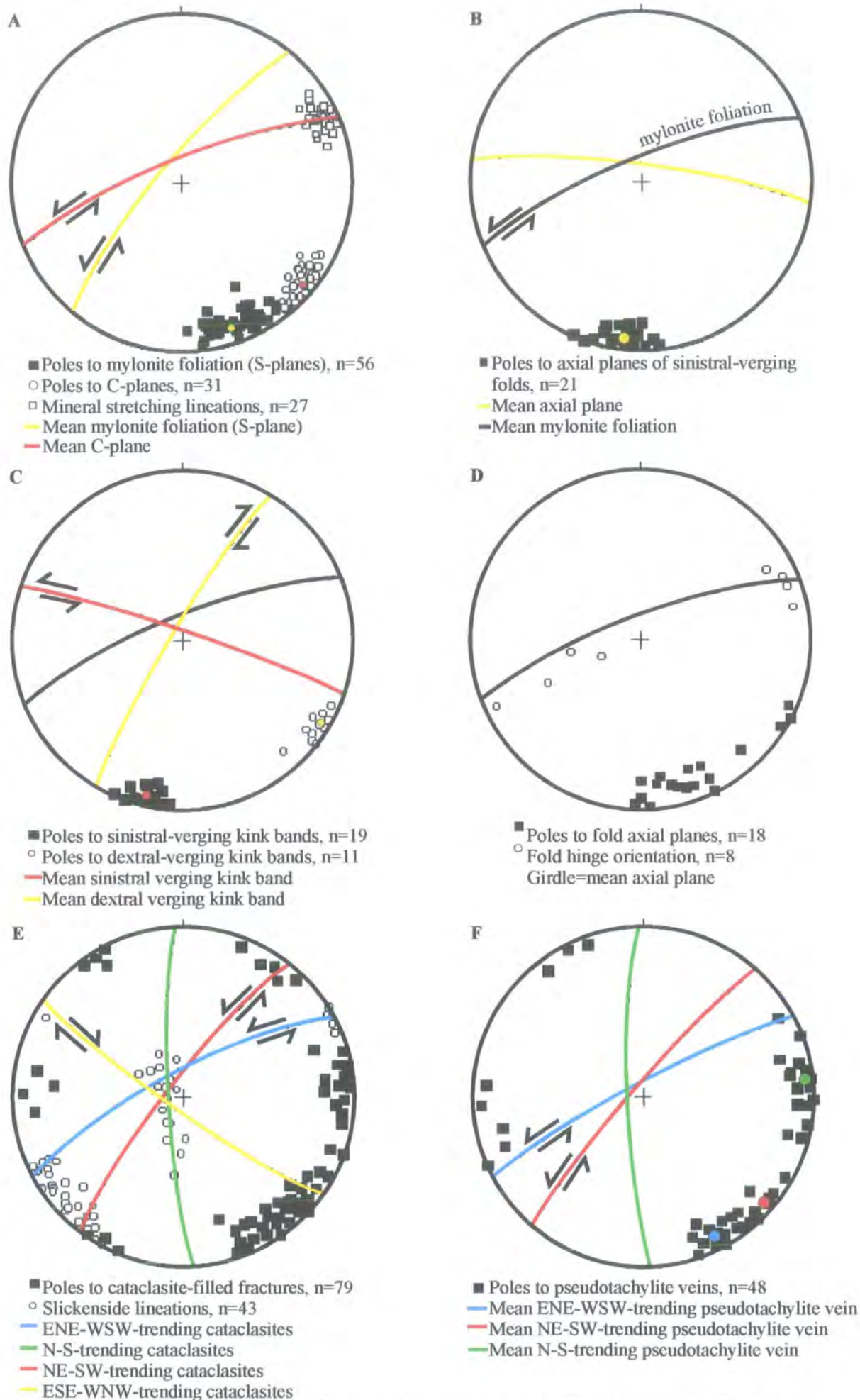


Figure 6.19 Stereographic projections of structural data collected southeast of the HSF core. (A) Poles to mylonite foliation, C-planes and lineations. (B) Poles to axial planes of sinistral-verging folds. (C) Poles to conjugate dextral and sinistral kink bands. (D) Sheath fold axial planes and hinge orientation. (E) Poles to cataclasite-filled fractures and slickenside lineations. (F) Poles to pseudotachylite veins.

In thin-section and in the field, the rocks display well-developed mylonite textures, with decreasing grain size and an increasing mica content towards the HSFP, giving rise to a platy appearance in the field (Plate 6.15 EFH).

At distances of less than 450m southeast of the HSFP, 5cm to 1m thick pegmatites are commonly exposed and increase in frequency towards the HSFP (Figure 6.18). The pegmatites are overprinted by an ENE-WSW-trending mylonite foliation defined by flattened and stretched aggregates of quartz and feldspar. On outcrop surfaces viewed parallel to the sub-horizontal lineation and normal to the foliation, the pegmatites display centimetre-scale S-C' fabrics and σ -type feldspar porphyroclasts (0.2cm to 1cm) which are consistent with sinistral shear. In the field, the pegmatites appear to contain a weaker mylonite fabric compared to the surrounding wall rock, probably due to variations in protolith grain size and/ or composition. The pegmatites are commonly folded and are oblique to the mylonitic S-C' fabric, which clearly overprints them (Figure 6.20), suggesting that the pegmatite dykes were intruded before the formation of the mylonite S-C' fabric. Pegmatites are increasingly common towards the HSFP, although they may only be recognised in thin-section as many of the protolith textures have been destroyed during intense mylonitisation.

At distances of less than 200m southeast of the HSFP, centimetre-scale S-C' fabrics are folded by centimetre-scale, steeply plunging folds (Figure 6.19B), which consistently display a sinistral sense of vergence (Plate 6.16). Quartz veins up to 1cm thick are commonly localised along the axial planes of the folds.

Quartz veining is present at distances of up to 300m southeast of the HSFP but is most intense at distances of less than 100m southeast of the HSFP (Figure 6.18). The foliation-parallel quartz veins are 1cm to almost 1m thick, laterally continuous and occur in clusters. In thin-sections cut parallel to the lineation and normal to the foliation, very strong mylonite fabrics are present. When viewed under a sensitive tint plate, the quartz grains display a strong preferred orientation consistent with sinistral shear.

Dark brown / grey microdiorite dykes are common at distances of up to 100m southeast of the HSFP (Plate 6.17; Figure 6.18). The dykes are 5cm to up to 1m in thickness and are orientated ENE-WSW. Some of the dykes are deformed by metre-scale isoclinal folds with sub-horizontal hinge orientations.

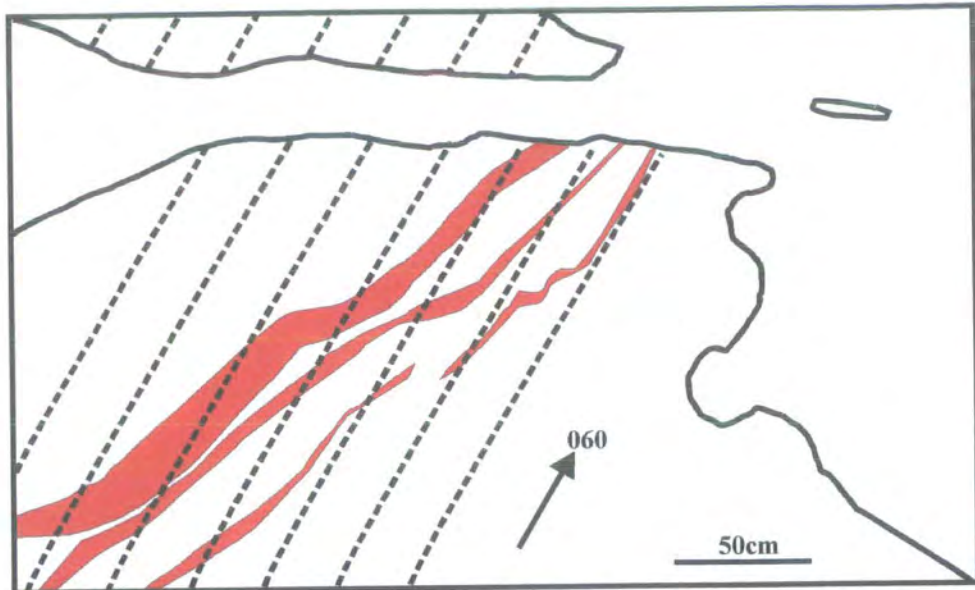


Figure 6.20 Field sketch of folded pegmatite dykes overprinted by well-developed mylonitic foliation (dashed lines), 400m southeast of the HSFP.

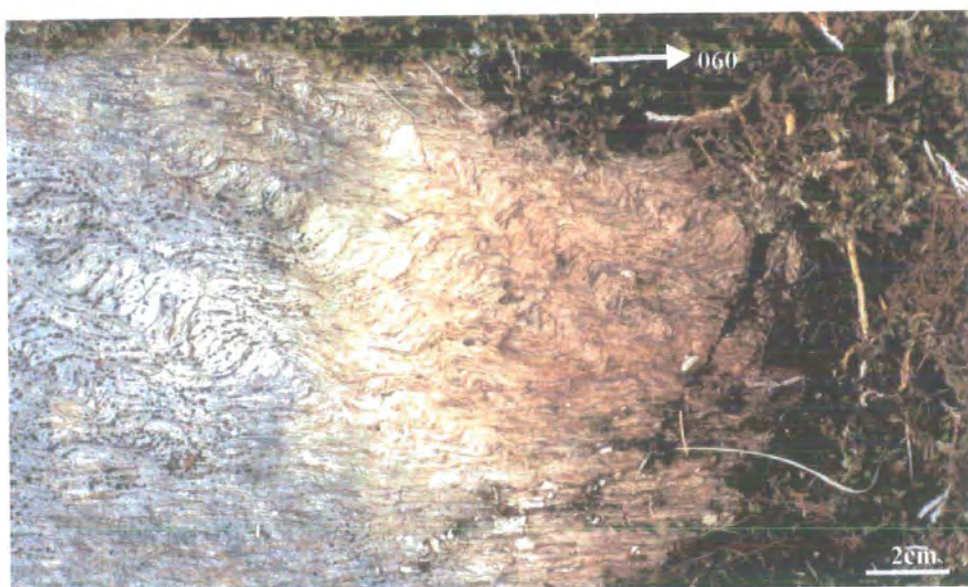


Plate 6.16 Plan view. Image to show centimetre-scale S-C' fabrics refolded by centimetre-scale, steeply plunging folds with a consistent sinistral sense of vergence, 215m southeast of HSFP.

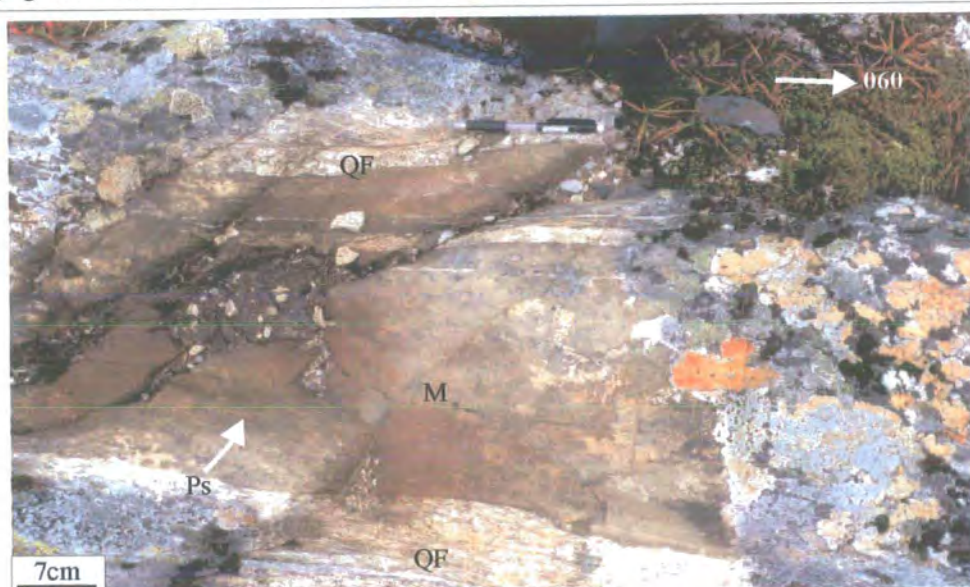


Plate 6.17 Plan view. Image to show 0.5m-thick mafic intrusion (M) with irregular ENE-WSW-trending contact surrounded by quartzo-feldspathic protomylonites (QF). In thin-sections cut parallel to the lineation and normal to the foliation, sub-millimetre-scale S-C' fabrics are consistent with sinistral shear. ENE-WSW-trending fractures are filled with pseudotachylite (Ps).

The intrusions are strongly overprinted by ultramylonite or mylonite fabrics and are strongly retrograded to a fine grained matrix of chlorite, biotite and muscovite, which surrounds porphyroclasts of quartz, epidote and magnetite (~35%). Sub-millimetre-scale S-C' fabrics consistent with sinistral shear are abundant in thin-sections cut normal to the foliation and parallel to the lineation.

Centimetre-scale, conjugate kink bands (Figure 6.19C) overprint the mylonite foliation, displaying both a sinistral and a dextral sense of vergence (Plate 6.18). It is inferred that the conjugate kink folds and sinistral S-C' fabrics accommodated N-S shortening and sinistral shear across anisotropic mylonites (see model described at Ollaberry, Shetland; section 3:1:1:5b)

At distances between 120m and 75m southeast of the HSFP, quartz veins and pegmatites are folded by centimetre- to metre-scale curvilinear folds with ENE-WSW-trending, sub-vertical axial planes (Figure 6.19D). The fold hinge orientations lie along a girdle sub-parallel to the mean axial plane and the mylonite foliation. When fold plunges are sub-horizontal, tight to isoclinal folds verge both up to the NW and to the SE. Steeply plunging folds consistently show a sinistral sense of vergence. The folds are similar to those exposed northwest of the HSFP and interpreted as sheath folds (Figure 6.16), which are consistent with sinistral shear.

Fault-related brittle deformation extends for approximately 100m southeast of the HSFP (Figure 6.18). Centimetre-thick pseudotachylite veins first appear 75m southeast of the HSFP and are commonly associated with mylonitised mafic intrusions (Plate 6.17). The pseudotachylite veins are much less common southeast of the HSFP compared to northwest of the HSFP. They are sub-vertical and trend either ENE-WSW to NE-SW or N-S (Figure 6.19F). The ENE-WSW- to NE-SW-trending pseudotachylite veins overprint and appear to localise along the pre-existing mylonite foliation (Plate 6.19ABC). The pseudotachylites occur adjacent to distinct slip surfaces and grade into a marginal cataclasite zone adjacent to the mylonitic host rock. Millimetre- to centimetre-scale injection veins nucleate along the slip surfaces and are generally orientated N-S (Plate 6.19A). N-S-orientated pseudotachylite veins commonly form in en échelon arrangements consistent with sinistral shear. Locally, ENE-WSW-trending pseudotachylite veins are offset along NNE-SSW-to NE-SW-trending sub-vertical fractures by 2cm to 10cm in a sinistral sense (Plate 6.19C).

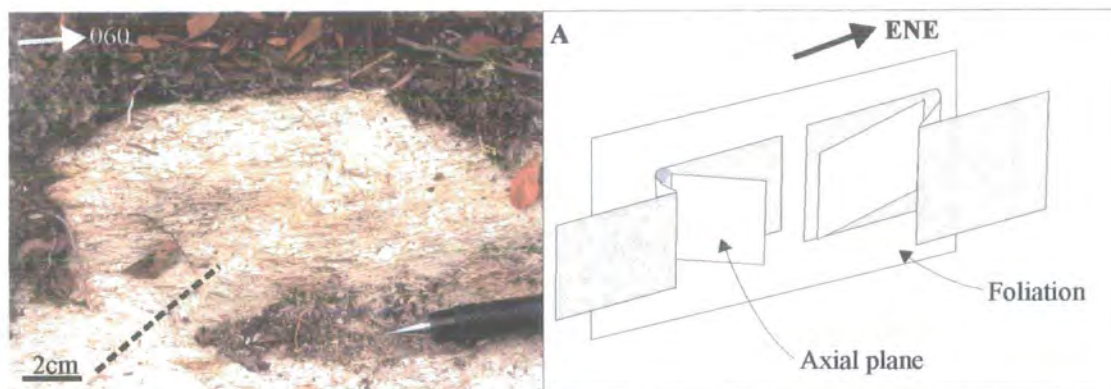


Plate 6.18 Plan view. Image to show centimetre-scale kink band with dextral sense of vergence. (A) Schematic sketch to show the geometric relationship of sinistral- and dextral-verging kink bands.

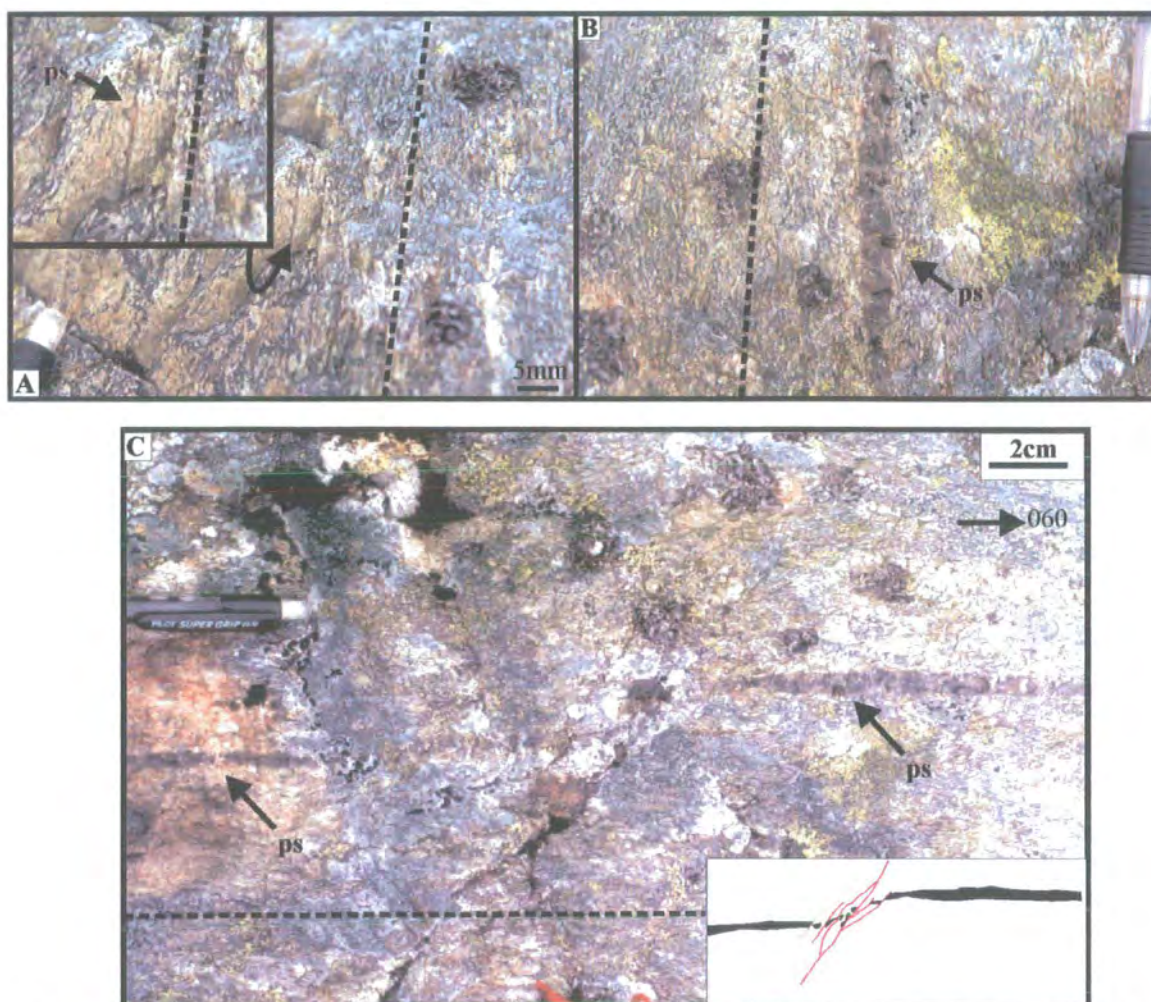


Plate 6.19 (A) & (B) Cross-sections through millimetre- to centimetre-thick pseudotachylites localising along the pre-existing mylonite foliation with N-S-orientated injection veins nucleating from planar fracture surface. (C) Plan view. Foliation-parallel pseudotachylite offset several centimetres by NE-SW-orientated, sub-vertical fractures with sub-horizontal slickenside lineations. Pseudotachylites (ps) arrowed. Dashed lines - trend of mylonite foliation.

At distances less than 50m southeast of the HSFP, ENE-WSW-trending faults filled with centimetre-thick cataclasite localise along the pre-existing mylonite foliation and link into braided networks of sub-vertical fractures (Plate 6.20). The cataclasite-filled fractures form three main clusters, N-S, NE-SW to ENE-WSW and ESE-WNW (Figure 6.19E). NE-SW-trending fractures with sub-horizontal slickenside lineations offset the mylonite foliation and quartz veins by 2cm to 2m in a sinistral sense (Plate 6.20A) and link into ENE-WSW-trending structures. The NE-SW-trending fractures are interpreted as R-type Riedel shears (Plate 6.20A&B; Figures 6.17, 6.21) formed as a result of sinistral strike-slip movement along the HSFP and sub-parallel structures. N-S-trending fractures form en échelon arrays and link into to NE-SW- to ENE-WSW-trending fractures or faults. They commonly display quartz slickenfibres, which step down the fault plane, indicating dip-slip normal movements. ESE-WSW-orientated fractures with sub-horizontal slickenside lineations display dextral strike offsets of 1cm to 5cm and are interpreted as R'-type Riedel shears. The geometrical configuration of W-dipping extensional fractures, R- and R'-type Riedel shears is consistent with sinistral transtension along the HSFZ.

Locally, NE-SW-orientated, sub-vertical fractures offset the mylonite foliation by 1cm to 5cm in a dextral sense (Plate 6.21). The fractures are associated with centimetre-scale kink bands located near the tip zones of the fractures, which display a dextral sense of vergence. The fractures contain sub-horizontal slickenside lineations and millimetre-thick zeolite and calcite veins. The zeolite and calcite veins fill sub-vertical fractures trending 130°, which display dextral strike-slip offsets of 2cm to 5cm of the mylonite foliation. It is unclear whether these fractures represent localised reactivation or local strain-rate variations within the HSFZ during sinistral transtension, and were then filled by later zeolite and calcite mineralisation. The zeolite- and calcite-filled fractures are also associated with NNE-SSW-orientated fractures, which display sinistral strike-slip offsets of 1cm to 2cm.

15m southeast of the HSFP, intensely fractured mylonites grade into a zone of brecciated mylonite cut by discrete cataclasites and pseudotachylites adjacent to the WBF core (Figure 6.18).

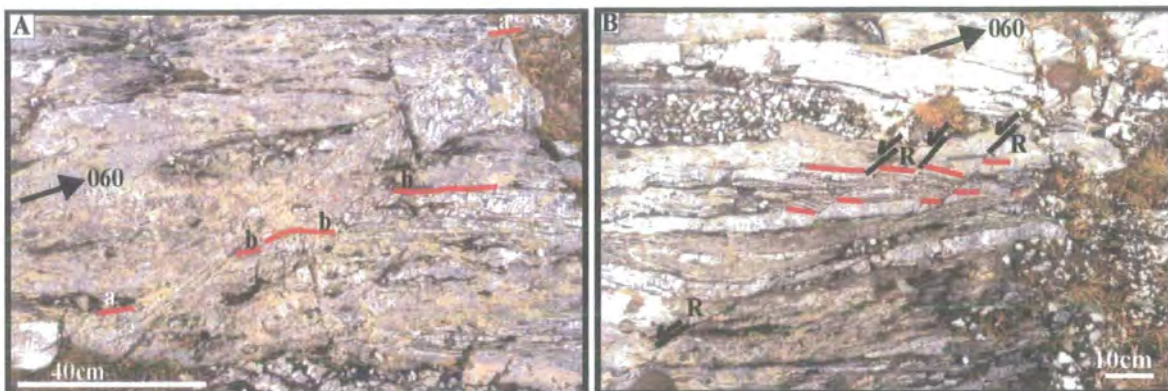


Plate 6.20 Plan view. Sub-vertical NE-SW-trending fractures with sub-horizontal slickenside lineations offset mylonitised quartz veins by 1cm to 1.5m in a sinistral sense. These fractures are interpreted as R-type Riedel shears formed as a result of sinistral strike-slip movements along the HSFP.

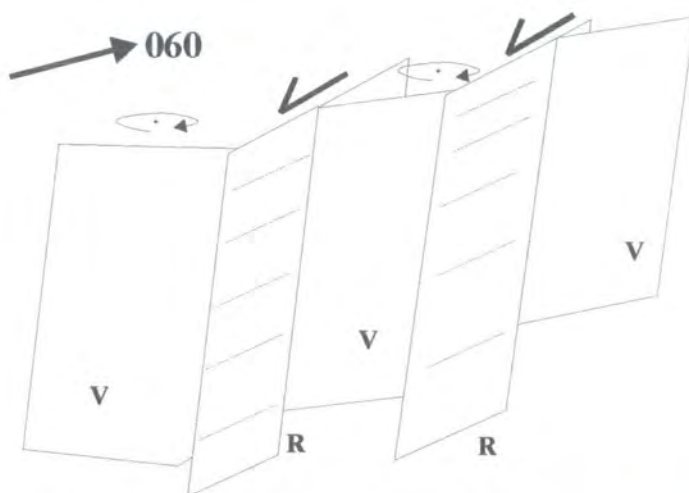


Figure 6.21 Schematic sketch to illustrate R-type Riedel shears (R) offsetting quartz veins (V) (Plate 6.20) with clockwise rotation northwest of the fracture surfaces to accommodate sinistral strike-slip offsets.

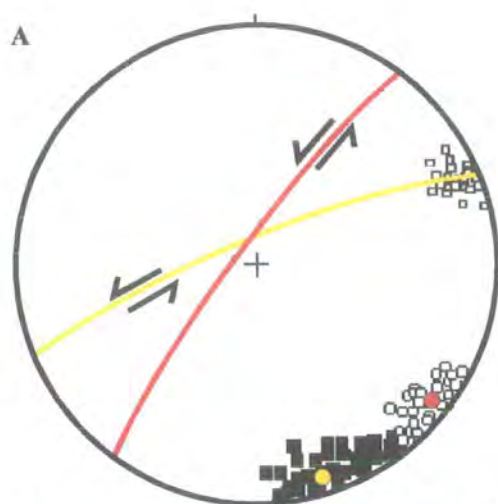


Plate 6.21 Plan view. NE-SW-orientated, sub-vertical fracture offsetting mylonitised quartz vein by 5cm in a dextral sense (7827 5737).

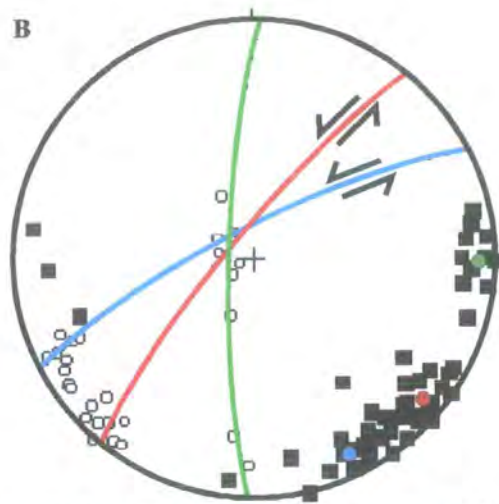
6:3:1:3c Hitra-Snåsa Fault core

In the Mefjellet area, the fault core is located in the central part of the HSFZ and corresponds to the 20m-wide region of most intense cataclastic deformation overprinting mylonites. The 20m-wide HSF core is well exposed at locality 7796 8719 and is illustrated by a schematic structural log (Figure 6.12). Here, the rocks comprise intensely fractured quartzo-feldspathic mylonites (Figure 6.22A), which are overprinted by 2cm to 40cm-thick breccia zones bounded by centimetre-thick epidote-rich cataclasites (Plate 6.22A&B). The breccia zones increase in frequency towards the HSFP (Hitra Snåsa Fault Plane; Figure 6.12). Centimetre-thick epidote-rich cataclasites trending NE-SW to ENE-WSW (Figure 6.22B) overprint the mylonite foliation and are spaced 3cm to 2m apart towards the outer parts of the fault core (Figure 6.12). The cataclasites commonly bound zones of brecciated mylonite. The cataclasites link into N-S-trending extensional cataclasites (Figure 6.22B), and increase in frequency towards the fault core where they are spaced on a millimetre- to centimetre-scale. Millimetre- to centimetre-thick pseudotachylite veins are common within the fault core (Figure 6.12). The pseudotachylite veins localise along the ENE-WSW-trending mylonite foliation and link into tensional structures (Figure 6.22C). Pseudotachylite veins both cross-cut and are present as clasts within the cataclasite matrix, suggesting that cataclasite and pseudotachylite development is coeval. Minor zeolite veins (millimetre-thick) transect the epidote-rich cataclasites.

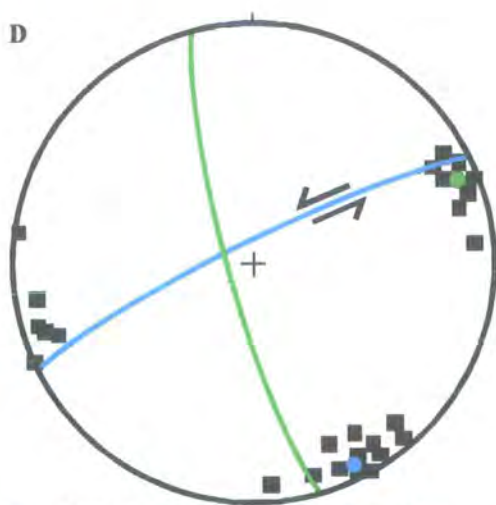
The best-exposed overprinting fault rock distribution and structural relationships within the HSF core are exposed at locality 7829 8741 (Figure 6.13). Here, quartzo-feldspathic mylonites display a strong ENE-WSW-orientated foliation (Figure 6.13B) defined by flattened and stretched aggregates of quartz, feldspar and muscovite with a sub-horizontal lineation defined by elongate quartz, feldspar and muscovite. The fine-grained mylonites are rich in muscovite and display a platy appearance (Plate 6.22C). Locally, layers of ultramylonite up to 20cm thick are developed. Feldspar porphyroclasts (1mm to 5mm in size) are wrapped by fine-grained millimetre-thick bands of fine-grained feldspar and muscovite aggregates interlayered with quartz-rich bands. On outcrop surfaces viewed parallel to the lineation and normal to the foliation, feldspar porphyroclasts display σ -type geometries consistent with sinistral shear (Plate 6.22C).



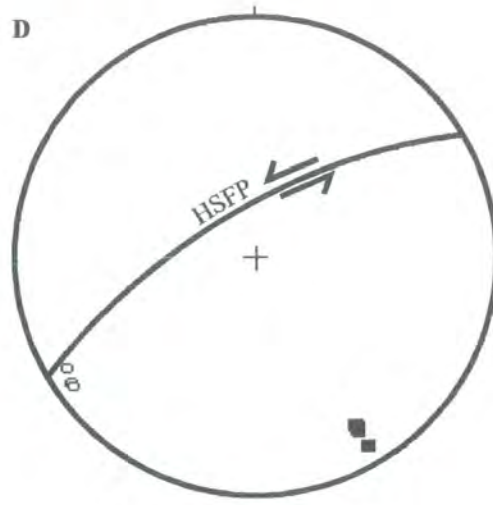
- Poles to mylonite foliation (S-planes), n=41
- Poles to C-planes, n=26
- Mineral stretching lineations, n=19
- Mean mylonite foliation (S-plane)
- Mean C-plane



- Poles to cataclasite-filled fractures, n=50
- Slickenside lineations, n=26
- ENE-WSW-trending cataclasites
- N-S-trending cataclasites
- NE-SW-trending cataclasites



- Poles to pseudotachylite veins, n=24
- Mean ENE-WSW-trending pseudotachylite vein
- Mean N-S-trending pseudotachylite vein



- Poles to HSFP, n=4
- Slickenside lineations, n=3

Figure 6.22 Stereographic projections of structural data collected within the core of the HSFZ. (A) Mylonite foliation (S-planes), C-planes and lineations. (B) Cataclasites and slickenside lineations. (C) Pseudotachylite veins. (D) HSFP and slickenside lineations.

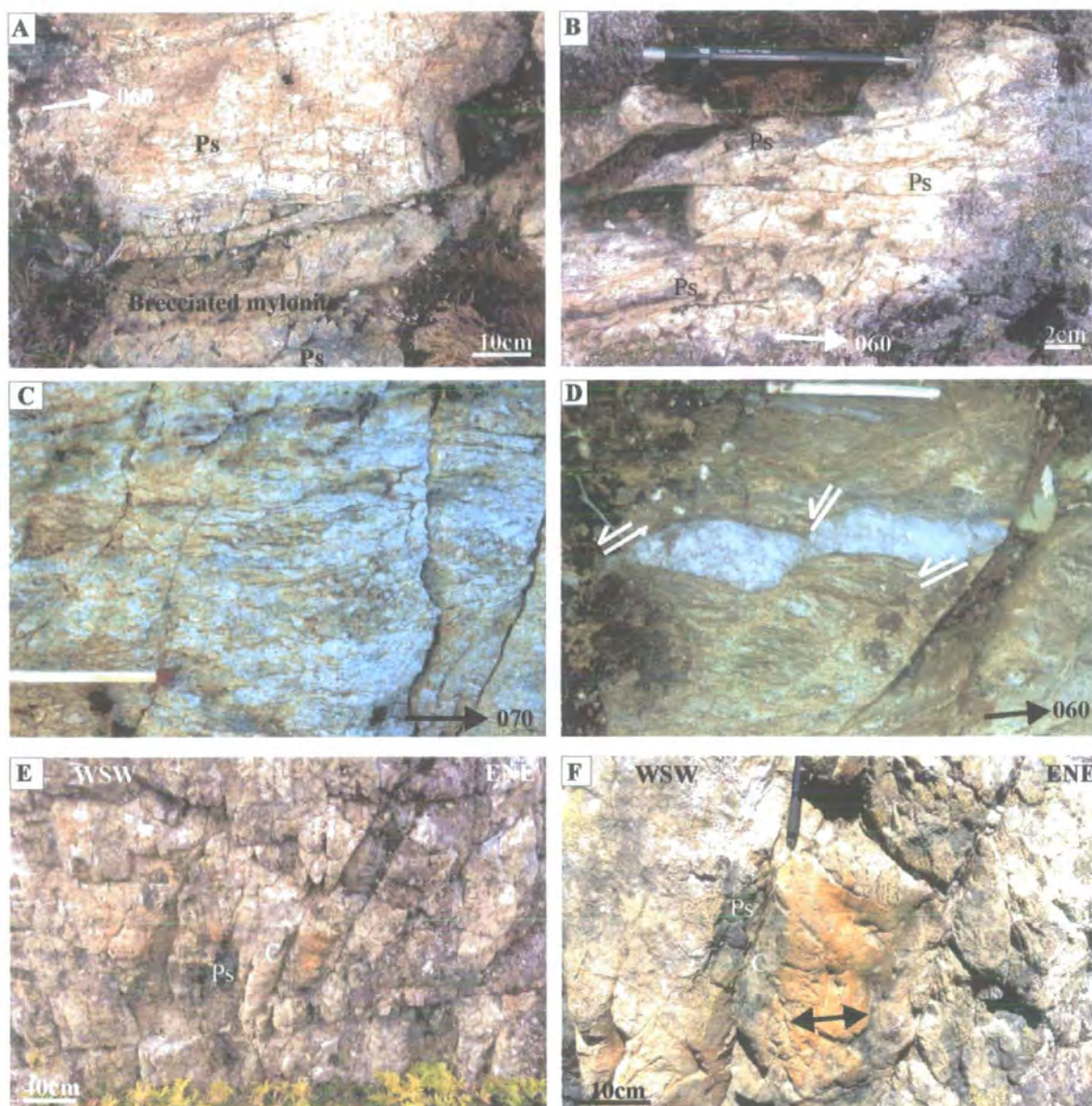


Plate 6.22 (A) & (B) Plan view. Brecciated mylonite adjacent to ENE-WSW- trending fractures filled with cataclasites and pseudotachylite (Ps), 8m northwest of HSFP. (C) Plan view. Mylonite with S-C' fabrics and σ -type porphyroclasts consistent with sinistral shear (6m south of HSFP; Figure 6.13). (D) Plan view. Millimetre-thick braided cataclasites orientated NE-SW to NNE-SSW display sinistral strike-slip offsets and are interpreted as R-type Riedel shears (6m south of HSFP; Figure 6.13) (E) View looking northwest onto sub-vertical HSFP and adjacent cataclasite (C) and pseudotachylite (Ps). Note the NE-SW- to NNE-SSW-trending sub-vertical fractures linking into HSFP. (F) Close-up image of sub-vertical HSFP to show sub-horizontal slickenside lineation (arrow) on polished surface on top of cataclasite (C) and pseudotachylite (Ps).

Millimetre- to centimetre-scale S-C' fabrics are abundant and are consistent with sinistral shear (Plate 6.6). The S-C' fabrics are refolded by centimetre-scale, steeply plunging, sinistrally verging folds (Figure 6.13). The intensely fractured mylonites are cross-cut by N-S- and NE-SW- to ENE-WSW-trending, epidote-rich cataclasites (Figure 6.13; Plate 6.6). The millimetre- to centimetre-thick cataclasites with sub-horizontal slickenside lineations form braided geometries and are spaced ~1mm to 40cm apart (Plate 6.22D). Centimetre-thick, N-S- and NE-SW- to ENE-WSW-trending pseudotachylite veins are locally well developed adjacent to thin cataclasites (Plate 6.6). The pseudotachylites nucleate from discrete slip surfaces and are flanked by thin cataclasite seams. NE-SW to ENE-WSW and N-S sub-vertical fractures are filled with either thin cataclasite or pseudotachylite. N-S-orientated fractures are less continuous and link into longer NE-SW- to ENE-WSW-trending fractures (Figure 6.13). NE-SW-trending fractures are interpreted as R-type Riedel shears formed as a result of sinistral movement along the HSFP. Breccia zones 20cm to 40cm-thick are developed locally where intense fracture networks are localised together with pseudotachylite veins. Millimetre-thick zeolite veins cross-cut and appear to localise along pre-existing cataclasites. Zeolite veins offset earlier formed cataclasites by 1cm to 5cm in an apparent dextral sense (Figure 6.13).

Within the centre of the HSF core, brecciated mylonite grades into a 2m-thick epidote-rich cataclasite (locally ultracataclasite) (Plate 6.5), with abundant pseudotachylite veining. The highly polished HSFP is orientated 060/71NW and contains slickenside lineations, which plunge shallowly to the WSW (Figure 6.22D; Plate 6.22E&F). NW-SE- and NNW-SSE- to N-S-orientated cataclasites (2cm to 20cm thick) curve and link into the HSFP. NW-SE-trending cataclasites contain sub-horizontal slickenfibres, which indicate sinistral strike-slip movements based upon the stepping direction of the quartz mineral fibres. NW-SE-trending cataclasites are interpreted as R-type Riedel shears formed as a result of sinistral strike-slip movement along the HSFP. NNW-SSE- to N-S- trending cataclasites contain dip-slip slickenside lineations (Figure 6.22B) and are extensional shears formed as a result of sinistral transtension along the HSFZ.

6:1:3:4 Kinematic summary and discussion

The kinematic evolution of the HSFZ at Mefjellet is summarised in Table 6.1.

Kinematic regime	Fault rocks / structures
4. Minor dextral strike-slip (localised reactivation, fault core remained inactive) (youngest)	<ul style="list-style-type: none"> ◦ Minor zeolite veining ◦ Dextral strike-slip offsets along NE-SW-trending fractures filled with zeolite
3. Sinistral transtension (291 ± 14 Ma)	<ul style="list-style-type: none"> ◦ Cataclasites ◦ Pseudotachylites ◦ Flow banding within pseudotachylites ◦ R- and R'-type Riedel shears ◦ W-dipping, N-S-trending extensional faults ◦ Slickenside lineations
2. Sinistral strike-slip (409 ± 12 Ma)	<ul style="list-style-type: none"> ◦ Mylonites ◦ S-C' fabrics ◦ σ- and δ-type porphyroclasts ◦ Sinistral-verging folds ◦ Sheath folds with sinistral vergence
Precursor basement structure prior to the formation of the HSFZ ? (oldest)	<ul style="list-style-type: none"> ◦ Pegmatite and mafic intrusions together with extensive quartz veining may indicate an igneous contact or zone of dyking

Table 6.1 Table summarising the kinematic evolution of the HSFZ at Mefjellet.

The HSFZ in the Mefjellet area comprises a 1 km-wide ductile shear zone (containing mylonites) formed during sinistral shear, with a narrow central fault core of coeval cataclasite and pseudotachylite formed during a later phase of sinistral transtension (Figure 6.23). The HSFZ comprises an anastomosing network of ENE-WSW-trending mylonites, which surround lenses of protomylonite and banded gneiss (in the outer parts of the shear zone). The mylonites overprint banded gneisses (section 6:2:1) exposed both to the northwest and to the southeast of the HSFZ. S-C' fabrics, σ -type porphyroclasts, sheath folds and small-scale steeply plunging folds developed within the mylonites are all consistent with sinistral shear (Figure 6.24). The mylonites that formed during this sinistral shear event are dated at 409 ± 12 Ma (Ar-Ar infrared laser ablation of syn-tectonic muscovite growths; this study, see section 7:2).

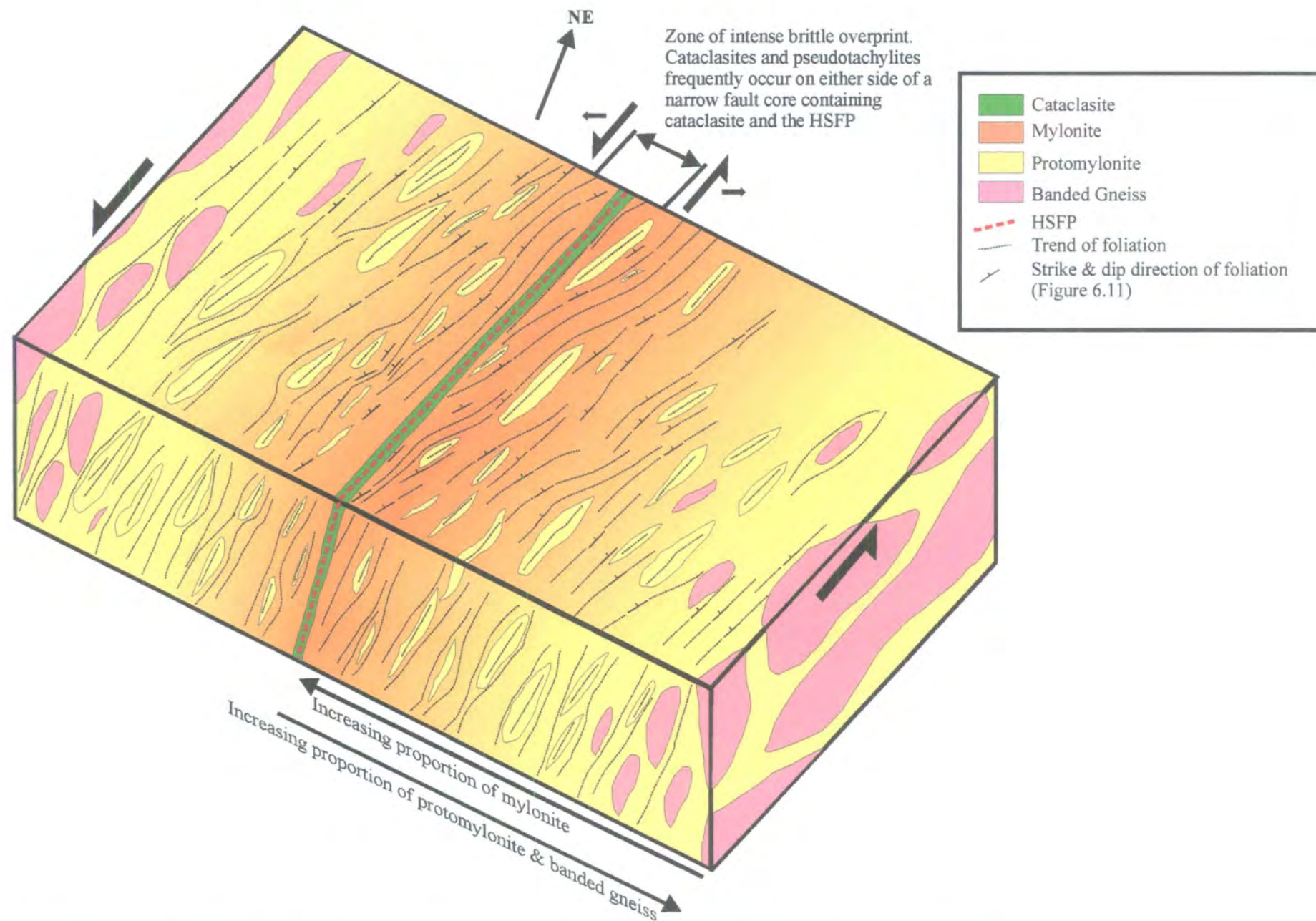


Figure 6.23 3D summary diagram to illustrate fault rock distribution and geometry within the HSFZ, Mefjellet. Not to scale.

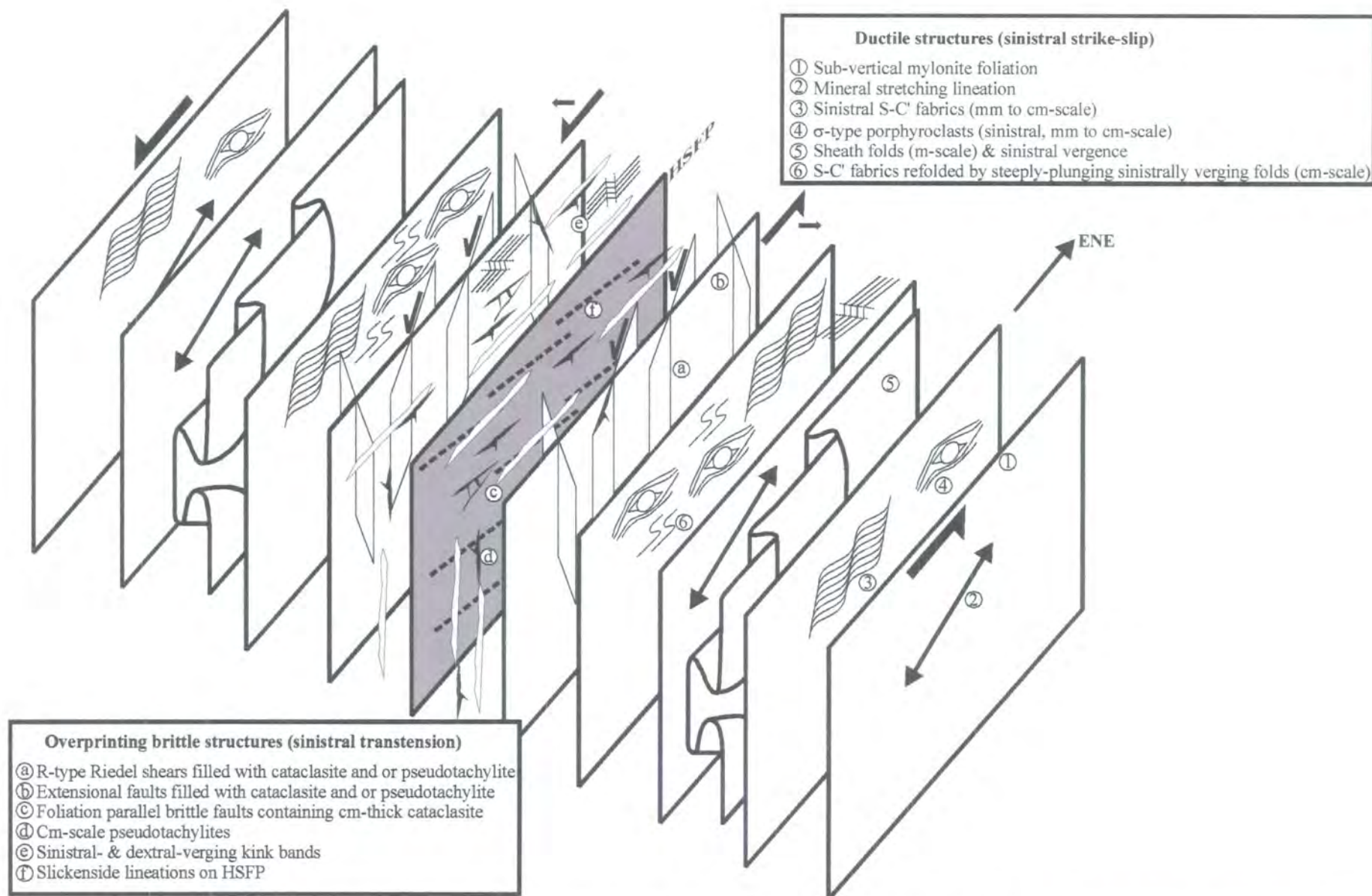


Figure 6.24 3D summary of ductile structures developed during sinistral strike-slip along the HSFZ, and overprinting brittle structures formed during sinistral transtension reactivation of the HSFZ, Mefjellet.

The occurrence of pegmatite and microdiorite dykes, and extensive quartz veining, which are clearly cross-cut by mylonite fabrics, and their increase in frequency towards the centre of the HSFZ, may indicate the presence of a precursor structure prior to the formation of the HSFZ. The dykes are restricted to the central part of the HSFZ, and have not been found outside the HSFZ within the protolith banded gneisses. Therefore, the 1km-wide ductile shear zone, which represents the earliest recognised deformation along the HSFZ, may have localised along a pre-existing basement structure, such as a deep-seated igneous contact or a zone of dyking.

Reactivation of the HSFZ led to the development of overprinting, foliation-parallel and cross-cutting cataclasites and pseudotachylites (Figure 6.23), together with the formation of W-dipping, N-S-trending extensional faults, which link into the HSFP, and other sub-parallel structures. The abundance of these extensional faults, which link into sinistral strike-slip ENE-WSW-orientated faults, indicates sinistral transtension. Other brittle structures include Riedel shears and slickenside and slickenfibres lineations, all of which are consistent with sinistral transtensional reactivation of the HSFZ (Figure 6.24). Pseudotachylites that formed during sinistral transtension are dated at 291 ± 14 Ma (Ar-Ar infrared laser ablation; this study, see section 7.2).

Locally, millimetre-thick zeolite mineralisation infills pre-existing NE-SW- to ESE-WNW-trending sub-vertical fractures; these veins carry sub-horizontal slickenside lineations. The fractures display dextral-strike slip offsets of several centimetres. Minor zeolite veining occurs in the HSF core, although there is no field evidence of dextral strike-slip reactivation within the HSF core itself in the Mefjellet area. These zeolite-filled fractures may represent localised reactivation of pre-existing structures, while the HSF core remained inactive.

It is difficult to gauge the displacement along the HSFZ as no reliable marker horizons exist. The same protolith is exposed on either side of the fault zone so lateral displacement can be no more than a few tens of kilometres.

6:3:2 Hammardalen quarry and road cut

The HSFZ is poorly exposed in a steep-sided wooded valley (Hammardalen, 20km WSW of Mefjellet). In the lower part of Hammardalen, a disused quarry and an ENE-WSW-trending road cut along the 719 road to Botngård provide good exposures, to the south and north of the HSFP trace, respectively (locality q; Figure 6.1; Figure 6.25). The central part of the HSFZ defines an ENE-WSW-orientated linear valley defined by streams and an alignment of lakes surrounded by cliffs and rocky crags. Both to the northwest and to the southeast of the HSFZ, gneisses belonging to the Banded Gneiss Complex of Fosen (see sections 6:2:1; 5:1:2 1) are exposed (Figure 6.1). At this locality, the true extent of the fault-related deformation is less clear due to the poverty of exposure.

6:3:2:1 Fault rocks

In this section, fault rocks are described in the order of their relative age (oldest to youngest; see section 6:3:2:2).

6:3:2:1a Protomylonite

Protomylonite-series rocks derived from quartzo-feldspathic banded gneisses (similar to those exposed at Mefjellet, section 6:3:1; section 6:2:1) are exposed at the Hammardalen quarry and road section (Figure 6.25). The grey-coloured quartzo-feldspathic mylonites contain approximately 50% feldspar, 25% quartz, 10% muscovite, 10% epidote and 5% chlorite and biotite, with minor amounts of sphene. Millimetre-scale bands of fine-grained feldspar and muscovite aggregates are interlayered with quartz-rich bands. The fine-grained matrix wraps around plagioclase, orthoclase and epidote / quartz aggregate porphyroclasts, which are typically 2mm to 3cm in length. The protomylonites contain a foliation defined by stretched and flattened aggregates of quartz, feldspar and mica. The proportion of matrix varies from 10% to almost 50%, so that the rocks can be classified as protomylonites.

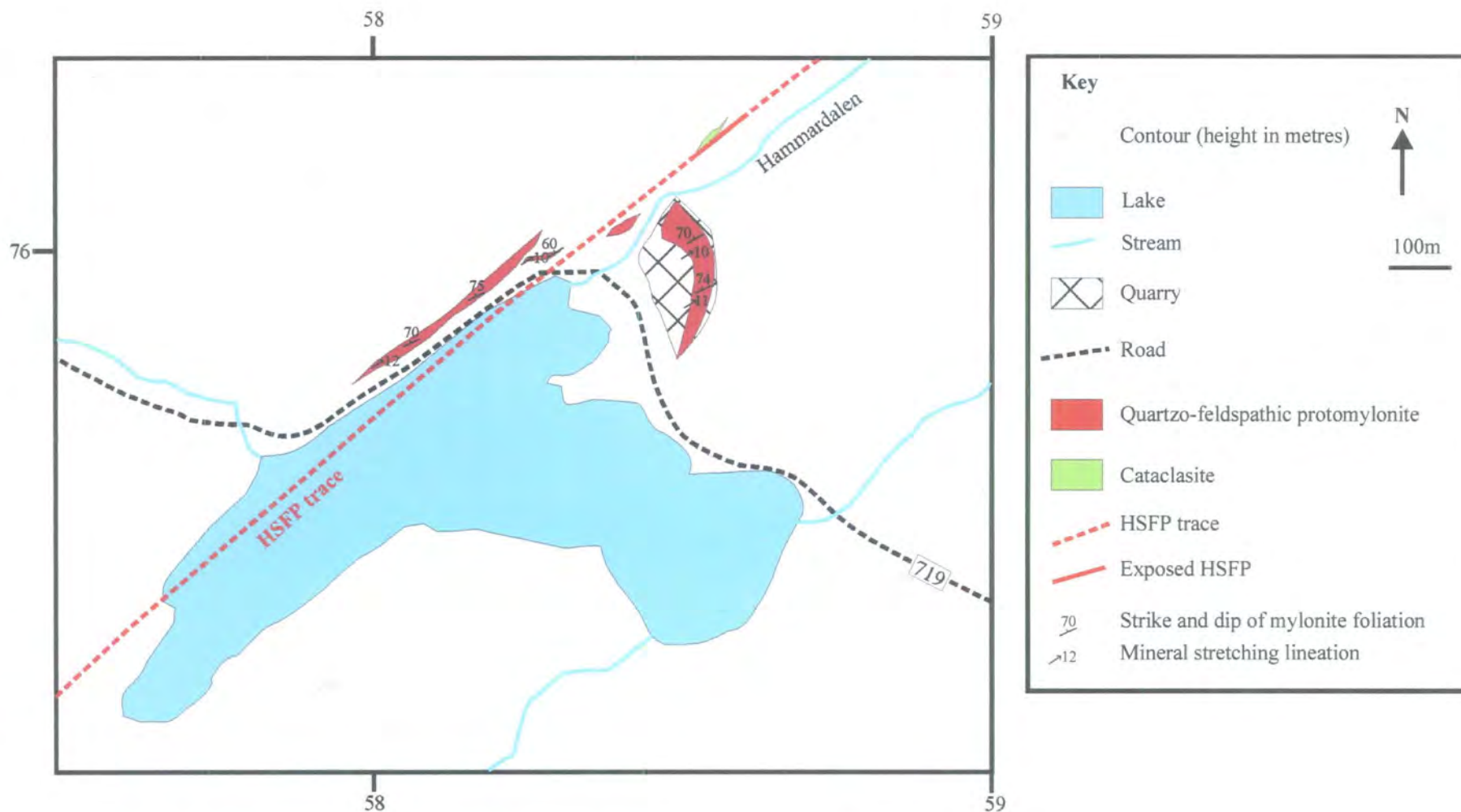


Figure 6.25 Geological outcrop map of the HSFZ at Hammardalen quarry. Located as q in Figure 6.1.

6:3:2:1b Cataclasite

Cataclastic-series rocks exposed in Hammardalen (Figure 6.25) are derived entirely from quartzo-feldspathic protomylonites. The cataclasites are pale-green in colour, comprising finely-comminuted clasts of mylonite, pseudotachylite, orthoclase, plagioclase, quartz, chlorite, epidote, muscovite and sphene set within a fine-grained cataclastic matrix. Randomly orientated clasts are angular to sub-angular, ranging from 5mm to less than 0.5mm in size. Feldspars are almost completely replaced by sericite grains within the fragmented protomylonite clasts. Pyrite grains less than 1mm to 5mm are disseminated through the matrix. The cataclasites possess no internal fabric and appear to be isotropic in the field on all scales of observation. Epidote and quartz veins cross-cut the cataclasites and occur locally as clasts within the cataclasite matrix. The proportion of matrix varies from approximately 50% to 90%, so that the rocks can be subdivided into cataclasites and ultracataclasites based upon the proportion of matrix.

6:3:2:2 Fault rock distribution and age relationships

To the northwest and southeast of the HSFP trace (Figure 6.25), centimetre-thick ENE-WSW- to NW-SE- and N-S-trending epidote veins and cataclasites cross-cut the protomylonites. Locally, millimetre-thick calcite and zeolite veins overprint the cataclasites, and appear to localise along pre-existing cataclasite-filled fractures.

A cataclasite, at least 1m thick, is exposed as rocky crags in a wooded area within Hammardalen (5855 7618). The cataclasites overprint and are derived entirely from quartzo-feldspathic mylonites. They are texturally very similar to those exposed within the centre of the HSF core at Mefjellet, and therefore represent the only exposures of the fault core at Hammardalen. Centimetre- to millimetre-scale quartz, zeolite and calcite veins transect the cataclasite.

6:3:2:3 Fault zone structure

In the quarry to the south of the HSFP trace and along a road cut to the north of the fault (Figure 6.25), the protomylonites (Plate 6.23A) display a foliation defined by flattened and stretched aggregates of quartz and feldspar, which trends ENE-WSW and dips steeply to the NW (Figure 6.26A). Lineations defined by elongate quartz, feldspar, mica and sphene plunge shallowly to the ENE (Figure 6.26A; Plate 6.23B). On outcrop surfaces viewed parallel to the stretching lineation and normal to the foliation, centimetre-spaced S-C' fabrics are abundant and are consistent with sinistral shear (Plate 6.23A). Locally, feldspar clasts display σ -type geometries consistent with sinistral shear. Steeply-plunging, centimetre-scale folds with a consistent sinistral sense of vergence refold the protomylonite fabric and shear bands (Plate 6.24). Axial planes are orientated E-W and dip steeply to the N (Figure 6.26B). The folds appear to nucleate from axial planar quartz veins (1cm to 3cm thick) which cross-cut the foliation.

Brittle deformation is widespread both north and south of the HSFP trace. Cataclasite-filled faults appear to localise along the pre-existing mylonitic foliation (Figure 6.27A; Plate 6.25C). Hammardalen quarry provides a NE-SW-trending cross-section where the faults are spaced between 1m and 5m apart (Plate 6.25A&B). The cataclasites contain sub-horizontal slickenside lineations (Figure 6.27A) and display braided geometries, where they link into sub-parallel and E-W-trending structures (Figure 6.27B). E-W-trending structures with sub-horizontal slickenside lineations and millimetre- to centimetre-thick cataclasite offset the mylonite foliation by 2cm to 1m in a sinistral strike-slip sense. The E-W structures display sinistrally verging drag folds and are interpreted as P-type Riedel shears formed as a result of sinistral strike-slip movements along the HSFP (Plate 6.25D). Foliation-parallel fault surfaces adjacent to cataclasites contain centimetre- to metre-scale grooves, which plunge shallowly to the WSW (Figure 6.28; Plate 6.26A-C). On fracture surfaces, quartz slickenfibres plunge moderately to the NE and overprint grooves (Plate 6.26AC&D). The slickenfibres are curved on a centimetre- to metre-scale (Plate 6.26A) and are consistent with sinistral oblique-reverse movements, based upon the stepping direction of the quartz mineral fibres (Plate 6.26D).

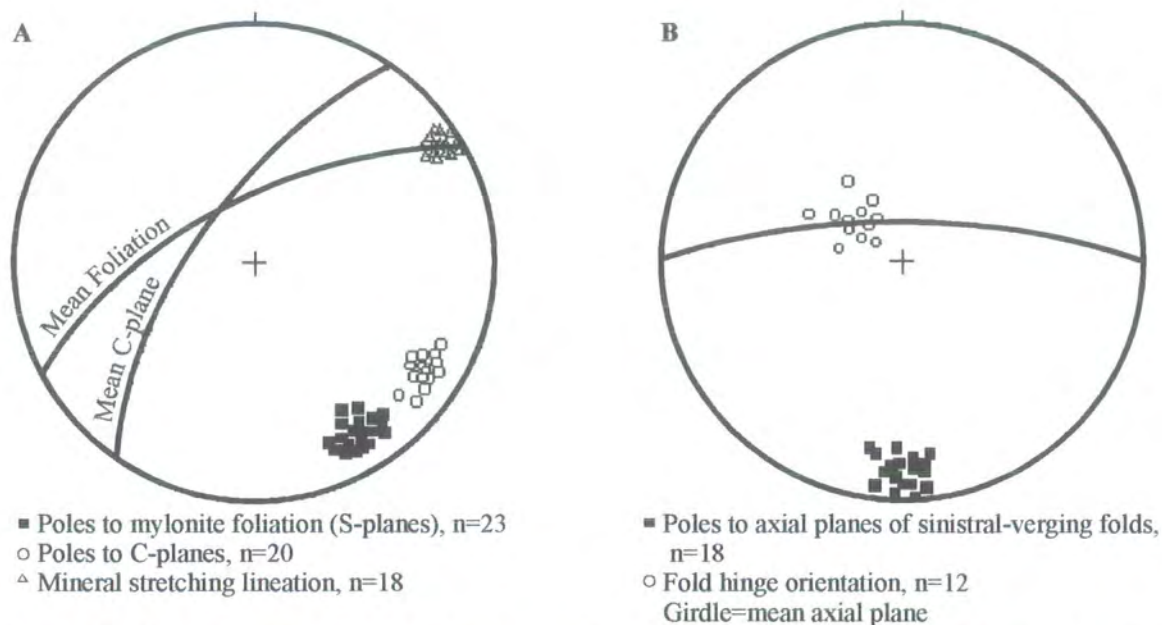


Figure 6.26 Stereographic projections of data collected in Hammardalen quarry and road section to show (A) mylonite foliation, shear bands and lineation and (B) Centimetre-scale sinistral-verging folds.

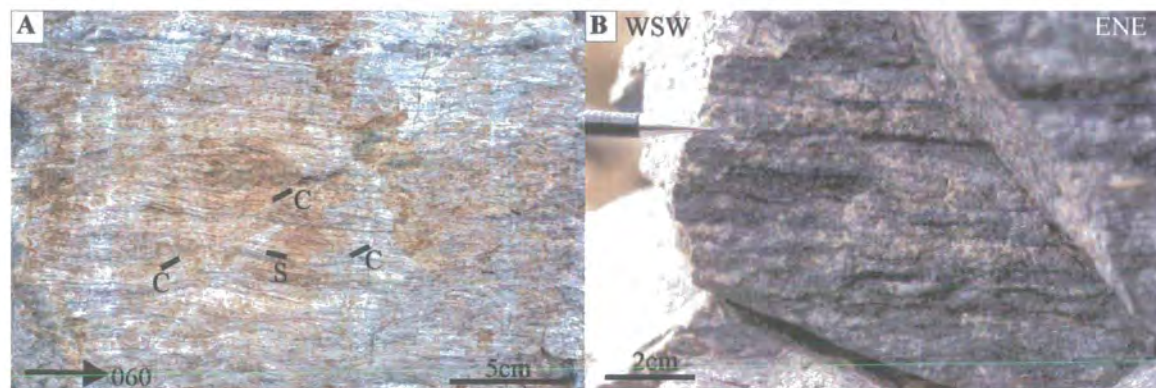


Plate 6.23 (A) Plan view. Image of protomylonite with centimetre-spaced S-C' fabric. C=C-planes, S= S-planes. (B) View of sub-vertical foliation plane. Image to show sub-horizontal lineation defined by elongate quartz, feldspar and mica grains.



Plate 6.24 Plan view. Image to show steeply-plunging centimetre-scale fold with a sinistral sense of vergence.

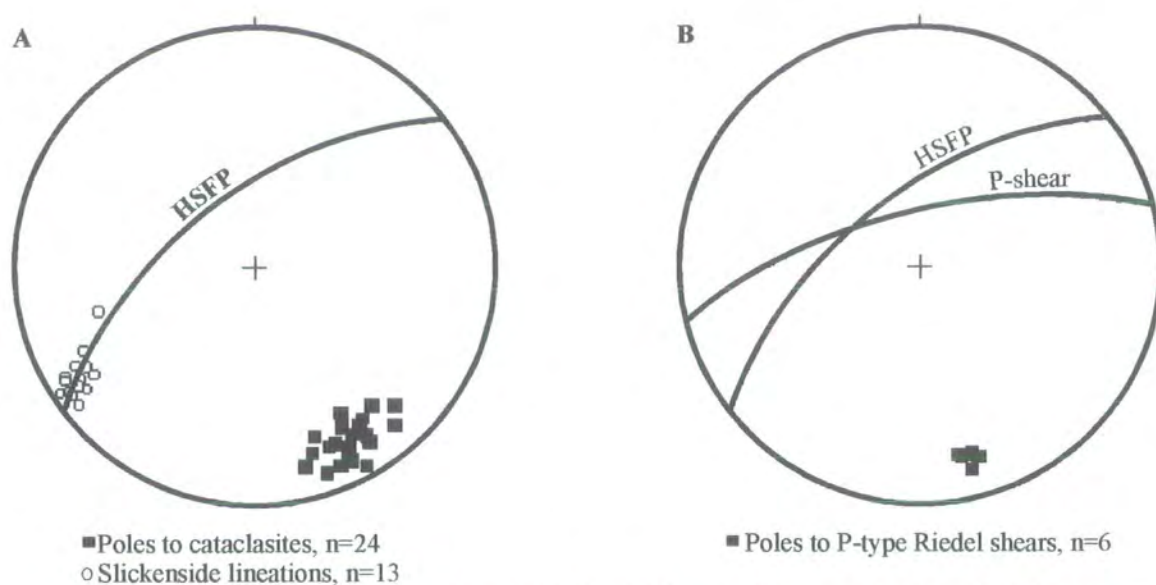


Figure 6.27 Stereographic projections of data collected in Hamnardalen quarry and road section to show (A) foliation-parallel cataclasites and (B) P-type Riedel shears.

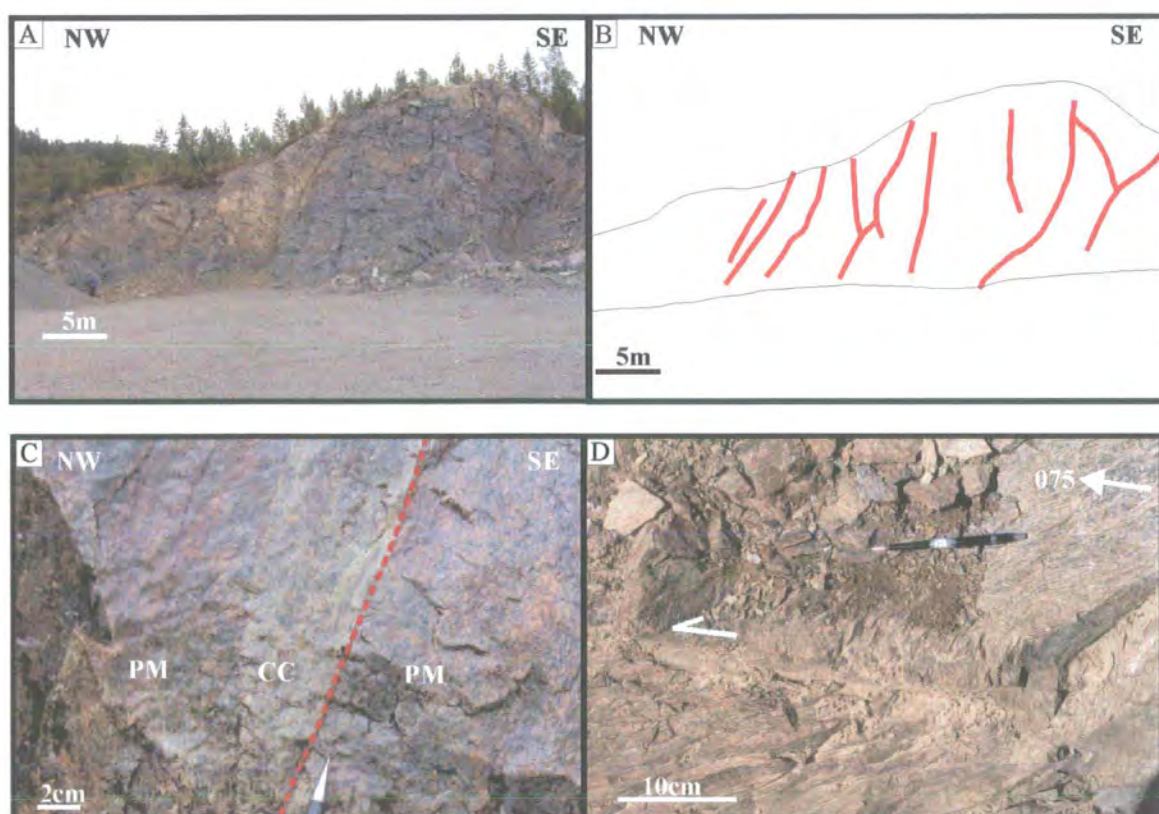


Plate 6.25 (A) View of sub-vertical quarry face, looking ENE. (B) Sketch of (A) to show the location of cataclasite-filled faults. (C) View of steeply dipping foliation-parallel cataclasite (CC) developed within protomylonite (PM). Dashed line - mylonite foliation. (D) Plan view. Image to show P-type Riedel shear with a sinistral strike-slip offset.

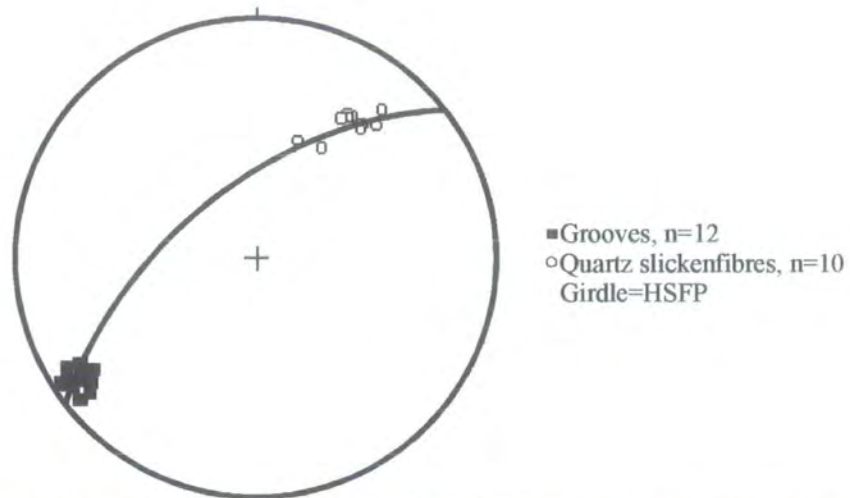


Figure 6.28 Stereographic projection to show the orientation of grooves and quartz slickenfibres on fault surfaces adjacent to cataclasites.

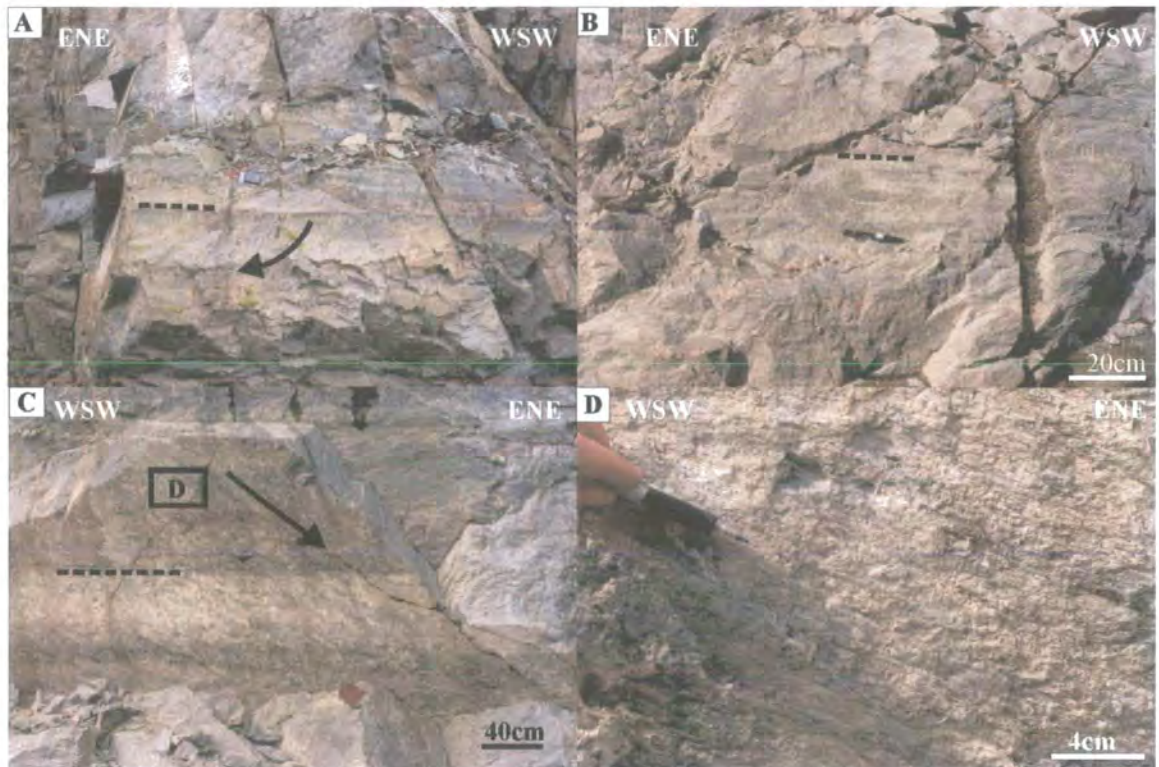


Plate 6.26 Views of ENE-WSW-trending fault surfaces which dip steeply to the NW (A) Fault surface (parallel to HSFP) with centimetre-scale grooves (dashed line) plunging shallowly to the WSW with curved quartz slickenfibres (arrow) on top, Hammardalen quarry, southeast of HSFP. (B) Centimetre-scale grooves on fault surface parallel to HSFP, Hammardalen quarry, southeast of HSFP. (C) Metre-scale sub-horizontal grooves on fault surface (dashed line) (HSFP parallel) overprinted by quartz slickenfibres (arrow) which plunge moderately to the ENE, road section northwest of HSFP. (D) Close up of slickenfibres located on (C) to show stepping direction is consistent with sinistral shear, road section northwest of HSFP.

Zeolite veins (1mm to 2cm) containing calcite cores are exposed north of the HSFP trace along the road section and appear to localise along pre-existing ENE-WSW- and N-S-trending cataclasites.

The HSFP itself is exposed adjacent to some rocky crags in the heavily wooded Hammardalen. The HSFP is orientated 052/65NW with slickenside lineations plunging shallowly to the WSW (6/235) (Figure 6.29; Plate 6.27C). On the north side of the HSFP, at least 1m of pale-green cataclasite derived from protomylonite is exposed (Plate 6.27A&B). The cataclasite is isotropic on all scales of observation in the field. Iron staining is ubiquitous within the cataclasite together with pyrite mineralisation. The cataclasite immediately to the north of the HSFP is weathered to a pale-grey coloured material (Plate 6.27D). Millimetre-scale quartz, calcite and zeolite veins cross-cut the cataclasite. Locally, the fault plane contains a maroon-coloured mineralisation, possibly zeolite.

The overprinting of sinistral oblique slickenfibres on top of sinistral strike-slip grooves in areas to the northwest and southeast of the HSFP, may reflect partitioning of localised sinistral transpression (Figure 6.30). Sub-horizontal grooves were formed during sinistral strike-slip movements, while sinistral-oblique slickenfibres were formed as a result of localised partitioning of sinistral transpression (Figure 6.30B). In places, the slickenfibres are curved, which reflects the along-strike change from sinistral strike-slip to sinistral-oblique reverse movements (Figure 6.30C).

6:3:2:4 Kinematic summary and discussion

The kinematic evolution of the HSFZ at the Hammardalen quarry and road section is summarised in Table 6.2.

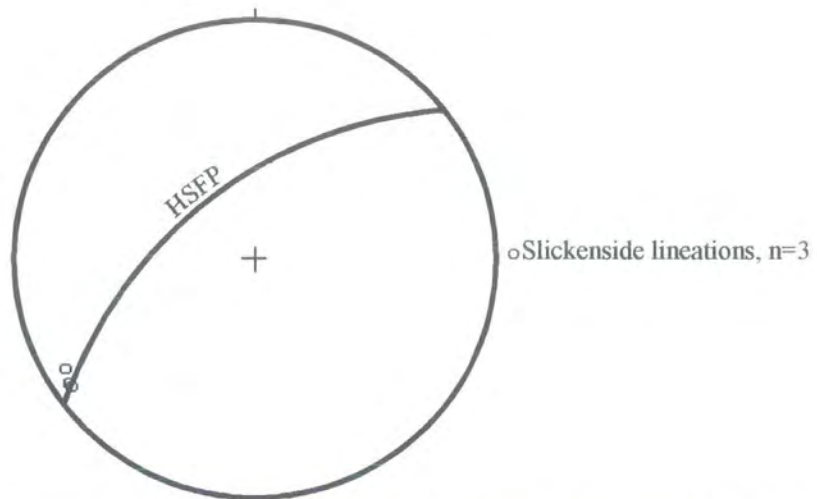


Figure 6.29 Stereographic projection of the HSFP and slickenside lineations in Hammardalen (5855 7618).

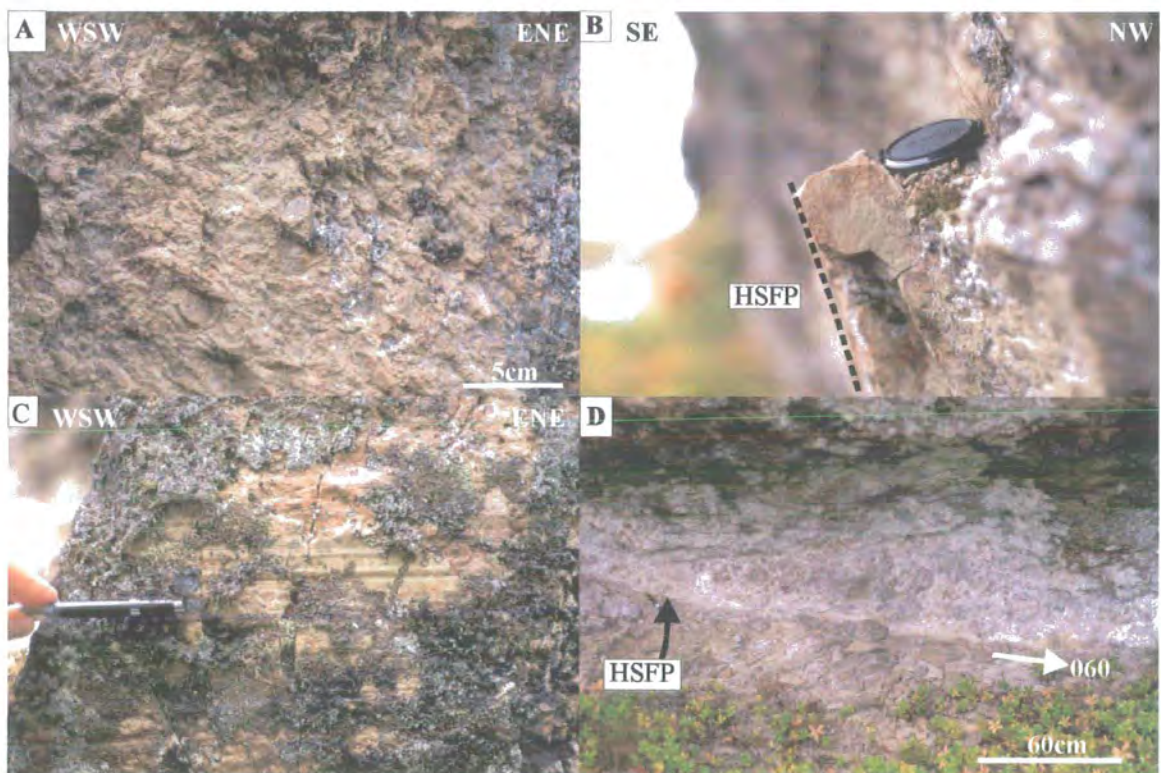


Plate 6.27 (A) Cataclasite 50cm northwest of the HSFP, Hammardalen (5855 7618). (B) Ultracataclasite adjacent to the HSFP. (C) Slickenside lineations on HSFP plunge shallowly to the WSW. (D) Plan view. Pale grey weathered zone adjacent to the HSFP.

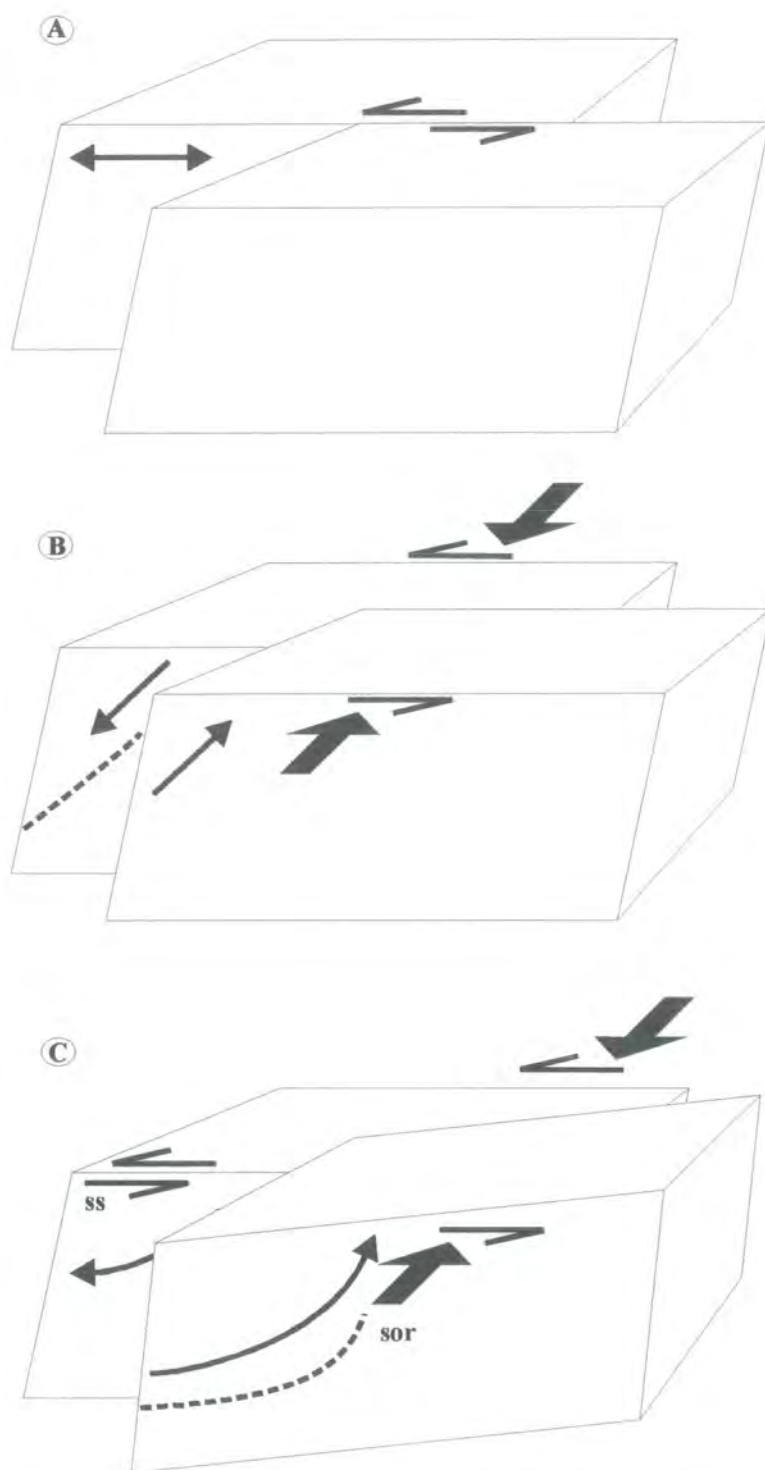


Figure 6.30 Model to explain sinistral strike-slip grooves which are overprinted by sinistral-oblique reverse quartz slickenfibres along fault surfaces which trend ENE-WSW and dip steeply to the NW. Split arrows indicate shear sense parallel to lineation. Large black arrows represent compression direction. (A) Sinistral strike-slip movements lead to the formation of groove marks (double-ended arrow). (B) Localised partitioning of sinistral transpression leads to sinistral-oblique reverse movements (dashed lines - slickenfibres) which overprint sinistral strike-slip movements. Arrows indicate relative motion of fault blocks (C) Curved slickenfibres (dashed line) may be produced by changes from sinistral strike-slip (ss) movements to sinistral-oblique reverse (sor) movements along strike of the fault surface.

Kinematic regime	Fault rocks / structures
3. ? (youngest)	<ul style="list-style-type: none"> ◦ Zeolite and calcite veining
2. Sinistral strike-slip with localised transpression	<ul style="list-style-type: none"> ◦ Cataclasites ◦ P-type Riedel shears ◦ Quartz slickenfibres ◦ Slickenside lineations ◦ Grooves ◦ Quartz slickenfibres
1. Sinistral strike-slip (oldest)	<ul style="list-style-type: none"> ◦ Mylonites ◦ Centimetre-spaced S-C' fabric ◦ σ-type porphyroclasts ◦ Steeply-plunging sinistral-verging folds

Table 6.2 Table summarising the kinematic evolution of the HSFZ at Hammarkalen.

The HSFZ in the Hammarkalen area shows protomylonites overprinting compositionally banded gneiss both to the northwest and to the southeast of the HSFP. The protomylonites represent the earliest fault-related deformation at this locality and were formed during sinistral shear (indicated by S-C' fabrics, folds and σ -type porphyroclasts). Later brittle deformation led to the formation of foliation-parallel faults and fractures containing cataclasites (quartz slickenfibres, P-type Riedel shears and slickenside lineations) consistent with sinistral strike-slip movements along the HSFP. Localised transpression to the northwest and southeast of the HSFP resulted in the overprinting of sinistral-oblique, reverse, quartz slickenfibres on top of sub-horizontal groove marks formed during sinistral strike-slip movements. A later phase of zeolite and calcite mineralisation fills pre-existing cataclasite-filled fractures and faults.

6:3:3 Follavatnet traverse and Brattreitelva stream section

The HSFZ is partially exposed along the north side of Follavatnet and along a wooded track and stream section along Brattreitelva (Figures 6.1, 6.31). The HSFP is unexposed in this area but can be traced on the Landsat™ image and geological maps from Mefjellet (section 6:3:1), which is 20km to the WSW. Here, the HSFP defines a series of linear lakes, streams and steep-sided valleys.

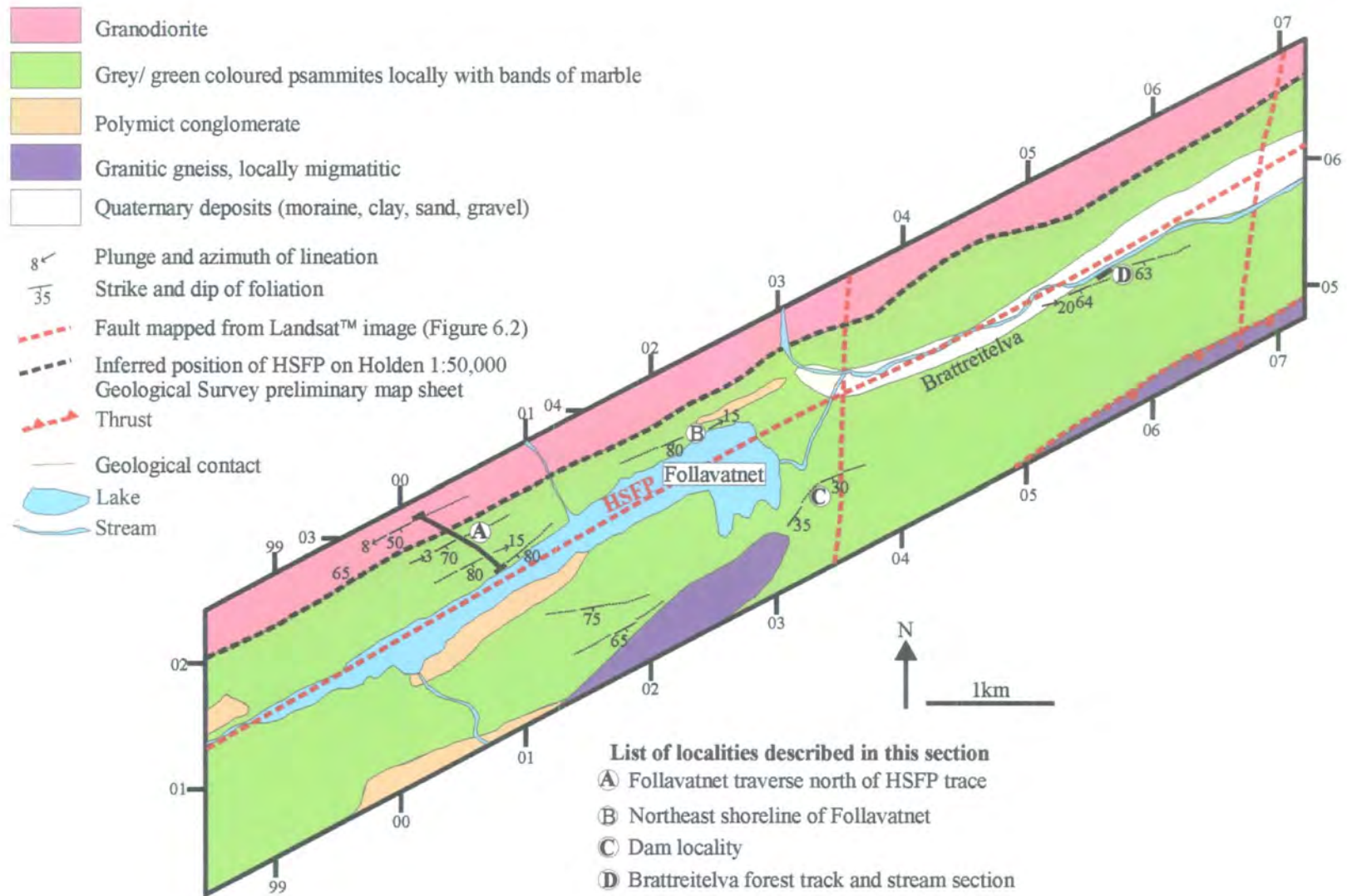


Figure 6.31 Geological map to show the location of the Follavatnet and Brattreitelva localities. Adapted from the preliminary 1:50,000 Holden sheet, NGU.

The Geological Survey maps show the HSFP 500m to 1km north of Follavatnet, separating psammities to the south from granodiorite to the north (Figure 6.31). This study suggests that the HSFP lies unexposed beneath Follavatnet and along Brattreitelva. The HSFP trace, interpreted from the Landsat™ image and geological maps compiled to the southwest, lies beneath Follavatnet and Brattreitelva. Field and thin-section observations support this interpretation and shows that fault-related deformation is clearly more intense along the northern shores of Follavatnet and along Brattreitelva than along the marked position of the fault on the Geological Survey map. The HSFZ is at least 600m wide at this locality and separates psammities occurring both to the northwest and to the southeast of the fault zone.

6:3:3:1 Fault rocks

6:3:3:1a Mylonites

Mylonitic rocks derived from granodiorite and a series of metasedimentary rocks comprising limestone, psammite and polymict conglomerates of uncertain origin, are poorly exposed to the north of Follavatnet and along Brattreitelva.

Mylonites derived from granodiorite

The grey-coloured, quartzo-feldspathic mylonites contain approximately 50% feldspar, 25% quartz, 10% muscovite, 10% epidote and 5% chlorite and biotite, with minor amounts of sphene. Millimetre-scale bands of fine-grained feldspar and muscovite aggregates are interlayered with quartz-rich bands. The fine-grained matrix wraps around plagioclase, orthoclase and epidote / quartz aggregate porphyroclasts, which are typically 2mm to 3cm in length. The mylonites contain a strong foliation defined by stretched and flattened aggregates of quartz, feldspar and mica. The proportion of matrix varies from 10% to almost 50%, so that the rocks can be subdivided into protomylonites and mylonites. The sub-vertical mylonitic foliation trends ENE-WSW and carries a sub-horizontal lineation defined by elongate quartz and feldspar together with aligned mica grains. On surfaces and in thin-sections viewed perpendicular to the mylonite foliation and parallel to the stretching lineation, σ - and δ -type porphyroclast geometries are well developed.

Mylonites derived from psammites and conglomerates

The green- to grey-coloured mylonites (Plate 6.28A&B) contain approximately 60% quartz, 15% feldspar, 20% muscovite and chlorite, and 5% epidote with minor amounts of calcite. Millimetre-scale bands of fine-grained quartz-rich bands are interlayered with chlorite and muscovite aggregates. The fine-grained matrix wraps around feldspar and host-rock porphyroclasts, which are typically 2mm to 10cm in length. The mylonites contain a strong foliation defined by stretched and flattened aggregates of quartz and mica. The proportion of matrix varies from 10% to almost 50%, so that the rocks can be subdivided into protomylonites and mylonites. The sub-vertical mylonitic foliation trends ENE-WSW and displays a sub-horizontal lineation defined by elongate quartz and aligned mica grains. On surfaces and in thin-sections viewed perpendicular to the mylonite foliation and parallel to the stretching lineation, σ - and δ -type porphyroclast geometries are well developed together with S-C'-type fabrics.

Mylonites derived from limestones (marbles) and schists

Marble mylonites interlayered with mylonites derived from schists are sporadically exposed along a wooded track and stream section in Brattreitelva. The mylonites display a strong millimetre- to centimetre-scale banding defined by variations in colour (blue, purple, white, yellow and pink) due to compositional variations. In thin-section, the mylonites comprise 95% fine-grained calcite grains (1 μ m to 0.25mm in length) with 5% quartz and white mica grains (~0.25mm) disseminated through the rock. The mylonites contain a foliation defined by flattened and stretched calcite grains with a lineation defined by elongate calcite grains. Stylolite surfaces formed as a result of dissolution are presently parallel to the foliation. In thin-sections cut parallel to the lineation and normal to the foliation, the calcite grains display a preferred orientation consistent with sinistral shear.

Dark grey to green coloured mylonites are derived from schistose rocks of uncertain origin. The mylonites comprise almost 100% fine-grained chlorite, biotite and muscovite, so that the rocks can be termed phyllonites (micaceous mylonite). The phyllonites contain a foliation and lineation defined by elongate mica grains.

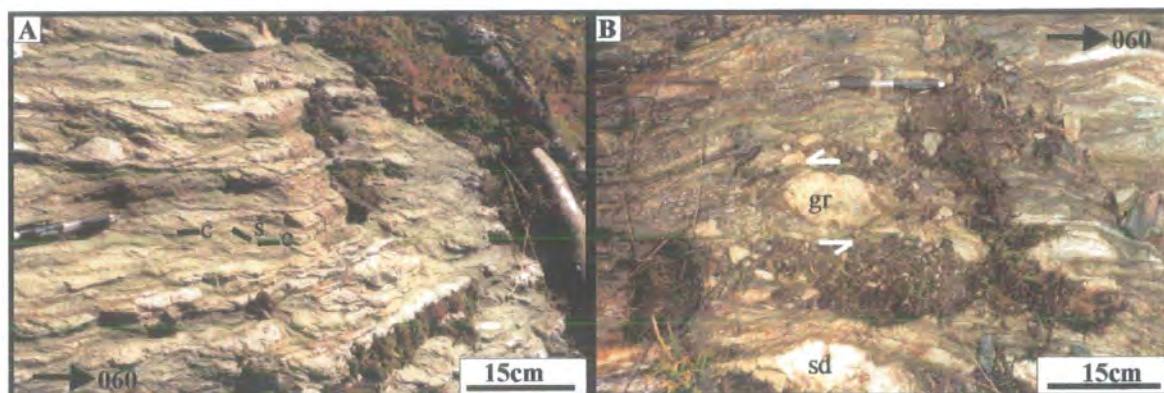


Plate 6.28 Plan view. (A) Mylonite derived from polymict conglomerate. Porphyroclasts of sandstone/psammite showing σ -type geometries consistent with sinistral shear are surrounded by fine-grained chlorite and muscovite interlayered with quartz-rich bands. Centimetre-scale S-C fabrics are abundant within the micaceous matrix and are consistent with sinistral shear (S, C). (B) Mylonite derived from polymict conglomerate. Large pebbles of granite (gr), sandstone (sd) and granodiorite are surrounded by green-coloured micaceous mylonite. Pebbles display σ -type geometries defined by fibrous overgrowths of mica are consistent with sinistral shear.

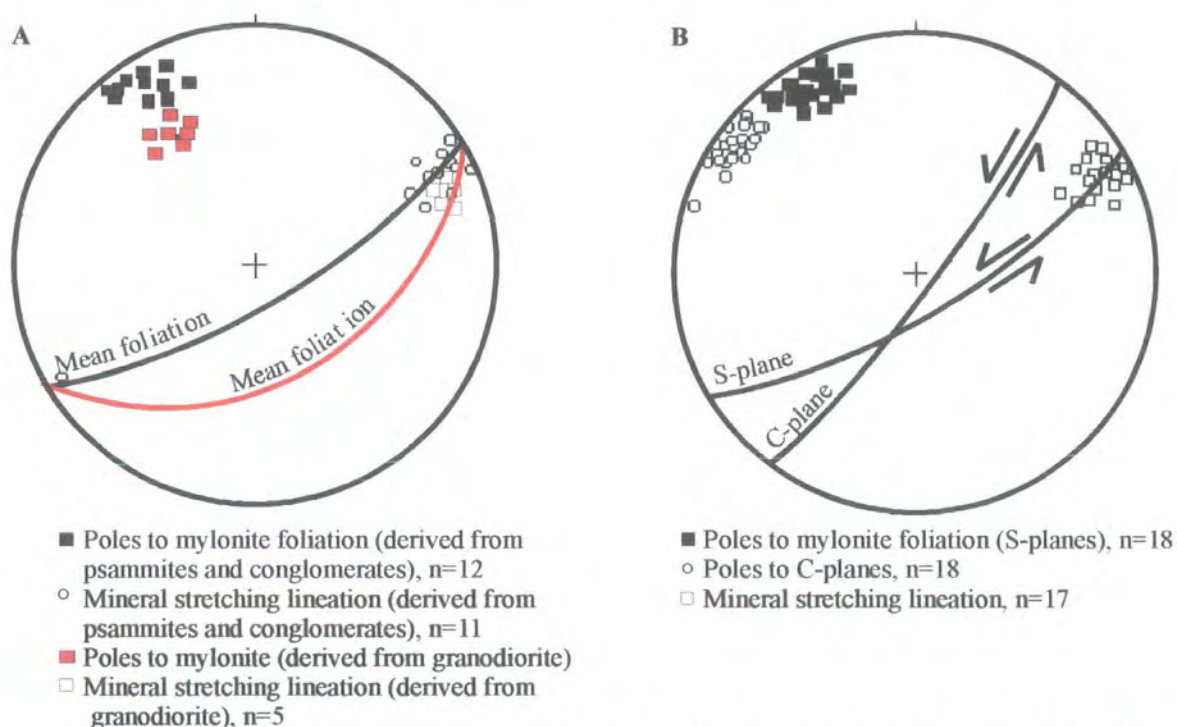


Figure 6.32 Stereographic projections of mylonite foliation and lineations northwest of the HSFP trace (A) Locality A. (B) Locality B.

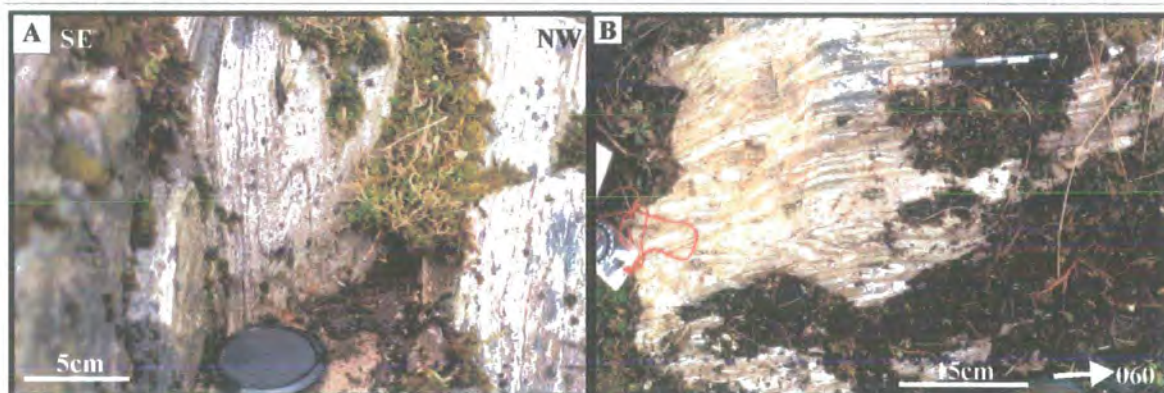


Plate 6.29 Mylonites derived from psammite (A) View of centimetre-scale tight- to isoclinal-folds which verge up towards the SE. (B) Plan view. Steeply-plunging centimetre-scale folds with a sinistral sense of vergence.

On outcrop surfaces viewed parallel to the lineation and normal to the foliation, millimetre- to centimetre-scale S-C' fabrics are well developed. Iron staining is ubiquitous.

6:3:3:2 Fault zone structure

The poorly-exposed HSFZ is at least 600m wide to the north of Follavatnet and along Brattreitelva. The HSFZ comprises a ductile shear zone containing mylonitised granodiorite together with slivers of mylonitised psammite, conglomerate, limestone (marble) and schist of uncertain origin. Limited brittle deformation overprints earlier formed fault rocks, exposed in a stream section along Brattreitelva towards the central part of the HSFZ.

6:3:3:2a NW of the HSFP trace [Locality A]

At 750m northwest of the HSFP trace (0018 0322), quartzo-feldspathic protomylonites overprint granodiorite. This is interpreted to represent the northwest limit of fault-related deformation. A foliation defined by stretched and flattened aggregates of quartz and feldspar trends ENE-WSW and dips moderately to the SE (060/50SE) (Figure 6.32A). A lineation defined by elongate quartz and feldspar grains together with aligned mica grains plunges shallowly to the WSW (8/240). In thin-sections cut parallel to the lineation and normal to the foliation, σ -type feldspar porphyroclasts (1mm to 5mm in diameter) are consistent with sinistral shear. The porphyroclasts represent 50% to 60% of the rock and are wrapped by fine-grained quartz-rich bands interlayered with fine-grained aggregates of muscovite and feldspar, so that the rocks can be classified as protomylonites. Later, overprinting, brittle deformation is virtually absent at this particular locality, both in the field and in thin-section.

Farther to the southeast, exposure is very poor. At 400m northwest of the HSFP trace (0056 0300), grey/ green mylonites derived from polymict conglomerates are exposed. Porphyroclasts and lenses of sandstone/ psammite (2cm to 20cm in length) are surrounded by anastomosing bands of fine-grained chlorite and muscovite

interlayered with quartz-rich bands (Plate 6.28A&B). A foliation defined by stretched and flattened quartz, chlorite and muscovite together with flattened pebbles of sandstone trends ENE-WSW and dips steeply to the SE (Figure 6.32A); and a lineation defined by elongate quartz and aligned mica grains plunges shallowly to the ENE. On outcrop surfaces viewed parallel to the lineation and normal to the foliation, sandstone/ psammite porphyroclasts display σ -type geometries consistent with sinistral shear (Plate 6.28B). Within the green-coloured micaceous-rich matrix, centimetre-spaced S-C' fabrics are consistent with sinistral shear.

Farther to the southeast (0080 0275), mylonitised psammites are commonly deformed by curvilinear centimetre-scale folds (Plate 6.29). When fold hinges are sub-horizontal, the almost isoclinal folds verge to the SE (Plate 6.29A). When the folds are steeply plunging they consistently show a sinistral sense of vergence (Plate 6.29B). The folds are interpreted to be curvilinear sheath folds formed during sinistral shear (c.f. Mefjellet section; section 6:3:1:3a).

Grey-coloured ultramylonites are exposed along the north side of Follavatnet (Plate 6.30A&B). In thin-sections viewed parallel to the lineation and normal to the foliation, millimetre-scale S-C' fabrics and σ -type porphyroclasts (0.5mm to 2mm) are consistent with sinistral shear. In plan view, centimetre-scale, ENE-WSW-trending isoclinal folds are common. In cross-section, centimetre-scale 'eye' structures and folds with both NW and SE vergence are common (Plate 6.30A&B). These structures are interpreted to be cross-sections through sheath folds formed during sinistral shear. Locally, the rocks are cross-cut by intense fracturing.

6:3:3:2b NW of the HSFP trace [Locality B]

At locality B (Figure 6.31), grey-coloured quartz-rich mylonites derived from psammites are exposed. A foliation defined by flattened and stretched aggregates of quartz together with aligned micas trends ENE-WSW and dips steeply to the SE (Figure 6.32B). A lineation defined by elongate quartz grains together with aligned mica plunges shallowly to the ENE. Centimetre-scale S-C' fabrics consistent with sinistral shear are common when viewed in outcrop surfaces viewed parallel to the lineation and normal to the foliation (Plate 6.31).

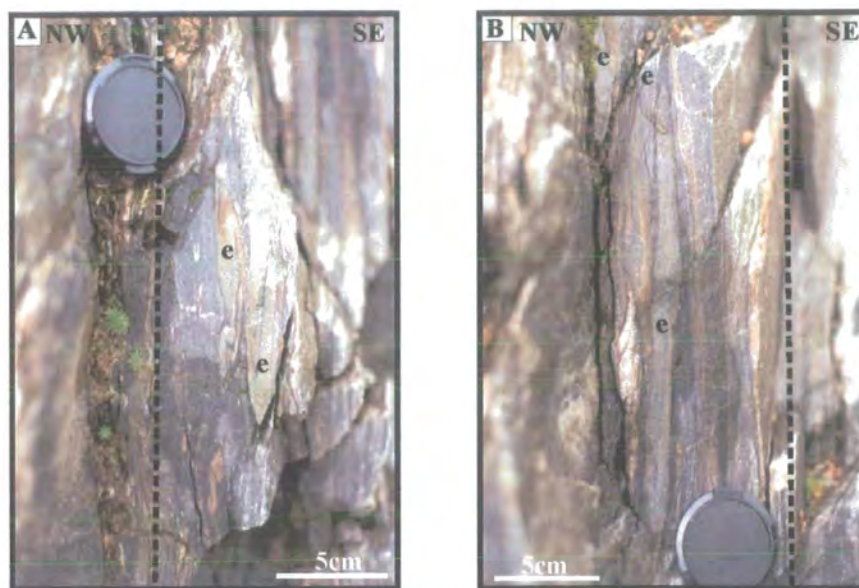


Plate 6.30 View of centimetre-scale 'eye' (e) structures within ultramylonites, which represent cross-sections through curvilinear folds with axial planes parallel to the steeply dipping foliation (dashed lines), northwest shoreline of Follavatnet. These folds are interpreted as sheath folds.



Plate 6.31 Plan view. Mylonitised psammite with centimetre-scale S-C' fabric consistent with sinistral shear, Locality B. Split arrows indicate shear sense parallel to lineation.

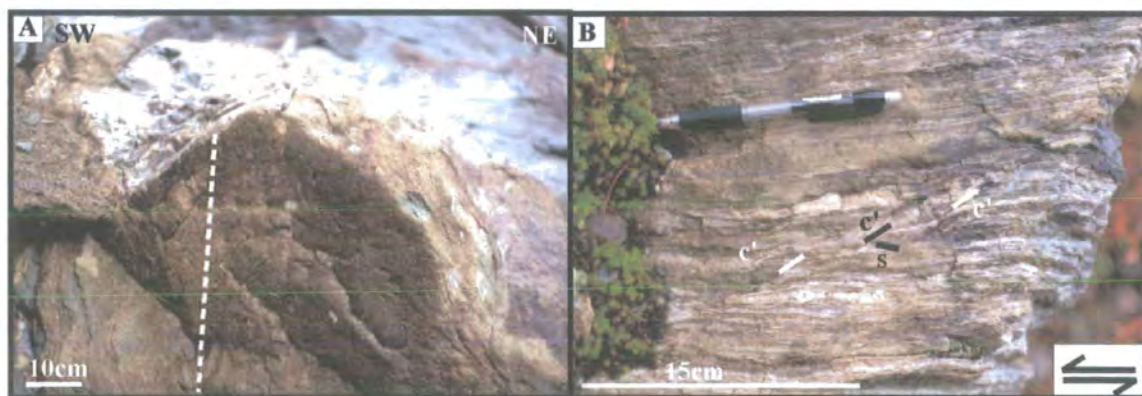


Plate 6.32 (A) Image to show psammite with ENE-WSW-trending open folds and axial planar fabric (dashed line) (locality C). (B) Plan view. Mylonite/ ultramylonite (locality D) derived from psammite with millimetre- to centimetre-scale S-C' fabric consistent with sinistral shear, Locality D. Split arrows indicate shear sense parallel to the lineation.

6:3:3:2c SE of the HSFP trace [Locality C]

At locality C (Figure 6.31; 750m southeast of the HSFP), green/ grey psammites are exposed. A foliation defined by flattened quartz aggregates trends ENE-WSW and dips shallowly to the SE; and a lineation defined by aligned quartz and mica grains plunges shallowly to the NE. The rocks are transected by ENE-WSW-trending open folds with sub-horizontal hinge orientations (Plate 6.32A). Near-vertical ENE-WSW-trending axial planar fabrics are locally well developed.

6:3:3:2d SE of the HSFP trace [Locality D]

To the southeast of the HSFP trace at locality D (Figure 6.31; Brattreitelva), a series of mylonites are derived from slivers of psammites, marbles and schists. Grey/ green mylonites derived from psammites (locality C) are very similar to those exposed at locality B. Millimetre-scale quartz-rich bands are interlayered with chlorite-rich bands and feldspar and muscovite aggregates. The foliation trends ENE-WSW and dips steeply to the SE and is defined by flattened and stretched quartz and feldspar together with aligned mica grains (Figure 6.33A). A lineation defined mainly by aligned mica grains plunge shallowly to the ENE. In thin-section and outcrop surfaces viewed parallel to the lineation and normal to the foliation, σ -type porphyroclasts and centimetre- to millimetre-scale S-C' fabrics are consistent with sinistral shear (Plate 6.32B). The S-C' fabrics are refolded by centimetre-scale steeply-plunging kink folds with a sinistral sense of vergence (Figure 6.33A). In thin-section, NE-SW, sub-millimetre thick cataclasites offset the mylonite foliation by several millimetres in an apparent sinistral sense.

Farther to the northeast along Brattreitelva, a series of intensely fractured marble mylonites are interlayered with phyllonites (derived from schists (Plate 6.33A&B)). Foliation within the marble, defined by stretched and flattened calcite grains and within the phyllonites defined by aligned chlorite, biotite and muscovite grains, trends ENE-WSW and dips steeply to the SE (Figure 6.33B). A lineation plunges shallowly to the ENE defined by aligned calcite (within marble mylonites) and mica (within phyllonite) grains.

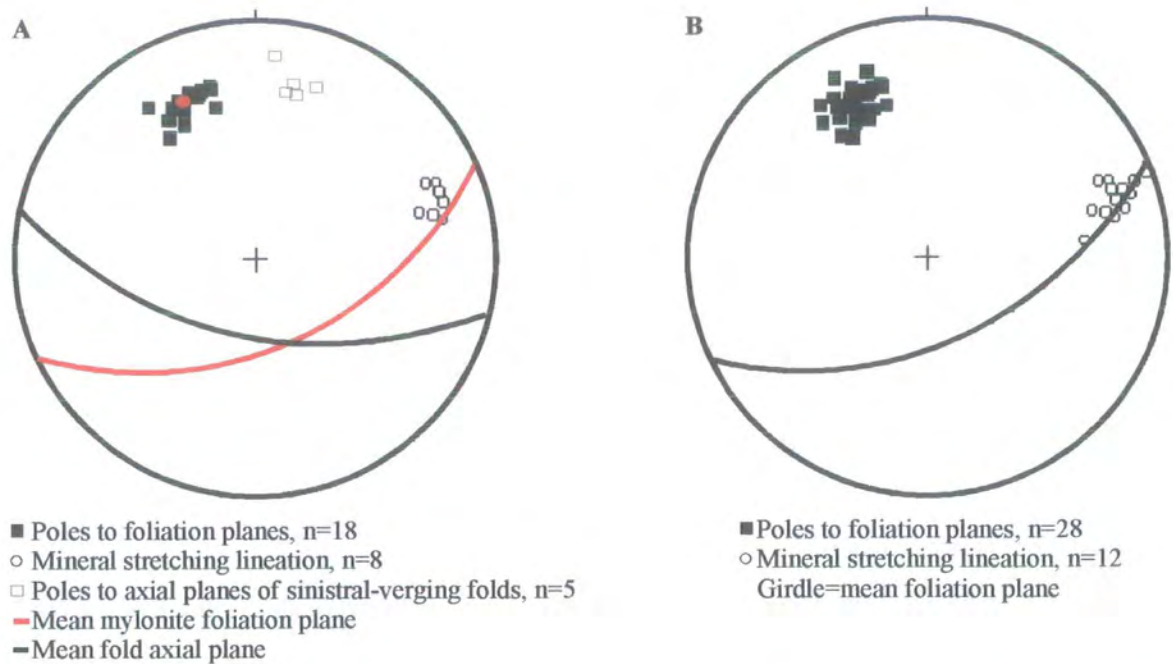


Figure 6.33 Stereographic projection to show structural data from locality D. (A) psammitic mylonite foliation, lineation and sinistral-verging folds. (B) marble mylonite and phyllonite foliation and lineation.

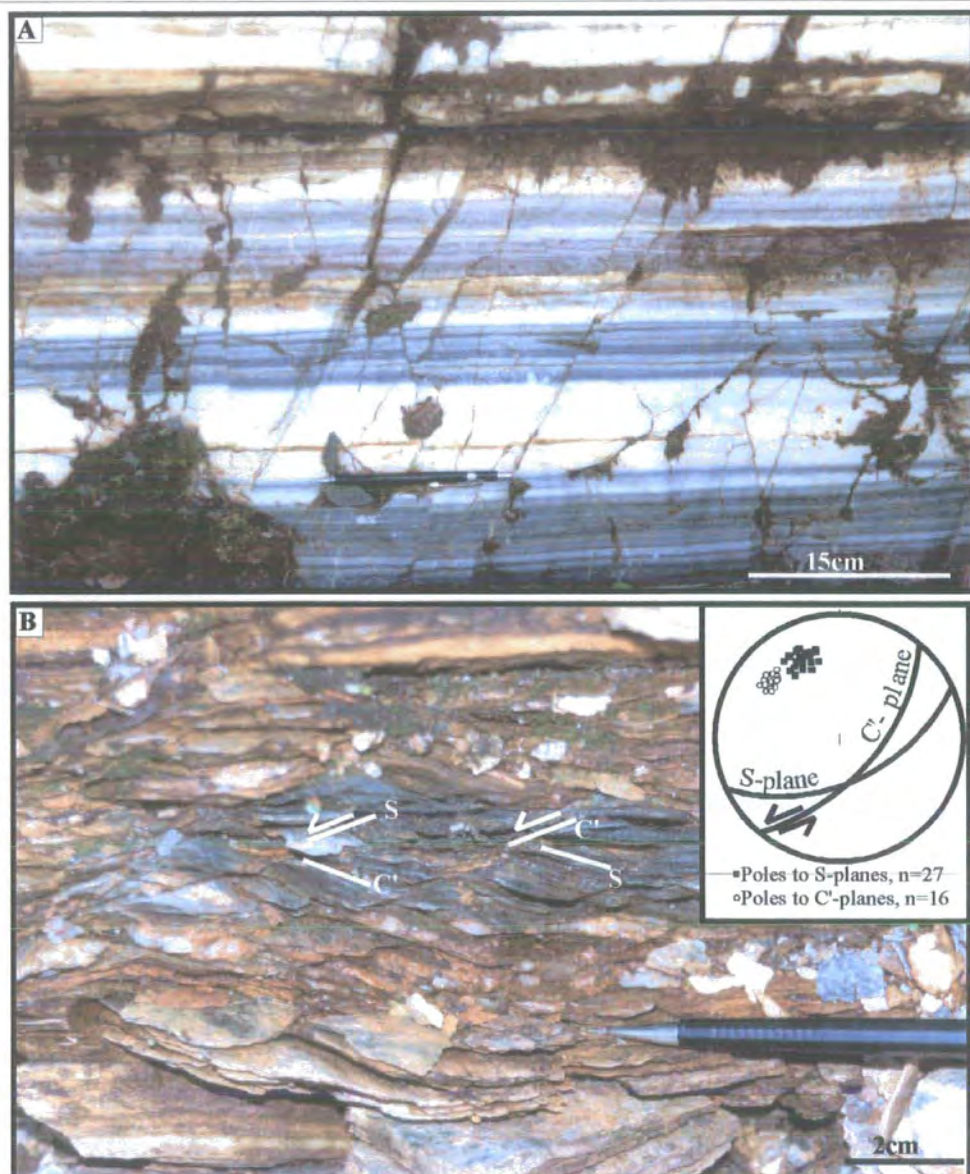


Plate 6.33 Plan view. (A) Marble mylonites, Locality D. (B) Centimetre-scale S-C' fabrics within phyllonites, Locality D.

The phyllonites display well-developed, centimetre-scale, S-C' fabrics consistent with sinistral shear (Plate 6.33B) in outcrop surfaces viewed parallel to the lineation and normal to the foliation. The marble mylonites do not display any S-C' fabrics or σ -type porphyroclast geometries (Plate 6.33A).

To the northeast in the stream section, marble mylonites display millimetre- to centimetre-scale isoclinal folds with ENE-WSW-trending, near-vertical axial planes (Plate 6.34A). Locally, the folds display a sinistral sense of vergence. Intense brittle deformation overprints the mylonite foliation at this locality. Sub-vertical foliation-parallel fractures with sub-horizontal slickenside lineations link into E-W trending fractures with sinistral strike-slip offsets of 2cm to 20cm (Plate 6.34C&D). The fractures are interpreted as P-type Riedel shears formed as a result of sinistral movements along the HSFP. The fractures commonly form braided geometries linking foliation-parallel structures. WNW-ESE-orientated sub-vertical fractures display dextral strike-slip offsets of a few centimetres (Plate 6.34B) and are interpreted as R'-type Riedel shears formed as a result of sinistral movement along the HSFP. Millimetre-thick, NNE-SSW-trending, tensional fractures are filled with calcite. Tensional calcite veins in this orientation are consistent with sinistral movement along the HSFP (Plate 6.34D).

6:3:3:4 Kinematic summary and discussion

The kinematic evolution of the HSFZ at Follavatnet and Brattreitelva is summarised in Table 6.3.

Kinematic regime	Fault rocks / structures
2. Sinistral strike-slip (youngest)	<ul style="list-style-type: none"> • P- and R'-type Riedel shears • Tensional calcite-filled veins
1. Sinistral strike-slip (oldest)	<ul style="list-style-type: none"> • Mylonites • Centimetre-spaced shear bands and S-C' fabrics • σ-type porphyroclasts • Steeply-plunging sinistral-verging folds

Table 6.3 Table summarising the kinematic evolution of the HSFZ at Hammarkalen.

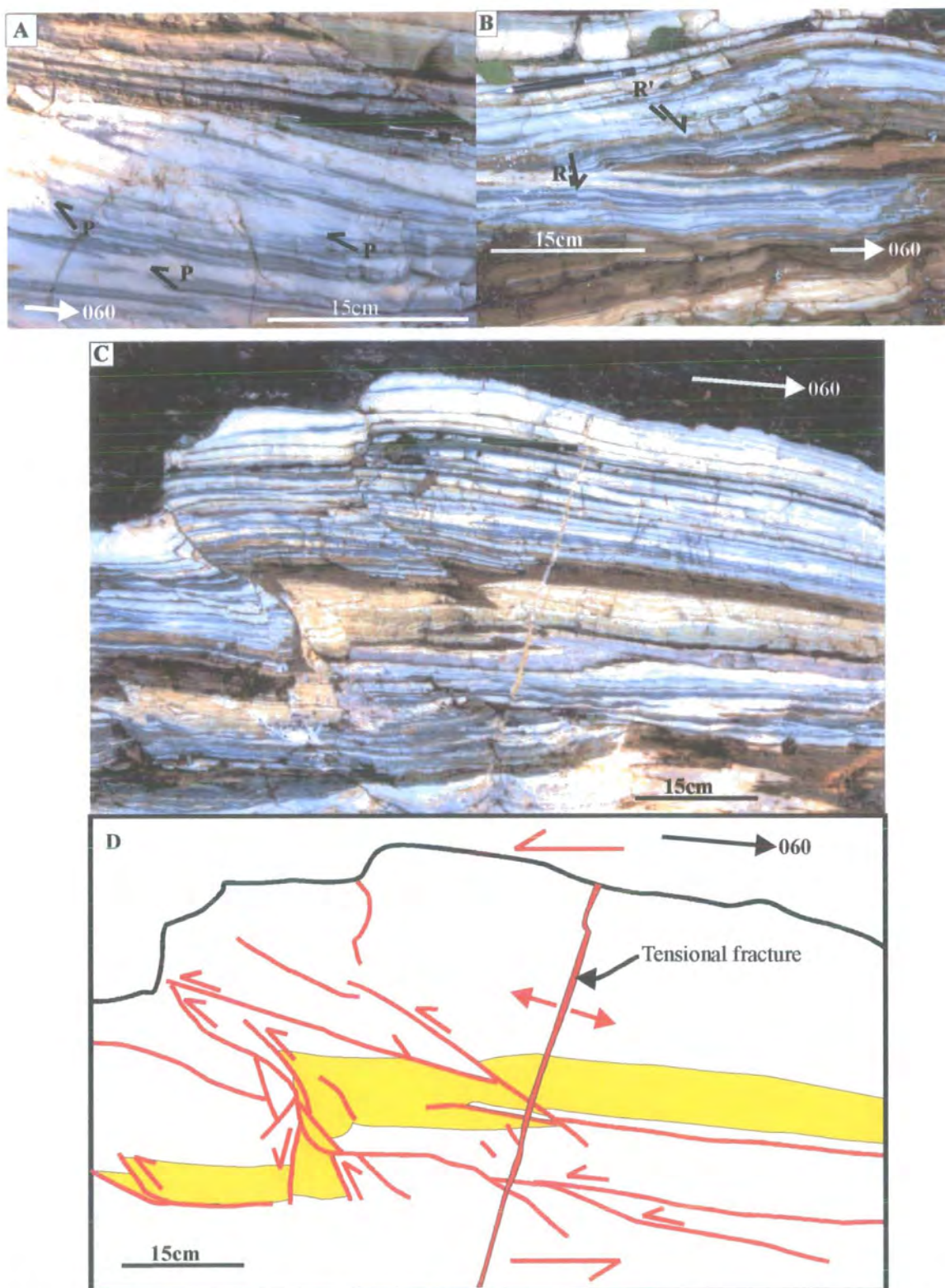


Plate 6.34 Plan view. (A) Marble mylonite with centimetre-scale isoclinal sinistral-verging folds and E-W-orientated fractures with sinistral strike-slip offsets. (B) ESE-WNW-trending fractures with dextral strike-slip offsets of a few centimetres. (C) Sub-vertical fractures forming braided geometries. Fractures orientated sub-parallel to the foliation link into E-W trending fractures with sinistral strike-slip offsets of 2cm to 20cm. E-W-trending fractures are interpreted as P-type Riedel shears. (D) Field sketch of the braided fracture networks shown in (C). All structures are found within Locality D.

The HSFZ in the Follavatnet and Brattreitelva area (Figure 6.31) is poorly exposed. Mylonites overprint slivers of granodiorite, psammite/ sandstone, conglomerate, schists and limestone to the northwest and southeast of the HSFP. The mylonites represent the earliest fault-related deformation at this locality and were formed during sinistral shear (S-C' fabrics, sinistral-verging folds, sheath folds and σ -type porphyroclasts). Later brittle deformation led to the formation of foliation-parallel faults and fractures (P- and R'-type Riedel shears) consistent with sinistral strike-slip movements along the HSFP.

6:4 The Verran Fault Zone: locality descriptions and structure

The Verran Fault Zone (VFZ) refers to a zone of rocks that are intensely deformed as a result of movement along the Verran Fault (VF) and includes all the faults between the main VF and the Elvdal Fault (EF) (Figure 6.34). Key components of the VFZ are exposed to the north of Verrasundet and in stream and road sections along Skaudalen to the southwest of Verrasundet (Figures 6.1, 6.34). In this section, the localities are generally described in order of decreasing distance to the VF plane (VFP) to illustrate the fault-normal variation in the geometry, cross-cutting relationships, spatial distribution and kinematic history exhibited by fault rocks within the VFZ.

Grønlie and Roberts (1989), Grønlie et al. (1991) and Bering (1992) have carried out the only detailed field studies to date of the VF to the north of Verrasundet. Lineament interpretations from Landsat™ images combined with analysis of aerial photographs and geological maps suggested a complex array of anastomosing faults, which display the geometric configuration of a dextral strike-slip fault zone (Grønlie and Roberts 1989). Grønlie and Roberts (1989) and Grønlie et al. (1991, 1994) interpreted a prolonged history of polyphase deformation varying from strike-slip through oblique-slip to dip-slip at different structural levels along the VF, north of Verrasundet. The VF was described as a 0.5 to 1km-wide ductile shear zone containing mylonites that was overprinted by polyphasal brecciation, hydrothermal alteration and pervasive veining (Grønlie and Roberts 1989; Grønlie et al. 1991).

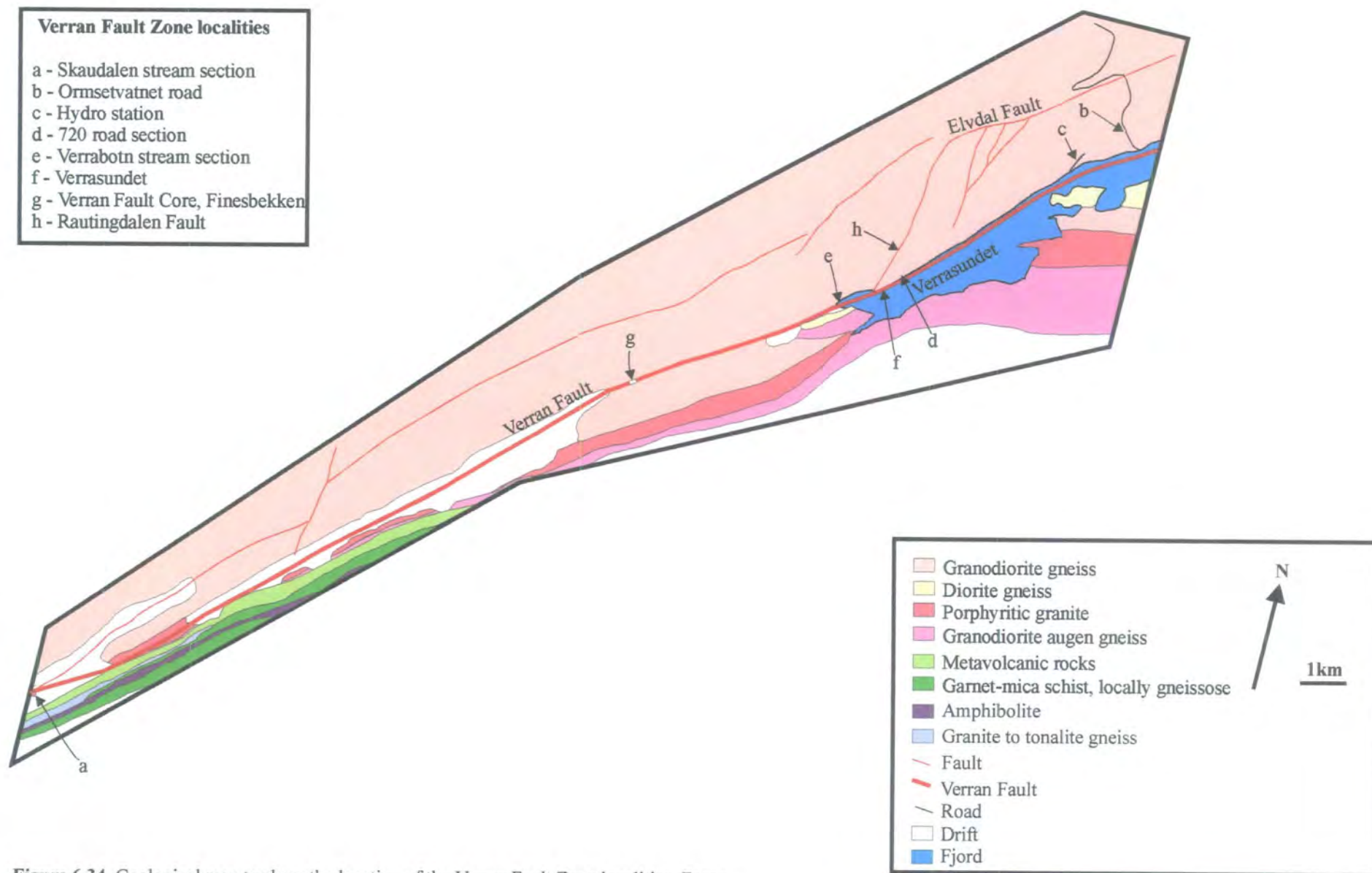


Figure 6.34 Geological map to show the location of the Verran Fault Zone localities, Fosen.

Fault-related deformation along the northern shoreline of Verrasundet was described as a 'crush zone', comprising cataclasites together with quartz-epidote breccias, which are cut by prehnite-matrixed cataclasites, which in turn are cut by extensive zeolite and calcite veining associated with brecciation (Grønlie and Roberts 1989). Grønlie et al. (1991) also described clasts of mylonite within cataclasites and N-S-trending pseudotachylites along the VF.

Bering (1992) measured slickenside lineations and other kinematic indicators on minor fault planes in selected areas to the north of Verrasundet. A system of slip vectors was established with an oblique-slip normal to pure dip-slip main component. The slip vectors, together with the minor fault plane orientations, were used to derive the deviatoric stress tensor responsible for the deformation. Bering (1992) concluded that the fault pattern along the VF is best interpreted as a set of dip-slip normal faults, which were formed during a pure crustal extension and not during strike-slip movements.

6:4:1 Air photograph interpretation of the Verran Fault Zone, N of Verrasundet

The air photograph (Figure 6.35) of the area to the north of Verrasundet illustrates the geometry of the VFZ on a hundreds of metres to kilometre scale. The VF trends ENE-WSW and defines the northern coastline of Verrasundet. To the south of Verrasundet, analysis of air photographs, together with field observations, suggests that the lineaments represent the regional foliation trend, which swings in an anticlockwise direction towards the VF. North of Verrasundet, the lineaments form 5 main orientations, ENE-WSW, NE-SW, NNE-SSW to N-S, NW-SE and E-W (Figure 6.35C). NW-SE- to E-W-trending structures appear to be shorter and less abundant than the more continuous and dominant ENE-WSW to NE-SW, NNE-SSW to N-S-orientated lineaments. The NNE-SSW- to N-S-trending lineaments (e.g. Rautingdalen Fault (RF); Figure 6.35B) splay from the VF and link into a series of ENE-WSW-trending lineaments farther north (e.g., Elvdal Fault; Figure 6.35B). The ENE-WSW-trending lineaments parallel to the main bounding structures are linked by a series of en échelon NNE-SSW- and NE-SW-trending lineaments on a variety of scales (Figure 6.35).

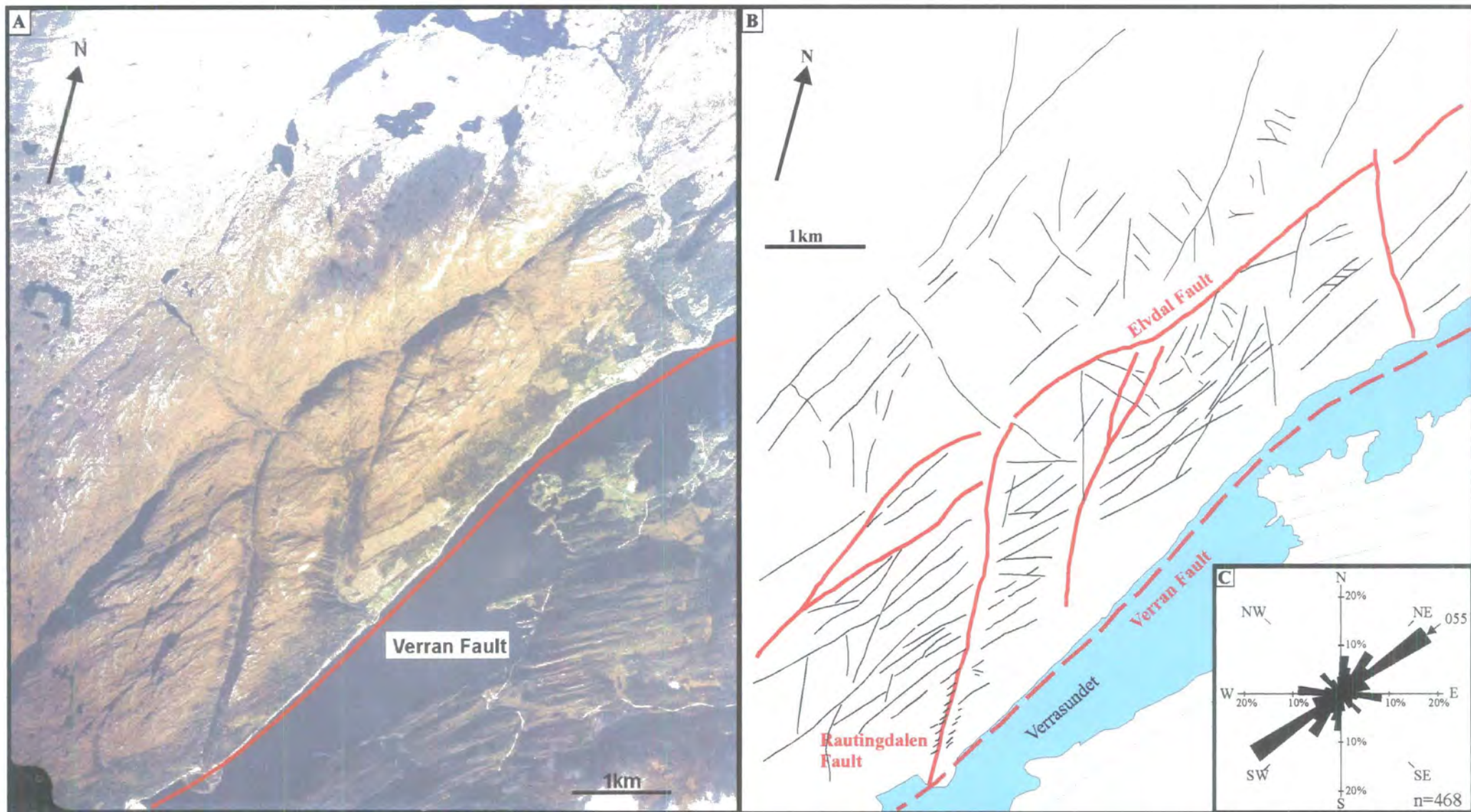


Figure 6.35 (A) Air photograph of the Verran Fault Zone north of Verrasundet. (B) Diagram to show the main lineaments on (A). Black lines=lineaments, Red lines=major lineaments. (C) Rose diagram of all lineaments on (A), after Sleight (2001).

6:4:2 Skaudalen stream section

The VFZ defines an ENE-WSW- to NE-SW-orientated flat-bottomed valley to the southwest of Verrasundet (Skaudalen). The VFZ is poorly exposed in a stream section (6183 6217) along the Skaudalen valley (locality a; Figure 6.34), which lies to the south of the VFP trace. At this locality, the true extent of the fault-related deformation is unclear due to the lack of exposure. The outcrops described in this section are important, as they preserve mylonites not generally preserved elsewhere within the existing limited exposures of the VFZ.

6:4:2:1 Protolith lithology

The stream section outcrops in Skaudalen (6183 6217) represent the only locality described where the fault rocks are not derived from compositionally banded gneisses of the Banded Gneiss Complex of Fosen (section 6:2:1). At this locality, fault rocks of the VFZ are entirely derived from a tectonised porphyritic granite, which is exposed to the south of Verrasundet (8330 7918; Figure 6.34).

The granite is grey in colour and medium to coarse grained with phenocrysts of plagioclase and orthoclase up to 3cm in length (Plate 6.35A). It is composed of approximately 40% orthoclase, 30% plagioclase, 20% quartz, and 10% biotite together with minor amounts of disseminated oxides and epidote grains. The granite is inequigranular and displays a porphyritic texture. Feldspars are replaced by aggregates of sericite, giving rise to a speckled appearance. The granite contains an ENE-WSW-trending foliation defined by flattened and stretched aggregates of quartz and feldspar. Lineations defined by elongate feldspar and quartz plunge shallowly to the SW.

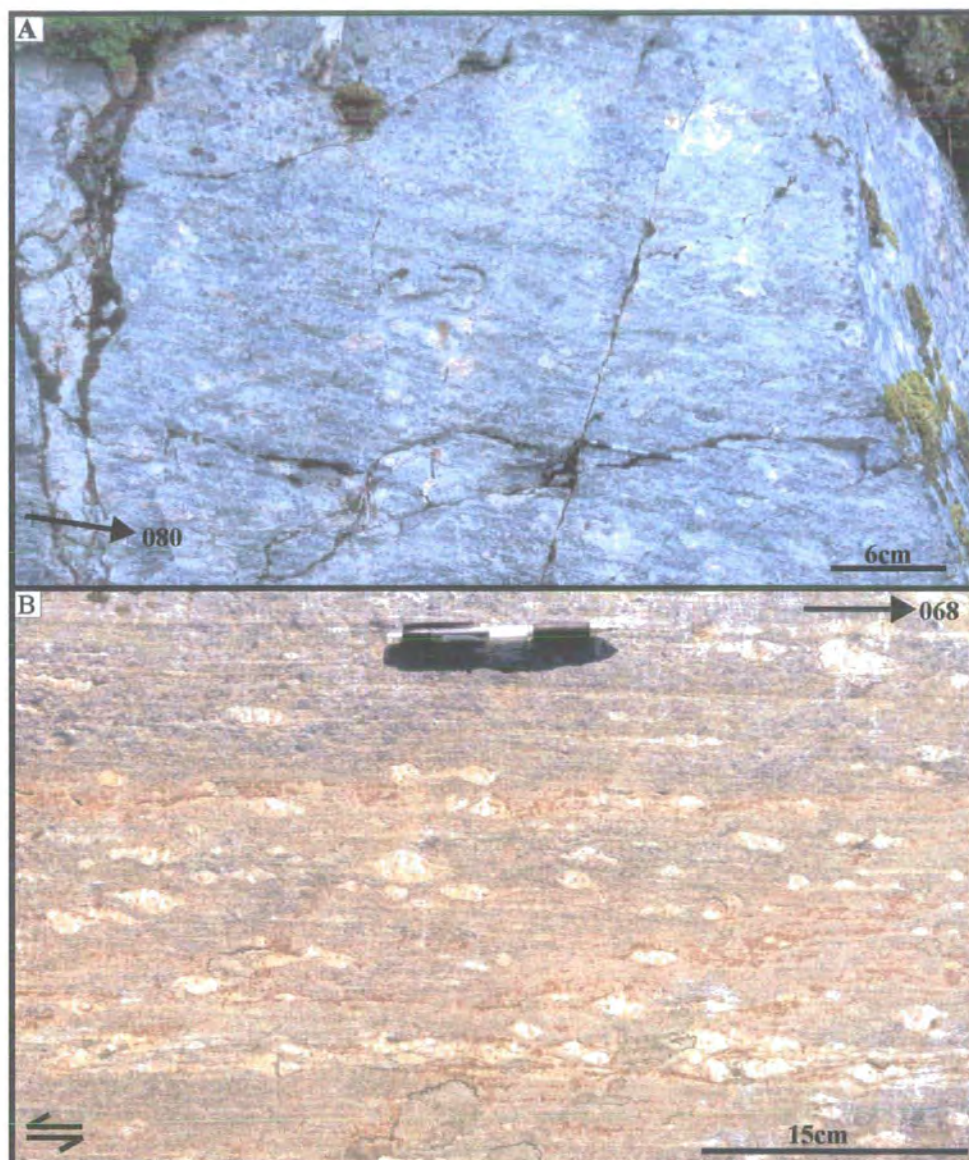


Plate 6.35 Plan view. (A) Tectonised granite exposed to the south of Verrasundet (8330 7918). (B) Mylonite derived from tectonised granite in (A), Skaudalen (6183 6217). Split arrows indicate shear sense parallel to lineation.

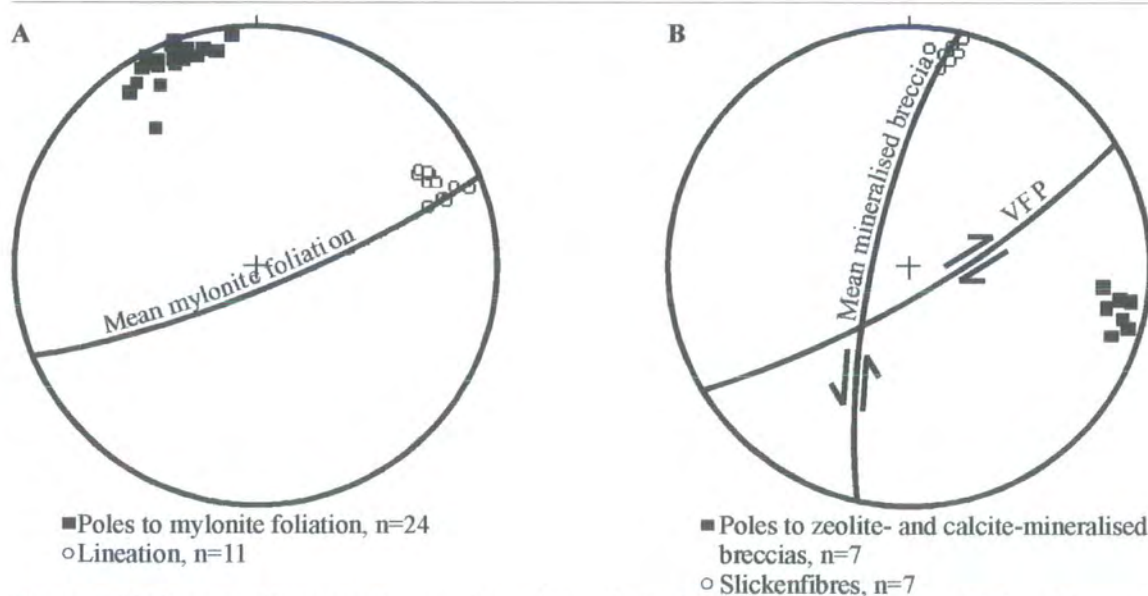


Figure 6.36 Stereographic projections to show (A) mylonite foliation and lineation, and (B) zeolite- and calcite-mineralised breccias and slickenfibres.

6:4:2:2 Fault rocks: nature, distribution and age relationships

In this section, fault rocks are described in the order of their relative age (oldest to youngest).

6:4:2:2a Mylonite

Mylonitic series rocks derived from porphyritic granite are exposed in the stream section. The grey-coloured, quartzo-feldspathic mylonites (Plate 6.35B) contain approximately 35% quartz, 35% muscovite and 20% feldspar together with minor amounts of calcite, epidote and clinozoisite. The relative abundance of minerals varies across the outcrops, due to differences in strain intensity, which induced retrograde metamorphic reactions within the mylonites. Millimetre-scale bands of fine-grained muscovite and feldspar aggregates are interlayered with quartz-rich bands. The fine-grained matrix wraps around plagioclase and orthoclase porphyroclasts, which are typically 2mm to 3cm in length. The mylonites contain a strong foliation defined by stretched and flattened aggregates of quartz, mica and feldspar. The proportion of matrix varies from 35% to almost 80%, so that the rocks can be subdivided into protomylonites and mylonites. The sub-vertical mylonite foliation trends ENE-WSW with a sub-horizontal lineation defined by elongate quartz and feldspar together with aligned mica grains. On surfaces and in thin sections viewed perpendicular to the mylonite foliation and parallel to the stretching lineation, σ - and δ -type porphyroclast geometries are well developed.

6:4:2:2b Zeolite- and calcite-mineralised breccias

NNE-SSW-trending brick-red to orange-coloured breccias occur in faults exposed within the stream section. Randomly orientated sub-angular to angular fragments of mylonite (0.5 to 3cm in size) are set within a fine- to coarse-grained interlocking matrix of calcite and zeolite grains. Randomly orientated calcite and zeolite veins (centimetre to millimetre scale) commonly nucleate from the fault surfaces which bound the breccias.

6:4:2:3 Fault zone structure

Mylonites and protomylonites derived from porphyritic granite display a well-developed foliation defined by flattened and stretched aggregates of quartz, mica and feldspar with lineations defined by elongate quartz, mica and feldspar grains. The mylonite foliation trends ENE-WSW and dips steeply to the SE, with lineations, that plunge shallowly to the ENE (Figure 6.36A). In outcrop surfaces viewed normal to the foliation and parallel to the lineation, feldspar porphyroclasts (up to 3cm in length) display σ - and δ -type geometries consistent with sinistral shear (Plate 6.35B). In thin-sections viewed parallel to the lineation and normal to the foliation, millimetre-scale S-C' fabrics are consistent with sinistral shear. Locally, the mylonites pass into centimetre- to metre-thick mylonites with a very strong L>S tectonite fabric, indicating constrictional strain (Figure 6.37). In plan view, porphyroclasts display linear augen structures up to 10cm in length.

Sub-vertical, NNE-SSW-trending faults (Figure 6.36B) cross-cut the mylonite foliation and are spaced between 1m and 5m apart. The faults contain centimetre-thick, brick-red to orange-coloured breccias comprising brecciated mylonite surrounded by calcite and zeolite mineralisation. The faults contain sub-horizontal slickenside lineations and display evidence for sinistral strike-slip movements based upon offsets and folding of the mylonite foliation (Figure 6.38). Randomly orientated millimetre- to centimetre-thick vein networks nucleate from the NNE-SSW-orientated faults. These faults are interpreted to have formed as sinistral strike-slip, R'-type, Riedel shears during dextral movement along the VF (Figure 6.38A).

6:4:2:4 Kinematic summary and discussion

The kinematic evolution of the VFZ at (6183 6217) along Skaudalen is summarised in Table 6.4.

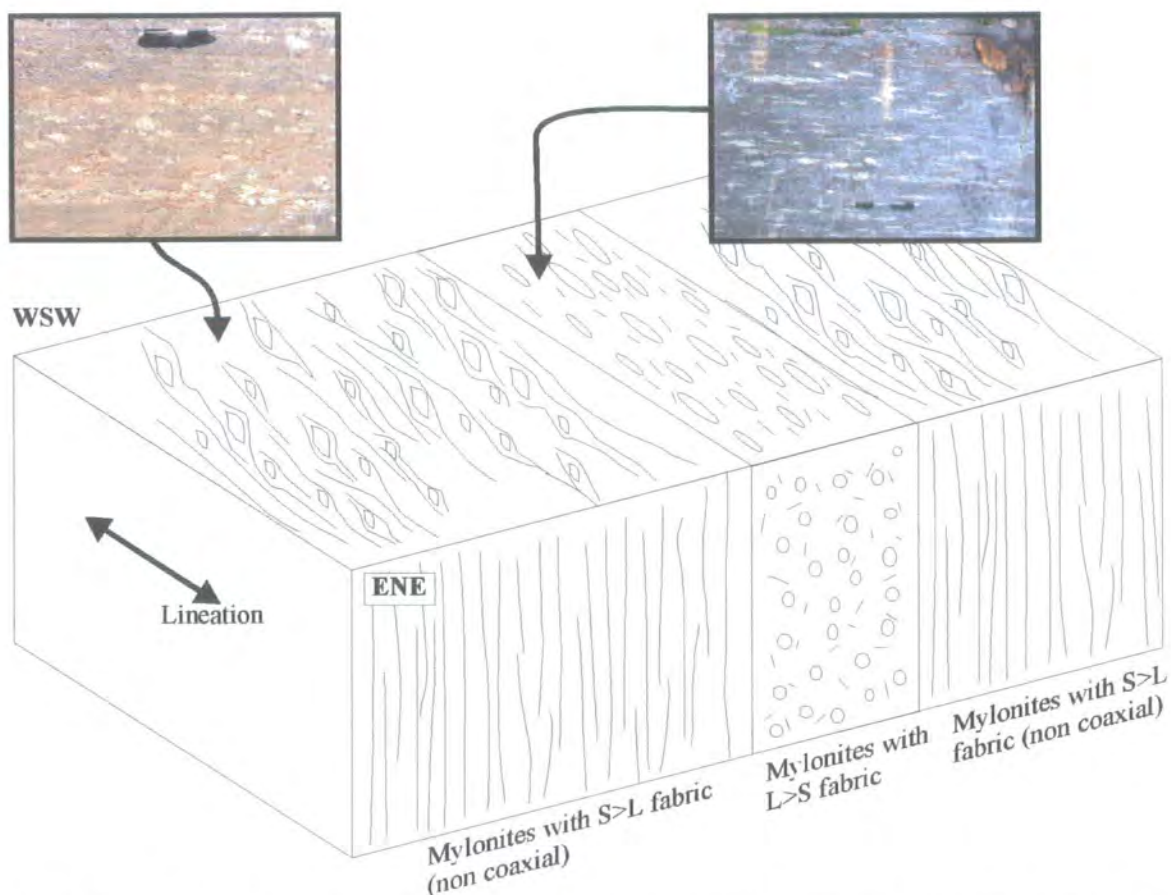


Figure 6.37 Not to scale. Schematic diagram to illustrate the spatial partitioning between mylonites with an S>L fabric and mylonites with an L>S fabric defined by linear feldspar augen.

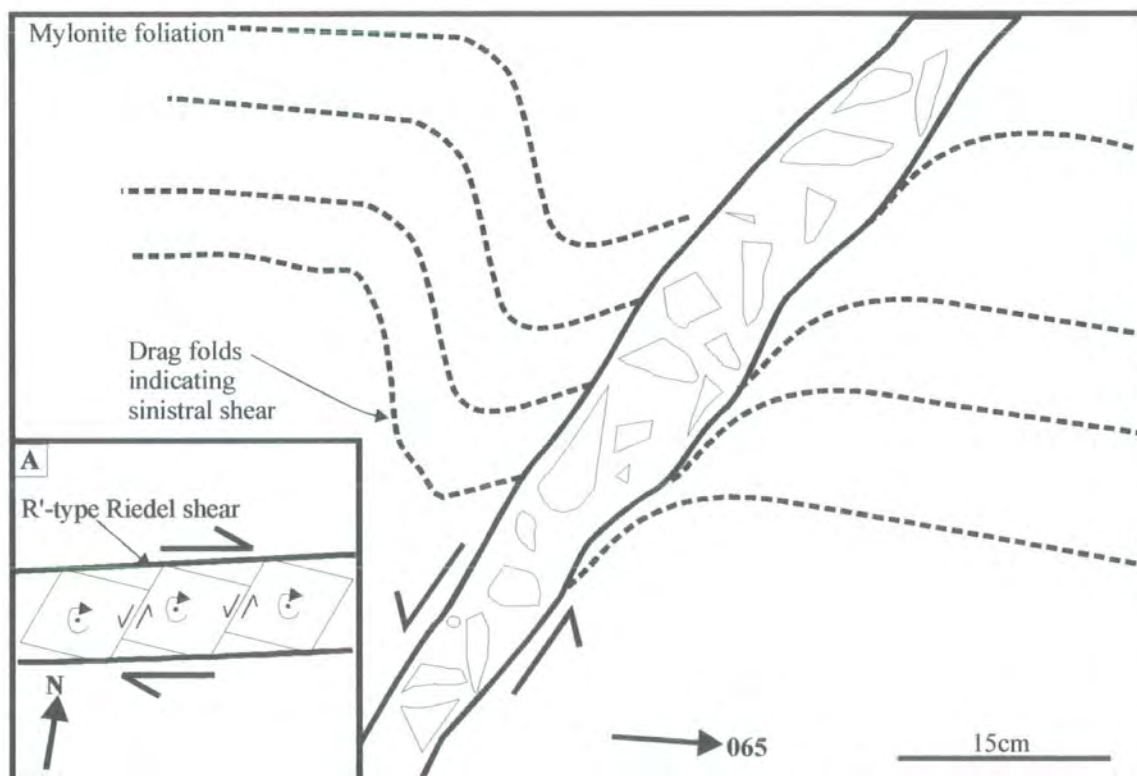


Figure 6.38 Plan view. Field sketch to show the geometry and kinematics of a zeolite- and calcite-mineralised breccia. Inset (A) shows that the breccias can be interpreted as R'-type Riedel shears formed during dextral strike-slip movements along the VFZ.

Kinematic regime	Fault rocks / structures
2. Dextral strike-slip (youngest)	<ul style="list-style-type: none"> NNE-SSW-trending zeolite and calcite matrixed breccias are interpreted as R'-type Riedel shears
1. Sinistral strike-slip (oldest)	<ul style="list-style-type: none"> Mylonites Feldspar porphyroclasts display δ- and σ-type geometries. Millimetre-scale S-C' fabrics

Table 6.4 Table summarising the kinematic evolution of the VFZ at (6183 6217), Skaudalen.

The VFZ along the Skaudalen valley is poorly exposed. Protomylonites and mylonites overprint porphyritic granite to the south of the VFP trace. The mylonites represent the earliest fault-related deformation within the VFZ and were formed during sinistral shear (σ - and δ -type porphyroclasts, S-C' fabrics). The switching between mylonites with an S>L fabric (non-coaxial strain) and those with an L>S fabric (constrictional strain) is possibly consistent with sinistral transtension (c.f. Krabbendam and Dewey 1998). Later brittle deformation led to the formation of NNE-SSW-trending zeolite- and calcite-matrixed breccias, which are interpreted as sinistral strike-slip, R'-type, Riedel shears formed during dextral strike-slip along the ENE-WSW-orientated VF.

6:4:3 Ormsetvatnet road section

Fault-related deformation extends for approximately 500m northwest of the VFP trace into granodiorite gneiss belonging to the Banded Gneiss Complex of Fosen (section 6:2:1). The Ormsetvatnet road section (locality b; Figure 6.34) provides a perpendicular sequence of road cuts through the outer parts of the VFZ.

6:4:3:1 Fault rocks: nature, distribution and age relationships

In this section, fault rocks are described in the order of their relative age (oldest to youngest).

6:4:3:1a Cataclasite

To the east of the road section, the gneisses are cut by NNE-SSW- and ENE-WSW-trending fractures which are filled with millimetre-thick cataclasites. The cataclasites are green in colour, comprising finely comminuted clasts of gneiss, orthoclase, plagioclase, quartz, chlorite, epidote and muscovite set within a fine-grained cataclastic matrix. Randomly orientated clasts are angular- to sub-angular, ranging from 2mm to less than 0.5mm in size. The cataclasites possess no internal fabric and appear to be isotropic in the field on all scales of observation. Epidote and quartz veins cross-cut the cataclasites and occur locally as clasts within the cataclasite matrix.

6:4:3:1b Zeolite- and calcite-mineralised breccias

ENE-WSW- and N-S-trending zeolite- and calcite-mineralised breccias occur in faults (Plate 6.36A), which cross-cut granodiorite gneiss and earlier formed cataclasite. The breccias are 1cm- to 50cm-thick, and vary in colour from pale grey, white and brown to orange in colour. The breccias comprise randomly orientated sub-angular to angular fragments (0.1 to 10cm in size) of gneiss set within a fine- to coarse-grained mineralised matrix of calcite and zeolite grains. The matrix comprises fibrous zeolite crystals (0.1mm to 0.5cm in size) which form interlocking mosaics with calcite grains (0.1 to 2cm in size). Randomly orientated calcite and zeolite veins (centimetre to millimetre thick) commonly cross-cut and occur as clasts within the mineralised breccias.

6:4:3:2 Fault zone structure

The Ormsetvatnet road section provides an insight into the structure and geometry of the outer part of the VFZ. Here, the gneissose foliation defined by flattened aggregates of quartz and feldspar trends ENE-WSW and dips steeply to the SE (Figure 6.39A). Elongate feldspar and quartz grains define a lineation which plunges shallowly to the ENE.

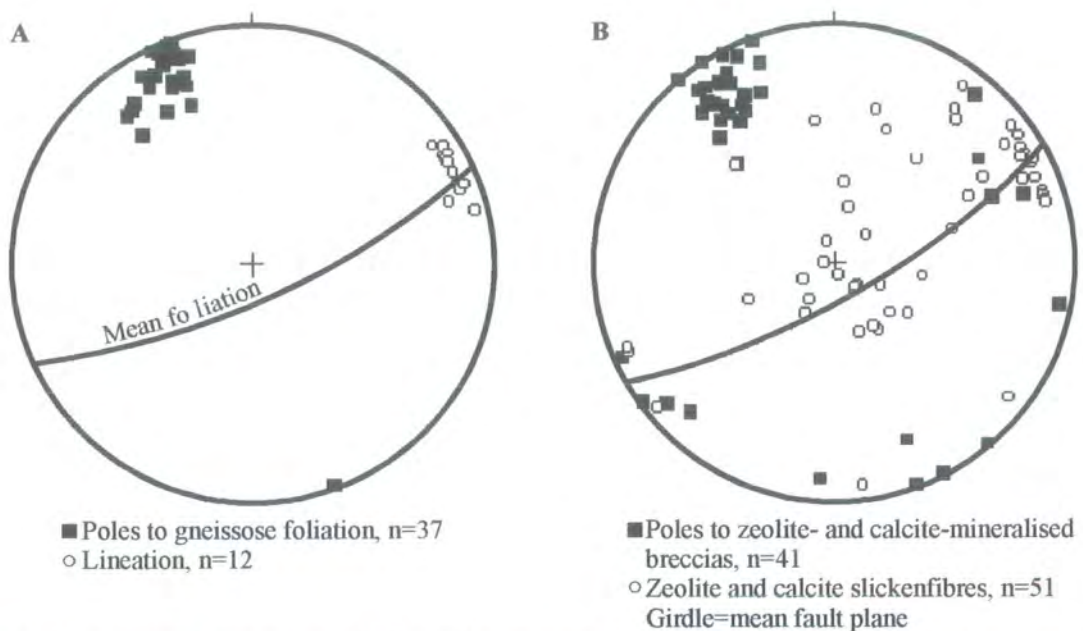


Figure 6.39 Stereographic projections to show (A) gneissose foliation and lineation, and (B) zeolite- and calcite-mineralised breccias and associated slickenfibres.

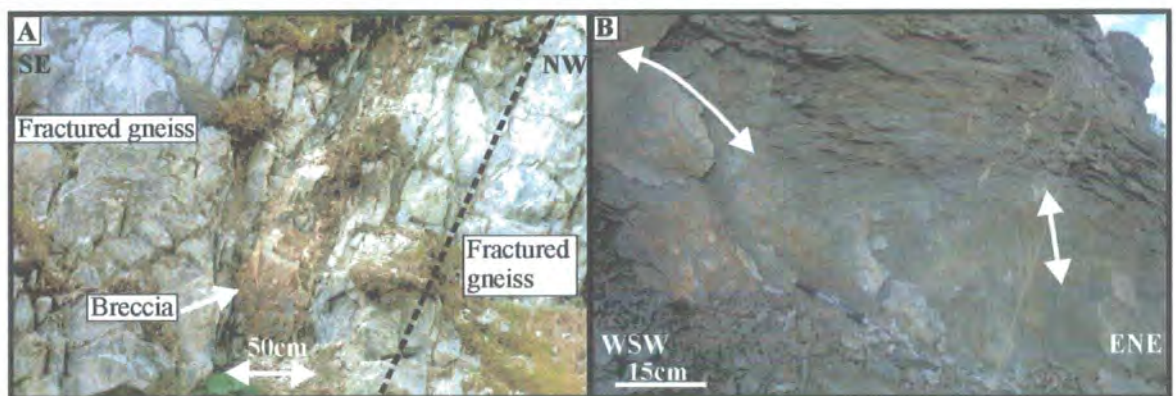


Plate 6.36 (A) View of zeolite- and calcite-mineralised breccia, which appears to localise along the pre-existing, near-vertical gneissose foliation (dashed line). (B) View of ENE-WSW-trending, SE-dipping fault surface to show dip-slip slickenfibres (white arrow) overprinted by curved oblique-dextral slickenfibres also shown by white arrow.

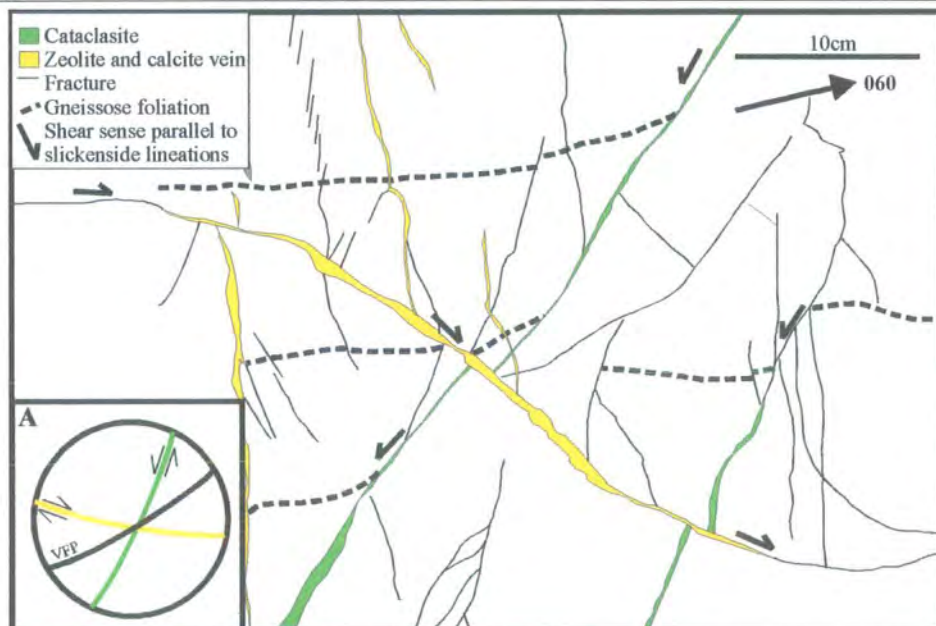


Figure 6.40 Plan view. NNE-SSW-trending, millimetre-thick cataclasites offset the gneissose foliation by 3cm to 2m in a sinistral sense, and are interpreted as R-type Riedel shears. ENE-WSW-trending zeolite and calcite veins offset the earlier-formed cataclasites by 1cm to 4cm in a dextral sense. Inset (A), stereographic projection to show mean cataclasite, mean zeolite and calcite vein and VFP trace (from VF core).

Two 50cm-thick amphibolite dykes occur parallel to the gneissose foliation, which have been sheared and retrograded to fibrous aggregates of biotite and epidote that surround polygonal aggregates of quartz. On outcrop surfaces viewed parallel to the lineation and normal to the foliation, centimetre-spaced shear bands are consistent with dextral shear. These sheared dykes are interpreted to have formed during late-Scandian regional shearing associated with the development of the regional-scale antiform, which lies between and pre-dates the VF and HSF (see section 6:2:2).

Fault-related deformation first appears approximately 500m northwest of the VFP trace. To the southwest, fracturing intensifies and defines metre-thick high-strain zones (intense fracturing) that are separated from metre-thick low-strain zones across ENE-WSW-trending, SE-dipping fracture surfaces localised along the pre-existing gneissose foliation.

At distances of 450m northwest of the VFP trace, 1cm- to 50cm-thick zeolite breccias are exposed. The breccias are spaced from 4m to 15m apart and are localised along the ENE-WSW-trending gneissose foliation (Plate 6.36A; Figure 6.39B). Most breccias are bounded by slickenfibres-covered fault planes, which indicate dip-slip normal and dextral strike-slip movements (Figure 6.39B), based upon the stepping of calcite and zeolite fibres. Dip-slip normal slickenfibres are consistently overprinted by dextral strike-slip slickenfibres (Plate 6.36B). Locally, the dextral strike-slip slickenfibres are curved in a clockwise sense when looking northwest onto fault surfaces, inferring that there has been a fault-normal rotation.

To the east of the road section, millimetre-thick NNE-SSW-trending cataclasites with sub-horizontal slickenside lineations link into foliation-parallel fractures. The cataclasites offset the gneissose foliation by 3cm to 2m in a sinistral sense (Figure 6.40) and are interpreted as R-type Riedel shears formed during sinistral strike-slip movements along the VFZ. ESE-WNW-trending zeolite and calcite veins (0.5cm to 1cm thick) with sub-horizontal slickenside lineations offset the cataclasites by 1cm to 4cm in a dextral sense (Figure 6.40). Tensional calcite and zeolite veins (1mm to 1cm) link into the ESE-WNW-orientated veins and trend NNW-SSE, displaying en échelon geometries.

6:4:3:3 Kinematic summary and discussion

The kinematic evolution of the VFZ along the Ormsetvatnet road section is summarised in Table 6.5.

Kinematic regime	Fault rocks / structures
2. Dip-slip normal (SE side down) followed by dextral strike-slip (youngest)	<ul style="list-style-type: none"> ENE-WSW-trending zeolite- and calcite-matrixed breccias with dip-slip normal and dextral strike-slip kinematic indicators
1. Sinistral strike-slip (oldest)	<ul style="list-style-type: none"> R-type Riedel shears filled with millimetre-thick cataclasites

Table 6.5 Table summarising the kinematic evolution of the VFZ along the Ormsetvatnet road section.

The outer parts of the VFZ contain millimetre-thick cataclasites consistent with sinistral strike-slip movements, which are overprinted by centimetre- to metre-thick zeolite- and calcite-mineralised breccias together with intense fracturing and veining. The breccias are bounded by discrete slickensided fault surfaces, which show evidence for dip-slip normal (SE side down) movements followed by a phase of dextral strike-slip movement.

6:4:4 Hydro station

The VFZ is partially exposed along a 60m long NE-SW-orientated road cut near the hydro station (8350 8115, locality c; Figure 6.34) to the north of the VP trace, which lies approximately 200m to the south in Verrasundet. Granodiorite gneisses belonging to the Banded Gneiss Complex of Fosen (section 6:2:1) are strongly affected by intense cataclasis.

6:4:4:1 Fault rocks: nature, distribution and age relationships

In this section, fault rocks are described in the order of their relative age (oldest to youngest).

6:4:4:1a Cataclasite

Irregular zones of centimetre-thick cataclasite together with quartz and epidote veining overprint intensely fractured and retrograde granodiorite gneiss. The cataclasites are green in colour, comprising finely comminuted clasts of gneiss, orthoclase, plagioclase, quartz, chlorite, epidote, muscovite and sphene set within an epidote-rich, fine-grained, cataclastic matrix. Randomly orientated clasts are angular to sub-angular, ranging from 5mm to less than 0.5mm in size. The cataclasites possess no internal fabric and appear to be isotropic in the field on all scales of observation. Epidote and quartz veins cross-cut the cataclasites and occur locally as clasts within the cataclasite matrix.

6:4:4:1b Zeolite- and calcite-mineralised breccias

Intense zones of brecciation cut by millimetre- to centimetre-thick zeolite and calcite veins overprint the earlier formed cataclasites. The brecciated gneiss is bounded by a network of linked ENE-WSW- and N-S-trending zeolite- and calcite-mineralised breccias, which occur along slickenfibres-covered fault planes (Plate 6.37A). The breccias are 2cm to 10cm thick (Plate 6.37B), pale grey to orange in colour and comprise randomly orientated, sub-angular to angular fragments (0.1 to 5cm in size) of gneiss set within a fine- to coarse-grained mineralised matrix of fibrous calcite and zeolite grains. Randomly orientated calcite and zeolite veins (centimetre to millimetre thick) commonly nucleate from the breccias.

6:4:4:2 Fault zone structure

Near the hydro station, brittle deformation is so intense that the protolith granodiorite gneisses are almost unrecognisable. Feldspars have a speckled appearance due to their breakdown to aggregates of sericite and clay minerals. Wide zones (2m to 5m) of intense brecciation and veining overprint centimetre-thick cataclasites. Zeolite- and calcite-mineralised breccias (Plate 6.37B) spaced from 10cm to 1m overprint the cataclasites and bound the zones of brecciated gneiss. The breccias are 2cm to 10cm thick and are bounded by discrete polished fault planes (Plate 6.37A).

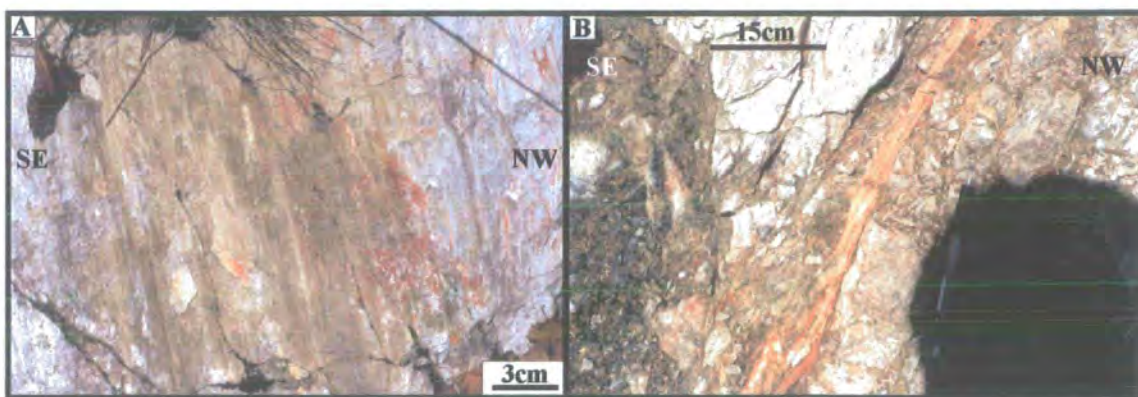


Plate 6.37 (A) View of dip-slip normal zeolite and calcite slickenfibres on NE-SW-trending, SE-dipping fault plane. (B) View of sub-vertical N-S-orientated zeolite- and calcite-mineralised breccia, with slickenfibres, which step down the fault plane, indicating dip-slip normal (W-side down) movements.

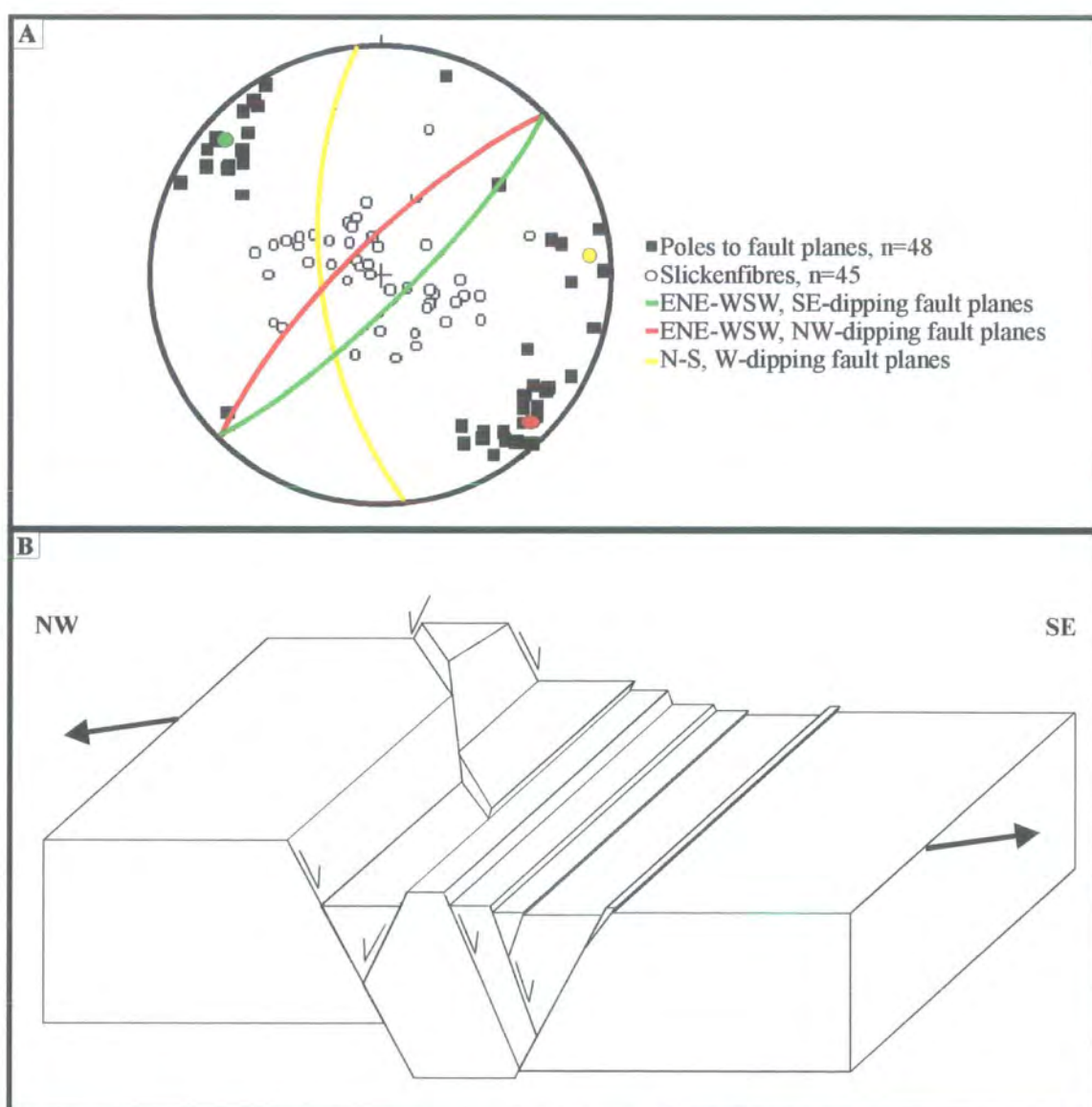


Figure 6.41 (A) Stereographic projection to show fault planes with slickenfibres, which bound zeolite- and calcite-mineralised breccias. (B) Not to scale. Schematic diagram to illustrate the geometrical and kinematic configuration of NE-SW-trending faults, which dip to the SE and NW, and N-S-trending faults, which dip to the W.

The fault planes form three main clusters, with mean girdles orientated 048/80SE, 048/80NW and 173/71W (Figure 6.41A). Well-developed, dip-slip, calcite and zeolite slickenfibres lineations are present on almost every fault plane. NE-SW-trending faults, which dip moderately to steeply to the SE, display calcite and zeolite slickenfibres, which step down the fault planes indicating dip-slip normal movements (SE-side down; Plate 6.37A). NE-SW-trending faults, which dip moderately to steeply to the NW, contain slickenfibres which step both up and down the fault planes indicating a combination of dip-slip normal (NW side down) and dip-slip (SE side down) reverse movements. The NW-dipping faults appear to be antithetic to the more continuous SE-dipping faults (Figure 6.41B). N-S faults, which dip steeply to the W, consistently display slickenfibres, which step down the fault plane indicating dip-slip normal movements. Locally, these faults led to reverse movements along some of the ENE-WSW-trending, NW-dipping antithetic faults (Figure 6.41B). Intense calcite and zeolite veining (millimetre to centimetre thick) nucleate from the breccias and cut the brecciated gneiss.

6:4:4:3 Kinematic summary and discussion

The kinematic evolution of the VFZ at the Hydro station (8350 8114) is summarised in Table 6.6.

Kinematic regime	Fault rocks / structures
1. Dip-slip normal (SE side down along main SE-dipping faults)	<ul style="list-style-type: none"> NE-SW-trending zeolite- and calcite-matrix breccias with dip-slip normal kinematic indicators

Table 6.6 Table summarising the kinematic evolution of the VFZ at the hydro station (8350 8114).

Outcrops of the VFZ near the hydro station display evidence of dip-slip normal offsets (SE side down), along NE-SW-trending faults. Here, the VFZ comprises zeolite- and calcite-mineralised breccias bounded by discrete slickenfibres-covered fault planes, which surround intensely fractured and locally brecciated retrograde gneiss.

6:4:5 Outcrops along the 720 road section

The 720 road section (locality d; Figure 6.34; Figure 6.42; Plate 6.38) to the east of the RF provides extensive exposures of cataclastically deformed rocks and mineralisation. The road section is orientated 040°, extends for approximately 750m and represents an oblique section through the VFZ, which trends ENE-WSW (Figure 6.42). Here, intense cataclastic deformation (Plate 6.38) overprints granodiorite gneiss of the Banded Gneiss Complex of Fosen (section 6:2:1).

6:4:5:1 Fault rocks: nature, distribution and age relationships

In this section, fault rocks are described in the order of their relative age (oldest to youngest).

6:4:5:1a Cataclasite

Along the NE-SW-orientated road section, anastomosing zones of ENE-WSW- and N-S-trending protocataclasite and cataclasite, ranging from less than 1cm to several metres in thickness, overprint intensely fractured granodiorite gneiss. The cataclasites are green in colour, comprising finely comminuted clasts of gneiss, orthoclase, plagioclase, quartz, chlorite, epidote, muscovite and sphene set within a fine-grained cataclastic matrix of the same. Randomly orientated clasts are angular to sub-angular, ranging from 5mm to less than 0.5mm in size. The cataclasites possess no internal fabric and appear to be isotropic in the field on all scales of observation. Epidote and quartz veins cross-cut the cataclasites and occur locally as clasts within the cataclasite matrix. The proportion of matrix varies from approximately 5% to 90%, so that the rocks can be subdivided into breccias, protocataclasites, cataclasites and ultracataclasites based upon the proportion of matrix.

6:4:5:1b Zeolite- and calcite-mineralised breccias

The cataclasites and fractured gneiss are overprinted by extensive zeolite and calcite veining (1mm to 10cm thick) associated with the development of zeolite- and calcite-mineralised breccias.

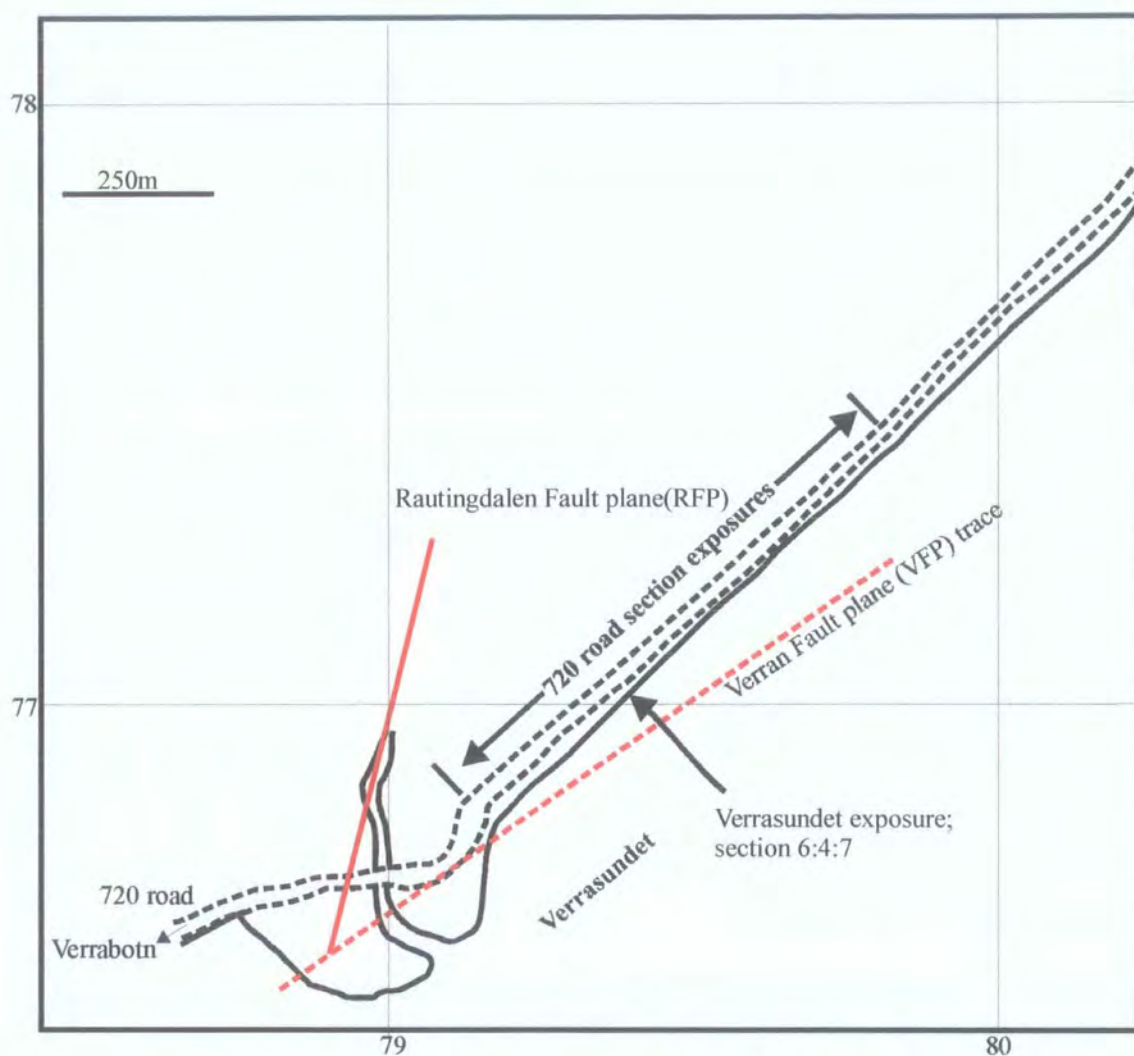


Figure 6.42 Map to show the location of the 720 road section exposures to the north of Verrasundet with respect to the VFP and RFP.



Plate 6.38 View of SE-dipping road cutting. Photograph taken halfway along the 720 road section exposures looking towards the southwest.

The breccias are pale grey, white, brown and orange in colour and comprise randomly orientated, sub-angular to angular fragments (0.1 to 10cm in size) of gneiss set within a fine- to coarse-grained mineralised matrix of calcite and zeolite grains. The matrix comprises fibrous zeolite crystals (0.1mm to 0.5cm in size) which form interlocking mosaics with calcite grains (0.1 to 2cm in size). Randomly orientated calcite and zeolite veins (centimetre to millimetre thick) commonly cross-cut and occur as clasts within the mineralised breccias.

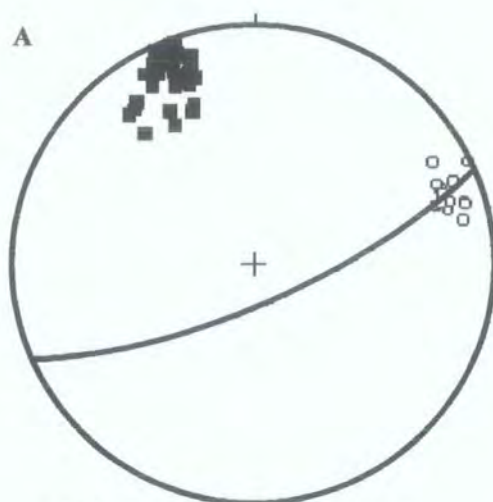
6:4:5:1c Grey fault gouge

Zeolite- and calcite-mineralised breccias are cross-cut by ENE-WSW-orientated grey fault gouges, which range from 1mm to 50cm in thickness. The grey fault gouge is incohesive and clay-like in appearance. It is very fine grained with no visible clasts present in the field. The gouge contains a lineation defined by the long axes of aligned clay minerals.

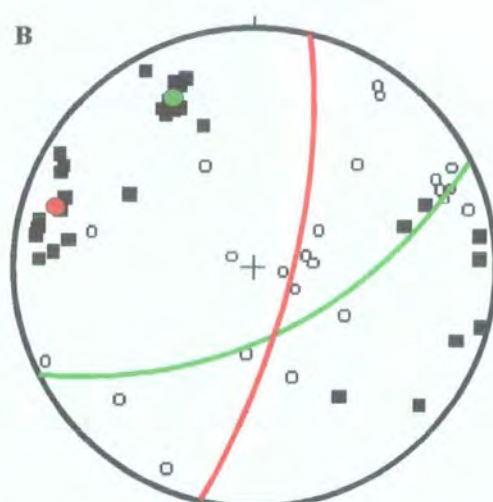
6:4:5:2 Fault zone structure

The granodiorite gneiss displays an ENE-WSW-trending, SE-dipping foliation defined by flattened aggregates of quartz and feldspar (Figure 6.43A). Lineations defined by elongate feldspar and quartz grains plunge shallowly to the ENE. Locally, the feldspars are almost completely replaced by grains of sericite, kaolin and illite, giving rise to a speckled appearance of the feldspars. The gneisses are overprinted by such intense cataclastic deformation that they are generally unrecognisable. Cataclastic deformation is most intense towards the southwest (closer to the ENE-WSW-trending VFP trace) and decreases to the northeast along the road section.

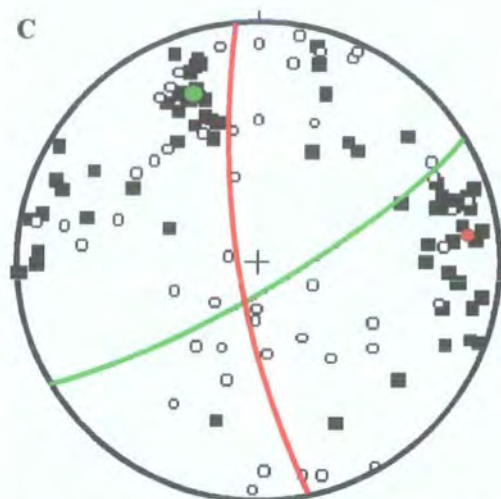
Cataclasites are the earliest recognised fault rocks along the road section. The cataclasites are from 1mm to several metres thick (towards the SW) and form anastomosing geometries around less deformed areas of granodiorite gneiss. They form two main clusters, (a) ENE-WSW-striking and SE-dipping and (b) N-S-trending which dip steeply to the E and W (Figure 6.43B).



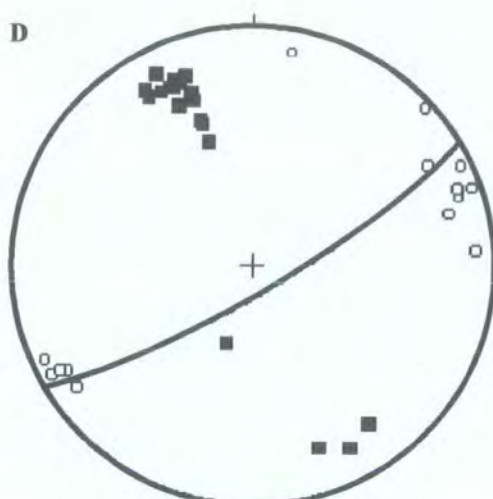
- Poles to gneissose foliation, n=53
- Lineation, n=20
- Girdle=mean foliation



- Poles to cataclasites, n=31
- Slickenfibres, n=23
- ENE-WSW-trending cataclasites
- N-S-trending cataclasites



- Poles to zeolite- and calcite-mineralised breccias, n=73
- Slickenfibres, 48
- ENE-WSW-trending breccias
- N-S-trending breccias



- Poles to grey-coloured fault gouge, n=20
- Lineations, n=14
- Girdle=mean fault gouge

Figure 6.43 Stereographic projections to show structural data collected along the 720 road section. (A) Gneissose foliation and lineation. (B) Cataclasite and slickenfibres. (C) Zeolite- and calcite-mineralised breccias and slickenfibres. (D) grey-coloured fault gouge and lineations.

ENE-WSW-trending cataclasites appear to localise along the pre-existing gneissose foliation and display sub-horizontal slickenfibres, which indicate sinistral strike-slip movements, based upon the stepping of the quartz and epidote fibres. N-S-striking cataclasites link into the ENE-WSW-trending structures and display dip-slip slickenfibre lineations. The quartz and epidote slickenfibres consistently step down the fault plane indicating dip-slip normal movements. The N-S-trending cataclasites are interpreted as extensional faults formed during sinistral transtension along the ENE-WSW-trending VFZ (Figure 6.44A).

Zeolite- and calcite-mineralised breccias (Plate 6.39A&C) overprint the earlier formed cataclasites. The breccias are 1m to 1cm in thickness and spaced from 1m to 3m apart. The breccias are bounded by discrete polished fault planes, which are commonly covered in slickenside and slickenfibre lineations. Extensive millimetre- to centimetre-thick zeolite and calcite veining nucleates from the breccias into intensely fractured retrograde gneiss (Plate 6.39A). The breccias form three main clusters (a) ENE-WSW-trending and SE-dipping, (b) N-S-trending which dip steeply to the W and E, and (c) ESE-WNW-trending (Figure 6.43C). ENE-WSW- and N-S-trending breccias localise along the ENE-WSW-orientated gneissose foliation and the pre-existing ENE-WSW- and N-S-trending cataclasites. Slickenside lineations show a large scatter and plot over the entire stereonet (Figure 6.43C). ENE-WSW-trending breccias display evidence of dip-slip normal movements, which are consistently overprinted by dextral strike-slip to oblique movements based upon the stepping direction of zeolite and calcite fibres. N-S-trending breccias (Plate 6.39C) consistently display zeolite and calcite slickenfibres, which indicate sinistral strike-slip movements, again based upon the stepping direction of the mineral fibres. These breccias are interpreted as R'-Type Riedel shears formed during dextral strike-slip movements along the ENE-WSW-trending VFZ (Figure 6.44B).

Towards the southwest of the road section, zeolite- and calcite-mineralised breccias are cross-cut by soft grey gouges (Plate 6.39B&D). The gouges trend ENE-WSW and dip mainly to the SE, with sub-horizontal lineations defined by aligned clay particles (Figure 6.43D). They are 1mm to 50cm thick and commonly form braided geometries. The gouges consistently display dextral strike-slip offsets of 30cm (Plate 6.39D) to 100m, depending on the thickness of the fault gouge.

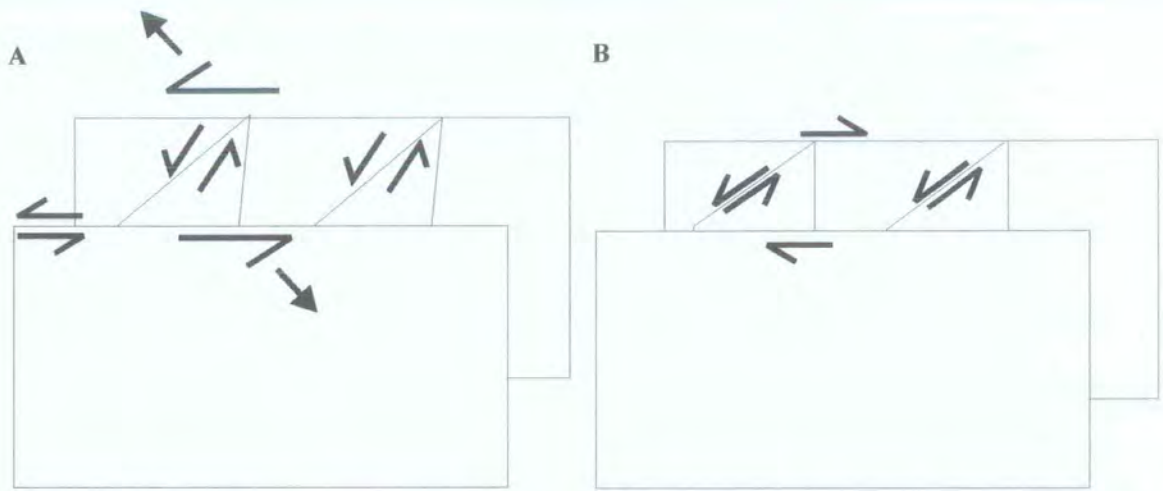


Figure 6.44 (A) Not to scale. Schematic diagram to show the geometry of cataclasites. Sinistral strike-slip, ENE-WSW-trending cataclasites link into N-S-trending extensional cataclasites during sinistral transtension along the VFZ. (B) Not to scale. Schematic diagram to show the geometry of zeolite- and calcite-mineralised breccias during dextral strike-slip phase, which post-dates dip-slip normal movements along the VFZ. Dextral strike-slip, ENE-WSW-trending breccias are linked by N-S-trending breccias, which are interpreted as R'-type Riedel shears that re-use and modify the pre-existing fault and fracture network.

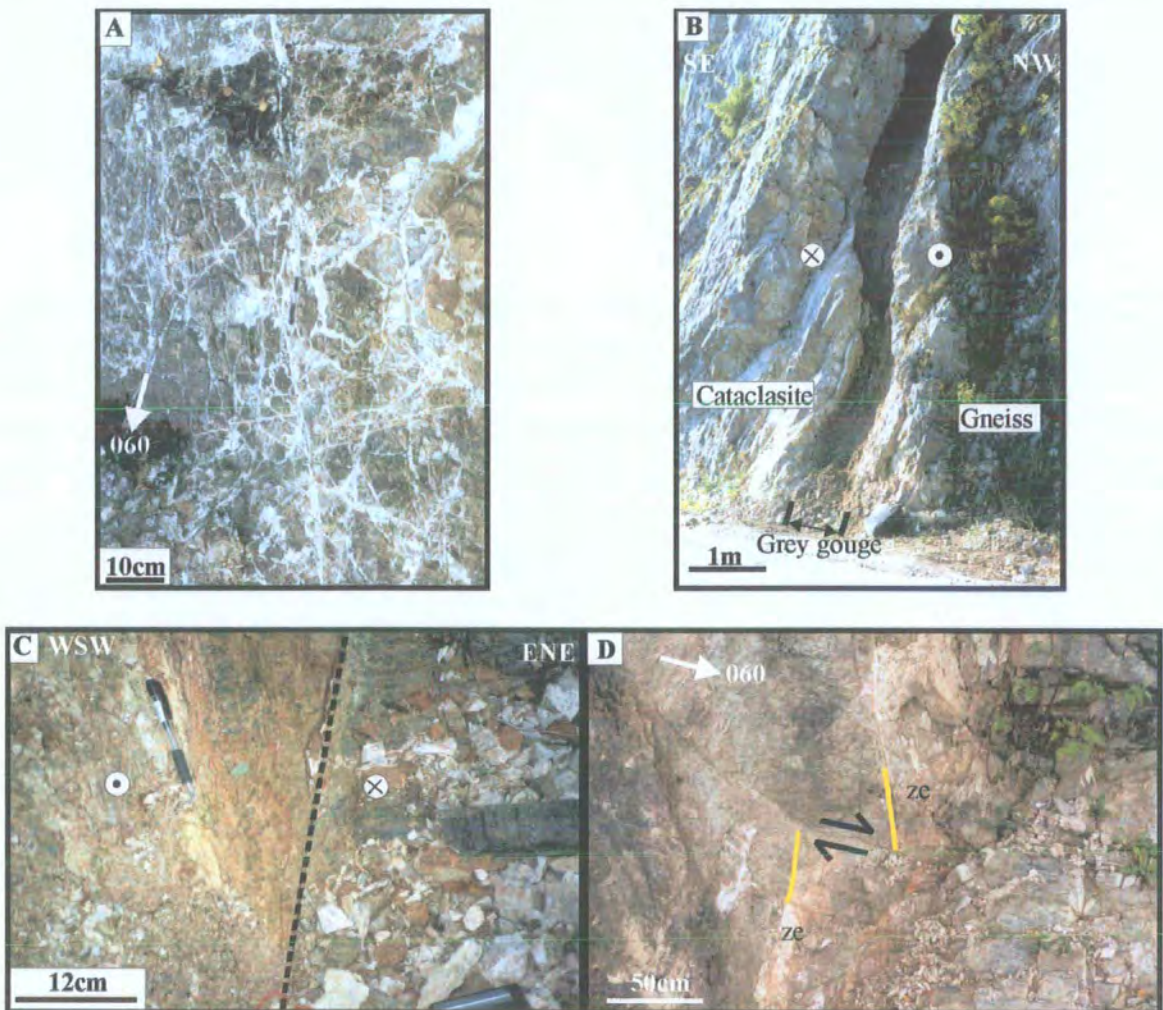


Plate 6.39 (A) Plan view. Intense millimetre- to centimetre-scale zeolite and calcite veining. (B) Cross-section through ENE-WSW-trending, SE-dipping grey fault gouge formed during dextral strike-slip movements along the VFZ. The fault gouge is 50cm-thick and separates cataclasite to the SE from fractured gneiss to the NW. (C) Cross-section across N-S-trending, W-dipping, zeolite- and calcite-mineralised breccia, which contains sinistral strike-slip slickenfibres. (D) Plan view. Millimetre-thick grey fault gouge, which offsets a N-S-trending zeolite- and calcite-mineralised breccia by 50cm in a dextral strike-slip sense.

Fault gouges to the southwest display centimetre-spaced shear bands consistent with dextral shear, on surfaces normal to the fault planes and parallel to the lineations. These gouges are interpreted to represent the most recent fault-related deformation exposed along the 720 road section.

6:4:5:3 Kinematic summary and discussion

The kinematic evolution of the VFZ along the 720 road section is summarised in Table 6.7.

Kinematic regime	Fault rocks / structures
3. Dextral strike-slip (youngest)	<ul style="list-style-type: none"> • Anastomosing gouges which trend ENE-WSW.
2. Dip-slip normal (SE side down) followed by dextral strike-slip	<ul style="list-style-type: none"> • ENE-WSW-trending zeolite- and calcite-mineralised breccias with dip-slip and dextral strike-slip slickenfibres • Sinistral strike-slip N-S-trending zeolite and calcite mineralised breccias, interpreted as R'-type Riedel shears.
1. Sinistral transtension (oldest)	<ul style="list-style-type: none"> • ENE-WSW-trending sinistral strike-slip cataclasites • Extensional N-S-trending cataclasites

Table 6.7 Table summarising the kinematic evolution of the VFZ along the 720 road section.

The VFZ along the road section contains a series of anastomosing cataclasites formed during sinistral transtension that are overprinted by intense veining associated with the development of zeolite and calcite mineralised breccias. These breccias were formed during a phase of dip-slip normal movement (SE side down) along the VFZ followed by a phase of dextral strike-slip faulting. The breccias are overprinted by anastomosing grey fault gouges, which were formed during a phase of dextral strike-slip movement.

6:4:6 Verrabotn stream section

The VFZ is well exposed in a stream section to the east of Verrabotn on the northern side of Verrasundet at 7830 7640 (locality e; Figure 6.34). Fault-related deformation and mineralisation overprints compositionally banded gneisses belonging to the Banded Gneiss Complex of Fosen (section 6:2:1).

6:4:6:1 Fault rocks: nature, distribution and age relationships

In this section, fault rocks are described in the order of their relative age (oldest to youngest).

6:4:6:1a Quartz and epidote cataclasites

N-S- and ENE-WSW-trending quartz- and epidote-matrixed cataclasites overprint intensely fractured granodiorite gneiss (Figure 6.45). The cataclasites range from 1cm to 10cm in thickness and are commonly flanked by irregular zones of breccia. N-S-trending, millimetre-thick chlorite veins commonly nucleate from the cataclasites. The cataclasites are green in colour, comprising finely comminuted clasts of gneiss, orthoclase, plagioclase, quartz, chlorite, epidote, muscovite and sphene, and are set within a fine-grained matrix of quartz and epidote grains. Randomly orientated clasts are angular to sub-angular, ranging from 1cm to less than 0.5mm in size. The cataclasites possess no internal fabric and appear to be isotropic in the field on all scales of observation. Epidote, quartz and chlorite veins cross-cut the cataclasites and occur locally as clasts within the cataclasite matrix. The proportion of matrix varies from approximately 5% to 70%, so that the rocks can be subdivided into breccias, protocataclasites and cataclasites based upon the proportion of matrix.

6:4:6:1b Zeolite- and calcite-mineralised breccias

Zeolite- and calcite-mineralised breccias (1mm to 15cm thick) overprint and appear to localise along the earlier formed N-S trending breccias and cataclasites (Figure 6.45).



Zeolite- and calcite-mineralised breccias contain clasts of quartz- and epidote-matrixed cataclasites, suggesting that the zeolite and calcite breccias are younger than the cataclasites. Centimetre- to millimetre-thick calcite and zeolite veins overprint and develop along the edges of the zeolite- and calcite-mineralised breccias. The breccias are pale grey to white in colour, comprising randomly orientated sub-angular to angular fragments (0.1 to 10cm in size) of gneiss and cataclasite, which are set within a fine- to coarse-grained mineralised matrix of calcite and zeolite grains. The matrix comprises fibrous zeolite crystals (0.1mm to 0.5cm in size) which form interlocking mosaics with calcite grains (0.1 to 2cm in size). Randomly orientated calcite and zeolite veins (centimetre to millimetre thick) commonly cross-cut and occur as clasts within the mineralised breccias.

6:4:6:1c Grey fault gouge

The breccias, cataclasites, zeolite- and calcite-mineralised breccias and veins are cross-cut by a series of millimetre- to centimetre-thick, ENE-WSW-trending, grey-coloured fault gouges (Figure 6.45). The grey gouges are lithologically similar to those exposed along the 720 road section (see section 6:4:5:1c for description).

6:4:6:2 Fault zone structure

The granodiorite gneiss displays an ENE-WSW-orientated, SE-dipping foliation defined by flattened aggregates of quartz and feldspar with sub-horizontal lineations defined by elongate feldspar and quartz grains (Figures 6.45, 6.46A). Centimetre-thick quartz- and epidote-matrixed cataclasites overprint and appear to localise along the pre-existing gneissose foliation (Figure 6.45). The cataclasites form braided networks, which link into NE-SW-trending structures. NE-SW-trending cataclasites link up with NNE-SSW-trending sub-vertical fractures, which display sinistral strike-slip offsets (Plate 6.40). These fractures are interpreted as R-type Riedel shears formed during sinistral strike-slip movements along the NE-SW-orientated cataclasites.

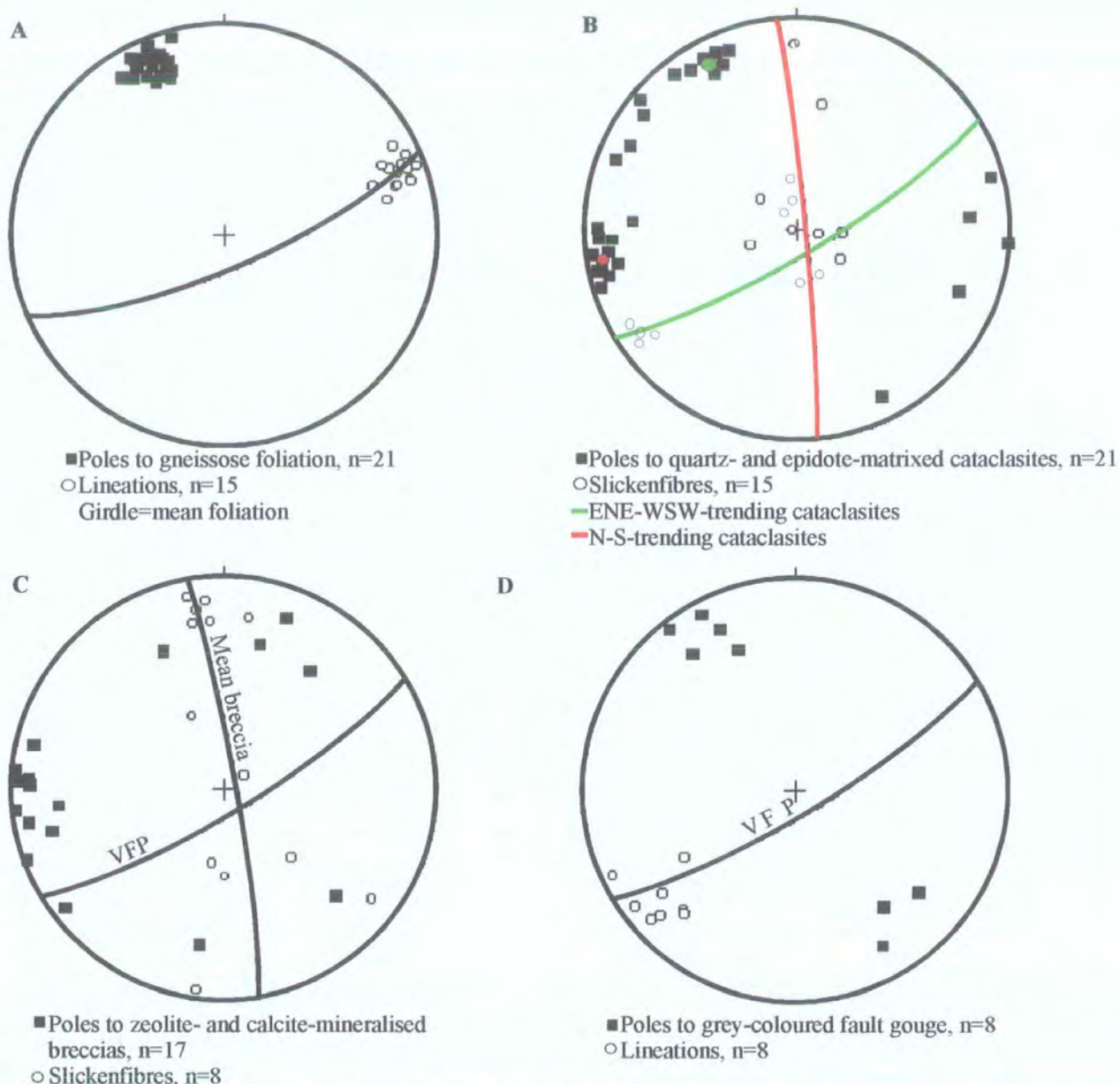


Figure 6.46 Stereographic projections to show (A) gneissose foliation and lineation, (B) quartz- and epidote-matrixed cataclasites and slickenfibres, (C) zeolite- and calcite-mineralised breccias and slickenfibres, and (D) grey gouge and lineations. All data collected from stream section map (Figure 6.45; 7830 7640).



Plate 6.40 Plan view. NE-SW-trending, sub-vertical cataclasite (cc) linked by sinistral strike-slip, R-type Riedel shears (R). Split arrows indicate shear sense parallel to slickenside lineations.

N-S-trending epidote- and quartz-matrixed cataclasites dip steeply to the E and W (Figure 6.46B) and link into NE-SW- to ENE-WSW-orientated cataclasites. The cataclasites contain sub-vertical slickenfibres (Figure 6.46B), which consistently indicate dip-slip normal movements based upon the stepping direction of quartz mineral fibres. The N-S-trending extensional cataclasites formed during sinistral transtension along the ENE-WSW-trending VFZ.

Zeolite- and calcite-mineralised breccias overprint and localise along the pre-existing quartz and epidote cataclasites (Figure 6.45). N-S-trending mineralised breccias (1mm to 15cm thick) dip steeply to the E and W (Figure 6.46C). Sub-horizontal slickenfibres indicate sinistral strike-slip movements based upon the stepping direction of the calcite mineral fibres. The N-S-trending breccias are interpreted as R'-type Riedel shears, which re-used pre-existing fractures and faults (Figure 6.45) during dextral strike-slip movements along the VFZ. Less common ENE-WSW-trending, mineralised breccias are 1cm to 3cm thick and contain dip-slip slickenside lineations (Figure 6.46C). Centimetre- to millimetre-thick calcite and zeolite veins overprint and develop along the edges of the earlier formed fault rocks (Figure 6.45). Millimetre- to centimetre-thick anastomosing grey gouges which trend ENE-WSW contain sub-horizontal lineations defined by aligned clay particles (Figures 6.46D; 6.45). The gouges offset the earlier-formed cataclasites, breccias, mineralised breccias and veins by 5cm to 40cm in a dextral sense.

6:4:6:3 Kinematic summary and discussion

The kinematic evolution of the VFZ in the stream section (7830 7640) E of Verrabotn is summarised in Table 6.8.

Kinematic regime	Fault rocks / structures
3. Dextral strike-slip (youngest)	<ul style="list-style-type: none"> ◦ Dextral strike-slip offsets along ENE-WSW-trending grey fault gouges
2. Dip-slip and Dextral strike-slip	<ul style="list-style-type: none"> ◦ ENE-WSW-orientated zeolite- and calcite-mineralised breccias with dip-slip slickenside lineations ◦ N-S-trending zeolite- and calcite-mineralised breccias are interpreted as R'-type Riedel shears
2. Sinistral transtension (oldest)	<ul style="list-style-type: none"> • NE-SW- to ENE-WSW-trending epidote- and quartz-matrixed cataclasites with sinistral strike-slip R-type Riedel shears • N-S-orientated quartz and epidote matrixed cataclasites indicate dip-slip normal movements. ◦ N-S-orientated chlorite veins

Table 6.8 Table summarising the kinematic evolution of the VFZ at the stream section (7830 7640), east of Verrabotn.

The earliest recognised fault-related deformation is recorded by the development of quartz- and epidote-matrixed cataclasites, which indicate sinistral transtensional movements for the VFZ. A phase of dip-slip and dextral strike-slip faulting was accompanied with the development of zeolite- and calcite-mineralised breccias, together with later veining. The most recent phase of fault-related deformation recognised in the field is dextral strike-slip, which led to the formation of a series of anastomosing grey fault gouges.

6:4:7 Verrasundet exposures

The VFZ is well exposed along the northern side of Verrasundet at 7921 7689 (Figure 6.42; locality f; Figure 6.34) to the north of the VFP trace, which lies less than 50m to the south beneath the fjord. Here, the fjord side comprises a rocky shoreline surrounded by 15-20m-high cliffs. Fault-related deformation overprints gneisses belonging to the Banded Gneiss Complex of Fosen (section 6:2:1).

The outcrops described in this section are important, as they represent the VFZ immediately to the north of the VF core.

6:4:7:1 Fault rock distribution and age relationships

All the fault rocks exposed along the northern shoreline of Verrasundet are lithologically and texturally similar to those exposed along the adjacent 720 road section (section 6:4:5:1; Figure 6.42). Compositionally banded granodiorite gneiss is overprinted by a series of centimetre- to millimetre-thick, ENE-WSW- and N-S-trending cataclasites (Figure 6.47). The cataclasites display anastomosing geometries, are spaced 3cm to 20cm apart and increase in frequency and thickness towards the fjord to the southeast. A 10cm-thick breccia grades into green-coloured cataclasites to the southeast (Figure 6.47). The cataclasite is at least 50cm thick and marks the actual coastline of the fjord. Zeolite and calcite veins 1mm to 20cm thick cross-cut the cataclasite and intensely fractured gneiss. In places, the veining is so intense that breccias form with a mineralised zeolite and calcite matrix (Figure 6.47).

6:4:7:2 Fault zone structure

The gneisses display a strong ENE-WSW-trending foliation, which dips steeply to the SE, and is defined by flattened aggregates of feldspar and quartz (Figure 6.48A). A lineation defined by elongate quartz and feldspar grains plunges shallowly to the ENE. Millimetre- to centimetre-thick braided cataclasites overprint and appear to localise along the pre-existing ENE-WSW-orientated gneissose foliation (Figures 6.47, 6.48B). N-S-trending cataclasites, which dip steeply to the E and W, link into the foliation-parallel cataclasites. This geometry is consistent with sinistral transtension along the VFZ. To the southeast, a 10cm-thick breccia grades into a green-coloured cataclasite (Figure 6.47). The cataclasite is at least 50cm thick and defines the coastline of the fjord. The actual coastline (adjacent to the cataclasite) is here defined by a sheer drop along an ENE-WSW-trending, near-vertical surface. Multiple generations of zeolite and calcite veining (1mm to 20cm thick) overprint and appear to localise along the earlier-formed ENE-WSW- and N-S-trending cataclasites (Plate 6.41A; Figures 6.47, 6.48B).

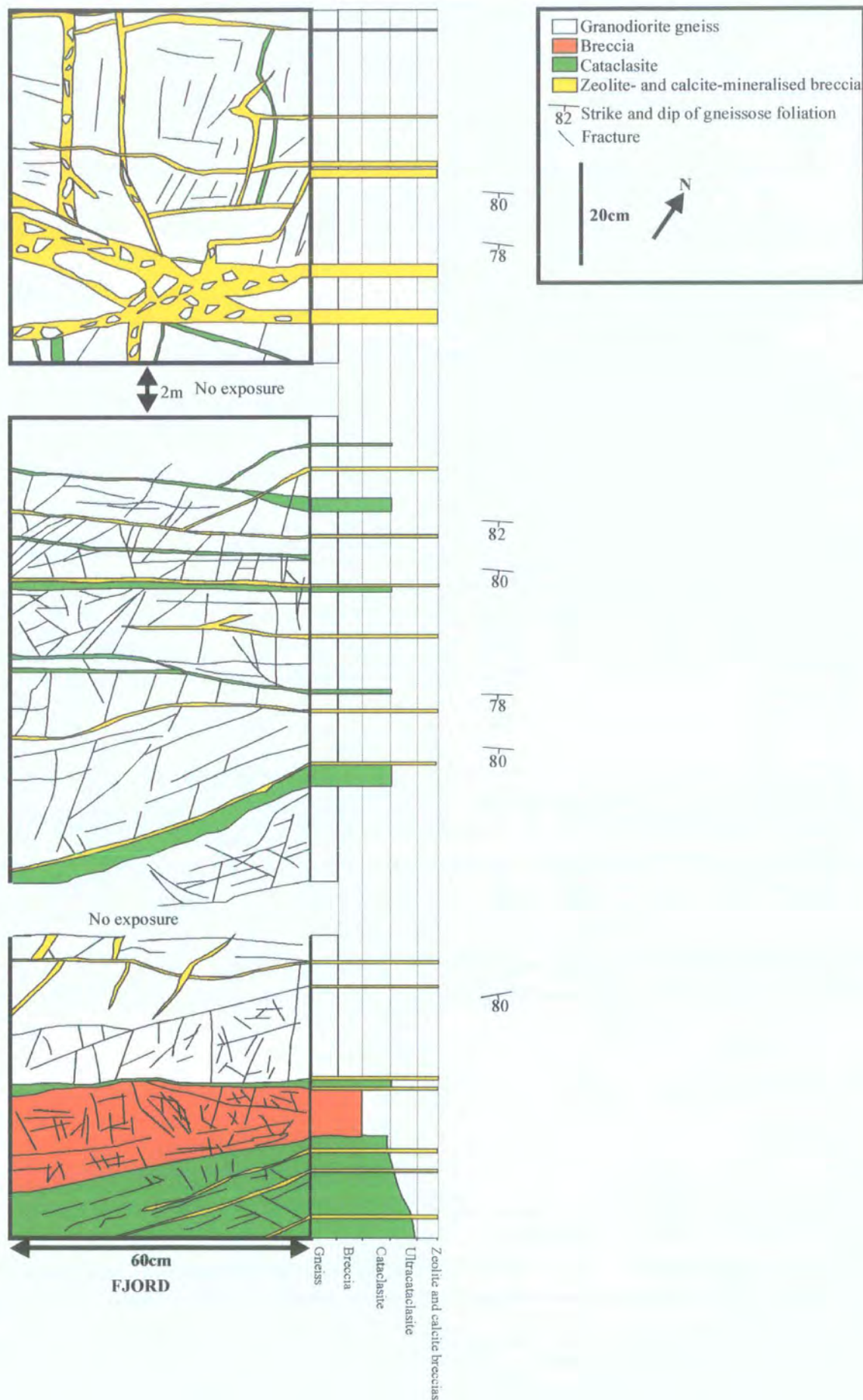


Figure 6.47 Structural log to show fault rock distribution, overprinting relationships and fault zone structure of the rocks exposed along the north side of Verrasundet (7921 7689).

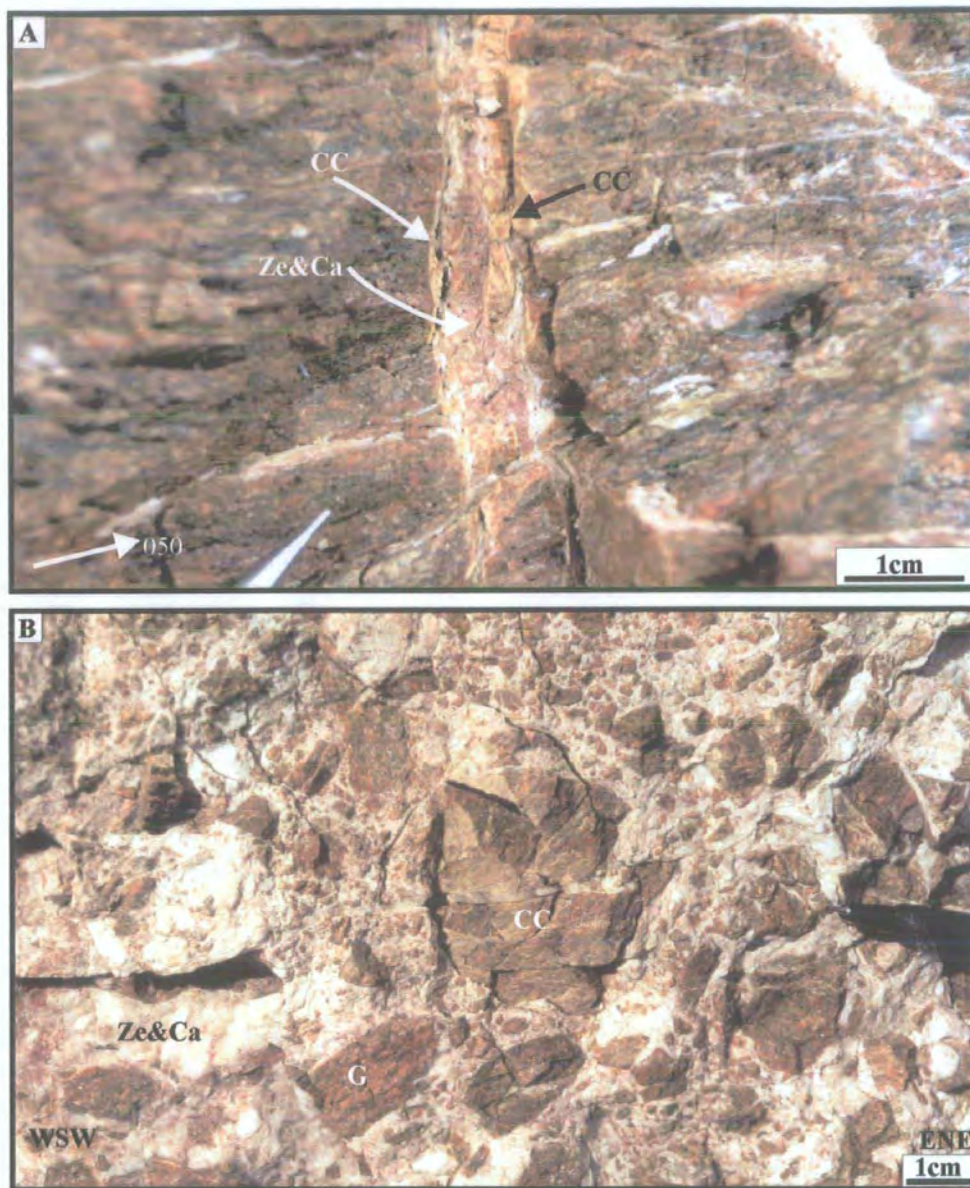


Plate 6.41 Plan view. (A) N-S-trending, millimetre-thick cataclasite (CC) overprinted by multiple phases of later zeolite and calcite (Ze&Ca) mineralisation. (B) Zeolite- and calcite-mineralised breccia (Ze&Ca) containing fragments of granodiorite gneiss (G) with cross-cutting cataclasites (CC).

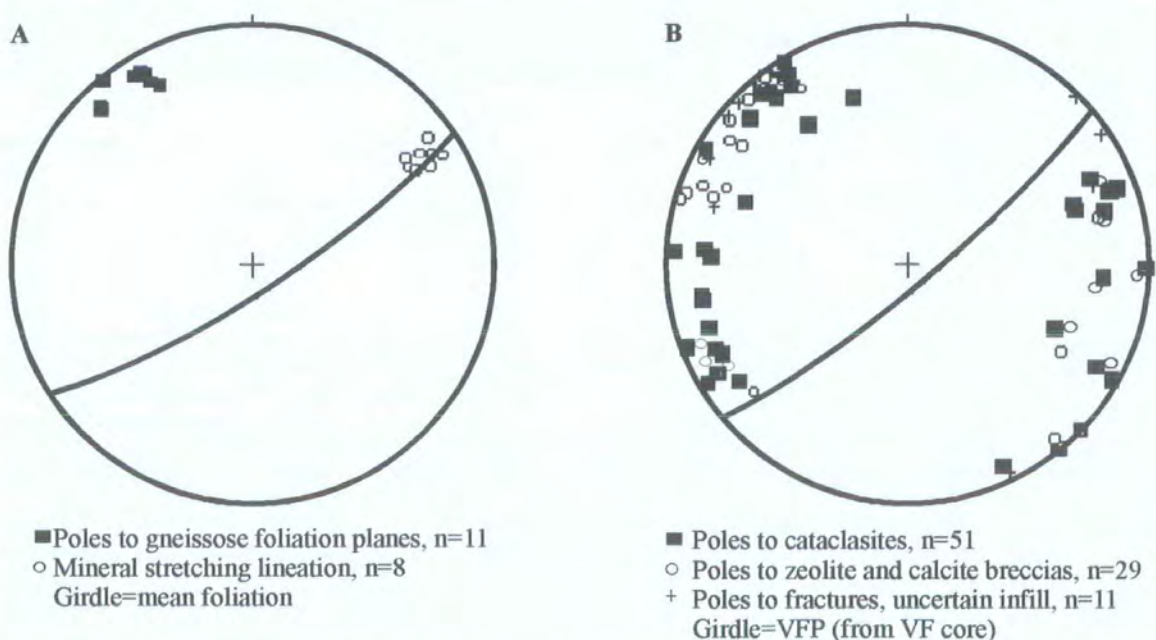


Figure 6.48 Stereographic projections to show (A) gneissose foliation and lineation, and (B) Cataclasites, zeolite and calcite breccias and fractures with uncertain infill, at the Verrasundet exposures (7921 7689).

Locally, the veining is so intense that irregular zones of zeolite and calcite breccias are developed. The breccias contain fragments of cataclasite, suggesting that they are younger than the cataclasites (Plate 6.41B). The breccias are overprinted by a later phase of randomly orientated, centimetre- to millimetre-thick, calcite and zeolite veins.

6:4:7:3 Kinematic summary and discussion

The kinematic evolution of the VFZ along the northern side of Verrasundet at 7921 7689 is summarised in Table 6.9.

Kinematic regime	Fault rocks / structures
2. ? (youngest)	• ENE-WSW- and N-S-trending zeolite- and calcite-matrixed breccias
1. Sinistral transtension (oldest)	• ENE-WSW- and N-S-trending cataclasites

Table 6.9 Table summarising the kinematic evolution of the VFZ along the shoreline on the northern side of Verrasundet (7921 7689).

The VFZ along the northern shoreline of Verrasundet (7921 7689) displays evidence for two phases of movement along the VFZ. Cataclasites represent the earliest fault rocks, which are interpreted to have formed during sinistral transtensional movements along the VFZ. These cataclasites are consistently overprinted by zeolite- and calcite-mineralised breccias, of uncertain kinematics at this locality. An ENE-WSW-trending, near-vertical, sheer drop adjacent to the cataclasite defines the coastline of the fjord. This surface may represent a major structural boundary within the VFZ, where the associated fault rocks of the VF core (section 6:4:8:2) have been eroded or lie beneath the fjord.

6:4:8 Verran Fault Core, Finesbekken

The only exposures of the VF core (7400 7320) are found in a stream section along Finesbekken to the southwest of Verrasundet (locality g; Figure 6.34). The fault core is located in the central part of the VFZ and corresponds to the region of most intense

fault-related deformation. It is defined by a continuous sequence of fault rocks that extends from the wall rocks on either side and across the VFP. Elsewhere, the VF core is eroded, submerged beneath the fjords (Verrasundet and Beitstadfjord) or concealed under the thick Quaternary glacial deposits that fill the ENE-WSW-orientated fertile valleys. The rocks described in this section are important, as they represent fault rocks of the VF core that are not exposed elsewhere and not previously described in the literature.

6:4:8:1 Fault rocks

In this section, fault rocks are described in the order of their relative age (oldest to youngest; see section 6:4:8:2).

6:4:8:1a Cataclasite

Cataclastic series rocks exposed within the VF core are derived entirely from granodioritic gneiss. The cataclasites are green in colour, comprising finely comminuted clasts of orthoclase, plagioclase, quartz, chlorite, epidote, muscovite and sphene set within a fine-grained, epidote-rich, cataclastic matrix (Plate 6.42A). Randomly orientated clasts are angular to sub-angular, ranging from 5mm to less than 0.5mm in size. The majority of the cataclasites possess no internal fabric and appear to be isotropic in the field on all scales of observation. Epidote, quartz, calcite and chlorite veins cross-cut the cataclasites and occur locally as clasts within the cataclasite matrix. The proportion of matrix varies from approximately 10% to 90%, so that the rocks can be subdivided into protocataclasites, cataclasites and ultracataclasites based upon the proportion of matrix present. Locally, the cataclasites contain a foliation defined by grain-size variations, pressure-solution seams and layers of dark-brown coloured gouge. The cataclasites are similar to those exposed at Verrasundet (see section 6:4:7), although they are enriched in epidote and contain layers of fault gouge.

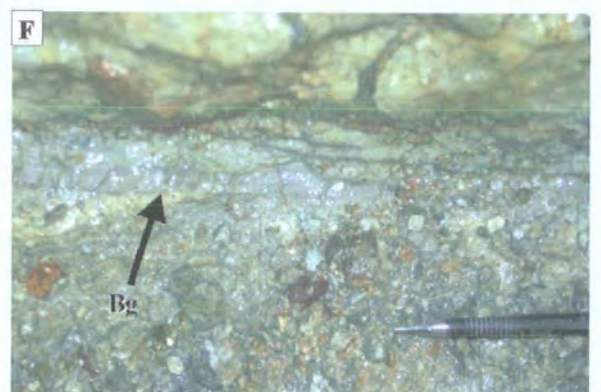
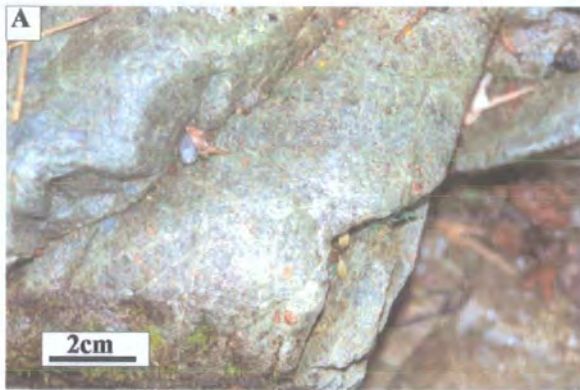


Plate 6.42 Plan view images of fault rocks within the VF core exposed in Finesbekken (7400 7320). (A) Cataclasite. (B) Pseudotachylite (Ps) bounding brecciated gneiss (Gn). (C) Dark brown to black indurated fault gouge (Ig). (D) Zeolite- and calcite-mineralised breccia. (E) Grey fault gouge. (F) Blue-grey fault gouge (Bg).

6:4:8:1b Pseudotachylite

Black to dark brown pseudotachylite veins derived from granodiorite gneiss are relatively uncommon within the VF core (Plate 6.42B). They are cohesive, glassy and very fine grained. They display a millimetre-scale colour banding, which probably reflects variations in grain size and/ or composition. The pseudotachylite veins display very straight boundaries and injection structures into the host-rock gneiss. They commonly occur adjacent to distinct slip surfaces and grade into a marginal cataclasite zone adjacent to the gneissose host rock.

6:4:8:1b Indurated gouge

Black to dark brown, indurated gouge (hardened by cementation or the effects of pressure and temperature (recrystallisation)) is exposed within the VF core (Plate 6.42C). In thin-section the gouge appears to be a brown-coloured, clay-rich isotropic paste containing sub-rounded clasts (0.1 to 0.5mm in size) of cataclasite, quartz, epidote and locally feldspar. XRD analyses (carried out by Laurence Warr, University of Heidelberg, Germany) show the gouge to be composed of chlorite, albite, quartz, epidote and pyrophyllite together with minor amounts of Ca-smectite. The gouge displays a millimetre-scale colour banding due to variations in the clast-to-matrix ratio and possibly composition.

6:4:8:1c Zeolite- and calcite-mineralised breccias

Pale-grey breccias are exposed within the VF core (Plate 6.42D). Randomly orientated, sub-angular to angular fragments of gneiss, cataclasite and indurated fault gouge (0.1 to 2cm in size) are set within a fine- to coarse-grained, mineralised matrix of calcite and zeolite grains. The matrix comprises fibrous zeolite crystals (0.1mm to 0.5cm in size) which form interlocking mosaics with calcite grains (0.1 to 2cm in size). Randomly orientated calcite and zeolite veins (centimetre to millimetre thick) commonly cross-cut and occur as clasts within the mineralised breccias.

6:4:8:1d Grey gouge

The grey gouge is incohesive and clay-like in appearance (Plate 6.42E). It is very fine grained, containing clasts (0.5mm to almost 1cm in size) of cataclasite, zeolite and

calcite breccias and granodiorite gneiss, together with pyrite mineralisation. The gouge contains a lineation defined by the long axes of aligned clay minerals. XRD analyses (carried out by Laurence Warr) show the finest grain-size fraction of the gouge to be composed of Ca-smectite, chlorite, calcite and orthoclase.

6:4:8:1e Blue-grey gouge

The blue-grey gouge is incohesive and clay-like in appearance (Plate 6.42F). It is very fine grained with no clasts visible in the field. The gouge has a strong lineation defined by the long axes of aligned clay minerals. XRD analyses (carried out by Laurence Warr) were not possible on this gouge due to the large amount of swelling clay minerals within the sample (e.g., Ca-smectite).

6:4:8:2 Fault rock distribution and age relationships

The fault core is located in the central part of the VFZ and corresponds to the region of most intense fault-related deformation. The most obvious movement plane of the VFZ is exposed within the Finesbekken stream section (Figures 6.49, 6.50). The fault plane (VFP) is orientated 058/86SE. Here, the fault core is approximately 4m wide (Figures 6.49) and is defined by a continuous sequence of fault rocks that extends from the wall rocks on either side and across the VFP. Figure 6.51 shows a schematic structural log across the fault core region based upon the section exposed in Finesbekken.

Northwest of the VFP, intensely fractured granodiorite gneiss is overprinted by millimetre- to centimetre-thick foliated cataclasites. The gneiss with foliated cataclasites grades into a 50cm-thick, epidote-rich cataclasite (Figures 6.49, 6.50, 6.51; Plate 6.42A), which is cut by millimetre-scale quartz, epidote and chlorite veining. In places, the cataclasite contains millimetre-thick, ENE-WSW-trending, dark-brown to black indurated gouges. To the southeast, the cataclasite is cut by a 5cm-thick brown to black indurated fault gouge (Figure 6.50; Plate 6.42B). The contact is irregular (Plate 6.42C) and the indurated fault gouge displays millimetre- to centimetre-scale, N-S injection vein geometries into the epidote-rich cataclasite.



Figure 6.49 1:200 scale cairn map of the exposures of the Verran Fault core along the Finesbekken stream at 7400 7320 to show the fault rock distribution and fault zone structure. A-A', B-B' and C-C' show the locations of structural logs in Figure 6.50.

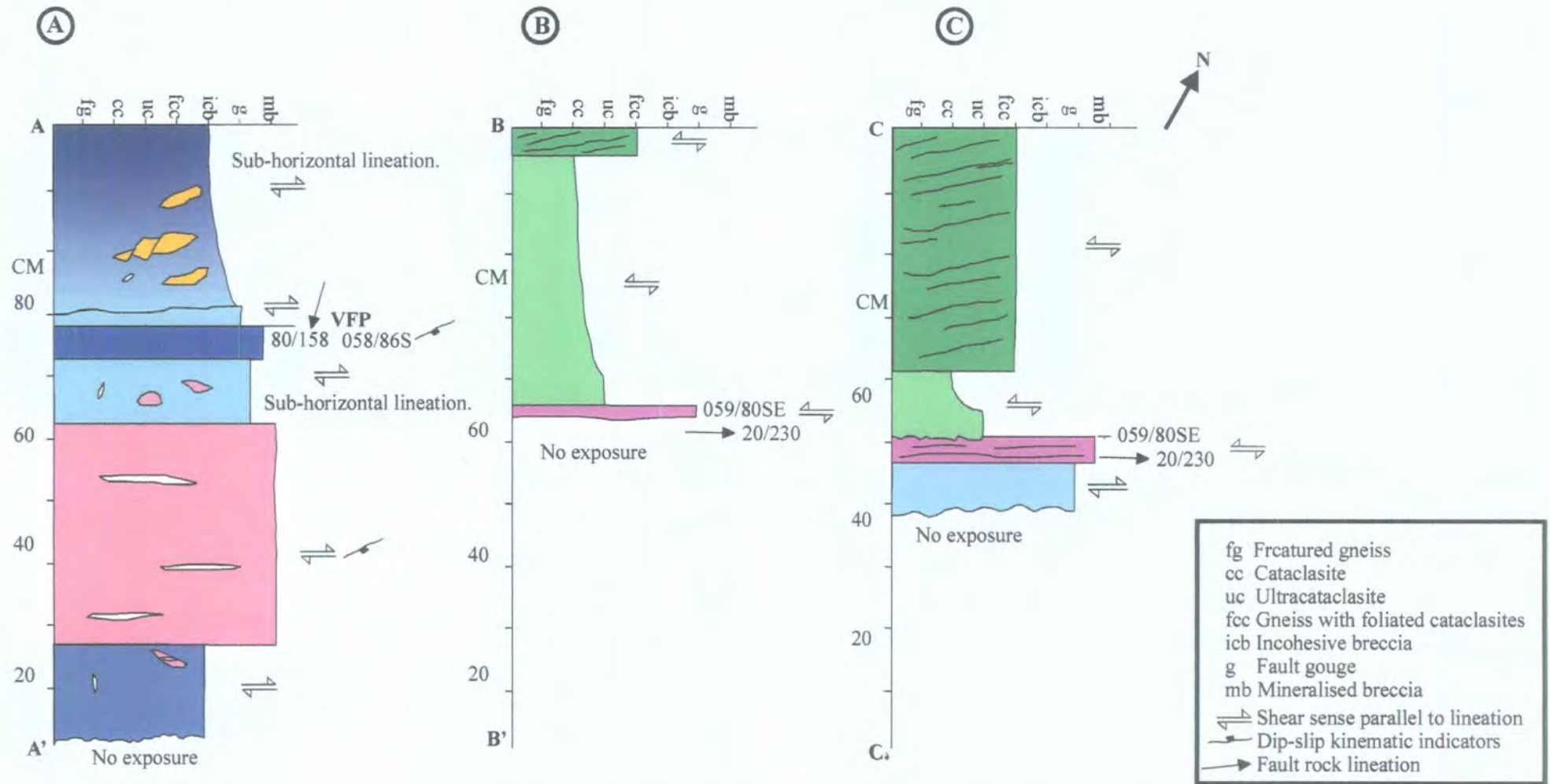


Figure 6.50 Plan view. Structural logs located on Figure 6.49 (Verran Fault core map) to illustrate fault rock distribution, overprinting relationships and structure within the Verran Fault core (7400 7320). Fault rock lithologies are the same as in Figure 6.49.

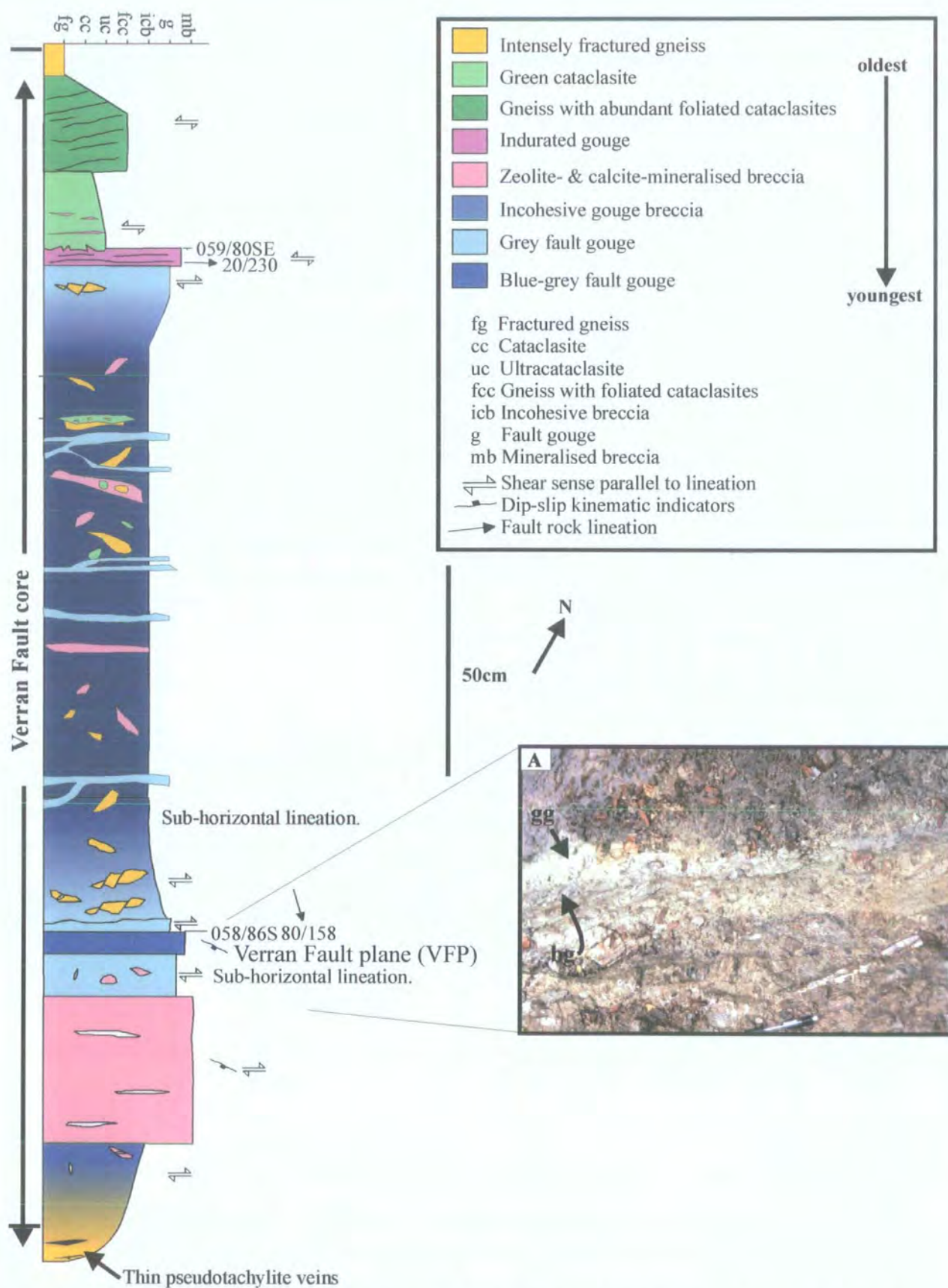


Figure 6.51 Plan view. Schematic structural log through the Verran Fault core based upon Figures 6.49 and 6.50 to illustrate fault rock distribution, overprinting relationships and fault zone structure. Inset (A), image to show blue-grey (bg) and grey gouges (gg).

The indurated fault gouge contains clasts of cataclasite, suggesting that the indurated fault gouge is the younger fault rock. The contact between the indurated fault and the soft grey gouge to the southeast is sharp and polished (059/80SE). The soft grey gouge contains fragments of earlier formed cataclasite, indurated gouge and zeolite/calcite mineralised breccia, suggesting that the gouge is younger than these fault rocks. It is at least 15cm thick, but the true thickness is unclear due to lack of exposure. To the southeast, the grey gouge is interpreted to grade into an incohesive breccia zone which is approximately 1.5m thick (Figure 6.51). The incohesive breccia sporadically crops out along the Finesbekken stream bed and contains fragments of earlier formed cataclasite, indurated gouge and mineralised (zeolite and calcite) breccia. Centimetre-thick, grey gouges cross-cut the incohesive breccia and commonly crop out beneath the water in the stream bed displaying ENE-WSW anastomosing geometries. On the southeast side of the stream, the incohesive breccia grades into a 30cm-thick grey gouge (Figures 6.49, 6.50, 6.51). Here, the grey gouge (Plate 6.42E) contains fragments (up to 30cm in length) of gneiss and zeolite and calcite mineralised breccia, suggesting that the grey gouge is younger than these fault rocks. Within the centre of the grey gouge, a 5cm-thick, blue-grey gouge cross-cuts the grey gouge (Figure 6.51; Plate 6.42F) and is interpreted to be the youngest fault rock within the VF core, corresponding to the VFP (058/86SE). To the southeast of the gouges, a 25cm-thick zeolite and calcite breccia is exposed (Figure 6.49, 6.50, 6.51). The breccia is cut by grey gouge to the northwest and an incohesive breccia on the southeast side. The incohesive breccia overprints and grades into intensely fractured gneiss to the southeast (Figure 6.51). Millimetre-thick cataclasites and pseudotachylites (Plate 6.42B; Figure 6.51) overprint the intensely fractured gneisses.

6:4:8:3 Fault zone structure

Granodiorite gneiss both to the northwest and southeast of the VF core contains an ENE-WSW-trending, SE-dipping foliation defined by flattened aggregates of feldspar and quartz (Figures 6.49, 6.52A). Lineations defined by elongate quartz and feldspar plunge shallowly to the ENE. ENE-WSW-trending, millimetre-thick cataclasites (Figure 6.52B) appear to localise along the pre-existing gneissose foliation both to the northwest and southeast of the VFP.

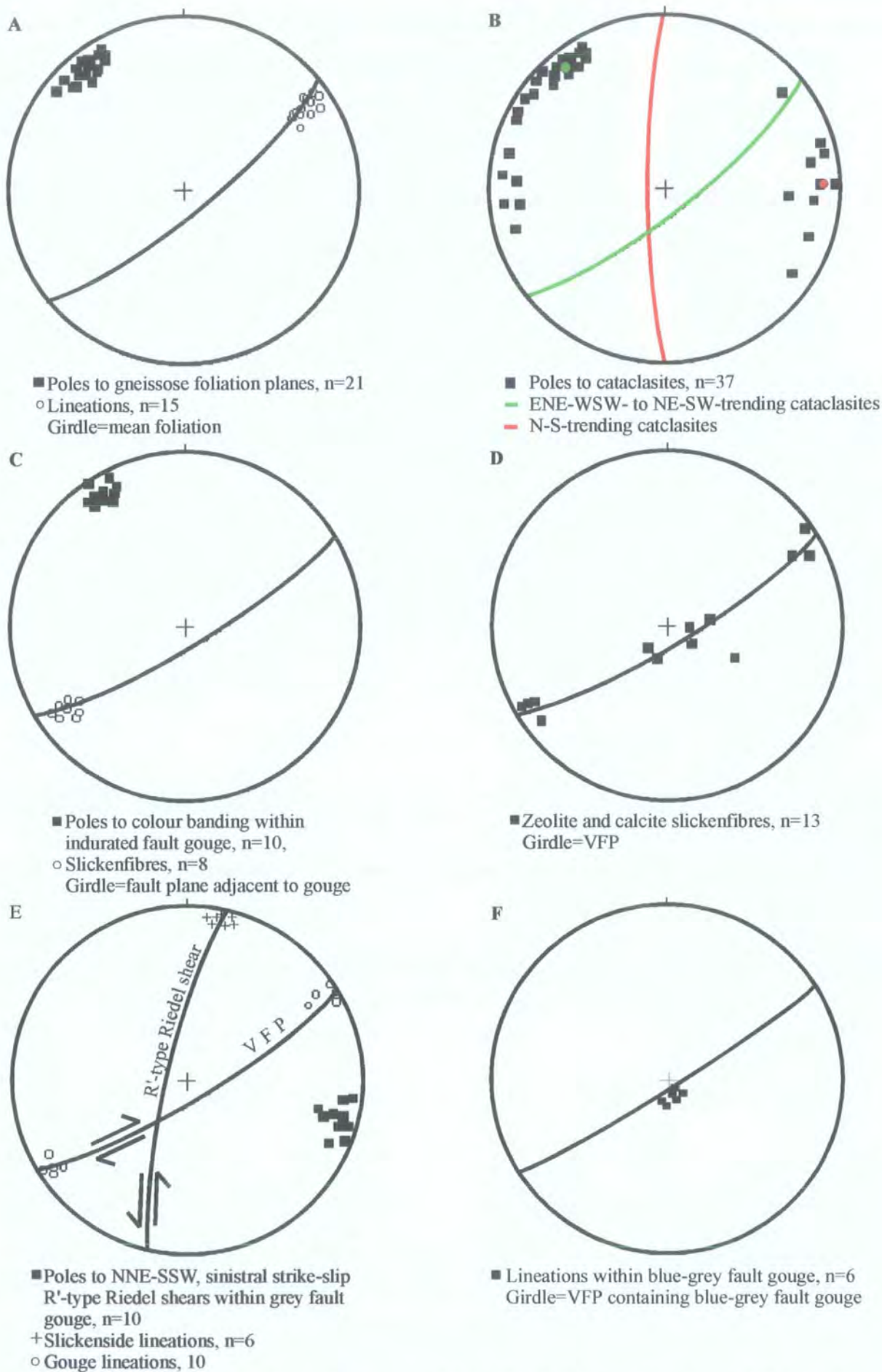


Figure 6.52 Stereographic projections to show structural data within the VF core. (A) gneissose foliation and lineation. (B) Millimetre-thick cataclasites. (C) Banding within brown to black indurated fault gouge and associated slickenfibres. (D) Slickenfibres associated with zeolite- and calcite-mineralised breccias. (E) R'-type Riedel shears and lineations within grey fault gouge. (F) Lineations within blue-grey fault gouge.

N-S- and NE-SW-trending cataclasites (Figure 6.52B) display braided geometries and commonly link into ENE-WSW-orientated cataclasites. ENE-WSW- and NE-SW-trending cataclasites contain sub-horizontal slickenside lineations. In thin-sections viewed parallel to the slickenside lineations and normal to the ENE-WSW-striking and steeply-dipping cataclasites, NE-SW-trending chlorite-filled linking fractures display braided geometries. The gneissose foliation is offset by up to 3cm in a sinistral sense along the NE-SW-orientated, chlorite-filled fractures, which are interpreted as R-type Riedel shears. The N-S-trending fractures display dip-slip slickenside lineations and kinematics consistent with extension. The R-type Riedel shears and N-S-trending extensional cataclasites were formed during sinistral transtension along the VFZ. In places, the cataclasites display a foliation defined by aligned clasts and a dark-brown colour banding. In thin-section, the foliation is defined by pressure-solution seams, grain size variations and slivers of dark-brown coloured indurated gouge. To the southeast of the VFP the gneisses are overprinted by millimetre- to centimetre-thick, foliation-parallel pseudotachylites (Plate 6.42B). They display very sharp boundaries, injection vein geometries and usually bound a 2-5cm-wide zone of brecciated gneiss. The pseudotachylites do not show any kinematic indicators in the field and are interpreted to be broadly coeval with the epidote-rich cataclasites.

On the north side of the VF core, intensely fractured gneisses cut by cataclasites, indurated fault gouge and pseudotachylites are overprinted by a 50cm-thick unit of epidote-rich cataclasite (Figure 6.49, 6.50, 6.51). The cataclasite contains no fabric and appears to be isotropic on all scales of observation in the field. To the southeast, the cataclasite grades into a 5cm-thick, brown to black, indurated fault gouge. The indurated fault gouge displays millimetre- to centimetre-scale injection veins into the adjacent cataclasite. It contains an ENE-WSW-trending colour banding, which dips steeply to the SE (Figure 6.52C) and is defined by grain size variations, compositional layers and the alignment of clasts. Backscatter SEM images show layers of Ca-smectite and pyrophyllite transected by sinistral-verging folds in polished blocks cut parallel to the slickenfibres lineations (Figure 6.52C) and normal to the foliation. The contact between the indurated fault and the soft grey gouge to the southeast is sharp and polished (059/80SE). Sub-horizontal quartz slickenfibres, which plunge

shallowly to the WSW (Figure 6.52C), indicate sinistral strike-slip movements based upon the stepping direction of the quartz mineral fibres.

The soft grey gouge is at least 15cm thick and grades southeastwards into a 1.5m-thick incohesive breccia, which contains slivers of calcite- and zeolite-mineralised breccia and fragments of cataclasite (Figure 6.51). The mineralised breccias form ENE-WSW-trending lenses, which dip steeply to the SE. SE-dipping surfaces of the mineralised breccias display dip-slip normal slickenfibres, which are consistently overprinted by dextral strike-slip slickenfibres (Figure 6.52D).

To the southeast, the incohesive breccia grades into a 30cm-thick grey gouge (Figures 6.49, 6.50, 6.51) which contains sub-horizontal lineations defined by the alignment of clay particles (Figure 6.52E). The gouge contains gneissose blocks up to 30cm in length. NNE-SSW-trending, sub-vertical fractures with sub-horizontal slickenside lineations offset the gneissose blocks by up to 30cm in a sinistral sense (Figure 6.52E; Plate 6.43A). These fractures are interpreted as sinistral strike-slip, R'-type, Riedel shears formed during dextral strike-slip movements along the VFZ. A thin (5cm-thick) blue-grey gouge orientated 058/86SE cross-cuts the grey gouge (Figures 6.49, 6.50, 6.51). The blue-grey gouge is interpreted to represent the most recent phase of regionally significant movement within the VFZ and is therefore interpreted to represent the VFP itself. The blue-grey gouge contains a lineation defined by aligned clay particles, which plunges steeply to the SE (80/158, Figure 6.52F; Plate 6.43B).

To the southeast of the gouges, a 25cm-thick zeolite- and calcite-mineralised breccia is exposed (Figures 6.49, 6.50, 6.51). Grey gouge to the northwest and an incohesive breccia to the southeast overprint the breccia. The incohesive breccia overprints and grades into intensely fractured gneiss to the southeast. Millimetre-thick grey gouges appear to localise along the pre-existing, ENE-WSW-trending cataclasites, indurated fault gouges and pseudotachylites within intensely fractured granodiorite gneiss, exposed to the southeast of the VF core (Figure 6.51).

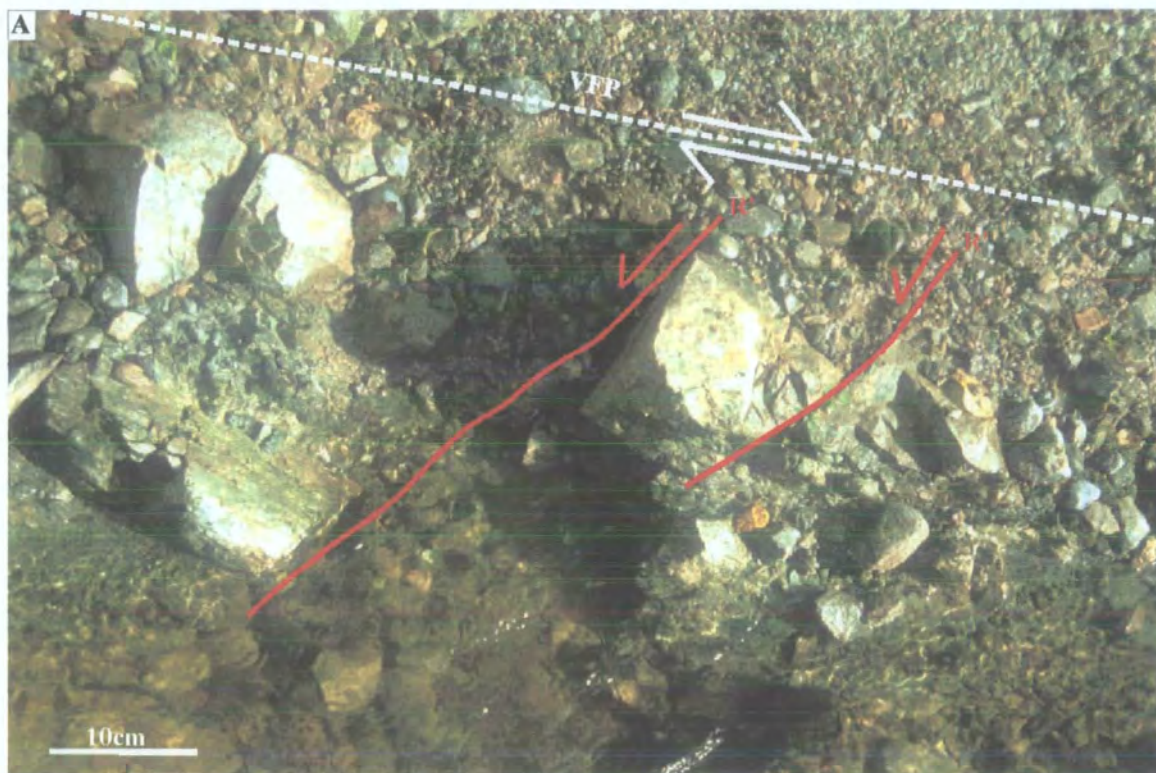


Plate 6.43 (A) Plan view. Sinistral strike-slip NNE-SSW-trending, sub-vertical fractures, offsetting gneissose blocks by up to 30cm within the grey fault gouge. (B) View of dip-slip lineations defined by aligned clay particles within the blue-grey fault gouge along VFP (059/86SE).

6:4:8:4 Kinematic summary and discussion

The kinematic evolution of the VFZ within the VF core exposed within the Finesbekken stream (7400 7320) is summarised in Table 6.10.

Kinematic regime	Fault rocks / structures
4. Dip slip (youngest)	<ul style="list-style-type: none"> ◦ Dip-slip lineations within thin blue-grey gouge
3. Dextral strike-slip	<ul style="list-style-type: none"> ◦ Grey gouge with sub-horizontal lineations ◦ R'-type Riedel shears offsetting gneissose blocks within gouge
2. Dip-slip normal (SE side down) followed by dextral strike-slip	<ul style="list-style-type: none"> ◦ ENE-WSW-trending zeolite- and calcite-mineralised breccias with dip-slip normal slickenfibres overprinted by dextral strike-slip slickenfibres
1. Sinistral transtension (oldest)	<ul style="list-style-type: none"> ◦ Cataclasites ◦ Pseudotachylites ◦ Indurated fault gouge ◦ Sinistral slickenfibres ◦ R-type Riedel shears and N-S extensional fractures ◦ Sinistral-verging folds within indurated gouge

Table 6.10 Table summarising the kinematic evolution of the VFZ within the VF core exposed within the Finesbekken stream (7400 7320).

The VF core is located in the central part of the VFZ and corresponds to the region of most intense fault-related deformation. It is approximately 4m wide (Figure 6.51) and is defined by a continuous sequence of fault rocks that extends from the wall rocks on either side and across the VFP. The rocks described in this section are important, as they preserve fault rocks and structures of the VF core not exposed elsewhere within the VFZ. The exposures within the fault core are interpreted to represent those immediately to the south of the Verrasundet exposures (7921 7689; see section 6:4:7, i.e., the cataclasites exposed at the extreme southeast of the Verrasundet locality correspond to those on the north side of Finesbekken). The fault rocks and structures

within the VF core display evidence for multiple reactivation through repeated localisation along pre-existing structures and fault rocks. The earliest fault rocks are cataclasites, indurated fault gouges and pseudotachylites formed during sinistral transtensional movements along the VFZ. Zeolite- and calcite-mineralised breccias were formed during dip-slip normal faulting followed by a phase of dextral strike-slip faulting. Anastomosing grey gouges surrounding zones of incohesive breccia formed during dextral strike-slip movements. The most recent phase of movement is recorded by a thin blue-grey gouge, which localises along the pre-existing grey gouge and was formed during a phase of dip-slip movement.

6:4:9 Rautingdalen Fault

The Rautingdalen Fault (RF) is one of the many, kilometre-scale, NNE-SSW-trending faults that links into the VF from the north (locality h; Figure 6.34; Figure 6.53). The RF is well exposed in a stream section of a steep-sided gorge, especially after a period of dry weather. Tree-covered rocky crags and cliffs (20 to 100m high) occur on either side of the stream section.

Grønlie et al. (1991) described the RF as a sigmoidal, NNE-SSW-trending structure formed at a high angle to the VF, providing spectacular outcrops of cataclastic series rocks as well as later zeolite mineralisation. Grønlie et al. (1991) described the entire bottom of the steep-sided valley as a 10m-wide zone of greenish cataclastic fault rock, comprising cataclasite, ultracataclasite, zeolite-matrix breccias and later zeolite and calcite veining.

6:4:9:1 Fault rocks

In this section, fault rocks are described in the order of their relative age (oldest to youngest; see section 6:4:9:3).

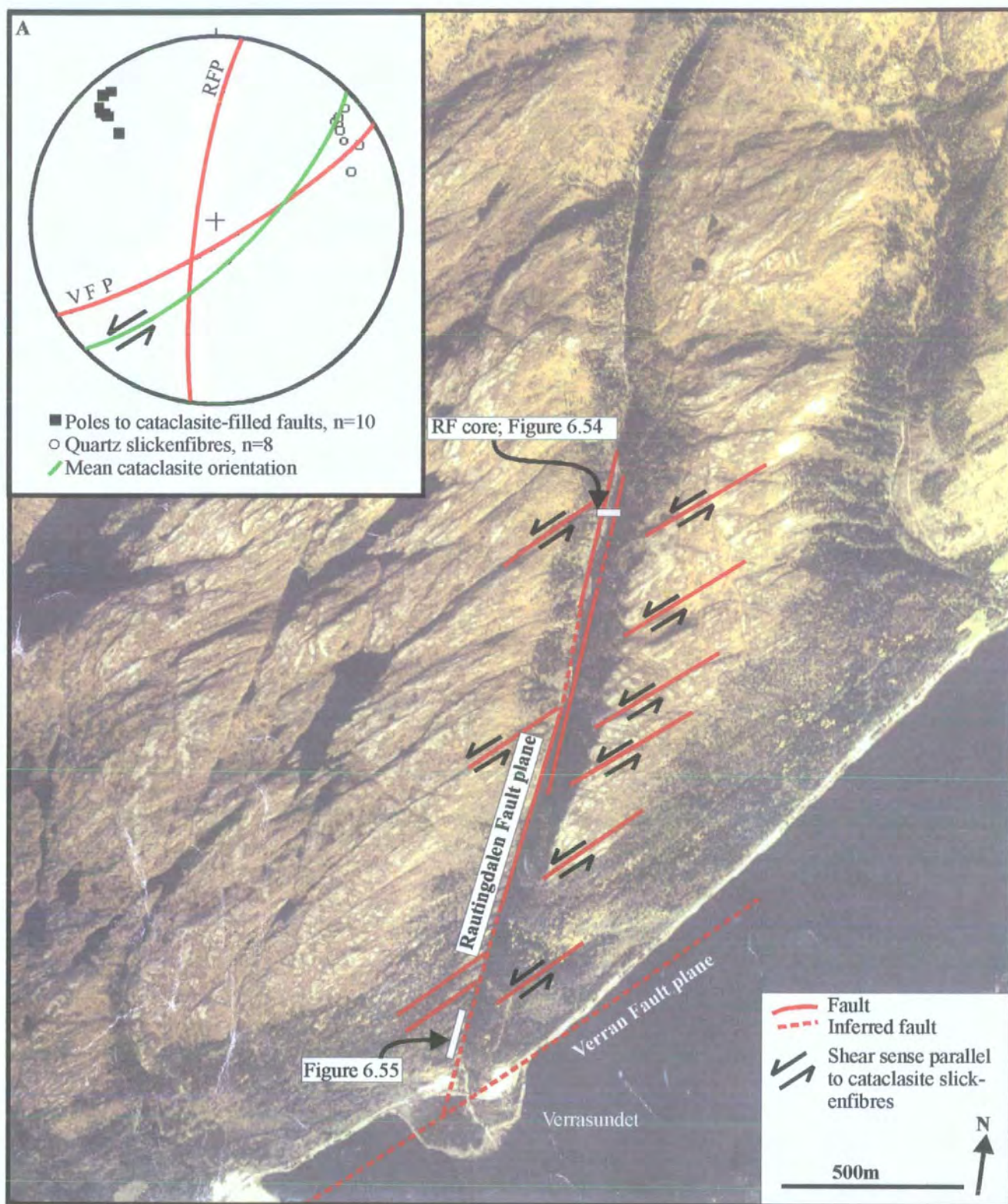


Figure 6.53 Air photograph to show the geometry of the RF and linking structures. (A) Inset. Stereographic projection to show sinistral strike-slip, cataclasite-filled faults relative to the RFP and VFP.

6:4:9:1a Cataclasite

Cataclastic series rocks are derived entirely from granodiorite gneiss. The cataclasites are usually pale-green in colour (Plate 6.44B), comprising finely comminuted clasts of gneiss, orthoclase, plagioclase, quartz, chlorite and epidote set within a fine-grained cataclastic matrix of the same. Randomly orientated clasts are angular to sub-angular, ranging from 5mm to less than 0.5mm in size. The cataclasites possess no internal fabric and appear to be isotropic in the field on all scales of observation. Epidote and quartz veins cross-cut the cataclasites and occur locally as clasts within the cataclasite matrix. The proportion of matrix varies from approximately 40% to 90%, so that the rocks can be subdivided into cataclasites and ultracataclasites based upon the proportion of matrix present. The cataclasites exposed along the RF are lithologically and texturally similar to those exposed along the VF core (section 6:4:8:1a) and the HSF core (section 6:3:1:1b).

6:4:9:1b Zeolite- and calcite-mineralised fault gouge

The pale grey mineralised fault gouge is fine grained, clay-rich and cohesive (Plate 6.44A). In thin-section and in the field, the gouge appears to be a clay-rich isotropic paste that has been cemented by zeolite (laumontite; Grønlie et al. 1991) and calcite mineralisation. Thin zeolite and calcite veins cross-cut the mineralised gouge.

6:4:9:1c Zeolite- and calcite-mineralised breccia

Pale grey to pink coloured breccias are exposed along the RF (Plate 6.44C). Randomly orientated, sub-angular to angular fragments (0.1 to 4cm in size) of gneiss, cataclasite and zeolite-mineralised fault gouge are surrounded by a fine- to coarse-grained, mineralised matrix of calcite and zeolite grains. The matrix comprises fibrous zeolite crystals (0.1mm to 0.5cm in size) which form interlocking mosaics with calcite grains (0.1 to 2cm in size). Late-stage calcite grains appear to fill in the remaining pore spaces within the breccias. The zeolite- and calcite-mineralised breccias are lithologically and texturally similar to those exposed throughout the VFZ.

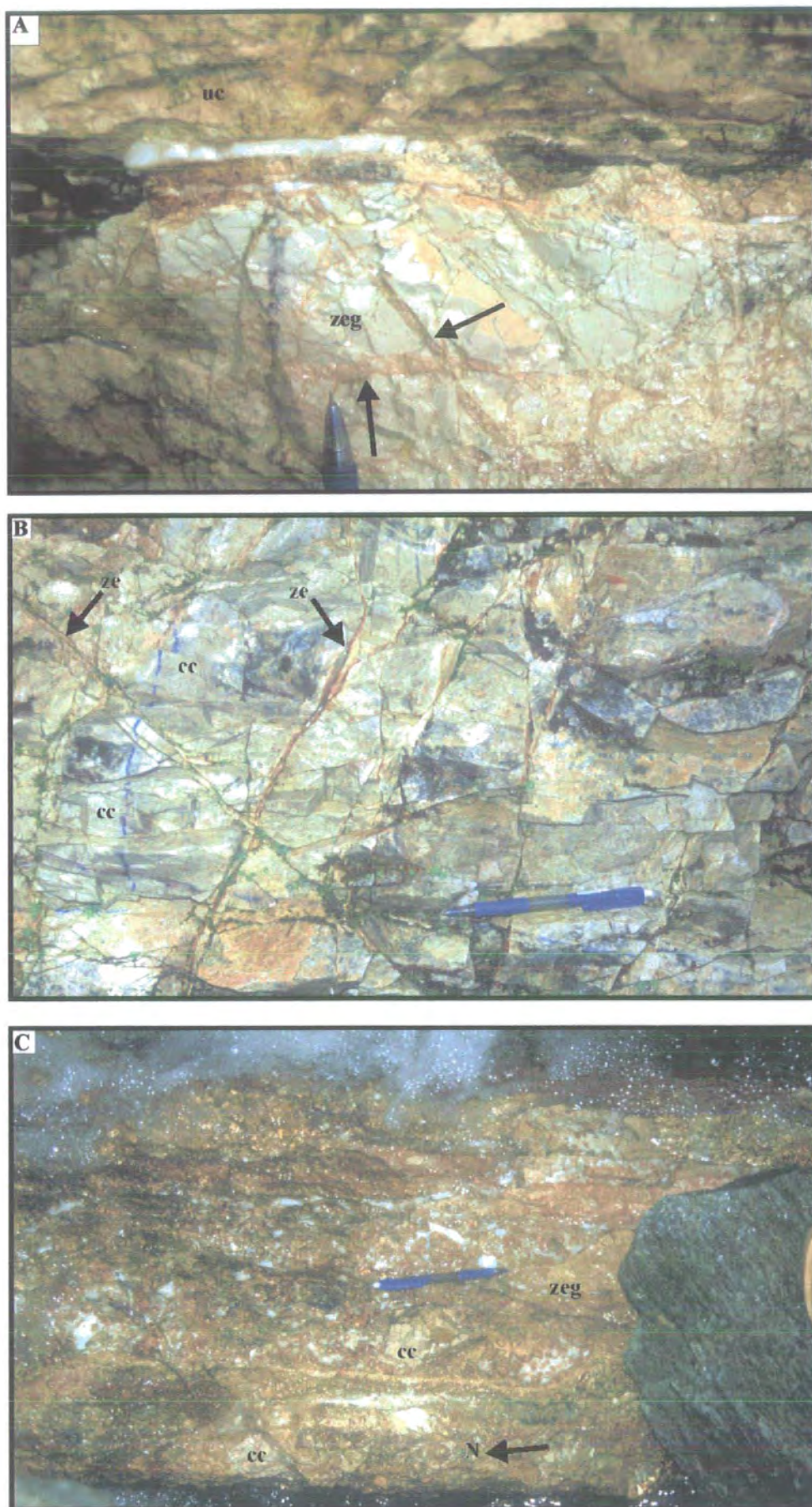


Plate 6.44 Plan view. Locations of A-C are shown in Figure 6.54. (A) Ultracataclasite (uc) overprinted by zeolite-mineralised gouge (zeg). The zeolite-mineralised gouge is transected by a series of zeolite and calcite veins (arrowed). (B) Cataclasite (cc) overprinted by a series of calcite and zeolite veins (ze-arrowed). (C) Zeolite- and calcite-mineralised breccia containing clasts of earlier-formed cataclasite(cc) and zeolite-mineralised gouge (zeg).

6:4:9:2 Fault rock distribution and age relationships

The fault core is best exposed at 7946 7872 (Figure 6.53) located in the central part of the RF and corresponds to the region of most intense fault-related deformation. The most obvious movement plane of the RF is exposed on the western side of the stream section (Figure 6.54). The fault plane (RFP) is orientated 008/81W. The fault core is approximately 8m wide (Figure 6.54) and is defined by a continuous sequence of fault rocks that extends from the wall rocks on either side and across the RFP.

Along the western margin of the RF, intensely fractured granodiorite gneiss is separated from a 20cm-thick unit of ultracataclasite by a sharp and polished RFP. The ultracataclasite is overprinted to the east by 30cm-thick zeolite- and calcite-mineralised gouge, which contains clasts of gneiss and earlier formed cataclasite (Figure 6.54). The mineralised gouge is cut by a series of randomly orientated, pale pink zeolite veins (1mm to 1cm thick; Plate 6.44A). Grønlie et al. (1991) described these as laumontite veins, based upon XRD analyses. Both the mineralised gouge and laumontite veins are cross-cut by a later phase of orange-coloured zeolite (stilbite; Grønlie et al. 1991) and calcite veins (1mm to 1cm thick; Figure 6.54). Farther east, a 1.2m-wide zone of pale green cataclasite overprints granodiorite gneiss. Millimetre- to centimetre-thick zeolite and calcite veins cross-cut the cataclasite (Figure 6.54; Plate 6.44B). The cataclasite grades eastwards into a 5m-wide zone of intensely fractured gneiss (locally brecciated) which is cut by a series of millimetre- to centimetre-thick, braided cataclasites. Millimetre-thick zeolite and calcite veins overprint both the cataclasite and the fractured gneiss. Farther east, the gneiss is bounded by a 2cm-thick zeolite- and calcite-mineralised gouge, which is overprinted eastwards by a 40cm-thick zeolite- and calcite-mineralised breccia further to the east (Figure 6.54). The zeolite- and calcite-mineralised breccia contains clasts of cataclasite and zeolite- and calcite-mineralised gouge (Plate 6.44C), suggesting that the zeolite- and calcite-mineralised breccia is the youngest fault rock.

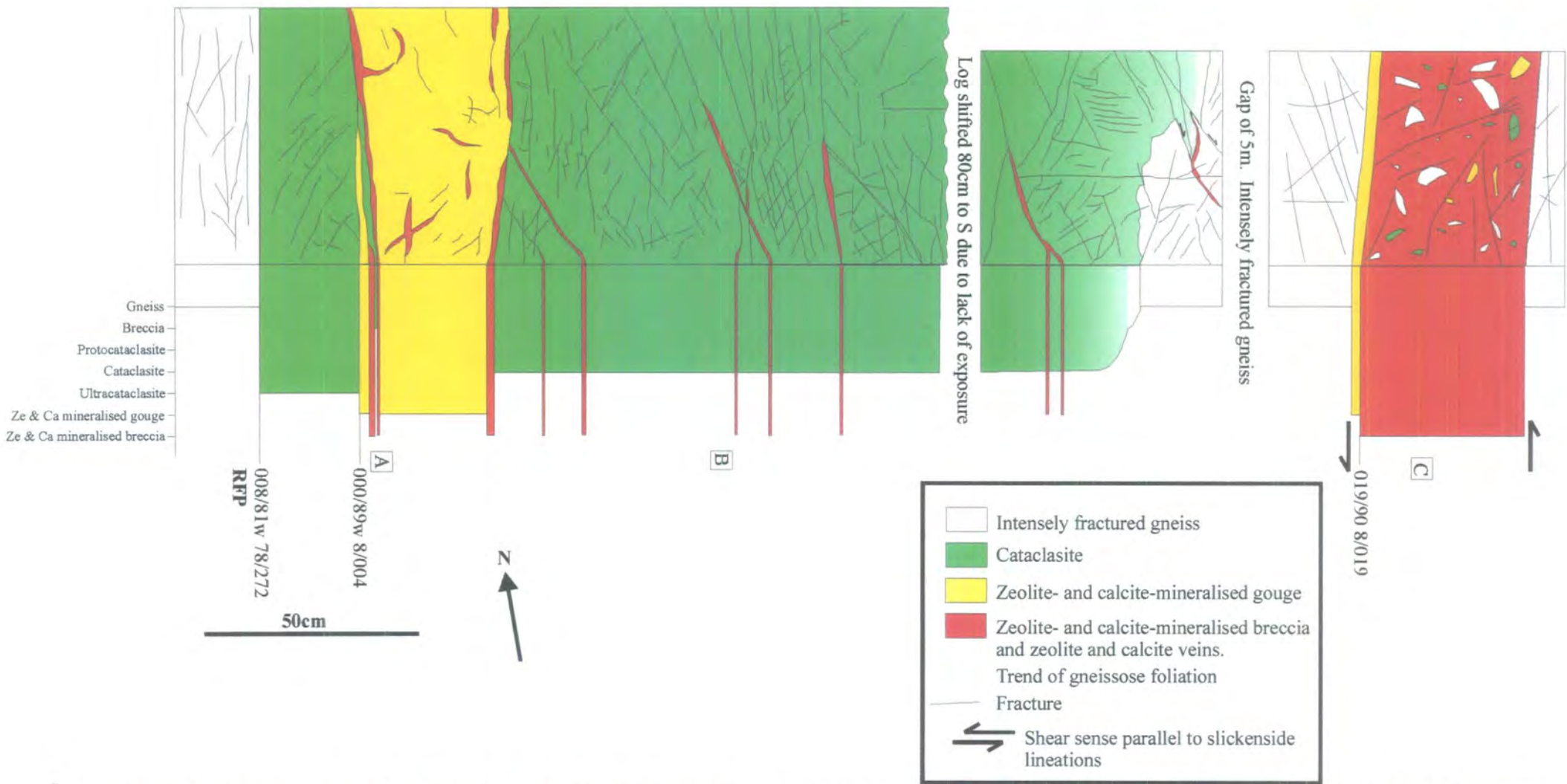


Figure 6.54 Plan view. Structural log through the Rautingdalen Fault core to illustrate overprinting relationships, fault rock distribution and fault zone structure. Located in Figure 6.53. (A), (B) and (C) refer to images within Plate 6.44.

6:4:9:3 Fault zone structure

The RF is a NNE-SSW-trending fault that dips steeply to the W and appears to link into the VF. Air-photograph interpretation combined with field mapping has identified a series of NE-SW-orientated faults spaced every 100 to 400m, that appear to link into the RF (Figure 6.53). The faults contain 10cm to 30cm of pale green cataclasite and display sinistral-strike-slip slickenfibres based upon the stepping direction of quartz mineral fibres (Figure 6.53A). These faults are interpreted as R-type Riedel shears formed during sinistral strike-slip movements along the VF.

In the wall rocks to the west of the RF, the granodiorite gneiss displays an ENE-WSW-trending, SE-dipping foliation defined by flattened aggregates of feldspar and quartz (Figure 6.55A). Lineations defined by elongate quartz and feldspar plunge shallowly to the ENE. The gneisses are intensely fractured and locally brecciated.

To the west of the RF, cataclasite-filled faults display ENE-WSW-trending braided geometries and overprint the fractured gneiss (Figure 6.55). The cataclasites contain sub-horizontal slickenfibres, which indicate sinistral strike-slip movements based upon the stepping direction of the quartz mineral fibres (Figure 6.55B). Zeolite- and calcite-mineralised breccias appear to both cross-cut and develop along the earlier formed cataclasite and gneissose foliation (Figure 6.55). The breccias are bounded by discrete fault planes which form three main clusters; a) ENE-WSW-trending which dip steeply to the SE, b) ENE-WSW-trending which dip steeply to the NW, and c) E-W to ESE-WNW, which range from steep to shallow dips to the NE (Figure 6.55C). The faults are spaced every 10cm to 5m and display a braided geometry surrounding slivers of intensely fractured gneiss (Figure 6.55). Zeolite and calcite slickenfibres form two main clusters; dip-slip, and a set that plunges shallowly to the ENE (Figure 6.55C). The sub-horizontal slickenfibres correspond to the intersection of NW- and SE-dipping faults, which trend ENE-WSW. The slickenfibres indicate contractional, extensional and dextral strike-slip movements (Figure 6.55) based upon the stepping direction of the mineral fibres. Dip-slip slickenfibres are consistently overprinted by dextral strike-slip slickenfibres along the ENE-WSW-trending faults.

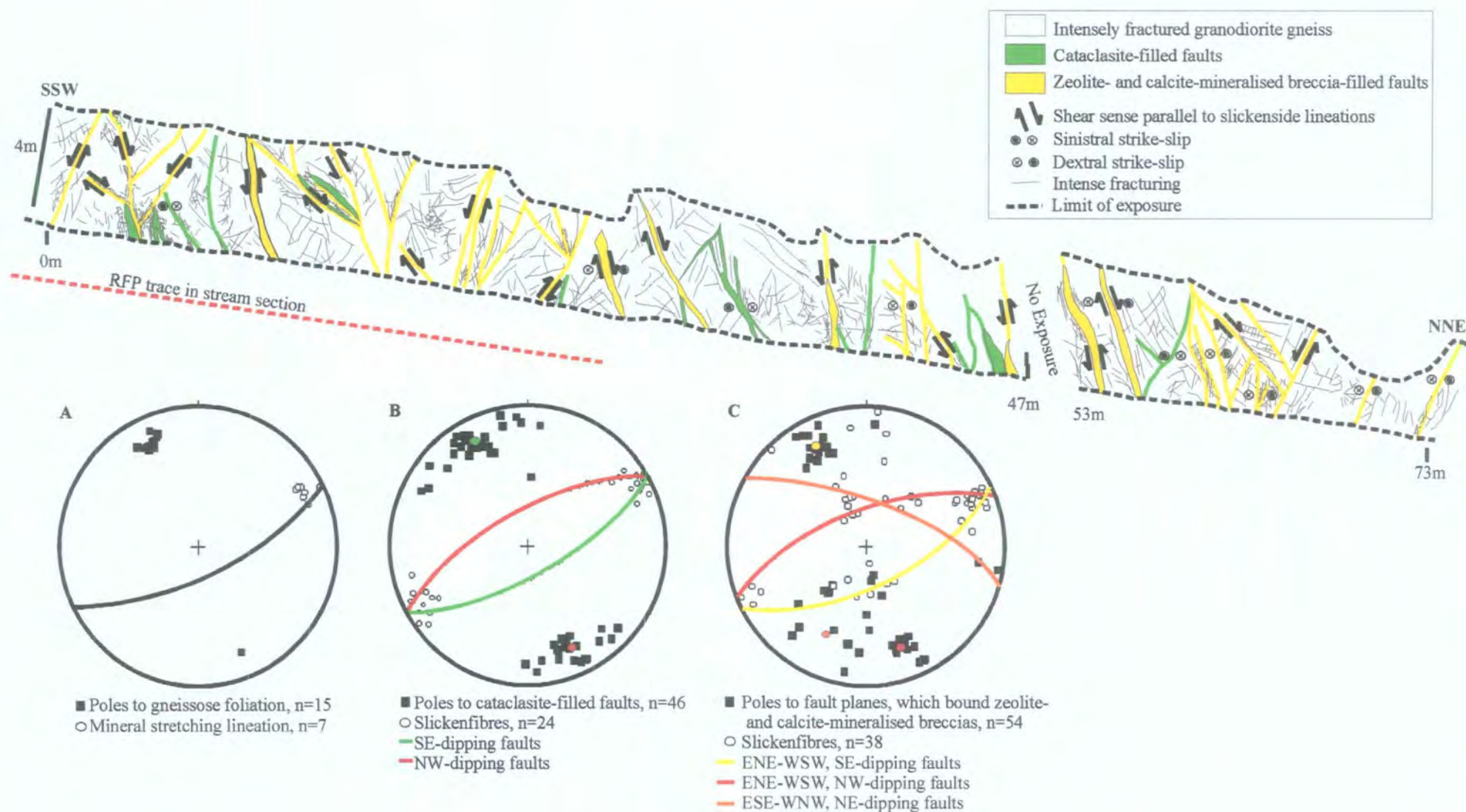


Figure 6.55 Structural cross-section orientated parallel to the RFP, located in Figure 6.53 to illustrate structure within wall-rocks 20m west of the Rautingdalen Fault core. (A) Stereographic projection to show gneissose foliation and lineations. (B) Stereographic projection to show cataclasite-filled faults and slickenfibres. (C) Stereographic projection of fault planes and slickenfibres, which bound zeolite- and calcite-mineralised breccias.

Along the western side of the RF, intensely fractured granodiorite gneiss is separated from a 20cm-thick unit of ultracataclasite by the RFP (Figure 6.54). The RFP is orientated 008/81W and contains quartz slickenfibres that step down the dip of the fault plane, which indicate dip-slip normal movements. The ultracataclasite is separated from a 30cm-thick zeolite- and calcite-mineralised gouge by a fault orientated 000/89W, which contains sub-horizontal slickenside lineations (Figure 6.54). Farther east, a 1.2m-wide zone of pale green cataclasite overprints granodiorite gneiss and in turn is cross-cut by millimetre- to centimetre-thick zeolite and calcite veins (Figure 6.54; Plate 6.44B). The cataclasite grades into a 5m-wide zone of intensely fractured gneiss, which is cut by a series of N-S-trending, millimetre- to centimetre-thick, braided cataclasites. Millimetre-thick zeolite and calcite veins appear to develop along the pre-existing cataclasite. To the east of the gneiss, a 2cm-thick zeolite mineralised gouge is separated from a 40cm-thick zeolite- and calcite-mineralised breccia (Plate 6.44C) by a fault plane orientated 019/90 (Figure 6.54). The fault plane contains zeolite and calcite slickenfibres, which indicate sinistral strike-slip movement based upon the stepping direction of the mineral fibres.

6:4:9:4 Kinematic summary and discussion

The kinematic evolution of the RF is summarised in Table 6.11.

Kinematic regime	Fault rocks / structures
2. Sinistral Strike-slip	<ul style="list-style-type: none"> NNE-SSW-trending zeolite- and calcite-mineralised breccia and gouge with sinistral slickenfibres
1. Dip-slip normal (oldest)	<ul style="list-style-type: none"> Cataclasite and ultracataclasite Quartz slickenfibres

Table 6.11 Table summarising the kinematic evolution of the RF.

The NNE-WSW-trending RF initiated as an extensional fault with the development of cataclasites. The RF formed as an extensional fault during sinistral transtension along the ENE-WSW-trending VFZ. Extensive zeolite and calcite veining was coeval with the development of zeolite- and calcite-mineralised breccias and gouges, which

formed during sinistral strike-slip reactivation along the RF. During this event the RF is interpreted as an R'-type Riedel shear which reactivated a pre-existing fault during dextral strike-slip movement along the ENE-WSW-trending VFZ.

6:5 Summary of the Verran Fault

The VF comprises a 0.5km-wide zone of intense cataclastic deformation together with hydrothermal alteration and mineralisation (Figure 6:56). The earliest fault rocks are rare mylonites formed during sinistral shearing that are only exposed at one locality along the VFZ (see section 6:4:2). These are correlated with mylonites along the HSFZ, as they display similar overprinting relationships, textures and microstructures (see sections 7:1:2, 7:4:2). Later cataclasite assemblages and indurated fault gouges and minor pseudotachylite veins were formed during sinistral transtension. During sinistral transtension, N-S-trending extensional faults such as the RF formed on all scales and linked into the sinistral strike-slip VF. This led to the development of an extensive fracture/ fault-related permeability and the present-day geometry of the MTFC. Later reactivation comprised dip-slip normal movements followed closely by dextral strike-slip movements, which led to the development of zeolite- and calcite-mineralised breccias and gouges. During dextral strike-slip movements along the VF, the N-S-trending faults (e.g., RF) were reactivated as sinistral strike-slip, R'-type Riedel shears to accommodate block rotations on a kilometre scale. Zeolite- and calcite-mineralised breccias and gouges are consistently cross-cut by grey gouges associated with dextral strike-slip. A blue-grey gouge represents the most recent phase of movement and contains a strong dip-slip lineation.

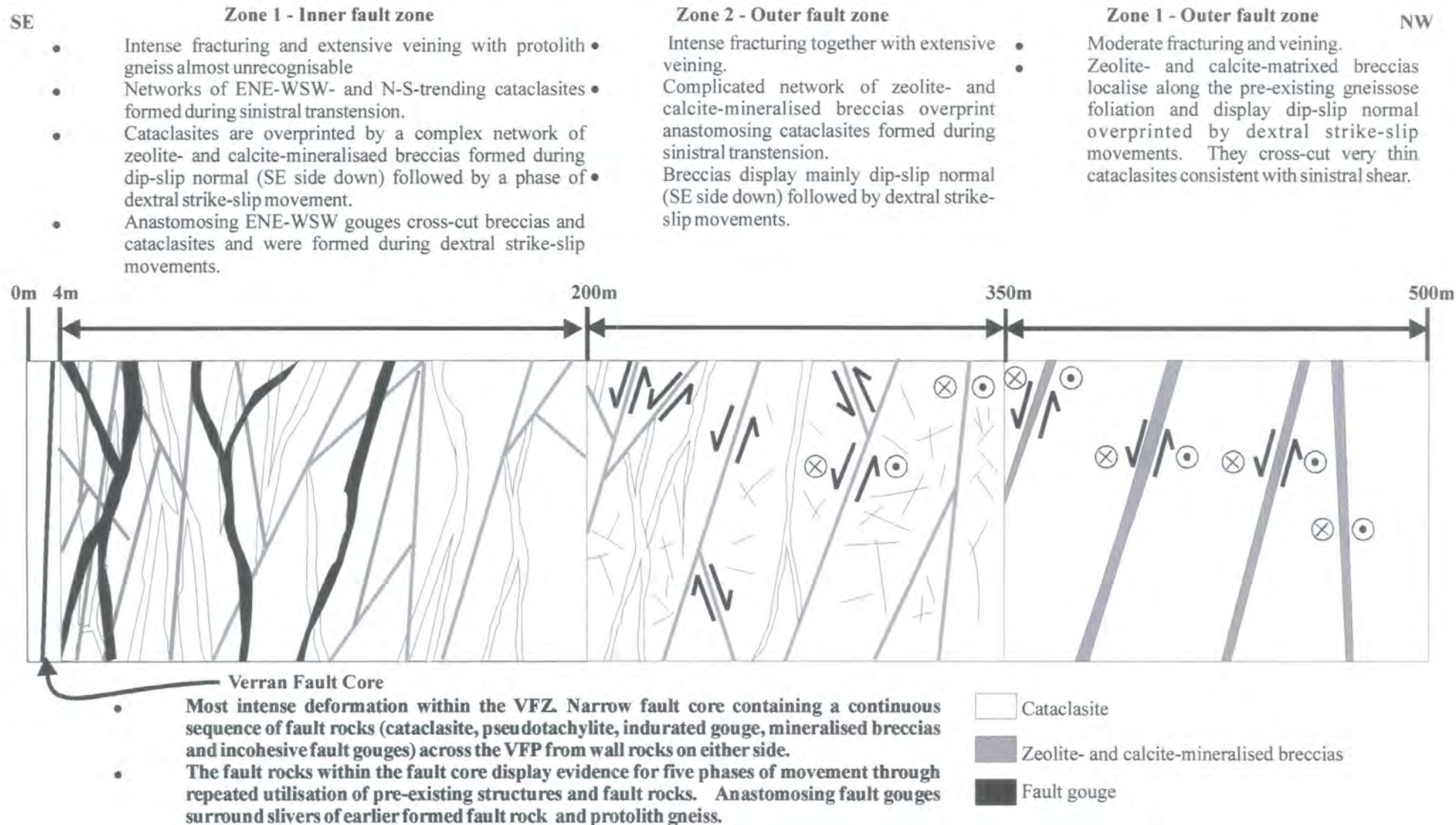


Figure 6.56 Schematic diagram to show the main component parts of the VFZ, based upon field descriptions and localities.

Chapter 7. Fault rock textures and microstructures: MTFC

The aim of this chapter is to provide a comprehensive description of fault rock microstructures and textures. In addition, $^{40}\text{Ar}/^{39}\text{Ar}$ laserprobe dating of pseudotachylite and host-rock mylonite samples will be discussed in order to constrain the timing of 'early' fault rocks formed along the MTFC. Fault rock dating and overprinting relationships (discussed in Chapter 6) combined with microstructural studies will be used to formulate a microstructural and textural evolution exhibited by the fault rocks (summarised in Chapter 8). This will provide an understanding of the processes and factors that control deformation, localisation and reactivation along the MTFC throughout geological time, that will be discussed in Chapter 8.

7:1 Hitra-Snåsa Fault Zone: textures and microstructures

The HSFZ comprises a 1km-wide ductile shear zone containing mylonites formed during sinistral shear, that are overprinted by later suites of coeval cataclasites and pseudotachylites formed during sinistral transtension. In the following section, textures and microstructures of protolith and fault rocks formed within the HSFZ will be described in order of age (oldest to youngest), based upon the field relationships described in Chapter 6.

7:1:1 Protolith

Quartzo-feldspathic banded gneisses of the Banded Gneiss Complex of Fosen are the protolith to fault rocks formed within the HSFZ. The gneisses typically comprise interlocking aggregates of equigranular feldspar (0.5mm to 1mm in size) interlayered with flattened polygonal aggregates of quartz (0.5mm to 1mm in size), which surround isolated pockets of biotite laths, epidote and rarely sphene and muscovite grains (Plate 7.1A&B). Feldspar (plagioclase, An_{55} and K-feldspar) and quartz constitute approximately 70% to 80% of the rock, with a feldspar to quartz ratio of 3:2.

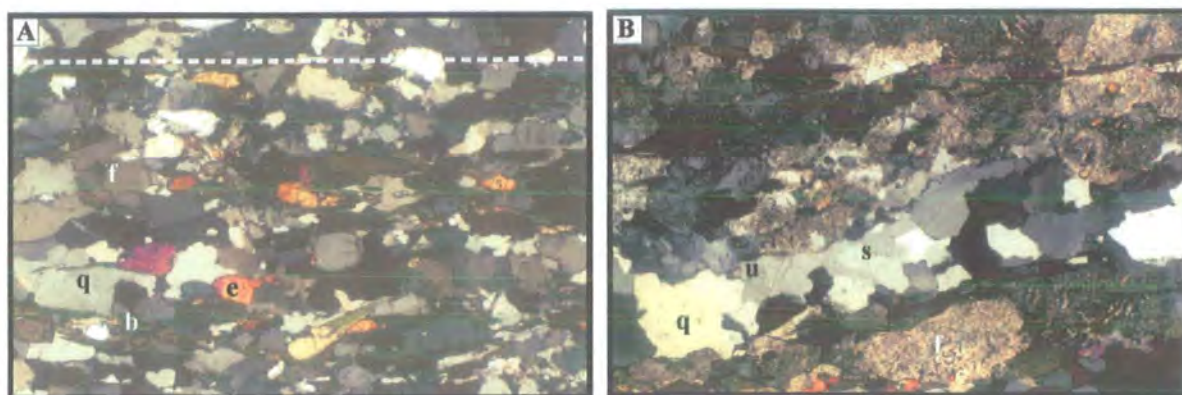


Plate 7.1 (A) Quartzo-feldspathic banded gneiss comprising interlocking aggregates of equigranular-feldspar grains (f) interlayered with polygonal aggregates of quartz (q). Epidote grains (e) and biotite laths (b) are scattered through the rock. The long axes of biotite laths together with flattened feldspar and quartz grains define a foliation (dashed line). (B) Feldspar-rich banded gneiss. Note the speckled appearance of feldspar grains (f), due to their breakdown to aggregates of sericite. Quartz grains (q) display undulose extinction (u) and poorly developed subgrains (s). Field of view 3.6 x 2.4mm, crossed polars.

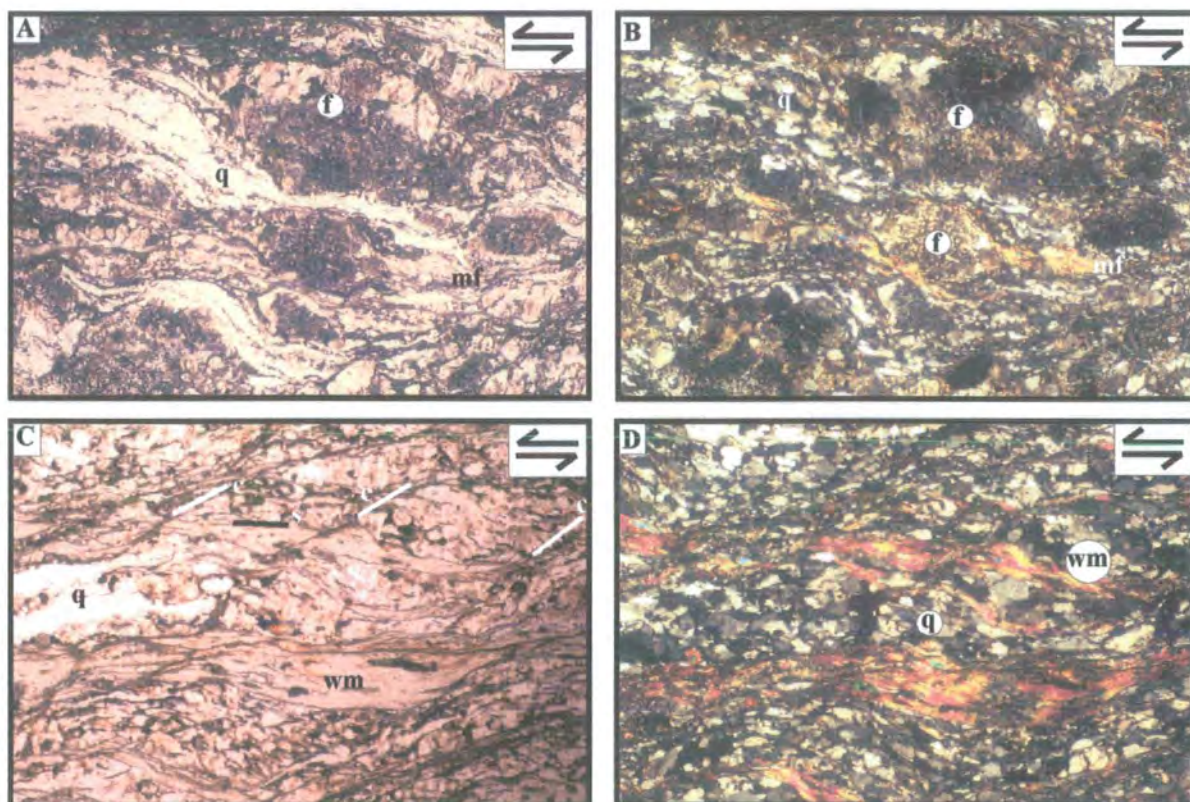


Plate 7.2 Split arrows indicate shear sense parallel to lineation. (A) & (B) 'Low'-strain mylonites from the HSFZ, Mefjellet. Quartzo-feldspathic mylonite comprising relatively undeformed but altered asymmetric feldspar (f) porphyroclasts (σ -type), which are surrounded by networks of polygonal quartz ribbons (q) and interlayered with fine-grained white mica and feldspar (mf). Field of view 3.6 x 2.4mm. (A) plane-polarised light, (B) crossed polars. (C) & (D) 'High'-strain mica-rich mylonite comprising polygonal quartz ribbons (q) interlayered with aggregates of fibrous white mica (wm), which wrap feldspar porphyroclasts. S-C' fabrics (s, c) are well developed and are consistent with sinistral shear. (C) plane-polarised light, (D) crossed polars. Field of view 3.6 x 2.4mm.

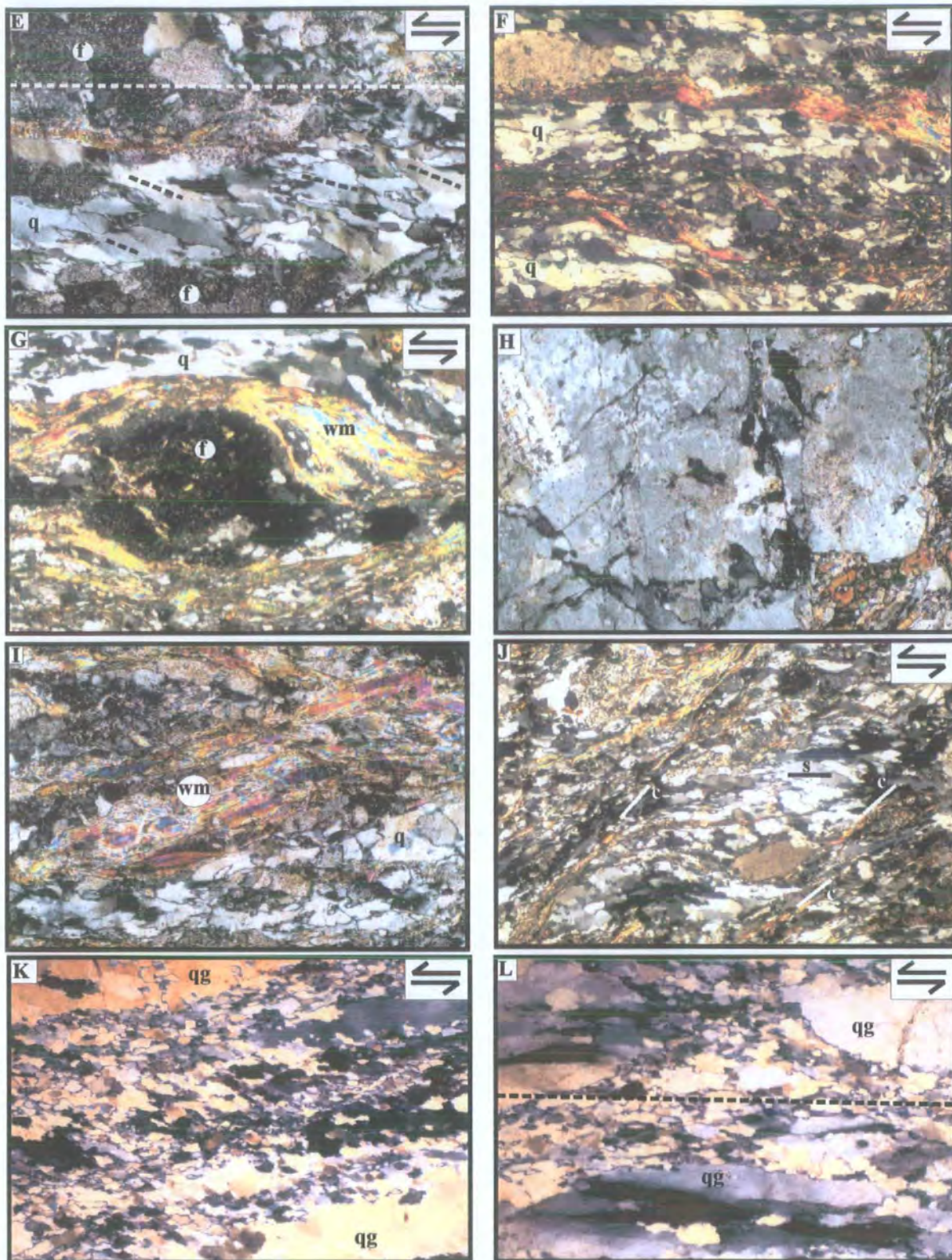


Plate 7.2 continued. (E) Partially sericitised feldspar grains (f) surrounded by a mantle of dynamically recrystallised quartz grains (q). Long axes of quartz grains (black dashed lines) are 15° clockwise of the macroscopic foliation trend (white dashed line), which is consistent with sinistral shear. Field of view 1.44×0.96 mm, crossed polars. (F) Ribbons of equigranular-polygonal aggregates of quartz grains (q) with a weak preferred orientation as a result of GBAR processes due to post-tectonic static recrystallisation. Field of view 3.6×2.4 mm, crossed polars. (G) σ -type feldspar porphyroblast (f) mantled by white mica (wm), quartz (q) and fine-grained feldspar. Field of view 3.6×2.4 mm, crossed polars. (H) Close-up of feldspar porphyroblast cut by intergranular fractures. Field of view 1.44×0.96 mm, crossed polars. (I) Close-up of white mica with well-developed subgrains (wm) interlayered with dynamically recrystallised quartz grains. Field of view 1.44×0.96 mm, crossed polars. (J) Mylonite with millimetre-scale S-C' fabric (s= s-splanes, c=s-planes). C-planes contain dynamically recrystallised white mica and quartz grains. Field of view 3.6×2.4 mm, crossed polars. (K) & (L) Mylonitised quartz veins. Large quartz grains (qq) surrounded by anastomosing networks of dynamically recrystallised quartz grains. Long axes of flattened quartz grains are parallel to the macroscopic foliation (dashed black line). Field of view 3.6×2.4 mm, crossed polars.

The feldspar grains display strong patchy undulose extinction and are partially altered to aggregates of fine-grained sericite and epidote. Alteration is limited and does not appear to increase with decreasing distance towards the HSFZ. Quartz grains also display strong patchy undulose extinction with poorly defined optical subgrains. Rare garnet porphyroblasts (0.5 to 1mm) are present within the gneiss and are partially retrogressed to aggregates of fibrous chlorite.

7:1:2 Mylonite

Mylonitic series rocks are common within the HSFZ. The best-developed mylonites are exposed on Mefjellet (section 6:3:1), along the northern shoreline of Follavatnet and along the Brattreitelva stream section (section 6:3:3).

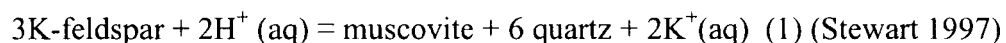
7:1:2:1 Mefjellet mylonites

Viscous deformation fabrics are present 500m to the northwest and southeast of the HSFP and overprint banded gneiss (section 7:1:1). Domains of mylonite comprise 'rigid' feldspar porphyroclasts, which are wrapped by a network of polycrystalline quartz ribbons and bands of fine-grained muscovite, chlorite and albitic feldspar (Plate 7.2A&B). When viewed under a sensitive tint plate, aggregates of quartz, muscovite and feldspar display strong preferred orientations. Towards the centre of the HSFZ, with increasing strain, the mylonites are finer grained and contain higher proportions of chlorite and white mica (Plate 7.2C&D) compared to coarser, lower-strain mylonites (Plate 7.2A&B). Biotite is progressively replaced with fibrous chlorite within higher-strain mylonites. At lower strains, mylonites consist of 55% feldspar, 25% quartz and 20% white mica and biotite (Plate 7.2A&B), whilst finer-grained, high-strain mylonites comprise 40% quartz, 35% white mica, 20% feldspar and 5% chlorite (Plate 7.2C&D).

Quartz ribbons display a variety of microstructures. Flattened quartz grains (~10µm in size) with aspect ratios between 2:1 to 5:1 are dominantly equigranular and display interlobate grain boundaries (Plate 7.2E). The long axes of the lobate grains are

orientated up to 40° in a clockwise direction to the trace of the macroscopic foliation, which is consistent with sinistral shear. Larger quartz grains (0.5mm to 0.1mm in size) display a strong irregular undulose extinction, deformation lamellae and well-developed subgrains. Subgrain boundaries commonly pass laterally into grain boundaries. The grain sizes of the subgrains are similar to the lobate quartz grains, indicating subgrain rotation as a mechanism of recrystallisation. Locally, the quartz ribbons comprise equigranular-polygonal aggregates, whereby individual grains (0.5mm to 0.3mm in size) display straight to faint undulose extinction and weak crystallographic preferred orientations (Plate 7.2F). These grains are thought to have formed as a result of grain-boundary area reduction (GBAR) processes consistent with post-tectonic static recrystallisation.

The relatively undeformed feldspar porphyroclasts (albite and K-feldspar) are commonly surrounded by mantles of polygonal aggregates of quartz and white mica (Plate 7.2G). Locally, fine-grained albite grains mantle the feldspar clasts, forming 'core' and 'mantle' structures, which is indicative of dynamic recrystallisation. The clasts display well-developed σ - and δ -type geometries consistent with sinistral shear. Feldspar porphyroclasts display sweeping undulose extinction and locally subgrains. Intergranular fractures and healed microcracks are a common feature within both the relict K-feldspar and albite clasts (Plate 7.2H). The clasts usually have a speckled appearance and irregular boundaries due to the breakdown to fibrous aggregates of white mica. At 'high' strains towards the central part of the HSFZ, feldspar is almost completely absent where it has apparently given way to growth of 'new' aligned grains of white mica together with relatively strain-free neoblasts of quartz, through the hydration reaction (1) below (reaction softening) (Plate 7.1D).



White mica forms multitudinous subgrains (Plate 7.2I), fine neoblasts and newly-aligned grains formed parallel to the macroscopic foliation. The newly-aligned grains form fibrous overgrowths around feldspar clasts and commonly define a well developed S-C' fabric, consistent with sinistral shear (Plate 7.2J). Mylonite textures clearly indicate that the white mica grains formed from the chemical breakdown of feldspar were syn-tectonic and formed during mylonitisation. White mica

overgrowths have been dated using an ^{40}Ar - ^{39}Ar laserprobe technique (described in section 7:2).

Thick (up to 1m) quartz veins are common towards the centre of the fault zone, where the mylonites are rich in muscovite. These are interpreted to have precipitated during the syn-tectonic breakdown of feldspar to muscovite and quartz (equation 1). Large flattened quartz grains (0.5mm to 0.1mm in size) are surrounded by a network of polygonal aggregates of lobate quartz grains ($\sim 10\mu\text{m}$ in size) (Plate 7.2K&L). Larger grains display sweeping undulose extinction, deformation lamellae and subgrains. The lobate quartz grains display aspect ratios of 2:1 to 5:1, sweeping undulose extinction and locally contain fine subgrains. The lobate grains are similar in size to the subgrains within the larger quartz grains, suggesting that the lobate grains formed by subgrain rotation recrystallisation.

7:1:2:1a Metamorphic conditions during mylonitisation

The mylonites comprise an assemblage of quartz, feldspar (K-feldspar and albite porphyroclasts, and fine-grained albitic feldspar), white mica, chlorite and epidote. The relative abundances of hydrous mineral phases (white mica, chlorite and epidote) in comparison with the relatively unmodified granodiorite gneisses, suggests that the hydrous minerals developed during localised retrograde metamorphism during mylonitisation. Textural evidence indicates that chlorite and white mica developed synchronously with sinistral shear. The coexistence of syn-tectonic growths of chlorite, white mica and fine-grained albite probably indicates mid-greenschist facies conditions (Yardley 1994).

7:1:2:1b Operative deformation mechanisms

Quartzo-feldspathic mylonites comprise 'rigid' feldspar porphyroclasts, which are wrapped by a network of polygonal quartz ribbons and bands of fine-grained white mica and feldspar. The porphyroclasts display relatively low aspect ratios and appear to be comparatively undeformed. In contrast, the quartz ribbons and muscovite-rich bands, which form an interconnected network, display comparatively high aspect ratios and appear to be very highly strained. Therefore, the mylonites display

interconnected weak-layer (IWL) microstructures (sections 1:6:4, 1:7:2:3a). These observations suggest that the rheological behaviour of the highly strained mylonitic fault rocks was primarily controlled by the rheological behaviour of the quartz ribbons and muscovite-rich bands (IWL) (Handy 1990).

Feldspars display sweeping undulose extinction, local subgrains and are locally mantled by fine-grained dynamically recrystallised albite. Most feldspars clasts are mantled by polygonal aggregates of quartz and fine-grained muscovite or, in many places, both minerals. They commonly display intergranular fractures and healed microcracks. With increasing strain, the feldspar grains chemically break down to aggregates of muscovite and quartz. Feldspar grains are primarily deformed by frictional sliding, accompanied with some dislocation glide and locally dynamic recrystallisation leading to the formation of 'core' and 'mantle structures'.

Polygonal quartz ribbons and muscovite display evidence for advanced dislocation creep and dynamic recrystallisation (e.g., subgrain rotation recrystallisation, section 1:6:2:2). Quartz displays sweeping undulose extinction, deformation lamellae and subgrains, which pass into aggregates of lobate quartz grains. Locally, strain-free polygonal grains are thought to develop in response to GBAR processes consistent with post-tectonic static recrystallisation. Muscovite forms multitudinous subgrains, fine-grained neoblasts and newly aligned grains formed due to the breakdown of feldspar

Deformation mechanisms within quartz and muscovite imply syn-tectonic temperatures greater than ~250-300°C, while frictional straining of feldspars puts an upper limit to probable temperature estimation, suggesting temperatures below 500°C (the temperature marking the onset of crystal plasticity in feldspar) (see section 1:6:3). Therefore, mylonites along the HSFZ formed at depths of 10-15km, assuming an average geothermal gradient of 30°C/km.

7:1:2:2 Follavatnet and Brattreitelva mylonites

Well-developed mylonites are exposed along the northern shoreline of Follavatnet and along the Brattreitelva stream section (section 6:3:3). The mylonitic rocks are derived from granodiorite and a series of metasedimentary rocks comprising limestone, psammite and polymict conglomerates of uncertain origin. Protoliths to the mylonites are largely unexposed within the study area. In the following sections, just the 'highest' strain mylonites are described. Those derived from granodiorite are microstructurally and texturally very similar to those described previously (Mefjellet mylonites; section 7:1:2:1).

7:1:2:2a Marble mylonite

Marble mylonites comprise porphyroclasts (~1mm in size) of calcite surrounded by polygonal aggregates of lobate calcite grains (<0.01mm in size) (Plate 7.3A). The lobate grains are equigranular and display aspect ratios of 2:1, and are aligned parallel to the macroscopic foliation. The calcite grains display undulose extinction and well-developed subgrain boundaries. Calcite porphyroclasts commonly display type 2, 3 and 4 twins (Passchier and Trouw 1996). In places, the matrix grades into ultrafine-grained polygonal aggregates of equidimensional calcite (~10µm in size). The grains are characterised by curved to straight boundaries and sharp extinction (Plate 7.3B). When viewed under a sensitive tint plate, the grains do not show a lattice-preferred orientation, which may indicate grain boundary sliding or 'superplasticity' (Rutter et al. 1994). Highly irregular surfaces occur parallel to the macroscopic foliation and are interpreted as stylolites formed as a result of pressure solution and removal of calcite.

Scattered quartz grains occur within the matrix. Isolated quartz grains show strong undulose extinction, poorly-developed subgrain boundaries and deformation lamellae (Plate 7.3A). The grains are flattened and display aspect ratios of 5:1, with their long axes parallel to the macroscopic foliation.

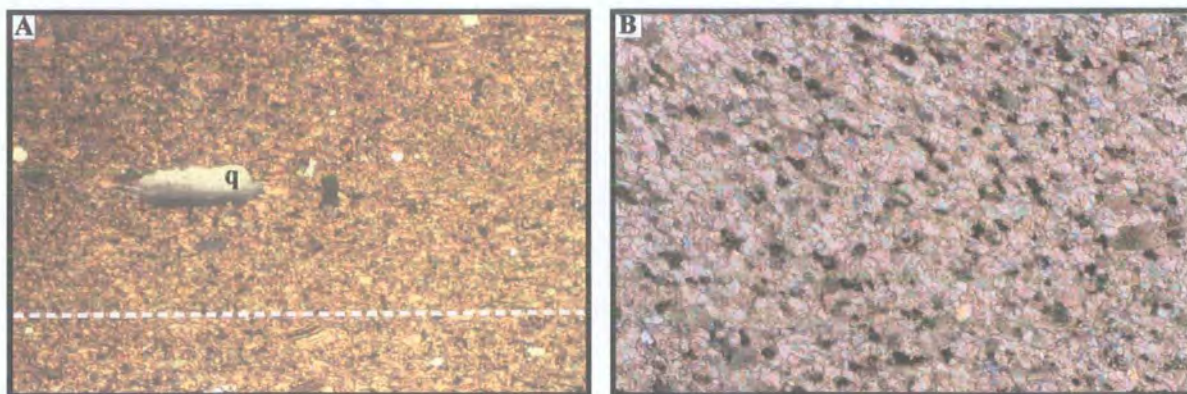


Plate 7.3 (A) Marble mylonite comprising fine-grained equigranular aggregates of lobate calcite grains. Long axes of the calcite grains are parallel to the macroscopic foliation (dashed line). Isolated quartz grains with long axes parallel to the macroscopic foliation display strong, sweeping, unulose extinction. Field of view 3.6x2.4mm, crossed polars. (B) Close-up of ultrafine-grained equidimensional calcite grains with curved to straight boundaries and sharp extinction. Field of view 1.44x0.96mm, crossed polars.

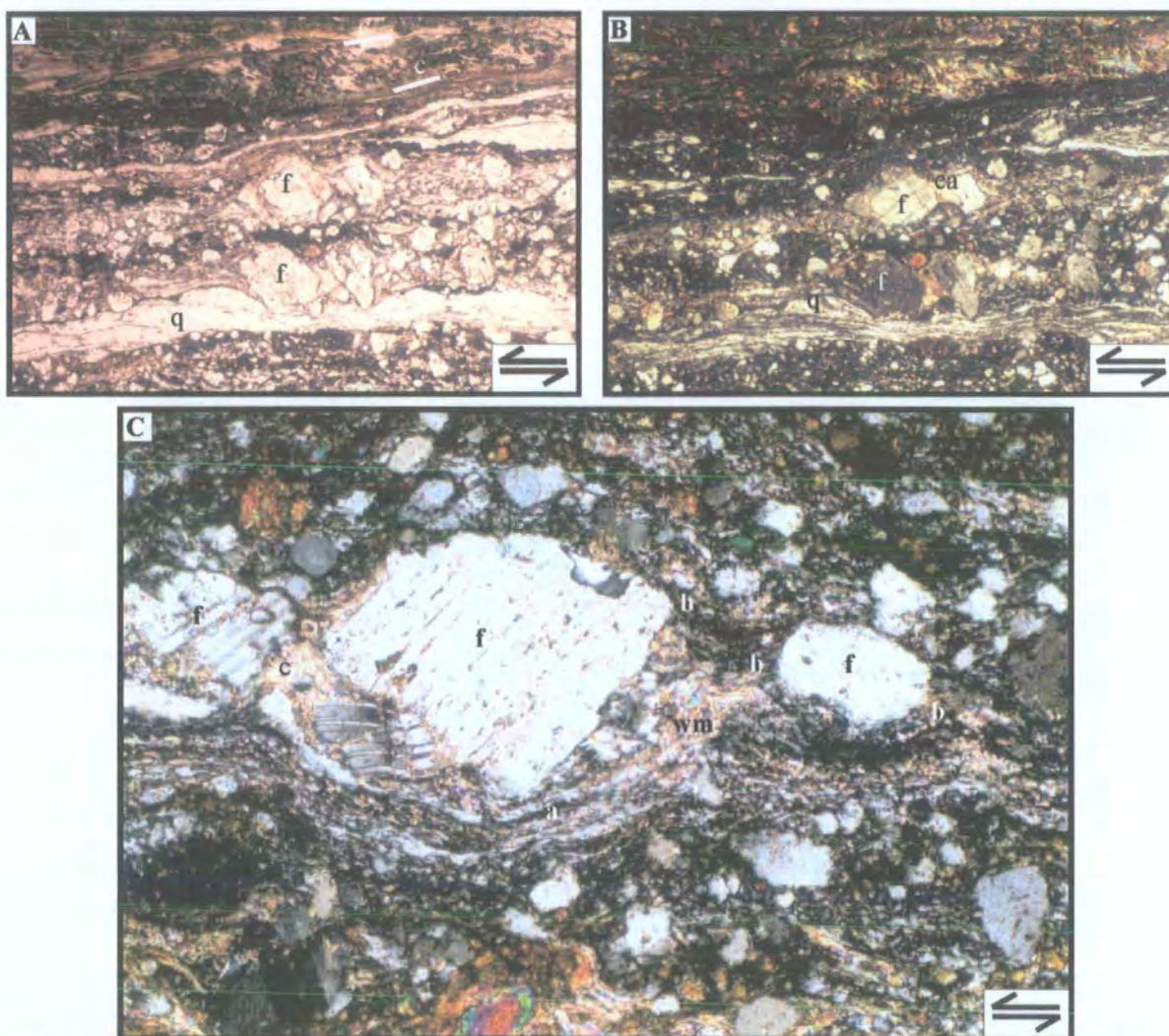


Plate 7.4 Quartz-feldspathic mylonites derived from psammite. (A) & (B) Mylonite comprising 'rigid' feldspar porphyroclasts (f) surrounded by polygonal quartz ribbons (q) interlayered with fine-grained feldspar (albite), white mica, chlorite and epidote. Feldspar clasts are boudinaged parallel to the foliation with calcite (ca) and mica filling the void between the boudinaged fragments. S-C' fabrics (c=c-planes) are present in mica-rich parts. Field of view 3.6x2.4mm. (A) plane-polarised light. (B) crossed polars. (C) Close-up of feldspar porphyroclast mantled by dynamically recrystallised albite (a) and white mica (wm). Feldspar porphyroclasts display 'beards' (b) of fibrous mica and neoblasts of albite. Tensional fractures filled with fibrous calcite (c) cross-cut the feldspar clasts. Field of view 1.44x0.96mm, crossed polars.

Operative deformation mechanisms

Calcite microstructures suggest a variety of deformation mechanisms. The marble mylonite matrix consists entirely of dynamically recrystallised grains, which display undulose extinction and subgrains indicative of dislocation creep. The finer-grained portion of the mylonite comprising ultrafine-grained equidimensional aggregates of randomly aligned calcite grains may have deformed by grain boundary sliding assisted by grain-boundary dissolution and growth. Calcite porphyroclasts also display type 2,3 and 4 twins which, coexisting together, indicate syn-tectonic temperatures of 250-300°C (section 1:6:3; Passchier and Trouw 1996). Isolated quartz grains display evidence for advanced dislocation creep, indicating syn-tectonic temperatures of greater than 250°C (Passchier and Trouw 1996). Therefore, the marble mylonites formed at depths of greater than 8km, assuming an average geothermal gradient of 30°C/km.

7:1:2:2b Mylonites derived from feldspathic psammites

These particular mylonites comprise 'rigid' feldspar (albite and K-feldspar) porphyroclasts (0.5mm to 2mm in size), which are wrapped by quartz ribbons and bands of fine-grained (~10µm) feldspar, white mica and chlorite (Plate 7.4A&B). When viewed under a sensitive tint plate, aggregates of quartz, feldspar and muscovite display strong preferred orientations.

Quartz ribbons are less than 1mm to 2cm in length and display aspect ratios greater than 20:1. They comprise polygonal aggregates of quartz grains (less than 10µm in size) with aspect ratios between 3:1 to 5:1. Quartz grains are inequigranular and display interlobate grain boundaries. Larger grains (0.3mm to 10µm) display a strong sweeping undulose extinction, deformation lamellae and well-developed optical subgrains. Larger grains are surrounded by anastomosing polygonal aggregates of lobate quartz grains (~10µm). The lobate quartz grains are equigranular and are a similar size to the subgrains within the 'larger' quartz grains. Lobate grain boundaries generally pass into well-developed subgrain boundaries within the 'larger' quartz grains. This is indicative of subgrain rotation recrystallisation. The long axes of the lobate grains are mainly parallel to the trace of the macroscopic foliation, but locally

the grains are orientated up to 20° in a clockwise direction to the trace of the macroscopic foliation, which is consistent with sinistral shear.

The clasts display well-developed σ - and δ -type geometries consistent with sinistral shear. Feldspar porphyroclasts display a sweeping undulose extinction and locally optical subgrains. The feldspar porphyroclasts commonly display 'core' and 'mantle' structures, where ultrafine-grained albite grains mantle the feldspar clasts (Plate 7.4C). Fibrous mica and feldspar neoblasts form strain shadows or 'beards' adjacent to the porphyroclasts indicating sinistral shear. Intergranular fractures and healed microcracks are a common feature within feldspar clasts. In places, the fractures develop as antithetic fractures displaying dextral offsets resulting in an asymmetric shape consistent with sinistral shear (e.g., Plate 7.4A). Locally, the clasts are boudinaged parallel to the foliation. Fibrous mica (white mica and chlorite, parallel to the macroscopic foliation) and calcite grains (Plate 7.4C) fill the fractures separating the boudinaged fragments. The feldspars usually have a speckled appearance due to the breakdown to fibrous aggregates of sericite.

White mica and chlorite generally form aggregates of multitudinous subgrains, fine neoblasts and newly aligned grains oriented parallel to the macroscopic foliation. S-C' fabrics are well developed within the mylonites, with the C'-planes defined by fine neoblasts of dynamically recrystallised white mica, chlorite and quartz.

Metamorphic conditions during mylonitisation

The mylonites comprise an assemblage of quartz, feldspar (K-feldspar and albite porphyroclasts, and fine-grained albitic feldspar), white mica, chlorite, epidote and calcite. The relative abundances of hydrous mineral phases (white mica, chlorite and epidote) within more highly-strained mylonites, suggests that the hydrous minerals developed during localised retrograde metamorphism during mylonitisation. Textural evidence indicates that chlorite, white mica and calcite developed synchronous with sinistral shear. The coexistence of syn-tectonic growths of chlorite, white mica, fine-grained albite and calcite probably indicates mid-greenschist facies conditions (Yardley 1994).

Operative deformation mechanisms

Quartzo-feldspathic mylonites comprise 'rigid' feldspar porphyroclasts which are wrapped by a network of quartz ribbons interlayered with bands of fine-grained feldspar and white mica. The porphyroclasts display relatively low aspect ratios and appear to be relatively undeformed. In contrast, the quartz ribbons and feldspar and mica-rich bands, which form an interconnected network, display comparatively high aspect ratios and appear to be very highly strained. These observations suggest that the rheological behaviour of the highly strained mylonitic fault rocks, which display IWL microstructures (section 1:6:4), was primarily controlled by the rheological behaviour of the fine-grained quartz ribbons and feldspar- and mica-rich bands (Handy 1990) that surround the 'rigid' porphyroclasts.

Polygonal quartz ribbons and mica display evidence for advanced dislocation creep and dynamic recrystallisation. Quartz displays sweeping undulose extinction, deformation lamellae and subgrains, which pass into aggregates of lobate quartz grains. Mica commonly forms multitudinous subgrains, fine-grained neoblasts and newly aligned grains deriving from the breakdown of feldspar.

Feldspars display 'core' and 'mantle' structures, where by feldspar porphyroclasts are mantled by fine-grained dynamically recrystallised albite. Sweeping undulose extinction and local subgrains are also present. The feldspar clasts commonly display intergranular fractures and healed microcracks. Feldspars are primarily deformed by frictional sliding, accompanied with some dislocation glide and limited dynamic recrystallisation leading to the formation of 'core' and 'mantle' structures.

Diffusive mass transfer (DMT) processes (section 1:6:2:1) are interpreted to have been operative in the finer-grained portions of the mylonite, where feldspar porphyroclasts may have acted as 'sources', whilst strain shadows of feldspar porphyroclasts acted as 'sinks' leading to the formation of fibrous growths of mica and albite neoblasts. Also, calcite and fibrous mica grains, which fill tensile fractures, are interpreted as DMT 'sinks'.

Deformation mechanisms within quartz and muscovite imply syn-tectonic temperatures greater than ~250-300°C, while frictional straining of feldspars with

localised dynamic recrystallisation and dislocation creep puts an upper limit to probable temperature estimation, suggesting temperatures below 500°C (the temperature marking the onset of crystal plasticity in feldspar) (section 1:6:3). Therefore, mylonitisation occurred at depths of 10-15km along the HSFZ, assuming an average geothermal gradient of 30°C/km.

7:1:3 Cataclasite

Pale-green coloured, cataclastic series rocks exposed within the HSFZ (Mefjellet; section 6:3:1) are derived entirely from quartzo-feldspathic mylonites. Within the central portion of the HSFZ, intensely fractured mylonite grades into brecciated mylonite and cataclasites, which are between 1mm and several metres thick and are usually bounded by discrete fault or fracture surfaces. The cataclasites localise along the pre-existing mylonite foliation on all scales of observation (thin-section to field) and are linked by cross-cutting Riedel-type structures.

The cataclasites comprise finely-comminuted clasts of mylonite, pseudotachylite, cataclasite, feldspar, quartz, chlorite, epidote, muscovite and sphene set within a fine-grained cataclastic matrix (Plate 7.5A&B). The proportion of matrix varies from approximately 10% to 90%, so that the rocks can be subdivided into protocataclasites, cataclasites and ultracataclasites based upon the proportion of matrix. In places, where the cataclastic matrix is finest, it is altered to a clay-rich optically isotropic paste. SEM analyses indicate that the clay minerals are predominantly pyrophyllite and illite. Randomly orientated clasts are angular to sub-angular, ranging from 5mm to less than 5µm in size, displaying a gradation from the coarsest to finest grain-size fractions (Plate 7.5A-D). Cataclasite fragments (less than 1mm in size) occur as clasts, suggesting a multiple generation of cataclasite formation or a prolonged period of cataclasis. The cataclasites possess no internal fabric and appear to be isotropic in thin section. Epidote and quartz veins cross-cut the cataclasites (Plate 7.5F) and occur as clasts within the cataclasite matrix, suggesting that veining is coeval with cataclasis. Veins of intergrown chlorite and white mica fibres also cross-cut the cataclasite (Plate 7.5E).

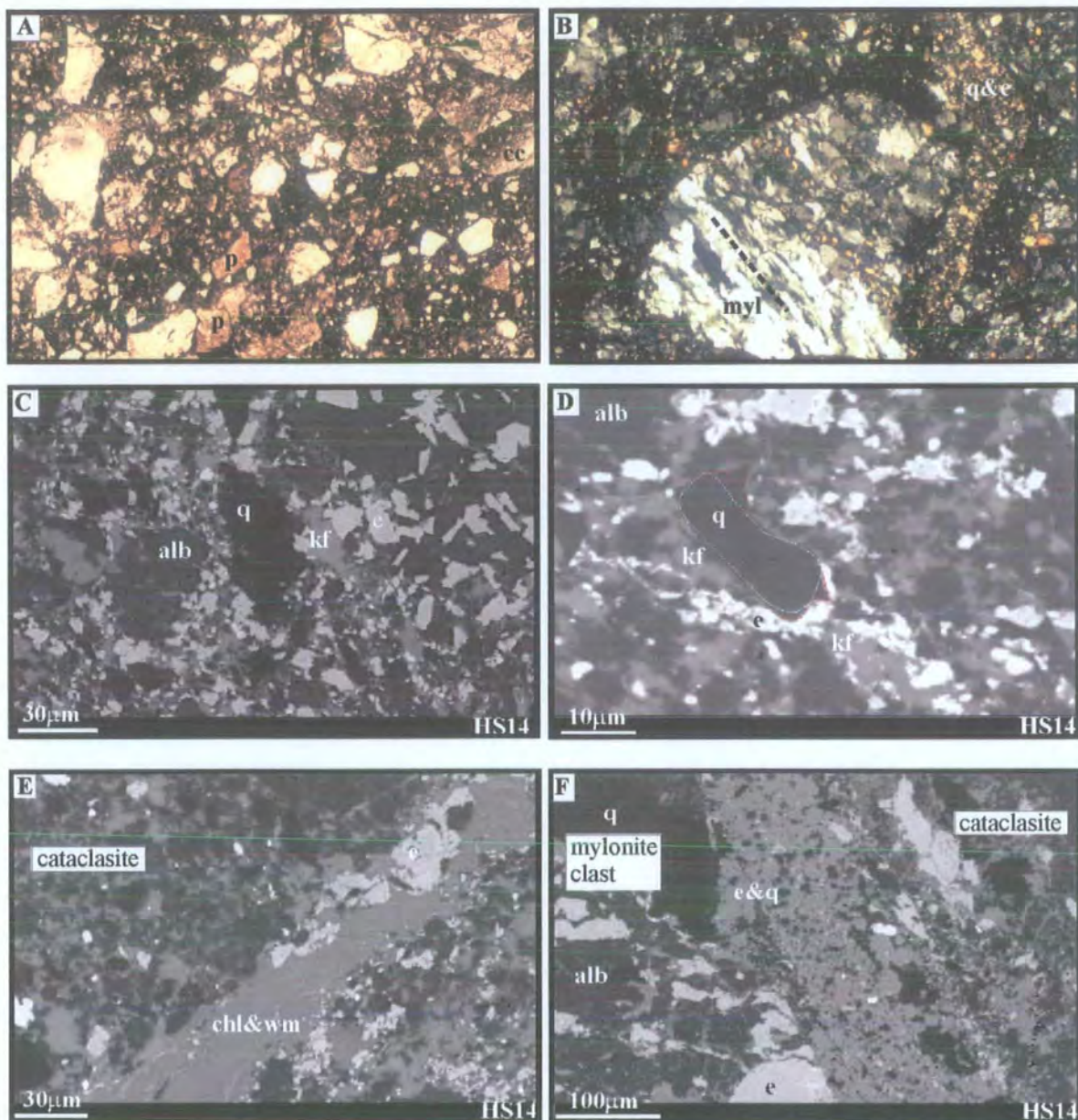


Plate 7.5 (A) Cataclasite comprising finely comminuted clasts of mylonite, pseudotachylite (p), cataclasite (cc), feldspar, quartz, chlorite, epidote and white mica set within a fine-grained cataclastic matrix. Field of view 3.6x2.4mm, plane-polarised light. (B) Cataclasite containing randomly orientated clasts of mylonite (myl, dashed line=foliation) and cross-cut by quartz and epidote vein (q&e). Field of view 3.6x1.4mm, crossed polars. (C) & (D) Backscatter SEM images of cataclasite matrix. Quartz (q) and K-feldspar grains (kf) 1 to 30 μ m in size display interlobate and irregular grain boundaries due to overgrowths as a result of pressure-solution processes which redistribute quartz and K-feldspar into voids and pore spaces (e=epidote, alb=albite) Fine dashed white line= original grain boundary. Fine dashed red line= overgrowth. (E) Backscatter SEM image to show vein filled with intergrown white mica and chlorite (chl&wm) transecting the cataclasite matrix (e=epidote). (F) Backscatter SEM image to show cataclasite cross-cut by epidote and quartz-filled vein (e&q) (e=epidote, q=quartz, alb=albite).

Pseudotachylite occurs both as cross-cutting veins and as clasts within the cataclastic matrix (Plate 7.5A), suggesting that pseudotachylite is broadly coeval with cataclasite development. Feldspar clasts are partially altered and are replaced by fine-grained aggregates of sericite and locally calcite. Both quartz and feldspar grains are cut by intergranular fractures and commonly display healed microcracks. Feldspars display patchy undulose extinction due to the effects of submicroscopic cataclasis.

Detailed studies show the cataclasite matrix to be composed of inequigranular fragments (1 μ m to 30 μ m) displaying interlobate grain boundaries (Plate 7.5C&D). Quartz and K-feldspar fragments display irregular grain boundaries and overgrowths as a result of pressure solution and redistribution of quartz and K-feldspar into voids and pore spaces (Plate 7.5D).

7:1:3:1 Operative deformation mechanisms

The dominant deformation mechanisms are considered to be cataclastic flow (mechanical disaggregation and grain-size diminution) in and between grains, grain boundary sliding and pressure solution. Quartz, feldspar and mica all deform by cataclasis, indicating temperatures of less than 250°C (section 1:6:3). Pressure solution also occurs at grain contacts leading to dissolution and precipitation of K-feldspar and quartz into voids and pore spaces, effectively sealing the rock to fluid infiltration. Pressure solution of quartz occurs at temperatures above 130°C. The presence of pyrophyllite and illite formed from the alteration of K-feldspar accompanied by pressure solution indicates temperatures of approximately 200°C (L. Warr. pers. comm., 2000). Therefore, cataclasites formed at temperatures between approximately 200° and 250°C or at depths of 6-8km assuming an average geothermal gradient of 30°C/km.

7:1:4 Pseudotachylite

Black to dark brown pseudotachylite veins derived from quartzo-feldspathic mylonites are well exposed within the HSFZ (Mefjellet; section 6:3:1). The

pseudotachylite veins are 1mm to 5cm thick and both localise along and locally cross-cut the mylonite foliation. The pseudotachylites commonly occur adjacent to distinct, sharp, straight contacts (Plate 7.6A) which are interpreted as slip surfaces and in places grade into a marginal cataclasite zone (100 μ m to 2mm thick) adjacent to the mylonitic host rock. Injection veins (Plate 7.6A) commonly nucleate from the veins and fracture surfaces into the mylonite host rock. Braided networks of R-type Riedel fractures, which are locally filled with fine-grained chlorite, display sinistral strike-slip offsets and link into the pseudotachylite veins or marginal cataclasite zones.

The pseudotachylites comprise randomly orientated, rounded to sub-rounded clasts (~30%) of feldspar, quartz, cataclasite and mylonite ranging from 20 μ m to 3cm in diameter, which appear to 'float' in an optically isotropic reddish brown to black aphanitic matrix (~70%) (Plate 7.6A). Quartz clasts are more common, larger and more angular than feldspar clasts, which display 'fuzzy' magmatic corrosion textures (Passchier and Trouw 1996). Microlites (10 μ m to 30 μ m in size) are common within the centre of the pseudotachylite veins, usually within the more K-feldspar composition glass (identified under SEM; Plate 7.6B&C). The microlites comprise ultrafine-grained clasts (1 μ m to 5 μ m in size) of quartz and feldspar, which are surrounded by coronas of radially arranged idiomorphic crystals of biotite, mica and feldspar. These are termed spherulites and are formed as a result of growth from a melt during devitrification. Locally, slivers (1mm to 2mm in length) of ultrafine-grained sericite aggregates appear to have formed due to alteration of the K-feldspar composition glass. The matrix is completely free of syn-tectonic mica, epidote and amphibole, and displays a sub-millimetre-scale colour banding, which is defined by compositional and clast to matrix variations (Plate 7.6D-F). In many veins the colour is different along the vein wall and in the interior, a feature which is interpreted to represent selective melting of the wall rock. Embayments of pseudotachylite occur where muscovite, epidote and rarely sphene were in contact with melt material. This is due to preferential corrosion of these minerals.

Flow structures are very common within the pseudotachylite veins. Within thicker pseudotachylite veins (2cm to 5cm thick) similar folds are common (Plate 7.6D) where the colour banding (compositional layering) within the vein thickens towards the hinge direction.

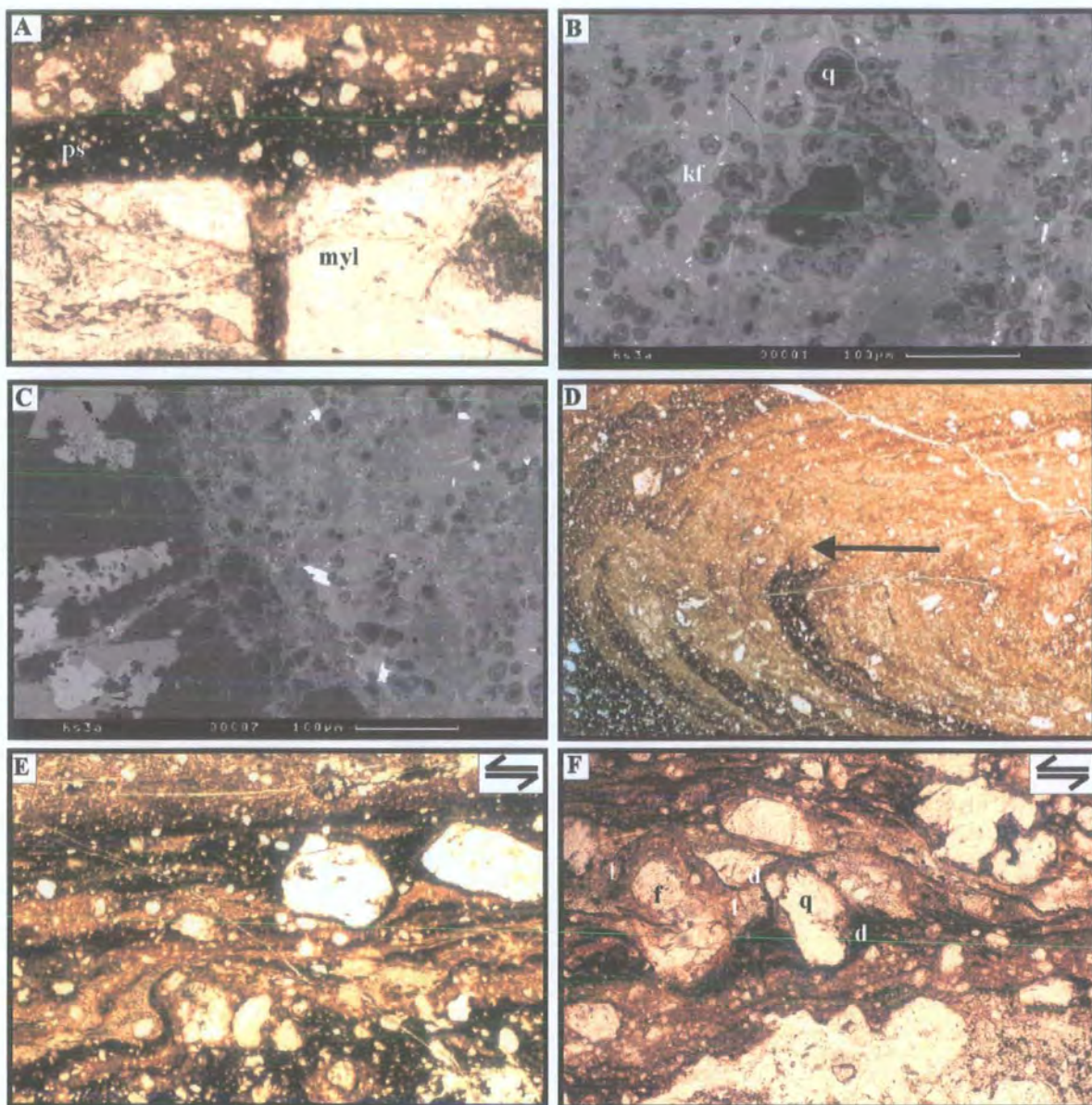


Plate 7.6 (A) Image of pseudotachylite vein (ps) containing sub-rounded to rounded clasts of quartz, feldspar and mylonite. The vein has a straight and sharp contact, and displays an injection structure into mylonite host-rock.(myl). Field of view 3.6x2.4mm, plane-polarised light. (B) Backscatter SEM image of pseudotachylite glass (K-feldspar composition, kf) containing microlites which overgrow ultrafine-grained quartz clasts (q). (C) Backscatter SEM image to show host-rock clast adjacent to pseudotachylite glass containing microlites. (D) Compositional banding in pseudotachylite displays millimetre-scale similar fold. Arrow indicates injection direction. (E) Close-up of pseudotachylite with compositional banding displaying sinistral-verging fold. Field of view 1.44x0.96mm, plane-polarised light. (F) Host-rock clasts display σ -type geometries defined by flow banding. Feldspar clasts (f) are wrapped by light-coloured glass (l), while quartz clasts (q) are wrapped by dark-coloured glass (d). The melt material that defines the σ -type geometries is interpreted to have formed from the melting of the clast it surrounds, and this melt never mixed with adjacent portions of the melt. Field of view 1.44x0.96mm, plane-polarised light.

The colour banding bends towards the centre of the vein and becomes straight and parallel to the contact near the margin. The intervals between the colour banding become larger towards the centre of the vein due to an increased flow velocity in the central parts. The closure direction of the folds probably indicates the injection direction (Plate 7.6D), where the veins are thinner near the limbs and thicker towards the fold hinge zone. Within thinner pseudotachylite veins (1mm to 2cm thick), colour banding (which reflects variations in composition) is transected by sub-millimetre-scale folds, which consistently display a sinistral sense of vergence in thin-sections cut parallel to sub-horizontal, cataclasite slickenside lineations and normal to the vein boundaries (Plate 7.6E). In places, quartz clasts display flow structures similar to σ -type porphyroclasts within mylonites, where colour banding appears wrap around the clasts (Plate 7.6F). Quartz clasts appear to be wrapped by dark-coloured melt, whereas feldspar clasts are enveloped by a lighter-coloured melt. The dark-coloured material is interpreted to have formed from melting of the quartz clast, and this melt appears to have never mixed with other adjacent components of the melt (Plate 7.6F).

7:1:4:1 Localisation mechanism and generation of pseudotachylite

Pseudotachylite veins appear to localise along the pre-existing mylonite foliation. They occur towards the centre of the HSFZ, where the mylonites are highly strained and as a result are finer grained and mica-rich. Foliation-parallel pseudotachylites die out laterally and pass into braided zones of fractures filled with cataclasite. The pseudotachylites formed as a result of high (seismic) strain rates along the HSFZ, which led to rapid frictional sliding (10^{-2} to 1 ms^{-1}) and resulted in localised melting ($>1000^\circ\text{C}$) (Spray 1995) of the wall rocks along the foliation-parallel fault networks. The pseudotachylites are interpreted to have formed within host-rock below $300\text{--}350^\circ\text{C}$ or at depths of less than $11.5\text{--}10\text{km}$ (using an average geothermal gradient of 30°C/km), as no argon loss was observed in the micas within the wall rocks (S.C. Sherlock, pers.comm. 2001; section 7:2).

7:2 $^{40}\text{Ar}/^{39}\text{Ar}$ laserprobe dating of pseudotachylite and host rock samples

Mylonites within the HSFZ, formed during sinistral shear, are overprinted by coeval pseudotachylite and cataclasite that also developed during sinistral shear. Samples were collected of the mylonite host rock and cross-cutting pseudotachylite (Mefjellet; section 6:3:1) to establish whether the overprinting sequence of kinematically similar fault rocks represents (a) fault zone exhumation during a single continuous phase of sinistral shear or (b) a younger phase of fault reactivation.

7:2:1 Sample preparation

Thick sections of the pseudotachylite veins and the host rock mylonite were prepared following the same procedure as for thin-sections, but were polished to a thickness of 300 to 400 μm , uncovered, and using a Canada-Balsam type, rather than epoxy, resin. Once polished, the thick sections are heated on a hot plate, thus melting the resin, and the rock chips are removed from the glass mount. Each rock chip is then cleaned in acetone to remove traces of resin.

Small pieces of each thick section were selected for irradiation. These measured approximately 5 x 5 mm, as dictated by the irradiation container. Pseudotachylite pieces were chosen to avoid the highest density of host-rock clasts within the matrix, and chosen to coincide with the broadest regions of pseudotachylite. From the host rock mylonite a section was chosen with a high density of white mica. Neither sample showed optical evidence for post-formation alteration in the form of chloritised veins or sericitisation of feldspathic minerals or micas.

Each chosen piece of sample was cleaned ultrasonically in alternate methanol and de-ionised water prior to packaging in aluminium foil packets for irradiation. The samples were irradiated at McMaster reactor (Canada) for 50 hours. The GA1550 biotite standard, with an age of 98.79 ± 0.96 Ma (Renne et al. 1998), was used to monitor the fast-neutron flux; the calculated J value is 0.012064 ± 0.0000632 . Analyses were corrected for blanks, ^{37}Ar decay and neutron-induced interference

reactions using the correction factors: $(^{39}\text{Ar}/^{37}\text{Ar})_{\text{Ca}} = 0.00065 \pm 0.0000033$, $(^{36}\text{Ar}/^{37}\text{Ar})_{\text{Ca}} = 0.000264 \pm 0.0000013$ and $(^{40}\text{Ar}/^{39}\text{Ar})_{\text{K}} = 0.0085 \pm 0.0$, and the mass discrimination value used was 283. Average blank levels were: $^{40}\text{Ar} = 0.008408 \pm 0.00086$, $^{39}\text{Ar} = 0.00143 \pm 0.00017$, $^{38}\text{Ar} = 0.0001 \pm 0.000049$, $^{37}\text{Ar} = 0.000227 \pm 0.000107$, $^{36}\text{Ar} = 0.000497 \pm 0.00013$.

7:2:2 Sample analysis

Laser spots of approximately 50µm in diameter were positioned in the pseudotachylite matrix, avoiding host-rock clasts. For the host rock, 50µm laser spots were positioned within white mica grains, where possible avoiding contamination by simultaneously analysing adjacent parts of other minerals within the section. Eight analyses of the host rock white micas and eleven of the pseudotachylite material were carried out. After every two sample analyses the blank levels were measured.

The samples were analysed at The Open University (U.K.) using a focused CW Nd-Yag infrared laser with an external shutter; the extracted argon isotopes ^{35}Ar to ^{41}Ar were measured in a MAP 215-50 noble gas mass spectrometer after cleaning for 5 minutes by two SAES AP10 getters operating at 400°C and room temperature to remove unwanted gas species. All calculated ages are reported with 2σ errors and intra-laboratory uncertainties (1.5 to 2%) have been calculated by statistical propagation of uncertainties associated with each isotopic ratio, correction factors and J value.

7:2:3 Results

Host rock: White mica within the mylonite host rock crystallised during mylonitisation (see section 7:1:2:1), and formed along C-planes, and as overgrowths around K-feldspar and albite porphyroclasts. The host rock ages, which are all analyses of white mica, range from 392 ± 3 to 431 ± 8 Ma and have an unweighted mean age of 409 ± 12 Ma (Table 7.1).

	$^{36}\text{Ar}/^{39}\text{Ar}$	\pm	$^{37}\text{Ar}/^{39}\text{Ar}$	\pm	$^{38}\text{Ar}/^{39}\text{Ar}$	\pm	$^{40}\text{Ar}/^{39}\text{Ar}$	\pm	$^{40}\text{Ar}^*/^{39}\text{Ar}$	\pm	Age (Ma)	\pm (2 σ)
Host rock	nd	nd	0.00177	0.00112	0.01089	0.00093	19.72972	0.04597	19.83903	0.39711	411	8
Host rock	0.00037	0.00146	0.00280	0.00128	0.01432	0.00106	19.28526	0.07246	19.17510	0.43799	399	8
Host rock	0.00107	0.00136	0.08629	0.00132	0.01418	0.00097	21.23678	0.07154	20.92080	0.40876	431	8
Host rock	0.00144	0.00249	0.06585	0.00238	0.01435	0.00177	20.10625	0.07967	19.68068	0.74052	408	14
Host rock	0.00244	0.00059	0.08299	0.00054	0.01318	0.00042	20.25495	0.03146	19.53364	0.17763	405	4
Host rock	0.00090	0.00099	0.01731	0.00085	0.01132	0.00071	19.73277	0.04166	19.46729	0.29616	404	6
Host rock	0.00118	0.00043	0.00661	0.00037	0.01258	0.00031	19.16408	0.02022	18.81464	0.12876	392	3
Host rock	0.00650	0.00123	0.79357	0.00224	0.01360	0.00087	22.37708	0.04743	20.45730	0.36569	423	7
									Mean		409	12
Pseudotachylite	0.00113	0.00108	0.21411	0.00131	0.01185	0.00042	14.24482	0.03360	13.91064	0.32201	298	7
Pseudotachylite	0.00481	0.00038	0.18445	0.00050	0.01280	0.00014	13.84417	0.01127	12.42261	0.11175	268	3
Pseudotachylite	0.00093	0.00015	0.24228	0.00033	0.01238	0.00008	13.56699	0.00809	13.29157	0.04532	286	2
Pseudotachylite	0.00166	0.00040	0.21245	0.00050	0.01246	0.00017	13.09578	0.01107	12.60662	0.12008	272	3
Pseudotachylite	0.00264	0.00092	0.18089	0.00127	0.01317	0.00036	14.47208	0.02089	13.69289	0.27153	293	6
Pseudotachylite	0.00081	0.00088	0.20133	0.00890	0.01348	0.00089	14.83380	0.62861	14.59439	0.67083	311	13
Pseudotachylite	0.00421	0.00023	0.39295	0.00074	0.01294	0.00018	14.27365	0.01248	13.03067	0.06877	280	2
Pseudotachylite	0.00102	0.00024	0.22686	0.00073	0.01235	0.00018	13.43516	0.01299	13.13474	0.07208	282	2
Pseudotachylite	0.00190	0.00110	0.17772	0.00321	0.01252	0.00085	14.13549	0.02726	13.57529	0.32696	291	7
Pseudotachylite	0.00106	0.00051	0.18010	0.00155	0.01238	0.00042	14.74310	0.01673	14.42869	0.15055	308	3
Pseudotachylite	0.00082	0.00017	0.23369	0.00023	0.01172	0.00009	14.67884	0.00750	14.43605	0.05126	308	2
									Mean		291	14

Table 7.1 Argon isotope and age data for the host-rock mica and pseudotachylite samples.

The inverse isochron correlation diagram is usually used to determine an intercept age where the data are scattered, and to determine the presence of excess ^{40}Ar (e.g., Heizler and Harrison 1988). In samples where no excess argon is present, the data form a trend and a line of best fit will intercept the Y axis at 0.0034, the inverse of the atmospheric $^{40}\text{Ar}/^{36}\text{Ar}$ ratio in nature (295.5, Steiger and Jäger 1977). Where excess ^{40}Ar is present, the data may form a trend which intercepts the Y axis at a much lower value. In the case of these data, there is insufficient atmospheric-derived ^{36}Ar to enable a correlation to be made (Figure 7.1), and is it therefore unsuitable for either determining an intercept age or the presence of excess ^{40}Ar .

The analysis of ^{37}Ar and ^{38}Ar may yield useful information about the chemistry of the samples, and any contaminating components that may affect the age. ^{38}Ar is a reactor-induced product of Cl, and may tell us whether or not the sample has been affected by chlorine-rich brines during alteration subsequent to host rock or pseudotachylite formation (e.g., Sherlock and Hetzel 2001). ^{37}Ar is a reactor-induced product of Ca, and may be used to determine the effect of calcic minerals such as plagioclase in each analysis, specifically whether host-rock plagioclase clasts or plagioclase microlites are present within the pseudotachylite melt (e.g., Sherlock and Hetzel 2001). In the host rock sample, the two highest ages (431 ± 8 Ma and 423 ± 7 Ma) also have the highest $^{37}\text{Ar}/^{39}\text{Ar}$ ratio (Table 7.1) and suggest that there is contamination from a calcic phase adjacent to the white mica which was analysed. The $^{38}\text{Ar}/^{39}\text{Ar}$ ratios do not vary with age (Table 7.1) and suggests that there has not been significant alteration by Cl-rich brines prior to host rock crystallisation.

Pseudotachylite: The pseudotachylite ages range from 268 ± 3 Ma to 311 ± 13 Ma, with an unweighted mean age of 291 ± 14 Ma (Table 7.1). The inverse isochron correlation diagram is also inappropriate for these samples since there is insufficient atmospheric argon in the samples to produce a correlation (Figure 7.1). The scatter in ages within the samples may be attributed to chemical heterogeneity. The $^{37}\text{Ar}/^{39}\text{Ar}$ ratios are significantly higher than those from the host rock white micas (Table 7.1) and is most likely due to the abundance of host rock pieces and clasts within the matrix (Figure 7.2). The $^{37}\text{Ar}/^{39}\text{Ar}$ ratios do not vary significantly and do not correlate with any age variation. This suggests that each analysis comprises a calcic component, which is beyond the resolution of the laser, similar to plagioclase microlites observed by Sherlock and Hetzel (2001).

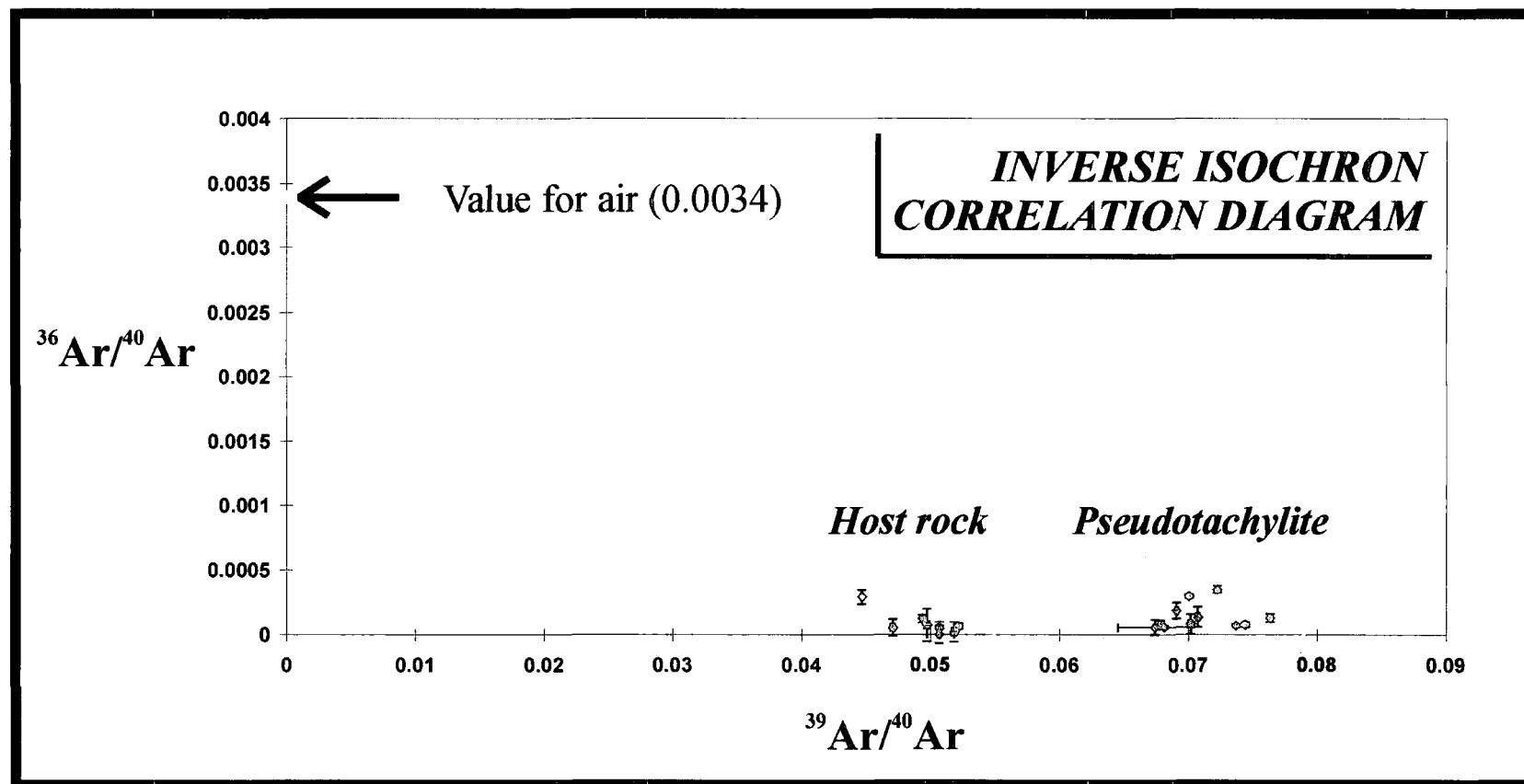


Figure 7.1 Inverse isochron correlation diagram for both host-rock micas and pseudotachylite laserprobe analyses. Neither of the two samples defines any trend due to the very low levels of atmospheric argon in the samples.

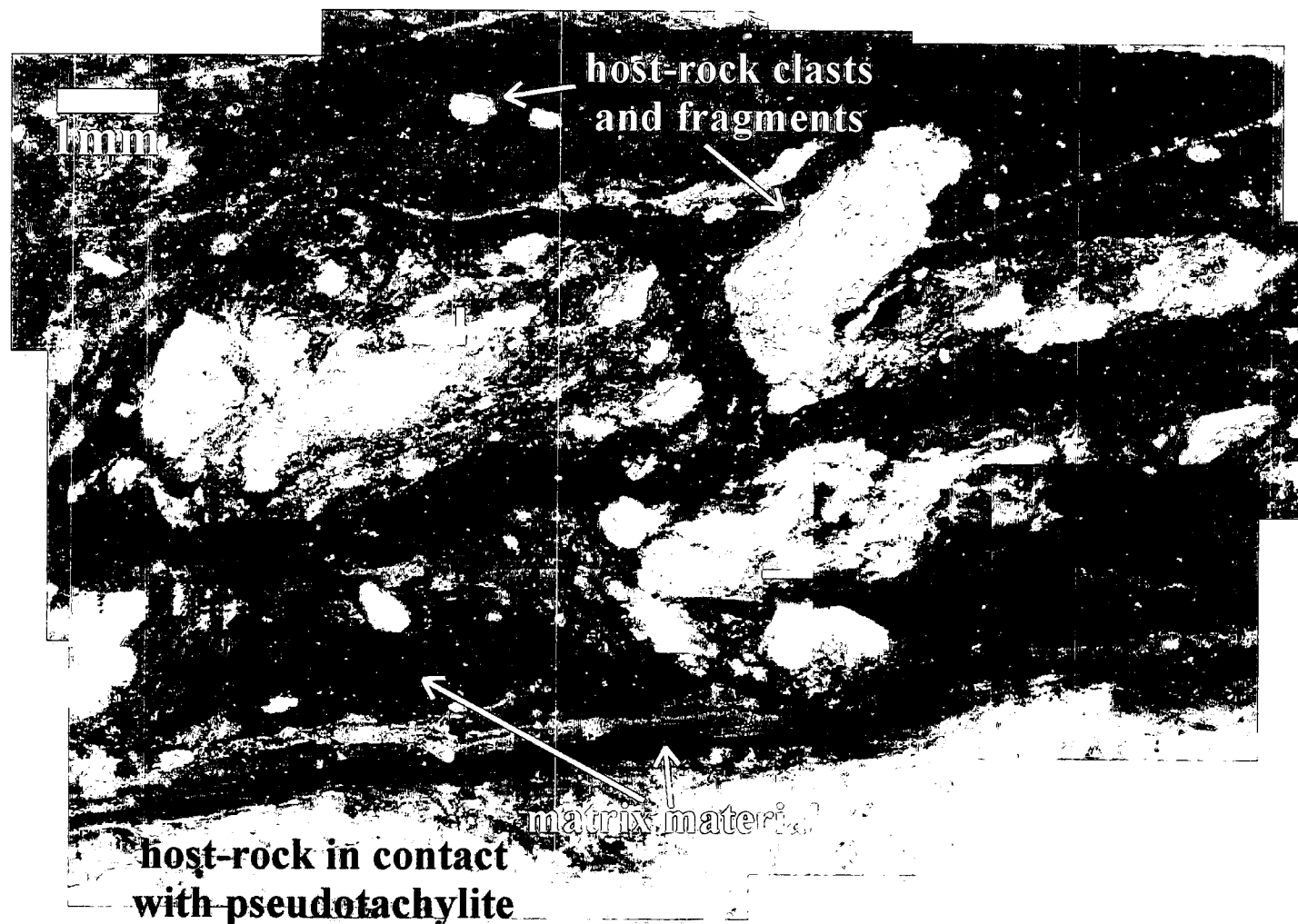


Figure 7.2 Photograph of the thick section of the pseudotachylite vein prior to removing it from the glass mount.

There is also no significant variation in $^{38}\text{Ar}/^{39}\text{Ar}$ ratio within the pseudotachylite analyses, and this does not appear to be a contributing factor to the scatter of ages within the sample.

Presenting all the ages as a cumulative probability curve allows a graphical comparison of all the ages (Figure 7.3). The host rock micas and pseudotachylite ages form two groups, around 400 Ma and 300 Ma respectively. The dominant peak within the host rock mica ages, at 410 Ma, corresponds closely to the mean age of 409 Ma for the sample. The two oldest ages, 431 Ma and 423 Ma, correspond to the highest $^{37}\text{Ar}/^{39}\text{Ar}$ ratios, and those ages younger than the mean age and the dominant age peak on Figure 7.3 may result from post-crystallisation argon loss. Since there is no isotopic evidence for the presence of chlorine-rich brines, and therefore alteration-induced argon loss, it is most likely to result from later low-temperature deformation. The pseudotachylite formed approximately 100 Ma after shear-zone cooling. Figure 7.3 is ambiguous in that the dominant age peak for pseudotachylite is at approximately 310 Ma, though comprises a single analysis.

The bulk of the pseudotachylite ages on Figure 7.3 ($n=6$), are in the range 280 to 295 Ma, coinciding with the mean age of 291 Ma. It is most likely that this corresponds to the crystallisation age of the pseudotachylite. The generally wide range of ages recorded by the pseudotachylite (spanning 39 Ma) may reflect the sample heterogeneity (Figure 7.2), though the small number of ages younger than the most likely crystallisation age of 291 Ma could be post-crystallisation argon-loss, which is not too unlikely given that the same is observed in the host rock white mica ages.

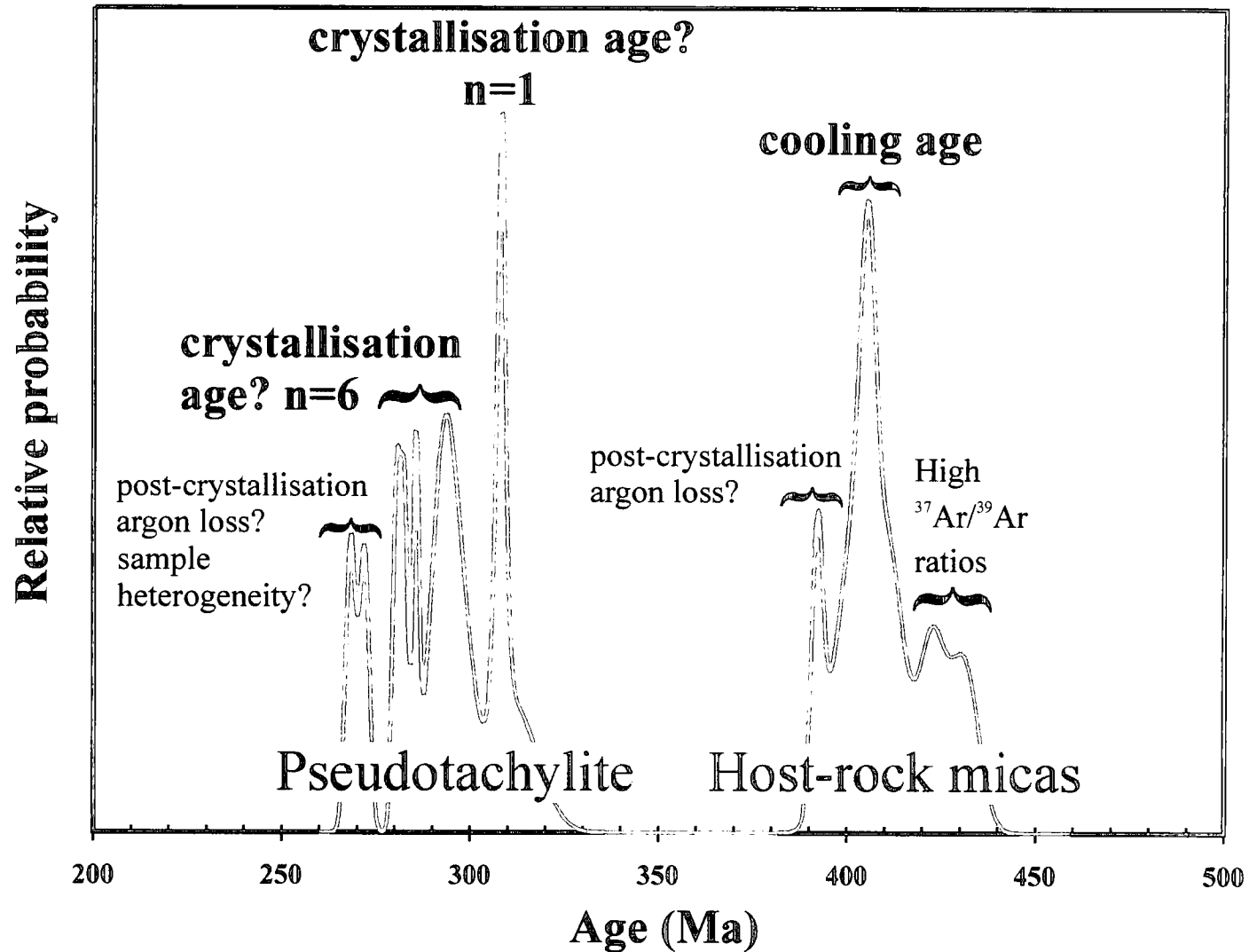


Figure 7.3 Relative probability plot of all data, from both the pseudotachylite and the host-rock micas.

7:3 Summary

- Sinistral strike-slip movements were associated with hydrous, upper greenschist-facies deformation and mylonitisation.
- Deformation was accommodated primarily by intracrystalline crystal plastic mechanisms, and was localised into mylonitised granodiorite gneiss.
- Age of white mica growth, $409 \pm 12\text{Ma}$, is interpreted to date mylonitisation
- Uplift / exhumation of the fault zone followed the cessation of viscous creep deformation mechanisms.
- Frictional, brittle reactivation of the HSFZ (sinistral transtension) led to the development of cataclasites and pseudotachylites, which localised in the central part of the fault zone (where the mylonites are finer-grained, mica-rich and display a strong foliation).
- This event is dated at $291 \pm 14\text{Ma}$ based on dates of pseudotachylite.

7:4 Verran Fault Zone: textures and microstructures

The VFZ comprises a 500m-wide zone of intense cataclastic deformation and mineralisation. Rare mylonites formed during sinistral shear along the VFZ are correlated with those along the HSFZ (section 6:5). Cataclasites, indurated fault gouge and minor pseudotachylites were formed during a later phase of sinistral transtension. Zeolite- and calcite-mineralised breccias and gouges formed during a series of later dip-slip normal and dextral strike-slip events.

7:4:1 Protolith

Compositionally banded gneisses of the Banded Gneiss Complex of Fosen are the protolith to most fault rocks formed within the VFZ. The gneisses comprise interlocking aggregates of equigranular feldspar (0.5mm to 1mm in size) interlayered with flattened polygonal aggregates of quartz (0.5mm to 1mm in size), which

surround isolated pockets of biotite laths, epidote and rarely sphene and muscovite grains (Plate 7.7A). Feldspar (plagioclase, An₅₅ and K-feldspar) and quartz constitute approximately 70% to 80% of the rock, with a feldspar to quartz ratio of 3:2. The feldspar grains display strong, patchy, undulose extinction and are partially altered to aggregates of fine-grained sericite and epidote. Within distances of less than 500m to the VF core, feldspar grains display a speckled appearance and are extensively altered to sericite, illite and pyrophyllite. The clays are interpreted to have formed as a result of the infiltration of aqueous fluids through the extensive fracture network adjacent to the VF, inducing alteration of unstable minerals formed at higher temperatures and pressures (Warr et al. 2001). Quartz grains also display strong, patchy, undulose extinction with poorly defined optical subgrains.

Tectonised granite is the protolith to the only mylonites exposed along the VFZ. The granite comprises interlocking aggregates of equigranular feldspar (albite and K-feldspar; 0.5mm to 1mm in size) interlayered with flattened polygonal aggregates of quartz (0.5mm to 1mm in size), which surround K-feldspar phenocrysts (up to 3cm in size) (Plate 7.7B). Biotite laths, which are partially chloritised, are scattered through the rock together with equant magnetite grains (~1mm in size). Feldspar (~55%) and quartz (~30%) constitute approximately 80% or more of the rock with biotite, chlorite and accessories (magnetite) forming the remainder. The feldspar grains display strong, patchy, undulose extinction, are partially altered to aggregates of fine-grained sericite and locally display myrmekite textures. Quartz grains also display strong, patchy, undulose extinction with poorly defined optical subgrains.

7:4:2 Mylonite

Mylonites are exposed at only one locality (6183 6217; section 6:4:2) along the VFZ. Here, the mylonites are derived from tectonised porphyritic granite (sections 7:3:1; 6:4:2:1) and are texturally similar to those exposed along the HSFZ.

The mylonites comprise little deformed feldspar (K-feldspar and albite) porphyroclasts (1mm to 3cm in size), which are wrapped by quartz ribbons and bands of fine-grained (~10µm in size) white mica and feldspar (Plate 7.8A&B).

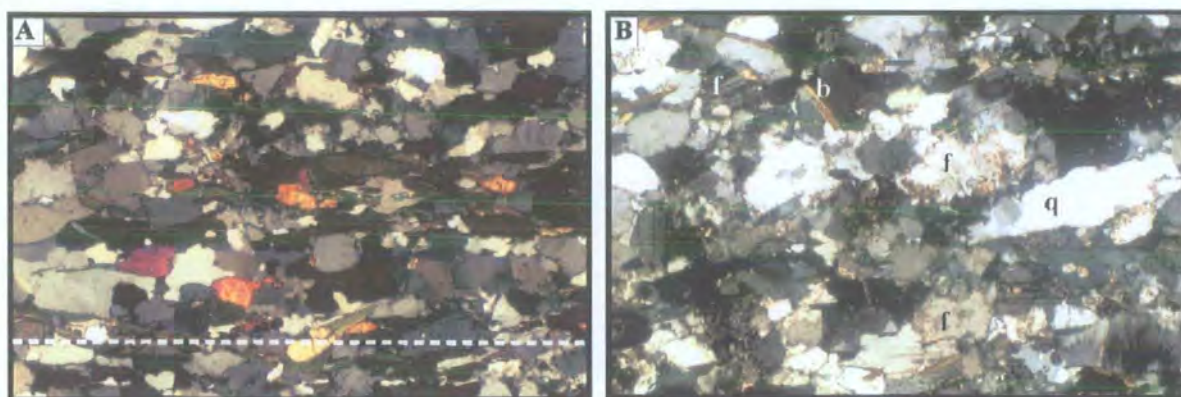


Plate 7.7 (A) Quartzo-feldspathic banded gneiss comprising interlocking aggregates of quartz (q) and feldspar (f). Epidote grains (e) and biotite laths are scattered through the rock. Foliation=dashed line. Field of view 3.6x2.4mm, crossed polars. (B) Tectonised granite comprising interlocking aggregates of feldspar (f) interlayered with polygonal aggregates of quartz (q). Feldspars are partially sericitised. Randomly orientated biotite laths (b) are scattered through the rock.

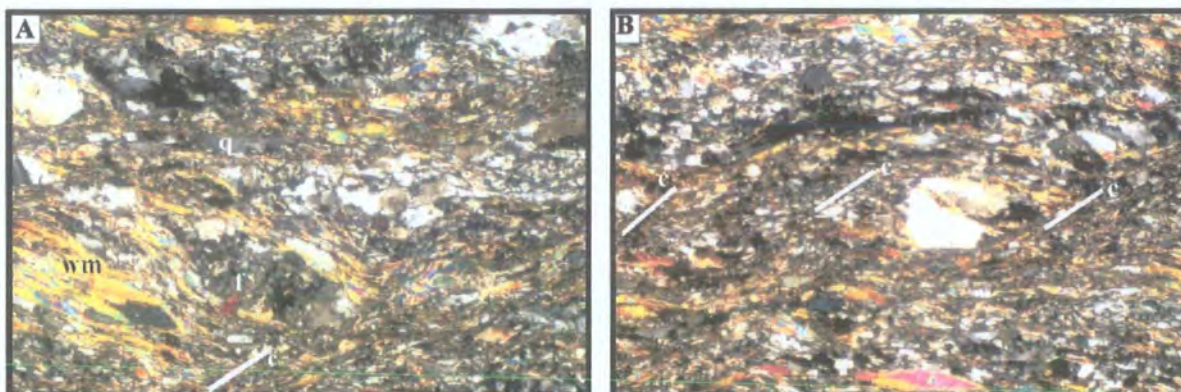


Plate 7.8 (A) & (B) Quartzo-feldspathic mylonites comprising feldspar porphyroclasts which are wrapped by quartz ribbons (q) interlayered with fibrous white mica (wm) and fine-grained feldspar. The mylonite displays a millimetre-scale S-C' fabric (c=c planes) consistent with sinistral shear. Field of view 3.6x2.4mm, crossed polars.

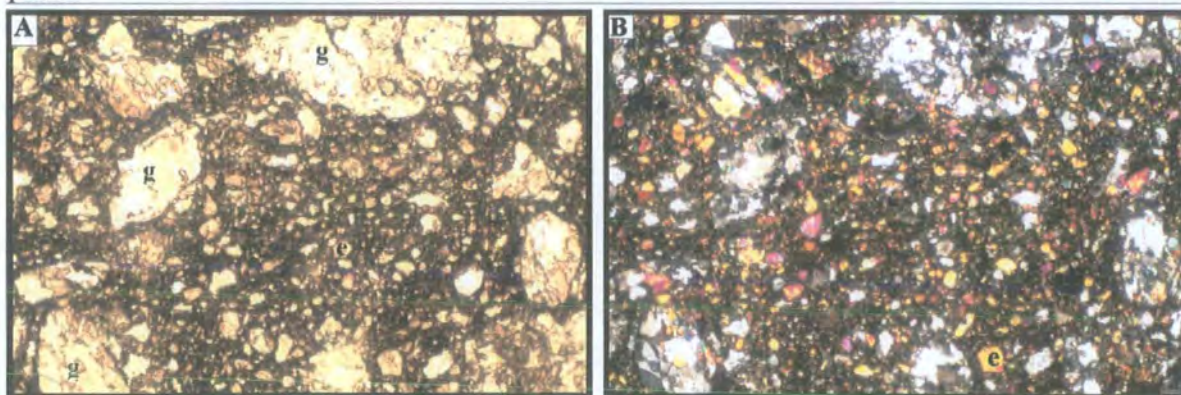
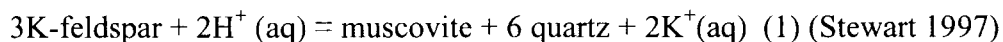


Plate 7.9 (A) & (B) Cataclasite from VF core comprising finely comminuted clasts of gneiss (g), cataclasite, feldspar, quartz, chlorite, epidote (e) and white mica set within a fine-grained epidote-rich cataclastic matrix, which has been partially altered to a clay-rich isotropic paste. Field of view 3.6x2.4mm, (A) plane-polarised light & (B) crossed polars.

Quartz, feldspar and white mica grains display a strong preferred orientation, when viewed under a sensitive tint plate.

Feldspar (K-feldspar and albite) porphyroclasts (1mm to 3cm in size) display a patchy undulose extinction, poorly-developed subgrains and flamed perthite textures. The clasts commonly contain intergranular fractures (filled with calcite and quartz), kinked twin planes and healed microcracks. In places, the feldspars display 'core' and 'mantle' structures, where fine-grained, dynamically recrystallised, albite grains mantle the porphyroclasts. Feldspar porphyroclasts also display irregular boundaries and pass into fine-grained, strain-free neoblasts of white mica (Plate 7.8A), possibly formed from the breakdown of feldspar; equation (1).



Quartz ribbons between 2mm to 2cm in length with aspect ratios of 20:1 comprise polygonal aggregates of lobate quartz grains (0.1mm to 10µm in size) (Plate 7.8A&B). Flattened quartz grains with aspect ratios of 2:1 to 5:1 are dominantly equigranular within individual layers. The long axes of the lobate grains are oriented between 5° and 30° in a clockwise direction to the macroscopic foliation, which is consistent with sinistral shear. Quartz grains display strong undulose extinction, deformation lamellae and subgrains boundaries. The grain size of the subgrains is similar to that of the smallest lobate quartz grains (~10µm).

White micas are thought to have been derived from the chemical break down of feldspar (cf. Mefjellet mylonites, section 7:1:2:1). They form countless grains, fine-grained neoblasts and newly aligned grains, which form syn-tectonic overgrowths around feldspar clasts. Larger, blade-like white micas display undulose extinction and well-developed subgrains. S-C' fabrics consistent with sinistral shear are abundant, with dynamically recrystallised white mica defining the C-planes.

7:4:2:1 Metamorphic conditions during sinistral shear

The mylonites comprise an assemblage of quartz, feldspar (K-feldspar and albite porphyroclasts, and fine-grained albitic feldspar), white mica and epidote. The relative abundances of hydrous mineral phases (white mica and epidote) compared to the relatively unmodified granodiorite gneisses, suggests that the hydrous minerals developed during localised retrograde metamorphism during mylonitisation. Textural evidence indicates that white mica developed synchronously with sinistral shear, due to the breakdown of feldspar. Deformation mechanisms within quartz, mica and feldspar indicate temperatures of around 300 to 500°C or mid to upper greenschist-facies conditions during mylonitisation (Yardley 1994).

7:4:2:2 Operative deformation mechanisms

Little deformed, apparently rigid, feldspar porphyroclasts that display relatively low aspect ratios, are surrounded by a fine-grained matrix comprising polygonal quartz ribbons interlayered with fine-grained white mica and feldspar. In contrast, quartz ribbons and bands of fine-grained feldspar and white mica, which form IWL microstructures (section 1:6:4, 1:7:2:3a), display comparatively high aspect ratios and appear to be very highly strained. This suggests that the rheological behaviour of the highly strained mylonitic fault rocks was primarily controlled by the quartz ribbons and interlayered fine-grained feldspar and white mica bands (Handy 1990).

Feldspars are primarily deformed internally by frictional sliding, accompanied by some dislocation glide and locally dynamic recrystallisation leading to the formation of 'core' and 'mantle' structures.

Polygonal quartz ribbons and white mica display evidence for advanced dislocation creep and dynamic recrystallisation (section 1:6:2:2). As a result, quartz displays sweeping undulose extinction, deformation lamellae and subgrains, which pass into aggregates of lobate quartz grains. White micas display undulose extinction,

subgrains and commonly form multitudinous grains, neoblasts and 'newly' aligned grains.

Frictional sliding within feldspars suggests syn-tectonic temperatures of below 500°C (the temperature that marks the onset of crystal-plasticity in feldspar), while deformation mechanisms within quartz and mica grains infer temperatures greater than ~250-300°C (section 1:6:3). Assuming an average geothermal gradient of 30°C/km, mylonites along the VFZ were probably formed at depths between 10 and 15km.

7:4:3 Cataclasite

Green-coloured cataclastic series rocks exposed within the VFZ are derived entirely from granodiorite gneiss (section 7:3:1). Within the central parts of the VFZ, intensely fractured gneiss grades into brecciated gneiss and anastomosing cataclasites, which are between 1mm and several metres thick and are usually bounded by discrete fault or fracture surfaces. The cataclasites localise along the pre-existing gneissose foliation on all scales of observation (thin-section to field) and are linked by cross-cutting, R-type Riedel shears consistent with sinistral shear.

The cataclasites comprise finely-comminuted fragments of gneiss, cataclasite, feldspar (albite and K-feldspar), quartz, chlorite, epidote and muscovite set within a fine-grained cataclastic matrix (Plate 7.9A&B). In places, where the cataclastic matrix is finest, it is altered to a clay-rich, optically isotropic paste. Randomly orientated clasts are angular to sub-angular, ranging from 5mm to less than 5µm in size, displaying a gradation from the coarsest to finest grain-size fractions. Cataclasite fragments (less than 2mm in size) are present within the matrix, suggesting a multiple generation of cataclasite formation or a prolonged period of cataclasis. The cataclasites generally possess no internal fabric and appear to be isotropic in thin-section. Epidote and quartz veins cross-cut the cataclasites and occur as clasts within the cataclasite matrix, suggesting that veining is coeval with cataclasis. Feldspar clasts are partially altered and are replaced by fine-grained aggregates of sericite. Both quartz and feldspar grains are cut by intergranular

fractures and commonly display healed microcracks. Feldspars and quartz display a patchy undulose extinction, possibly due to submicroscopic cataclasis. These cataclasites are very similar in texture and microstructure to those found along the HSFZ.

The fault core is located in the central part of the VFZ and corresponds to the region of most intense fault-related deformation. It is defined by a continuous sequence of fault rocks that extends from the wall rocks on either side and across the VFP (see section 6:4:8). Within the VF core, the cataclasite matrix is different from those outside the fault core due to the high proportion of epidote grains within the matrix within the VF core (Plates 7.9A&B, 7.10A). In thin-section, the cataclasite matrix appears to be altered to a clay-rich isotropic paste. SEM studies show the matrix to be composed of inequigranular fragments (1 μ m to 10 μ m in size) of K-feldspar, albite and quartz together with 'newly' formed epidote, chlorite and pyrophyllite grains (1 μ m to 10 μ m in size) (Plate 7.10A).

In gneissose wall rocks to the south of the core of the VF, millimetre-thick cataclasites display a colour banding defined by bands of opaque grains and clay material (Plate 7.10B). The bands of opaques are interpreted to represent the residue left by dissolution and removal of silica during pressure-solution processes. Quartz and feldspar fragments also display irregular grain boundaries, when viewed under high magnification, as a result of pressure solution and dissolution of quartz and feldspar. Calcite and zeolite veins (~0.1mm thick) consistently transect the cataclasites.

7:4:3:1 Operative deformation mechanisms

The dominant deformation mechanisms appear to be cataclastic flow (mechanical disaggregation and grain-size diminution) in and between grains, grain boundary sliding and pressure solution. Quartz, feldspar and mica all deform by cataclasis, indicating temperatures of less than 250°C (section 1:6:3; Passchier and Trouw 1996).

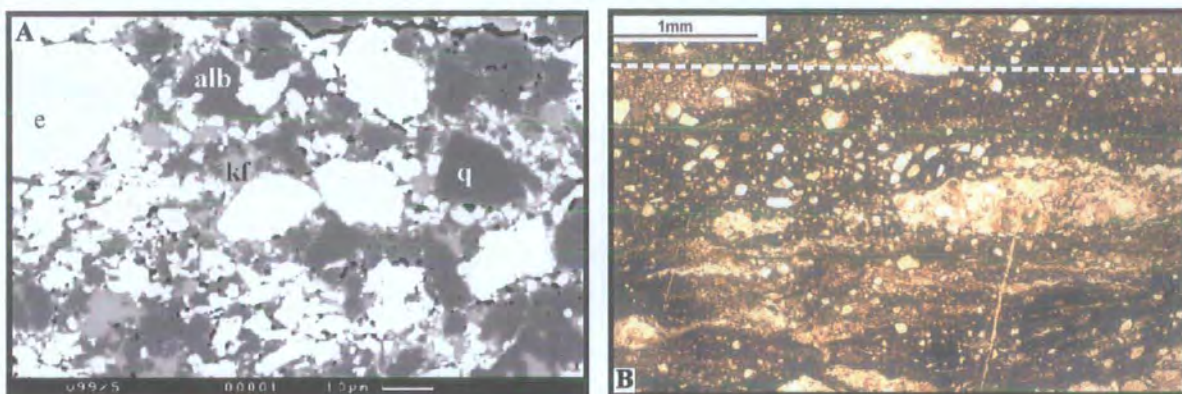


Plate 7.10 (A) Backscatter SEM image to show cataclasite matrix within the VF core. Inequigranular fragments of K-feldspar (kf), albite (alb) and quartz (q) appear to be supported by 'newly' mineralised epidote grains (B) Cataclasite with a fault-parallel colour banding defined by bands of opaque grains and clay material. Field of view 3.6x2.4mm, plane-polarised light.

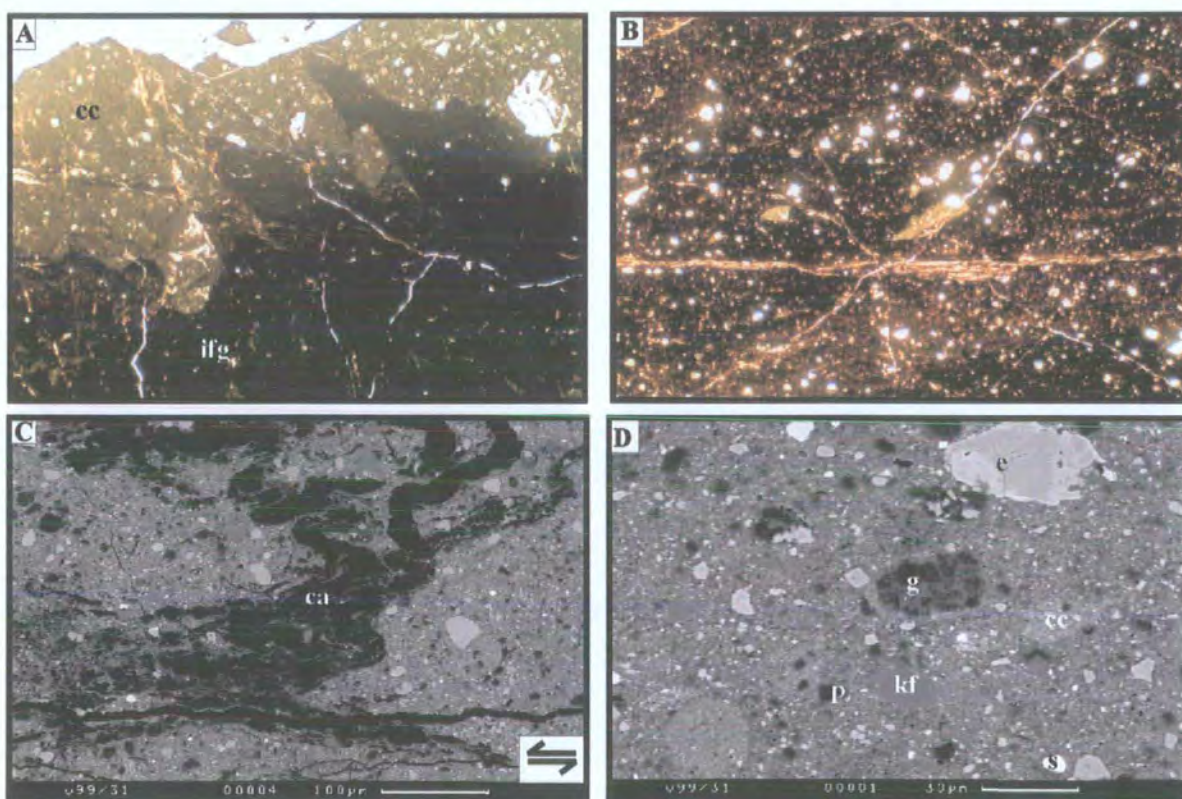


Plate 7.11 (A) Large-scale image to show irregular contact and injection vein structures of indurated fault gouge (ifg) into adjacent cataclasite (cc), which has been highly altered to a clay-rich paste. Field of view 14.4x9.6mm, plane-polarised light. (B) Image of indurated fault gouge, which comprises sub-rounded to rounded clasts of cataclasite, quartz, epidote and, in places, feldspar set within a dark-brown coloured matrix, which appears to be an isotropic paste, composed predominantly of clay minerals. Field of view 3.6x2.4mm, plane-polarised light. (C) Backscatter SEM image of indurated fault gouge. Ca-smectite (ca) layers display sinistral-verging folds, VF core. (D) Close-up backscatter SEM image of indurated fault gouge from the VF core. Fragments of epidote (e), pyrophyllite (p), cataclasite (cc), gneiss (g), k-feldspar (kf), sphene (s) and quartz lie within an ultrafine-grained clay-rich matrix (ca-smectite & pyrophyllite), which is not possible to image on the SEM.

Pressure solution also occurs at grain contacts leading to dissolution and removal of silica from cataclasites within the VF core and precipitation in voids, pore spaces and as veins within cataclasites outside the VF core (see major element geochemistry of cataclasite in section 7:6). Pressure solution of quartz occurs at temperatures above 130°C (Passchier and Trouw 1996). The presence of pyrophyllite, which is formed from the breakdown of K-feldspar indicates temperatures of approximately 200°C (L. Warr pers. comm. 2000). Therefore, the cataclasites along the VFZ formed at temperatures between approximately 200° and 250°C or depths of 6-8km assuming an average geothermal gradient of 30°C/km.

7:4:4 Indurated fault gouge

Indurated, black to brown fault gouge is exposed within the VF core. The development of the indurated fault gouge is broadly coeval with the development of cataclasites and was formed during sinistral strike-slip movements along the VFZ (see section 6:4:8). The term 'indurated' refers to post-tectonic lithification of the fault gouge, as a result of recrystallisation and cementation.

In thin-section, the gouge appears to be a dark-brown, clay-rich, isotropic paste containing sub-rounded to rounded clasts (0.1mm to 0.5mm in size) of cataclasite, quartz, epidote and locally feldspar (Plate 7.11A&B). The gouge displays a sharp and highly irregular contact with the adjacent cataclasite. Millimetre-scale injection veins of gouge appear to have nucleated into the adjacent epidote-rich cataclasite (Plate 7.11A). The gouge displays a sub-millimetre-scale colour banding, which reflects variations in grain size and the clast to matrix ratio.

SEM studies show the matrix to be composed of clasts of K-feldspar, epidote, quartz, chlorite, white mica, 'newly' formed pyrophyllite and ultracataclasite, which range from less than 1µm to 10µm in size (Plate 7.11C&D). The finest grain sizes and textures are not possible to image on the SEM. The gouge contains anastomosing layers of Ca-smectite, which are approximately 10µm to 100µm thick. The layers of Ca-smectite (formed from the breakdown of feldspar) commonly display folds (micrometre-scale) with a consistent sinistral sense of vergence (Plate 7.11A).

7:4:4:1 Operative deformation mechanisms

The dominant deformation mechanism is cataclastic flow (mechanical disaggregation and grain-size diminution) in and between grains, grain boundary sliding and pressure solution. Quartz, feldspar and mica all deform by cataclasis, indicating temperatures of less than 250°C. The presence of pyrophyllite, which is formed from the breakdown of K-feldspar, indicates temperatures of approximately 200°C (L. Warr pers.comm., 2000). Ca-smectite probably formed from the breakdown of albite, based on XRD analyses carried out by L. Warr (University of Heidelberg), and occurs at temperatures of between 80° and 150°C (Frey 1988). Therefore, the cataclasites along the VFZ formed at temperatures between approximately 80° and 200°C or at depths of 3-7km assuming an average geothermal gradient of 30°C/km.

7:4:5 Zeolite- and calcite-mineralised breccia

Zeolite- and calcite-mineralised breccias are common within the VFZ. In thin-section, randomly orientated clasts of gneiss, cataclasite, quartz, feldspar and epidote are set within a fine- (1µm to 10µm in size) to coarse-grained (0.5mm to 1mm in size) matrix of intergrown zeolite and calcite grains (Plate 7.12A-D). The breccias are both cross-cut by and contain clasts of zeolite and calcite veins (Plate 7.12A), suggesting multiple vein generation during brecciation.

Larger zeolite grains (~1mm) display undulose extinction and are cut by numerous intergranular fractures (Plate 7.12D). Calcite grains commonly display type 1 and 2 twinning (Plate 7.12C), indicating temperatures of less than 200°C (Passchier and Trouw 1996). Grønlie et al. (1994) identified the zeolites as laumontite, stilbite and analcite using XRD analyses.

7:4:5:1 Operative deformation mechanisms

The dominant deformation mechanisms are cataclastic flow (mechanical disaggregation and grain-size diminution) in and between grains, grain boundary sliding and hydrofracturing due to elevated pore-fluid pressures.

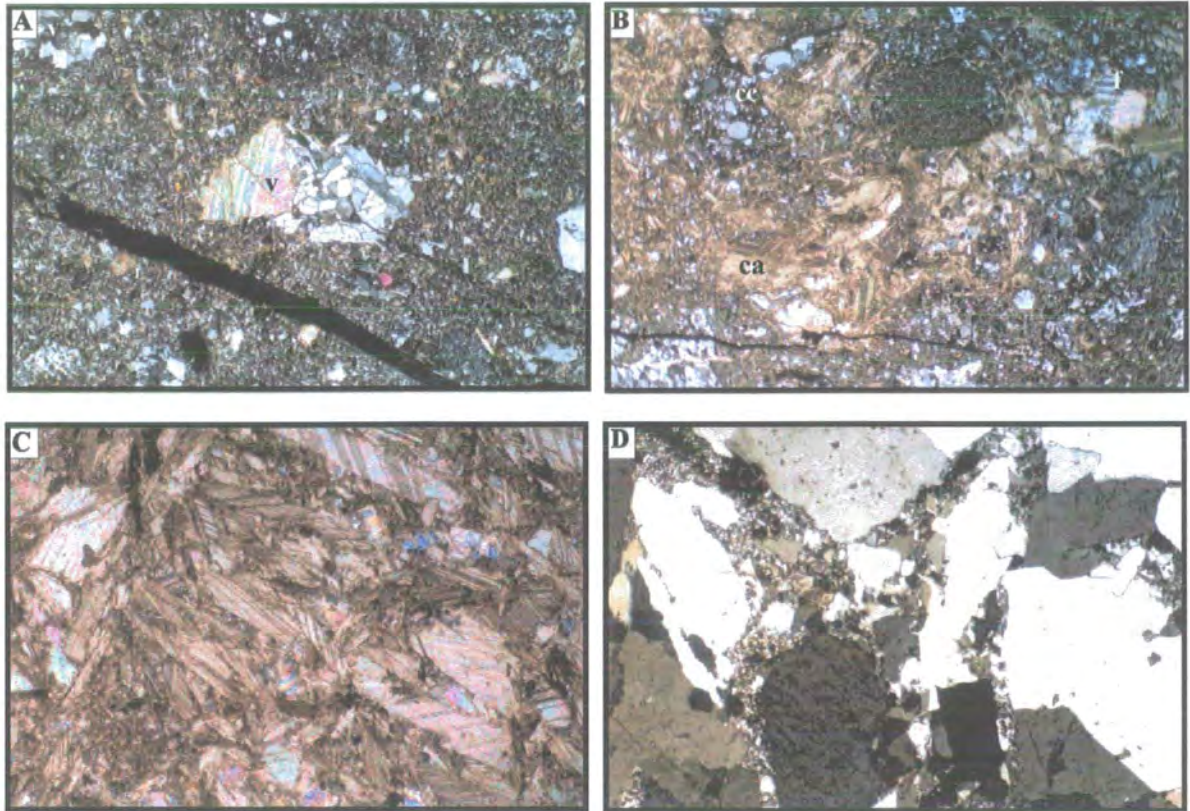


Plate 7.12 (A) & (B) Large-scale images of zeolite- and calcite- (ca) mineralised breccias. The breccias contain randomly orientated fragments of gneiss, cataclasite (cc), zeolite and calcite veins (v), feldspar (f), quartz and epidote which lie within a matrix of fine- to coarse-grained interlocking blades of calcite (ca) and zeolite. Field of view 14.4x9.6mm, crossed polars. (C) Image of randomly orientated fibrous calcite grains displaying interlocking textures within breccia matrix. Field of view 3.6x2.4mm, crossed polars. (D) Image of interlocking mosaic of zeolite grains within the breccia matrix, which are cut by a series of fine-grained zeolite veins. Field of view 3.6x2.4mm, crossed polars.

Calcite deformation twins indicate temperatures of less than 200°C (section 1:6:3). The coexistence of stilbite, laumontite and analcite indicates temperatures of between 100° and 160°C (Frey 1988). Therefore, zeolite- and calcite-mineralised breccias are interpreted to have formed at depths of 3 to 5km, assuming an average geothermal gradient of 30°C/km.

7:4:6 Grey fault gouge

Optical microscopy of incohesive, grey-coloured, fault gouges exposed within the VF core was impossible due to the difficulty involved in making thin-sections.

XRD analyses carried out by L.Warr (University of Heidelberg, Germany) show the grey gouge to be dominantly composed of Ca-smectite. The clays form as a result of the infiltration of aqueous fluid during frictional deformation, inducing alteration of unstable minerals formed at higher temperatures and pressures (Warr et al. 2001). Calcite, K-feldspar and possibly chlorite are also present. The grey gouge does not contain albite (which has reacted away to form Ca-smectite; L.Warr pers. comm., 2000), pyrophyllite and epidote. In the absence of TEM, due to the fine grain sizes, it is impossible to elucidate deformation mechanisms.

7:4:7 Blue-grey fault gouge

As in the case of the grey gouge, optical microscopy of the incohesive, blue-grey, fault gouges exposed within the VF core was impossible, due to the difficulty involved in making thin-sections.

XRD analyses were attempted by L.Warr (University of Heidelberg, Germany), but were impossible due to the swelling nature of the sample. The swelling probably indicates a high Ca-smectite content (L.Warr, pers.comm., 2000; see above section).

7:5 Summary

- Sinistral strike-slip movements were associated with hydrous, upper greenschist-facies deformation and mylonitisation.
- Deformation was accommodated primarily by intracrystalline crystal plastic mechanisms, and was localised into mylonites.
- Uplift / exhumation of the fault zone followed the cessation of viscous deformation mechanisms.
- Brittle reactivation (sinistral transtension) of the VFZ led to the development of cataclasites, minor pseudotachylites and indurated fault gouge, together with the creation of a large fracture-controlled permeability.
- Post-tectonic alteration of the wall-rocks to sericite, illite and pyrophyllite, due to the post-tectonic influx of hydrous fluid through the extensive fracture network.
- Several later phases of reactivation and localisation along the pre-existing fault rocks. Frictional deformation at depths of less than 5km, led to the formation of zeolite- and calcite-mineralised breccias, and a series of Ca-smectite-rich fault gouges.

7:6 Major element geochemistry of fault rocks

A representative suite of host rock (gneiss for VF and mylonite for HSF) and cross-cutting cataclasites were selected from key exposures along the VF and HSF (Table 7.2). These samples were selected in order to gain an improved understanding of changes in rock chemistry and the fluid-rock interaction during cataclasis along the VF and the HSF. The whole-rock major element compositions were determined using X-ray fluorescence (XRF) techniques. Protolith and fault-rock samples were analysed for ten standard major elements (SiO_2 , Al_2O_3 , Fe_2O_3 , MgO , CaO , Na_2O , K_2O , TiO_2 , MnO , P_2O_5) using XRF fusion disks. The mean major element composition for each group of samples was calculated (Table 7.3) and the results are summarised in Figure 7.4.

Sample	Location	Rock type	Kinematic regime
VL1	North of Verrasundet	Granodiorite gneiss	N/A
V99/19	Ormsetvatnet road	Granodiorite gneiss	N/A
V99/20	Ormsetvatnet road	Granodiorite gneiss	N/A
VC11	Verrasundet	Cataclasite	Sinistral strike-slip
V99/25	Verrasundet	Cataclasite	Sinistral strike-slip
V99/5A	Verran Fault core	Cataclasite	Sinistral strike-slip
V99/5B	Verran Fault core	Cataclasite	Sinistral strike-slip
HS50	Mefjellet	Protomylonite	Sinistral strike-slip
HS46	Mefjellet	Mylonite	Sinistral strike-slip
HS42	Mefjellet	Mylonite	Sinistral strike-slip
HS4	Mefjellet	Cataclasite	Sinistral strike-slip
HS9	Mefjellet	Cataclasite	Sinistral strike-slip
HS14	Mefjellet	Cataclasite	Sinistral strike-slip

Table 7.2 Summary of the locations, rock type and kinematic regime of each of the samples.

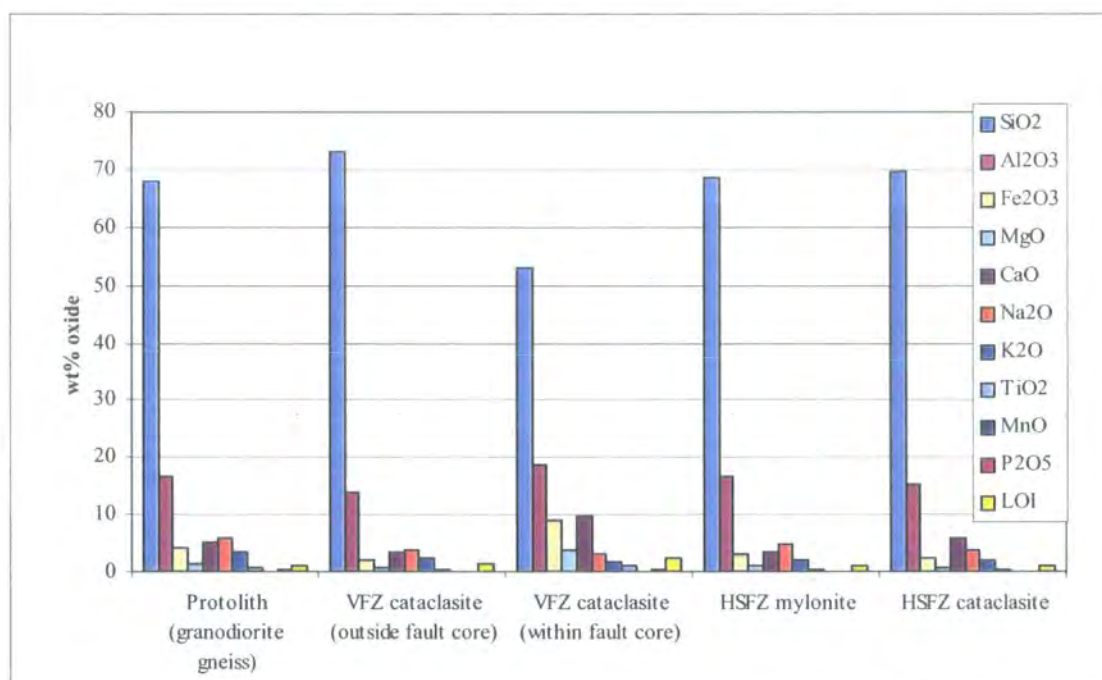


Figure 7.4 Mean major element compositions for the protolith, VFZ cataclasites (outside & inside fault core), HSFZ mylonites and HSFZ cataclasites.

	SiO ₂	Al ₂ O ₃	Fe ₂ O ₃	MgO	CaO	Na ₂ O	K ₂ O	TiO ₂	MnO	P ₂ O ₅	Total	LOI
VL1	69.59	16.14	2.57	0.87	2.5	5.64	2.41	0.317	0.051	0.124	100.21	0.782
V99/19	65.66	16.9	3.32	1.1	5.86	3.5	2.53	0.604	0.067	0.15	99.69	0.936
V99/20	69.1	15.99	3.08	0.96	3.67	4.51	2.727	0.404	0.067	0.128	100.41	1.59
V99/20	67.29	17.16	3.1	0.99	3.46	4.21	2.645	0.696	0.06	0.143	99.75	1.59
VC11	71.84	14.6	2.03	0.68	3.83	3.91	2.327	0.438	0.031	0.118	99.81	1.54
VC11	73.01	13.94	2.08	0.72	3.72	4.27	2.493	0.388	0.036	0.107	100.77	1.54
V99/25	74.56	13.24	2.08	0.81	3.09	3.59	2.707	0.267	0.036	0.108	100.49	1.13
V99/5A	52.37	18.88	9.07	3.73	9.83	3.19	1.796	1.131	0.148	0.39	100.53	2.25
V99/5B	53.29	18.62	8.7	3.68	9.65	3.19	1.857	1.071	0.141	0.365	100.57	2.29
HS50	69.96	16.47	2.4	0.72	3.39	4.96	2.462	0.314	0.058	0.108	100.85	0.82
HS46	67.38	17.11	3.41	0.87	4.05	5.04	2.086	0.425	0.056	0.148	100.57	0.75
HS42	68.71	16.52	3.47	1.06	2.97	4.89	2.088	0.48	0.0072	0.147	100.41	1.72
HS42	68.27	16.31	3.49	1.06	3.01	4.89	2.107	0.485	0.073	0.139	99.84	1.72
HS4	72.64	13.91	1.73	0.36	7.87	2.71	1.117	0.183	0.053	0.071	100.65	1.84
HS9	68.55	15.9	3.06	0.97	4.8	4.56	2.166	0.411	0.067	0.141	100.63	1.01
HS14	68.15	15.99	2.93	0.78	5.05	4.1	2.815	0.391	0.062	0.135	100.85	0.77

Table 7.3 Major element compositions in wt% of samples from the HSFZ and VFZ.

	SiO ₂	Al ₂ O ₃	Fe ₂ O ₃	MgO	CaO	Na ₂ O	K ₂ O	TiO ₂	MnO	P ₂ O ₅	LOI
VFZ cataclites outside fault core	5.23	-2.62	-1.96	-0.57	-1.62	-2.03	-0.93	-0.31	-0.05	-0.07	0.24
VFZ cataclites within fault core	-15.08	-1.34	4.86	2.40	4.58	-2.76	-1.61	0.43	0.06	0.20	1.17
HSFZ mylonite	0.67	2.20	-0.83	-0.38	-1.81	-1.01	-1.25	-0.25	-0.03	-0.05	0.00
HSFZ cataclasite	1.87	0.05	-1.45	-0.60	0.74	-2.16	-1.40	-0.35	-0.02	-0.07	0.11

Table 7.4 Mean protolith-normalised major element compositions for the VFZ cataclites, HSFZ mylonites and HSFZ cataclites.

7:6:1 Major element composition

The major element compositions (Figure 7.4) are dominated by SiO_2 and Al_2O_3 , which reflects the abundance of silicates, such as feldspar, quartz, white mica, chlorite and epidote, which are characteristic of granodiorite gneiss. The concentration of SiO_2 varies considerably (from 73 wt% in cataclasites outside VF core to 53 wt% in cataclasites within VF core), although Al_2O_3 is less variable (19 wt% in cataclasites within the VF core to 14 wt% in cataclasites outside the VF core). The other major elements are present in much lower concentrations (typically <10 wt%). The ratio of wt% Fe_2O_3 (total iron) to MgO is approximately 2:1 in both the mylonite and the cataclasite. The concentration of CaO is variable (from approximately 3% in mylonites along the HSFZ to approximately 10% in cataclasites within the VF core). The concentration of Na_2O (typically between 3 and 6 wt%) is greater than that of K_2O . TiO_2 , MnO and P_2O_5 are most abundant in cataclasites within the VF core, although overall the variation in the concentrations of these elements is small. Loss-on-ignition (LOI) is negligible in all rocks except for cataclasites within the VF core, which is 2.3 wt%.

7:6:2 Protolith-normalised composition

The variation in the concentrations of the less abundant major elements may not be apparent due to the high concentrations of SiO_2 and Al_2O_3 . An alternative approach is to calculate the amount of enrichment or depletion of the major elements relative to the protolith (e.g., Condie and Sinha 1996). The major element composition of each fault rock was normalised to the granodiorite gneiss protolith (Table 7.4). The data have been summarised by calculating the mean protolith-normalised compositions for each fault rock and the results are presented on a major element enrichment-depletion diagram (Figure 7.5).

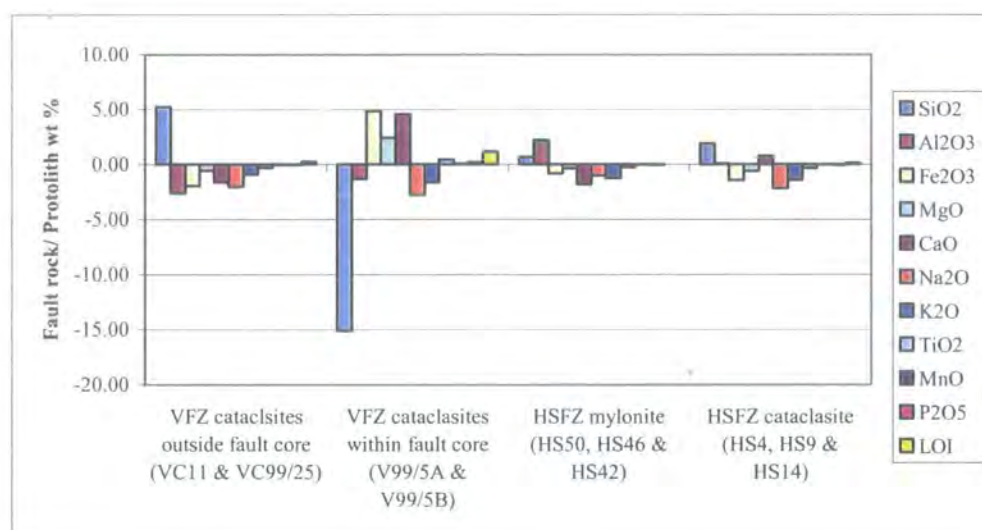


Figure 7.5 Mean protolith-normalised major element compositions for the VFZ cataclasites outside the fault core, inside the fault core, HSFZ mylonites and HSFZ cataclasites.

Concentrations of SiO_2 are enriched by ~ 5 wt% within cataclasites outside the VF core, 0.7 wt% within mylonites along the HSFZ and ~ 2 wt% within cataclasites along the HSFZ. Cataclasites within the VF core are depleted by ~ 15 wt% SiO_2 . The apparent loss in SiO_2 is consistent with the breakdown of plagioclase and K-feldspar to white mica, epidote, $\text{SiO}_2(\text{aq})$, $\text{Na}^+(\text{aq})$ and $\text{K}^+(\text{aq})$ (e.g., $2 \text{ oligoclase} + 3 \text{ K-feldspar} + \text{H}_2\text{O} + 8\text{H}^+(\text{aq}) \rightarrow 4 \text{ sericite} + \text{epidote} + 22 \text{ SiO}_2(\text{aq}) + 8 \text{ Na}^+(\text{aq})$; Imber 1998). Additional SiO_2 loss probably occurred by dissolution of quartz and feldspar along clay-rich seams. SiO_2 enrichment within cataclasites outside the VF core could be a result of precipitation of SiO_2 due to result of pressure solution and removal of SiO_2 from cataclasites of the adjacent fault core (section 7:4:3). SiO_2 concentrations within the mylonites along the HSFZ are similar to those within the gneissose protolith. Cataclasites along the HSFZ are enriched by $\sim 2\%$ in SiO_2 concentrations. This could be a result of the release of SiO_2 during the breakdown of albite and K-feldspar to muscovite and subsequent precipitation within the cataclasites (Wibberley 1999) within the HSFZ, due to the lower fracture-controlled permeability compared to the VFZ.

Al_2O_3 concentrations within the mylonites are very similar to those within the gneissose protoliths. Cataclasites within the HSFZ and outside the VF core display slight depletions in Al_2O_3 (1.3 and 2.6 wt%, respectively). The depletions could be due to dissolution of K-feldspar and plagioclase or breakdown to white mica.

Cataclasites within the VF core are enriched in Al_2O_3 by approximately 2 wt%, a feature which is probably associated with the growth of epidote and other aluminosilicates.

Fe_2O_3 and MgO concentrations are slightly depleted within HSFZ mylonites, HSFZ cataclasites and VFZ cataclasites outside the VF core, whilst cataclasites are enriched by 5 wt% for Fe_2O_3 and 2.4 wt% for MgO. The enrichment of MgO and Fe_2O_3 within the VF is consistent with chlorite and epidote growth, and the presence of opaque grains.

The alkali metals (Na_2O and K_2O) are depleted in all fault-rock samples, due to the breakdown of plagioclase and K-feldspar. The greatest depletion occurs within cataclasites within the VF core due to dissolution of feldspar.

TiO_2 , MnO and P_2O_5 are slightly depleted in mylonites, cataclasites along the HSFZ and cataclasites outside the VF core. Within cataclasites of the VF core, TiO_2 , MnO and P_2O_5 are slightly enriched probably due to the growth of apatite and opaque minerals.

Loss-on-ignition (LOI) is slightly higher in all fault-rock samples and reflects the breakdown of anhydrous mineral phases (e.g. feldspar) to syn-tectonic, OH-bearing, mineral phases (e.g., epidote, white mica and pyrophyllite).

Chapter 8. Discussion and Conclusions

Detailed field and microstructural studies (Chapters 3, 4, 6 and 7) have demonstrated that the Walls Boundary Fault Zone and the Møre-Trøndelag Fault Complex are long-lived structures that have experienced a prolonged history of repeated reactivation. The aims of this chapter are:

- To summarise and discuss the kinematic, textural and microstructural evolution of the Walls Boundary Fault System and the Møre-Trøndelag Fault Complex.
- To discuss the regional tectonic setting from mid Palaeozoic to Tertiary times and possible fault zone linkages of the WBF and MTFC.
- To discuss localisation and weakening processes that may control fault reactivation.
- To present a model of fault-rock exhumation and preservation along multiply reactivated faults.

8:1 The Walls Boundary Fault System

8:1:1 Kinematic evolution and fault-rock sequence

The aim of this section is to synthesise the kinematic evolution of the WBFS based upon the field relationships discussed in Chapter 3. Timing, regional implications and displacement magnitudes are discussed in section 8:1:2.

The earliest recognised fault-related deformation within the WBFS occurred along the WBFZ and led to the development of mylonites, blastomylonites, cataclasites and foliated cataclasites (Figure 8.1), which are only partially preserved in a series of fault-bounded blocks (e.g., Sullom, Lunnister and the Ness of Hagggrister, section 3:1:2 and Sand to Seli Voe, section 3:1:7).

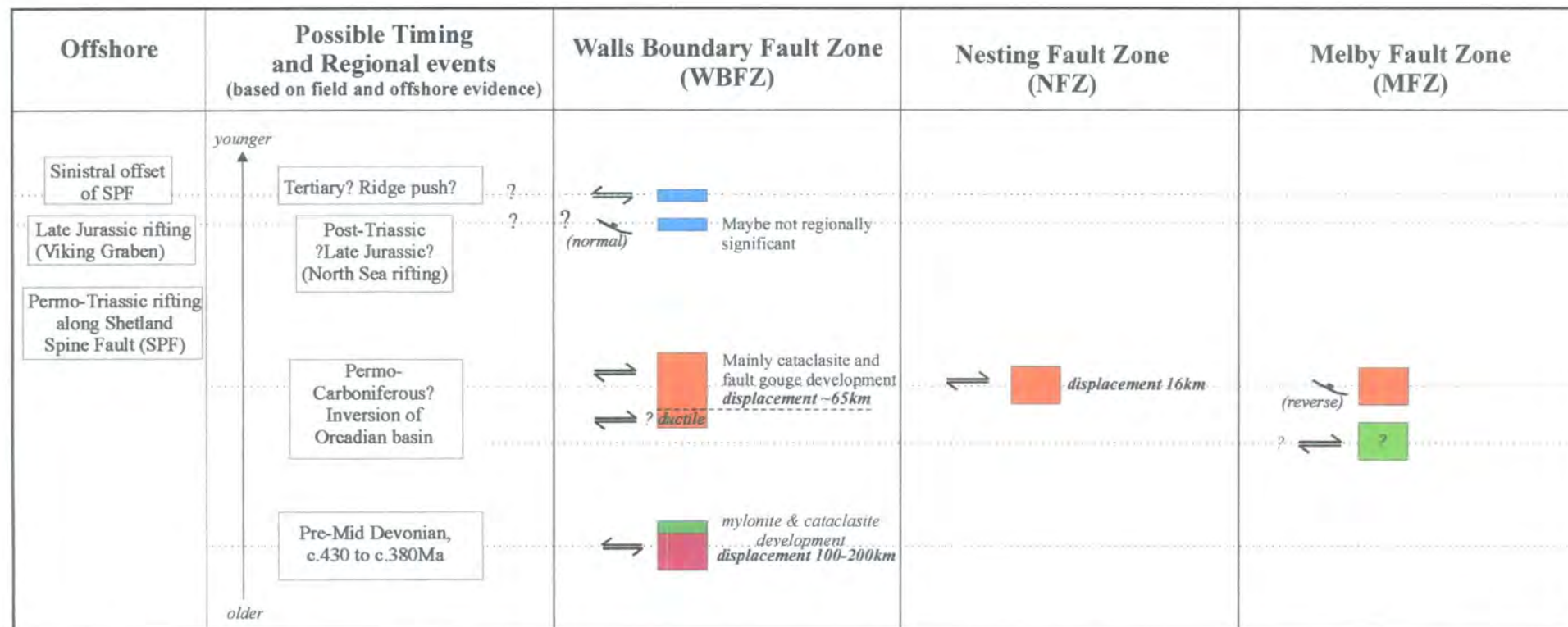


Figure 8.1 Diagram to show the relative kinematic histories for the Walls Boundary, Nesting and Melby Fault (discussed in section 8:1:1) with suggested timings based on field and offshore evidence (discussed in section 8:1:2).

Mylonites formed during sinistral strike-slip movements are overprinted by a series of foliation-parallel and cross-cutting cataclasites and locally pseudotachylites, all of which formed during sinistral shear. The cataclasites are interpreted to have formed during syn-tectonic exhumation of the fault zone, which led to a switch from viscous to frictional deformation mechanisms (section 8:1:3). However, in the absence of fault-rock dating, it is possible that they developed during a later phase of sinistral strike-slip (c.f. MTFC, section 7:2). East of the WBF at the Ness of Haggrister, granodiorite of the Graven Complex contains xenoliths of protomylonites (section 3:1:2), suggesting that intrusion of the granodiorite (c.400Ma; see section 2:1:5:1) post-dated mylonitisation. Cataclasites west of the WBFZ on the island of Papa Little are transected by pegmatite dykes of the Northmaven Complex (c.360Ma; see section 2:1:5:2). At Red Ayre (section 3:1:8), a large xenolith of mylonite containing foliation-parallel cataclasites and pseudotachylites was mapped within the Sandsting granite (c.360Ma, section 2:1:5:2), suggesting both mylonites and overprinting cataclasites pre-date intrusion of the Sandsting granite. However, foliated cataclasites exposed at Brae Isthmus (section 3:1:3) formed during sinistral shear cross-cut granodiorite (c.400Ma). Also, most intrusions to the east of the WBFZ display a N-S-trending magmatic foliation suggesting that late-Caledonian deformation was still active during the emplacement of these intrusions. The fact that there seems to be a close spatial association of granites along the trace of the WBFZ and that the intrusions contain a magmatic fabric may imply that emplacement occurred during sinistral shear, although no direct evidence was observed within the granites during the present study. Granitic intrusions west of the WBFZ do not contain any magmatic fabrics and clearly post-date sinistral movements (xenoliths of mylonite and cataclasite at Red Ayre, section 3:1:8 and pegmatites which cross-cut cataclasites on Papa Little, section 3:1:4) along the WBFZ, suggesting that sinistral movements must be older than c.360Ma and are very likely to be late-Caledonian. It should be noted that many of the granite ages on Shetland were determined using K-Ar whole-rock or mineral techniques (Miller and Flinn 1966; Flinn 1985 and references therein), and therefore the exact ages of the intrusions are uncertain.

A major phase of dextral strike-slip brittle faulting overprints a dextral strike-slip ductile event at several localities (e.g., Ollaberry, section 3:1:1, Ness of Haggrister, section 3:1:2, and Aith Voe, section 3:1:5). In the absence of direct fault-rock dating,

it is possible that the kinematically similar ductile and brittle fault rocks formed either during the same event as the fault zone was being exhumed or during separate kinematic phases. The only constraints on the relative age are exposed along the west coast of Aith Voe (section 3:1:5). Here, dextral shear fabrics within N-S-trending, phyllonitic fault rocks are cut by an E-W-orientated dolerite dyke which is offset along later, N-S-orientated, gouge-filled fractures. The age of the dyke is unknown but is possibly Permo-Carboniferous based on its orientation and composition. However, due to the lack of evidence at other localities it is unclear how representative these relationships are.

The most significant phase of dextral strike-slip reactivation (Figure 8.1) led to the development of a 500m to 2km-wide zone of braided sub-vertical faults associated with broad zones of cataclasis and the development of fault gouge. During this event a series of kilometre-scale positive and negative flower structures were formed along the strike of the fault zone (e.g., Sullom, Lunnister and the Ness of Haggrister, section 3:1:2, Ness of Bixter, section 3:1:6 and Seli Voe to Sand 3:1:7). This phase of faulting cross-cuts the youngest rocks exposed on Shetland (i.e., Sandsting granite, c.360Ma) and therefore must be post-Devonian. Offset units of Queyfirth Group to the west of the WBF are exposed at Ollaberry (section 3:1:1) and the Ness of Haggrister (section 3:1:2) and to the east of the WBF at the Ness of Bixter (section 3:1:6) and Seli Voe to Sand (section 3:1:7), inferring a minimum dextral strike-slip offset of 35km.

At the Ness of Bixter (section 3:1:6), incohesive fault gouge within the WBF core that formed during dextral strike-slip movements is cross-cut by a metre-wide pegmatite intrusion. Xenoliths of fault gouge are present within the pegmatite, which is interpreted to have been emplaced along the fault during dilatancy related to dextral strike-slip movements. Direct dating of this pegmatite would constrain the age of dextral strike-slip movements along the WBFZ.

Subsequent dip-slip and sinistral strike-slip reactivation of the WBFZ was localised entirely within pre-existing fault gouges located in the central part of the WBFZ (fault core) (Figure 8.1). Therefore, these events are only recognised where parts of the fault core are exposed. The regional extent of the dip-slip event is unclear as it is only

recorded in the incohesive gouge at the Ness of Haggrister (see Table 3.10, section 3:1:9) and therefore may only represent localised reactivation. However, this is by far the best-preserved fault core section and any dip-slip reactivation may not have been recognised at other localities due to the lack of exposure. The youngest phase of movement, sinistral strike-slip, occurs within the central part of the WBF core along the WBF and is recognised at several localities along the strike of the fault zone (Ness of Haggrister, section 3:1:2, Brae Isthmus, section 3:1:3 and Papa Little, section 3:1:4).

The NF is the second most significant fault in terms of displacement within the WBFS. It splays from the WBF offshore to the south of Seli Voe and links back into the WBF offshore and to the north of Ollaberry. The NF is dominated by a 300m-wide zone of cataclasis with the development of fault gouge assemblages, which formed during a single phase of dextral strike-slip movement. Earlier sinistral displacements and fault rocks are not preserved. The present study supports the interpretation of the NF by Flinn (1977) as a dextral strike-slip fault along which a 16km displacement occurred (Figure 8.1). No structures associated with later movements were recognised along the NF in this study.

The MF is the third regionally significant fault. It is a poorly exposed, NE-SW-trending, reverse fault associated with the development of fault gouge (Figure 8.1). No later structures were recognised along the MF in this study. Earlier fault rocks comprise strike-slip (uncertain shear sense) phyllonites exposed within the basement rocks to the east of the MF. Due to the poor level of exposure of this fault the kinematic history is uncertain.

8:1:2 Timing, regional implications and displacement magnitudes

The WBF is a near vertical, N-S-trending, multiply reactivated fault which cross-cuts the whole crust and offsets the Moho by several kilometres vertically (McGeary 1989; McBride 1994b).

Onshore, Flinn (1977) mapped a gouge-filled fracture containing sub-horizontal slickensides, which he interpreted to represent the latest movement on the WBF. Flinn (1977) also noted that the WBF lies within broad zones of cataclasis, subsidiary faulting and localised folding, which is consistent with the results of the present study. Slices of mylonite were recognised along the trace of the WBF (Flinn 1977; Conroy 1996), which Flinn (1977) related to an earlier fault, possibly the GGF, which was active before the WBF along the same line. Flinn (1977, 1992) concluded that the WBFZ was a dextral transcurrent fault of Mesozoic age, with an offset of 65km based on the matching of aeromagnetic anomalies on either side of the fault offshore. Mykura and Phemister (1976) concluded that the Fair Isle sandstone to the east of the WBF was lithologically similar to that exposed west of the WBF on the Walls Peninsula, supporting a post-Devonian dextral offset of c.65km. In a more recent study, Marshall (2000), constrained the age of the Walls Group, which was previously thought to be Lower to Middle Devonian, to Givetian (385Ma). This provides a direct correlation of the Walls sandstones to the Fair Isle sandstones east of the WBF and supports the lithological comparisons of Mykura and Phemister (1976) and Rogers et al. (1989). This confirms a dextral strike-slip offset along the WBF of c.65km, which is in broad agreement with the present study where a minimum, post-Devonian, 35km dextral strike-slip offset has been recognised (Figure 8.1).

Flinn (1992) pointed out that a displacement of c.65km in Shetland cannot die out along strike within 240km to Inverness and suggested that displacement was taken up on the Helmsdale Fault. Underhill (1993) dismissed this correlation on the basis that the Helmsdale Fault formed as a basin-bounding normal fault to a major half-graben structure in the Moray Firth, of Late Jurassic age. Underhill (1993) even questioned whether there was any field evidence to support a Mesozoic dextral offset of c.65km since this figure was based upon matching aeromagnetic anomalies, which were thought to be offset regions of Jurassic rocks, on either side of the fault (Flinn 1992). It is true that offshore, to the south of Shetland, the WBF is observed to cut Permo-Triassic rocks (McGeary 1989), suggesting post-Triassic movement. However, the present study has identified a late sinistral strike-slip event which post-dates dextral movement, thus accounting for the offshore observations (Figure 8.1).

A more likely explanation, however, is that the dextral movement on the WBF occurred before the Mesozoic. Field studies of structures within the sandstones of the Walls Group have identified a Permo-Carboniferous inversion event (Coward et al. 1989; Séranne 1992a). A series of kilometre-scale, NNW-SSE-trending folds, thrusts and reverse faults are developed, which post-date intrusion of the Sandsting granite (c.360Ma). These have been related to similar structures within the Orcadian basin on Orkney and in northern Scotland, that are thought to be related to Variscan tectonics. An E-W to NE-SW compression is inferred, which is compatible with dextral transpression (e.g. Ollaberry, section 3:1:1) along the WBF and the NF. Therefore, it is possible that dextral strike-slip movement along the WBF was related to Permo-Carboniferous inversion.

Offshore, Ritchie et al. (1987) suggested a net 15km sinistral movement along the WBF based upon an offset of the Shetland Spine Fault (SPF) to the north of Shetland (Figure 8.2). If this relationship is correct, then dextral movement on the WBF must have pre-dated movements on the SPF. The SPF was active in the Permo-Triassic and associated with a c.6km-thick syn-rift succession (Doré et al. 1999 and references therein). A thin sequence of Late Jurassic sedimentary rocks with only minor thickness variations overlies the Middle Jurassic unconformity and seismic sections provide very little evidence of Jurassic age syn-rift deposits (Doré et al. 1999). Therefore, the main phase of faulting along the SPF was of Permo-Triassic age. This supports a Permo-Carboniferous age for the dextral movement along the WBF (pre-dating the SPF). The apparent 15km sinistral offset of the SPF is also consistent with the most recent phase of movement (post-Triassic sinistral strike-slip) recognised onshore along the WBF in this study (Figure 8.1). This is consistent with the work of Conroy (1996) who also recognised the most recent sinistral strike-slip event.

When the dextral offset is restored, it is clear that there is no matching of pre-Devonian basement rocks across the WBF on Shetland. Flinn (1977, 1992) suggested a 100-200km sinistral offset based on differences in the metamorphic basement on either side of the fault. The Caledonian front (exposed west of the WBF), which is marked by a series of alternating slices of Lewisian gneiss and Moine metasedimentary rocks, is bound to the west by a ductile thrust that is thought to be the equivalent of the Moine Thrust of Northwest Scotland (Pringle 1970).

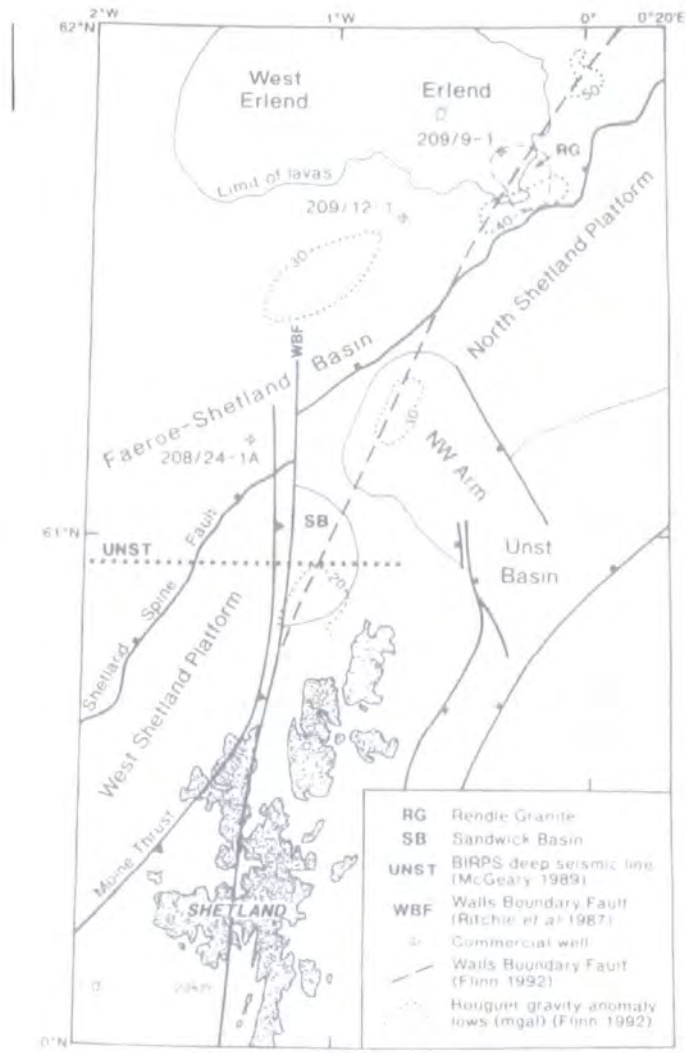


Figure 8.2 Geological sketch map illustrating the location of the WBF and the apparent sinistral offset of the Shetland Spine Fault (SPF) to the north of Shetland (after Ritchie et al. 1987).

This structure was interpreted by Flinn (1969, 1977, 1992) to intersect the WBF at depth to the north of Shetland, and does not pass through Shetland or to the south on the east side of the WBF, suggesting an initial sinistral offset of 100-200km. This sinistral event is the earliest recognised event in the present study (e.g., blastomylonites, mylonites and cataclasites at Sand to Seli Voe, section 3:1:7 and Lunnister, section 3:1:2) and is consistent with the observations of Flinn (1977, 1992).

Field evidence in the present study indicates that this sinistral event initiated before c.400Ma (intrusion of eastern late-orogenic granites) and ceased before c.360Ma (intrusion of western post-orogenic granites) (section 8:1:1). Séranne (1992a) noted the occurrence of syn-depositional, ENE-WSW-trending folds and sinistral shearing along ENE-WSW- to NE-SW-trending detachment faults within the Walls sandstones (c.385Ma). These structures seem to be consistent with active sinistral shear along the WBF during this time (c. 385Ma). Roddom et al. (1989) inferred a Carboniferous / Permian age for the formation of mylonites along the WBF, based on ^{40}Ar - ^{39}Ar (whole-rock) step heating. However, it is clear from the present study that the mylonites are derived from banded gneiss and are preserved as xenoliths within granodiorite (c.400Ma) and granite (c.360Ma), indicating that the mylonites could not be of Carboniferous/ Permian age.

It has long been thought that the offshore continuation of the WBF to the south of Shetland links with the Great Glen Fault (GGF) in Scotland (Flinn 1961). McBride (1994a) mapped a stepover structure between the WBF and the GGF, which was consistent with late-Caledonian, sinistral, strike-slip movements. A recent study of the emplacement of the Clunes Tonalite during sinistral shear has constrained early movements along the GGF to c.430Ma (U-Pb on zircon) (Stewart et al. 2001). Sinistral movements along the GGF are thought to have ceased by c.400Ma (Rogers et al. 1989; Stewart 1997) based upon the presence of Devonian sedimentary rocks which unconformably overlie the GGF. Therefore, the timing of early sinistral movements recognised along the WBF (before c.400Ma to c.385Ma) in the present study is broadly contemporaneous with that along the GGF (c.430 to c.400Ma). Also, displacement magnitudes estimated for the GGF during sinistral movements are thought to be c.100-200km (Stewart et al. 1997; Stewart 1997 and references therein), which is consistent with estimates for the WBF in Shetland (Flinn 1977, 1992).

A post-Devonian, dextral, strike-slip offset of c.30km was recognised along the GGF in the Inverness area, based upon a restoration of the Devonian sedimentary rocks (Rogers et al. 1989). It was argued that much of the dextral displacement (c.20km) probably took place during Late Carboniferous inversion of the Orcadian basin (see Rogers et al. 1989 and references therein for discussion). This is broadly coeval with dextral movements recognised along the WBF in the present study. However, as pointed out by Flinn (1992), a c.65km dextral displacement in Shetland cannot die out along strike within 240km to Inverness. This suggests that some of the displacement was taken up on other structures to the south of Shetland, and possibly along some of the N-S-trending, Permo-Carboniferous dextral faults described on Orkney (e.g., Coward et al. 1989).

Thomson and Underhill (1993) concluded that less than 10km of net dextral movement had occurred along the GGF since the Jurassic. However, the most recent movement recognised along the WBF in the present study is post-Triassic, sinistral strike-slip. This is clearly inconsistent with earlier interpretations and therefore suggests that these faults were not linked during post-Triassic times.

Flinn (1977, 1992) described the Nesting Fault (NF) as a splay of the N-S-trending WBF, which accommodated some strike-slip displacement as the WBF changed strike. Flinn (1977) suggested a 16km dextral displacement based upon the interpretation of units offset on geological maps. This is consistent with the present study, where only a dextral strike-slip event is preserved which led to the development of fault gouge assemblages.

The MF has long been considered to be a strike-slip fault despite there being no direct evidence of such movement reported in the literature (e.g., Mykura 1976; Mykura and Phemister 1976; Mykura 1991). Donovan et al. (1976) proposed a dextral strike-slip offset of a 'considerable amount' based upon reconstructing Devonian palaeogeography. Flinn (1977) described the MF as a series of polished SE-dipping surfaces arranged in an en échelon fashion with slickenfibres indicating reverse motion. Rogers et al. (1989) suggested that the fault is an inverted syn-depositional normal fault. A major, dextral, strike-slip displacement was implied by Séranne

(1992a) based upon his maps and fold axis orientations within the Devonian sedimentary rocks, which were thought to have formed during Carboniferous inversion of the Orcadian Basin. Conroy (1996) interpreted the outcrops to the east of the MF trace to display evidence for dextral shear overprinted by strong cataclastic deformation. The present study supports Flinn (1977), who recognised the MF as a reverse fault. However, the present work cannot rule out an earlier dextral strike-slip movement as strike-slip phyllonites are developed locally in the basement to the east of the fault.

8:1:3 Textural and microstructural evolution

The aim of this section is to summarise the textural and microstructural evolution exhibited by fault rocks along the WBFZ as a basis for the discussion of possible fault-zone weakening mechanisms (section 8:4).

Primary, sinistral, strike-slip movements were associated with the development of blastomylonites, upper greenschist-facies mylonites and localised pseudotachylite, that are preserved in two deeply-exhumed, fault-bounded blocks. These blocks are part of two, distinct, kilometre-scale, 'positive' flower structures, exposed at (a) Seli Voe to Sand (section 3:1:7) and (b) Sullom, Lunnister and the Ness of Haggrister (section 3:1:2), which were probably exhumed during later dextral strike-slip movement along the WBFZ (see section 8:5). The best-exposed mylonites are exposed at Lunnister (section 3:1:2).

At Lunnister, a series of felsic and mafic mylonites are derived from compositional banded gneisses (Figure 8.3). The gneisses display a granoblastic texture where feldspar grains form interlocking aggregates that isolate quartz, hornblende and micas (section 4:1:1). The onset of viscous creep in feldspar typically occurs at $\sim 450^{\circ}\text{C}$ while in quartz and micas it occurs at $\sim 300^{\circ}\text{C}$ (section 1:6:3). Thus, at any given temperature, feldspar is significantly stronger than quartz. These observations, together with the textures described in section 4:1:1, suggest that the banded gneiss displays a load-bearing framework (LBF) microstructure (section 1:6:4; Handy 1990), where the rheology of the rock is controlled by the rheology of the feldspar grains.

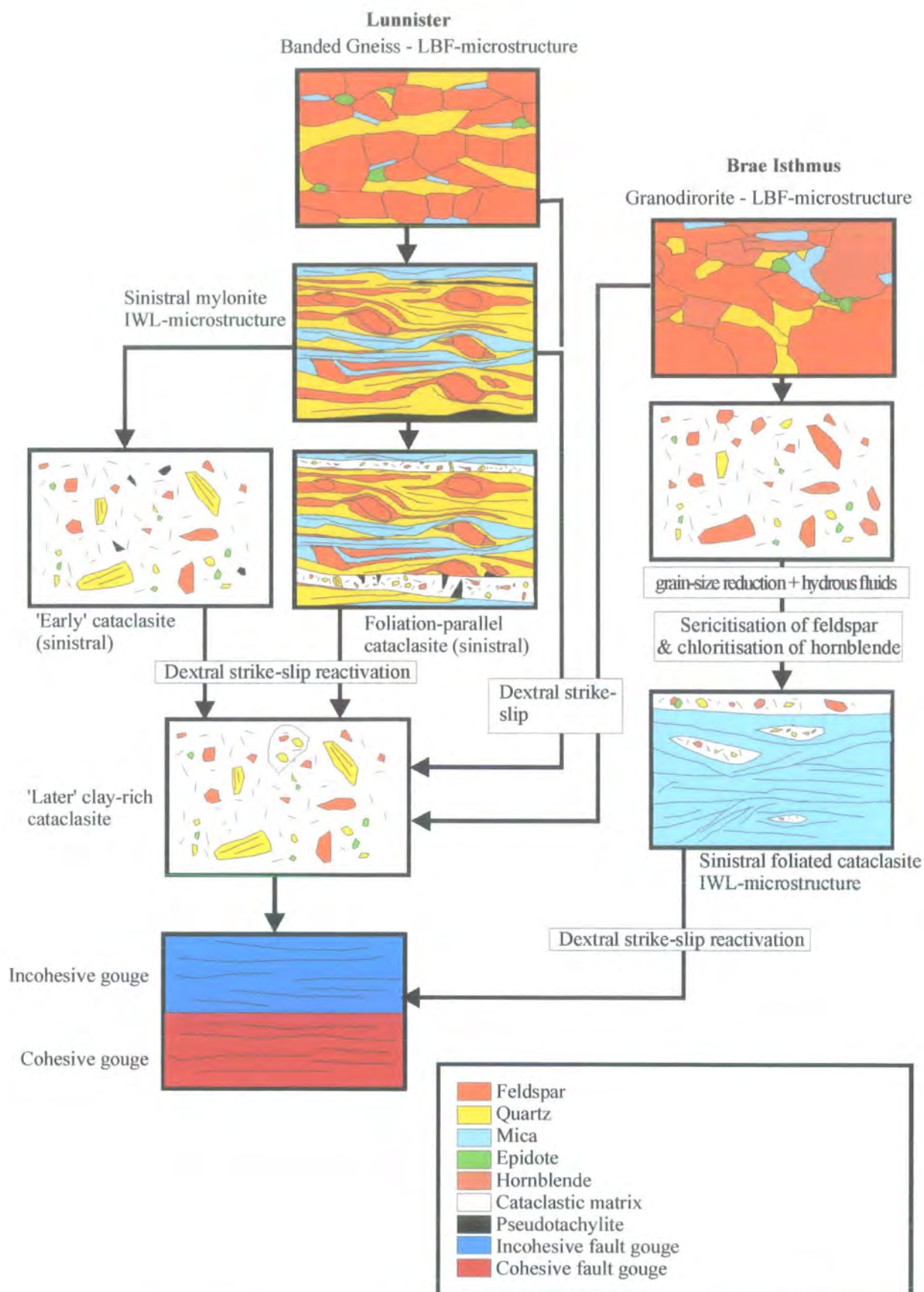


Figure 8.3 Schematic diagram to illustrate the textural evolution of the primary and secondary fault rocks at Lunnister and Brae Isthmus.

The mylonites comprise 'rigid' feldspar and or hornblende porphyroclasts, which are wrapped by an interconnected network of polycrystalline quartz ribbons and bands of ultrafine-grained feldspar, sericite and biotite. The porphyroclasts display relatively low aspect ratios ($<5:1$) and appear to be relatively undeformed internally. In contrast, the polycrystalline quartz ribbons and bands of ultrafine-grained feldspar, sericite and biotite display comparatively high aspect ratios ($<100:1$), appear to be very highly strained and form an interconnected weak-layer (IWL) microstructure (Figure 8.3; section 1:6:4). These observations suggest that the rheological behaviour of the highly strained mylonitic fault rocks was primarily controlled by the rheological behaviour of the quartz ribbons and ultrafine-grained feldspar (Handy 1990). The breakdown of the LBF to an IWL-microstructure was strain induced and caused by crystal-plastic deformation of quartz, and fracturing and dynamic recrystallisation of feldspar (section 4:2:1:2).

The quartz grains preserved in the mylonites display evidence for widespread dynamic recrystallisation. These observations are consistent with deformation of quartz at temperatures of between 400°C and 700°C (see section 1:6:3; Passchier and Trouw 1996). The microstructures associated with feldspars (fracturing & frictional sliding) suggest that deformation took place between 400°C and 500°C. Therefore, mylonitisation is postulated to have occurred at upper greenschist facies or temperatures of between 400°C and 500°C and depths of 13-16km, around the level of the frictional to viscous transition (section 1:6:5) (assuming an average geothermal gradient of 30°C/km). As mentioned in section 4:2:1:2d, the geothermal gradient may have been elevated, given the presence of late-Caledonian granitic intrusions along the trace of the WBFZ in Shetland (section 2:1:5). Therefore, mylonitisation could have taken place at shallower depths.

Exhumation of the fault zone (maybe during continued sinistral strike-slip movements) promoted a transition from viscous creep to mainly frictional deformation mechanisms, leading to the localisation of sinistral cataclasites along the mylonite foliation and the formation of cataclasites derived from granodiorite (e.g., Brae Isthmus, section 3:1:3) and gneiss (Figure 8.3). Quartz and feldspar deform by cataclasis, indicating temperatures of between 250°C and 300°C or depths of 8.5 to

10km (see section 1:6:3) (assuming an average geothermal gradient of 30°C/km). However, in the absence of direct fault-rock dating, it may be possible that the cataclasites formed during a later phase of sinistral strike-slip movement.

Locally (e.g., at Brae Isthmus; section 3:1:3), the influx of hydrous fluid led to the development of phyllosilicate-rich, foliated cataclasites, the textures of which are consistent with sinistral shear (Figure 8.3; section 4:2:2:2). Cataclastically deformed feldspar and hornblende have broke down to sericite and chlorite in the presence hydrous fluids (see section 4:2:2:2). Foliated cataclasites comprise isolated quartz, feldspar, hornblende and cataclasite slivers, which are wrapped by a network of intergrown sericite and chlorite that appear to form an IWL-microstructure (sections 1:6:3, 1:7:2:3a). These observations are consistent with the overall rheological behaviour of the foliated cataclasites having been controlled by deformation within the interconnected network of phyllosilicate grains (Handy 1990).

Dextral strike-slip reactivation of the WBFZ led to the development of a sequence of extensive cataclasite and fault-gouge assemblages, which display evidence for a progressive, syn-tectonic shallowing of the fault zone (Figure 8.3). Cataclasites indicate temperatures of 150°C to 300°C or depths of 5-10km (assuming an average geothermal gradient of 30°C/km) (sections 4:3:1 to 4:3:4). Fault gouges indicate temperatures of less than 150°C or depths of less than 5km (section 4:3:5).

8:2 The Møre-Trøndelag Fault Complex

8:2:1 Kinematic evolution, fault-rock sequence and timing

The aim of this section is to summarise the kinematic evolution of the MTFC based upon field relationships (Chapter 6), microstructural and textural studies, and fault-rock dating (Chapter 7).

The two principal bounding structures of the MTFC, the HSF and VF, lie along the steeply dipping limbs of a regional-scale antiformal structure (section 6:2). Field

evidence shows that these faults are superimposed upon and therefore post-date the regional fabrics associated with the development of the fold.

Field studies of fault rock distribution, overprinting relationships and fault-zone structure (described in Chapter 6) have elucidated a prolonged and heterogeneous kinematic history for the MTFC. Kinematic events have been correlated along the main faults of the MTFC based on overprinting relationships, and microstructural and textural studies (Chapter 7). Direct fault-rock dating of the earliest recognised fault rocks along the HSF has helped constrain the timing of early kinematic events along the MTFC. The kinematic history and structural evolution of the MTFC is summarised in Figures 8.4 and 8.5.

The HSFZ is a 1km-wide, ductile, sinistral shear zone that contains mylonites, with a narrow central zone of cataclasite and pseudotachylites formed during sinistral shear (section 6:3:1). Syn-tectonic mica overgrowths formed during mylonitisation of the banded gneiss have been dated at 409 ± 12 Ma (Figures 8.4, 8.5; section 7:2). The occurrence of pegmatite and microdiorite dykes, and extensive quartz veining, which are clearly cross-cut by mylonite fabrics, and their increase in frequency towards the centre of the HSFZ (section 6:3:1), may indicate the presence of a precursor structure prior to the formation of the HSFZ. Therefore, the 1km-wide ductile shear zone, which represents the earliest recognised deformation along the HSFZ, may have localised along a pre-existing basement structure, such as a deep-seated igneous contact or a zone of dyking. Cross-cutting pseudotachylite veins coeval with cataclasites developed during a phase of sinistral transtension and are dated at 291 ± 14 Ma (Figures 8.4, 8.5; section 7:2). The cataclasites and pseudotachylites are the youngest significant fault rocks present along the HSFZ (Figure 8.4). Later, localised dextral strike-slip reactivation occurred along minor zeolite-filled fractures. The exposures on Mefjellet (section 6:3:1) display little evidence for dextral strike-slip reactivation, whilst localities to the southwest (Hamardalen; section 6:3:2) and to the northeast (Follavatnet and Brattveit; section 6:3:3) display increased amounts of late-stage zeolite and calcite mineralisation together with minor dextral strike-slip kinematics.

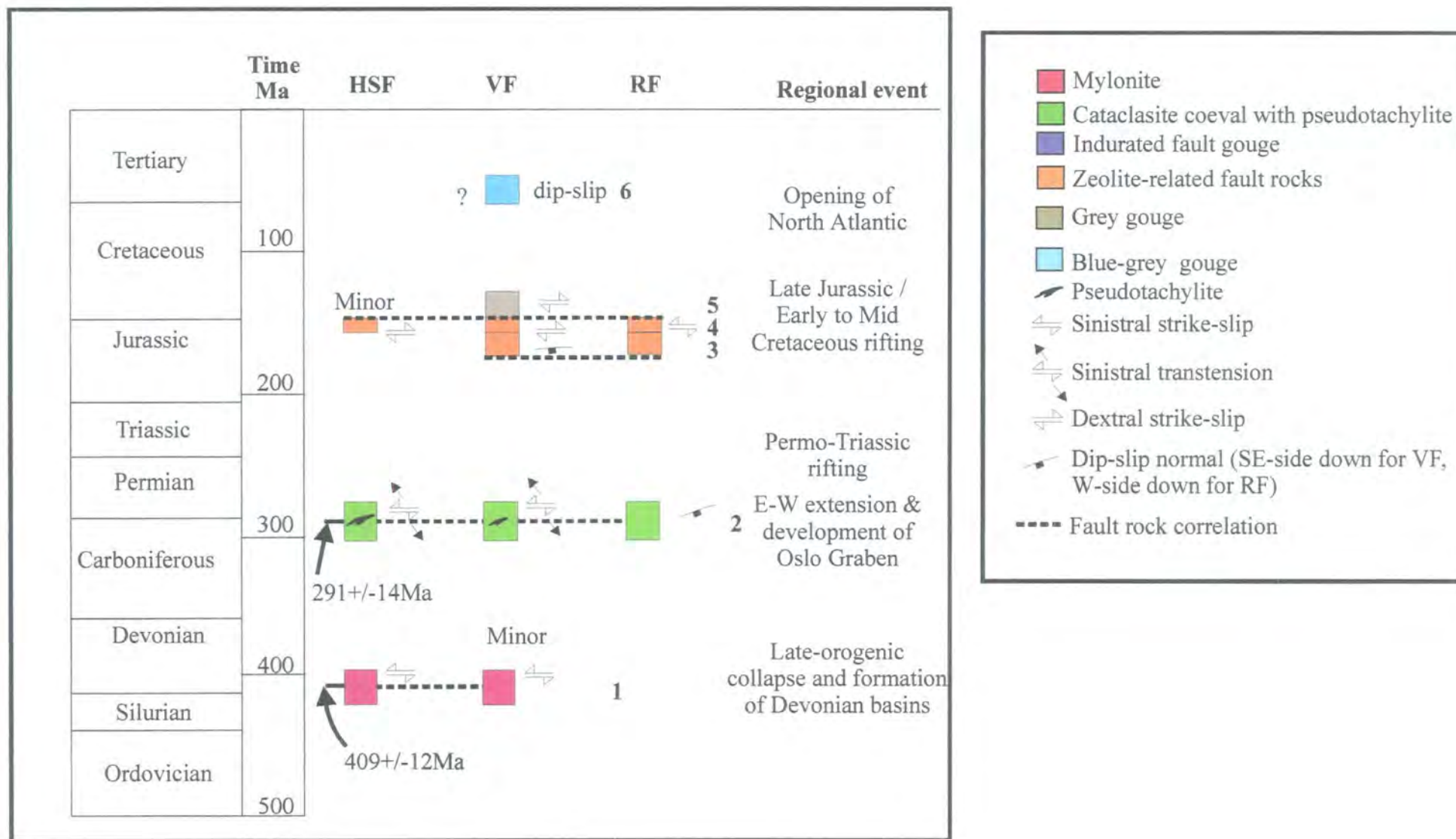


Figure 8.4 Time diagram to show fault-rock correlation, kinematic evolution and timing for the HSF, VF and RF of the MTFC. Fault-rock correlation based upon fault rock distribution, overprinting relationships and fault-zone structure. Timing based upon fault-rock dating (mylonite and pseudotachylite along the HSF; see section 7:2) and previous work (mainly offshore stratigraphic relationships with the MTFC; section 5:3).

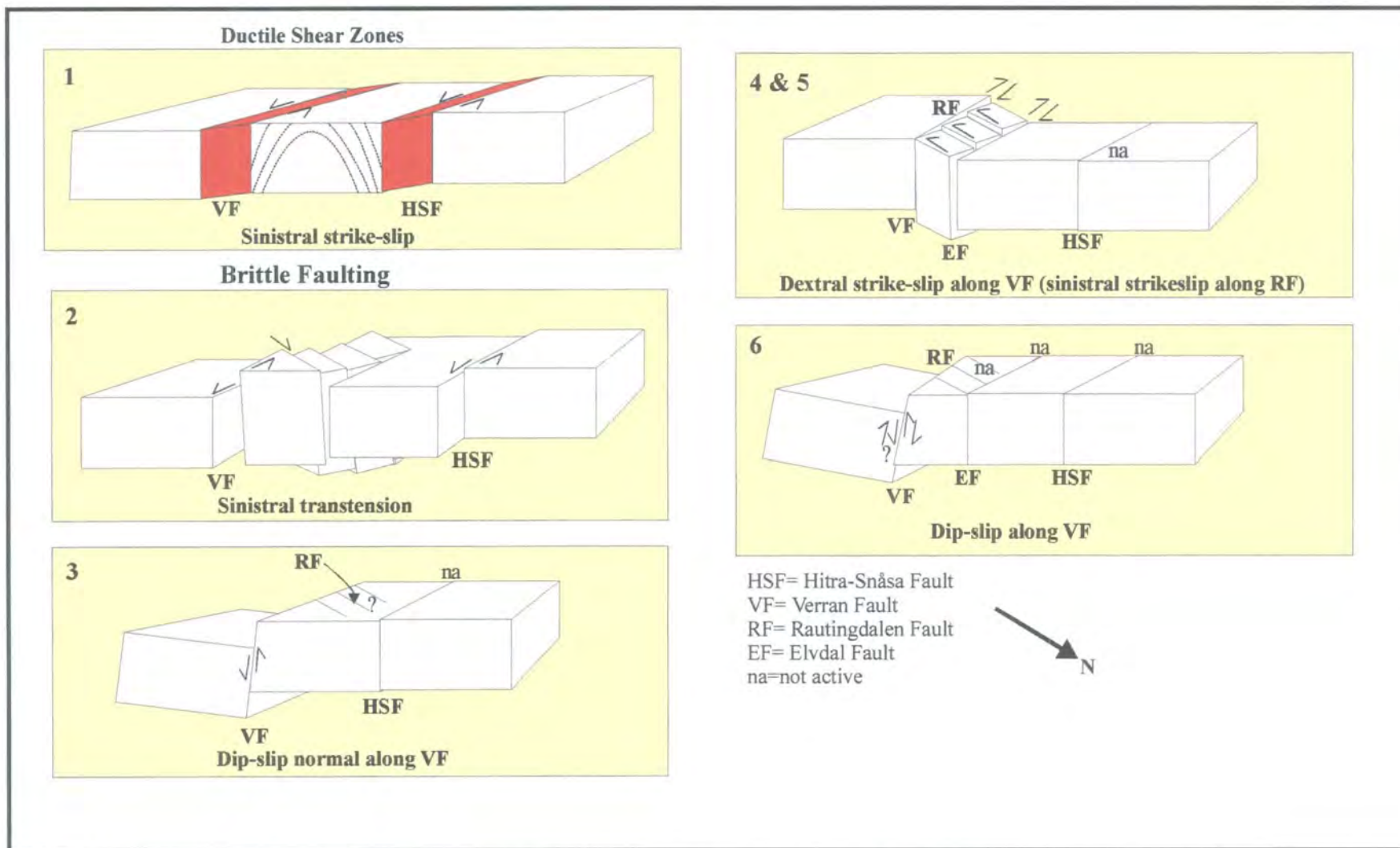


Figure 8-5 Schematic diagram to show the structural evolution of MTFC (1-6 refer to those events on Figure 8.4).

It is, therefore, possible that the HSFZ was locally reactivated to different degrees in certain fault zone segments along strike, although there are no complete sections through the fault core to the southwest or northeast of Mefjellet to prove or disprove this.

The VFZ comprises a 0.5km-wide zone of intense cataclastic deformation together with extensive hydrothermal alteration and mineralisation of the wall rocks. The earliest fault rocks are rare mylonites formed during sinistral shearing (Figures 8.4, 8.5) that are exposed at only one locality along the VFZ (see section 6:4:2). These are correlated with mylonites along the HSFZ (Figure 8.4), as they display similar overprinting relationships, textures and microstructures (see sections 7:1:2; 7:4:2). Later cataclasite assemblages and indurated fault gouges (not found along the HSF), and minor pseudotachylite veins, were formed during sinistral transtension. During this phase of sinistral transtension, a series of N-S-trending extensional faults, such as the RF, formed on all scales and linked into the sinistral strike-slip, ENE-WSW-trending VF. This led to the development of an extensive fracture/ fault-related permeability and the present-day, brittle-fault geometry of the MTFC. Later reactivation comprised dip-slip normal movements followed closely by dextral strike-slip, which led to the development of extensive zeolite- and calcite-mineralised breccias and gouges (Figures 8.4, 8.5). During the dextral strike-slip movements along the VF, the N-S-trending faults (e.g., RF) were reactivated as sinistral strike-slip, R'-type Riedel shears to accommodate block rotations on a kilometre scale (Figure 8.5). This event is interpreted to be of Late Jurassic to Early Cretaceous age based upon sedimentary and structural relationships within the Beitstadfjorden Basin (Bøe and Bjerkli 1989) (see section 5:3:2:1). The zeolite- and calcite-mineralised breccias and gouges are consistently cross-cut by grey gouges, also associated with dextral strike-slip. A blue-grey gouge represents the most recent phase of movement and contains a strong dip-slip lineation.

8:2:1:1 Summary

These two major faults seem to have broadly initiated as sinistral shear zones that formed part of a single system during Early Devonian times (409 ± 12 Ma). Permo-

Carboniferous sinistral transtensional reactivation (291 ± 14 Ma) along the MTFC led to the development of cataclasites, pseudotachylites and indurated fault gouges. The location of reactivation shifted towards the VF during the Mesozoic, while the HSF remained mainly inactive. Along the VF and N-S linking structures (eg., RF), multiphase brecciation, mineralisation and gouge development occurred during a sequence of dip-slip and dextral strike-slip (sinistral along N-S structures) movements not recognised along the HSF.

8:2:2 Timing, regional implications and displacement magnitudes

There have been many, partly conflicting accounts of the kinematic history of the MTFC in the literature. The earliest recognised movement based on field evidence is ductile, sinistral strike-slip, which has generally been regarded as Devonian age (Grønlie and Roberts 1989; Torsvik et al. 1989; Grønlie et al. 1991; Séranne 1992b; Roberts 1998a). This is consistent with the earliest recognised fault-related deformation described in the present study and dated at 409 ± 12 Ma (Figure 8.4). Some authors have suggested that a precursor fault in the basement may have caused deflections (to the NE) in the regional E- to SE-directed thrust transport during the Scandian orogeny (Grønlie and Roberts 1989; Séranne 1992a)

The early sinistral movements on the MTFC are broadly coeval with an unconformity in the Hitra Basin, which separates Uppermost Silurian rocks from Lower Devonian sedimentary rocks, and also with top-SW movements along the Høybakkken detachment. The latter structure is situated to the north of the MTFC and developed synchronous with the deposition of Lower to Middle Devonian sedimentary rocks. Top-SW, ductile shear zones in the Banded Gneiss Complex (BGC) of southwest Fosen are dated at 389 ± 6 and 386 ± 6 Ma (Rb-Sr, muscovite; Piasecki and Cliff 1988), and are thought to be broadly contemporaneous with early movements along the MTFC and late-orogenic collapse. These dates are broadly similar to those of the present study. Séranne (1992a) suggested that during the sinistral strike-slip movements, Devonian basins formed in extensional detachments within releasing bends along the MTFC.

In western Norway, HP/UHP metamorphic rocks dated between 400 and 420Ma are juxtaposed against Middle Devonian sedimentary rocks (c.390Ma) across W-dipping detachments. Krabbendam and Dewey (1998) suggested sinistral transtension with an increasing transtensional angle towards the MTFC as an exhumation mechanism for the Western Gneiss Region (WGR). In the present study, structures and fabrics contemporaneous with the regional-scale antiformal structure which lies between the VF and the HSF in the basement gneisses are consistent with regional sinistral transtension (section 6:2). Field evidence suggests that the sinistral strike-slip shear zones of the MTFC are superimposed on this regional fold structure. The findings of the present study are thus consistent with the Krabbendam and Dewey (1998) model of transtensional collapse at c.400Ma. However, in a more recent study, Terry et al. (2000) suggested that contraction was still going on at depth at c.401Ma, while at the same time sedimentary rocks were being deposited in the extensional Hitra Basin, situated north of the MTFC. Hence, sinistral movements on the MTFC were coeval with the early stages of extensional collapse, that was occurring in some places at the same time as subduction of Baltica beneath Laurentia, with its associated UHP metamorphism.

Braathen et al. (2000) suggested that north of the MTFC, bi-directional opposed extension led to the exhumation of the Central Norway Basement Window, whereas to the south unidirectional (top-WSW) extension dominated. As a result, Braathen et al. (2000), suggested that the MTFC formed as a sinistral strike-slip transfer structure between the SW-dipping Høybakken detachment and the NE-dipping Kollstraumen detachment, to the southwest and northeast, respectively (Figure 8.6). Extensional movements along the Kollstraumen and Høybakken detachments related to late-orogenic collapse are dated at c.400Ma, which fits in with the timing of sinistral shear along the MTFC in the present study.

Gilotti and Hull (1993) disagreed with published geological maps and observed the same rock type on either side of the HSF, suggesting that displacements could not have been large along the HSF. This is consistent with the present study, inferring that displacements along the MTFC can be no more than several tens of kilometres.

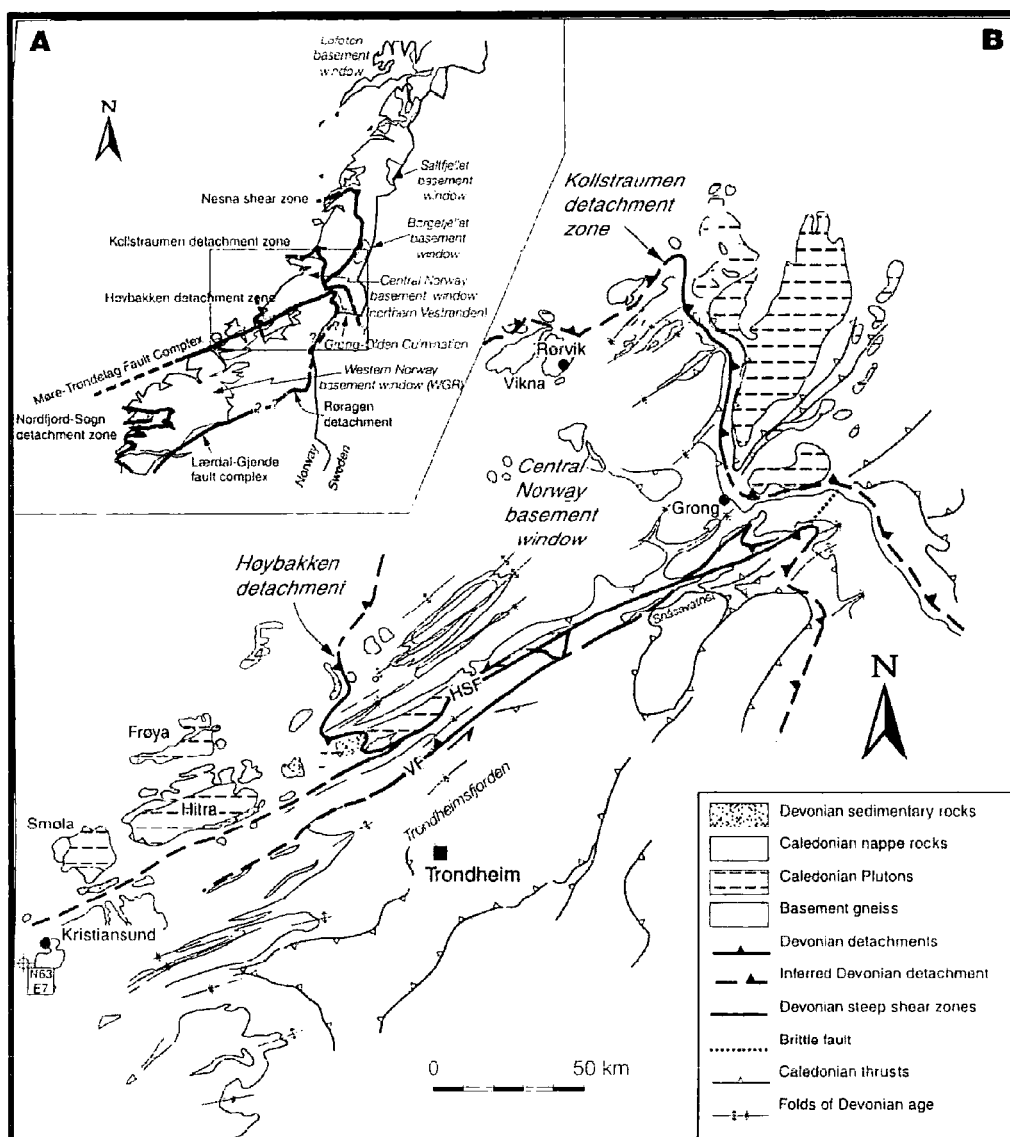


Figure 8.6 (A) Sketch map of central parts of the Scandinavian Caledonides, highlighting basement windows and Early-Middle Devonian faults and shear zones. (B) Tectonic map of Trondheimsfjorden, locating MTFC, and the Høybakken and Kollstraumen detachment zones. HSF - Hitra-Snåsa Fault, VF - Verran Fault (After Braathen et al. 2000).

Later brittle reactivations along the MTFC have been described as Late Devonian/ Early Carboniferous, Permian, Late Jurassic/ Early Cretaceous and Late Cretaceous/ Early Tertiary based upon isotopic (Sm-Nd, K-Ar) and fission track dating, and palaeomagnetic studies (Figure 8.7; Torsvik et al 1989; Grønlie and Torsvik 1989; Grønlie et al. 1990, 1994; Smith 1995).

Grønlie and Roberts (1989) and Grønlie et al. (1991) recognised an initial, ductile, sinistral strike-slip event overprinted by three generations of brittle structures. The earliest, sinistral strike-slip brittle structures were considered to be of Late Devonian /Early Carboniferous age. The earliest brittle reactivation recognised in the present study is associated with sinistral transtension (Figure 8.4), which has been dated to Permo-Carboniferous age (291 ± 14 Ma). This sinistral transtensional event has not previously been described in the literature and is coeval with E-W extension and the development of the N-S-trending Oslo Rift (Pedersen et al. 1995; Heeremans et al. 1996; Torsvik et al. 1998). K-feldspar thermochronology in southern Norway indicates rapid cooling with possibly 2-4 km of exhumation during the Permo-Carboniferous (~300 Ma) (Dunlap and Fossen 1998), which is coeval with the development of the Oslo Rift and sinistral transtension along the MTFC.

Grønlie and Roberts (1989) noted that the locus of reactivation switched to the VF. This is corroborated by the present study, where the HSF appears to have largely remained inactive in post Permo-Carboniferous times (Figure 8.4). The next phase of reactivation recognised in this study was dip-slip normal followed by dextral strike-slip movements along the VF, which was associated with extensive zeolite mineralisation. Grønlie and Roberts (1989) and Grønlie et al. (1991) also recognised these events and their association with zeolite mineralisation. The dip-slip normal movement is interpreted to be of post-Mid Jurassic age, based upon a 250 m-thick Jurassic succession in the hangingwall of the VF in the Beitstadvjorden basin (Bøe and Bjerkli 1989). This event is coeval with Late Jurassic to Early Cretaceous rifting in the North Sea. Offshore to the southwest, the MTFC apparently defines the southern margin of the Møre Basin. There, the MTFC comprises a series of fault-controlled ridges, highs and half-grabens (Grunnaleite and Gabrielsen 1995).

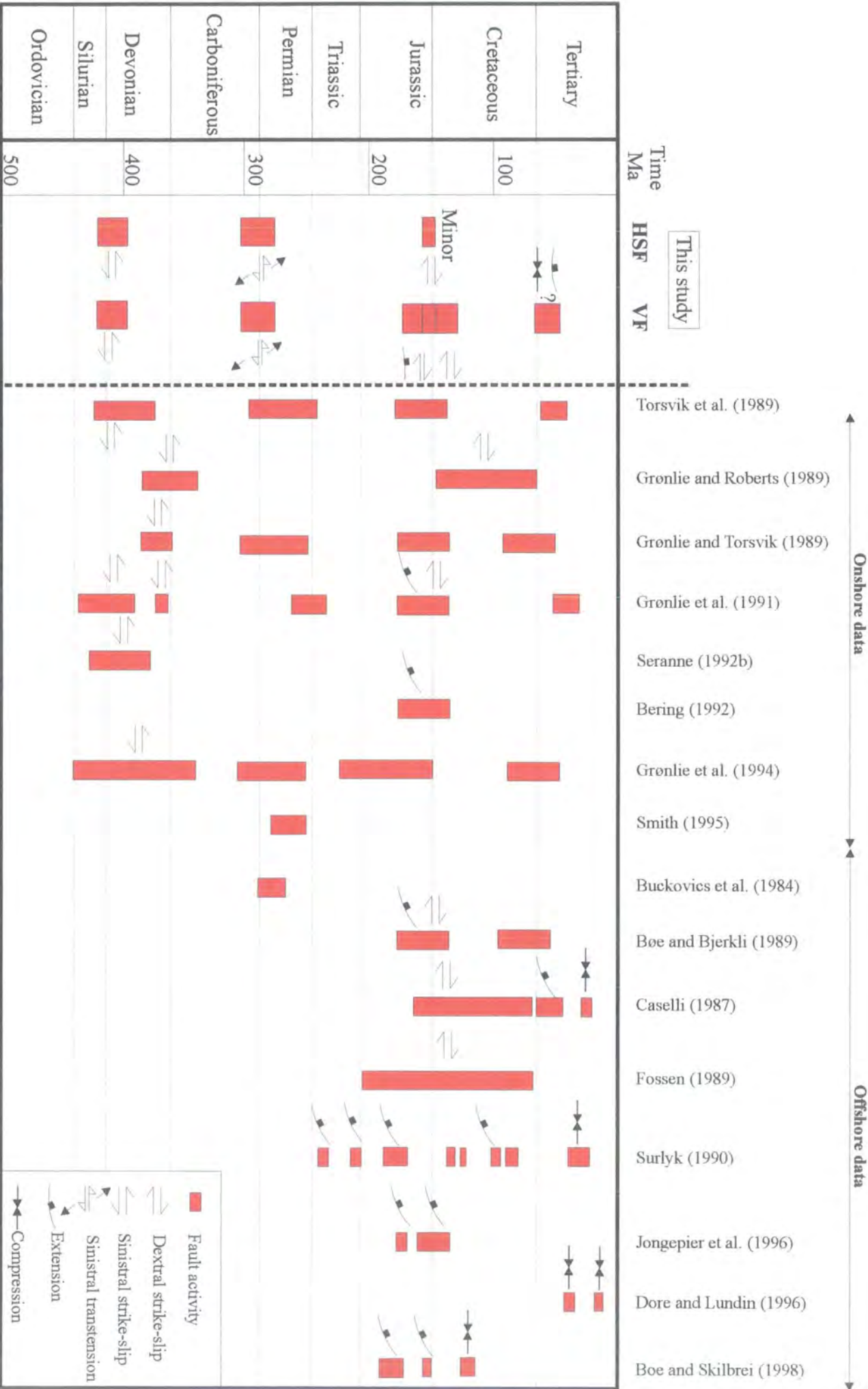


Figure 8.7 Diagram to compare the kinematic history of the MTFC from this study to previous work.

The vertical throw of the near base Cretaceous is c.5km, which was interpreted to be related to late Mid to Early Cretaceous rifting, as post-Lower Cretaceous sedimentary rocks onlap onto the truncated fault blocks (Grunnaleite and Gabrielsen 1995).

Bøe and Bjerkli (1989) also recognised a later phase of dextral strike-slip movement based upon N-S-trending folds and a series of sinistral offsets of the VF trace by N-S-trending faults within the Beitstadfjord Basin, inferring dextral strike-slip movements along the VF that are consistent with the present study (zeolite fault rocks, Figure 8.4). Bøe and Bjerkli (1989) also suggested that these N-S-trending folds were transected by the VF and inferred a later event, possibly Early Cretaceous or Tertiary. This is consistent with the present study where a later phase of dextral strike-slip (post-dating zeolite) and dip-slip faulting are recognised (Figure 8.4). These relationships were also recognised in the Edøyfjorden Basin to the southwest of Fosen (Bøe and Bjerkli 1989). In the Edøyfjorden Basin (section 5:3:2:2), both the VF and the HSF were recognised to have dip-slip normal displacements of no more than 1km.

The age of the latest phase of reactivation along the MTFC is uncertain. Several authors have recognised NE-SW compressional structures within the Møre Basin of Mid-Tertiary age (Figure 8.7). A NW-SE compression across the MTFC is consistent with the most recent dip-slip phase recognised in this study. Other authors have suggested an Early Cretaceous inversion event along the MTFC (Grunnaleite and Gabrielsen 1995; Bøe and Bjerkli 1998). Fission-track dating of fluorite mineralisation in one area, east of Beitstadfjord, has yielded a Late Cretaceous to Tertiary age for this hydrothermal activity (Grønlie et al. 1990). In a recent study, Pascal and Gabrielsen (2001) noted that the MTFC separates an area with abundant Cenozoic compressional structures to the north (e.g., Møre Basin, Doré and Lundin 1996) from an area of relative tectonic quiescence to the south (e.g., northern North Sea). Stress modelling suggests that the MTFC acted as a shield to SE-directed ridge push forces to the south (Pascal and Gabrielsen 2001), inferring oblique or reverse movements, possibly consistent with the most recent (dip-slip; Figure 8.4) movement recognised in this study.

Pascal and Gabrielsen also suggested a recent dextral strike-slip component along the MTFC based on present-day stress patterns observed on the Norwegian continental

shelf. Other authors have stated that the MTFC is still tectonically active offshore to the south of the Møre Basin (Ringdal 1983; Bungum et al. 1991; Lindholm et al. 1995).

8:2:3 Textural and microstructural evolution

The aim of this section is to summarise the textural and microstructural evolution exhibited by fault rocks along the MTFC as a basis for the discussion of possible fault-zone weakening mechanisms (section 8:4).

The earliest recognised, fault-related deformation along the HSF and the VF led to the development of upper greenschist-facies mylonites consistent with sinistral shear (Figure 8.8). The mylonites are derived from banded gneiss along the HSF and tectonised granite along the VF. Both protoliths are characterised by granoblastic textures where feldspar grains form interlocking aggregates that isolate quartz, epidote and micas. The onset of viscous creep in feldspar typically occurs at $\sim 450^{\circ}\text{C}$, while in quartz and micas it occurs at $\sim 300^{\circ}\text{C}$. Thus, at any given temperature, feldspar is significantly stronger than quartz and mica. These observations, together with the textures described in section 7:1:1 and 7:4:1, suggest that both protoliths display a LBF-microstructure (section 1:6:4), where the rheology of the rock is controlled by the rheology of the feldspar grains.

The quartzo-feldspathic mylonites comprise 'rigid' feldspar porphyroclasts, which are wrapped by a network of polygonal quartz ribbons and bands of fine-grained white mica and feldspar. The porphyroclasts display relatively low aspect ratios and appear to be comparatively undeformed. In contrast, the quartz ribbons and muscovite-rich bands, which form an interconnected network, display comparatively high aspect ratios and appear to be very highly strained. The mylonites thus display IWL-microstructures (Figure 8.8; sections 1:6:4, 1:7:2:3a). These observations suggest that the rheological behaviour of the highly strained mylonitic fault rocks was primarily controlled by the rheological behaviour of the quartz ribbons and muscovite-rich bands (IWL) (Handy 1990). Also, highly-strained mylonites along both the VF and the HSF display widespread evidence for the syn-tectonic retrogression of feldspar to white mica.

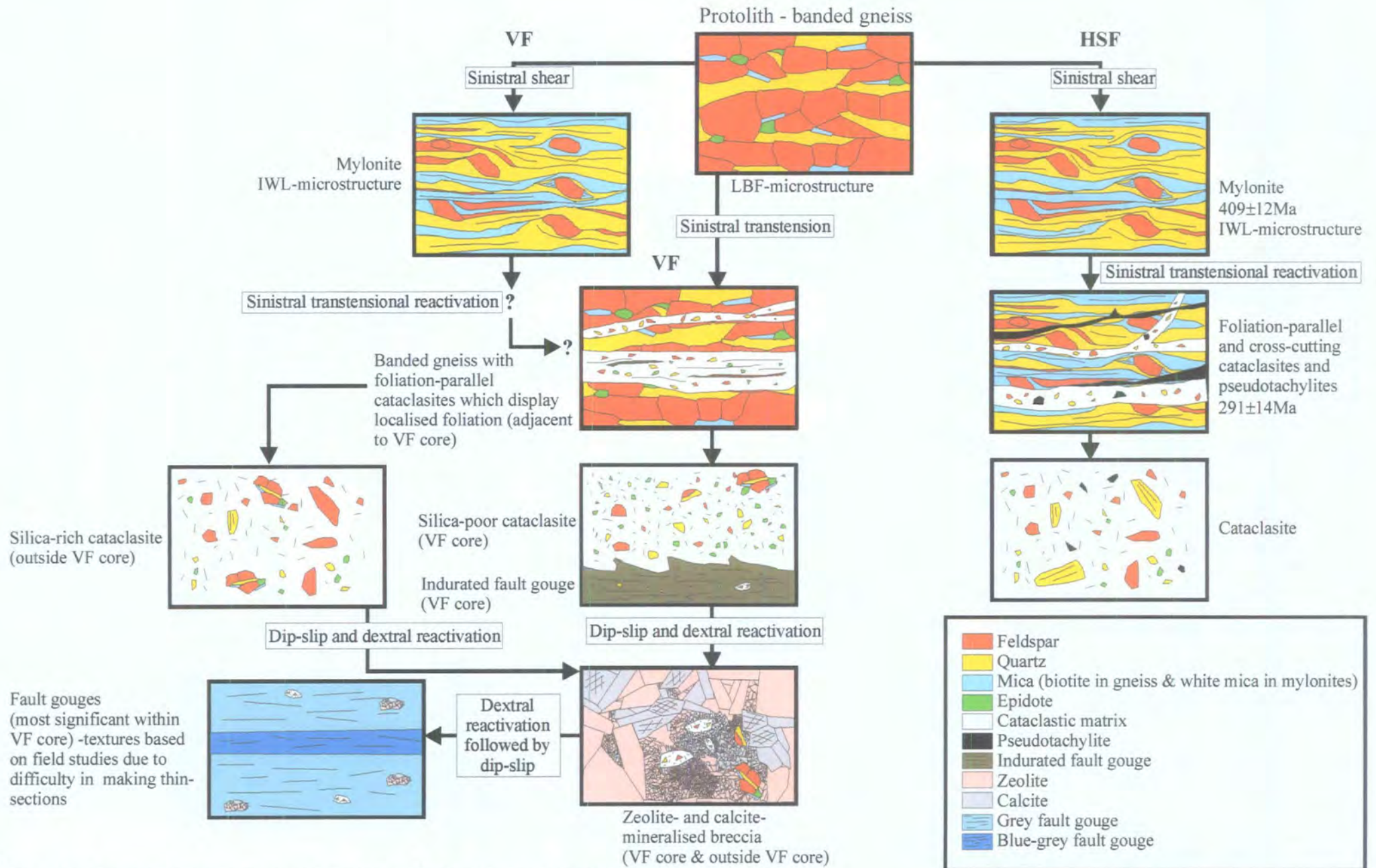


Figure 8.8 Schematic diagram to illustrate the evolution of fault rock textures along the VF and HSF.

Therefore, the age of white mica growth, $409 \pm 12\text{Ma}$, is interpreted to date mylonitisation along the HSF. The breakdown of the LBF to an IWL-microstructure was strain induced and caused by crystal-plastic deformation of quartz and fracturing and retrogression of feldspar to 'weaker' white mica (sections 7:1:2:1, 7:4:2).

The quartz and mica grains display evidence for widespread dynamic recrystallisation. This is consistent with syn-tectonic temperatures greater than $\sim 250\text{--}300^\circ\text{C}$, while the frictional straining of feldspars places an upper limit on probable temperature estimation, suggesting temperatures below 500°C (the temperature marking the onset of crystal plasticity in feldspar) (see section 1:6:3). Mylonites along the HSFZ therefore formed at depths of 10-15km or around the level of the frictional to viscous transition (1:6:5) (assuming an average geothermal gradient of 30°C/km).

Uplift / exhumation of the fault zone followed the cessation of the viscous creep deformation mechanisms.

Frictional, brittle reactivation of the HSFZ (sinistral transtension) led to the development of cataclasites and pseudotachylites, which localised in the central part of the fault zone parallel to the foliation (where the mylonites are finer-grained, mica-rich and display a strong foliation) (Figure 8.8). This event is dated at $291 \pm 14\text{Ma}$ based on $^{40}\text{Ar}\text{--}^{39}\text{Ar}$ ages of pseudotachylite (section 7:2). The dominant deformation mechanisms are considered to be cataclastic flow (mechanical disaggregation and grain-size diminution) in and between grains, grain boundary sliding and pressure solution. Quartz, feldspar and mica all deformed by cataclasis, indicating temperatures of less than 250°C (section 1:6:3). The presence of pyrophyllite and illite, formed from the alteration of K-feldspar accompanied by pressure solution indicates temperatures of approximately 200°C (L. Warr. pers. comm., 2000). The pseudotachylites formed as a result of high strain rates along the HSFZ, which led to rapid frictional sliding and resulted in localised melting of the wall rocks along the foliation-parallel fault networks. The pseudotachylites are interpreted to have formed within the host-rock below $\sim 300^\circ\text{C}$ at depths of less than 10km (using an average geothermal gradient of 30°C/km), as no argon loss was observed in the micas within the wall rocks (S.C. Sherlock, pers.comm. 2001; section 7:2).

Brittle reactivation (sinistral transtension) of the VFZ led to the development of cataclasites, minor pseudotachylites and indurated fault gouge, together with the creation of a large fracture-controlled permeability (Figure 8.8). Wall-rocks along the VFZ suffered intense post-tectonic alteration to sericite, illite and pyrophyllite, due to the post-tectonic influx of hydrous fluid through the extensive fracture network. The dominant deformation mechanisms appear to be cataclastic flow (mechanical disaggregation and grain-size diminution) in and between grains, grain boundary sliding and pressure solution. Quartz, feldspar and mica all deformed by cataclasis, indicating temperatures of less than 250°C (section 1:6:3; Passchier and Trouw 1996).

Cataclasites within the VF core are depleted (~15wt%) in SiO₂ while cataclasites outside the fault core are enriched (~5wt%) in SiO₂ (Figure 8.8). This depletion within the VF core is interpreted to be the result of fluid-assisted DMT processes, which remove silica from the fault core and precipitate it in voids within cataclasites outside the fault core. LOI is also greatest within the VF core cataclasites, possibly inferring a greater volume loss than the other fault rocks (c.f. Condie and Sinha 1996). Fluid-rich conditions along the VF may also explain the lack of pseudotachylites along the VF compared to the relatively 'dry' HSF. The presence of pyrophyllite in the coeval indurated fault gouge, which is formed from the breakdown of K-feldspar, indicates temperatures of approximately 200°C (L. Warr pers. comm. 2000). Therefore, the cataclasites along the VFZ formed at temperatures between approximately 200° and 250°C or at depths of 6-8km, assuming an average geothermal gradient of 30°C/km.

Several later phases of reactivation and localisation occurred along and within the pre-existing fault rocks of the VFZ but not along the HSF (Figure 8.8). Frictional deformation at depths of less than 5km led to the formation of zeolite- and calcite-mineralised breccias, and a series of Ca-smectite-rich fault gouges.

8:3 Regional synthesis and possible fault-zone linkages

It has been suggested in the literature, based on apparent offshore trends, that the MTFC and the WBF may have been linked at some stage during their evolution and subsequent reactivation (Norton et al. 1987; Ziegler 1987; Grønlie and Roberts 1989; Séranne 1992b; Blystad 1995). This is apparently consistent with the present study as early movements along both the WBF and the MTFC are sinistral. If applied to pre-Devonian times, this correlation would conflict with traditional Caledonian models, since it would require linkage of shears intersecting Baltican and Laurentian basement complexes that were originally situated on opposite sides of the Iapetus Ocean (Doré et al. 1997a). It therefore seems more reasonable to suggest that these structures could have become linked during the Mesozoic, or at earliest in Mid Palaeozoic (earliest Devonian) time (e.g., Grønlie and Roberts 1989), or that the correlation could be based upon a chance alignment of structures. A more thorough understanding of the regional tectonic framework from Late Palaeozoic to Mesozoic times is therefore needed in order to assess possible fault-zone linkages between the WBF and the MTFC.

The Caledonides along the North Atlantic margin developed as a result of the closure of the Iapetus Ocean. Two major continental landmasses collided, Laurentia to the west and Baltica to the east, and a microcontinent (Avalonia) to the south, to form the supercontinent Laurussia (Figure 8.9; Soper et al. 1992). At c.440Ma, nappe stacking was well underway in the Scottish Highlands, while Baltica was rotating anticlockwise and moving northwestwards and Avalonia was migrating northwards. Baltica eventually collided with Laurentia by c.420Ma, resulting in intense thrusting in the Scandinavian (Scandian phase), East Greenland and Scottish Caledonides (Figure 8.9). In Norway convergence was still occurring at depth while late-orogenic collapse was active at upper crustal levels. It is inferred that a major network of NE-SW, sinistral, strike-slip faults developed due to the oblique nature of convergence (Soper et al. 1992). During these times, both the WBF and the MTFC appeared to have initiated as sinistral strike-slip structures. Early movements along the WBF are thought to have taken place at c.430 to c.380Ma, while movements along the MTFC occurred during the period c.410 to c.390Ma.

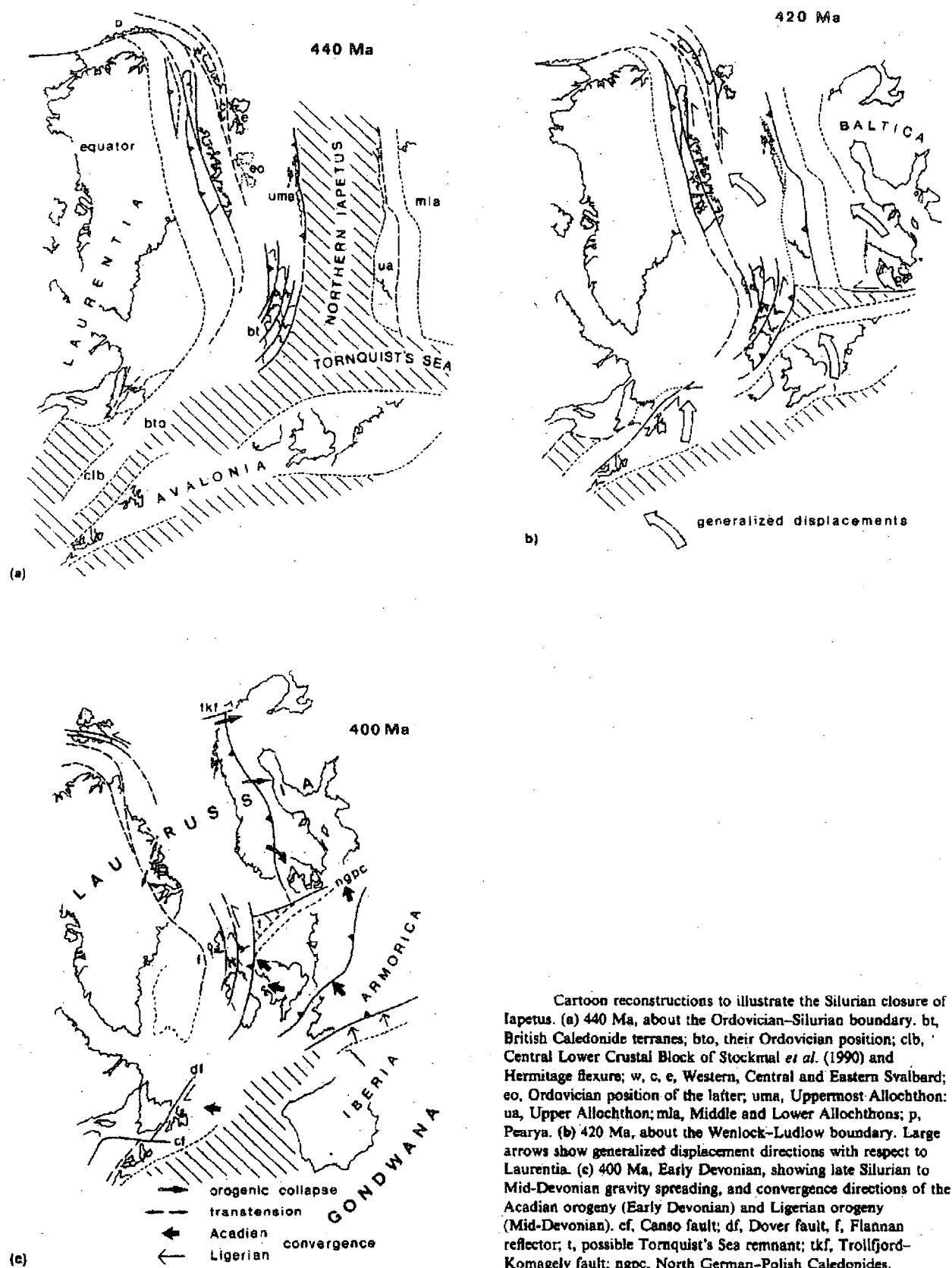


Figure 8.9 Cartoon sketches to illustrate the closure of the Iapetus Ocean from 440 to 400 Ma (after Soper et al. 1992).

The fact that these movements are kinematically similar and occurred at broadly the same time suggests that they could theoretically be linked. The formation of the MTFC was probably related to late-orogenic collapse in Central Norway due to the close association of the Høybakken detachment (Braathen et al. 2000) and regional sinistral transtensional collapse as proposed by Krabbendam and Dewey (1998). Early sinistral movements along the WBF (c.430Ma) were probably related to oblique convergence. However, sinistral movements continued to c.380Ma and therefore could also be related to late-orogenic collapse, as suggested by Séranne (1992a). In view of the regional tectonic framework during these times, many faults of a similar orientation (NE-SW) would have displayed similar kinematics. It seems that the formation of the WBF and MTFC were related to the same regional tectonic processes and therefore shared similar kinematics (Figures 8.1, 8.4). However, there seems to be no compelling reason to justify fault linkages solely on the basis that they share a similar regional tectonic origin.

Both the WBF and the MTFC were reactivated in Permo-Carboniferous times (Figures 8.1, 8.4). During the Permo-Carboniferous, the Gondwana continent together with a series of microplates (e.g., Iberia, Armorica and Alpine) moved northwards and collided with the Laurussian plate (Baltica, Laurentia, Avalonia), resulting in the Variscan orogeny and the formation of the Pangea supercontinent (Figure 8.10; Warr 2000). In the British Isles, the most intense Variscan deformation resulted in the E-W-trending thrust and fold belts of Southwest England and South Wales. To the south of Britain, a braided zone of E-W-trending dextral strike-slip faults formed due to continued oblique convergence (Arthaud and Matte 1977). In Scotland, the final stages of the Variscan orogeny led to inversion (NE-SW to E-W compression) of the earlier formed Devonian and Carboniferous basins (Coward et al. 1989). Farther north, in East Greenland and Norway, E-W extension (Figure 8.11) led to extensive magmatism and the development of a series of rift basins (e.g., Oslo Graben, Heeremans et al. 1996). At these times, sinistral transtension occurred along the MTFC, whilst dextral strike-slip movements characterised the WBF (Figures 8.1, 8.4). It thus seems unlikely that the structures were linked during the Permo-Carboniferous, as sinistral transtension along the MTFC was related to regional E-W extension, whilst dextral strike-slip movements along the WBF were related to NE-SW compression and inversion of the Orcadian basin (Figures 8.1, 8.4).

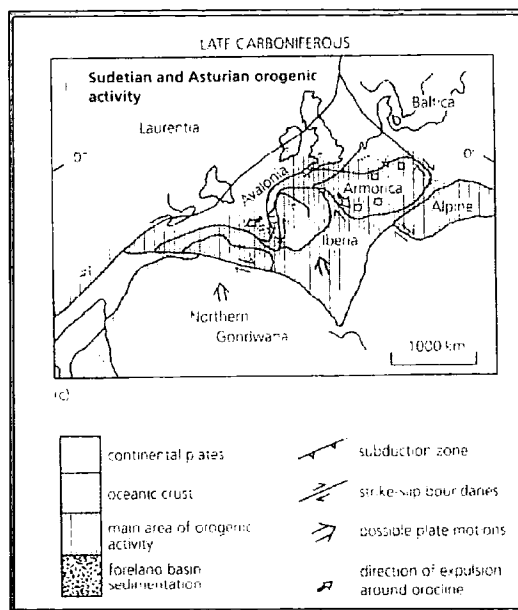


Figure 8.10 Schematic diagram to show the final amalgamation of Pangea in the Late Carboniferous (after Warr 2001).

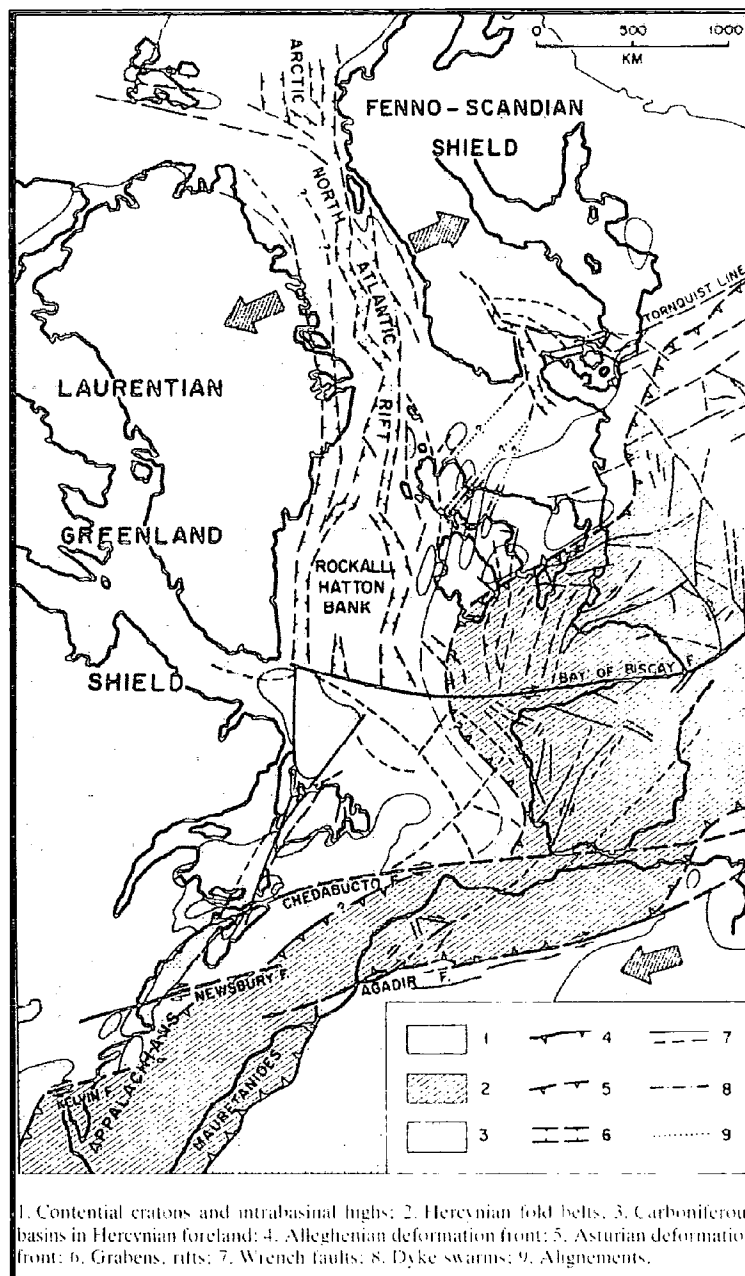


Figure 8.11 Permo-Carboniferous tectonic framework of the North Atlantic region (after Ziegler 1982).

More extensive rifting occurred in Permo-Triassic and Late Jurassic / Early Cretaceous times in the North Atlantic region. Permo-Triassic rifting formed a series of rift basins (e.g., West Shetland and Unst Basins, Figure 8.12) which display no consistent extension direction, suggesting a mosaic-like fragmentation of the inherently unstable supercontinent of Pangea (Doré et al. 1999). No evidence of Permo-Triassic extension along the WBF and the MTFC has been identified in this study.

The most extensive period of rifting occurred in the Late Jurassic / Early Cretaceous and led to the development of a series of N-S-trending rift basins (e.g., Viking Graben, East Greenland Rift and the Halten Terrace) under a component of E-W regional extension (Figure 8.13). The Shetland Platform was uplifted in the footwall of the Viking Graben during this event. In the Early to Mid Cretaceous, as Atlantic spreading propagated northwards, the extension direction switched to ENE-WSW resulting in a series of NE-SW basins (e.g., Møre and Faroe-Shetland Basins, Figure 8.13). During the Late Jurassic or Early to Mid Cretaceous, the ENE-WSW-trending MTFC experienced a period of extension followed by dextral strike-slip movements (Figure 8.4). Linkages of the WBF and MTFC are unlikely during these times as there appears to be little evidence of significant extensional movements along the WBF at this time; and there is an absence of faults of Jurassic to Cretaceous age on the Shetland Platform.

Final continental break up along the North Atlantic margin occurred during the Eocene and was associated with extensive magmatism in the Faroe-Shetland and Møre Basins (Figure 8.13). The most recent movements along the MTFC and WBF are difficult to resolve in the regional tectonic framework. It is possible that sinistral movements along the N-S-trending WBF (Figure 8.1) are related to ESE-directed ridge push forces during post-Eocene times associated with spreading in the North Atlantic. Ridge push forces would also invoke a reverse movement along the MTFC (Figure 8.4), which is broadly consistent with the most recent movement detected in the present study. However, this is beyond the scope of this thesis and would require vigorous analysis of the structures offshore.

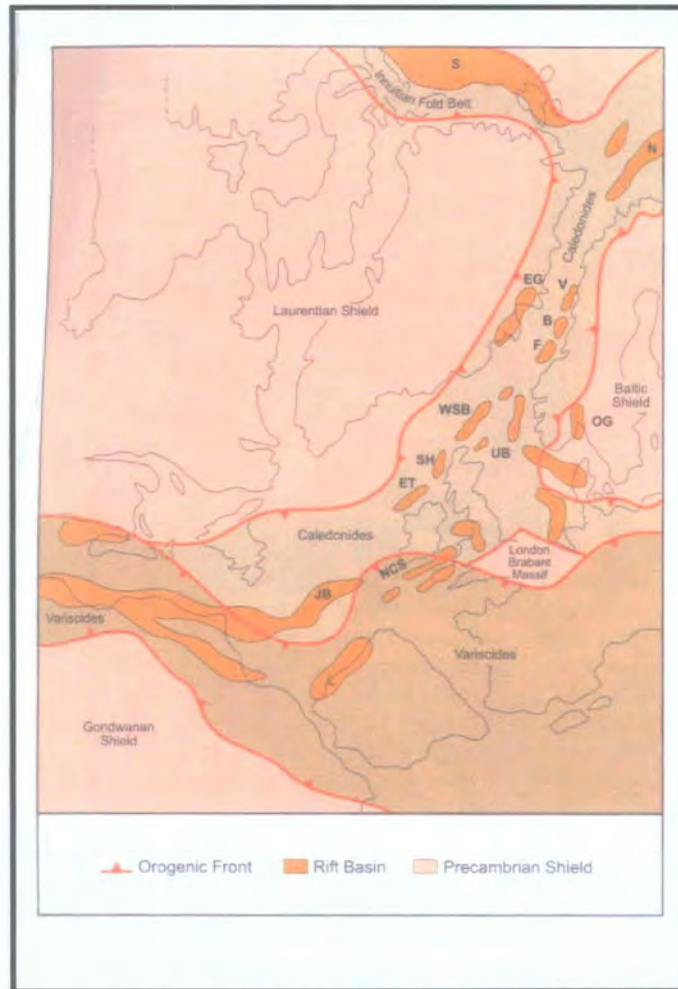


Figure 8.12 Pangean orogenic belts and Permo-Triassic basins (after Doré et al. 1999). S - Sverdrup Basin, N - Nordkapp Basin, EG - East Greenland Rift, V - Viking Graben, B - Bronnoysund Basin, F - Froan Basin, WSB - West Shetland Basin, UB - Unst Basin, ET - Erris Trough, OG - Oslo Graben, NCS - North Celtic Sea Basin, JB - Jeanne D'arc Basin.

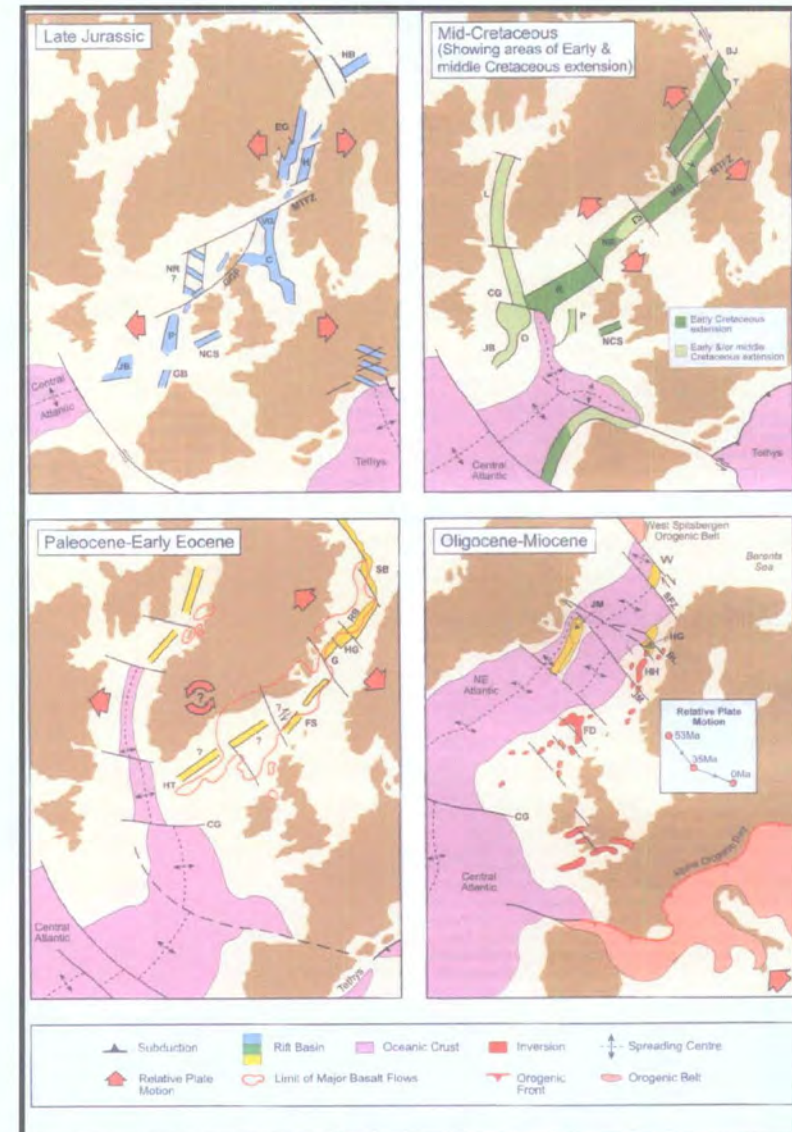


Figure 8.13 Plate reconstructions of the North Atlantic region - Late Jurassic, mid-Cretaceous, Paleocene and mid-Cenozoic, indicating relative plate motion, contemporaneous rifts and areas of inversion (after Doré et al. 1999). VG - Viking Graben, EG - East Greenland Rift, H - Halten Terrace, MB - More Basin, FS - Faeroe Shetland Basin.

8:4 Localisation and weakening processes

Field evidence acquired during this study has shown that both the MTFC and the WBFZ preserve evidence of repeated localisation or reactivation over long periods of geological time, suggesting that reactivation often occurs in preference to the formation of new structures. This suggests that reactivated fault zones may be weak relative to their surroundings. Several authors have suggested that operative weakening mechanisms along long-lived reactivated fault zones must affect the main load-bearing regions or the strongest parts of the lithosphere (upper mantle and mid crust). Recent studies of deeply-exhumed, crustal-scale, reactivated fault zones (Butler 1995; Imber et al. 1997; Stewart et al. 1997, 1999, 2000; Imber 1998; Holdsworth et al. 2001) have identified long-term weakening mechanisms such as *foliation weakening*, *reaction softening* and the onset of *fluid-assisted diffusional creep*. These processes are thought to shallow and narrow the frictional to viscous creep transition within the fault zone and, therefore, weaken the fault zone, resulting in these structures being more susceptible to reactivation in the long term (Figure 8.14).

Relatively little attention has been paid to the geometric controls on fault reactivation (Walsh et al. 2001). Walsh et al. (2001) argued that the geometrical properties of the fault system, such as size, position, orientation and connectivity, could be the principal control for reactivation. Many of the previous studies on fault-zone weakening have concentrated on large, well-connected, crustal-scale faults (Butler 1995; Imber et al. 1997; Stewart et al. 1997, 1999, 2000; Imber 1998; Holdsworth et al. 2001). Therefore, both the geometrical properties of these structures and the presence of 'weak' fault rocks may control fault reactivation. Large connected faults will thus be expected to form an effective IWL-structure. Numerical modelling has also shown that localisation can occur along faults that contain relatively 'strong' fault rocks, if the fault is of a sufficient size (Walsh et al. 2001).

The aim of the following sections is to provide some insights into the geometrical controls and potential long-term weakening mechanisms along the MTFC and WBFZ.

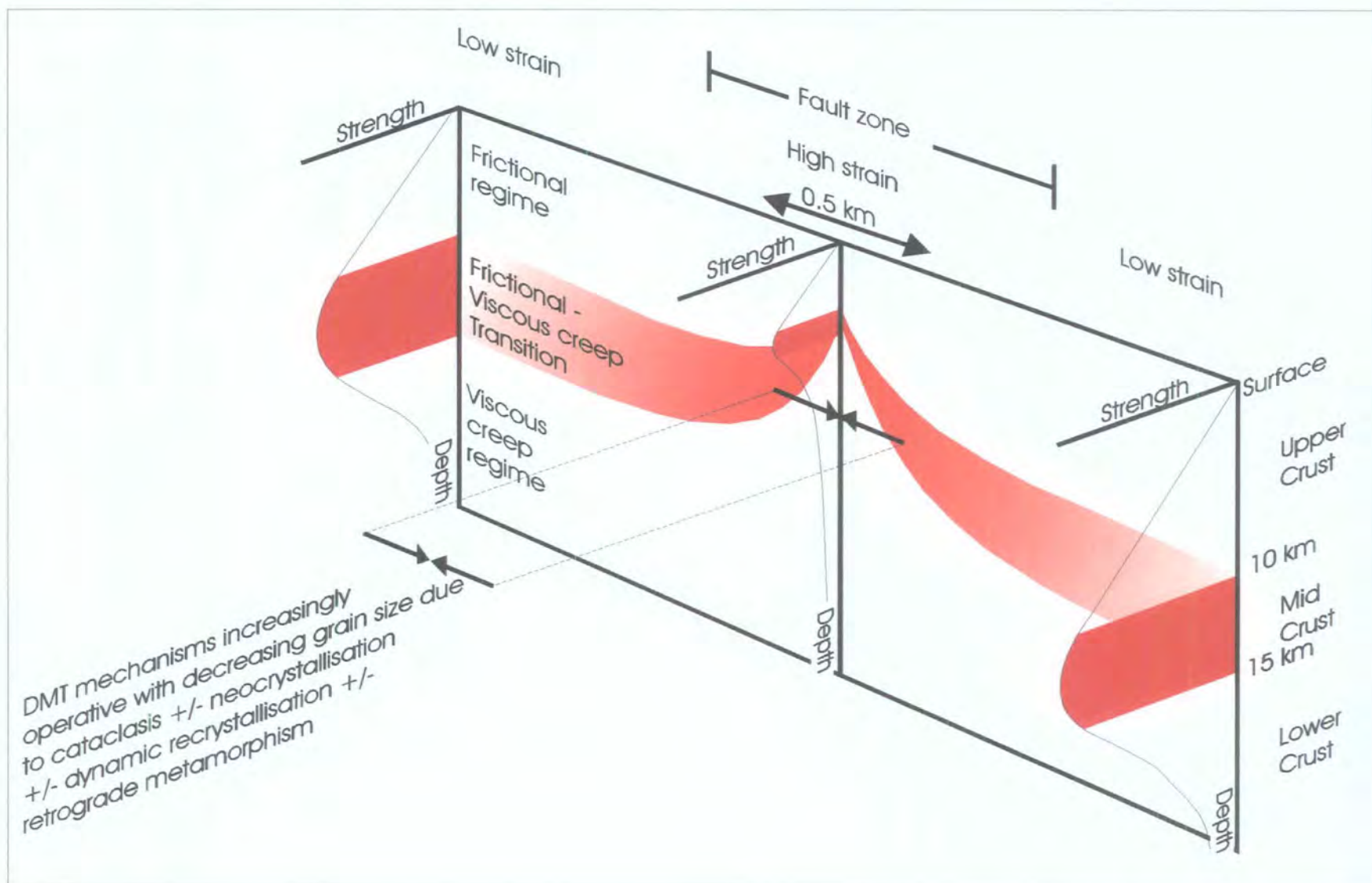


Figure 8.14 Schematic three-dimensional strength vs. depth profiles through a vertical, crustal-scale fault zone and adjacent wall rocks based in part upon text of Schmid and Handy (1991). In high-strain fault strands, the grainsize-controlled switch from frictional cataclasis to diffusional viscous creep leads to a shallowing of the transition zone and to weakening. The frictional to viscous transition narrows as the strain localises into the interconnected network of high-strain fault strands and the weakening rapidly spreads to affect the entire fault zone (compare protolith/low-strain and high-strain strength curves) (after Stewart et al. 2000).

8:4:2 'Weak' fault rocks

Many studies of reactivated, basement fault zones have suggested that the presence of 'weak' fault rocks near or around the level of the frictional to viscous creep transition may control later reactivation of the structure. In the present study, microstructural and textural investigations of fault rocks formed at or around this level have provided some insights into weakening mechanisms.

The two most important mechanisms identified in the present study are (a) *foliation weakening*, and (b) *reaction softening*.

Foliation weakening was observed within the earliest fault rocks (mylonites) formed along the WBFZ and the MTFC. The protolith gneisses along both the WBFZ and the MTFC display granoblastic textures, where strong minerals such as feldspar and hornblende isolate pockets of relatively 'weak' minerals such as quartz and micas. The rheology of these protoliths is controlled by the rheological behaviour of the strong minerals, and thus forms a LBF-microstructure (section 8:1:3, 8:2:3). As the rock starts to deform, the strong minerals (e.g., hornblende and feldspar) remain rigid and deform primarily by fracturing (Handy 1990). At the same time, the relatively weak minerals (e.g., quartz and mica) deform in a crystal-plastic manner. The plastically deformed minerals become stretched with increasing strain to such an extent that the weak phase becomes interconnected, and wraps around isolated, rigid porphyroclasts. This is known as an IWL-rheology, where the rheology of the interconnected weak phase controls the rheology of the rock. Therefore, the strain-induced breakdown of the LBF to an IWL-microstructure, known as foliation weakening, constitutes an important long-term weakening mechanism along the MTFC and the WBFZ.

Within the mylonites along the MTFC, *reaction softening*, through the chemical breakdown of feldspar, in the presence of hydrous fluids, to highly aligned aggregates of white mica, will enhance the process of foliation weakening (Jordan 1987; Handy 1990; Imber et al. 1997). White mica has a lower activation energy than feldspar with respect to dislocation glide, and is therefore weak over a wide range of crustal depths.

Along the WBFZ, *reaction softening* is an important process within early-formed cataclasites exposed at Brae Isthmus (section 4:2:2:2). Grain-size reduction by cataclasis promoted the influx of hydrous fluids by grain-scale dilatancy and the subsequent reaction softening of feldspar and hornblende to aggregates of sericite and chlorite. This led to the development of foliated cataclasites, which display an IWL-microstructure. These processes were widely recognised along the Outer Hebrides Fault Zone (Imber et al. 1997, 2001) and the Great Glen Fault Zone (Stewart et al. 2000; Holdsworth et al. 2001), and were thought to lead to the onset of grain-size sensitive, diffusion-dominated, diffusional creep, which led to a shallowing and narrowing of the frictional to viscous transition (Figure 8.14). The importance of the rocks exposed at Brae Isthmus is uncertain as it is difficult to ascertain whether these rocks are truly characteristic of the WBFZ. It is impossible to say whether this constitutes an important weakening process, due to the lack of evidence in outcrops along the WBFZ and the MTFC. It is possible that these rocks were once more widespread along the WBFZ but have been uplifted and eroded away or cut out by later reactivation along the WBF. This process was not observed in fault rocks along the MTFC, possibly due to the large amount of exhumation and erosion of the fault zones, thus exposing the wrong structural level, or that these processes did not occur at all along the MTFC (see discussion in next section).

Other studies have suggested that the presence of clay-rich fault gouge significantly weakens fault zones (Zoback et al. 1987; Morrow et al. 1992; Rice 1992; Wintsch et al. 1995). Along both the MTFC and the WBFZ, later reactivations were associated with the development of smectite-rich fault gouges. Experimental data suggest that smectite-rich fault gouges have a very low frictional strength, and are therefore very weak relative to the surrounding wall rocks (Byerlee 1978). However, the presence of these gouges is not likely to control fault reactivation at depth, as smectite is only stable at temperatures of less than 200°C or at depths of less than 6km (assuming an average geothermal gradient of 30°C/km) (Frey 1988). Water-swelling, impermeable clay minerals (e.g., smectite) also lead to a build up of pore-fluid pressure along fault zones and may promote fault valve behaviour (section 1:5:2). An increase in pore-fluid pressure causes a decrease in the effective normal stress across a pre-existing fault surface, and therefore causes brittle failure under differential stress conditions

that, in dry rocks, would otherwise be stable. Wintsch et al. (1995) stated that high pore-fluid pressures are very unlikely to be maintained in the long term and, thus, any weakening would only be effective in the short term.

Pegmatite intrusions are found within fault gouge along the WBFZ. Scholz (1990) suggested that the frictional resistance to brittle failure may drop if the fault is filled with hot fluid or magma. Handy et al. (2001) concluded that the introduction of melts may lead to localisation and short-term, syn-tectonic weakening, but on its own is unlikely to be important over long periods of geological time, as any short-term weakening would be counteracted by the effects of magma crystallisation.

8:4:2 Geometric controls on reactivation

Studies of the two main bounding structures of the MTFC may provide insights into the geometrical controls of fault reactivation. It has been well documented in this study that the HSF and the VF show heterogeneous kinematic histories. Both structures were initiated as ductile shear zones (Figures 8.4, 8.5), which led to the development of texturally and microstructurally similar fault rocks (Figure 8.8). Both structures were then reactivated during sinistral transtension. Brittle faulting along the VF led to the development of extensive, N-S-orientated, linking structures (Figure 8.5) and a well-developed and wide zone of fracturing. Early-formed fractures and faults along the centre of the VF tend to be longer and more connected over a wide zone (~500m) (Sleight 2001). Conversely, early-formed fractures and faults tend to be shorter and connected over a much narrower zone (<100m) along the HSF (Sleight 2001). Therefore, during brittle reactivation, the VF was more evolved and more connected than the HSF. Consequently, the subsequent reactivation of the VF and not the HSF, may have been controlled primarily by the geometrical properties of the fault zone (c.f. Walsh et al. 2001).

Fault rocks along each fault are similar (Figure 8.8), although the VF seems to have experienced significantly higher volumes of fluid flow (mineralisation and fluid-assisted DMT processes). Hence, the fluid-rich VF is highly reactivated, whilst the relatively dry HSF experienced only minor reactivation. Fluid-rich conditions along

the VF are consistent with the operation of *fluid-assisted reaction softening* (of cataclasites) and *fluid-assisted diffusional creep* at depth (section 8:4:1; c.f. Imber et al. 1997; Stewart et al. 2000; Holdsworth et al. 2001), and that geological evidence may not be preserved at the present level of exposure. This fluid flow may also be explained by the presence of a more connected and wider zone of fracturing along the VF compared to the HSF. Therefore, are the fluids along the VF the cause of reactivation (fluid-related weakening at depth), or are they simply an effect of reactivation (fluid channelling through well-connected fracture network)? The present study is unable to prove or disprove whether the fluids along the VF are the cause or effect of fault reactivation, in the absence of direct evidence for the operation of *fluid-assisted reaction softening* (of cataclasites) and *fluid-assisted diffusional creep* at the present level of exposure. Any weakening of the fault rocks at depth may therefore be a function of fluid flow through the pre-existing fracture network, suggesting a complex interaction between the geometrical properties of the fault network and fault-zone weakening mechanisms.

8:5 Exhumation and preservation of fault rocks along multiply reactivated faults

Fault-rock textures along both the MTFC and the WBFZ show a progressive, lower-temperature origin with time due to exhumation processes. In other words, early, higher-temperature, fault-rock textures are typically mylonitic, having formed in the viscous regime, whilst later reactivations are typically cataclastic and formed in the frictional regime. Exhumation of fault zones can occur during periods of tectonic quiescence along the actual fault zone, but can also be syn-tectonic. Syn-tectonic exhumation leads to fault-rock assemblages which formed during the same kinematic event, showing evidence of passing through progressively shallow crustal levels with time.

Fault-rock preservation is fundamentally different along the strike-slip WBFZ and MTFC. Later reactivations along the WBFZ tend to be associated with much larger displacements (tens of kilometres) than the MTFC (no more than a few tens of kilometres).

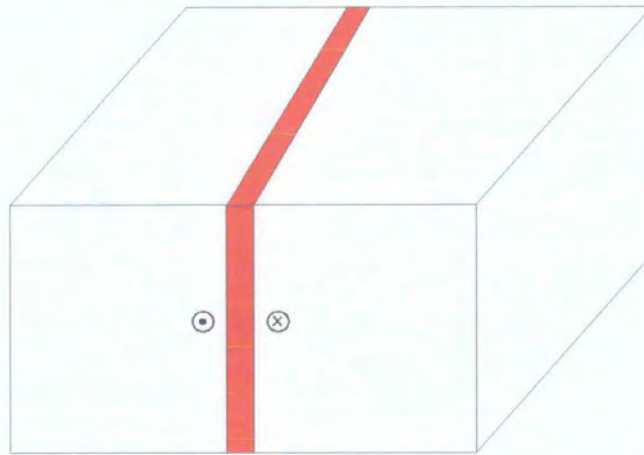
Along the WBFZ, early sinistral strike-slip, mylonitic fault rocks are preserved in two deeply-exhumed, fault-bounded blocks. These blocks are part of two, distinct, kilometre-scale, 'positive' flower structures, exposed at (a) Seli Voe to Sand (section 3:1:7) and (b) Sullom, Lunnister and the Ness of Haggrister (section 3:1:2), which were progressively exhumed during later dextral strike-slip movements along the WBFZ associated with the development of fault gouge and cataclasite assemblages (see section 8:1:1). Conversely, only later fault rocks are preserved in 'negative' flower structures formed at releasing bends along the WBF (e.g., Ness of Bixter, section 3:1:6). The 'positive' flower structures are interpreted to have formed in the compressional bends of the WBFZ (see sections 3:1:2, 3:1:7; Figure 8.15). Therefore, due to the large magnitudes of the later reactivations along the WBF, earlier fault rocks are cut out and are not preserved in the wall rocks, but instead are preserved in deeply exhumed, fault-bounded blocks in compressional bends along the strike of the fault zone (Figure 8.15). Hence, the preservation of early fault rocks along large-magnitude, sub-vertical, reactivated, strike-slip fault zones seems to be controlled by fault-related exhumation.

Displacement magnitudes along the MTFC are smaller (no more than a few tens of kilometres) than those along the WBFZ. Here, later reactivations repeatedly localise within the earlier formed fault rocks of the fault core. As displacements are relatively small, fault rocks are preserved in sequence within the wall rocks adjacent to the fault core (Figure 8.16) and are not cut out by later movements. Also, the fault rocks do not display a progressive, syn-tectonic shallowing of the fault zone, as flower structures are not developed along small-magnitude, strike-slip, fault zones. Here, fault-rock textures derived from different structural levels were formed during different kinematic events separated by long periods of tectonic quiescence along the actual fault zone, during which time exhumation occurred due to erosion and other regional-scale processes. As a result, fault-rock textures along large-displacement, sub-vertical, strike-slip fault zones are much more likely to record a progressive syn-tectonic shallowing of the fault zone compared to small-displacement fault zones, where flower structures are not developed.

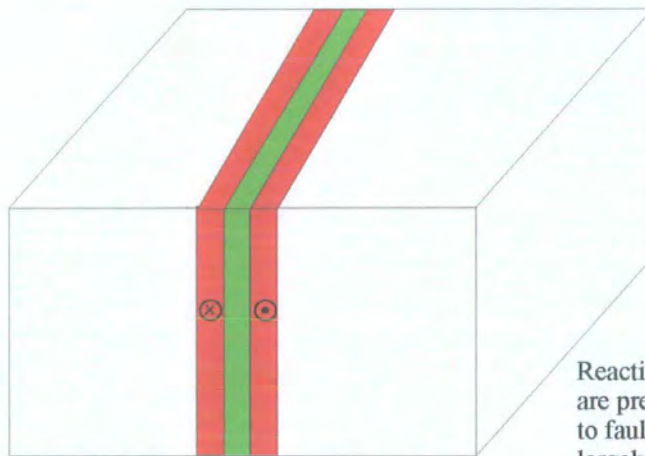


Figure 8.15 Models of fault-rock exhumation and preservation for a large-magnitude, strike-slip (sub-vertical) reactivated fault zone, e.g., WBF. (A) Model to show fault-controlled exhumation of early fault rocks within 'positive' flower structure. (B) Preservation of early fault rocks in fault-bounded blocks along strike, adjacent to later fault rocks.

Formation of early fault rocks



Early fault rocks
 Later fault rocks



Reactivation - early fault rocks are preserved in wall rocks adjacent to fault core & flower structures are largely absent.

Figure 8.16 Model to show preservation of successive generations of fault rocks adjacent to fault core, along reactivated, strike-slip (sub-vertical), fault zone with relatively small displacements, e.g., MTFC.

The nature and preservation of early fault rocks along reactivated, sub-vertical, strike-slip fault zones therefore seems to depend upon the nature and magnitude of later reactivations. Along large-magnitude, reactivated, strike-slip fault zones, earlier-formed fault rocks are often cut out and are preserved in uplifted fault-bounded blocks that are parts of 'positive' flower structures. Conversely, along small-magnitude, reactivated, strike-slip fault zones, where flower structures are not developed, earlier fault rocks are preserved in sequence adjacent to the fault core which contains younger fault rocks.

8:6 Conclusions

- Reactivated faults are complex but their geometric and structural evolution can be unravelled with detailed field, textural and microstructural studies.
- The MTFC comprises two major fault strands: the Hitra-Snåsa Fault and the Verran Fault. These two faults seem to have broadly initiated as part of a single system of sinistral shear zones during Early Devonian times (409 ± 12 Ma). Sinistral transtensional reactivation (Permo-Carb; 291 ± 14 Ma) of the ENE-WSW-trending HSF and VF led to the development of cataclasites and pseudotachylites together with the formation of N-S-trending faults leading to the present day brittle fault geometry of the MTFC. Several later phases of reactivation were focused along the VF and N-S linking structures during the Mesozoic probably related to Mid-Late Jurassic / Early Cretaceous rifting and Late Cretaceous / Early Tertiary opening of the North Atlantic.
- The WBF initiated as a late-Caledonian sinistral strike-slip fault (c.100-200km) associated with the development of mylonites and cataclasites. Dextral strike-slip reactivation (c.65km) in the Permo-Carboniferous related to inversion of the Orcadian Basin and led to the development of cataclasite and fault gouge assemblages. Later dip-slip and finally sinistral strike-slip (c.15km, Tertiary?) reactivation localised within earlier formed fault gouges.
- It seems that the formation and reactivation of the WBF and MTFC were related to broadly similar regional tectonic processes and therefore to some extent share similar kinematics. The MTFC and WBF are both persistently reactivated but

superficially similar geometries or alignments should not be used to correlate structures, in the absence of direct kinematic evidence.

- Displacements along the MTFC and WBFZ are repeatedly localised along the earlier formed fault rocks. In the case of reactivated, sub-vertical, strike-slip fault zones the preservation of these rocks also depends on the architecture and magnitude of later reactivations.
- This study shows that both the geometrical properties of the fault network and fault-zone weakening mechanisms are important in understanding the controlling factors on fault reactivation.

References

- Allen, K.C. 1976. Devonian spores from outer Trøndelag, Norway. *Norsk Geologisk Tidsskrift* **56** (4), 437-448.
- Andersen, T. B. 1998. Extensional tectonics in the Caledonides of southern Norway, an overview. *Tectonophysics* **285**, 333-351.
- Andrews, I. J. 1985. The Deep-Structure of the Moine Thrust, Southwest of Shetland. *Scottish Journal of Geology* **21**(2), 213-217.
- Andrews, I. J. & others, a. s. 1990. United Kingdom regional report: the geology of the Moray Firth. BGS.
- Arthaud, F. & Matte, P. 1977. Late Paleozoic strike-slip faulting in southern Europe and northern Africa. *Geological Society of America Bulletin* **88**, 1305-1320.
- Badley, M. E., Price, J. D., Rambech Dahl, C. & Agdestein, T. 1988. The structural evolution of the northern Viking Graben and its bearing upon extensional modes of basin formation. *Journal of the Geological Society* **145**, 455-472.
- Beach, A. 1979. Pressure solution as a metamorphic process in deformed terrigenous sedimentary rocks. *Lithos* **12**, 51-58.
- Beach, A. 1980. Retrogressive metamorphic processes in shear zones with special reference to the Lewisian complex. *Journal of Structural Geology* **2**(1/2), 257-263.
- Bergfjord, E. 1989. Den strukturelle utvikling i den devoske Fosen-gruppen og dens underlag, Ørlandet, Sør-Trøndelag. Unpublished Cand. Scient. thesis, University of Bergen.
- Bering, D. 1992. The orientation of minor fault plane striae and the associated deviatoric stress tensor as a key to the fault geometry in part of the Møre-Trøndelag Fault Zone, on-shore, central Norway. In: *Structural and Tectonic Modelling and its application to Petroleum Geology* (edited by Larsen, R. M., Brekke, H., Larsen, B. T. & Talleras, E.). *NPF Special Publication* **1**. Elsevier, Amsterdam, 83-90.
- Blystad, P. 1995. Structural elements of the Norwegian continental shelf. *Norwegian Petroleum Directorate Bulletin* **8**.

Bøe, R., Atakan, K. & Sturt, B. A. 1989. The style of deformation in the Devonian rocks on Hitra and Smøla. *Norsk geologiske undersøkelse Bulletin* **414**, 1-19.

Bøe, R. & Bjerkli, K. 1989. Mesozoic Sedimentary-Rocks in Edøyfjorden and Beitstadfjorden, Central Norway, Implications for the Structural History of the Møre-Trøndelag Fault Zone. *Marine Geology* **87**(2-4), 287-299.

Bøe, R. & Skilbrei, J. R. 1998. Structure and seismic stratigraphy of the Griptane area, Møre Basin margin, mid-Norway continental shelf. *Marine Geology* **147**, 85-107.

Braathen, A., Nordgulen, O., Osmundsen, P. T., Andersen, T. B., Soli, A. & Roberts, D. 2000. Devonian, orogen-parallel, opposed extension in the Central Norwegian Caledonides. *Geology* **28**, 615-618.

Brekke, H. 2000. The tectonic evolution of the Norwegian Sea continental margin, with emphasis on the Vøring and Møre basins. In: *Dynamics of the Norwegian Margin* (edited by Nottvedt, A.) **167**. Geological Society, London, Special Publication.

Brodie, K. & Rutter, E. H. 1985. On the relationship between deformation and metamorphism with special reference to the behaviour of basic rocks. In: *Kinetics, Textures and Deformation, Advanced Physical Chemistry* (edited by Thompson, A. B. & Rubie, D.) **4**, 138-179.

Brodie, J. & White, N. 1994. Sedimentary basin inversion caused by igneous underplating: Northwest European continental shelf. *Geology* **22**, 147-150.

Buckovics, C., Cartier, E.G., Shaw, W.D. & Ziegler, P.A. 1984. Structure and development of the mid-Norway continental margin. In: *Petroleum Geology of the North European margin* (edited by Spencer, A.M. et al). Graham & Trotman, London, 407-423.

Bungum, H., Alsaker, A., Kvamme, L. B. & Hansen, R. A. 1991. Seismicity and seismotectonics of Norway and nearby continental shelf areas. *Journal of Geophysical Research* **96**(2), 2249-2265.

Butler, C. A. 1995. Basement Fault Reactivation: The Kinematic Evolution of the Outer Hebrides Fault Zone, Scotland. Unpublished PhD thesis, University of Durham.

Byerlee, J. D. 1978. Friction of rocks. *Pure and Applied Geophysics* **116**, 615-626.

Caselli, F. 1987. Oblique-slip tectonics, mid-Norway shelf. In: *Petroleum geology of north west Europe* (edited by Brooks, J. & Glennie, K. W.). Graham & Trotman, London.

Claesson, S. & Roddick, J. C. 1983. $^{40}\text{Ar}/^{39}\text{Ar}$ data on the age and metamorphism of the Ottfjället dolerites, Saerv Nappe, Swedish Caledonides. *Lithos* **16**(1), 61-73.

Cobbold, P. R. & Quinquis, H. 1980. Development of sheath folds in shear regimes. *Journal of Structural Geology* **2**(1/2), 119-126.

Conroy, D. A. 1996. The Structure and Kinematic History of the Walls Boundary Fault Zone in Shetland. Unpublished PhD thesis, Queens University Belfast.

Condie, K.C. & Sinha, A.K. 1996. Rare earth and other trace element mobility during mylonitization: A comparison of the Brevard and Hope Valley shear zones in the Appalachian Mountains, USA. *Journal of Metamorphic Geology* **14** (2), 213-226.

Coward, M. P., Enfield, M. A. & Fisher, M. W. 1989. Devonian basins of Northern Scotland: extension and inversion related to Late Caledonian - Variscan tectonics. In: *Inversion Tectonics* (edited by Cooper, M. A. & Williams, G. D.). *Special Publication* **44**. Geological Society, London, 275-308.

Dallmeyer, R. D. 1990. $^{40}\text{Ar}/^{39}\text{Ar}$ mineral age record of a polyorogenic evolution within the Seve and Koli nappes, Trøndelag, Norway. *Tectonophysics* **179**, 199-226.

Dallmeyer, R. D., Johansson, L. & Möller, C. 1992. Chronology of Caledonian high-pressure granulite-facies metamorphism, uplift, and deformation within northern parts of the Western Gneiss region, Norway; with Suppl. Data 92-10. *Geological Society of America Bulletin* **104**(4), 444-455.

David, F., Walker, L., Lee, M. R. & Parsons, I. 1995. Micropores and micropermeable texture in alkali feldspars: geochemical and geophysical implications. *Mineralogical Magazine* **59**, 505-534.

Davidson, C., Schmid, S. M. & Hollister, L. S. 1994. Role of melt during deformation in the deep crust. *Terra Nova* **6**, 133-142.

Dewey, J. F., Hempton, M. R., Kidd, W. S. F., Saroglu, F. & Sengor, A. M. C. 1986. Shortening of continental lithosphere: the neotectonics of Eastern Anatolia - a young collision zone. In: *Collision Tectonics* (edited by Coward, M. P. & Ries, A. C.). *Special Publication* **19**. Geological Society, London, 3-37.

Donovan, R. N., Archer, R., Turner, P. & Tarling, D. H. 1976. Devonian palaeogeography of the Orcadian Basin and the Great Glen Fault. *Nature* **259**, 550-551.

Doré, A. G. & Lundin, E. R. 1996. Cenozoic compressional structures on the NE Atlantic margin: nature, origin and potential significance for hydrocarbon exploration. *Petroleum Geoscience* **2**(4), 299-311.

Doré, A. G., Lundin, E. R., Fichler, C. & Olesen, O. 1997a. Patterns of basement structure and reactivation along the NE Atlantic margin. *Journal of the Geological Society* **154**, 85-92.

Doré, A. G., Lundin, E. R., Birkeland, O., P.E., E. & Jensen, L. N. 1997b. The NE Atlantic Margin: implications of late Mesozoic and Cenozoic events for hydrocarbon prospectivity. *Petroleum Geoscience* **3**, 117-131.

Doré, A. G., Lundin, E. R., Jensen, L. N., Birkeland, O., Eliassen, P. E. & Fichler, C. 1999. Principal tectonic events in the evolution of the northwest European Atlantic margin. In: *Petroleum Geology of Northwest Europe: Proceedings of the 5th Conference* (edited by Fleet, A. J. & Boldy, S. A. R.). Geological Society, London, 41-61.

Drury, M. R. & Urai, J. L. 1990. Deformation-related recrystallization processes. *Tectonophysics* **172**, 235-253.

Duindam, P. & Hoorn, B. V. 1987. Structural evolution of the West Shetland continental margin. In: *Petroleum Geology of Northwest Europe* (edited by Brooks, J. & Glennie, K.). Graham & Trotman, 765-773.

Dunlap, W. J. & Fossen, H. 1998. Early Palaeozoic orogenic collapse, tectonic stability, and late Palaeozoic continental rifting revealed through thermochronology of K-feldspars, Southern Norway. *Tectonics* **17**(4), 604-620.

Dunning, G. R. & Pedersen, R. B. 1988. U/Pb ages of ophiolites and arc-related plutons of the Norwegian Caledonides; implications for the development of Iapetus. *Contributions to Mineralogy and Petrology* **98**(1), 13-23.

Etheridge, M. A., Wall, V. J. & Vernon, R. H. 1983. The role of the fluid phase during regional metamorphism and deformation. *Journal of Metamorphic Geology* **1**, 205-226.

Etheridge, M. A. 1986. On the reactivation of extensional fault systems. *Philosophical Transactions of the Royal Society of London* **A317**, 179-194.

Evans, B. & Goetze, C. 1979. The temperature variation of hardness of olivine and its implication for polycrystalline yield stress. *Journal of Geophysical Research* **84**(B10), 5505-5524.

Evans, D., Chester, J. A., Deegan, C. E. & Fannin, N. G. T. 1981. The offshore geology of Scotland in relation to the IGS Shallow Drilling Programme, 1970-78. I.G.S. no. 82/12, HMSO, London, 1-36.

Flinn, D. 1954. On the time relations between regional metamorphism and permeation in Delting, Shetland. *Quarterly Journal of the Geological Society of London* **110**(438), 177-201.

Flinn, D. 1958. On the nappe structure of north-east Shetland. *Quarterly Journal of the Geological Society of London* **114**(453), 107-136.

Flinn, D. 1961. Continuation of the Great Glen Fault beyond the Moray Firth. *Nature* **191**, 589-591.

Flinn, D. 1969. A geological interpretation of the aeromagnetic maps of the continental shelf around Orkney and Shetland. *Journal of Geology* **6**(2), 279-292.

Flinn, D. 1977. Transcurrent faults and associated cataclasis in Shetland. *Journal of the Geological Society* **133**, 231-248.

Flinn, D. 1979. Basement-cover relations in Shetland. In: *The Caledonides of the British Isles; reviewed* (edited by Harris, A. L., Holland, C. H. & Leake, B. E.). *Special Publication* **8**. Geological Society, London, 109-115.

Flinn, D. 1985. The Caledonides of Shetland. In: *The Caledonide Orogen - Scandinavia and Related Areas* (edited by Gee, D. G. & Sturt, B. A.). John Wiley & Sons Ltd, 1159-1171.

Flinn, D. 1988. The Moine rocks of Shetland. In: *Later Proterozoic stratigraphy of the northern Atlantic regions* (edited by Winchester, J. A.). Chapman & Hall.

Flinn, D. 1992. The History of the Walls Boundary Fault, Shetland - the Northward Continuation of the Great Glen Fault From Scotland. *Journal of the Geological Society* **149**, 721-726.

Flinn, D., Miller, J. A., Evans, A. C. & Pringle, I. R. 1968. On the age of sediments and contemporaneous rocks of western Shetland. *Scottish Journal of Geology* **4**, 10-19.

Flinn, D., Miller, J. A. & Roddom, D. 1991. The age of the Norwick hornbelndic schists of the Unst and Fetlar and the obduction of the Shetland ophiolite. *Scottish Journal of Geology* **27**(1), 11-19.

Flinn, D., May, F., Roberts, J. F. & Treagus, J. E. 1972. A revision of the stratigraphic succession of the East Mainland of Shetland. *Scottish Journal of Geology* **8**(4), 335-343.

Fossen, H. 1989. Indication of transpressional tectonics in the Gullfaks oil-field, northern North Sea. *Marine and Petroleum Geology* **6**(1), 22-30.

Frey, M. 1988. *Low temperature metamorphism*. Blackie & son Limited, Glasgow and London.

Gabrielsen, R. H. & Ramberg, I. B. 1979. Fracture patterns in Norway from Landsat imagery: results and potential use. In: *Proceedings of the Norwegian Sea Symposium*, Tromso, Norway.

Gabrielsen, R. H., Odinsen, T. & Grunnaleite, I. 1999. Structuring of the Northern Viking Graben and the Møre Basin; the influence of basement structural grain, and the particular role of the Møre-Trøndelag Fault Complex. *Marine and Petroleum Geology* **16**(5), 443-465.

Gale, G. H. & Roberts, D. 1974. Trace element geochemistry of Norwegian lower Palaeozoic basic volcanics and its tectonic implications. *Earth and Planetary Science Letters* **22**(4), 380-390.

Gautneb, H. & Roberts, D. 1989. Geology and petrochemistry of the Smøla-Hitra Batholith, Central Norway. *Norges geologiske undersokelse Bulletin* **416**, 1-24.

Gee, D. G., Guezou, J. C., Roberts, D. & Wolff, F. C. 1985. The central-southern part of the Scandinavian Caledonides. In: *The Caledonide Orogen-Scandinavian and Related Areas* (edited by Gee, D. G. & Sturt, B. A.). John Wiley & Sons.

Gilotti, J. A. & Hull, J. M. 1993. Kinematic stratification of the central Scandinavian Caledonides. *Journal of Structural Geology*, 629-645.

Grønlie, A. & Roberts, D. 1989. Resurgent strike-slip development along the Hitra-Snåsa and Verran Faults, Møre-Trøndelag Fault Zone, Central Norway. *Journal of Structural Geology* **11**(3), 295-305.

Grønlie, A. & Torsvik, T. H. 1989. On the Origin and Age of Hydrothermal Thorium-Enriched Carbonate Veins and Breccias in the Møre-Trøndelag Fault Zone, Central Norway. *Norsk Geologisk Tidsskrift* **69**(1), 1-19.

Grønlie, A., Harder, V. & Roberts, D. 1990. Preliminary Fission-Track Ages of Fluorite Mineralization Along Fracture-Zones, Inner Trondheimsfjord, Central Norway. *Norsk Geologisk Tidsskrift* **70**(3), 173-178.

Grønlie, A., Nilsen, B. & Roberts, D. 1991. Brittle deformation history of fault rocks on the Fosen Peninsula, Trøndelag, Central Norway. *Norges geologiske undersøkelse Bulletin* **421**, 39-57.

Grønlie, A., Naeser, C. W., Naeser, N. D., Mitchell, J. G., Sturt, B. A. & Ineson, P. R. 1994. Fission-Track and K-Ar Dating of Tectonic Activity in a Transect Across the Møre-Trøndelag Fault Zone, Central Norway. *Norsk Geologisk Tidsskrift* **74**(1), 24-34.

Grunnaleite, I. & Gabrielsen, R. H. 1995. Structure of the Møre Basin, mid-Norway continental margin. *Tectonophysics* **252**, 221-251.

Hancock, P.L. 1985. Brittle Microtectonics – Principles and Practice. *Journal of Structural Geology* **7**(3-4), 437-457.

Handy, M. R. 1989. Deformation Regimes and the Rheological Evolution of Fault Zones in the Lithosphere - the Effects of Pressure, Temperature, Grainsize and Time. *Tectonophysics* **163**(1-2), 119-152.

Handy, M. R. 1990. The Solid-State Flow of Polymineralic Rocks. *Journal of Geophysical Research* **95**, 8647-8661.

Handy, M. R. 1992. Correction and Addition to "The Solid-State Flow of Polymineralic Rocks". *Journal of Geophysical Research* **97**(B2), 1897-1899.

Handy, M. R., Mulch, A. R., Rosenau, M. & Rosenberg, C. L. 2001. The role of fault zones and melts as agents of weakening, hardening and differentiation of the continental crust: a synthesis. In: *The Nature and Tectonic Significance of Fault Zone Weakening* (edited by Holdsworth, R. E., Strachan, R. A., Magloughlin, J. F. & Knipe, R. J.). *Special Publication* **186**. Geological Society, London, 305-332.

Hanmer, S. & Passchier, C. 1991. Shear sense indicators: a review. *Geological Survey of Canada Paper* **90**, 1-71.

Harris, A. L. 1991. The Growth and Structure of Scotland. In: *Geology of Scotland* (edited by Craig, G. Y.). Geological Society, London.

Harris, A. L., Haselock, P. J., Kennedy, M. J. & Mendum, J. R. 1994. The Dalradian supergroup in Scotland, Shetland and Ireland. In: *A revised correlation of Precambrian rocks in the British Isles* (edited by Gibbons, W. & Harris, A. L.). Geological society, London.

Heeremans, M., Larsen, B. T. & Steel, H. 1996. Palaeostress reconstruction from kinematic indicators in the Oslo Graben, southern Norway: new constraints on the mode of rifting. *Tectonophysics* **266**, 55-79.

Heizler, M. T. & Harrison, T. M. 1988. Multiple-trapped argon isotope components revealed by $^{40}\text{Ar}/^{39}\text{Ar}$ isochron analysis. *Geochemica et Cosmochimica Acta* **52**, 1295-1303.

Hesthammer, J., Johansen, T. E. S. & Watts, L. 2000. Spatial relationships within fault damage zones in sandstone. *Marine and Petroleum Geology* **17**, 873-893.

Hitchen, K. & Ritchie, J. D. 1987. Geological review of the West Shetland area. In: *Petroleum Geology of North West Europe* (edited by Brooks, J. & Glennie, K.). Graham & Trotman, 737-749.

Hobbs, B.E., Means, W.D. & Williams, P.F. 1976. An outline of structural geology. John Wiley & Sons, New York.

Hobbs, B. E., Mulhaus, H.-B. & Ord, A. 1990. Instability, softening and localization of deformation. In: *Deformation mechanisms, Rheology and Tectonics* (edited by Knipe, R. J. & Rutter, E. H.). *Special Publication* **54**. Geological Society, London.

Holdsworth, R. E. 1989. The geology and structural evolution of a Caledonian fold and ductile thrust zone, Kyle of Tongue region, Sutherland, northern Scotland. *Journal of the Geological Society* **146**, 909-823.

Holdsworth, R. E. 1994. Structural Evolution of the Gander Avalon Terrane Boundary - a Reactivated Transpression Zone in the NE Newfoundland Appalachians. *Journal of the Geological Society* **151**, 629-646.

Holdsworth, R. E., Strachan, R. A. & Harris, A. L. 1994. Precambrian rocks in northern Scotland east of the Moine Thrust: the Moine supergroup. In: *A revised correlation of Precambrian rocks in the British Isles* (edited by Gibbons, W. & Harris, A. L.). Geological Society, London.

Holdsworth, R. E., Butler, C. A. & Roberts, A. M. 1997. The recognition of reactivation during continental deformation. *Journal of the Geological Society* **154**, 73-78.

Holdsworth, R. E., Stewart, M., Imber, J. & Strachan, R. A. 2001. The structure and rheological evolution of reactivated continental fault zones: a review and case study. In: *Continental Reactivation and Reworking* (edited by Miller, J. A., Holdsworth, R. E., Buick, I. S. & Hand, M.). *Special Publication* **184**. Geological Society, London, 115-137.

Hollister, L. S. & Crawford, M. A. 1986. Melt-enhanced deformation: a major tectonic process. *Geology* **14**, 558-561.

Hutton, D. H. W. & McErlean, M. 1991. Silurian and Early Devonian sinistral deformation of the Ratagain Granite, Scotland; constraints on the age of Caledonian movements on the Great Glen fault system. *Journal of the Geological Society* **148**, 1-4.

Imber, J. 1998. Deformation and fluid-rock interaction along the reactivated Outer Hebrides Fault Zone, Scotland. Unpublished PhD thesis, University of Durham.

Imber, J., Holdsworth, R. E., Butler, C. A. & Lloyd, G. E. 1997. Fault-zone weakening processes along the reactivated Outer Hebrides Fault Zone, Scotland. *Journal of the Geological Society* **154**, 105-109.

Imber, J., Holdsworth, R. E., Butler, C. A. & Strachan, R. A. 2001. A reappraisal of the Sibson-Scholz fault zone model: The nature of the frictional to viscous ("brittle-ductile") transition along a long-lived, crustal-scale fault, Outer Hebrides, Scotland. *Tectonics* **20**(5), 601-624.

Johansson, L. 1986. Basement and cover relationships in the Vestranden-Grong-Olden region, Central Scandinavian Caledonides: petrology, age relationships, structures and regional correlation. Unpublished PhD thesis, University of Lund, Sweden.

Johansson, L., Schoberg, H. & Solyom, Z. 1993. The age and regional correlation of the Svecofennian Geitfjell Granite, Vestranden, Norway. *Norsk Geologisk Tidsskrift* **73**(2), 133-143.

Johns, C. R. & Andrews, I. J. 1985. The petroleum geology of the Unst Basin, North Sea. *Marine and Petroleum Geology* **2**, 361-372.

Johnson, H., Richards, P. C., Long, D. & Graham, C. C. 1993. *The geology of the northern North Sea*. BGS, London.

Jongepier, K., Rui, J. C. & Grue, K. 1996. Triassic to Early Cretaceous stratigraphic and structural development of the northeastern Møre Basin margin, off mid-Norway. *Norsk Geologisk Tidsskrift* **76**(4), 199-214.

Jordan, P. G. 1987. The deformation behaviour of bimineralic limestone-halite aggregates. *Tectonophysics* **135**, 185-197.

Kjerulf, T. 1870. Om Trondhjems stifts geologi. *Nyt Magazin for Naturvitenskap, Christiania* **18**, 1-79.

Knipe, R. J. 1989. Deformation mechanisms - recognition from natural tectonites. *Journal of Structural Geology* **11**, 127-146.

Krabbendam, M. & Dewey, J. F. 1998. Exhumation of UHP rocks by transtension in the Western Gneiss Region, Scandinavian Caledonides. In: *Continental Transpressional and Transtensional Tectonics* (edited by Holdsworth, R. E., Strachan, R. A. & Dewey, J. F.). *Special Publication* **135**. Geological Society, London, 159-181.

Law, R. D. 1990. Crystallographic fabrics: a selective review of their applications to research in structural geology. In: *Deformation Mechanisms, Rheology and Tectonics* (edited by Knipe, R. J. & Rutter, E. H.). *Special Publication* **54**. Geological Society, London, 335-352.

Lindholm, C. D., Bungum, H., Bratli, R. K., Aadnoy, B. S., Dahl, N., Torudbakken, B. & Atakan, K. 1995. Crustal stress in the northern North Sea as inferred from borehole breakouts and earthquake focal mechanisms. *Terra Nova* **7**(1), 51-59.

Lloyd, G. E. & Knipe, R. J. 1992. Deformation mechanisms accommodating faulting of quartzite under upper crustal conditions. *Journal of Structural Geology* **14**(2), 127-143.

Magloughlin, J. F. 1992. Microstructural and chemical changes associated with cataclasis and frictional melting at shallow crustal levels: the cataclasite-pseudotachylyte connection. *Tectonophysics* **204**, 243-260.

Magloughlin, J. F. & Spray, J. G. 1992. Frictional melting processes and products in geological materials; introduction and discussion. *Tectonophysics* **204**(3-4), 197-204.

Mares, V. M. & Kronenberg, A. K. 1993. Experimental deformation of muscovite. *Journal of Structural Geology* **15**, 1061-1075.

Marshall, J. E. A. 2000. Devonian (Givetian) miospores from the Walls Group, Shetland. In: *New Perspectives on the Old Red Sandstone* (edited by Friend, P. F. & Williams, B. J.). *Special Publication* **180**. Geological Society, London, 473-483.

McBride, J. H. 1994a. Investigating the crustal structure of a strike-slip "step-over" zone along the Great Glen Fault. *Tectonics* **13**(5), 1150-1160.

McBride, J. H. 1994b. Structure of a Continental Strike-Slip-Fault From Deep Seismic- Reflection - Walls Boundary Fault, Northern British Caledonides. *Journal of Geophysical Research-Solid Earth* **99**(B12), 23985-24005.

McCaig, A. M. & Knipe, R. J. 1990. Mass-transport mechanisms in deforming rocks: Recognition using microstructural and microchemical criteria. *Geology* **18**, 824-827.

McGeary, S. 1989. Reflection Seismic Evidence for a Moho Offset Beneath the Walls Boundary Strike-Slip-Fault. *Journal of the Geological Society* **146**, 261-269.

Miller, J. A. & Flinn, D. 1966. A survey of the age relations of Shetland rocks. *Journal of Geology* **5**(1), 95-116.

Möller, C. 1988. Geology and metamorphic evolution of the Roan area, Vestranden, Western Gneiss region, central Norwegian Caledonides. *Norges geologiske undersøkelse Bulletin* **413**, 1-31.

Molnar, P. 1988. Continental tectonics in the aftermath of plate tectonics. *Nature* **335**, 131-137.

Morrow, C. A., Radney, B. & Byerlee, J. 1992. Frictional strength and the effective pressure law of montmorillonite and illite clays. In: *Fault Mechanics and Transport Properties of Rocks* (edited by Evans, B. & Wong, T.-F.). Academic Press, New York, 69-88.

Mykura, W. 1976. *British Regional Geology - Orkney and Shetland*. BGS, Edinburgh.

Mykura, W. 1991. Old Red Sandstone. In: *Geology of Scotland* (edited by Craig, G. Y.). Geological Society, London.

Nordgulen, O., Bickford, M. E., Nissen, A. L. & Worthman, G. L. 1993. U-Pb zircon ages from the Bindal Batholith, and the tectonic history of Helgeland nappe complex, Scandinavian Caledonides. *Journal of the Geological Society* **150**, 771-783.

Norton, M. G., McClay, K. R. & Way, N. A. 1987. Tectonic evolution of Devonian basins in northern Scotland and southern Norway. *Norsk Geologisk Tidsskrift* **67**, 323-338.

Oftedahl, C. 1972. A sideritic ironstone of Jurassic age in Beitstadfjorden, Trøndelag. *Norsk Geologisk Tidsskrift* **52**(2), 123-124.

Oftedahl, C. 1975. Middle Jurassic graben tectonics in mid Norway. In: *Proceedings of the Symposium on the Jurassic of the northern North Sea*. Norwegian Petroleum Society, Stavanger, 1-13.

Oliver, N. H. S. 1996. Review and classification of structural controls on fluid flow during regional metamorphism. *Journal of Metamorphic Geology* **14**, 477-492.

Osmundsen, P. T., Andersen, T. B., Markussen, S. & Svendby, A. K. 1998. Tectonics and sedimentation in the hangingwall of a major extensional detachment; the Devonian Kvamshesten Basin, western Norway. *Basin Research* **10**(2), 213-234.

Pascal, C. & Gabrielsen, R. H. 2001. Numerical modelling of Cenozoic stress patterns in the mid-Norwegian margin and the northern North Sea. *Tectonics* **20**(4), 585-599.

Passchier, C. W. & Trouw, R. A. J. 1996. *Micro-tectonics*. Springer-Verlag, Berlin.

Pedersen, L. E., Heaman, L. M. & Holm, P. M. 1995. Further constraints on the temporal evolution of the Oslo Rift from precise U-Pb zircon dating in the Siljan-Skrim area. *Lithos* **34**, 301-315.

Phemister, J. 1979. The Old Red Sandstone intrusive complex of Northmaven, Shetland. I.G.S. Ref. 78/2, OHMS.

Piasecki, M. A. J. & Cliff, R. A. 1988. Rb-Sr dating of strain-induced mineral growth in two ductile shear zones in the Western Gneiss Region of Nord-Trøndelag, Central Norway. *Norsk geologiske undersøkelse Bulletin* **413**, 33-50.

Pringle, I. 1970. The structural geology of the North Roe area of Shetland. *Journal of Geology* **7**(1), 147-170.

Renne, P. R., Swisher, C. C., Deino, A. L., Karnet, D. B., Owens, T. L. & DePaolo, D. J. 1998. Intercalibration of standards, absolute ages and uncertainties in $^{40}\text{Ar}/^{39}\text{Ar}$ dating. *Chemical Geology* **145**(117-152).

Rice, J. R. 1992. Fault stress states, Pore Pressure Distributions, and the weakness of the San Andreas Fault. In: *Fault mechanics and Transport Properties of Rocks* (edited by Evans, B. & Wong, T. F.). Academic Press, 476-503.

Richards, P. C. 1990. The Early to Mid-Jurassic evolution of the northern North Sea. In: *Tectonic events responsible for Britain's oil and gas reserves* (edited by Hardman, R. F. P. & Brooks, J.). *Special Publication* **55**. Geological Society, London, 191-205.

Riedel. 1929. Zur Mechanik geologischer Brucherscheinungen. Ein Beitrag zum Problem der "Fiederspaltten". *Centralblatt für Mineralogie, Geologie, und Paleontologie* **Part B**, 354-368.

Ringdal, F. 1983. Seismicity of the North Sea area. In: *Seismicity and seismic risk in the offshore North Sea area; NATO advanced research workshop* (edited by Ritsema, A. R. & Guerpinar, A.). D. Reidel Publ. Co.

Ritchie, J. D., Hitchen, K. & Mitchell, J. G. 1987. The offshore continuation of the Moine Thrust north of Shetland as deduced from basement isotopic ages. *Scottish Journal of Geology* **23**, 163-173.

Ritchie, J. D. & Hitchen, K. 1993. Discussion on the location and history of the Walls Boundary Fault and Moine thrust north and south of Shetland. *Journal of the Geological Society* **150**, 1003-1008.

Roberts, D. 1983. Devonian Tectonic Deformation in the Norwegian Caledonides and its Regional Perspectives. *Norges geologiske undersøkelse* **380**, 85-86.

Roberts, D. 1988. The terrane concept and the Scandinavian Caledonides; a synthesis. *Norges geologiske undersøkelse Bulletin* **413**, 93-99.

Roberts, D. 1998a. High-strain zones from meso- to macro-scale at different structural levels, Central Norwegian Caledonides. *Journal of Structural Geology* **20**(2-3), 111-119.

Roberts, D. 1998b. Geology of the Fosen Peninsula and Trondheimsfjord: a synopsis and excursion guide. NGU.

Roberts, D., Grenne, T. & Ryan, P. D. 1984. Ordovician marginal basin development in the central Norwegian Caledonides. In: *Marginal basin geology; volcanic and associated sedimentary and tectonic processes in modern and ancient marginal basins* (edited by Kokelaar, B. P. & Howells, M. F.). *Special Publication* **16**. Geological Society, London, 233-244.

Roberts, D. & Gee, D. G. 1985. An introduction to the structure of the Scandinavian Caledonides. In: *The Caledonide Orogen-Scandinavia and Related Areas* (edited by Gee, D. G. & Sturt, B. A.). John Wiley & Sons.

Roberts, D., Walker, N., Slagstad, T., Solli, A. & Krill, A.G. 2002. U-Pb zircon ages from the Bymarka ophiolite, near Trondheim, Central Norwegian Caledonides, and regional implications. *Norsk Geologisk Tidsskrift* **82**, 000-000 (in press).

Roddam, D. S., Miller, J. A. & Flinn, D. 1989. Permo-Carboniferous mylonite formation in the Walls Boundary Fault system, Shetland. *Proceedings of the Yorkshire Geological Society* **47**(4), 339-343.

Rogers, D. A., Marshall, J. E. A. & Astin, T. R. 1989. Devonian and Later Movements On the Great Glen Fault System, Scotland. *Journal of the Geological Society* **146**, 369-372.

Rubie, D. C. 1990. Mechanisms of reaction-enhanced deformability in rocks. In: *Deformation processes in minerals, ceramics and rocks* (edited by Barber, D. J. & Meredith, P. G.). Cambridge University Press, 262-294.

Rutter, E. H. 1983. Pressure solution in nature, theory and experiment. *Journal of the Geological Society* **140**, 725-740.

Rutter, E. H. & Brodie, K. 1985. Experimental deformation of serpentinite under conditions of syn-tectonic dehydration. *Abstracts of the international conference on tectonics and structural processes*, Utrecht, 45-46.

Rutter, E. H. 1986. On the nomenclature of mode of failure transitions in rocks. *Tectonophysics* **122**, 381-387.

Rutter, E. H., Holdsworth, R. E. & Knipe, R. J. 2001. The nature and tectonic significance of fault-zone weakening: an introduction. In: *The Nature and Tectonic Significance of Fault Zone Weakening* (edited by Holdsworth, R. E., Strachan, R. A., Magloughlin, J. F. & Knipe, R. J.). *Special Publication* **186**. Geological Society, London.

Schmid, S. M. & Handy, M. R. 1991. Towards a Genetic Classification of Fault Rocks: Geological Usage and Tectonophysical Implications. In: *Controversies in Modern Geology* (edited by Muller, D. W., McKenzie, J. A. & Weissert, H.). Academic Press, London.

Scholz. 1990. *The mechanics of earthquakes and faulting*. Cambridge University Press.

Schouenborg, B. E., Johansson, L. & Gorbatshev, R. 1991. U-Pb zircon ages of basement gneisses and discordant felsic dykes from Vestranden, westernmost Baltic Shield and central Norwegian Caledonides. *Geologische Rundschau* **80**, 121-134.

Séranne, M. & Seguret, M. 1987. The Devonian basins of western Norway: tectonics and kinematics of an extending crust. In: *Continental Extensional tectonics* (edited by Coward, M. P., Dewey, J. F. & Hancock, P. L.). *Special Publication* **28**. Geological Society, London, 537-548.

Séranne, M. 1992a. Devonian extensional tectonics versus Carboniferous inversion in the northern Orcadian basin. *Journal of the Geological Society* **149**, 27-37.

Séranne, M. 1992b. Late Paleozoic kinematics of the Møre-Trøndelag Fault Zone and adjacent areas, Central Norway. *Norsk Geologisk Tidsskrift* **72**(2), 141-158.

Shea, W. T. J. & Kronenberg, A. K. 1993. Strength and anisotropy of foliated rocks with varied mica contents. *Journal of Structural Geology* **15**, 1097-1121.

Sherlock, S. C. & Hetzel, R. 2000. A laser-probe $^{40}\text{Ar}/^{39}\text{Ar}$ study of pseudotachylite from the Tambach Fault Zone, Kenya: direct isotopic dating of brittle faults. *Journal of Structural Geology* **23**, 33-44.

Sibson, R. H. 1977. Fault rocks and fault mechanisms. *Journal of the Geological Society* **133**, 191-213.

Sibson, R. H. 1977b. The Outer Hebrides Thrust: Its Structure, Mechanism and Deformation Environment. Unpublished PhD thesis, University of London.

Sibson, R. H. 1980. Transient discontinuities in ductile shear zone. *Journal of Structural Geology* **2**, 165-171.

Sibson, R. H. 1983. Continental fault structure and the shallow earthquake source. *Journal of the Geological Society* **140**, 741-767.

Sibson, R. H. 1990. Conditions for fault-valve behaviour. In: *Deformation mechanisms, Rheology and Tectonics* (edited by Knipe, R. J. & Rutter, E. H.). *Special Publication* **54**. Geological Society, London, 15-28.

Sibson, R. H. 1993. Load-strengthening versus load-weakening faulting. *Journal of Structural Geology* **15**(2), 123-128.

Sibson, R. H. 1996. Structural permeability of fluid-driven fault-fracture meshes. *Journal of Structural Geology* **18**(8), 1031-1042.

Sibson, R. H., Moore, J.M. & Rankin, A.H. 1975. Seismic pumping – a hydrothermal fluid transport mechanism. *Journal of the Geological Society* **131**, 653-659.

Siedlecka, A. 1975. Old Red Sandstone Lithostratigraphy and Sedimentation of the Outer Fosen Area. *Norges geologiske undersokelse*, 1-35.

Silver, P. G. 1996. Seismic anisotropy beneath the continents: Probing the depths. *Annual Review of Earth and Planetary Sciences* **24**, 385-432.

Simpson, C. & Schmid, S. M. 1983. An evaluation of criteria to deduce the sense of movement in deformed rocks. *Geological Society of America Bulletin* **94**, 1281-1288.

Sleight, J. M. 2001. Fracture Characteristics from Two Reactivated Basement Fault Zones: examples from Norway and Shetland. Unpublished PhD thesis, University of Durham.

Smith, P. M. 1995. Geological setting of mineralization along the Verran Fault Zone, central Norway. Unpublished PhD thesis, Imperial College of Science, Technology and Medicine.

Soper, N. J., Strachan, R. A., Holdsworth, R. E., Gayer, R. A. & Greiling, R. O. 1992. Sinistral transpression and the Silurian closure of Iapetus. *Journal of the Geological Society* **149**, 871-880.

Spray, J. G. 1988. Thrust-related metamorphism beneath the Shetland Islands oceanic fragment, Northeast Scotland. *Canadian Journal of Earth Sciences* **25**(11), 1760-1776.

Spray, J. G., Dunning, G. R. & Jones, J. 1991. A U/Pb age for the Shetland Islands oceanic fragment, Scottish Caledonides : evidence from the anatectic plagiogranites in 'layer 3' shear zones. *Geological Magazine* **128**(6), 667-671.

Spray, J. G. 1995. Pseudotachylyte Controversy - Fact or Friction. *Geology* **23**(12), 1119-1122.

Steel, R., Siedlecka, A. & Roberts, D. 1985. The Old Red Sandstone basins of Norway and their deformation: a review. In: *The Caledonide Orogen-Scandinavian and Related Areas* (edited by Gee, D. G. & Sturt, B. A.). John Wiley & Sons.

Steel, R. & Ryseth, A. 1990. The Triassic-Early Jurassic succession in the northern North Sea: megasequence stratigraphy and intra-Triassic tectonics. In: *Tectonic events responsible for Britain's oil and gas reserves* (edited by Hardman, R. F. P. & Brooks, J.). *Special Publication* **55**. Geological Society, London, 139-168.

Steiger, R. H. & Jäger, E. 1977. Subcommittee on geochronology: Convention on the use of decay constants in geo- and cosmochronology. *Earth and Planetary Science Letters* **36**, 359-361.

Stephens, M. B., Furnes, H., Robins, B. & Sturt, B. A. 1985. Igneous activity within the Scandinavian Caledonides. In: *The Caledonide Orogen-Scandinavian and Related Areas* (edited by Gee, D. G. & Sturt, B. A.). John Wiley & sons.

Stephens, M. B. & Gee, D. G. 1989. Terranes and polyphase accretionary history in the Scandinavian Caledonides. In: *Terranes in the Circum-Atlantic Paleozoic orogens* (edited by Dallmeyer, R. D.) **230**. Geological Society of America, 17-30.

Stewart, M. 1997. Kinematic evolution of the Great Glen Fault Zone, Scotland. Unpublished PhD thesis, Oxford Brookes University.

Stewart, M. Strachan, R.A. & Holdsworth, R.E. 1997. Direct field evidence for sinistral displacements along the Great Glen Fault Zone: Late Caledonian reactivation of a regional basement structure? *Journal of the Geological Society* **154**, 135-139.

Stewart, M., Strachan, R. A. & Holdsworth, R. E. 1999. Structure and early kinematic history of the Great Glen Fault Zone, Scotland. *Tectonics* **18**(2), 326-342.

Stewart, M., Holdsworth, R. E. & Strachan, R. A. 2000. Deformation processes and weakening mechanisms within the frictional-viscous transition zone of major crustal-scale faults: Insights from the Great Glen Fault Zone, Scotland. *Journal of Structural Geology* **22**, 543-560.

Stewart, M., Strachan, R. A., Martin, M. W. & Holdsworth, R. E. 2001. Constraints on early sinistral displacements along the Great Glen Fault Zone, Scotland: structural setting, U-Pb geochronology and emplacement of the syn-tectonic Clunes tonalite. *Journal of the Geological Society* **158**, 821-830.

Strachan, R. A. 1994. Evidence in North-east Greenland for Late Silurian-Early Devonian regional extension during the Caledonian Orogeny. *Geology* **22**(10), 913-916.

Sturt, B. A. & Roberts, D. 1991. Tectonostratigraphic relationships and obduction histories of Scandinavian ophiolite terranes. In: *Ophiolite genesis and evolution of the oceanic lithosphere Petrology and Structural Geology* (edited by Peters, T., Nicolas, A. & Coleman, R. J.). Kluwer Academic Publishers, 745-769.

Surlyk, F. 1990. Timing, style and sedimentary evolution of late Palaeozoic-Mesozoic extensional basins of East Greenland. In: *Proceedings of Tectonic events responsible for Britain's oil and gas reserves* (edited by Hardman, R. F. P. & Brooks, J.). *Special Publication* **55**. Geological Society, London, 107-125.

Sutton, J. & Watson, J. V. 1986. Architecture of the continental lithosphere. *Philosophical Transactions of the Royal Society, London* **A317**, 5-12.

Terry, M. P., Robinson, P., Hamilton, M. A. & Jercinovic, M. J. 2000. Monazite geochronology of UHP and HP metamorphism, deformation and exhumation, Nordoyane, Western Gneiss Region, Norway. *American Mineralogist* **85**, 1651-1664.

Thirlwall, M. F. 1979. The petrochemistry of the British Old Red Sandstone volcanic province. Unpublished PhD thesis, University of Edinburgh.

Thomson, K. & Underhill, J. R. 1993. Controls on the development and evolution of structural styles in the Inner Moray firth Basin. In: *Petroleum Geology of North West Europe* (edited by Parker, I. J.). Geological Society, Bath.

Torsvik, T. H., Sturt, B. A., Ramsay, D. A., Grønlie, A., Roberts, D., Smethurst, M., Atakan, K., Bøe, R. & Walderhaug, H. J. 1989. Palaeomagnetic constraints on the early history of the Møre-Trøndelag Fault Zone, Central Norway. In: *Palaeomagnetic Rotations and Continental Deformation* (edited by Kissel, K. & Laj, C.). Kluwer Academic Publishers, 431-457.

Torsvik, T. H., Eide, E. A., Meert, J. A., Smethurst, M. A. & Walderhaug, H. J. 1998. The Oslo Rift: new palaeomagnetic and $40\text{Ar}/39\text{Ar}$ age constraints. *Geophysical Journal International* **135**, 1045-1059.

Tucker, R.D., Bradley, D.C., Straeten, C.A.V., Harris, A.G., Ebert, J.R. & McCutcheon, S.R. 1998. New U-Pb zircon ages and the duration and division of Devonian time. *Earth and Planetary Science Letters* **158** (3-4), 175-186

Tullis, J. & Yund, R. A. 1980. Hydrolytic weakening of experimentally deformed Westerly granite and Hale albite rock. *Journal of Structural Geology* **2**, 439-451.

Twiss, R. J. & Moores, E. M. 1992. *Structural geology*. W. H. Freeman, New York.

Underhill, J. R. 1991. Implications of Mesozoic Recent Basin development in the western Inner Moray Firth, UK. *Marine and Petroleum Geology* **8**(3), 359-369.

Underhill, J. R. 1993. Discussion on the location and history of the Walls Boundary Fault and Moine thrust north and south of Shetland. *Journal of the Geological Society* **150**, 1003-1008.

Vigran, J. O. 1970. Fragments of a Middle Jurassic flora from northern Trøndelag, Norway. *Norsk Geologisk Tidsskrift* **50**, 193-214.

Vrolijk, P. & van der Pluijm, B. A. 1999. Clay gouge. *Journal of Structural Geology* **21**, 1039-1048.

Walsh, J. J., Childs, C., Meyer, V., Manzocchi, T., Imber, J., Nicol, A., Tuckwell, G., Bailey, W. R., Bonson, C. G., Watterson, J., Nell, P. A. & Strand, J. 2001. Geometric controls on the evolution of normal fault systems. In: *The Nature and Tectonic Significance of Fault Zone Weakening* (edited by Holdsworth, R. E., Strachan, R. A., Magloughlin, J. F. & Knipe, R. J.) *Special Publication* **186**. Geological Society, London, 157-170.

Warr, L. N. 2000. The Variscan Orogeny: the welding of Pangea. In: *Geological History of Britain and Ireland* (edited by Woodcock, N. H. & Strachan, R. A.). Blackwell Science Ltd, Oxford, 271-297.

Warr, L. N. & Cox, S. 2001. Clay mineral transformations and weakening mechanisms along the Alpine Fault, New Zealand. In: *The Nature and Tectonic Significance of Fault Zone Weakening* (edited by Holdsworth, R. E., Strachan, R. A., Macgloughlin, J. F. & Knipe, R. J.). *Special Publication* **186**. Geological Society, London, 85-101.

Watson, J. 1984. The Ending of the Caledonian Orogeny in Scotland - Presidents Anniversary Address 1983. *Journal of the Geological Society* **141**(MAR), 193-214.

Watterson, J. 1975. Mechanism for the persistence of tectonic lineaments. *Nature* **253**, 520-521.

Wheeler, J. 1987. The significance of grain-scale stresses in the kinetics of metamorphism. *Contributions to Mineralogy and Petrology* **17**, 397-404.

White, S. 1976. The effects of strain on the microstructures, fabrics, and deformation mechanisms in quartzites. *Philosophical Transactions of the Royal Society, London* **283**, 69-86.

White, S. H., Burrows, S. E., Carreras, N. D., Shaw, N. D. & Humphreys, F. J. 1980. On mylonites in ductile shear zones. *Journal of Structural Geology* **2**(1/2), 175-187.

White, S. H., Bretan, P.G. & Rutter, E.H. 1986. Fault-Zone Reactivation : Kinematics and Mechanisms. *Philosophical Transactions of the Royal Society of London* **317**(1539), 81-97.

Wibberley, C. A. J. 1999. Are feldspar-to-mica reactions necessarily reaction-softening processes in fault zones? *Journal of Structural Geology* **21**, 1219-1227.

Williams, H. R. 1987. Stick-slip model for kink band formation in shear zones and faults. *Tectonophysics* **140**, 327-331.

Williams, P. F., Goodwin, L. B. & Ralser, S. 1994. Ductile Deformation Processes. In: *Continental Deformation* (edited by Hancock, P. L.). Pergamon Press, Oxford, 1-27.

Wintsch, R. P., Christoffersen, R. & Kronenberg, A. K. 1995. Fluid-Rock Reaction Weakening of Fault Zones. *Journal of Geophysical Research* **100**(B7), 13021-13032.

Yardley, B. W. D. 1994. *An introduction to Metamorphic Petrology*. Longman Scientific and Technical, London.

Ziegler, P. A. 1982. *Geological atlas of Western and Central Europe*. Elsevier for Shell Internationale Petroleum.

Ziegler, P. A. 1987. Evolution of the Arctic-North Atlantic borderlands. In: *Petroleum geology of north west Europe*. Graham & Trotman, London, 1201-1204.

Zoback, M. D., Zoback, M. L., Mount, V. S. & ten others. 1987. New evidence on the state of stress on the San Andreas fault system. *Science* **238**, 1105-1111.

